Xenophagy in response to Gram-positive *Staphylococcus aureus* and Gram-negative *Salmonella enterica* sv. Typhimurium

A thesis presented by

Ohood Aqeed Radhi

In fulfilment of the requirement for the degree of

Doctor of Philosophy

June 2018

Strathclyde Institute of Pharmacy and Biomedical Sciences

University of Strathclyde

Declaration

This thesis is the result of the author's original research. It has been composed by the author and has not been previously submitted for examination which has led to the award of a degree. The copyright of this thesis belongs to the author under the terms of the United Kingdom Copyright Acts as qualified by University of Strathclyde Regulation 3.49.

Due acknowledgment must always be made of the use of any material contained in, or derived from, this thesis.

Signed: Ohood Aqeed Radhi

Date: 01/06/2018

Acknowledgements

I thank Allah (SWT) for giving me the ability to complete my studies to this level. Firstly, I would like to express my sincere gratitude to my supervisor, Dr Edmond Chan for all his help and the continuous support of my PhD study, for his patience, motivation, and immense knowledge. His guidance has continually helped me in the research and writing of this thesis. I would also like to thank my second supervisor, Dr Jun Yu who aided me with the microbiology side of my project. Besides my supervisors, I would like to thank my assessor, Professor Susan Pyne for her insightful comments and encouragement, and also for the previous stimulating discussion which has given me incentive to further widen my research perspectives.

My acknowledgements also go to the Ministry of Higher Education in Iraq for awarding me the scholarship and providing me with the opportunity to study abroad to undertake my PhD degree in the United Kingdom. Also, thanks to Al Kufa University in Iraq and the Nursing faculty, which gave me this opportunity to develop my skills through study at Strathclyde University.

Last but not least, I wish to extend my thanks to all members of my family, in particular my husband for his prayers and giving me the strength to achieve my dream to obtain such success. I also would like to thank my sisters and my brothers for their support throughout the duration of my PhD. I also cannot forget my son Yasir, who makes me happy even when I am stressed. Finally, I offer my kind regards to all of my friends for every moment we have spent together abroad.

Publications

Papers

Lysosomotropism depends on glucose: a chloroquine resistance mechanism Abdul

Gallagher, L. E., **Radhi, O. A**., Abdullah, M. O., McCluskey, A. G., Boyd, M. and Chan, E. Y. W. 24 Aug 2017 In: Cell Death and Disease. 8, 14 p., e3014.

Verbal presentation

Ohood A. Radhi, Jun Yu and Edmond Y.W. Chan (2016). Xenophagy in response to gram-positive *Staphylococcus aureus* and gram-negative *Salmonella enterica* sv. Typhimurium. SIPBS research day. University of Strathclyde, Glasgow, UK.

Poster presentation

Ohood A. Radhi, Jun Yu and Edmond Y.W. Chan (2015). Xenophagy in response to gram-positive *Staphylococcus aureus* and gram-negative *Salmonella enterica* sv. Typhimurium. SIPBS student day. University of Strathclyde, Glasgow, UK.

Ohood A. Radhi, Jun Yu and Edmond Y.W. Chan (2017). Xenophagy in response to gram-positive *Staphylococcus aureus* and gram-negative *Salmonella enterica* sv. Typhimurium. SIPBS research day. University of Strathclyde, Glasgow, UK. (Poster Prize).

Contents

List of Tables

List of Figures

List of Abbreviations

agr	accessory gene regulator
AMBRA1	autophagy and beclin 1 regulator 1
AMPK	AMP-activated protein kinase
AP3D1	Adaptor-related protein complex 3 delta 1
ARHGAP28	Rho-Type GTPase-Activating Protein 28
ATG	autophagy gene regulators
Bcl-2	B-cell lymphoma 2
Bif-1	Bax interacting factor 1
cAMP	Cyclic adenosine monophosphate
Cas9	CRISPR-associated protein 9
CD164	Cluster of differentiation 164
CDC	Centres for Disease Control and Prevention
c-di-AMP	Cyclic-di-adenosine monophosphate
CFU	Colony forming unit
CRISPRs	Clustered Regularly Interspaced Short Palindromic Repeats
DAZL	Deleted in Azoospermia-Like
DMEM	Dulbecco's modified eagle's medium
DSB	Double-strand break
EBSS	Earle's balanced salt solution
EGFP	Enhanced Green Fluorescent Protein
EPAC	Exchange protein activated by cAMP
ER	Endoplasmic reticulum
ERES	ER exit sites
FBS	Fetal bovine serum
FDR	False discovery rate
FIP200	FAK family interacting protein of 200 kD
GABARAP	Gamma-aminobutyric acid receptor associated proteins
GeCKO	Genome-scale CRISPR Knock-Out
gRNA	guide RNA
HDR	homology-directed repair

Hla	α-hemolysin or α-toxin
InlK	Internalin K
IRF8	Interferon Regulatory Factor 8
IsaB	Immuno-dominant surface antigen B
KLHL17	Kelch-Like 17
LAMP	Lysosome-associated membrane proteins
LLO	Listeriolysis O
LLOME	Leucyl-Leucyl-O-Methyl ester
LRSAM1	E3 ubiquitin ligase leucine-rich repeat and sterile α motif-containing 1
MaGeck	model-based Analysis of Genome-wide CRISPR/Cas9 Knockout
MEF	Mouse embryonic fibroblasts
MGE	mobile genetic elements
MOI	Multiplicity of infection
mTOR	Mechanistic target of rapamycin
mTORC1	Mechanistic target of rapamycin complex 1
MVP	Major Vault Protein
NADPH oxidase	nicotinamide adenine dinucleotide phosphate-oxidase
NGS	Next Generation Sequencing
NHEJ	non-homologous end joining
NLRC4	NLR family CARD domain-containing protein 4
NLRs	nucleotide-binding oligomerization domain-like receptors or NOD-Like Receptors
PAM	Protospacer Adjacent Motif
PAMPs	pathogen-associated molecular patterns
PAS	Pre-autophagosomal structure
PI3K	Phosphoinositide 3-kinase
PI3K-III	class III phosphatidylinositol 3-kinase autophagy nucleation complex
PI3P	Phosphatidylinositol 3-phosphate
PLEKHM1	Pleckstrin homology domain-containing protein family member 1
PRRs	pattern recognition receptors
PSMα	phenol soluble modulin alpha
RAPGEF3	Rap Guanine Nucleotide Exchange Factor 3
RRA	robust ranking aggregate
SaPI	*Staphylococcus aureus* Pathogenicity Islands

SCC	Staphylococcal cassette chromosome
SCV	Salmonella-containing vacuoles
Sifs	*Salmonella*-induced filaments
SQSTM1	sequestome 1
TAK1	Transforming growth factor beta-activated kinase 1
TALENs	Transcription activator-like effector nucleases
TBK1	TANK-binding kinase 1
TRIM	Tripartite motif
TSB	Tryptic soy broth
TSC	tuberous sclerosis complexes
TTSS	Type three secretion system
ULK	Unc-51 like autophagy activating kinase
UVRAG	UV radiation resistance-associated gene protein
VPS41	Vacuolar protein sorting 41
WIPI	WD-repeat protein interacting with phosphoinositides
wt	wild type
ZFNs	Zinc Finger Nucleases

Abstract

Autophagy is an important process for cell survival in the human body, which plays a critical role in fighting infections. Some infections exploit the autophagic system and are often promoted by autophagy. Recent evidence has suggested that *Staphylococcus aureus* has specialised mechanisms to evade xenophagy, thus allowing bacterial survival and replication within autophagosomes, leading to eventual cell death. ULK1 is a serine/threonine kinase that plays an essential role during the early steps of autophagosome biogenesis, but its roles during xenophagy following *Staphylococcus aureus* infection have been unclear. ULK1 represents an excellent candidate for drug targeting to control autophagy under various settings.

This study aimed to investigate the role of autophagy in defence against two disease-causing bacteria that are known for their ability to damage cells: *Salmonella enterica* sv. Typhimurium and *Staphylococcus aureus*. A further aim was to study the role of the ULK1 complex in xenophagy following infection by *Staphylococcus aureus* and furthermore to test ULK1 inhibitors as a novel therapy to restrict MRSA infection in cells. In addition, in this project, CRISPR genetic selection approaches were developed, aimed to find new host cell genes required for *Staphylococcus aureus* and *Salmonella enterica* sv. Typhimurium infection.

The results indicated two different roles of autophagy: 1) to provide a protective niche for MRSA, and 2) to provide a mechanism to fight infection by *Salmonella enterica* sv. Typhimurium. Importantly, treatment of cells with a ULK1/2 small molecule inhibitor strongly inhibited cell killing following infection by MRSA. However, ULK1/2 inhibition made cells more sensitive to cell death following infection by *Salmonella enterica* sv. Typhimurium. Thus, ULK1 inhibitors may be a novel therapeutic method for fighting infection by MRSA.

Also, in this project, we found that screening with a freely available CRISPR-Cas9 library successfully identified the host genes essential for the toxicity of cells by MRSA (NCTC8325) or *Salmonella enterica* sv. Typhimurium. This was confirmed by functional validation and may open the door for novel putative therapeutic targets in future.

Chapter 1

Introduction

1.1. Autophagy

1.1.1. Introduction to autophagy

The term autophagy is derived from the Greek word which means self-eating. The first reported usage of the term autophagy was by Belgian cell biologist Christian de Duve in 1963, during his studies of the lysosome (for which he received the Nobel Prize in 1974) (Klionsky, 2008). Autophagy is a catabolic process that plays a vital role in the degradation of damaged organelles by engulfing them into a double membrane vesicle termed an autophagosome, which is then delivered to the lysosome (Bento et al., 2016). Autophagy has multiple essential intracellular quality control roles in recycling cellular compartments and removal of damaged organelles in response to different stress conditions, such as nutrient limitation, viral infection, and oxidative stress (as reviewed in (Filomeni et al., 2015, Mercer et al., 2018).

By classical classifications, there are three main forms of autophagy in mammalian cells termed: macroautophagy, microautophagy and chaperone-mediated autophagy (CMA). During macroautophagy, cytoplasmic contents become enclosed in a double membrane structure termed the autophagosome that then fuses with the lysosome (Martens, 2016). On the other hand, during microautophagy, components are directly internalised into the lysosome by invagination (inward folding of the lysosomal membrane) (Li et al., 2012). During chaperone-mediated autophagy (CMA), proteins with a KFERQ-like motif are recognised by Hsp70 chaperones on the lysosome, where they pass through the lysosomal membrane-associated protein 2 (LAMP-2A) macromolecular complexes into the lysosome for degradation processes (Bandyopadhyay et al., 2008, Orenstein and Cuervo, 2010). In contrast with these, macroautophagy, herein referred to simply as autophagy, is the predominant canonical pathway under most physiological situations and has been the best characterised and understood. Microautophagy and chaperone-mediated autophagy will not be discussed in this study.

1.1.2. Mechanism of autophagy

The full mechanism of autophagy can be divided into distinct steps. Firstly, the initiation step features formation of the isolation membrane (phagophore). The phagophore extends and elongates to take up and enclose cell components, such as organelles, malformed proteins, long-lived proteins and ribosomes. In addition, more recent studies have shown important roles of organelle-phagy where autophagy can selectively target

endoplasmic reticulum (ER), lysosome and the nucleus (Mochida et al., 2015, Maejima et al., 2013, Smith et al., 2017).

Phagophore extension eventually forms a double bilayer membrane-enclosed autophagosome. The autophagosome containing cargo next undergoes fusion with the lysosome (as reviewed in (Bento et al., 2016, He and Klionsky, 2009). In the final stages of autophagy, the autophagosomal contents are degraded by lysosomal acid proteases and permeases, and transporters export amino acids back into the cytoplasm to use in metabolism and building macromolecules (as reviewed in (Yang and Klionsky, 2010, Gallagher et al., 2016).

The steps of autophagy initiation are regulated by sequential action of a network of gene products which have been collectively named autophagy gene regulators (ATG). Genetic studies in yeast have identified 41 ATG genes (so far) that are required for autophagy, most of which have been conserved from yeast to mammals (Harnett et al., 2017). The core autophagy factors have been classified into four functional groups: 1) the ATG1/ULK1 kinase complex; 2) the class III phosphatidylinositol 3-kinase (PI3K) complex containing ATG14; 3) the ATG9 trafficking system; and 4) two ubiquitin-like conjugation systems that control ATG8/LC3 and ATG5-ATG12 modifications (Reggiori et al., 2012).

1.1.3. Regulation mechanisms and signalling pathways of autophagy

1.1.3.1 Regulation of initiation

1.1.3.1.1. ULK1 complex

ATG1/ULK1 kinase activation initiates autophagy. In fact, ATG1/ULK1 kinase has been proposed to be autophagy's most upstream regulator. ULK1 is a serine/threonine protein kinase that represents the mammalian orthologue of the yeast ATG1. Based on the findings of our group's past work, the role of ULK1 is crucial for autophagy. For example, our group found that RNAi-mediated suppression of ULK1 alone could inhibit autophagy in cell lines indicating that ULK1 is likely to be the major form in many systems (Chan et al., 2007). ULK1 is situated on chromosomes 12q24.3 with a predicted 112 kDa molecular size. The regions of the ULK1 protein include a C-terminal interacting domain, a serine-proline rich region and an N-terminal kinase catalytic domain.

ULK1 functions to promote autophagy initial steps; therefore, ULK1 has been proposed to be a potential target to inhibit the pro-survival autophagy pathways, for example, in cancer (Chen et al., 2014). The kinase activity of ULK1 has been shown to be important

for the initiation of autophagy, for instance by blocking enzymatic activity using chemical inhibitors and kinase-dead mutants, causing an autophagic flux block (Egan et al., 2015, Petherick et al., 2015, Chan et al., 2009).

ULK1 and ULK2 in cells appear to be constitutively in complexes with no less than three proteins, which include ATG13, FIP200 and ATG101 (Mizushima, 2010, Mercer et al., 2018). By studies of cells from knockout, it was established that the FIP200 subunit was absolutely necessary for autophagy (Hara et al., 2008). Moreover, ATG13 is essential for autophagy as demonstrated in siRNA experiments (Hosokawa et al., 2009, Jung et al., 2009). In addition, both ATG13 and FIP200 are needed for proper ULK1 localisation to sites of isolation membrane formation (Ganley et al., 2009, Hara et al., 2008, Hosokawa et al., 2009). Adding ATG13 or FIP200 recombinant proteins increased the kinase activity of recombinant ULK1 *in vitro*, clearly showing that both of these two proteins positively promote overall activity of a ULK1 complex (Ganley et al., 2009, Jung et al., 2009, Hosokawa et al., 2009).

The interaction between ULK1 and ATG13 appears to be direct (Hosokawa et al., 2009, Jung et al., 2009). However, the FIP200/ULK1 interaction mechanism is more uncertain. It was suggested that ATG13 could mediate binding between ULK1 and FIP200 (Hosokawa et al., 2009, Jung et al., 2009). However, FIP200 alone has also been shown to have the capability of binding with ULK1 (Ganley et al., 2009). ATG13 and FIP200 have been found to bind the ULK1 C-terminal domain (Hosokawa et al., 2009, Jung et al., 2009).

ATG101 was subsequently identified as a member of the core ULK1 complex (Mercer et al., 2009). The interaction between ATG101 protein and ULK1 was not direct, but via a bridging interaction with ATG13 (Hosokawa et al., 2009, Mercer et al., 2009). ATG101 helps maintain ULK1 basal phosphorylation and promotes its stabilisation along with that of ATG13 (Hosokawa et al., 2009, Mercer et al., 2009).

From the above, we can conclude that ATG13 binds directly with ULK1 and FIP200, mediating the interaction between these two proteins. However, it was also observed that FIP200 can bind ULK1. Moreover, ATG101 interacts with the complex through ATG13.

1.1.3.1.2. Upstream regulation of ULK1

In the current model, ULK1 receives signals downstream of the main cellular energy sensors to regulate autophagy (Chan et al., 2007, Hosokawa et al., 2009, Jung et al., 2009). In this model, autophagy initiation is tightly controlled by the ULK1 complex, sensing upstream signals from MTOR complex 1 (MTORC1) and AMPK (Hosokawa et al., 2009, Kim et al., 2011). A mechanism of ULK1 regulation by AMPK and mTORC1 has been proposed based on several studies over the last 10 years (Figure 1.1).

MTOR is a serine-threonine kinase that takes part in several cell processes including protein synthesis, migration and proliferation (Saxton and Sabatini, 2017). MTOR is a main regulator of the nutrient signalling pathway and is a central inhibitor of autophagy (Laplante and Sabatini, 2012, Efeyan et al., 2013). It has been established that MTOR can be found in two different complexes: MTORC1 (MTOR complex 1) and MTORC2 (MTOR complex 2). A number of published reports have asserted that only mTORC1, but not mTORC2, is compatible with the ULK1 complex (Saxton and Sabatini, 2017).

MTORC1 detects variations in the amounts of cellular amino acids by means of a lysosomal sensing system (Goberdhan et al., 2016). MTORC1 is usually active under nutrient-rich conditions. Activated MTORC1 signals to the ULK complex by means of direct interaction between ULK1 and Raptor (Ganley et al., 2009, Hosokawa et al., 2009, Jung et al., 2009). Multiple phosphorylation events occur following this association. MTORC1 leads to phosphorylation of both ULK1/2 and mATG13 leading to a potent inhibition of the kinase activity of both of these components and subsequent inhibition of autophagic activity (Ganley et al., 2009, Hosokawa et al., 2009, Jung et al., 2009). Further studies have revealed that ULK1 is phosphorylated by mTORC1 on serine 757, 638 and 758 (Cemma et al., 2011, Shang et al., 2011), and of ATG13 at serine 258 (Puente et al., 2016).

MTORC1 disassociates from the complex upon nutrient starvation leading to dephosphorylation of ULK1/2 and mATG13. In addition to autophosphorylation, ULK1/2 also phosphorylates mATG13 and FIP200 components of the complex (Ganley et al., 2009). Through this direct interaction, therefore, MTOR controls activity of the ULK complex and autophagy in mammalian cells.

The energy sensor AMP activated protein kinase (AMPK) is a further regulator of autophagy and, more particularly, the ULK complex. AMPK functions in all eukaryotes and maintains cellular homeostasis in response to intracellular energy levels. AMPK has

been suggested to play a main function in autophagy induction via Raptor and TSC1/2 complex phosphorylation to deactivate MTOR (Gwinn et al., 2008, Inoki et al., 2003b).

TSC2 is a GTPase activating protein (GAP), which accelerates GTPase activity of Rheb. AMPK can phosphorylate TSC2, and this brings about the GTP hydrolysis of Rheb leading to its inactivation (Inoki et al., 2003a). For that reason, AMPK can inhibit mTORC1 and thereby promote autophagy. There are further pathways linking AMPK to MTORC1 regulation. Gwinn et al. (2008) explained that AMPK is capable of phosphorylating the MTORC1 binding protein Raptor at two distinct sites (Ser792 and Ser722), which is then followed by binding to 14-3-3 proteins and inhibition of mTORC1 (Gwinn et al., 2008). In addition, AMPK binds ULK1 directly, leading to the phosphorylation of both ULK1 and ATG13 (Puente et al., 2016). The binding between AMPK and ULK1 was mapped to the proline/serine-rich domain of ULK1 at residues 654-828. This region was found to be necessary for AMPK-dependent regulation of autophagy (Lee et al., 2010). In fact, AMPK has been found to phosphorylate multiple ULK1 sites, including (most notably) S317, S467, S555, T574, S637 and S777, which has been generally proposed to activate ULK1 and induce autophagy (Kim et al., 2011, Egan et al., 2011).

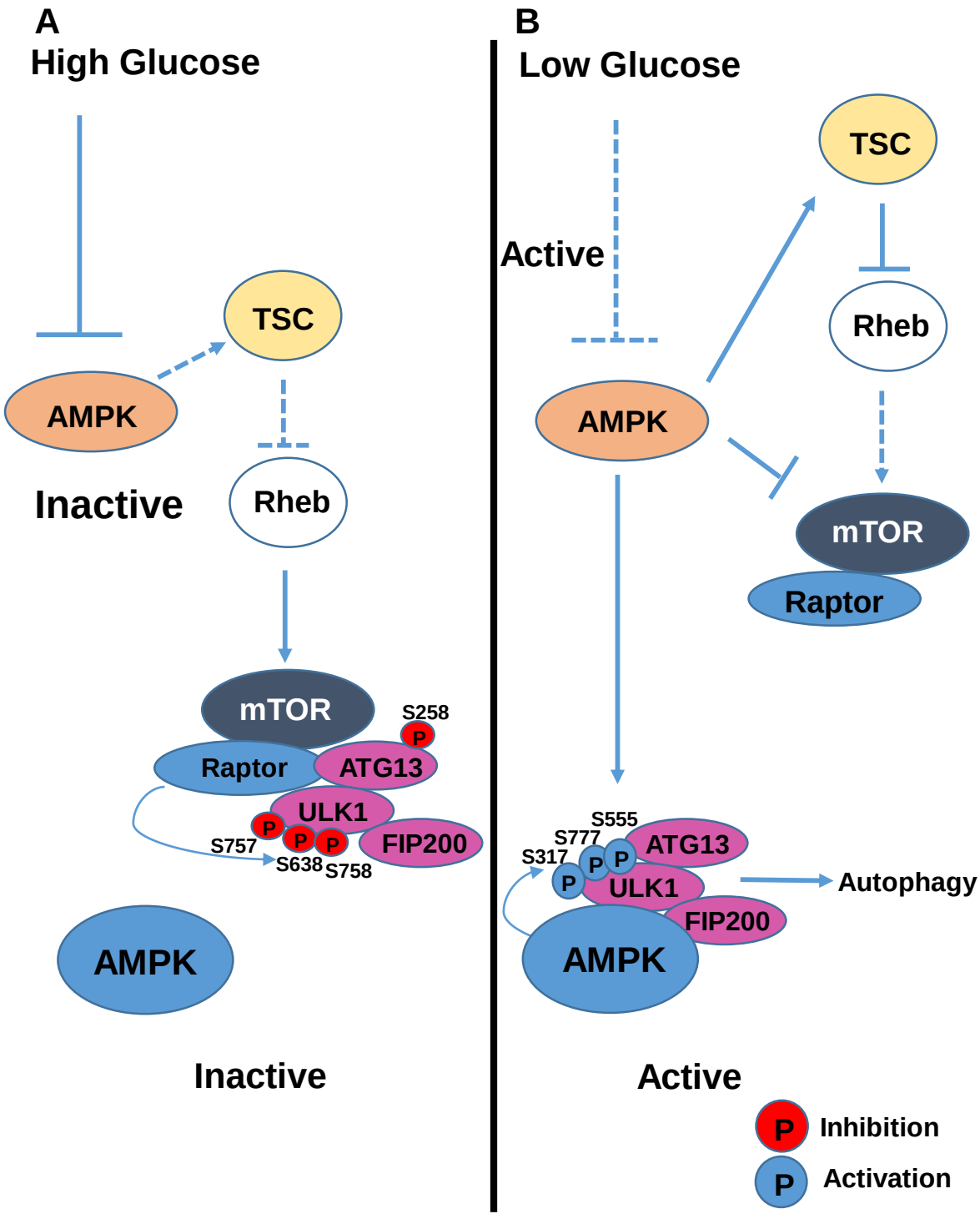

Figure 1.1: The mechanism of ULK1 regulation by AMPK and mTORC1.
A) In nutrient rich conditions, mTORC1 is bound to ULK1 through Raptor. mTORC1 phosphorylates multiple residues of ULK1 that constrains the activity of ULK1. Among these are S757, S638 and S758 phosphorylation, which further constrains the binding of AMPK.
B) Upon nutrient deprivation, mTORC1 is inactivated. Activated AMPK plays a role in the downregulation of mTORC1 through phosphorylating TSC2 and Raptor. There is disassociation of mTORC1 from ULK1 while dephosphorylation of S757 promotes binding of AMPK. Multiple ULK1 sites which include S317, S555 and S777 are phosphorylated by AMPK, while ULK1 is activated, leading to autophagy induction. Figure adapted from (Kim et al. 2011).

1.1.3.1.3. Downstream regulation by the ULK1 complex

The activated ULK1/2 complex promotes autophagy, and one primary pathway has been shown to involve activation of the type III phosphatidylinositol 3-kinase autophagy nucleation complex (PI3K) (otherwise recognised as VPS34) (Russell et al., 2013). To activate autophagy, there are several phosphorylation events that occur through association of ULK1 with PI3K as depicted in Figure 1.2. VPS34 forms a stable complex with p150 (VPS15 orthologue) and Beclin-1. The ULK1 protein directly phosphorylates Beclin-1 at Ser14, resulting in activated VPS34 activity, PI3P production and autophagy initiation (Russell et al., 2013). ULK1 was also shown to phosphorylate ATG14L at Ser29 to bring about increased VPS34 activity and autophagy induction (Wold et al., 2016, Park et al., 2016). Other findings have suggested that ULK1 phosphorylates VPS34 on Ser249, although the exact functional role of this event is uncertain (Egan et al., 2015).

Interestingly, Beclin-1 has been reported to bind several other proteins that can either increase (ATG14L, UVRAG, Bif1, and AMBRA-1) or decrease (Bcl2, BclxL, Rubicon) autophagic activity (Sun et al., 2008, Di Bartolomeo et al., 2010, Itakura et al., 2008, Liang et al., 2006, Matsunaga et al., 2009, Pattingre et al., 2009, Zalckvar et al., 2009, Zhong et al., 2009, Takahashi et al., 2007). Also, ULK1 has been shown to control the VPS34 complex via AMBRA1 (Di Bartolomeo et al., 2010). AMBRA was discovered to be a potential molecular link between the two kinases and a substrate of ULK1. In this system, AMBRA was shown to tether the Beclin-1/VPS34 complex to microtubules. Upon starvation, ULK1 could phosphorylate AMBRA and release it from microtubules, which would allow the whole PI3KC3 complex to translocate to the autophagy initiation sites and induce autophagy (Di Bartolomeo et al., 2010).

The association of Beclin-1 to different factors appears to control the extent or localisation of VPS34 activity and therefore autophagy. One key Beclin-1 binding protein is UVRAG. UVRAG is interesting as this protein has been shown to stimulate autophagy by competitively binding Beclin-1 away from ATG14L interactions (Itakura et al., 2008, Matsunaga et al., 2009). Also, UVRAG can bind to Bif-1, which is suggested to have the capability to bind to membranes and change their shape. Bif-1 is thought to have this capability because of its N-BAR domain which can promote curvature of the membrane (Itoh and De Camilli, 2006). The anti-apoptotic protein Bcl-2 also has been shown to bind Beclin-1 and this interaction negatively controls autophagy (Levine et al., 2008). Phosphorylation of Bcl-2 by c-Jun N-terminal kinase 1 (JNK-1) and also death-

associated protein kinase (DAPK) causes disassociation of Bcl-2 and Beclin-1 stimulating autophagy (Wei et al., 2008).

Once activated, the ATG14-Beclin 1-VPS34 complex generates phosphatidylinositol 3-phosphate (PI3P) at autophagosome membrane nucleation sites. Sites of concentrated PI3P on membranes therefore drive the recruitment of PI3P-binding effectors that trigger initiation of phagophore assembly (Sun et al., 2008). More recently, VPS34 has been proposed to further act in a feedback loop with the ULK1 complex. Generation of PI3P can lead to increased recruitment or stabilisation of ULK1 via a lipid-binding domain existing in ATG13 (Karanasios et al., 2013).

In yeast, the key downstream PI3P-binding effector is comprised of the ATG18/ATG2 complex (Obara and Ohsumi, 2008). In mammals, members of the ATG18 homologous WIPI family (for example WIPI2b) have been characterised as the PI3P binding autophagy effectors that promote phagophore assembly at sites linked to the cellular endomembrane network (Polson et al., 2010). Furthermore, ATG16L1 directly binds WIPI2b. Mutation experiments and ectopic localisation of WIPI2b to plasma membrane show that WIPI2b is a PI3P effector upstream of ATG16L1 and is required for LC3 conjugation and starvation-induced autophagy through recruitment of the ATG12–5-16L1 complex (Dooley et al., 2014).

1.1.3.1.4. Phagophore assembly site formation

As PI3P is generated and assembly factors are recruited, autophagosome formation begins at the phagophore assembly site. In yeast, there is a corresponding assembly site which is also known as the pre-autophagosomal structure (PAS). In mammalian cells, the membrane source (or localisation) of the phagophore assembly site is still a continuing matter of debate. Strong arguments have been presented for the role of the endoplasmic reticulum (ER) in the initiation of autophagy. A number of findings have further detected that endoplasmic reticulum (ER) exit sites (ERES) (specialised ER regions where proteins are sorted into the secretory system), play the key role in the formation of autophagosomes (Axe et al., 2008, Hayashi-Nishino et al., 2009). While ERES may be a predominant site based on the wide base of evidence, it is unlikely to be the sole source across all cell types or situations. For example, other groups have suggested that the mitochondrial outer membrane may be another source of the isolation membrane (Hailey et al., 2010, Hamasaki et al., 2013).

Of importance, the Golgi apparatus and post-Golgi compartments which contain ATG9 also contribute to the formation of the autophagosome membrane (Ohashi and Munro, 2010, Mari et al., 2010). ATG9, which is well conserved from yeast to mammals, is the only transmembrane protein of all the ATG regulatory factors. ATG9-containing membranes are often vesicles that engage in a dynamic cycling pattern, moving from numerous peripheral sites (primarily Golgi) to deliver new membrane for autophagosome formation at the assembly site (Gelino and Hansen, 2012, Saitoh et al., 2009, Geng et al., 2008). Several ATG proteins have important functions in the regulation of ATG9 cycling in yeast autophagy. For example, it was discovered in initial studies that ATG27 can be seen shuttling between the Golgi complex, PAS and mitochondria. With ATG27 mutation, ATG9 is limited to mitochondria. In addition, ATG23 also helps modulate this cycling pattern (Legakis et al., 2007). All these three proteins (ATG9, ATG23 and ATG27) cycle between the PAS and the other sites, and depend upon one another for this movement. Also, ATG9, ATG23 and ATG27 play a role in ATG protein retrieval from the PAS (Legakis et al., 2007).

In mammalian cells, an analogous system regulates ATG9 localisation. The ULK1 complex, once at the assembly site, serves to generally recruit other ATG proteins needed for autophagosome formation (such as Beclin1 and WIPI). Interestingly, the trafficking of mammalian ATG9 to form autophagosomes was found to be ULK1-dependent as initially shown by Young et al. (2006). The authors explored changes in the mATG9 protein localisation during autophagy induction. It was found that mATG9 is localised in juxta-nuclear structures recognised as a trans-Golgi network in addition to peripheral puncta structures (shown to be endosomes) (Young et al., 2006). Upon starvation, the juxta-nuclear portion of mATG9 was reduced while the peripheral fraction increased. These changes suggested translocation of mATG9 to endosomes upon starvation and autophagy. Moreover, mATG9 co-localised with LC3, showing the processing of the puncta structures into autophagy vesicles. The mATG9 translocation was repressed by ULK1 knockdown. Knockdown of ATG13 to block the ULK1 complex also inhibited proper cycling of ATG9-containing vesicles (Chan et al., 2009).

ULK1 has, in recent times, been found to act synergistically with the protein kinase SRC, to phosphorylate ATG9, thereby encouraging the ATG9-positive vesicles translocation to the autophagy sites of initiation (Zhou et al., 2017).

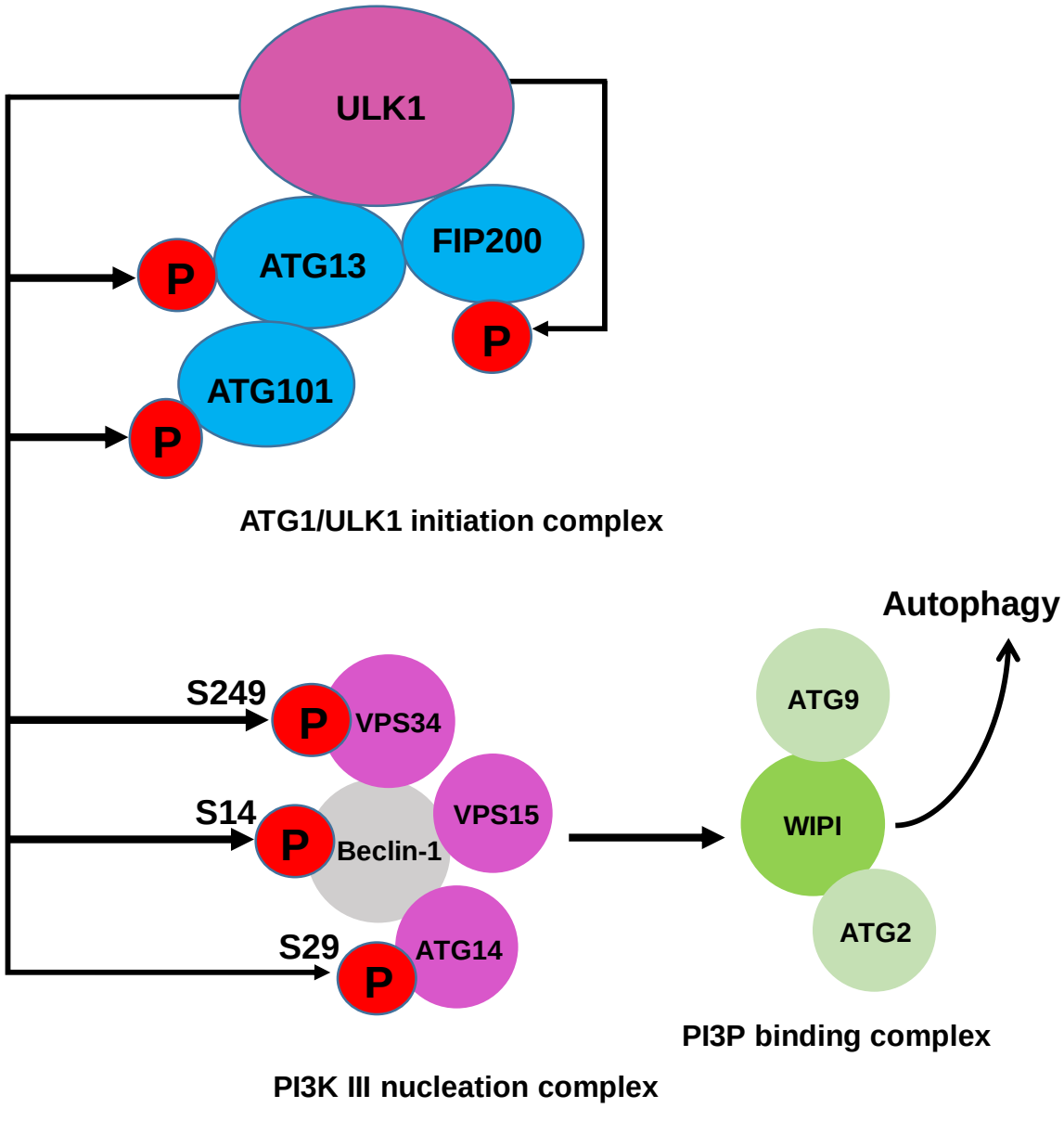

Figure 1.2: Downstream regulation by the ULK1 complex. ULK1 phosphorylates Beclin-1 at Ser14, resulting in activated VPS34 activity, PI3P production and autophagy initiation. ULK1 also phosphorylates ATG14L at Ser29 to bring about increased VPS34 activity and autophagy induction. Additionally, ULK1 phosphorylates VPS34 on Ser249.

1.1.3.2. Elongation

Once the initial phagophore is formed, the next stage is to expand and elongate the membrane to generate a double-membrane enclosed vesicle called the autophagosome. The elongation step is driven by the biochemical modifications of the ATG7-ATG10 pathway. This pathway leads to activation of the first core ubiquitin-like conjugation reaction which promotes formation of an ATG12-ATG5-ATG16L oligomeric complex on the initiating autophagosomal membranes (Fujita et al., 2008).

The stepwise assembly of this complex begins when ATG12 becomes activated by ATG7 (E1 ubiquitin activating enzyme-like), which is then transferred to ATG10 (E2 ubiquitin activating enzyme-1like). ATG12 is finally covalently linked to ATG5. The ATG12-ATG5 complex then forms a higher order molecular complex consisting of 4 x [ATG12-ATG5-ATG16L] structures (Fujita et al., 2008, Mizushima et al., 2001). Elongation of the isolation membrane and autophagosomal closure involves the ATG7-ATG3 complex that catalyses the second ubiquitin-like reaction involving ATG8 family proteins.

In mammalian cells, there are a range of different members of the ATG8 family, which are subdivided into the LC3 and GABARAP families, and include LC3A, LC3B, LC3C, GABARAP, GABARAPL1 and GABARAPL2 (Weidberg et al., 2010, Shpilka et al., 2011). However, Microtubule-associated protein 1 light chain 3 B (LC3B) remains, to date, the best characterised representative (Martens, 2016). In this second conjugation system, pro-LC3 is first cleaved by ATG4, leading to the formation of cytosolic, inactive, LC3-I. LC3-I is then conjugated to phosphatidylethanolamine (PE) via the function of ATG7 (E1-like reaction) which next transfers LC3-I to ATG3 (E2-like reaction) leading to conjugation to PE to form active LC3-II (Kabeya et al., 2000).

LC3 lipidation is fundamental for the association with the membrane. It has been shown that ATG5-ATG12/ATG16L complex recruits ATG3 and LC3 to the plasma membrane and functions as a scaffold for LC3 lipidation (Fujita et al., 2008). It was also suggested that the ATG5-ATG12/ATG16L complex could be instrumental as 3-lik enzyme for LC3 (Hanada et al., 2007, Fujita et al., 2008). Recently, ULK1 has also been suggested to regulate the ubiquitin-like conjugation machinery. ULK1 was reported to phosphorylate the protease ATG4B, which converts pro-LC3 to LC3-I (Pengo et al., 2017). Phosphorylation of ATG4B at ser316 by ULK1 results in inhibition of ATG4B catalytic activity, although the precise consequences of this on autophagy are still not clear.

ATG8 members like LC3B provide a critical link between the autophagosome membrane and specific capture of autophagy cargo. Cellular cargo is commonly targeted to autophagosomes by adaptor proteins such as p62 (also known as SQSTM1 (sequestosome 1)) or NBR1 (which were the two key members initially identified). Multiple classes of autophagy adaptor proteins have now been characterised, which bind to ubiquitinated cellular targets. The adapter proteins generally contain an LC3-interacting region (LIR). This short linear motif was first identified in p62, but this motif has been repeatedly found in a range of proteins from mammals and yeast (Ichimura et al., 2008, Noda et al., 2010). The LIR motif binds to the nascent phagophore through their interaction with LC3 proteins, thereby defining the mechanism to specifically target multiple types of cargo to autophagy degradation (Yoo and Jung, 2018, Lazarou et al., 2015, Lamark et al., 2017). In relation to our project, adaptor-mediated targeting of intracellular bacteria for autophagy has emerged as a prominent pathway (and this system will be discussed in further detail below).

The LC3/GABARAP proteins also play a critical role of recruiting other autophagy regulatory factors to the phagophore. In relation to this thesis, Atg8/LC3 interacts with the Atg1/ULK1 complexes via LIR motifs (termed AIM, Atg8-interacting motif, in yeast). This interaction occurs via LIR in the disordered regions of Atg1/ULK1 (Kraft et al., 2012, Alemu et al., 2012). Interestingly, an LIR motif is also found in mammalian ATG13 (Alemu et al., 2012). The ATG13 LIR crystal structure bound to LC3 has been characterised (Suzuki et al., 2014). In this mechanism, the role proposed for these interactions is to ensure that the ULK complex has stable association with the phagophore via binding ATG8 family proteins.

1.1.3.3. Maturation and fusion

As described above, the initial phagophore elongates to eventually completely surround the cytosolic components and create new autophagosomes (Fujita et al., 2008). LC3-II does not separate from the autophagosome, unlike the ATG16 complex, and remains attached until autophagosome fusion with the lysosome. In this regard, it has been proposed that LC3-II may play a vital role in the closure of autophagosomes (Fujita et al., 2008). In addition to their role in closure, the GABARAP and LC3 sub-families are believed to take part in other autophagosome biogenesis, such as autophagosome expansion, and sequestration of selective autophagy cargo. ATG8 proteins function in the expansion of isolation membrane, for instance, by serving as tethering or fusion aspects, as proposed previously (Weidberg et al., 2011), or by recruiting and triggering

the remaining ATG proteins, as presented earlier (Kraft et al., 2012, Joachim et al., 2015). Other more recent data highlight a range of roles. It was found in one system that LC3/GABARAP proteins are primarily involved in autophagosome-lysosome fusion, with, interestingly, a less prominent role in formation of autophagosomes (Nguyen et al., 2016).

Fusion of autophagosomes with the vacuole takes place in yeast as a proposed single event. In contrast, maturation of autophagosomes in mammalian cells has been proposed to take place through several fusion events with diverse endosome populations, such as early endosomes and multi-vesicular bodies, together with late endosomes and lysosomes (Reggiori and Ungermann, 2017). Proton pumps and enzymes vital for the degradation of cargo, and proteins needed for the fusion within the next vesicle form, would be delivered by successive steps. Overall, a dramatically more dynamic and complex system is therefore proposed in mammalian cells.

For regulatory mechanisms, the small Rab GTPases and soluble N-ethylmaleimide–sensitive factor attachment protein receptors (SNAREs) are the two main groups of factors controlling membrane trafficking (Galluzzi et al., 2017). It has been found that the SNARE protein syntaxin-17 plays a key role by inserting into the autophagosome membrane and mediating fusion with the lysosome. This mechanism involves a unique C-terminal tandem transmembrane domain in syntaxin-17. Syntaxin-17 thereby goes on to bind its cognate SNARE and the homotypic fusion and protein sorting (HOPS)-tethering complex (Jiang et al., 2014).

The autophagy pathway is closely interconnected to endocytic degradative pathways, as evidenced by several protein regulatory machineries that coordinate these membrane trafficking routes. One of these includes Rab7, which constitutes the late endosomal/lysosomal Rab GTPase (Stenmark, 2009, Hutagalung and Novick, 2011). Various downstream effectors of Rab7 have been characterised, and an example of these includes Rab7-interacting lysosomal protein (RILP) (Cantalupo et al., 2001). RILP functions by interacting with the HOPS VPS41 subunit and recruiting the whole HOPS complex onto the late endosomal compartment (Lin et al., 2014). The HOPS complex and Rab7 thereby coordinate the fusion of endosomes and autophagosomes with lysosomes.

The interaction between the pleckstrin homology domain that contains protein family member 1 (PLEKHM1), a lysosomal adaptor, and the HOPS complex provides a further direct mechanism to regulate trafficking from autophagy. This pathway involves a LC3-interacting region (LIR) in PLEKHM1 that mediates binding directly with LC3-ATG8 on autophagosomal membranes (McEwan et al., 2015a). This mechanism agrees with other data showing LC3/GABARAPs and recruitment of adaptor proteins (such as PLEKHM1) to fully formed autophagosomes in order to facilitate autophagosome–lysosome fusion (Stolz et al., 2014, McEwan et al., 2015a, Nguyen et al., 2016). These results imply that LC3/GABARAPs make an important contribution in late fusion stages after formation of the autophagosome. As related to xenophagy, interestingly, *Salmonella enterica* sv. Typhimurium utilises a complex containing PLEKHM1, Rab7 and VPS41 (HOPS) to mobilise tethering of the phagolysosome membranes to the SCV. This mechanism thereby helps form a protective niche for proliferation in the primary cells and tissues (as demonstrated in infected mice) (McEwan et al., 2015b). The subversion of host cell autophagy/xenophagy by bacterial pathogens will be further detailed later in this introduction.

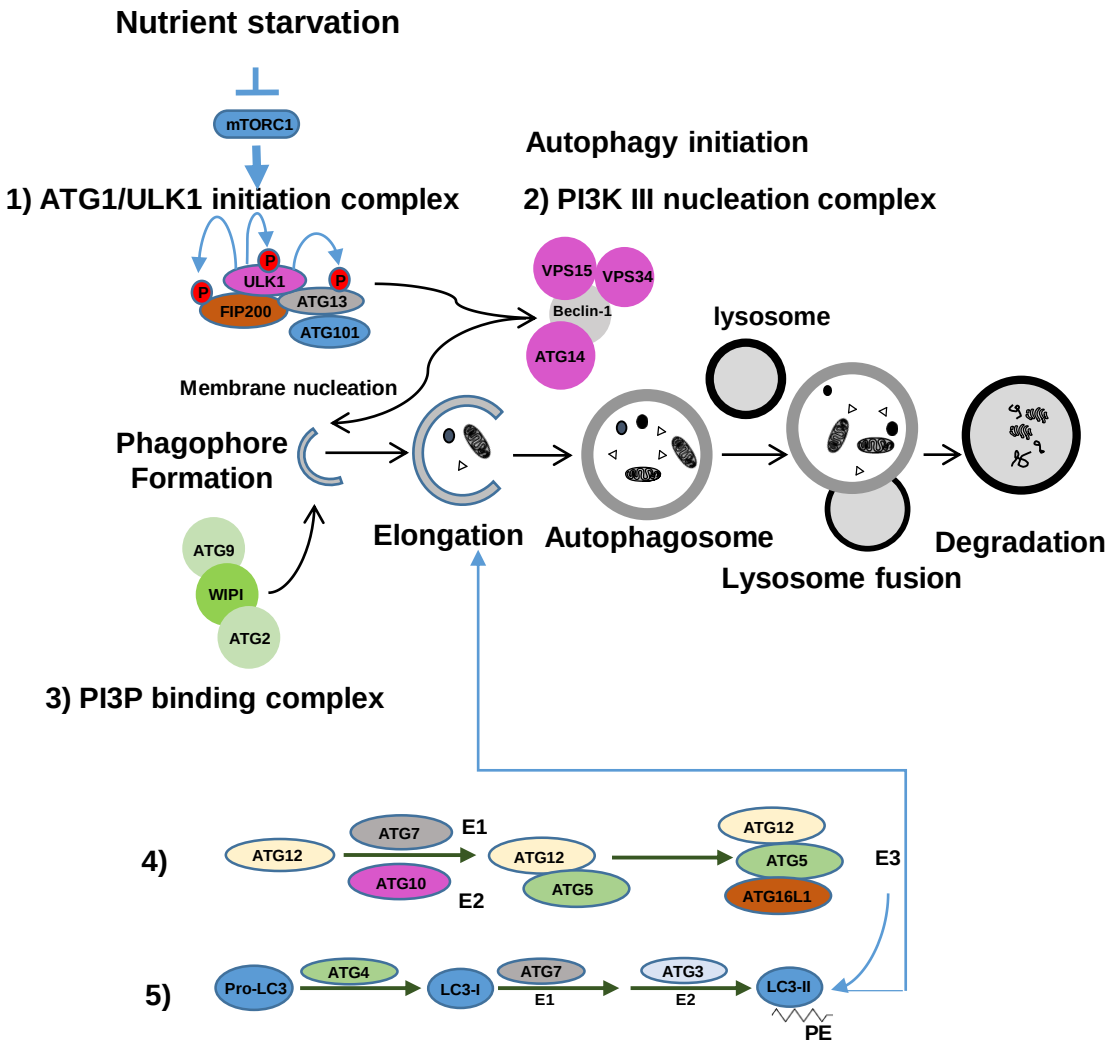

Figure 1.3: Autophagy involves a stepwise series. autophagy induction, membrane nucleation, phagophore formation, autophagosome elongation, lysosome fusion, and degradation. These steps are controlled by: 1) the ATG1/ULK1 initiation complex; 2) the PI3K III nucleation complex; 3) the PI3P-binding complex; 4) the ATG5-ATG12 conjugation system; and 5) the ATG8/LC3 conjugation system. In the latter, LC3 is cleaved by ATG4 to form LC3-I and is then conjugated with phosphatidylethanolamine to become LC3-II, which is incorporated into pre- autophagosomal membranes.

1.2. Specific autophagy

The characterisation of autophagy was originally made as a cytosolic bulk degradation pathway, which was induced by glucagon and amino acid deprivation in liver cells (Takeshige et al., 1992, Ashford and Porter, 1962, Novikoff and Essner, 1962, De Duve and Wattiaux, 1966, Mortimore and Schworer, 1977, Schworer and Mortimore, 1979). The main role in this context was to assist in the recycling of building blocks in order to maintain metabolic balance. Autophagy in this system was understood to be non-selective towards its substrates or cargos (Kopitz et al., 1990).

On the other hand, it has become better appreciated over the last ten years that autophagy also makes a contribution to intracellular homeostasis in non-starved cells through the selective degradation of cargo. This selective degradation forms a part of cellular quality control by removing material that would be harmful to the cell, such as aggregated proteins (Pankiv et al., 2007), damaged mitochondria (Wong and Holzbaur, 2014, Heo et al., 2015, Lazarou et al., 2015), excess peroxisomes (Kim et al., 2008, Deosaran et al., 2013), invading pathogens (Thurston et al., 2009, Zheng et al., 2009, Wild et al., 2011) and damaged lysosomes (Maejima et al., 2013) and also reviewed in (Kraft et al., 2009, Khaminets et al., 2016, Rogov et al., 2014). Additionally, autophagy was also able to remodel the ER during homeostatic response pathways engaged by ER stress (Smith et al., 2017).

1.2.1. Xenophagy

The main role of autophagy has been understood to be degradation of cell components in response to nutrient starvation. In addition to this recycling function, autophagy is now understood to also have essential roles in the innate immunity against a variety of infectious agents, such as bacteria, viruses, fungi and parasites (Levine et al., 2011). Autophagy of intracellular pathogens (as a specialised pathway) has been termed xenophagy, derived from the Greek meaning “strange eating”.

Generally, xenophagy involves formation of autophagosome phagophores to engulf invading organisms and restrict their growth, in addition to delivery of entrapped pathogenic organisms to the lysosome for degradation (Knodler and Celli, 2011, Gomes and Dikic, 2014). Xenophagy therefore results in degradation and clearance of pathogenic microorganisms (and also liberation of metabolites that have been utilised during pathogen infection). This xenophagy response supports multiple needs in the host

defence mechanism to limit bacteria growth, reduce infection for other cells and promote cell survival of the host cell (Devenish and Lai, 2015). Accumulating evidence indicates that autophagy and ATG genes play an essential role in this process, as expected, although evolution has led to development of specific roles.

The earliest reported example for autophagy targeting bacteria was in polymorphonuclear leukocytes from guinea pigs infected with *Rickettsia conorii*, observed more than two decades ago (Rikihisa, 1984). Since then, this basic autophagy response has been further observed for many types of bacteria from a range of studies *in vitro*. However, it is becoming apparent that xenophagy responses can vary depending on the type of infection and invading pathogens. Invading bacteria can be classified as cytosolic if they inhabit the cytoplasm of host cells, such as Group A *Streptococcus* (GAS) (Barnett et al., 2013). A bacterial infection can also be vacuolar, if post-infection they reside mostly in a vacuole, which they tailor to their own survival by release of bacterial proteins (Knodler and Celli, 2011) such as, *Mycobacterium tuberculosis* (Deretic, 2008), and *Salmonella enterica* sv. Typhimurium (Thurston et al., 2012).

Many studies have indicated that bacteria can also escape or move from the vacuoles to freely reside in the host cytoplasm, but these bacteria can then be effectively and easily captured into autophagosomes. For instance, streptolysin O is secreted by GAS to break down the vacuole membrane, thus allowing the bacteria to get into the cytosol (Nakagawa et al., 2004). Following access to the cytoplasm, these bacteria can thereafter be attacked and neutralised by autophagy. Several GAS bacteria are then engulfed inside a multilamellar compartment where they die as a result of successive fusion with the lysosome (Nakagawa et al., 2004).

Numerous groups have suggested that even if invading pathogens are able to hide within vacuoles, the bacteria may still be targeted by autophagic machinery. A perfect example of this is with *Mycobacterium tuberculosis.* Mycobacteria evade the immune system of the host cell by hiding within a vacuole and preventing fusion with the lysosome. However, the bacteria can then be targeted by autophagy capture of the entire phagosome when the cells are further stimulated by IFNγ, or treated with the autophagy activator rapamycin (Gutierrez et al., 2004).

In the case involving *Salmonella enterica* serovar Typhimurium (*Salmonella enterica* sv. Typhimurium), the bacteria are targeted by autophagy while the Salmonella-containing

vacuoles (SCVs) become damaged (Birmingham et al., 2006). About 20% of the population of intracellular bacteria were observed to be LC3 (+) (meaning targeted by autophagy) at one-hour post-infection. Indeed, Autophagy has been shown to control the growth of bacteria, as cells lacking autophagy (ATG5-deficient MEFs) are more permissive of the growth of *Salmonella enterica* sv. Typhimurium than wild-type MEF (Birmingham et al., 2006). The targeted *Salmonella enterica* sv. Typhimurium became fully enclosed in multilamellar structures, visible by electron microscopy, at one hour post-infection due to autophagic bacterial capture (Zheng et al., 2009). From the initial studies, it was concluded that autophagy has the ability to target intracellular bacteria for degradation, whether they hide within vacuoles or break free into the cytosol. However, further detailed analysis has shown that the trafficking of *Salmonella* is complex with multiple routes, as summarised later in a separate section (see Figure 1.5).

1.2.1.1. The association of innate immunity and xenophagy activation

The innate immune system is activated after infection by pathogens and induces inflammation to protect the host (Kawai and Akira, 2009). Pattern recognition receptors (PRRs) are key players of the innate immune system, sensing Pathogen-associated molecular patterns (PAMPs), such as lipopolysaccharide (LPS) and flagellin, and play a critical role in induction of the inflammatory response. Toll-like receptors (TLRs) represent host-surface PAMP recognition receptors (PRRs) that are activated by their cognate PAMPs (Delgado et al., 2009).

PRRs work in concert with autophagy; for example, during activation of TLR4 by bacterial LPS (Xu et al., 2007). TLR activation enhances the interaction of the TLR adaptors MyD88 and Trif with Beclin 1. Consequently, the binding of Beclin 1 by Bcl-2 is reduced leading to an increase in autophagy (Shi and Kehrl, 2008). Also, TLR4 has led to TANK binding kinase 1 (TBK1) mediated phosphorylation of Optineurin (OPTN), which increases the ability of this cargo receptor to bridge LC3 and ubiquitinated *Salmonella enterica* sv. Typhimurium (Wild et al., 2011). Other intracellular innate immune receptors have been described to work in concert with autophagy: nucleotide-binding oligomerization domain 1 (NOD1) and NOD2 (members of the NOD-like receptor (NLR) family). It was found that NOD1 and NOD2 NLRs recognise bacterial peptidoglycans (Travassos et al., 2010). In macrophages, NOD1 and NOD2 NLRs thereby further signal intracellularly to activate autophagy by recruiting ATG16L1 to the plasma membrane at the entry site of invading *Shigella flexneri* and *Listeria monocytogenes* leading to their efficient sequestration in autophagosomes (Travassos et al., 2010, Irving et al., 2014,

Homer et al., 2012, Cooney et al., 2010, Chauhan et al., 2015). Therefore, immune signalling and xenophagy are coordinated by PRRs at the plasma membrane, at least for certain bacteria.

1.2.1.2. Inflammasomes in response to bacterial infection

Inflammasomes are a family of multiprotein complexes that lead to activation of caspase-1, thus eliciting maturation and release of critical pro-inflammation cytokines from the IL-1 family, such as IL-1β and IL-18. Inflammasomes function to detect the molecular patterns of pathogens to cause innate immunological responses of inflammation and are responsible for host defence against a number of infectious agents (Perry et al., 2007). Conversely, over-activated inflammatory reactions via inflammasomes can result in pathogenesis and damage. For this reason, inflammatory responses have to be tightly regulated at different levels during the activation of host immune protection against invading pathogens, while at the same time preventing host damage. Evidence has demonstrated that autophagy also takes part in the fine control of inflammatory responses in order to prevent pathogenic stimuli and potential damage (Deretic, 2012, Qin et al., 2016, Ma et al., 2017).

The main inflammasome component features an NLR, an intracellular sensor that takes part in recognising and responding to danger signals and microbes (Davis et al., 2011, Vladimer et al., 2013). Four types of inflammasome complexes have been described: NLR family, pyrin domain-containing 1 (NLRP1), NLRP3, IPAF and AIM2. A large body of evidence indicates that autophagy can be stimulated by inflammasomes after infection. For instance, NLRP3 has been found to enhance autophagy after infection by *Pseudomonas aeruginosa* in macrophages (Deng et al., 2016). These results suggested that autophagy mediated by NLRP3 was critical for the clearance of bacteria in cells.

In addition, activation of NLR and TLR can lead to the initiation of NF-κB signalling and transcriptional activation of inflammatory genes (Liu et al., 2017). For instance, *Salmonella*-triggered inflammation was a product of multiple immune pathways including the activation of pattern-recognition modules like TLRs and NOD receptors. Furthermore, *Salmonella* pathogenicity effectors contributed to the induction of NF-κB activity (Ashida et al., 2014, Keestra et al., 2013). The E3 ubiquitin ligase LUBAC was found to remodel and amplify the ubiquitin platform present on cytosolic *Salmonella* to recruit the NF-κB essential modulator (NEMO) and autophagy receptors (Fiskin et al., 2016, van Wijk et al., 2017, Noad et al., 2017). By this mechanism, LUBAC promotes

cytokine production via NF-κB to work together with xenophagy in the restriction of bacterial proliferation. Therefore, these examples show how inflammasomes can promote xenophagy and cytokine production to fight infection.

However, inflammasome pathways are further complex. Autophagy can also play the opposite role in controlling excessive inflammation by mediating mitochondrial integrity or removal of aggregates that signal inflammasome activators. In the event of influenza A infection, NOD2 serves to detect the viral RNA to facilitate the elimination of damaged mitochondria through induction of ULK1 phosphorylation to limit excessive NLRP3 activation (Lupfer et al., 2013). Furthermore, autophagy inducers suppress IL-1β and IL-18 production mediated by NLRP3 and this suppression helps to alleviate tissue damage due to inflammation (Shaw et al., 2013, Guo et al., 2014, Abderrazak et al., 2015).

The above studies highlight the multiple pathways linking xenophagy upstream and downstream to infection and inflammation. Details in the mechanisms underlying autophagic control of the immune response are still unclear. In relation to this research project, our GeCKO library screening detected several candidates functioning in immunity. Future investigation from our screen could help to clarify the fundamental role of autophagy in the immune response and provide a molecular basis for innovative drug development.

1.2.1.3. Bacterial targeting via the autophagic pathway (Ubiquitin)

Ubiquitin serves an essential function to tag proteins for the purpose of degradation by the proteasome and, furthermore, for the aggregation of proteins for lysosomal degradation (Shaid et al., 2013). Studies conducted in the recent past have shown a function of ubiquitin in the selective elimination of intracellular infection through the process of autophagy (Li et al., 2016). For instance, intracellular *Salmonella*, *Shigella* and *Listeria* are all tagged by ubiquitin in the cytosol (Fiskin et al., 2016, Dupont et al., 2009, Pei et al., 2017). Poly-ubiquitinated proteins accumulate on bacteria that enter the host cell cytosol. This ubiquitination is now a well-characterised signal for xenophagy to recognise the invading bacterium, requiring adaptor proteins to bridge the targeted bacteria to LC3 on autophagosome elongation membranes (Zheng et al., 2009).

Studies of antibacterial xenophagy have uncovered at least four key adaptors that directly mediate interaction between ubiquitin and LC3: p62/SQSTM1 (Pankiv et al., 2007, Zheng et al., 2009), NBR1 (Kirkin et al., 2009), OPTN (Wild et al., 2011) and

NDP52 (nuclear dot protein 52 kDa, also called CALCOCO2) (von Muhlinen et al., 2012, Ivanov and Roy, 2009). These adaptor proteins all contain ubiquitin binding domains (UBDs) which are distinct. For example, during xenophagy, OPTN recognises M1- or K63-linked ubiquitin chains present on bacteria, while, NDP52 binds ubiquitylated cargo via its ubiquitin-binding zinc finger. On the other hand, p62 recognises K63-linked ubiquitin chains via its ubiquitin-associated (UBA) domain (Wild et al., 2011, Thurston et al., 2009, Zheng et al., 2009, Verlhac et al., 2015).

Through their UBDs, the adaptor proteins are then bound to the nascent phagophore through their interaction with LC3 proteins via LIR motifs (Noda et al., 2008, Randow and Youle, 2014). p62 has recently been found to take part in autophagy regulation through the induction of the biogenesis of autophagosome. In this further novel mechanism, p62 promotes its own delivery, and that of other cargoes, to the autophagosome via its ZZ-binding domain. Besides its function in autophagy regulation, p62 thereby functions to mediate the crosstalk between the Ub-proteosome system and autophagy (Cha-Molstad et al., 2017). More information about ubiquitin and adaptor proteins will be discussed in detail in relation to *Salmonella enterica* sv. Typhimurium infection in the section below.

1.2.1.4. The ability of bacteria to evade autophagy

Despite the cellular xenophagy pathways that serve to kill bacteria, most microorganisms have also evolved to use a range of different strategies to evade or exploit autophagy for survival and replication in a host. Therefore, identification of host cell interaction mechanisms exploiting autophagy may provide new insights and strategies for therapeutic intervention in infectious diseases (Yuk et al., 2012).

The ability of a pathogen to subvert the autophagy process can occur through multiple pathways. One of these ways is the production of virulence factors that allow the bacteria to avoid being recognised by the autophagy machinery. This method of subverting degradation via autophagy is by far the best studied and is employed by those pathogens that are able to escape from vacuoles into the cytosol. Examples such as *Shigella flexneri* and *Listeria monocytogenes* are briefly summarised below (but note there are other types of autophagy subversion; for example, *Yersinia pseudotuberculosis* (Moreau et al., 2010) and *Legionella pneumophila* (Amer and Swanson, 2005)).

Autophagic capture can be evaded in the cytosol by *Shigella flexneri*. The IcsA protein expressed on the surface of *Shigella flexneri* (utilised to promote actin-based motility) is

a direct target for autophagy by binding to the autophagy component ATG5. However, IcsB, another bacterial protein secreted by a type 3 secretion system, competitively binds to IcsA and masks it from recognition by ATG5 and the autophagy pathway (Ogawa et al., 2005). Therefore, *Shigella* has evolved to rely on IcsB for autophagy evasion and survival.

Listeria monocytogenes is another bacterium that can avoid autophagy recognition. *Listeria* is known to be able to subvert the autophagy system in different ways, depending on whether a high or a low amount of Listeriolysis O (LLO) is secreted (Figure 1.4). The *Listeria monocytogenes* are found in the cytosol where they express high amounts of Listeriolysin O (LLO). The presence of ActA protein (normally found on the bacterial surface and involved in actin-based motility and cell-to-cell-spread) leads to the protection of this bacteria from autophagy recognition (Yoshikawa et al., 2009). The presence of ActA on the bacterial surface also prevents ubiquitination. This mechanism further prevents the recruitment of adaptor molecules, which in turn prevents detection of *Listeria* by autophagy (Perrin et al., 2004). In the absence of ActA, the intracellular *Listeria monocytogenes* are also masked from the autophagic recognition by internalin K (InlK). This mechanism is achieved through a major vault protein (MVP) complex interaction with the host (Dortet et al., 2011). When both protection virulence factors (ActA and InlK) are targeted, the bacteria become vulnerable. Overall, the use of virulence factors for protein camouflage in order to be undetectable by autophagy appears to be a widely used and effective strategy for intracellular survival.

It should, however, be noted that if the amount of LLO expressed is low, *Listeria* cannot evade the phagosome. In this case, a spacious Listeria-containing phagosome (SLAP) is produced and the bacteria slowly replicate over time (Birmingham et al., 2008). Moreover, fusion of SLAP with lysosomes is blocked, and thus this blocks the degradation of the vacuole content. The SLAP formation occurs via the Listeria adhesion protein (LAP) pathway (Cemma and Brumell, 2012). Overall, mechanisms are in place for persistent infection of *Listeria monocytogenes* under both low and high LLO levels.

Other bacteria have evolved further ways to prevent the autophagosome from fusing with a lysosome to avoid the degradative processes and destruction (Levine et al., 2011, Powers and Bubeck Wardenburg, 2015). For instance, *Staphylococcus aureus* can produce α-toxin (also known as hemolysin) to help promote bacterial replication in an autophagosome niche (O'Keeffe et al., 2015, Schnaith et al., 2007). More recently,

another *Staphylococcus aureus* virulence factor Immuno-dominant surface antigen B (IsaB) was shown to play an important role in inhibiting fusion with lysosomes to create a double membrane autophagosome protective niche (Liu et al., 2015). Xenophagy subversion by *Staphylococcus aureus* is the focus of this thesis and will be further introduced later in this chapter.

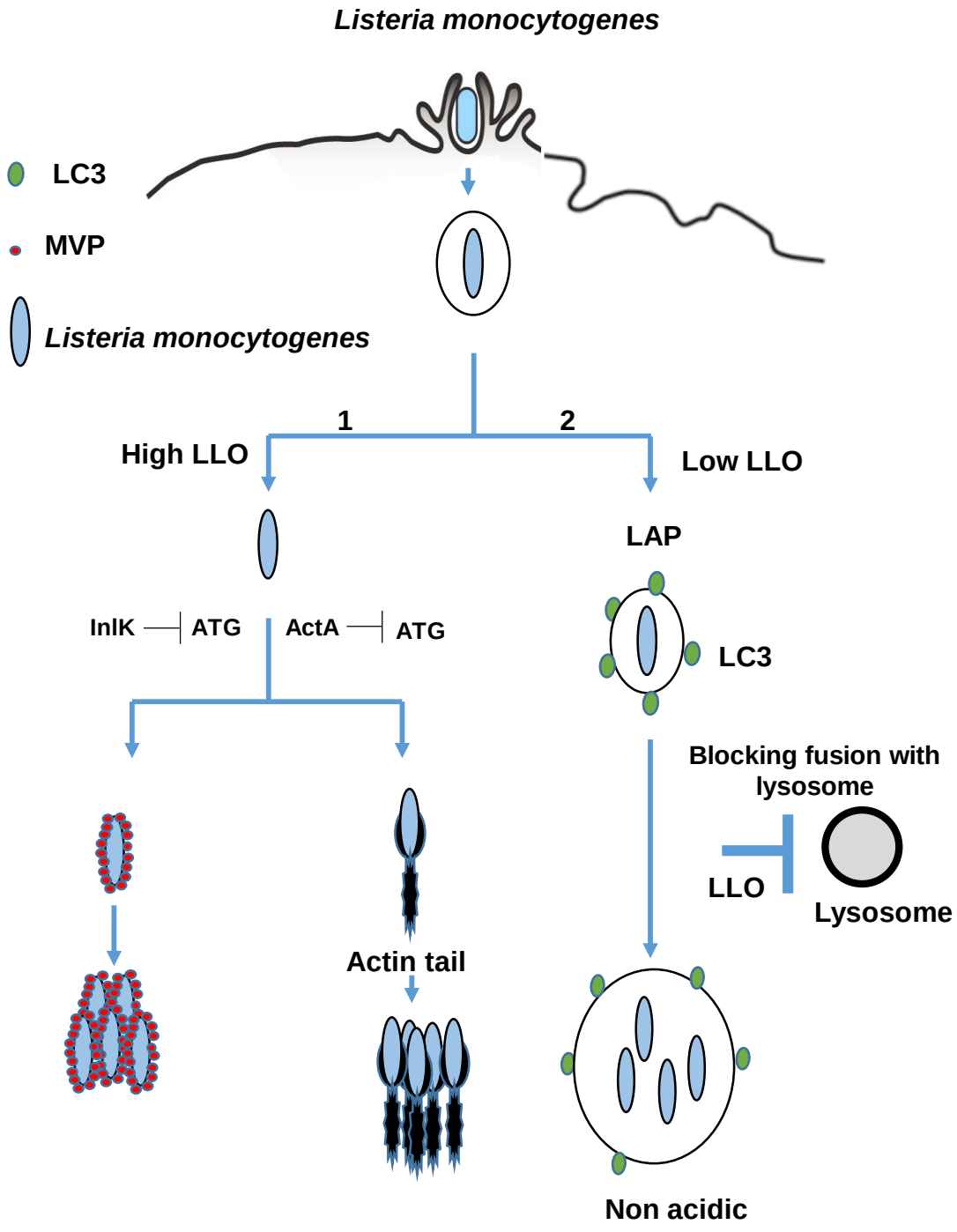

Figure 1.4: Overview of subverting autophagy by *Listeria monocytogenes*. Upon the entry of *Listeria* in the cell, expression of Listeriolysin O (LLO) begins. Depending on the amount of LLO:
1) There is an option on the part of the bacteria for an actin tail to be created for motility through ActA (High LLO). It is possible for bacteria to be masked by ActA. Therefore they will not be ubiquitinated and recognized by the autophagy machinery. MVPs are also recruited by InlK, which, in turn, masks the bacteria. Bacteria masked by MVPs are not ubiquitinated and not recognized by the autophagy machinery.
2) A membrane carrying LC3 can also capture *Listeria* (low LLO). The fusion of the vacuole that was created with lysosomes is prevented by the excreted LLO while there is transformation of the vacuole into a spacious *Listeria* containing phagosome (SLAP). Figure adapted from (Cemma and Brumell 2012) & (Dortet.,et al. 2011).

1.3. Pathogen interactions with host cells via autophagy

1.3.1. *Salmonella enterica* sv. Typhimurium

Salmonella enterica sv. Typhimurium are small rod-shaped Gram-negative intracellular bacteria belonging to the Enterobacteriaceae family. Infection with this bacteria generally begins with the ingestion of contaminated food or water so that *Salmonella* reach the intestinal epithelium, followed by colonisation of the small and large intestine resulting in gastroenteritis. The symptoms include vomiting, diarrhoea, headache and fever (Fabrega and Vila, 2013). *Salmonella enterica* sv. Typhimurium can also disseminate from the intestine and produce serious, sometimes fatal, infections in a number of systemic organs to affect a significant number of patients in both developed and developing countries (Kariuki et al., 2006, Kozak et al., 2013, Keestra-Gounder et al., 2015). According to the CDC, about 40,000 cases of Salmonellosis are recorded each year in the United States alone and approximately 400 deaths each year arise due to acute Salmonellosis (Fabrega and Vila, 2013). *Salmonella enterica* sv. Typhimurium has become gradually resistant to traditional antibiotics, leading to serious concerns of potential spread of antibiotic resistant determinants to other bacteria (Wattiau et al., 2011).

1.3.1.1. *Salmonella enterica* sv. Typhimurium pathogenicity

A combination of bacterial genetic and cell biology studies indicated that *Salmonella* can use specific virulence mechanisms to induce host cell death during infection (Guiney, 2005). *Salmonella* has acquired a large number of virulence genes and other pathogenicity determinants via horizontal gene transfer (McClelland et al., 2001). The majority of the genes coded for these virulence factors are located within highly conserved, genomic sequences known as *Salmonella* pathogenicity islands (SPI). Thus far, five SPIs have been reported to make a major contribution to pathogenesis (Fabrega and Vila, 2013, Schlumberger and Hardt, 2006). Additional virulence factors are also found in the pSLT (stably inherited virulence plasmid). Adhesion proteins, flagella, and biofilm-related proteins all contribute significantly in determining the overall virulence of the *Salmonella* pathogen (Fabrega and Vila, 2013, Latasa et al., 2005, Ledeboer et al., 2006, Mazurkiewicz et al., 2008, Stecher et al., 2004, Kolde et al., 2012).

SPI-1 encodes several effector proteins (such as SipBCD) that are required for bacterial penetration of the epithelial cells of the intestine. These factors mediate actin cytoskeletal rearrangements and hence internalisation of the bacteria. These effectors are

translocated into the host cell via a type III secretion system, termed T3SS-1 (Haraga et al., 2008). SPI-2 encodes factors of T3SS-2 which functions to secrete effector proteins, such as SifA, PipB2, SseJ, SopD2, SseF, SseG, SpvC, SspH1 and SseL, SteC, SpvB, SspH2 and SrfH, that enable *Salmonella* vacuolar movement across the membrane of the SCV (Haraga et al., 2008, Jennings et al., 2017).

Salmonella enterica sv. Typhimurium harbours three additional pathogenicity islands, SPI-3, SPI-4 and SPI- 5, which are primarily required for growth and survival of bacteria within the host in the systemic phase of disease. Additionally, identified virulence factors encoded by SPI-5 appear to mediate the inflammation and chloride secretion which characterise the enteric phase of disease (Marcus et al., 2000).

The pSLT-type plasmid encodes virulence-associated genes which are known to play a significant role during the later stages of the infection process and contribute to the intracellular growth at sites beyond the intestine (Marcus et al., 2000). Also, *Salmonella enterica* sv. Typhimurium has been found to harbour hybrid plasmids. One example, pUO-stRV2, is approximately 140kb in size and may have originated from the pSLT plasmid with the acquisition of a complex, antimicrobial locus involved in multiple antibiotic resistance of *Salmonella enterica* sv. Typhimurium (Herrero et al., 2008).

1.3.1.2 Cell invasion to form intracellular *Salmonella enterica* sv. Typhimurium

When *Salmonella enterica* sv. Typhimurium enters the human body from contaminated food or water, most of the pathogen is killed by the acidic conditions in the stomach. However, a fraction of the bacteria may survive and progress to the intestine. *Salmonella enterica* sv. Typhimurium uses flagella to swim towards the surface of the epithelial cells and bacterial factors promote attachment to the epithelial cell surface (LaRock et al., 2015, Fabrega and Vila, 2013). Thus, *Salmonella enterica* sv. Typhimurium uses its two type III secretion systems (T3SS) to invade epithelial cells, and then typically resides in the *Salmonella*-containing vacuole (SCV) (Brumell et al., 1999).

The SPI-1 encodes for factors that drive host-cell invasion through the formation of needle-like structures that inject further different effector proteins. These injected virulence factors induce actin cytoskeleton rearrangements to facilitate the cell invasion (Haraga et al., 2008). Then, *Salmonella enterica* sv. Typhimurium uses the type III secretion system -2 (T3SS-2) to begin injecting another range of effector proteins across the vacuole. These effectors manipulate the host vacuole, and modify the lipid and

protein content of the SCV. This induces morphological changes, including membrane associated actin polymerization and endosomal tubulation of the vacuolar membrane. By way of this process, the bacteria are protected inside their vacuole from the host intracellular defence mechanisms (LaRock et al., 2015, Haraga et al., 2008).

The process of *Salmonella* infection can be studied mechanistically in cultured host cells. As shown in Figure 1.5, the intracellular fates of *Salmonella enterica* sv. Typhimurium during *in vitro* infection can show four major routes (Birmingham et al., 2006, Huang and Brumell, 2014, Scheidel et al., 2016). **In population (1)**, most of the bacteria enter the classical SCVs. These are organelles that have acquired lysosomal markers, for instance, LAMP-1. Maturation of the SCV is altered by the intracellular bacteria to evade the defensive systems of the host induced by phagocytosis; for instance, the delivery of NADPH oxidase, induction nitric oxide and fusion with lysosomes (Brumell and Grinstein, 2004, Holden, 2002, Buchmeier and Heffron, 1991, Vazquez-Torres et al., 2000, McGourty et al., 2012). By 6–8 hours after infection of cultured cells, *Salmonella enterica* sv. Typhimurium replication is accompanied by the formation of long, membranous structures that emanate from the SCV, called *Salmonella*-induced filaments (Sifs) (Garcia-del Portillo et al., 1993, Brumell et al., 2001, Birmingham et al., 2005).

The extension of these filaments begins from the *Salmonella* effector-covered vacuoles, such as SifA. For example, a very important role for SifA was found in SCV membrane maintenance and for replication of bacteria in macrophages (Beuzon et al., 2000). The loss of the SCV several hours after uptake was discovered following infection of *Salmonella* SifA-mutant and bacteria were found to be freely in the cytosol. Therefore, SifA was clearly important for SCV membrane maintenance and for the bacteria's replication in macrophages. The role of SifA in the maintenance of SCV integrity makes it critical for the prevention of autophagy initiation. The survival of *Salmonella enterica* sv. Typhimurium also requires phosphoinositide 3-phosphate (PI(3)P) modulation by myotubularin 4 (MTMR4). In this way, PI(3)P regulation is also essential for SCV integrity and stability, thus playing an additional role in autophagy modulation (Teo et al., 2016).

In population (2), it can be noted that usually the autophagy machinery does not recognise the majority of the SCV inside the host cells. However, there are several mechanisms for the autophagy machinery to detect invading *Salmonella* and induce a xenophagy response. It is proposed that the TTSS effectors destroy some (~ 20%) of the SCV early after infection (~1 hour), thereby leading to a significant level of autophagy

induction (Birmingham et al., 2006). Due to SCV damage, *Salmonella* can escape into the cytoplasm to obtain nutrients for rapid growth (Brumell et al., 2002).

The first eat-me signal – Ubiquitin: The bacteria that escape the SCV stay in the cytosol. These bacteria are then recognised by the ubiquitination system and become surrounded by ubiquitinated proteins to form a targeting signal (Perrin et al., 2004, Wang et al., 2018). Interestingly, ubiquitin has been found to target *Salmonella* inside damaged SCV, as well as cytosolic *Salmonella* (Scheidel et al., 2016). A host ubiquitin E3 ligase, leucine-rich repeat and sterile α-motif-containing 1 (LRSAM1), was found to have a key role in generating the bacteria-associated ubiquitin signals for *Salmonella enterica* sv. Typhimurium (Huett et al., 2012, Ng et al., 2011). NDP52, the ubiquitin-binding xenophagy adaptor, can also directly interact with LRSAM1 which may help for a positive-reinforcement cycle (Huett et al., 2012).

LRSAM1-ubiquitination was suggested to favour K6 and K27 linkages of ubiquitin residues (Huett et al., 2012). However, the coating around *Salmonella* was found to contain multiple types of linkages including chains associated with linear ubiquitin, K63 and K48 branching (van Wijk et al., 2012, Fujita et al., 2013). This pattern suggests other E3 ubiquitin ligases may be involved in ubiquitination of *Salmonella*. Recently, in addition to LRSAM1, other E3 ligases have been identified for *Salmonella* ubiquitylation including LUBAC (Linear Ubiquitin chain Assembly Complex), catalytic subunit HOIP and ARIH1 (Ariadne RBR E3 Ubiquitin Protein Ligase 1) (Noad et al., 2017, Polajnar et al., 2017). The *Salmonella* outer surface K48 and M1-linked ubiquitin chains were predominantly produced by ARIH1 and LUBAC/HOIP, respectively (Noad et al., 2017, Polajnar et al., 2017).

Ubiquitination is now a well-appreciated signal for xenophagy through ubiquitin binding adaptor proteins that bridge to LC3 on autophagosome membranes (Shahnazari and Brumell, 2011, Zheng et al., 2009, Marcus et al., 2000, Yuk et al., 2012, Thurston et al., 2009). Recently, LUBAC was found to remodel and amplify the ubiquitin platform present on cytosolic *Salmonella* to recruit autophagy receptors (Noad et al., 2017). A wide range of adaptor proteins have been shown to target ubiquitinated *Salmonella* including p62 (Zheng et al., 2009) and NDP52 (Thurston et al., 2009), which function together with OPTN (Wild et al., 2011). These three receptors of autophagy are proposed to be non-redundant and, also, each is independently recruited to the same bacteria. These receptors appear to work together in protecting cells from the highly replicating cytosolic

Salmonella (Zheng et al., 2009, Thurston et al., 2009, Wild et al., 2011, Cemma et al., 2011). When two of these receptors were depleted, a non-additive strong effect on *Salmonella* replication was observed (Cemma et al., 2011, Wild et al., 2011). Therefore, there seems to be participation of these three receptors at different steps within the same pathway, with distinct roles in LC3 and ubiquitin binding.

Further studies have demonstrated that Tax1-binding protein 1 (TAX1BP1), a novel type of autophagy receptor, plays a critical role in xenophagy of *Salmonella* (Tumbarello et al., 2015). The role of TAX1BP1 was observed to be different from the other receptors of autophagy: NDP52, p62 and OPTN. Concurrent NDP52 and TAX1BP1 depletion resulted in an additive effect on *Salmonella* replication. It therefore appears that NDP52 and TAX1BP1 display partially redundant roles in xenophagy and that TAX1BP1 can serve to compensate NDP52 knockdown.

As an adaptor protein, p62 is well characterised as one of the core autophagy components involved around ubiquitination. Recently, the E3 ligase RNF26 has been shown to promote ubiquitination of p62 in the UBA domain. The ubiquitination was suggested to increase the interaction of p62 with other adaptors of ubiquitin, for instance, TOLLIP, thereby facilitating vesicular sorting of cargo (Jongsma et al., 2016). Interestingly, ubiquitinated p62 acts as a scaffold to recruit downstream adaptors to bacteria at early time points and then helps maintain a stable complex (Heath et al., 2016). In this study, RNF166 ubiquitinates p62 at residues K91 and K189. Interestingly, these events involve atypical ubiquitin chains that are K29- and K33-linked. Overall, RNF166 mediated ubiquitin ligase activity facilitates p62's role in the xenophagic degradation of intracellular bacteria (Heath et al., 2016).

In order for *Salmonella* to be efficiently cleared, phosphorylation events directed by TANK binding kinase 1 (TBK1) are required. TBK1 is an IKK-related kinase responsible, overall, for the maturation of the autophagosome. TBK1 carries out this critical function by phosphorylating OPTN and enhancing OPTN interaction with LC3, thereby restricting intracellular growth of *Salmonella enterica* sv. Typhimurium (Wild et al., 2011, Morton et al., 2008, Rogov et al., 2013). OPTN binds LC3 via its LIR N-terminal motif, which is located next to S177. Phosphorylation of OPTN at S177 facilitates LC3B binding affinity by altering the hydrogen bonding network, as shown by NMR studies (Wild et al., 2011). In addition, it has been demonstrated that TBK1 can phosphorylate S513 and S473 in OPTN to promote binding of Ub chains (Heo et al., 2015). Interestingly, this TBK1-driven

enhanced binding affinity significantly increases rates of cytosolic *Salmonella* xenophagy.

The second eat-me signal – Galectin 8: Galectin 8 is a cytosolic lectin capable of recognising the β-galactoside portion of glycolipid (normally localised to the plasma membrane surface and luminal face of endosomes). Importantly, in this context, damage to the SCV membrane exposes β-galactoside on the inner membrane surface. It was demonstrated that Galectin 8 is recruited to the SCV and further binds NDP52 (Thurston et al., 2012, Li et al., 2013). NDP52 therefore serves as an adaptor protein capable of bridging the damaged SCV as substrate. The Galectin 8–NDP52 complex, thus, succeeds in recruiting LC3-PE and the autophagosome membrane.

NDP52 has been found to further recruit TBK1 to ubiquitinated bacteria via a complex with the adaptor proteins, Nap1 and Sinbad (Thurston et al., 2009). It was found that the recruitment of TBK1 to *Salmonella enterica* sv. Typhimurium through Galectin 8 and K48- or K63-linked ubiquitin chains serves to enhance xenophagy capture (as observed via recruitment of WIPI2) to restrict bacterial proliferation (Thurston et al., 2016). This signalling mechanism thereby links SCV damage to a phosphorylation pathway to promote antibacterial xenophagy and *Salmonella* growth restriction in mammalian cells.

Recently, it has been shown that NDP52 plays a dual role in autophagy. This implies that NDP52 actively targets bacteria to the autophagosomes during the process of autophagy initiation and further ensures the degradation of pathogens through the process of regulating autophagosome maturation (Verlhac et al., 2015). It is interesting that both the NDP52 and OPTN are capable of facilitating the maturation of autophagosomes via the function of myosin VI adaptor proteins. Indeed, this mechanism has been shown to speed the clearance of *Salmonella enterica* sv. Typhimurium via xenophagy (Tumbarello et al., 2015).

Once the damaged SCV is ubiquitin-tagged and recognised by autophagy membranes, xenophagy can proceed. Indeed, core autophagy machinery constituents including ATG14L, ATG16L1, ULK1/FIP200 and ATG9, have been shown to be targeted to the SCV. Each one of these pathways was shown to contribute independently in limiting the intracellular growth of *Salmonella enterica* sv. Typhimurium (Kageyama et al., 2011). In agreement, LC3-PE targeting of bacteria interestingly can occur independently of ULK1,

Beclin 1 and ATG9 complexes. Thus, LC3 can target SCVs by non-canonical pathways, but additional canonical pathways also contribute (Kageyama et al., 2011).

The current understanding indicates several autophagy pathways contribute towards intracellular anti-bacterial function. The emerging picture shows multiple mechanisms, but further roles seem likely. *Salmonella* xenophagy was recently shown to involve FBXO27, a glycoprotein-specific F-box protein that forms a subunit of the SCF (SKP1/CUL1/F-box protein) ubiquitin ligase complex. SCF^{FBXO27} ubiquitinated exposed glycoproteins and this resulted in accelerated recruitment of autophagic machinery (Yoshida et al., 2017). In this project, unbiased screening was used to search for potential new xenophagy factors involved during *Salmonella* infection.

In population (3), it has also been shown that damaged SCVs can be targeted to lysosomes via a Ca2+ dependent signalling for degradation. The detection and targeting of the damaged SCV was dependent on pores formed by virulence factors of the T3SS. These pores led the Ca2+ to flux from the Ca2+ rich SCV into the cytosol. Lysosomal associated synaptotagmin (SytVII) next became activated by this elevation in cytosol Ca2+. In this way, the damaged SCV thereby underwent direct fusion with the lysosome leading to degradation and restriction of intracellular *Salmonella* growth (Roy et al., 2004).

In population (4), *Salmonella enterica* sv. Typhimurium, in addition, can be targeted by the LC3-associated phagocytosis (LAP) pathway. It has been shown that NADPH oxidase and ROS are necessary for effective direct recruitment of the autophagy protein LC3 to bacteria (Huang et al., 2009). Furthermore, DAG (diacylglycerol) can be generated on the SCV and this production led to efficient LC3 recruitment to bacteria (Shahnazari et al., 2010). In fact, DAG-positive bacteria were not associated with ubiquitin or p62. Inhibiting both DAG and p62 pathways led to an additive inhibitory effect on LC3 recruitment to the bacteria. These results suggest that the DAG pathway and the p62 ubiquitin-adaptor pathway both contribute independently to the recruitment of LC3 to *Salmonella enterica* sv. Typhimurium. For the LC3 selection of bacteria, the downstream effector of DAG, protein kinase Cδ (PKCδ) was important (Shahnazari et al., 2010). PKCδ can trigger NADPH oxidase by direct phosphorylation of the complex (Fontayne et al., 2002). These studies further demonstrate that DAG dependent LC3 targeting of bacteria involves a PKCδ–NADPH oxidase–ROS pathway.

The mechanism for translocation of DAG to the SCV remains unclear. The SPI-1 T3SS of *Salmonella enterica* sv. Typhimurium is needed for DAG localisation on SCVs, suggesting that one of the bacterial effectors, or the membrane destruction triggered by T3SS pore-forming activity, is needed. It is also unclear if LAP takes place before canonical autophagy targets *Salmonella enterica* sv. Typhimurium. ROS production is very fast after bacterial (*Listeria monocytogenes*) attack (peaking at ~10 min post-infection) (Lam et al., 2011), and the presence of DAG with *Salmonella enterica* sv. Typhimurium peaks at 30 min after infection (Shahnazari et al., 2010). Similarly, it has been proposed that ROS could lead to destruction of SCV membranes. Therefore, activation of LAP signalling could take place much earlier than activation of the ubiquitin-adaptor autophagy pathway.

Overall, autophagy plays a key role in restricting infection by *Salmonella enterica* sv. Typhimurium. *Salmonella*, nonetheless, have mechanisms to counteract and inhibit selective autophagy, for example, through expression of SseL. SseL is a T3SS effector, which acts as a de-ubiquitinase. SseL activity lowers autophagic flux and promotes the replication of bacteria (Mesquita et al., 2012). This pathway has been suggested to cause disassembly of entire K63-linked chains thereby impairing recruitment of xenophagy adaptors. This pathway could also target particular host proteins like oxysterol-binding protein (OSBP) directly (Pruneda et al., 2016). S100A6 and HNRPK (heterogeneous nuclear ribonuclear protein K) are included among other SseL substrates (Sontag et al., 2016, Nakayasu et al., 2015). Therefore, in each infected cell there is a dynamic interplay between invading *Salmonella* and intracellular defence mechanisms, featuring host cell ubiquitination and xenophagy versus bacterial virulence factors.

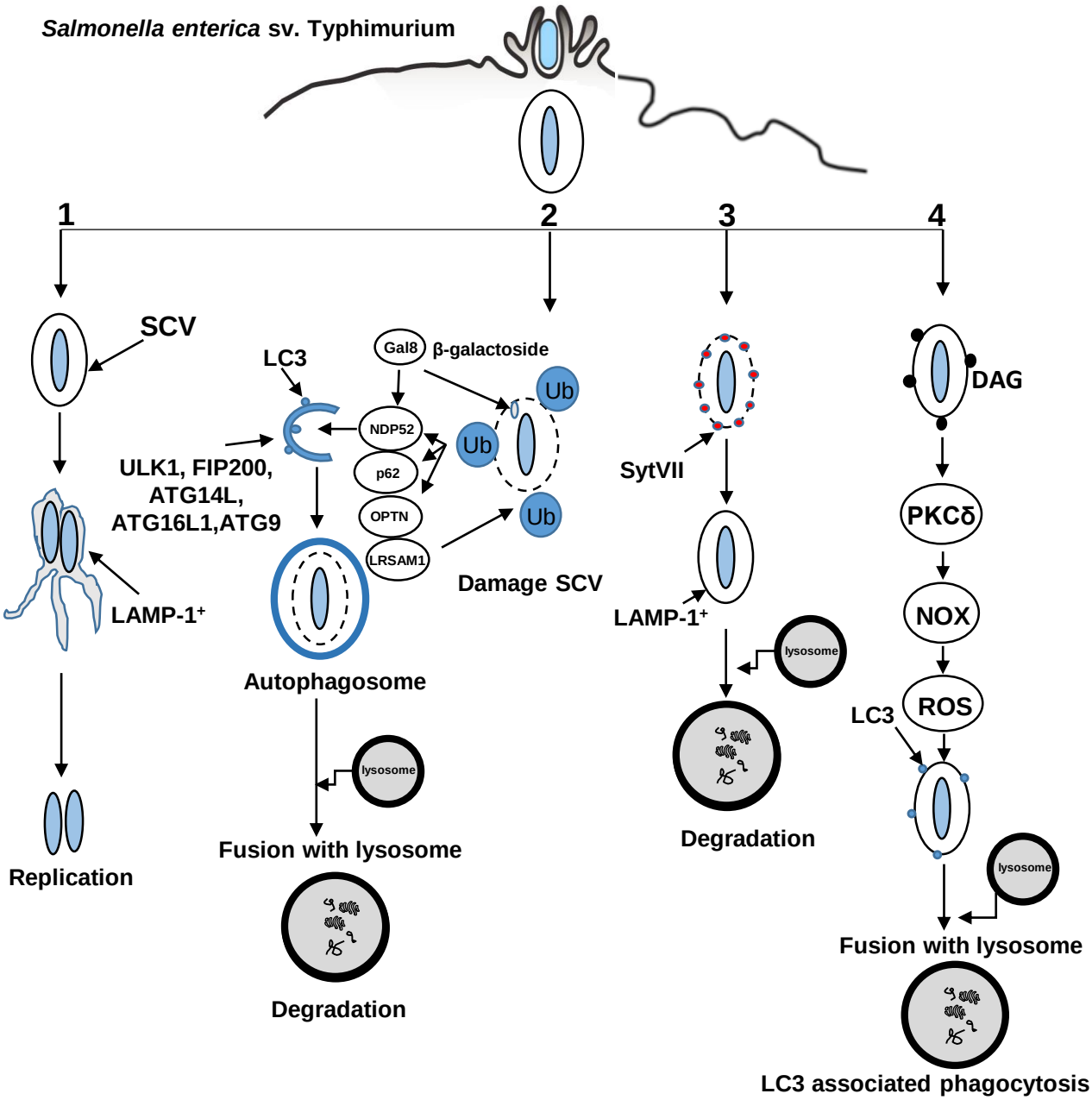

Figure 1.5: Model of the interaction between *Salmonella enterica* sv. Typhimurium and host cells. The bacteria reside in a Salmonella-containing vacuole (SCV) after invading epithelial cells.

1) It is within the SCVs that the majority of *S. typhimurium* take up residence where vacuolar markers like lysosomal associated membrane protein (LAMP)-1 are acquired immediately after infection. Manipulation of SCV maturation takes place in order for a permissive environment for the replication of bacteria (that includes Sifs formation) to be established.

2) Initially upon infection (less than one hour), the membrane of a subset of SCVs is damaged and the bacterium is exposed to the cytoplasm, where it becomes linked to ubiquitylated proteins within a procedure dependent on E3 ubiquitin ligase leucine-rich repeat and sterile α motif-containing 1 (LRSAM1). The recruitment of adaptor proteins to the SCV that includes p62, NDP52 and optineurin (OPTN) is produced by attachment to ubiquitin, and interaction with LC3, finally leading to autolysosome formation. The damaged SCV membrane also exposes β-galactoside to the cytoplasm and recruits galectin 8, which binds to NDP52 and further recruits LC3.

3) Lysosomes are recruited to damaged SCVs in a calcium sensor, SytVII-dependent manner. The fusion of the lysosomes with the damaged SCV then takes place for the repair and probable delivery of the degradative lysosomal enzymes to the vacuolar compartment.

4) Diacylglycerol (DAG) is also recruited by a subclass of bacteria less than one hour of post infection, to the unimpaired SCVs. Protein kinase Cδ (PKCδ), responsible for the activation of NADPH oxidase (NOX), as well as for the promotion for the production of reactive oxygen species (ROS), is activated by DAG and, in turn, induces LC3 linked phagocytosis. Figure adapted from (Birmingham et al., 2006) & (Huang and Brumell 2014).

1.3.2 *Staphylococcus aureus*

Staphylococcus aureus are Gram-positive bacteria from the family Staphylococcaceae. The species *aureus* refers to the fact that colonies often have a golden colour when grown on solid media. Mannitol salt agar media is considered to be a selective medium to allow growth of these bacteria (Stapleton and Taylor, 2002). *Staphylococcus aureus* are commensal bacteria that are commonly carried by humans. About 20% of healthy individuals are chronically colonised with *Staphylococcus aureus*, while 60% are intermittent carriers (Foster, 2004). *Staphylococcus aureus* can further infect a number of human tissues in a pathogenic manner leading to many pathologies such as abscess formation, septicaemia, endocarditis and pneumonia (Alva-Murillo et al., 2014, Loffler et al., 2014). These bacteria have a tendency infect wounds, bone and joints. The majority of these infections can become life threatening because this pathogen has developed multiple evasion strategies to survive intracellularly for different periods of time. Therefore, it is important to understand the mechanisms which allow *Staphylococcus aureus* to colonise and proliferate continually inside cells (Alva-Murillo et al., 2014).

1.3.2.1 Staphylococcal pathogenicity

The *Staphylococcus* virulence factors that promote infection (and interact with autophagy) are all encoded by the bacterial genome. The *Staphylococcus* genome consists of approximately 2,500 genes, reflecting a combination of the core genome along with lateral acquired genes. The core genome contains all genes responsible for common basal housekeeping functions (for example, metabolism, nucleic acid synthesis and replication). This core genome has high conservation in terms of sequence and structure (Alibayov et al., 2014). In contrast, non-essential sequences are found as mobile genetic elements scattered in the genome.

The accessory component of the *Staphylococcus* genome contains a higher degree of genetic variations across the species and encodes a diverse range of virulence and resistance factors for drug and metal interactions, substrate utilisation and alternative metabolism pathways (Kuroda et al., 2001). The accessory genes are contained in a number of exogenous mobile genetic elements (MGE), which allow horizontal transfer between strains, and these represent about 15 % of the full *Staphylococcus aureus* genome. MGE plays an essential role in genome plasticity and allows for rapid adaptation to environmental stress and selection conditions (Alibayov et al., 2014). The identification and characterisation of MGE are essential to understand how

Staphylococcus aureus adapts to cause disease, its relative diversity, and how *Staphylococcus aureus* infections might eventually be contained and targeted.

The Staphylococcal cassette chromosome (SCC) element is one of several DNA mobile genetic elements which inserts into the *Staphylococcus* genome. The SCC element integrates at the unique site termed attBscc. There are five types of SCC and all these members vary in length, structure and content. Types I-III are associated with hospital acquired methicillin-resistant *Staphylococcus aureus* (HA-MRSA), also known as Epidemic MRSA (EMRSA). EMRSA includes characterised strains such as ST250-MRSA-I and ST239-MRSA-III.

All SCC types share inverted and direct repeats, which allow for the SCC to serve as a carrier for the *mecA* gene (O'Hara et al., 2008). Of critical importance, the *mecA* gene product provides resistance to methicillin, penicillin, as well as other β-lactam antibiotics (Ito et al., 2014). As such, the widely reported drug resistance of *Staphylococcus aureus* is based on the *mecA* which encodes an alternative penicillin-binding protein (PBP2a/PBP2′) with reduced affinity to methicillin, as compared to normal PBP. The capacity of methicillin to inhibit *Staphylococcus aureus* cell wall synthesis is therefore reduced due to this decreased affinity in resistant strains (Chatterjee and Otto, 2013).

Pathogenicity islands (SaPI) are a further distinct set of exogenous mobile genetic elements on the chromosomes of all *Staphylococcus* species. SaPI elements encode integrase, resistance, virulence genes and genes encoding super antigens, which are responsible for food poisoning or host adaptation. The SaPI genes are also very important in bacterial evolution and these are horizontally transferred at very high frequencies by specific Staphylococcal helper phages (Alibayov et al., 2014).

1.3.2.2. Methicillin resistant *Staphylococcus aureus* (MRSA)

MRSA is now well understood to be a prominent cause of nosocomial infections and a general health concern globally (Chatterjee and Otto, 2013, Hogea et al., 2014). MRSA infections occur predominantly in hospitals, leading to the HA-MRSA classification mentioned above. Nevertheless, there is also a recognised increasing threat from the prevalence of community-acquired MRSA (CA-MRSA) infections (Jappe et al., 2008, Otto, 2010, Ito et al., 2014).

With HA-MRSA or CA-MRSA, the bacteria inevitably spread through skin contact and potentially can get into the bloodstream leading to sepsis, the primary cause for shock and circulatory collapse (Ito et al., 2014). MRSA can spread further to other tissues, such as kidney, lung, liver, heart and bone marrow, with severe clinical complications caused by endocarditis, osteomyelitis and urethritis (Haim et al., 2010). MRSA is becoming more difficult to treat because of the evolving resistance to known effective antibiotics, therefore resulting in high mortality rates (Westling, 2009). Newly evolved strains can also show poor response to vancomycin (Fasihi et al., 2017) and daptomycin (Pader et al., 2016), the proposed last resort drugs for treating *Staphylococcus aureus* infection (Ruiz-Ramos et al., 2017, Howden et al., 2011).

1.3.2.3 Intracellular *Staphylococcus aureus*

It has long been recognised that *Staphylococcus aureus* plays out a large part of its life cycle and infectious stages extracellularly, but the importance of intracellular *Staphylococcus aureus* has become better appreciated. The adherence of *Staphylococcus aureus* to host cells is essential for asymptomatic chronic colonisation and overt disease (Sinha and Fraunholz, 2010). Non-professional phagocytes cells (NPPCs) such as epithelial, endothelial cells, fibroblasts, osteoblasts, kidney cells and keratinocytes can be infected by *Staphylococcus aureus* following invasion through a “zipper-type” internalisation mechanism (Strobel et al., 2016, Edwards et al., 2010, Jett and Gilmore, 2002, Ahmed et al., 2001).

The invasion is initiated by the adherence of *Staphylococcus aureus* to the cellular surface through Fibronectin (FN)-binding proteins A and B which bind to host fibronectin (often found in host serum or secreted by fibroblasts) with an incredibly high affinity. Fibronectin serves as a linking molecule between host cells and bacteria, since fibronectin, in turn, binds to integrins (normally α5β1) on the host cell surface. This bacteria adherence induces polymerization of intracellular actin, resulting in the engulfment by the plasma membrane, and ultimately the formation of bacteria-containing phagosomes in the cell similar to the process in professional phagocytes (Alva-Murillo et al., 2014, Fraunholz and Sinha, 2012, Krut et al., 2003). Internalisation has been found to be extremely slow during *Staphylococcus aureus* infection (Schroder et al., 2006). Therefore, *Staphylococcus* has been found to remain attached to host membranes for up to 45 minutes prior to internalisation. This extensive adherence time of *Staphylococcus aureus* might allow the bacteria to produce cell-damaging toxins,

possibly in a quorum sensing mechanism, to promote internalisation (Schroder et al., 2006).

The overall fate of the host cell after *Staphylococcus aureus* invasion depends on the balance between multiple pathways in a dynamic interaction (as summarised in Figure 1.6). Following invasion, some strains of *Staphylococcus aureus* have defence mechanisms including resistance to low pH and escape from the phagosome. This escape is through destruction of the phagosomal membrane, which would yield access to the cytoplasm with milder conditions close to pH 7 (route 1 in Figure 1.6). On the other hand, some strains are rapidly killed by non-professional phagocytes upon close contact and fusion with lysosome (route 2) (Sinha and Herrmann, 2005).

Pathogenic strains of *Staphylococcus aureus*, after invasion of host cells, are well understood to release a range of bacterial toxins and pro-inflammatory factors into the intracellular environment, causing inflammatory and cytotoxic effects to the cell host (Loffler et al., 2014). The main virulence factor deployed is α-hemolysin (hla), a pro-inflammatory pore-forming toxin. Hla toxin eventually kills cells via apoptosis-dependent pathways, initially through formation of pores that allow the exchange of monovalent ions, resulting in cell stress, and DNA fragmentation (Loffler et al., 2014, Mestre et al., 2010, Sinha and Fraunholz, 2010). Expression of hla and other factors is driven by the accessory gene regulator (*agr*) system, a quorum sensing bacterial gene expression pathway (route 3) (Loffler et al., 2014). The interaction of *Staphylococcus aureus* virulence factors with autophagy, the focus of this thesis, is further discussed in detail in a later section.

Importantly, if *Staphylococcus* virulence factors are down-regulated or poorly expressed, bacteria can remain intracellular for a long period of time, leading to persistence and resistance in the host cells (Loffler et al., 2014). It is also understood that certain subpopulations, called “small colony variants“, are difficult to detect and treat; and small colony variants are better adapted to survive intracellularly in the host cell compared with normal Staphylococcal strains (Sendi and Proctor, 2009). All small colony variants known so far are functionally deficient in the *agr* system, thus failing to produce the potent *agr*-regulated virulence factors. These strains appear to increase in their internalisation of the cell host and also can show resistance to the defences of these cells (as well as reduced stimulation of host defences) (routes 4 and 5) (Garzoni and Kelley, 2009, Sendi and Proctor, 2009).

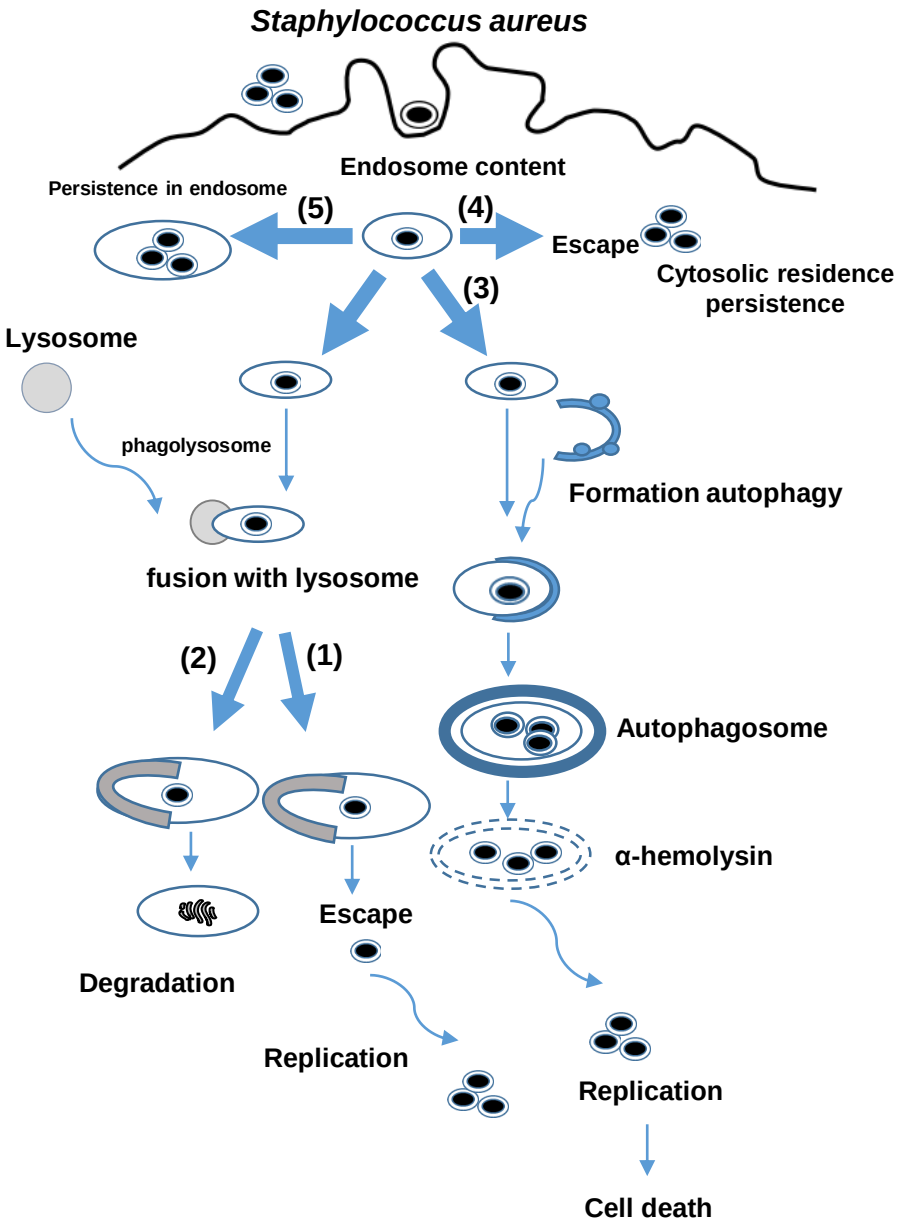

Figure 1.6: Schematic diagram depicting *Staphylococcus aureus* internalization and possible intracellular fates. There are a number of proposed scenarios: (1) survival within the lysosomal compartment, (2) destruction, (3) envelopment of the endosome by double-membrane autophagosome, (4) rapid escape from the endosomal compartment, and (5) persistence within the endosome. Infected host cells might rapidly undergo apoptosis or necrosis manifesting as cytotoxic effects or, alternatively, show little or no cytotoxicity. Figure adapted from (Garzoni and Kelley 2009).

1.3.2.4 *Staphylococcus aureus* and its interaction with autophagy

While anti-bacterial xenophagy has been better characterised with different types of bacteria (for example *Salmonella*), to date, there have been fewer studies on the association between *Staphylococcus aureus* and autophagy. This, therefore, represents a poorly understood, yet clinically important, area of autophagy research.

Evidence has highlighted the importance of a subversion pathway during which *Staphylococcus aureus* invades host cells and then become sequestered into autophagosomes. The current model describes how *Staphylococcus aureus*, via the function of virulence factors, critically inhibits autophagosome fusion with lysosomes. This mechanism thus creates a protective environment in which *Staphylococcus aureus* survives and replicates. After replication, it has been observed that *Staphylococcus aureus* breaks out of the autophagosome-derived replicative niche through the action of α-haemolysin and escapes into the cytoplasm to then induce cell death (Campoy and Colombo, 2009). After inducing cell lysis, *Staphylococcus aureus* disperses and goes on to infect neighbouring cells. Therefore, in this model, the intracellular replicative niche plays a major role in supporting the overall infection process of the tissue.

1.3.2.4.1 *Staphylococcus aureus* exploits autophagy factors to form a niche for replication in non-professional phagocytic cells

Upon getting into close proximity with the cell surface of the host, *Staphylococcus aureus* engages via fibronectin- and collagen-binding proteins found on the bacterial cell wall. Next, the bacteria are internalised into the cell. *Staphylococcus aureus* then must exist within phagosomes that escape fusion with the lysosomal compartment (Kahl et al., 2000).

With regard to the role of autophagy, the key study has been from Schnaith et al. (2007), which initially analysed the intracellular transport of *Staphylococcus aureus* in HeLa cells through electron microscopy. At 1.5 hours after infection, bacteria were present in a Rab7-positive phagosomal compartment connected to multilamellar membranes. Within three hours after infection, these membranes surrounded most of the phagosomes and a double membrane-like autophagic membrane enclosed the bacteria. Autophagic marker protein GFP-LC3 was also seen on these compartments, as exhibited by confocal microscopy. Later, the majority of the *Staphylococcus aureus* were observed to

be free in the cytoplasm. Hence, this demonstrates that the pathogen escapes from the autophagosomes into the cell cytoplasm of the host. The appearance of bacteria in the cytoplasm corresponds to signs of cell death.

The number of intracellular bacteria was markedly increased by the pre-incubation with the autophagy-inducer rapamycin. Therefore, this indicates that *Staphylococcus aureus* replication is promoted by autophagy. On the other hand, bacterial intracellular growth was reduced after treatment with wortmannin (as an inhibitor of autophagy). Similarly, *Staphylococcus aureus* replication was reduced in cells deficient for the key autophagy protein ATG5.

Remarkably, an *agr*-deficient strain was not enclosed by multilamellar membranes and did not co-localise with LC3 at any post-infection time studied. It was therefore proposed that *agr*-mutant *Staphylococcus aureus* was unable to induce an autophagic response in the host cell. Furthermore, phagosomes, which contained wt *Staphylococcus aureus*, hardly co-localised with the lysosomal protein LAMP-2, while the *agr*-deficient mutant clearly acquired this marker. Therefore, one or more *agr*-dependent factors appears to inhibit the fusion between bacteria contining autophagosome compartments and the lysosomes. Lysotracker labelled the *agr*-deficient bacterium in contrast to wt *Staphylococcus aureus*. Therefore, wt bacteria also have pathways to evade lysosomal acidification.

On the cytotoxic effects of *Staphylococcus aureus,* it is worth mentioning that these bacteria induced death of HeLa cells without caspase activation. Overexpression of apoptosis inhibitor XIAP did not prevent the cell lysis and death caused by *Staphylococcus aureus*. However, cell death was inhibited by Bcl-2 overexpression. Since Bcl-2 suppresses autophagy through attachment to the autophagy protein Beclin-1, it was hypothesised that *Staphylococcus aureus* causes an autophagic type of cell death (also referred to as Type II cell death). Indeed, cells infected with *Staphylococcus aureus* showed a marked vacuolization, which suggested autophagic cell death. These results taken together show a dynamic balance. *Staphylococcus aureus* averts the autophagosomal compartment maturation and avoids both lysosomal acidification and fusion, and escapes to the cytoplasm to then induce a later stage of autophagy-dependent cell death (Schnaith et al., 2007).

1.3.2.4.2 *Staphylococcus aureus* exploits autophagy factors to form a niche for replication in professional phagocytic cells

Although classically considered as extracellular bacteria, *Staphylococcus aureus* can live within various non-professional phagocytic host cells, enabling tissue persistence and relapsing disease (Garzoni and Kelley, 2009, Rollin et al., 2017). Strikingly, *Staphylococcus* can also manipulate professional phagocytes by living in neutrophils and macrophages as reviewed in (Horn et al., 2017). Evidence has been shown to support formation of an intracellular survival niche by subversion of autophagy in professional phagocytes. By use of the bone marrow derived dendritic cells (BMDC), O'Keeffe et al. (2015) demonstrated that professional DCs have the potential to kill *Staphylococcus aureus*. It should, however, be noted that *Staphylococcus aureus*, such as strain PS80 (clonal complex type 3), has the capacity to evade DC (and macrophage) death by manipulation of autophagic pathways. These strains have high levels of *agr* that enable autophagosome accumulation so *Staphylococcus* were not rapidly killed in BMDCs, thus eventually causing cytotoxic effects. On the other hand, strains with low levels of *agr*, for example SH1000 (clonal complex 8), lacked the capacity to accumulate autophagosomes and were rapidly killed by BMDCs. By use of *in vivo* systemic infection, it was demonstrated that *Staphylococcus aureus* has the potential to avoid phagocytic cell death and to survive within phagocytes. Importantly, this pathway correlated with *in vivo* persistence in the periphery. This overall role is critically *agr* dependent (in agreement with the Schnaith et al. niche model).

From the above studies, we can conclude that *agr* wt strains of *Staphylococcus aureus* are capable of blocking autophagic flux, leading to the accumulation of halted autophagosomes. Within these autophagosomes, bacteria are protected from destruction, thus providing an intracellular survival niche within non-professional and professional phagocytes cells, which ultimately facilitates dissemination. wt *agr Staphylococcus aureus* strains and *agr* mutant strains were studied in this project in non-professional phagocytes (epithelial) cells.

1.3.2.4.3 The role of α-haemolysin and cAMP in induction of autophagy following *Staphylococcus aureus* infection

α-haemolysin is required for the activation of the autophagic pathway in *Staphylococcus aureus*-infected cells. In 2010, Mestre et al. reported that α-haemolysin was critical for the activation of the autophagic pathway when Chinese hamster ovary (CHO) cells were

infected with wild-type strains of *Staphylococcus aureus*. These authors described the build-up of activated LC3-II in infected cells as a result of a dysfunctional autophagy pathway. The *agr*-mutant strains were incapable of inducing autophagy (as was reported by Schnaith et al., 2007). Furthermore, mutant strains were localised to an acidic compartment unlabelled by LC3. In this study, additional experiments were conducted utilising purified α-haemolysin toxin. These studies showed the dependence of the toxin-dependent autophagic response on ATG5 and calcium signalling. In contrast, autophagy was not dependent on phosphatidylinositol-dependent kinase (PI3K) and Beclin-1, thereby indicating an autophagic response that fitted non-canonical classification (Mestre et al., 2010). Class III PI3K and Beclin-1 are essential for autophagy initiation via the canonical pathway.

Cyclic adenosine monophosphate (cAMP) is an important secondary messenger that controls multiple types of intracellular pathways. Interestingly, cAMP plays a major role in α-hemolysin-induced autophagy following infection by *Staphylococcus aureus* (Mestre and Colombo, 2012). Administration of cAMP to α-hemolysin-treated cells, as well as *Staphylococcus aureus* infected cells, led to a decrease in autophagy. cAMP-regulated Rap Guanine Nucleotide Exchange Factor 3 (RAPGEF3/EPAC) stimulation of the small GTPase Rap2b, which was suggested to be the pathway to suppress autophagy, and not the cAMP target: protein kinase A (PKA). For the mechanism, it was shown that Rap2b had the ability to increase the level of intracellular calcium, thereby resulting in activation of the host cell protease, calpain, which led to restriction of autophagy (Williams et al., 2008). There was a reversal of cAMP negative regulation on autophagy when activation of calpain was restricted in α-toxin-treated cells. The authors proposed that this represented a fundamental mechanism where cellular cAMP and Rap2b restricted autophagy activation (Mestre and Colombo, 2012). In any event, the above study shows that a cAMP pathway can inhibit the xenophagy response following *Staphylococcus aureus* infection. In relation to this project, we also examined different *Staphylococcus aureus* strains to compare their effect on autophagy and to understand how bacterial genotype (and gene products) affect the host cell.

1.3.2.4.4. Rab GTPases and the *Staphylococcus* autophagy pathway

Rab GTPases participate at multiple steps in the formation of phagosomes following *Staphylococcus aureus* infection. For example, *Staphylococcus aureus* has been found to travel through early phagosomes associated with Ra22b and Rab5, which then

matured to late stage vesicles marked by LAMP-1 and Rab7 (Seto et al., 2011), as reviewed in (Lopez de Armentia et al., 2016).

More recent studies have shown that internalised *Staphylococcus aureus* can re-model membranes to produce tubular structures marked with Rab1b and Rab7, and by the autophagy ATG8 member LC3 at an early post-infection stage (Lopez de Armentia et al., 2017). As shown by live cell imaging, these tubular structures were exceedingly dynamic, and extend, branch and increase in length. These tubules have been termed *Staphylococcus aureus* induced filaments (Saf) (analogous with structures formed during *Salmonella* infection). In addition, the authors showed that the development of Saf depends on the integrity of microtubules, activity of the motor protein Kinesin-1 (Kif5B), and the Rab-interacting lysosomal protein (RILP).

Previously, these researchers had detailed that α-hemolysin was responsible for the activation of the autophagic pathway induced by the bacteria (Mestre and Colombo, 2012). In their current report (Lopez de Armentia et al., 2017), they were further able to show that LC3 translocates to the membrane of Saf and that α-hemolysin is the toxin that induces this tubule Saf formation. Strikingly, in agreement with their other work, increasing the levels of intracellular cAMP significantly repressed Saf biogenesis. It was surprising to note that, in this report, the researchers demonstrated that formation of tubular structures from the phagosome seemed to be required for effective bacteria replication. The above findings suggest that *Staphylococcus aureus* takes advantage of intracellular trafficking, modulating multiple types of Rab GTPases on the phagosome/ autophagosome membrane in order to create protective niche.

1.3.2.4.5 The role of canonical autophagy during *Staphylococcus aureus* infection

Based on our discussion so far, autophagy is critical for *Staphylococcus aureus* to form a replicative niche. What type of autophagy is involved? We summarised above one study that showed *Staphylococcus* non-canonical autophagy that was PI3K- and Beclin1-independent (Mestre et al., 2010). In contrast, a study conducted by Mauthe et al. (2012) using microscopy high content analyses supported a role for canonical autophagy following *Staphylococcus aureus* infection (Mauthe et al., 2012). In this study, infection of cells with *Staphylococcus aureus* strains USA300, HG001 and SA113 all stimulated autophagy. These strains became entrapped in intercellular PI3P enriched vesicles that were decorated with human WIPI-1, an essential PI3P effector of canonical autophagy and a membrane associated protein of both early phagophores and complete

autophagosomes. Also, *agr*-positive *Staphylococcus aureus* (USA300, HG001) strains were more efficiently entrapped in WIPI-1 positive autophagosomes in comparison to the *agr*-negative bacteria (SA113). When confocal and electron microscopy were used, it was found that there were single and multiple Staphylococci entrapped that had gone through the process of cell division. Also, there was an increase in the number of WIPI-1 positive autophagosome-like vesicles entrapping Staphylococci under lysosomal inhibition by bafilomycin A1 and also after blocking PIKfyve-mediated PtdIns(3,5)P2 generation by YM201636. These results suggested that WIPI-1 and PI3P lipid generation are very important during xenophagy of *Staphylococcus aureus*. This study thereby suggests that invading *Staphylococcus aureus* cells become entrapped in canonical autophagosome-like WIPI-1 positive vesicles targeted for lysosomal degradation in non-professional host cells.

Cyclic-di-adenosine monophosphate (c-di-AMP) is a bacterial second messenger produced by human pathogens. It is involved in regulating a number of physiological processes including potassium transport (Fahmi et al., 2017). Cyclic di-adenosine monophosphate (c-di-AMP) is a recently discovered signalling molecule important for the survival of *Staphylococcus aureus* (Zeden et al., 2018, Bowman et al., 2016). More recently, it was found that c-di-AMP could function as a vita-PAMP that induces STING dependent endoplasmic reticulum (ER) stress to protect mice against gram-positive infection (Moretti et al., 2017). This ER-stress response involved a mechanism with inactivation of mTOR and activation of canonical autophagy. This autophagy removes stressed ER regions, a process termed ER-phagy (Moretti et al., 2017). Interestingly, the *Staphylococcus aureus* strain involved in this study was a MSSA type strain (ATCC29213). We also used this same strain in this project and these bacteria indeed induced an autophagy response.

From these two studies, it is becoming more apparent that the cell response following *Staphylococcus aureus* infection can involve canonical autophagy. In accordance with this idea, in this project we studied the role of the ULK1 initiation complex (part of the canonical core pathways) following infection by *Staphylococcus aureus.* The aim was to work towards the development of ULK1 inhibitors as a novel therapy to fight MRSA infection via blocking autophagosome formation as a way of preventing the Staphylococcal replication niche.

1.3.2.4.6. Other *Staphylococcus* virulence factors that induce autophagy

While much data have been collected supporting a key role for α-haemolysin in promoting autophagy, other recent results demonstrate that other virulence factors are involved (Liu et al., 2015). This work suggested that Immuno-dominant surface antigen B (IsaB) also plays a role in activation and manipulation of autophagy. These authors discovered that IsaB expression was elevated in transmissible MRSA. Wild-type IsaB strains inhibited autophagic flux (similar to the existing model) to promote bacterial survival and elicit inflammation in THP-1 cells and mouse skin. MRSA isolates with higher IsaB expression showed decreased autophagic flux, while MRSA isolates with the lowest IsaB expression showed more autophagic flux. Furthermore, recombinant IsaB rescued the virulence of the IsaB deletion strain. These results reveal that IsaB is another critical virulence factor that inhibits autophagic flux, thereby allowing MRSA to evade host degradation and replicate. These findings further suggest that IsaB may be a suitable target for preventing or treating MRSA infection.

From the above, we can conclude that *Staphylococcus aureus* virulence factors play a critical role in inducing and subverting autophagy. So far, two factors have been discovered: IsaB and *agr*. In the future, it is possible that further factors will be discovered. Therefore, it may be difficult to fully deactivate all *Staphylococcus aureus* virulence factors as a strategy to fight infection. On the other hand, understanding how this bacteria interacts with host cells may lead to novel knowledge on pathways that could eventually suggest new effective strategies.

1.3.2.4.7. Selective autophagy is induced following Staphylococcal infection

Consistent with the idea of specific autophagy shown with *Salmonella*, a study by Neumann et al. (2016) was able to demonstrate selective xenophagy following *Staphylococcus aureus* infection (Neumann et al., 2016). This event was proposed to occur when there is phagosomal escape and *Staphylococcus aureus* within the host cell cytoplasm. The results suggest that *Staphylococcus aureus* becomes ubiquitinated leading to recruitment of OPTN, p62/SQSTM1 and NDP52 receptor proteins, which promotes the formation of phagophore. Also, in agreement, this study confirmed that *Staphylococcus aureus* in murine fibroblasts prevents autophagosome fusion with lysosomes. More specifically, *Staphylococcus aureus* blocked autophagy through phosphorylation of mitogen-activated protein kinase 14 (MAPK14/p38α).

Interestingly, in this system, the induction of autophagy was not critical for *Staphylococcus aureus* survival, and intracellular replication was observed in the host cell cytosol after escape from the autophagosomes. These observations contrast with Schnaith et al. (2007), which showed that *Staphylococcus aureus* subverted autophagy for its intracellular survival. Importantly, these two studies used different *Staphylococcus aureus* strains. However, the extent to which such differences can be attributed to the bacterial strains or host cells must be researched further. Neumann et al. (2016) focused their studies on using strain SH1000, which belongs to the clonal complex 8 category. Overall, this study establishes adaptor-mediated autophagy targeting of intracellular *Staphylococcus aureus* as a prominent pathway. The role of ubiquitin-adaptor autophagy was also investigated in our project following infection by *Salmonella enterica* sv. Typhimurium and *Staphylococcus aureus*. Furthermore, we performed studies with clonal complex 8 and other strains of *Staphylococcus aureus.*

1.3.2.4.8 Autophagy is a key tolerance mechanism during *Staphylococcus aureus in vivo* infection

The literature above mainly focused on bacteria–host cell interactions from *in vitro* cell culture studies. The *Staphylococcus aureus* infection process, as it takes place *in vivo,* is an important consideration. *In vivo*, a critical pathway is understood to involve α-haemolysin and its interaction with A Disintegrin and Metalloproteinase domain-containing protein 10 (ADAM10), which serves as its receptor (Wilke and Bubeck Wardenburg, 2010). Upon binding ADAM10 on endothelial and epithelial cells, α-haemolysin disrupts tissue integrity and promotes bacterial dissemination through induction of pore-formation and cleavage of cadherins. Interestingly, the level of ADAM10 was increased in endothelial cells from ATG16L1^{HM} (hypomorph) mice, which are deficient in autophagy compared with wt. These data together suggest that autophagy functions to offer protection through limiting ADAM10 levels and toxin-mediated damage in endothelial cells (Maurer et al., 2015a, Maurer et al., 2015b). Importantly, USA300 infection models demonstrated that ATG16L1^{HM} mice showed more severe pneumonia and sepsis following infection.

As a critical point, ATG16L1^{HM} mice showed stronger tendencies to survive (resistance) when they were infected with mutant toxin-deficient *Staphylococcus aureus* strains. Overall, according to the authors, these results illustrate how autophagy can play a critical role in limiting *in vivo* infection and toxin sensitivity via modulation of receptor

levels. However, autophagy plays an opposite role in supporting *Staphylococcus aureus* infection in cases where strong pathogenic effects of toxin are removed, consistent with the replication niche model proposed earlier from *in vitro* data.

The role of the ADAM10 toxin receptor has been highlighted through other *in vitro* studies. A genome-wide loss-of-function screen utilising CRISPR/Cas9 technology was performed to identify the host factors necessary for α-haemolysin susceptibility in human myeloid cells (Virreira Winter et al., 2016). This screen discovered ADAM10 in agreement with its established role. In addition, this screen also identified, as top hits, three other proteins: Sys1 Golgi trafficking protein (SYS1), ADP-ribosylation factor 1 (ARFRP1), and tetraspanin-14 (TSPAN14). In agreement, these three proteins regulate presentation of ADAM10 on the plasma membrane post-translationally. Therefore, this cell culture screen further supports a critical role of ADAM10 in determining α-haemolysin toxicity during a *Staphylococcus* infection.

1.3.2.4.9. Summary of *Staphylococcus aureus* interactions

In summary, we can conclude that the interaction of *Staphylococcus aureus* (and likely all infectious pathogens) with autophagy will show multiple behaviours when considering *in vitro* and *in vivo* systems. *In vitro* interactions happen within the first few hours while *in vivo* infections involve multiple cell types over days. In one sense, autophagy helps to develop a niche for this pathogen when considering just the bacteria-host cell interaction. Conversely, autophagy also modulates expression of the cell surface receptor proteins involved in pathogenic effects from bacterial toxins, which can be illustrated during in vivo infection.

After reviewing the literature, we have integrated the information on interactions of *Staphylococcus aureus* with autophagy in Figure 1.7. During *Staphylococcus aureus* infection, a major role is played by the formation of an intracellular replicative niche for *Staphylococcus aureus* under control of virulence factors (Fraunholz and Sinha, 2012). The importance of autophagy has been to help form this protective niche. *Staphylococcus aureus* hijacks, modifies and uses autophagy membrane structures to promote bacterial survival (Schnaith et al., 2007).

During infection of a host cell, *Staphylococcus aureus* travels after internalisation through an early phagosome with Ra22b and Rab5, which quickly mature to a late stage marked by LAMP-1 and Rab7 (Seto et al., 2011). The α-haemolysin secreted by the bacteria

makes the phagosomal membrane permeable, which then stimulates autophagy. Subsequently, autophagosomes are recruited to the leaky phagosome (Mestre et al., 2010). There is overall inhibition of lysosomal fusion so the autophagosome fails to mature, enabling the *Staphylococcus aureus* to replicate inside (Schnaith et al., 2007). Thereafter, tubular structures emerge from the *Staphylococcus aureus* containing phagosome. These are marked with the small GTPases Rab1b and Rab7 and by the autophagic protein LC3, which are required for efficient bacteria replication (Lopez de Armentia et al., 2017). At a later stage, phenol soluble modulin alpha (PMSα) facilitates *Staphylococcus aureus* to move to the cytoplasm leading to cell lysis to infect neighbouring cells (Grosz et al., 2014). It is notable that during *in vivo* infection, autophagy offers overall protection by limiting expression of the toxin receptor ADAM10, in particular on endothelial cells (Maurer et al., 2015a, Maurer et al., 2015b). Thus, proposals to modulate autophagy to control *Staphylococcus aureus* infection will need to consider these time and cell contexts.

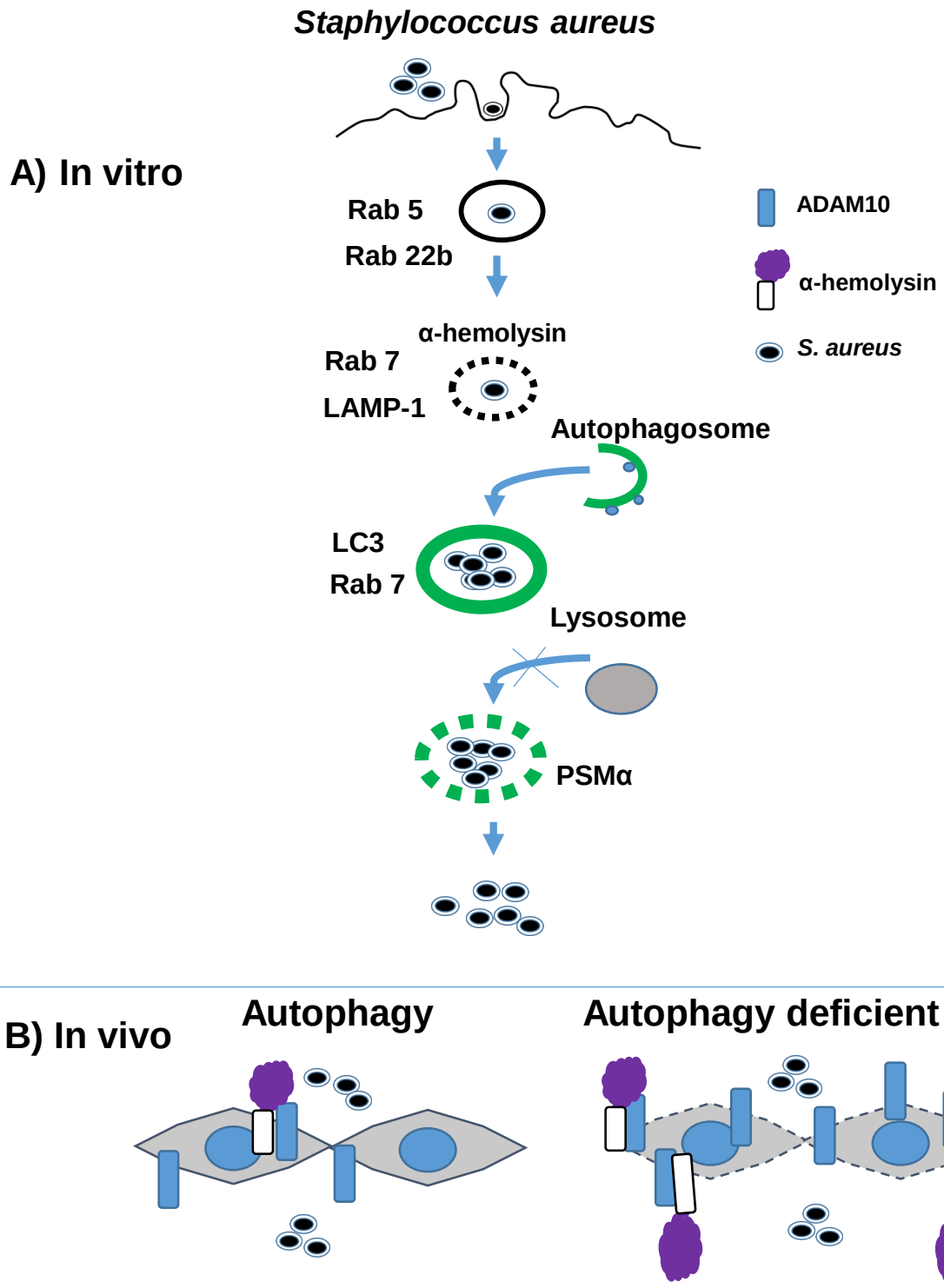

Figure 1.7: The physiologic interaction of *Staphylococcus aureus* with autophagy.
A) In vitro**:** *Staphylococcus aureus* transits through an early phagosome with Rab5 and Rab22b that quickly maturates (15 min p.i.) to a late compartment marked by Rab7 and LAMP-1. α-hemolysin is secreted by the bacteria and causes membrane damage. Autophagy is stimulated by the toxin and autophagosomes are recruited to the damage phagosome. *Staphylococcus aureus* replicates inside autophagosomes that do not mature to autophagolysosomes due to the inhibition of lysosomal fusion. Then, phenol soluble modulin alpha (PSMα) mediates *Staphylococcus aureus* escape to the cytoplasm, where bacteria continue replicating. Figure adapted from (Lopez de Armentia et al., 2016).
B) In vivo: autophagy plays a critical role in tolerance following infection by *Staphylococcus aureus*. Autophagy functions offer protection through limiting the toxin's damage by decreasing the level of ADAM10 receptor. Figure adapted from (Maurer et al., 2015).

1.4. Hypothesis and aims

The emergence of multi-drug resistance in bacteria is a major concern compelling researchers to explore further treatment strategies. New drugs that kill or attenuate bacteria will likely lead to further resistance. Another developing strategy is to discover the interaction between the bacteria and host cells, in order to understand how the pathogen reduces the host defence systems and causes infection. This new knowledge could lead to new host-directed therapies to fight bacterial infections.

Therefore, we advance the hypothesis that targeting the genes which are required for *Staphylococcus aureus* or *Salmonella enterica* sv. Typhimurium infection may develop a novel therapeutic means aimed to fight bacterial infection through the development of host-directed therapies.

This project has three major aims:

1- To study the xenophagy response induced by *Staphylococcus aureus* as compared with the better understood xenophagy programme induced following infection with Gram-negative *Salmonella enterica* sv. Typhimurium. This comparison was performed because the autophagy response to *Staphylococcus aureus* infection was relatively poorly understood, as compared with *Salmonella enterica* sv. Typhimurium. This, therefore, was important to establish the experimental system.

2- To develop ULK1 inhibitors as drugs to fight MRSA infection via blocking autophagosome formation and formation of the Staphylococcal replication niche.

3- To find novel genes in host cells required for *Staphylococcus aureus* infection using the CRISPR Cas9 genome-wide genetic selection approach.

Chapter 2

Materials and Methods

2. Material and methods

2.1. Eukaryotic cells

2.1.1. Eukaryotic cell culture

In this project, eukaryotic cell lines described in Table 2.1 were used. All of these were cultured in Dulbecco's modified Eagle's medium (DMEM) (Lonza, BE12-614F) complete media supplemented with 10% FBS (Biosera, S1900-050), 4mM L-glutamine (Lonza, BE17-605E) and 0.01 units /L of penicillin/streptomycin (Lonza, 17-602E). A penicillin/streptomycin (P/S) free variant of this media was also used in this study during bacterial infection stages. All cells were grown in an incubator set at 37^{o}C with 5% CO_2. All cell culture plastics were bought from Greiner. All cell lines were sub-cultured twice a week depending on requirements.

NO.	Cell Type	Reference
1	Human Embryonic Kidney (HEK) 293A	Invitrogen, R705-07
2	Henrietta Lacks (HeLa)	European Collection of Cell Cultures
3	ATG5 knock-out (-/-) mouse embryonic fibroblasts (MEFs) and matched wild type MEFs.	(Kuma et al., 2004)

Table 2.1 A list of eukaryotic cell lines grown within this investigation

2.1.2. Eukaryotic cell preparation for infection

One day prior to infection, required cell lines were plated at set densities as described below. All cell lines were grown in flasks (or 10 cm plates) until confluent before plating. Once confluent, the cells were washed with PBS (Lonza, BF17-516F) and then detached from the surface by Trypsin/EDTA (Lonza, BE17-161E). Cells were counted using a haemocytometer and plated at varying densities depending on the experiment. Lower densities were plated for imaging experiments using glass coverslips. Penicillin/streptomycin free media DMEM was used when plating cells. Plated cells were left to attach in this media overnight at 37^{o}C with 5% CO_2.

For experiments which required glass coverslips, 1.0 thickness coverslips (Agar L4096-1) were first sterilised with 70% ethanol for 60 seconds. Wells were then washed twice with sterile dH_2O. For most experiments, cells were seeded onto 24-well plates at a

density of 0.1 x 10^6 cells per well. In experiments where cell lysates were to be run on gels, 12-well plates were used at a density of 0.4 x 10^6 cells per well.

2.2. Bacterial strains, growth and infection conditions

2.2.1. Bacterial strain

Five separate strains of *Staphylococcus aureus* were used to infect cells in this project. (Tables 2.2 and 2.3).

NO.	Name	MSSA/MRSA	Accessory gene regulator (*agr*)	Reference
1	*S. aureus* subsp. ATCC®29213TM	Methicillin Sensitive *S.aureus* (MSSA)	Present	ATCC (American Type Culture Collection).
2	Wild type MRSA epidemic 78 strain (EMRSA78)	Methicillin Resistant *S.aureus* (MRSA)	Present	(Raghukumar et al., 2010) Obtained from Jun Yu (U Strathclyde)
3	Wild type MRSA strain (NCTC8325)	Methicillin Resistant *S.aureus* (MRSA)	Present	(Schnaith et al., 2007) Obtained from Public Health England, National Collection of Type Cultures
4	NRS144	*agr*-mutant	*agr*-mutant	(Kreiswirth et al., 1983). Obtained from Jun Yu (U Strathclyde)

Table 2.2 A description of the *Staphylococcus aureus* strains used within this investigation

Clonal complex	Strain	Reference
CC8	EMRSA 6	(Sangal et al., 2012) Obtained from Jun Yu (U Strathclyde)

Table 2.3 HA-MRSA strains used throughout this study

All *Staphylococcus aureus* strains were grown at 37ºC on mannitol salt agar plates (OXOID 1106008). This media was prepared and sterilised and then poured into sterile petri dishes. For liquid cultures, *Staphylococcus aureus* was grown in tryptic soy broth (TSB) (Fluka analytical, 22092-500G), which was also prepared and sterilised according to standard protocols and then dispensed into sterile tubes.

Furthermore, *Salmonella enterica* sv. Typhimurium was used in this study.

NO.	Name	Code	Reference
1	*Salmonella enterica* sv. Typhimurium	NCTC 13347	(Zheng et al., 2009) Obtained from Public Health England, National Collection of Type Cultures

Table 2.4 *Salmonella enterica* sv. Typhimurium strains used in this study

Salmonella were grown at 37ºC on nutrient agar plates (OXOID 1655783) which was prepared and sterilised according to standard protocols and poured into sterile petri dishes. For liquid cultures, *Salmonella* were grown in tryptic soy broth (TSB) (Fluka analytical, 22092-500G) which was prepared and sterilised according to standard protocols and then dispensed into sterile tubes.

2.2.2. Long-term storage and recovery of bacterial stocks

One colony from an overnight bacterial culture plate was added to a glycerol stock tube (Microbank™ - Yellow (80 vials) PL.170/Y). After five minutes, the tubes were vortexed, the media pipetted off and stored immediately at -80°C until required. When bacteria were needed, this glycerol stock was removed from -80°C, cells were scraped with a sterile inoculation loop and then streaked onto an agar plate. For bacteria which have an antibiotic plasmid resistance, these were streaked onto agar plates containing ampicillin (100 µg/ml). The frozen stock was returned immediately to -80°C. Plates were inverted

and incubated in a 37°C bacterial incubator overnight. Agar plates with cultures were wrapped in Parafilm and stored inverted at 4°C (for up to a maximum of three weeks).

2.2.3. The transformation of *Salmonella enterica* sv. Typhimurium with EGFP plasmid

Overnight cultures were diluted 1:100 into 10 ml of fresh tryptic soy broth (TSB) and incubated until OD600 = 0.5 (detected using cell density meter (CO8000)). After reaching OD=0.5, cultures were chilled on ice for 20 minutes. These cells were harvested by centrifugation for 10 minutes at 2500 rpm (4 ^{o}C). The pellets were re-suspended in 10 ml of ice-cold sterile 10% glycerol/water. Then, they were re-centrifuged for 10 minutes at 2500 rpm and re-suspended again in 500 µl 10% glycerol. Next, after separating into 200 µl ice-cold tubes, EGFP (1 µg/ml) plasmid was added. The transformation was done using electroporation by transferring cells+DNA to an ice-cold 2-mm electroporation cuvette (Bio-Rad) which pulsed on the EC2 programme. The cells were immediately transferred to 1 ml of TSB and incubated for one hour with shaking at 37^{o}C and then concentrated to 300 µl. After this process, 40 µl or 100 µl were plated on LB agar media including 100 mg/ml ampicillin and incubated at 37^{o}C.

2.2.4. Bacteria preparation for infection

2.2.4.1. Staphylococcal preparation for infection

One day prior to infection, overnight cultures were set up with the required bacterial strains. A single colony from an agar plate was cultured overnight at 37^{o}C in 5 ml tryptic soy broth (TSB). For infections, overnight culture was diluted in 5 ml of fresh TSB. The dilution used (typically 1:100 for *Staphylococcus aureus*) gave an initial OD600 reading of approximately 0.1, which was called Time=0. The dilutions were then incubated at 37^{o}C with shaking until the OD600 measured was 0.3 ± 0.05. Depending on the OD measured and the multiplicity of infection (MOI) required, volumes of bacterial culture were added to 1.5 ml centrifuge tubes and spun at 5000 rpm for 10 minutes to isolate bacterial pellets.

Varying MOIs were used for different types of experiments: normally 100 MOI for imaging experiments and 100 and 200 MOI for biochemistry signalling experiments. The supernatant was then removed and the pellets were re-suspended in 100 µl Pen/Strep-free DMEM media to be added to mammalian host cells.

Example calculation

If the OD600 of bacterial culture grown was 0.32 and the desired MOI was 100, then the calculation would be as follows:

Volume of bacterial culture required to infect one well at desired MOI =

(0.3 * 100 MOI) / 0.32 = 93.75 µl of bacterial culture per well

If, for example, 10 wells were being infected, then 937.5 µl of bacterial culture would be centrifuged and the pellets would be resuspended in 1 ml of complete media.

2.2.4.2. *Salmonella* preparation for infection

One day prior to infection, overnight cultures were made up of the required bacterial strains. A single colony from an agar plate was cultured overnight at 37°C in 5ml tryptic soy broth (TSB). For infections, *Salmonella* were sub-cultured (1:33 diluted) in 10 mL of TSB broth (for example, 300µL overnight culture + 10000µL fresh TSB) for 3 hours at 37°C with shaking. This resulted in the *Salmonella experimental stock culture* (used below), which is at OD600 of approximately 1.2–1.5, corresponding to approximately 1 * 10^8 bacteria/ml.

2.2.5. Infecting cells

2.2.5.1. Infecting cells with *Staphylococcus*

100µl of bacteria/DMEM suspension (described above) was added to each well of a 12 well plate containing 1 ml Pen/Strep-free DMEM supplemented with 10% foetal bovine serum and incubated for an hour. After this hour, 0.05 mg/ml gentamicin was added. This inhibited growth of any extracellular bacteria and this point was designated the 0-hour time point. The plates were returned to the 37°C incubator.

2.2.5.2. Infecting cells with *Salmonella*

For use, the *Salmonella* bacteria experimental stock cultures (described above) were further diluted 1:100 in Pen/Strep-free DMEM supplemented with 10% foetal bovine serum. Cell medium was removed from mammalian cell wells and 1 ml of bacteria-containing Pen/Strep-free DMEM was added. Cell infection/invasion proceeded for 20 minutes at 37°C. After 20 minutes, the media was changed into fresh Pen/Strep-free DMEM supplemented with 10% foetal bovine serum and further incubated at 37°C for 30 minutes. After this 30 minutes, the media was further removed and exchanged with

Pen/Strep-free DMEM supplemented with 10% foetal bovine serum containing gentamicin (0.05mg/ml gentamicin) and incubated for a further hour for cover slip /imaging experiments; or 72 hours for cell killing experiments.

2.2.6. Fixing and Giemsa staining

Seventy-two (72) hours after infection, the cells were fixed with 10% Formalin (SIGMA SLBK3646V) /PBS for 15 minutes. After fixation, cell wells were changed into a 1:1 mix of PBS: methanol (1 min). The PBS: methanol was removed and then 1 ml of diluted Giemsa stain (Fluka BCBK8476V) was added. After five minutes, the plates were washed with water and dried by aspiration. To quantify Giemsa stain, 1 ml of 30% Acetic acid/water was added to each well to dissolve the cells/stain. The solute from each well was transferred to a cuvette and absorbance read at 560nm. In an alternate way, the solute from each well was transferred to a 96 well plate and read in a plate reader at ABS 560nm. Giemsa blue uptake represented the % of viable cells after infection.

2.2.7. Bacterial Colony forming unit (CFU) assay

Once the desired time point was reached, infected mammalian host cells were washed with PBS once and then 0.5ml of 0.05% Triton X 100 solution (Sigma, T-9284) (diluted in PBS) was added to each well. During the next steps, the cell well plates were incubated on ice. Cells were lysed and removed from the bottom of the wells by pipetting. Next, cell lysates were diluted 100 X (into PBS) and, of this, 50 µl was plated on MSA agar. These plates were incubated overnight at 37^{o}C. Colonies grown overnight were then counted and the overall CFU (colony forming units) was calculated using the following equation:

CFU = number of colonies / volume of lysate (ml) normalised by dilution factor

Example Calculation.

If 100 colonies were counted after 50 µl of a 1/100 dilution of lysates was plated, then the calculation would be as follows: =

(100 / 0.05 ml) X 100 = 200,000 CFU/ml.

2.2.8. Induction, block and inhibition of autophagy

Where indicated, drugs or alternative media were added to the wells in order to induce, inhibit or block autophagy. For the induction of autophagy via amino acid starvation, EBSS, containing 0.05 mg/mL of gentamicin (if the experiment involved bacterial

infection), was added to the cells (after a PBS wash). Autophagy flux was blocked by the addition of 25 μM Chloroquine (Sigma, C6628) or 10 nM Bafilomycin to the media.

MRT68921 is a potent and dual ULK1/2 inhibitor with IC50 of 2.9 nM and 1.1 nM, ULK1 and ULK2 activity, respectively (Petherick et al., 2015). This drug was used in this project in order to inhibit autophagy (10 μM final concentration). In addition, three related MRT analogues (MRT216403, MRT239016 and MRT238993) derived from MRT68921 were obtained in collaboration from B. Saxty, Medical Research Council (MRC), and College of Life Science at the University of Dundee / LifeArc.

The ULK1 inhibitory compounds SBI-0206965 (Egan et al., 2015), and "KS1 drug" (compound #6 in(Lazarus and Shokat, 2015)) were synthesised in collaboration with Prof. N. Tomkinson, Strathclyde Pure and Applied Chemistry. These drugs were used in this study at high (10 μM) or low (1 μM) concentrations.

2.3. Western blotting

2.3.1. Cell Lysis

At the desired time point, cell well plates were placed on ice and media were aspirated. 30μl of lysis buffer was added to each well, consisting of TNTE (150 mM NaCl, 5mM EDTA, 0.3% TX100 + EDTA-free protease inhibitor (Roche, 05892791001) (protease inhibitor added fresh, prior to use). A cell scraper removed all lysates from the surface of the well. All of the lysates were stored at -80^{o}C in until further processing.

2.3.2. Western blot protocol to resolve endogenous LC3 using NuPAGE gel or other protein using hand-poured BIS-TRIS gels

Samples stored at -80^{o}C were thawed on ice and centrifuged at 12000 RPM (15,000 x g) for three minutes at 4^{o}C to pellet cell debris. 15 μl of each sample was then mixed with 7.5 μl of 1.5x concentrated Laemmli sample buffer (LSB) (94 mM Tris pH 6.8, 30% Glycerol, 3% SDS and 5% BME). Samples were then heated at 95^{o}C for five minutes.

Once heated, the samples were resolved on pre-cast gels for LC3 immunoblotting (NuPAGE® 4-14% Bis-Tris Gel (NPO335BOX)) for 40 minutes at 180 volts using NuPAGE® MES Running Buffer (Invitrogen, NP0002).

Alternatively, processed lysates were loaded on hand-poured Bis-Tris gels made up of 10% acrylamide lower stack and 5% acrylamide upper stack gels prepared accordingly using 30% Acrylamide stocks [National Diagnostics, EC-890]. Gel internal buffering was comprised of 0.33M final Bis-Tris [Sigma, #B9754]. These gels were run for one hour at

150V using MES-SDS running buffer (NOVEX life technologies, #NP0002). A 26–180 KDa molecular marker (Sigma, SDS7B2) was used as standard (Table 2.5).

The proteins were transferred to PVDF-FL Millipore membranes. Once protein transfer was confirmed using Ponceau S and washed with water, membranes were trimmed into appropriate sections. Once cut, membranes were blocked in a 5% milk solution (in 1X TBS) (0.15 M NaCl, 24.7 mM Tris pH 7.4) for an hour. After this hour, the membranes received three five-minute washes in 1X TBS.

Then, the membranes were incubated with diluted primary antibody (Table 2.6) at 4^{o}C overnight. After this, the membranes were given three five-minute washes in 1X TTBS (0.15 M NaCl, 24.7 mM Tris pH 7.4 and 0.05% Tween 20) and then stained with the appropriate secondary antibody (Table 2.6) for an hour (diluted 1:4000 in 1XTBS). Finally, the membranes were given three five-minute washes in 1XTTBS, and then they were analysed and quantified using the LICOR odyssey infrared imager and Image Studio v2.0 software. Blots were quantified typically as ratios of protein over the loading control actin, with the exception of LC3-II, which was quantified as a ratio of LC3-II/LC3-I protein. Real protein expression was calculated as sample signal minus background signal.

Pre-stained protein	**Weight (Da)**
α2–macroglobulin from human blood plasma	180,000
β-galactosidase from *E.Coli*	116,000
Lactoferrin from human milk	90,000
Pyruvate kinase from rabbit muscle	58,000
Fumarase from porcine heart	48,500
Lactic dehydrogenase from rabbit muscle	36,500
Triosephosphate isomerase from rabbit muscle	26,600

Table 2.5 Sigma molecular weight marker proteins

Protein	Weight (kda)	Primary antibody	Secondary antibody
Actin	48kda	Mouse monoclonal (Ab-5) [BD Bioscience #612657]; 1:1000, final [0.25 µg/ml], dilution in TBS	Alexa Fluor® 680 goat anti-mouse IgG (H+L) [Thermo Scientific, A-21057]; final [0.4µg/ml], dilution in TBS
LC3II	17kda	Mouse monoclonal (clone 5F10) [Nanotools #0231-100] 1:200, final [0.5µg/ml], dilution in TBS	Alexa Fluor® 680 goat anti-mouse IgG (H+L) [Thermo Scientific, A- 21057]; final [0.4µg/ml], dilution in TBS
ATG13	70kda	monoclonal Rabbit D4P1K (Cell signaling, #13273) 1:1000 dilution in (5% w/v BSA ,1X TBS, 0.1% TWEEN 20)	Dylight 800 conjugated goat anti rabbit igG, (Thermo scientific), dilution in TBS
ULK1	120kda	Rabbit monoclonal (Cell signaling, #D8H5)1:1000 dilution in (5% w/v BSA, 1X TBS, 0.1% TWEEN 20).	Dylight 800 conjugated goat anti rabbit igG, (Thermo scientific), dilution in TBS

Table 2.6 Primary and Secondary Antibodies for western blot analyses. Dilution factors, incubation conditions and final concentrations (where available) indicated

2.4. Imaging experiments for immunofluorescence and confocal microscopy

2.4.1. Fixing cells grown on coverslips

At the desired time point after infections and treatments, cells were fixed onto the coverslips as described below. The media was aspirated off and the cells were washed with PBS. The cells were then fixed by the addition of 3.2% paraformaldehyde (Agar Scientific (R1026)) diluted with PBS for 20 minutes at room temperature. Cells were then rinsed in PBS and stored at 4^{o}C.

2.4.2. Staining for protein A on the surface of *Staphylococcus aureus* strains, p62/Sequestosome1, LC3, LAMP2, ATG13

Cells were first permeabilised with a 0.2% solution of Triton X100 (Sigma, T-9284) (diluted in PBS) for five minutes. Cells were then washed with PBS and blocked in 2 g/L (i.e. 0.2%) porcine gelatin (Sigma, G9136) (diluted in PBS) for 20 minutes. Antibody incubation chambers were set up consisting of parafilm layered on the bottom of a light safe enclosed box. On this parafilm, 50µl drops of diluted primary antibody were displaced as follows: 1/1000 anti-protein A (mouse antibody) (Sigma, P2921-2ML); anti-p62/SQSTM1 1/500 (BD Transduction Laboratories purified mouse anti-p62); LAMP-2 1/500 (purified mouse anti-human CD107b), LC3 Polyclonal rabbit (Cell signalling, #2775) or ATG13 monoclonal Rabbit D4P1K (Cell signalling, #13273) (all diluted in blocking solution). After blocking, each coverslip was placed with cells face down onto primary antibody and incubated at room temperature for 20 minutes.

A similar chamber was set up for the secondary antibody (1/500 solution of Alexa Fluor 555®- goat anti-mouse IgG (H+L) (Invitrogen, A21422)) for anti-Protein A, anti-p62 and anti-LAMP2 or alternatively, with Alexa 555 anti-rabbit (Invitrogen, #1037302) for anti-LC3 and anti-ATG13. After staining with primary antibody, coverslips were washed three times in PBS and then placed, cells face down, on 50 µl of the appropriate secondary antibody. The coverslips were stained with secondary antibody for 20 minutes. Coverslips were then washed three times in PBS, blotted dry carefully and mounted onto a microscope slide using 8µl of MOWIOL.

All images were captured on a Leica TCS SP5 confocal microscope fitted with a HCX PL APO CS-63x-1.4NA objective and a HyD GaAsP detection system under the following setting: speed (200Hz), line average (4), frame average (1) and lasers: DAPI (PMT1), YFP (HYD), Alexa 555 (HYD4). For spot counting, Epi-fluorescence upright microscopy (Nikon Eclipse) E600 was used under an X60 1.40 NA objective lens fitted with appropriate standard filter blocks.

2.5. The criteria of quantitation, the measured readout, and the statistical tests

Activation of autophagy was quantified by calculating the ratio of LC3-II to LC3-I using the Li-COR Odyssey system and Image Studio v2.0 software. Other proteins such as ULK1 and ATG13 were quantified typically as ratios of protein over the loading control actin. For each densitometer measurement, an identical ellipsis was drawn and the intensity quantified. The local background for each band was also analysed and subtracted from the band intensity to give a more accurate and precise quantification.

The number of Gal3 or ATG13 puncta was counted from 50 infected cells captured by a Leica TCS SP5 confocal microscope for Gal3 using LAS AF Lite or epifluorescence microscopy for ATG13. Fifty (50) infected cells were captured from different fields for three coverslips and the average of three independent experiments was taken.

Also, the number of infected cells which had LC3 or p62 puncta was counted as above using epifluorescence microscopy and then the cells' percentage was calculated as the number of infected cells having LC3, P62, or LAMP-2 spots divided by the total number of infected cells in the same field multiplied by 100.

All statistical analysis, the unpaired t-test, and 1-way ANOVA with Tukey multiple comparison tests were done using GraphPad Prism-4 software (GraphPad Software Inc., USA).

2.6. Molecular experiments

2.6.1. CRISPR-Cas9 mediated knockout in HEK293A cells

CRISPR-Cas9 mediated knockout was used in order to target genes for validation or focused studies.

Oligonucleotides containing gRNA sequences targeting genes were cloned individually into lentiGuide-Puro vector using standard protocols as summarised below.

LentiGuide-Puro plasmid (Addgene #52961) (Sanjana et al., 2014) was digested with BsmB1 (Biolabs #R0580S) and then purified on an agarose gel using the QIAquick gel extraction kit (Qiagen) according to the manufacturer's instructions. Following this, a sample of this product was checked by agarose gel for correct size and purity.

Forward and reverse primer oligonucleotide sequences were ordered (corresponding to sequences in the CRISPR2-Gecko library (genome engineering.org/gecko) (Table 2.7) and resuspended in sterile water at a stock concentration of 100 µM then diluted to give 50nM final concentrations.

For annealing, 1 µl for each primer dilution was mixed with 1 µl 10X T4 ligation buffer (New England Biolabs, B0202S), and 7 µl water (10 µl total). Reactions were annealed by a Thermo-cycler program (95^{o}C 5 mins, followed by a reduction in temperature to 25^{o}C at a rate of 6^{o}C/min).

For ligation of the annealed oligos with digested lentiGuide-Puro plasmid, 50 ng digested plasmid was mixed with 1 µl above diluted oligonucleotides, 1 µl 10X ligation buffer and 0.5 µl T4 DNA ligase (Biolabs #M0202S) in a final volume of 10 µl. Ligations were carried out overnight at 16^{o}C. Then, 5 µl from the ligated product was transformed into chemically competent DH5α *E. coli* (100 µl) (Invitrogen #12297016) using standard heat shock conditions (20 mins on the ice, 37^{o}C/40 secs, 1 min on ice). Transformed *E. coli* were transferred on LB-Ampicillin plates according to a standard molecular biology protocol, and bacterial colonies were isolated after growth overnight.

Multiple *E. coli* colonies were picked and grown overnight in 2 ml LB-Amp and DNA plasmids were purified using QIAprep Spin miniprep kit (Qiagen #27104). A sample from DNA plasmid was digested and checked by agarose gel for size. DNA concentration was measured by using a NanoDrop ND2000 (Thermo Fisher Scientific, USA). Lastly, correct DNA (gRNA) sequence was confirmed with Sanger sequencing using primer LKO1.5' (GACTATCATATGCTTACCGT) (GATC Biotech service, SupremeRunTM).

Lentiviruses were generated using HEK293FT packaging cells by transfection via using Lipofectamine 2000 (as described in detail in Section 2.6.2). HEK293A Cas9 cells were transduced with neat viral supernatant (as described in detail in Section 2.6.3) and left to grow for 48 hours. Transduced cells were selected using puromycin (2µg/ml) for two days. We worked with cell pools generated after transduction with CRISPR-Cas9 lentivirus leading to a heterogeneous population. Then, cells were plated for bacterial infection (as described in 2.2.5.1 and 2.2.5.2) to test if this gene has a role in MRSA or *Salmonella enterica* sv. Typhimurium infection. After various time points of infection, cell viability was read by AlamarBlue (as described in Section 2.6.4). Then, the percentage of cells surviving was calculated as cell viability with bacterially infected cells divided by full (uninfected) cell viability x 100.

For the production of a stable HEK293A Cas9-Blast cell line, lentivirus was produced by transfecting HEK293T cells using Lipofectamine 2000, as described in a later section. The virus was used to transduce the HEK293A cells. Cells were selected in 10 µg/ml blasticidin for one week. To confirm Cas9 expression, cells were plated on coverslips and stained with FLAG M2 antibody (Sigma, Cat no. F3165). Cas9 protein expression was analysed using an epi-fluorescent microscope. The Cas9 protein construct contains a FLAG-tagged (DYKDDDDK Tag) (Vector Addgene: 52962).

Sequence name	Oligo sequence (5´-3´)
DAZLHGLibA_12369_F	CACCGCTTCTGGTAAAATATAGCCT
DAZLHGLibA_12369_R	AAACAGGCTATATTTTACCAGAAGC
DAZLHGLibA_12370_F	CACCGAAGATAATCACTGATCGAAC
DAZLHGLibA_12370_R	AAACGTTCGATCAGTGATTATCTTC
DAZLHGLibA_12371_F	CACCGAGAAGCTTCTTTGCTAGATA
DAZLHGLibA_12371_R	AAACTATCTAGCAAAGAAGCTTCTC
DAZLHGLibB_12356_F	CACCGTCATCAGCTGCAACCAGCCA
DAZLHGLibB_12356_R	AAACTGGCTGGTTGCAGCTGATGAC
DAZLHGLibB_12357_F	CACCGTGGTTGCAGCTGATGAGGAC
DAZLHGLibB_12357_R	AAACGTCCTCATCAGCTGCAACCAC
DAZLHGLibB_12358_F	CACCGCCTCCAACAAAAACAGTGTT
DAZLHGLibB_12358_R	AAACAACACTGTTTTTGTTGGAGGC
CD164HGLibA_08248_F	CACCGGCAGCTGTTTCGACCTTCAC
CD164HGLibA_08248_R	AAACGTGAAGGTCGAAACAGCTGCC
CD164HGLibA_08249_F	CACCGGTGCCAACAGCCAATTCTAC
CD164HGLibA_08249_R	AAACGTAGAATTGGCTGTTGGCACC
CD164HGLibA_08250_F	CACCGAACACGACAGACTTCTGTTC
CD164HGLibA_08250_R	AAACGAACAGAAGTCTGTCGTGTTC
CD164HGLibB_08241_F	CACCGTCCAAGACAGTTACTACATC
CD164HGLibB_08241_R	AAACGATGTAGTAACTGTCTTGGAC
CD164HGLibB_08242_F	CACCGAACAGTTAGTGATTGTCAAG
CD164HGLibB_08242_R	AAACCTTGACAATCACTAACTGTTC
CD164HGLibB_08243_F	CACCGACCTGATGTAGTAACTGTCT
CD164HGLibB_08243_R	AAACAGACAGTTACTACATCAGGTC
ARHGAP28HGLibA_02746_F	CACCGCCACTTATCGCATTCTGAAC
ARHGAP28HGLibA_02746_R	AAACGTTCAGAATGCGATAAGTGGC
ARHGAP28HGLibA_02747_F	CACCGCCAGTTCAGAATGCGATAAG
ARHGAP28HGLibA_02747_R	AAACCTTATCGCATTCTGAACTGGC
ARHGAP28HGLibA_02748_F	CACCGTGCTTCAGTTAAGCCAAATC
ARHGAP28HGLibA_02748_R	AAACGATTTGGCTTAACTGAAGCAC
ARHGAP28HGLibB_02744_F	CACCGAATGTTCAGAAAACCAGATT
ARHGAP28HGLibB_02744_R	AAACAATCTGGTTTTCTGAACATTC
ARHGAP28HGLibB_02745_F	CACCGAATGACAGCTCTTCAGCCTC

ARHGAP28HGLibB_02745_R	AAACGAGGCTGAAGAGCTGTCATTC
ARHGAP28HGLibB_02746_F	CACCGTGAAGTGTCTTATTCAGAAA
ARHGAP28HGLibB_02746_R	AAACTTTCTGAATAAGACACTTCAC
ATG13GLibA_03466_F	CACCGTTTACCCAATCTGAACCCGT
ATG13GLibA_03466_R	AAACACGGGTTCAGATTGGGTAAAC
ATG13GLibA_03468_F	CACCGGACTGTCCAAGTGATTGTCC
ATG13GLibA_03468_R	AAACGGACAATCACTTGGACAGTCC

Table 2.7 Different gRNA oligo forward and reverse sequences

2.6.2. Stable expression in eukaryotic cells via transduction with retro- or lentivirus vectors

Two different plasmids were used throughout this project to generate stable eukaryotic cell transduction with plasmids for overexpression.

To produce retrovirus, small (60mm) dishes of HEK293FT cells were seeded (which yielded ~60 % confluence the next day) in standard “D10” media (DMEM supplemented with 10% foetal bovine serum). Transfection was performed using Lipofectamine 2000 (Life Technologies). For one dish, 6.4µl of Lipofectamine 2000 was diluted in 320µl OptiMEM (Life Technologies) and left for five minutes. In another tube, 400µl of OptiMEM was mixed with 2 µg of pMXs-IP-EGFP-hAtg13 (Addgene: 38191) or pMXs-puro GFP-p62 (Addgene: 38277) + 0.5 µg of MDG-VSVG (packaging plasmid) + 1 µg of pMDLG (viral replication components) (kind gift from F. Randow, MRC Laboratory of Molecular Biology (LMB), Cambridge, UK).

The Lipofectamine/OptiMEM was mixed with the DNA/OptiMEM and left for 20 minutes before adding it to the HEK293FT cells. After four hours the media was changed to 5ml normal D10. After 48 hours the media was removed, supplemented with polybrene (8 µg/ml) and filtered through a 0.22µm Steriflip filter (HV/PVDF low protein binding membrane).

For transduction, HEK293 or HeLa target cells were grown in 12-well plates with about 50% confluency. The media was aspirated and 500µl of retrovirus containing plasmid was added to each cell line. These cells were incubated at 37^{o}C for one hour and then replenished with a further 0.5 ml of fresh D10 media (without polybrene). The following day, cells were exchanged into D10 media containing puromycin 2 µg/ml for GFP-

p62, and GFP-ATG13, in order to remove non-transduced cells. When the control (no virus) cells were killed by this antibiotic, the transduction cells were used for experiments.

2.6.3. Generated stable eukaryotic cells knockdown of autophagy-related protein ULK1

ULK1 pLKO shRNA (TRCN0000000835) vector was purchased from Open Biosystems. Lentiviruses containing the ULK1 shRNA were made in HEK293FT cells using LipofectamineTM 2000 (Life Technologies), as described above by using (pCMV-VSVG, and psPAX2) as packaging plasmid. The cells were transduced with lentivirus, following the same procedure as described above.

2.6.4. Lipofectamine 2000 Transient Transfection of Galectin3

HeLa cells were grown in 24-well plates with glass coverslips. These coverslips were washed with ethanol, followed by washing twice with sterile H_2O. Transient transfection with Lipofectamine 2000 was achieved by following the manufacturer's recommended guidelines. However, slight adjustments were made to optimise the transfection efficiency. The transfection complex was prepared using OptiMEM (Life Technologies). For each well (2 µg) of plasmid DNA of pEGFP-hGal3 (Addgene: 73080) was re-suspended in 50µl of OptiMEM. In another centrifuge tube, 0.8µl of Lipofectamine 2000, the reagent, was added to 40µl of OptiMEM. Both tubes were left for five minutes at room temperature. The contents of the two tubes were carefully mixed and incubated at room temperature for a further 20 minutes, and subsequently 160 µl of additional OptiMEM was added to this mixture. Then, the cells media were aspirated and 250µl of transfection mix added to each well. The mix was left to incubate for two hours in a humidified atmosphere (5% CO2) at 37^{o}C, then the transfection mix was aspirated and replaced with full media. After 24 hours of incubation, the cells were stimulated to use for experiments.

2.7. Method: Genome wide CRISPR/CAS9 screen (GeCKO libraries in one vector system)

2.7.1. Library amplification

GeCKO pooled libraries were first amplifed to a concentration and amount sufficient to generate lentivirus. For that, the gRNA pooled library in lentiCRISPRv2 (1-vector system) was purchased from Addgene (1000000048) and amplified as recommended by the Feng Zhang Lab protocols, as performed in collaboration with Helgason and Holyoake, of the University of Glasgow.

Briefly, GeCKO libraries A and B (50 ng/µL) were electroporated into Lucigen Endura (TM) electrocompetent cells as per the manufacturer's instructions. Bacteria were expanded on solid media and DNA was extracted by Maxiprep. Following DNA extraction, gRNA representation was checked using next generation sequencing, to ensure no guides had been lost or over amplified, which may introduce bias to the screen. For NGS, two PCR steps were performed. The first PCR amplified lentiCRISPR gRNAs and the second PCR step attached Illumina adaptors and barcodes to the samples. Analysis from this initial sequencing confirmed 99.98% representation from both Library A and Library B in the amplified plasmid library. Therefore, essentially all gRNAs were well represented and no skewed bias was shown.

2.7.2. Lentivirus production

To produce sufficient lentivirus for the whole screen, 12 small (60mm) dishes of HEK293FT cells were seeded (which yielded ~60 % confluence the next day) in standard "D10" media (DMEM supplemented with 10% foetal bovine serum). Transfection was performed using Lipofectamine 2000 (Life Technologies). For each dish, 6.4µl of Lipofectamine 2000 was diluted in 320µl OptiMEM (Life Technologies) and left for five minutes. In another tube, 400µl of OptiMEM was mixed with 2 µg of GeCKO v2 lentiCRISPR plasmid library (1 µg Library A+ 1 µg Library B) (Addgene) (Shalem et al., 2014) + 0.5 µg of pCMV-VSVG (packaging plasmid) + 1 µg of psPAX2 (viral replication components, Addgene 12260). Note: 2 µg of shRNA LKO ATG13-129 was used instead of GeCKO library plasmid for optimisation experiments.

The Lipofectamine/OptiMEM was mixed with the DNA/OptiMEM and left for 20 minutes before adding it to the HEK293FT cells in a total volume of 2 ml OptiMEM. After four hours, the media was changed to 5ml normal D10. After 60 hours the media was removed, supplemented with polybrene (8 µg/ml) and filtered through a 0.22µm Steriflip filter (HV/PVDF low protein binding membrane), and frozen at -80^{o}C.

2.7.3. Cell virus transduction by spinfection or without spinfection

For the standard (non-spinfection) method, on day 1, cells of interest were seeded in 12-well plates at 3,000,000 per well. On day 2, the cells were transduced with 100% (neat), 50% or 20% concentration diluted virus (0.5ml total volume/well). Virus dilutions were performed using D10 media supplemented with 8 µg/ml polybrene. After adding the virus, the cells were incubated at 37^{o}C for one hour and then replenished with a further 0.5 ml of fresh D10 media (without polybrene).

For plates with spinfection, the cells were centrifuged in a 12-well plate at 2,000 rpm for one hour at 37^{o}C, before being replenished with 0.5 ml of fresh D10 media (without polybrene).

After virus transduction, on day 3, the cells were split: one well was divided equally into two wells (12-well plates). On day 4, the cells were exchanged into D10 media containing puromycin 2 µg/ml to remove the non-transduced cells. The resulting cell viability (correlating to levels of transduction and effective virus titre) were measured by AlamarBlue in parallel replicate control wells as follows. Cell viability in cells treated with CRISPR lentivirus was measured by incubating cells in AlamarBlue reagent according to manufacturer's protocols at 37^{o}C for four hours (by adding from a 10x final concentration stock) and then reading with a plate reader (544nm excitation, 590nm emission).

2.7.4. Determination of viral titre

To measure viral titres, HEK293A target cells were infected with different volumes of virus. In respect of each dilution, 3 million cells in a 12-well plate were plated and then infected with different volumes of virus (500 µl, 250 µl and 125 µl) (all diluted to a total volume of 500 µl in D10 medium including polybrene (8 µg/mL)). After overnight

incubation, each well was split into two wells (6-well plate), with and without puromycin (2 µg/ml). When the non-infected cells treated with puromycin were 100% dead, the titre was determined by reading cell viability as measured by AlamarBlue as described above. The percentage of transduction was then calculated as cell viability = (reading from replicate with puromycin / reading from replicate without puromycin) x 100. From this calculation, it was found that the 250 µl amount of virus allowed roughly 50% of the cells to survive. The multiplicity of infection (MOI) was, in this case, designated as 0.5, as explained in Chapter 5.

2.7.5. Viral infection, puromycin selection

In order to have good representation of all guides in the starting population of cells, we ensured at least 300x coverage for each guide, as recommended in the protocol. The GeCKO Library A and B together contain approximately 120,000 gRNAs. Therefore, we used initially $80x10^6$ target cells for transduction. Using an MOI of 0.5, after puromycin (2 µg/ml) selection should yield 40 $x10^6$ cells. This equates to over 300 cells with every single gRNA. Therefore, $80x10^6$ 293A cells were seeded in 12-well plates at a cell concentration of $3x10^6$/mL. The total volume of media required per well was 1 mL. Therefore, cells were infected with the 250 µl of lentiviral supernatant plus 250 µl of polybrene (8 µg/mL) media. The cells were incubated for one hour with the virus. Following the incubation period, another 500 µl of normal media was added without polybrene and then the cells were incubated overnight.

The following day, each 2-well combination was pooled in one dish (75mm) and incubated for one week with puromycin (2 µg/ml) media for selection. Media were changed frequently (3–4 days) and refreshed with puromycin media to remove dead cells. After one week of incubation, cells were amplified to $60x10^6$ per condition. So, for five conditions (untreated control, infection with 2x MRSA and infection with 2x *Salmonella enterica* sv. Typhimurium), we required 300 $x10^6$ cells from the 40 $x10^6$ surviving cells.

2.7.6. Bacterial infection for positive selection screen

After the cell amplification, 60 x10^6 of untreated control cells were collected, counted and frozen for genomic DNA analysis (to determine initial representation of each gRNA). Remaining cells were re-plated in dishes (75mm) with Pen/Strep-free regular media for infection with MRSA or *Salmonella enterica* sv. Typhimurium. Most of the cells were killed by MRSA or *Salmonella enterica* sv. Typhimurium and very few cells survived. These few cells were amplified for one week, collected and counted. The pellets were frozen for genomic DNA isolation.

2.7.7. Amplification and identification of gRNA sequences

Following thawing of cell pellets (all control and treated samples done together), DNA was isolated with a QIAamp DNA Blood Maxi Kit as per the manufacturer's protocol (Qiagen, cat no: 51192). DNA concentration and purity were measured using a Nanodrop ND2000 (Thermo Fisher Scientific, USA) (Table 2.8).

Sample	No. of cells /million	DNA concentration ng/µL	Quality (260/280)
Control	60	227.7	1.91
CRISPR Screen post NCTC8325 set one	126	193.6	1.92
CRISPR Screen post S. Typhimurium set one	79	549.5	2.03
CRISPR Screen post NCTC8325 set two	100	298.6	1.92
CRISPR Screen post NCTC8325 set two	100	492.8	1.95
CRISPR Screen post S. Typhimurium set two	86	309.8	1.95

Table 2.8 CRISPR screen gDNA concentration

PCR for amplification of the gRNA sequences were performed in two steps to add barcodes and adapters for deep sequencing. For the first PCR, the amount of input genomic DNA (gDNA) for each sample was calculated as per Shalem et al. (2014) as follows: in order to achieve 300X coverage over the GeCKO library, 130 µg of DNA was used per sample (assuming 6.6 µg of gDNA for 10^6 cells). Therefore, for each sample, 13 separate 100 µl reactions were performed with 10 µg genomic DNA per reaction using Herculase II Fusion DNA Polymerase (Agilent). The primer sequences used to amplify lentiCRISPR gRNA (Feng Zhang Lab) are publicly available (http://genome-engineering.org/gecko/?page_id=15.).

v2Adaptor_F	AATGGACTATCATATGCTTACCGTAACTTGAAAGTATTTCG
v2Adaptor_R	TCTACTATTCTTTCCCCTGCACTGTtgtgggcgatgtgcgctctg

These primers were suspended for a working concentration of 10 µM. Each PCR reaction was set up with a total volume of 100 µL. For this reaction, 20 µL of 5X buffer, 1 µL of dNTPs, 10 µg of template DNA, 2.5 µL of 10 µM of v2Adaptor_F and v2Adaptor_R, final concentration 0.5 µM and 1 µL of polymerase were mixed (volume completed to 100 µl with nuclease-free water). PCR1 reaction was amplified with the following conditions: Initial denaturation: 95°C for 2 minutes, denaturation: 95°C for 20s, annealing: 60°C for 20s, extension: 72°C for 30s, 20 cycles. Final extension: 72°C for 30s. The 13 PCR amplicons for same biological sample were pooled.

The second PCR was performed to attach the Illumina adaptors and to barcode the samples. These primers were re-suspended in sterile water at a working concentration of 10 µM. Each sample was set up in 12 reactions using 12 different forward primers (F01-F12, as below). The forward primers had staggered sequences, which were 1-9bp different in order to increase the complexity of the library for sequencing. The same reverse primer was used in the 12 reactions for each specific biological condition.

For example: Sample 1:

F01+R01, F02+R01, F03+R01, F04+R01, F05+R01, F06+R01, F07+R01, F08+R01, F09+R01, F10+R01, F11+R01 and F12+R01.

For multiple samples, different reverse primers were used. The 12 reverse primer sequences (R01-R12) are on the GeCKO website. In this project, we needed four reverse sequences for four samples, so we used R04, 05, 06, and 08.

Forward

F01	AATGATACGGCGACCACCGAGATCTACACTCTTTCCCTACACGACGCTCTTCCGATCTtAAGTAG AGtcttgtggaaaggacgaaacaccg
F02	AATGATACGGCGACCACCGAGATCTACACTCTTTCCCTACACGACGCTCTTCCGATCTatACACG ATCtcttgtggaaaggacgaaacaccg
F03	AATGATACGGCGACCACCGAGATCTACACTCTTTCCCTACACGACGCTCTTCCGATCTgatCGCG CGGTtcttgtggaaaggacgaaacaccg
F04	AATGATACGGCGACCACCGAGATCTACACTCTTTCCCTACACGACGCTCTTCCGATCTcgatCAT GATCGtcttgtggaaaggacgaaacaccg
F05	AATGATACGGCGACCACCGAGATCTACACTCTTTCCCTACACGACGCTCTTCCGATCTtcgatCG TTACCAtcttgtggaaaggacgaaacaccg
F06	AATGATACGGCGACCACCGAGATCTACACTCTTTCCCTACACGACGCTCTTCCGATCTatcgatT CCTTGGTtcttgtggaaaggacgaaacaccg
F07	AATGATACGGCGACCACCGAGATCTACACTCTTTCCCTACACGACGCTCTTCCGATCTgatcgat AACGCATTtcttgtggaaaggacgaaacaccg
F08	AATGATACGGCGACCACCGAGATCTACACTCTTTCCCTACACGACGCTCTTCCGATCTcgatcga tACAGGTATtcttgtggaaaggacgaaacaccg
F09	AATGATACGGCGACCACCGAGATCTACACTCTTTCCCTACACGACGCTCTTCCGATCTacgatcg atAGGTAAGGtcttgtggaaaggacgaaacaccg
F10	AATGATACGGCGACCACCGAGATCTACACTCTTTCCCTACACGACGCTCTTCCGATCTtAACAAT GGtcttgtggaaaggacgaaacaccg
F11	AATGATACGGCGACCACCGAGATCTACACTCTTTCCCTACACGACGCTCTTCCGATCTatACTGT ATCtcttgtggaaaggacgaaacaccg
F12	AATGATACGGCGACCACCGAGATCTACACTCTTTCCCTACACGACGCTCTTCCGATCTgatAGGT CGCAtcttgtggaaaggacgaaacaccg

Reverse

R04	CAAGCAGAAGACGGCATACGAGATCATGATCGGTGACTGGAGTTCAGACGTGTGCTCTTCCGA TCTcgatTCTACTATTCTTTCCCCTGCACTGT
R05	CAAGCAGAAGACGGCATACGAGATCGTTACCAGTGACTGGAGTTCAGACGTGTGCTCTTCCGA TCTtcgatTCTACTATTCTTTCCCCTGCACTGT
R06	CAAGCAGAAGACGGCATACGAGATTCCTTGGTGTGACTGGAGTTCAGACGTGTGCTCTTCCGA TCTatcgatTCTACTATTCTTTCCCCTGCACTGT
R08	CAAGCAGAAGACGGCATACGAGATACAGGTATGTGACTGGAGTTCAGACGTGTGCTCTTCCGA TCTcgatcgatTCTACTATTCTTTCCCCTGCACTGT

PCR2 was set up as a 100 µL reaction using 5µL of the PCR product from the first PCR (in each of the 12 reactions). This used the entire DNA sample from the first PCR to maintain representation of the guides.

Similar to PCR1, each PCR2 reaction was 20 µL of 5X buffer, 1ul of dNTPs, 5µL of PCR1 product, 2.5 µL of 10 µM of v2Adaptor_F and v2Adaptor_R (final concentration 0.5 µM) and 1ul of polymerase (with nuclease-free water to make final volume 100 µl). The same thermocycler parameters were used as for PCR1.

Three PCR2 products (equal to 300µl) were pooled to purify and concentrate 5x on columns using the QIAquick purification kit as per the manufacturer's instructions. The resulting amplicon from PCR2 had an expected length of 340bp. All products were run on 2% agarose mini gels (1 g of agarose powder in 50 mL of 1x TBE buffer). 10µL of PCR product was mixed with 2 µL loading dye (6x) and was loaded into each well of the gel next to 100 bp DNA ladder and run at 100V for one hour. After running, the gel was documented by ultraviolet (UV) transilluminator and camera (ChemiDoc).

For gel extraction, in order to remove excess primers, the 340bp product was excised and extracted using a QIAquick gel extraction kit as per the manufacturer's instructions. Finally, PCR2 products from the same biological condition were pooled and passed to collaborators at Glasgow University Polyomics for measurement of the DNA concentration using a NanoDrop ND2000 and then sequenced on a NextSeq500 (Illumina): 30M reads for control sample, 10M reads for samples after positive selection. The raw analysis was performed in collaboration by Dr. Pawel Herzyk (Glasgow University Polyomics).

2.7.8. Statistical analysis

For data mining analysis, the Model-based Analysis of Genome-wide CRISPR/Cas9 Knockout (MaGeck) algorithm (Li et al., 2014) was used to generate gene scores from individual gRNAs, performed in collaboration by Dr. Pawel Herzyk (Glasgow University Polyomics). This statistical analysis uses combined p-value ranks of all gRNAs belonging to the same gene. MaGeck scores whether these ranks are significantly different from a purely random rank distribution. MaGeck analysis generates a gene summary that includes: Ranked aggregate RRA score, p-value, simple ranking of the gene, and the number of 'good' gRNAs after the positive selection. These details are discussed in detail in Chapter 5.

Chapter 3

Results

Xenophagy following infection by *Staphylococcus aureus* and *Salmonella enterica* sv. Typhimurium

3. Xenophagy following infection by *Staphylococcus aureus* and *Salmonella enterica* sv. Typhimurium

3.1. Introduction

Autophagy is a cellular process that results in the elimination of damaged or destroyed organelles and intracellular aggregates (Yu et al., 2018). However, a wide range of studies have shown different roles of autophagy in response to bacterial infection, demonstrating the complexity of pathogen-host cell interactions. Autophagy has been shown to degrade and restrict the replication of some bacteria (Birmingham et al., 2006, Gutierrez et al., 2004, Zhao et al., 2008, Py et al., 2007, Nakagawa et al., 2004). In contrast, other types of bacteria have been shown to require autophagy membrane transport for their replicative cycle (Starr et al., 2012, Mestre et al., 2010, Mestre and Colombo, 2012, Schnaith et al., 2007).

3.1.1. Xenophagy following infection by *Salmonella enterica* sv. Typhimurium

Generally, more studies have been performed on the xenophagy response following infection with *Salmonella enterica* sv. Typhimurium and this pathogen has become the best understood in terms of interaction with host cells. Following invasion of host cells, *Salmonella enterica* sv. Typhimurium remains inside a membrane vacuole, which is then remodelled to form a custom niche suitable for survival and replication. This specialised compartment has been termed the Salmonella-containing vacuole (SCV) and is promoted by bacterially encoded virulence factors such as TTSSs. When this vacuole becomes damaged through the action of the “needle-like” structure of the SPI-1 T3SSs (Birmingham et al., 2006), Galectin 8 can bind to the damaged vacuole and then recruit NDP52 followed by LC3-PE, thus inducing autophagy (Thurston et al., 2012). Alternatively, it is also possible for the damaged membrane SCVs to target lysosomes via a Ca2+-dependent mechanism, where a damaged SCV can be recognised and be degraded by a host cell (Roy et al., 2004).

Due to SCV damage, *Salmonella* escapes into the cytoplasm and are recognised by the ubiquitin system. The bacteria become encircled by the ubiquitinated proteins (Perrin et al., 2004). This ubiquitination is a well-characterised signal for xenophagy, requiring adaptor proteins to bridge the targeted bacteria to LC3 on autophagosome elongation membranes (Shahnazari and Brumell, 2011, Zheng et al., 2009, Yuk et al., 2012). This xenophagy response has been shown to be especially dependent upon

the ULK1, Atg9L and the Atg14L regulatory complexes, leading to formation of autophagy membranes around Salmonella-containing vacuoles so that the growth of *Salmonella enterica* sv. Typhimurium within SCV can be restricted (Kageyama et al., 2011). Accordingly, autophagy is important for the restriction of *Salmonella enterica* sv. Typhimurium growth in human host cells and the elimination of the free bacteria and damaged vacuoles. Interestingly, the *Salmonella* SPI-2 system also excretes a deubiquitinase (SseI) that reduces ubiquitinated aggregates on structures close to the damaged SCV to suppress recruitment of the autophagy adaptor SQSTM1, thereby providing a resistance mechanism to sustain replication in cells (Mesquita et al., 2012).

3.1.2. Xenophagy following infection by *Staphylococcus aureus*

While anti-bacterial xenophagy has been well characterised in response to *Salmonella enterica* sv. Typhimurium, to date, there are fewer studies on the relationship between *Staphylococcus aureus* and autophagy. *Staphylococcus aureus* causes several infections in human beings that range from mild skin symptoms to life-threatening conditions (Tong et al., 2015). Recently, infections caused by *Staphylococcus aureus* have displayed increased resistance to drugs, therefore complicating treatment strategies and creating a formidable public health concern.

Lately evolved strains can also show poor response to vancomycin (Fasihi et al., 2017) and daptomycin (Pader et al., 2016), the proposed last resort drugs for treating *Staphylococcus aureus* infection (Ruiz-Ramos et al., 2017, Howden et al., 2011). The efficacy evaluation of antibiotics used for the treatment of Staphylococcal infections found that just a fraction prevented replication of intracellular bacteria. At concentrations above the minimum inhibitory concentration, some of the antibiotics were largely ineffective at stopping intracellular bacteria replication (Qazi et al., 2004). The redevelopment of the infection caused by *Staphylococcus aureus* after the patient has had initial antibiotic treatment appears to be the critical medical issue. It can therefore be hypothesised that redevelopment or relapse of an infection may be caused by the inability of the antibiotic to the access the infection site and, particularly, *Staphylococcus aureus* residing in the intracellular niche.

Evidence has highlighted the importance of autophagy in supporting a protective niche for *Staphylococcus aureus*. Therefore, the normally protective autophagy pathway is critically subverted during *Staphylococcus aureus* invasion for the needs of the pathogen. The current model describes how *Staphylococcus aureus* uses virulence factors to inhibit the normal autophagosome fusion with lysosomes, creating a protective environment in which *Staphylococcus aureus* survives and replicates. After replication, *Staphylococcus aureus* breaks out of the autophagosome-derived replicative niche through the action of α-haemolysin and escapes into the cytoplasm to induce cell death (Campoy and Colombo, 2009). After inducing cell lysis, *Staphylococcus aureus* disperses and goes on to infect neighbouring cells (Liu et al., 2015, Schnaith et al., 2007). Expression of IsaB and *agr* by *Staphylococcus aureus* have been shown to be critical steps for subverting the autophagic machinery (Liu et al., 2015, Schnaith et al., 2007). However, other studies have shown evidence for degradation of intracellular *Staphylococcus* via autophagy to provide protection for the host cell (Mauthe et al., 2012). Therefore, the role of autophagy during *Staphylococcus aureus* infection appears to involve a dynamic or context-dependent balance that is not fully understood.

3.1.3. Aim and objectives

Details of the autophagy-*Staphylococcus aureus* interaction need to be clarified, as better understanding in this area could have potential medical applications. The experiments in this chapter aimed to study the xenophagy response induced by *Staphylococcus aureus* as compared with the better understood xenophagy programme induced following infection with gram-negative *Salmonella enterica* sv. Typhimurium. We decided to use HeLa and HEK293A cell lines as well-studied autophagy and xenophagy cell models for this project.

Our objectives were to:

1. Study activation of autophagy following infection by *Staphylococcus aureus* as compared with *Salmonella enterica* sv. Typhimurium.
2. Investigate the role of p62/sequestosome 1 as a potential adaptor molecule between ubiquitinated *Staphylococcus aureus*.
3. Investigate the modulation of lysosomes during *Staphylococcus aureus* infection.
4. Investigate the endomembrane damage in host cells following infection with *Staphylococcus aureus*.
5. Analyse host cell killing by *Staphylococcus aureus* as compared with *Salmonella enterica* sv. Typhimurium.
6. Investigate the role of Atg5 in xenophagy following infection by *Staphylococcus aureus.*

3.2. Results

3.2.1. Activation of autophagy following infection by *Staphylococcus aureus* as compared with *Salmonella enterica* sv. Typhimurium

3.2.1.1. Activation of autophagy in HeLa cells

Firstly, to observe how different bacterial pathogens activate the autophagic pathway, we tested xenophagy in response to *Staphylococcus aureus* as compared to the better characterised pathogen, *Salmonella enterica* sv. Typhimurium, through a biochemical western blot assay using HeLa cells. For this, autophagy was monitored by LC3 western blotting. LC3 is synthesised and cleaved during autophagy to generate mature LC3-I which is lipidated during autophagy activation to generate the LC3-II form which associates with autophagosomes (Kabeya et al., 2000).

Although autophagy has a significant role in protecting the host from pathogen infection, it has been suggested that the autophagic pathway can conversely also be beneficial to produce an intracellular niche for *Staphylococcus aureus* (Schnaith et al., 2007, O'Keeffe et al., 2015, Mestre et al., 2010). Therefore, inhibition of autophagy might have opposite effects on different bacterial pathogens. It was critical for our project to compare how gram-positive *Staphylococcus aureus* and gram-negative *Salmonella enterica* sv. Typhimurium activate xenophagy. In the initial experiments, we compared *Staphylococcus aureus* (ATCC29213) and *Salmonella enterica* sv. Typhimurium (NCTC13347), which both served as reference strains during xenophagy in infected HeLa, as a representative type of host cell (Birmingham et al., 2006, Schnaith et al., 2007).

HeLa cells were infected with ATCC29213 *Staphylococcus aureus* using an infection protocol based on the previous report by Schnaith et al. (2007). For simplicity and to directly compare, HeLa cells were infected with *Salmonella enterica* sv. Typhimurium using the same protocol. Briefly, both pathogens were grown until OD=0.3 and cells were infected using MOI 200 at 37^{o}C for three hours after which gentamicin was added to deactivate the extracellular bacteria (Figure 3.1A).

To compare xenophagy responses with other more standard forms of autophagy, the cells were treated as control with either: 1) EBSS (Earle's Balanced Salt Solution)

which represents full starvation of nutrients (amino acid and serum) to stimulate typical autophagy, or 2) the autophagy/lysosome inhibitor chloroquine. Importantly, more accumulation of LC3-II was seen when cells were infected with ATCC29213, as compared to starvation (typical form of autophagy) (Figure 3.1A). Incubation of HeLa cells with 25 µM of chloroquine to block the autophagy/lysosomal pathway led to similar levels of accumulated LC3-II. This drug is a routine positive control to help identify elevated levels of LC3-II (Gallagher et al., 2017). During a typical starvation response, LC3 is activated to form LC3-II, which is then quickly degraded via the lysosome illustrating autophagic flux. The high levels of LC3-II observed following *Staphylococcus aureus* infection could therefore show very high levels of LC3 activation, or alternatively inhibited degradation leading to strong LC3-II accumulation.

Surprisingly, *Salmonella* infection did not produce similar levels of LC3-II. To further explore, we repeated the comparison but used a reported xenophagy protocol using *Salmonella enterica* sv. Typhimurium from Birmingham et al. (2006). In this *Salmonella* protocol, cells are infected with bacteria (1:100 dilution of OD= 1.2 - 1.5 culture) for 20 minutes and then changed into fresh P/S-free media for 30 minutes. After these steps, cells are further changed into P/S-free media contain gentamicin (0.05 mg/ml) and incubated for 10 minutes to stop the infection process (Figure 3.1B). Results showed that infection with *Salmonella enterica* sv. Typhimurium using this reported *Salmonella*-specific protocol also did not lead to LC3-II accumulation. Interestingly, infection with *Staphylococcus aureus* using this second protocol did not lead to LC3-II accumulation, maybe because one hour was insufficient time to stimulate strong autophagy. Previous work has found *Staphylococcus aureus* sequestered within double membrane autophagosome only after three hours post infection (Schnaith et al., 2007). Overall, xenophagy responses following *Staphylococcus aureus* and *Salmonella enterica* sv. Typhimurium infection were dramatically different.

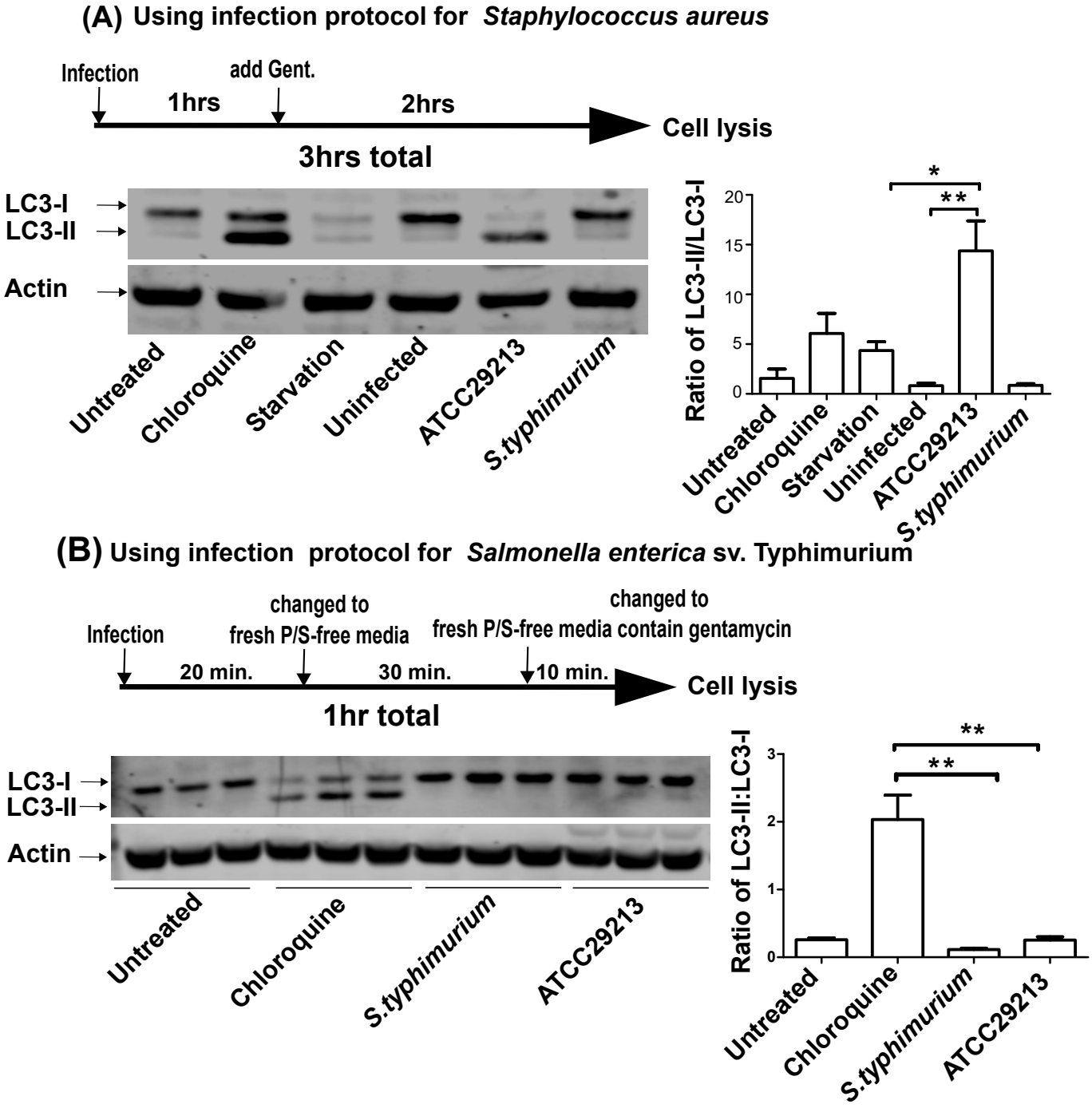

Figure 3.1: Activation of autophagy in HeLa cells following invasion of *Staphylococcus aureus* and *Salmonella enterica* sv. Typhimurium. HeLa cells were seeded and infected with *Staphylococcus aureus* (ATCC29213) or *Salmonella enterica* sv. Typhimurium (NCTC13347) with diffrent protocols.

(A) In the "*Staphylococcus* protocol", bacteria were grown until OD=0.3 and infected cells at MOI 200 and then incubated at 37^{O}C for 3 hours with gentamicin (0.05 mg/ml) which was added after 1hr in order to stop the bacterial infection as shown in top diagram.

(B) In the "*Salmonella* protocol", bacteria were grown until OD= 1.2 - 1.5 and used to infect cells at 1:100 dilution for 20 min. and then changed to fresh P/S-free media for 30 min. Cells were then changed to fresh P/S-free media contain gentamicin (0.05 mg/ml) as shown.

As control, other wells were treated with EBSS (AA starvation, typical autophagy) or chloroquine 25 μM. For all treatments, cells were incubated at 37^{O}C for 3 hours (A) or 1 hour (B). Cell lysates were resolved by NUPAGE gel electrophoresis and the proteins were probed with anti-LC3 antibody. Activation of autophagy was detected by calculating the ratio of LC3-II / LC3-I. The average from 3 samples ± SD is shown. P value from one-way ANOVA with Tukey multiple comparison test. Each experiment was done three times on different days.

3.2.1.2. A comparison of autophagy induction between different strains of *Staphylococcus aureus*

We next wanted to examine how different strains compared in their effect on autophagy to understand how *Staphylococcus aureus* genotype (and gene products) affect the host cell. HeLa cells were infected with *Staphylococcus aureus* strains ATCC29213 (agr-WT), NCTC8325 (agr-WT), NRS144 (partial agr-deficient mutant of NCTC8325) (Schnaith et al., 2007), and D393 (Sangal et al., 2012), under comparable conditions. In addition, an epidemic strain of *Staphylococcus aureus*, MRSA-78, which is multiresistant to antibiotics (oxacillin, cefotaxime, and cefuroxime and ciprofloxacin) was also studied (Raghukumar et al., 2010). Epidemic MRSA is a major problem in hospital-acquired infections and we wondered if this increased risk was linked to a stronger host cell response.

We found that the three strains of virulent *Staphylococcus aureus* (ATCC29213, NCTC8325, and epidemic MRSA-78) were able to strongly induce LC3-II accumulation following infection of HeLa cells (Figure 3.2). However, the *Staphylococcus aureus* NRS144 strain which lacks the *agr* (accessory gene regulator) only led to partial activation. D393, a clinical isolate with a clonal complex 8 genotype, also did not induce autophagy. These results suggest that the autophagic response depends on the presence of *agr* and the CC8 strain lacks a particular factor such as *agr* which underlies the difference in effect with host cell autophagy. This was confirmed later by O'Keeffe et al. (2015). We also again found that *Salmonella enterica* sv. Typhimurium did not stimulate autophagy (LC3-II levels).

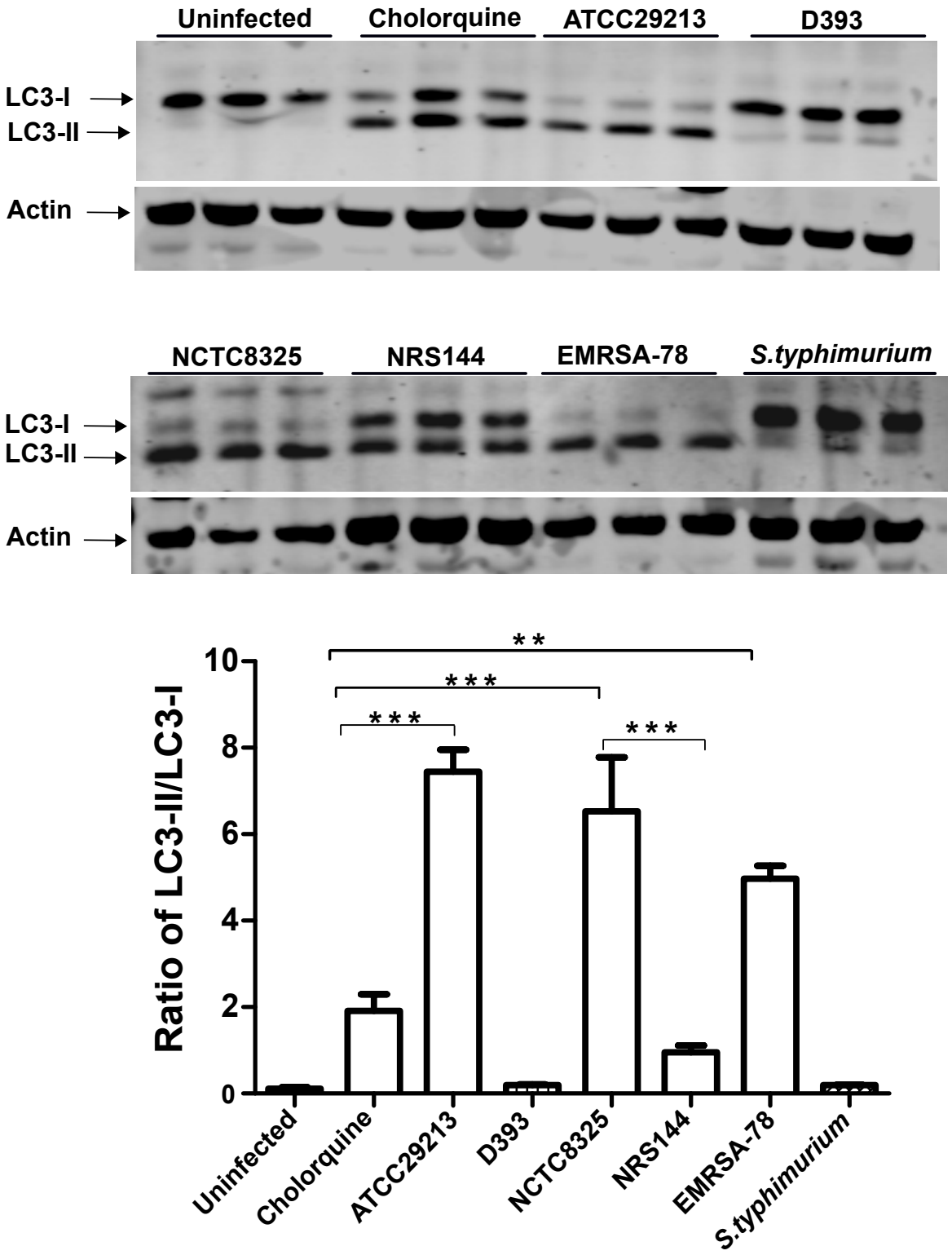

Figure 3.2: Different strains of *Staphylococcus aureus* activate autophagy in HeLa cells to different levels. Cells were infected with ATCC29213, D393 clonal complex 8, NCTC8325, NRS144 agr mutant, and EMRSA-78 and *Salmonella enterica* sv. Typhimuriumin triplicate. These cells were seeded and infected at MOI 200 and incubated at 37^{O}C with gentamicin (added after one hour of infection). As control, 25 μM of chloroquine was added to another 3 wells. After further 3 hour incubation, cells were lysed and analysed for LC3 lipidation as described in Figure 3.1. The average from 3 samples ± SD is shown. P value from one-way ANOVA with Tukey multiple comparison test. This experiment was done two times in different days.

3.2.1.3. Analysis of autophagy membrane formation in HeLa cells following invasion of *Salmonella enterica* sv. Typhimurium

As introduced earlier, many studies have reported that autophagy is involved as a defence mechanism for clearing *Salmonella enterica* sv. Typhimurium resulting in reduced bacterial survival (Birmingham et al., 2006, Wild et al., 2011, Zheng et al., 2009, Verlhac et al., 2015, Thurston et al., 2009). Our studies, described above, surprisingly did not find any accumulation of activated LC3-II (a marker of autophagy) following infection of HeLa cells by *Salmonella enterica* sv. Typhimurium using biochemical western blot. Earlier studies of *Salmonella enterica* sv. Typhimurium and autophagy have been performed exclusively with imaging of infected cells. We proposed that autophagy/xenophagy was activated in our HeLa experiments following *Salmonella enterica* sv. Typhimurium invasion, but maybe at a level below detection by blotting. Therefore, it was important to use imaging with our HeLa cell system to clarify the differences.

First, as control, it was confirmed that HeLa cells formed a basal level of LC3 positive membrane structures dispersed in the cytoplasm (uninfected cells), and that the number, size, and staining intensity all greatly increased when chloroquine was added to the cells to block the autophagy/lysosome pathway. Chloroquine led to massive accumulation of LC3-stained autophagosomal structures (Figure 3.3).

To investigate the activation of xenophagy, HeLa cells were infected with *Salmonella enterica* sv. Typhimurium using the *Salmonella* protocol and then fixed and stained with LC3 antibody. One clear result was that large-sized LC3 structures strongly formed following infection with *Salmonella*. *Salmonella enterica* sv. Typhimurium showed close contact with LC3 puncta. Many LC3-labelled membranes appeared to elongate around the bacteria and others surrounded the bacteria completely. From these observations, it was obvious that there is an active association between *Salmonella enterica* sv. Typhimurium and LC3 (Figure 3.4). These results confirmed the activation of autophagy by microscopy following infection with *Salmonella enterica* sv. Typhimurium.

In regard to *Staphylococcus aureus*, autophagy membrane formation following the invasion of these bacteria has been studied previously in our lab by a Masters level student (S. Davidson). Using stable expressing GFP-LC3/293A cells, it was observed

that more GFP-LC3 membranes had formed around invading EMRSA-15 and ATCC29213 *Staphylococcus aureus* (see supplementary Figure 7.1,2,3 for more details).

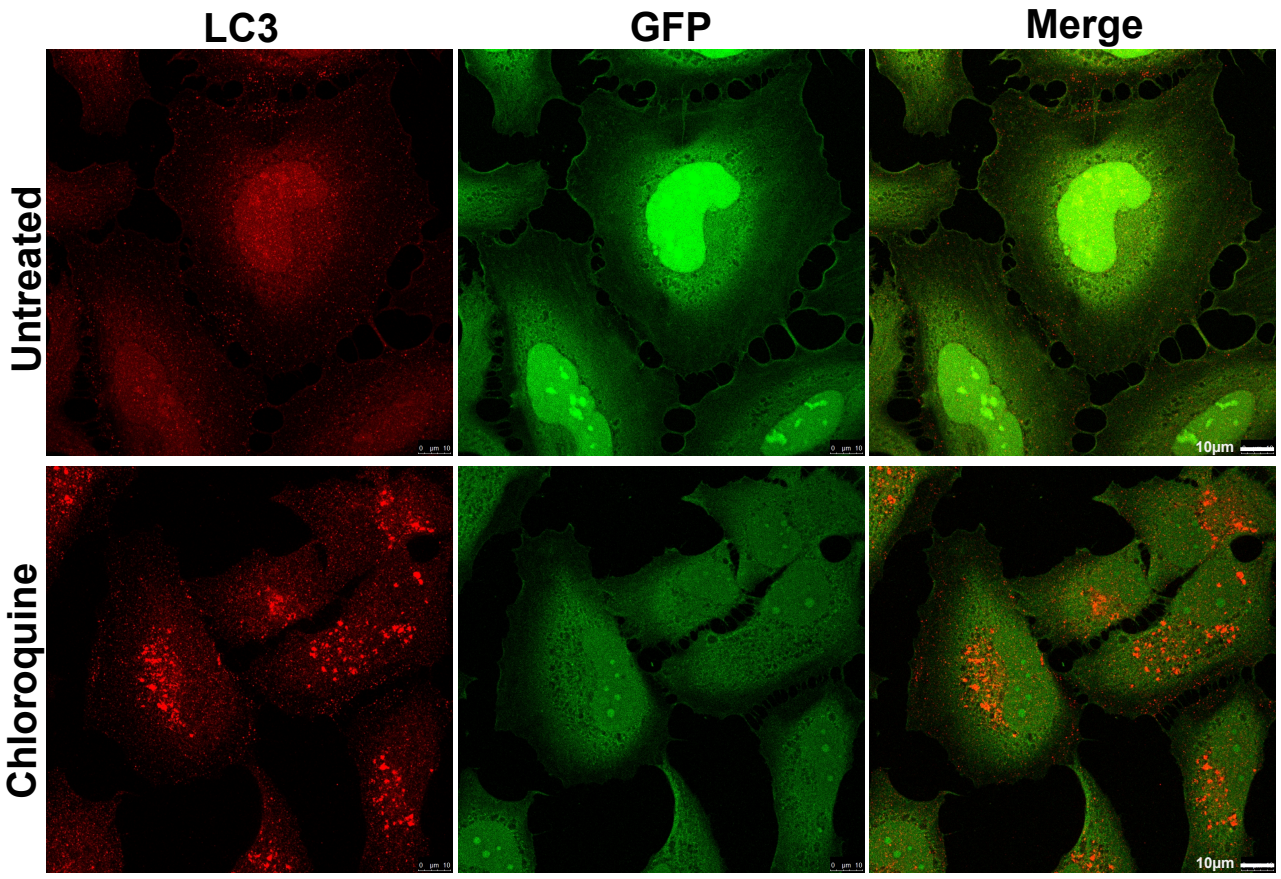

Figure 3.3: Autophagosomes labelled with LC3 in control treated HeLa cells. Cells were either left untreated or treated with chloroquine (25 µM) and incubated for 3 hours before fixation and staining with anti LC3 antibody. GFP channel (for bacteria, see Figure 3.4) also shown to indicate that cells were not infected. Cells were observed by confocal microscopy. Scale bar: 10 µm.

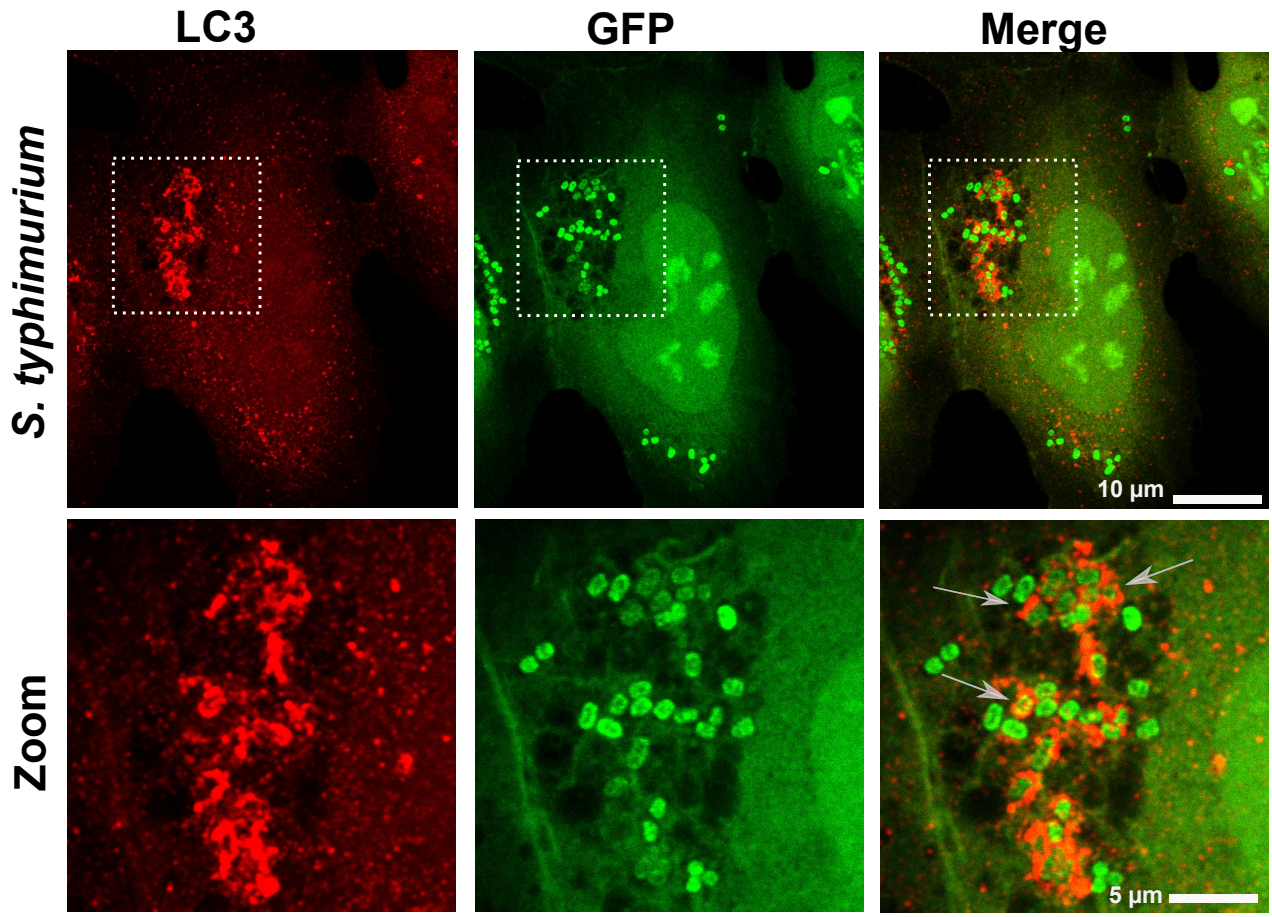

Figure 3.4: The activation of autophagy in HeLa cells following invasion of *Salmonella enterica* sv. Typhimurium. HeLa cells were plated on glass coverslips then infected with 1:100 MOI of GFP expressing *Salmonella enterica* sv. Typhimuriumand incubated at 37^{O}C for 1hr before fixation and staining with anti-LC3 antibody. Infection was via the "*Salmonella* protocol". Cells were observed by confocal microscopy. The arrow shows the co-localization of this bacteria with LC3. Scale bar: 10 and 5 µm.

3.2.1.4. Infection with *Staphylococcus aureus*, but not *Salmonella enterica* sv. Typhimurium, is associated with increased accumulation of LC3-II lapidating overtime

Staphylococcus aureus was previously shown to be enclosed by autophagosomes in non-professional and professional phagocytic cells (O'Keeffe et al., 2015, Schnaith et al., 2007). These autophagosomes provide a niche for the intracellular survival of *Staphylococcus aureus* through blocking of autophagic flux. The blocking of autophagic flux results in a build-up of autophagosomes, where *Staphylococcus aureus* can replicate and eventually escape into the cytoplasm, ultimately leading to host cell death (Mestre et al., 2010, O'Keeffe et al., 2015, Schnaith et al., 2007, Liu et al., 2015, Lopez de Armentia et al., 2017).

To test if the clinical isolates of *Staphylococcus aureus* in our studies also manipulated the autophagic process, we studied the accumulation of LC3-II over time following infection. HeLa cells were infected with ATCC29213 at MOI 100 and then incubated at 37^{o}C for one to six hours. In one case, infections were allowed to fully continue without gentamicin. For comparison, gentamicin was added after one hour of interaction between *Staphylococcus aureus* and host HeLa cells.

Accumulation of LC3-II appeared in HeLa cells following ATCC29213 infection after two hours (without any added gentamicin) (Figure 3.5, top). Levels of LC3-II increased further with longer incubation, for example by three hours. On the other hand, when *Staphylococcus aureus*/HeLa cell interactions were allowed to take place for just one hour before addition of gentamicin (bottom), activated LC3-II was only mildly detected at the three-hour time point (two hours post gentamicin). LC3 accumulation only became very strong after the six-hour time point. These results suggest that a portion of bacterial/host cell interaction (leading to autophagy) took place within one hour of incubation. Further incubation of these infected cells led to higher levels of autophagy which gradually built up; for example, up to six hours after initial infection. When no gentamicin was added to the experiment, levels of autophagy were generally higher, possibly due to a combination of continued bacterial replication outside of cells and continued invasion. These results indicate that levels of autophagy can increase depending on levels and duration of infection.

To study the accumulation of activated LC3 over time following infection by *Salmonella enterica* sv. Typhimurium, we used imaging, since this was the clearest way to detect this xenophagy response. HeLa cells were infected following the *Salmonella* protocol and then fixed after different times of bacterial interaction (20 minutes, 1–5 hrs) and stained with LC3 antibody. As a control, untreated HeLa cells were included to confirm that HeLa cells had a basal level of LC3 positive membrane structures present dispersed in the cytoplasm. Cells were also treated with chloroquine to confirm that the number, size, and staining intensity of LC3 all greatly increased when chloroquine was added to the cells to block the autophagy/lysosome pathway.

We found that the percentage of cells with LC3 puncta was increased in one hour and after one hour this percentage was reduced and absent in four hours, suggesting that these cells had normal autophagic flux (Figure 3.6). Taken together, these results indicated inhabited autophagy flux following infection by *Staphylococcus aureus* leading to accumulation of LC3. Compared with *Salmonella enterica* sv. Typhimurium infection, normal autophagy flux leads to prevention of the accumulation of LC3.

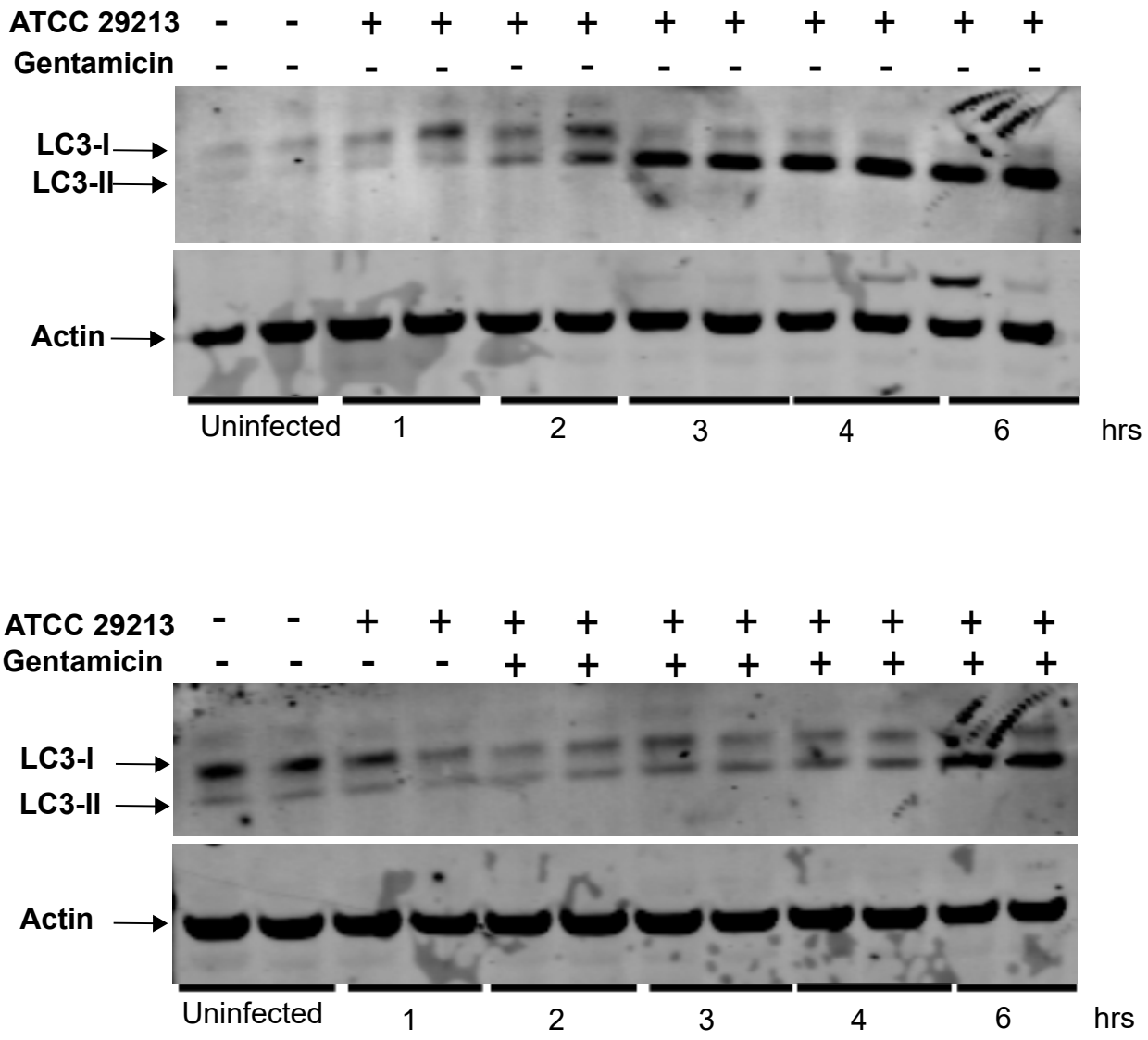

Figure 3.5: The accumulation of LC3-II over time following infection by *Staphylococcus aureus*. HeLa cells were seeded in 12 well plates and infected with ATCC29213 at MOI 100. The plates were incubated at 37^{O}C for up to 6hrs with or without adding gentamicin (0.05 mg/ml). Gentamicin was added 1hr after infection. Cells were then lysed and analysed for LC3 lipidation as described in Figure 3.1. Each experiment was done two times.

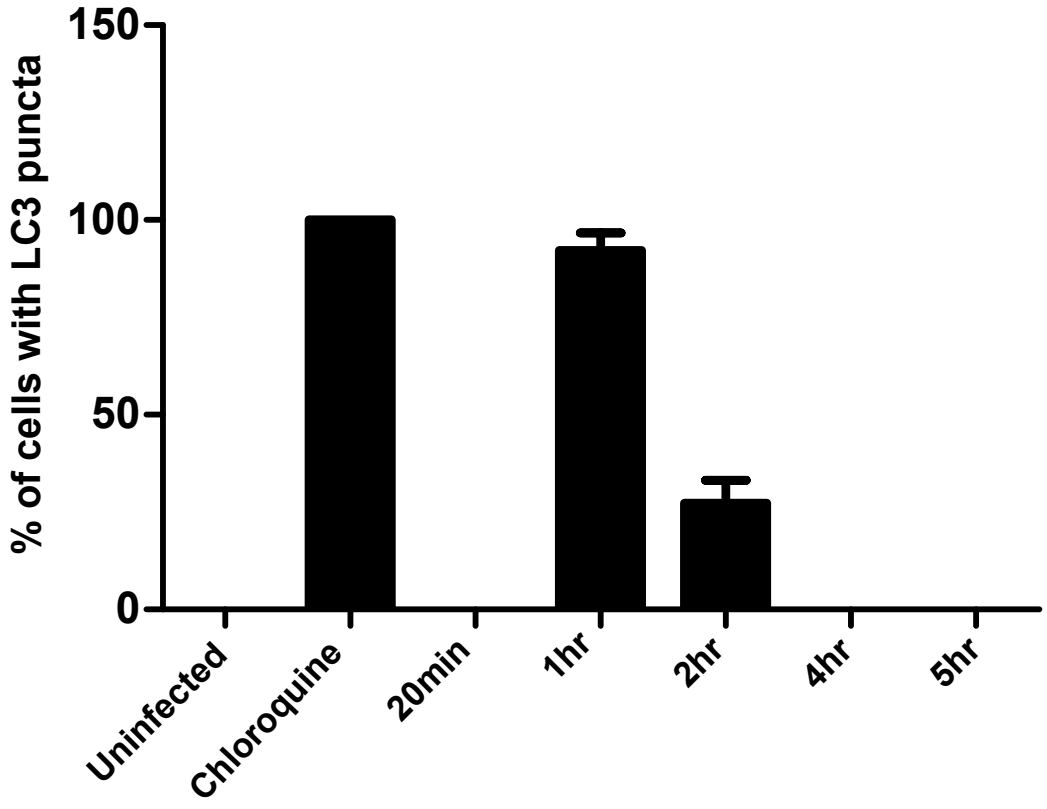

Figure 3.6: The reduction of LC3 puncta over time following infection with *Salmonella enterica* sv. Typhimurium. HeLa cells were plated on glass coverslips then infected with 1:100 MOI of GFP expressing *Salmonella enterica* sv. Typhimurium and incubated at 37^{O}C for 20 min., 1, 2, 3, or 5hrs before fixation and staining with anti-LC3 antibody. The number of infected cells which had LC3 puncta was counted using epifluorescence microscopy and then the cells' percentage was calculated as the number of infected cells having LC3 puncta divided by the total number of infected cells in the same field multiplied by 100. The average from 3 samples ± SD is shown. This experiment was done three times.

3.2.2. Investigating the role of p62/sequestosome1 as an adaptor molecule in targeting *Staphylococcus aureus* as compared with *Salmonella enterica* sv. Typhimurium to autophagosomes

Our above results with LC3 suggested that the xenophagy membrane trafficking response occurred at different rates following infection by *Staphylococcus* as compared with *Salmonella*. We investigated this difference using another autophagy marker. The consensus in the literature is that autophagy adaptor molecules are important in targeting invading bacteria. These adaptor proteins are able to bind to both ubiquitinated targets and LC3-II, consequently creating a bridge between cargos and forming autophagosomal membranes (Zheng et al., 2009). p62 is the earliest described adaptor protein implicated in the delivery of ubiquitinated *Salmonella enterica* sv. Typhimurium to the lysosome. p62 interacts with light chain 3 (LC3) and is recruited to ubiquitinated cytosolic bacteria via its UBA domain (Pankiv et al., 2007).

The role of ubiquitin is not well understood, particularly during *Staphylococcus aureus* infection. Therefore, we wanted to investigate whether p62 is recruited to *Staphylococcus aureus* as compared with *Salmonella enterica* sv. Typhimurium after invasion of host cells. Adaptor molecules showing co-localisation with *Staphylococcus aureus* or *Salmonella enterica* sv. Typhimurium would indicate ubiquitination of bacterial coat proteins.

First, as a control, it was confirmed that HeLa cells have a basal level of p62 positive structures present dispersed in the cytoplasm (uninfected cells) and that the number, size and staining intensity all greatly increased when chloroquine was added to the cells to block the autophagy/lysosome pathway. Chloroquine led to massive accumulation of ubiquitinated proteins and autophagosomal structures (Figure 3.7).

To investigate activation of the p62 pathway during xenophagy responses, HeLa cells were infected with three different types of *Staphylococcus aureus* (strains NCTC8325, D393 or NRS144). Alternatively, cells were infected with *Salmonella enterica* sv. Typhimurium for one hour using its specific infection method. One clear result was that large-sized p62 structures strongly formed following infection with NCTC8325 wt *Staphylococcus aureus*. However, while increases in p62 were obvious, we could not detect the expected clear co-localisation between p62 and invading bacteria in the cytoplasm (Figure 3.8). These results suggest that p62 may have been acting as an adaptor molecule for polyubiquitinated *Staphylococcus aureus* that we did not detect

with the Hoechst DNA stain. By contrast, only normal p62 structures formed following infection with D393 or NRS144, possibly because these strains lacked key virulence factors and did not activate the autophagy process (as shown in our other western blot experiments).

Thus, to further explore the role of p62 with NCTC8325 wt *Staphylococcus aureus*, we used stably expressing GFP-p62 Hela cells to allow detection of *Staphylococcus aureus* with anti-protein A antibody. Using this approach, we found again that large-sized p62 structures strongly formed following infection with NCTC8325 wt *Staphylococcus aureus*. However, the bacteria did not co-localise with p62 (Figure 3.9).

On the other hand, HeLa cells infected with *Salmonella enterica* sv. Typhimurium led to large-sized p62 structures in close contact with *Salmonella enterica* sv. Typhimurium, and some of the p62 structures elongated laterally, along with the bacteria, and other completely surrounded the bacteria. However, p62 structures formed following infection with NCTC8325 did not directly co-localise with MRSA. They could often be seen just next to the individual *Staphylococcus aureus*. This suggests clear ubiquitination of *Salmonella enterica* sv. Typhimurium coat proteins (Figure 3.10).

Collectively, these results confirm the role of p62/sequestosome1 as an adaptor molecule in targeting *Salmonella enterica* sv. Typhimurium that have invaded the cell cytoplasm. Large structures of p62 without co-localisation with MRSA (NCTC8325) may be because the p62 was targeting other proteins (or organelles) that became damaged during the bacterial infection.

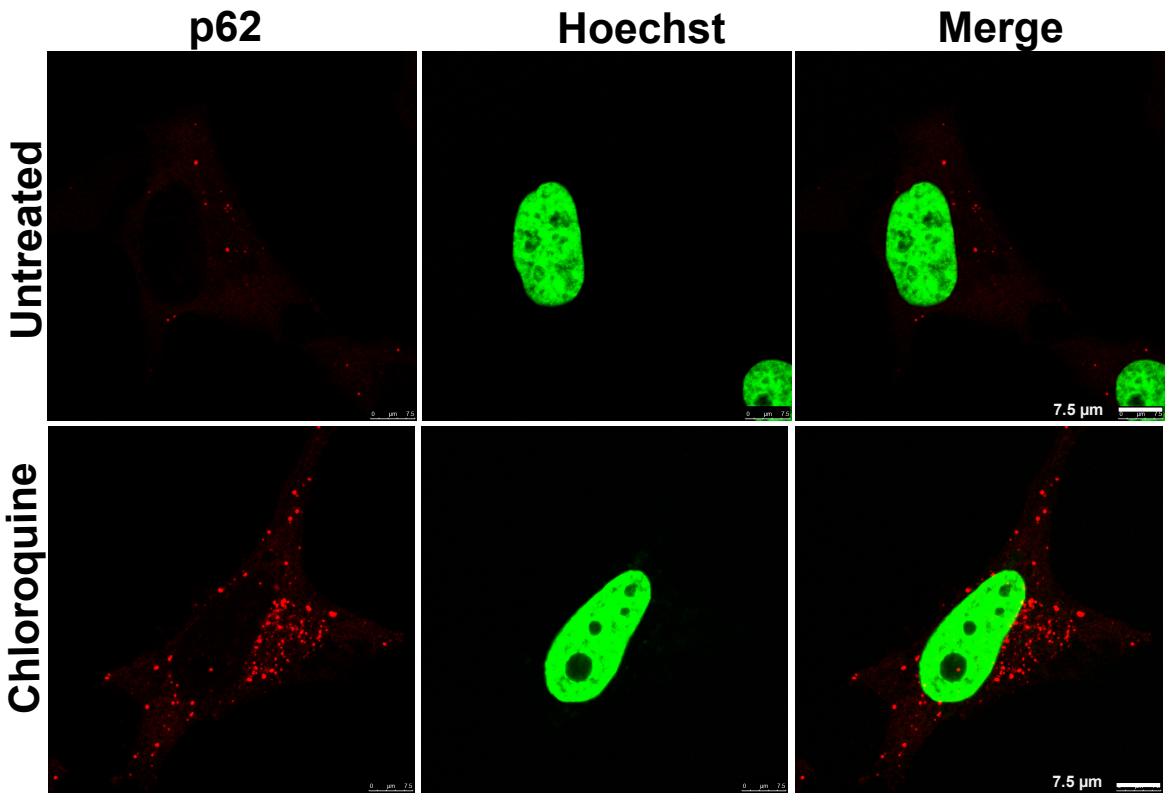

Figure 3.7: Autophagosomes labelled with p62/SQSTM1 in control treated HeLa cells. HeLa cells were plated on glass coverslips. For these control experiments, cells were either left untreated or treated with chloroquine (25 µM) and incubated for 3hrs before fixation and staining with anti-p62/SQSTM1 antibody. Cells were observed by confocal microscopy. Scale bar: 7.5 µm.

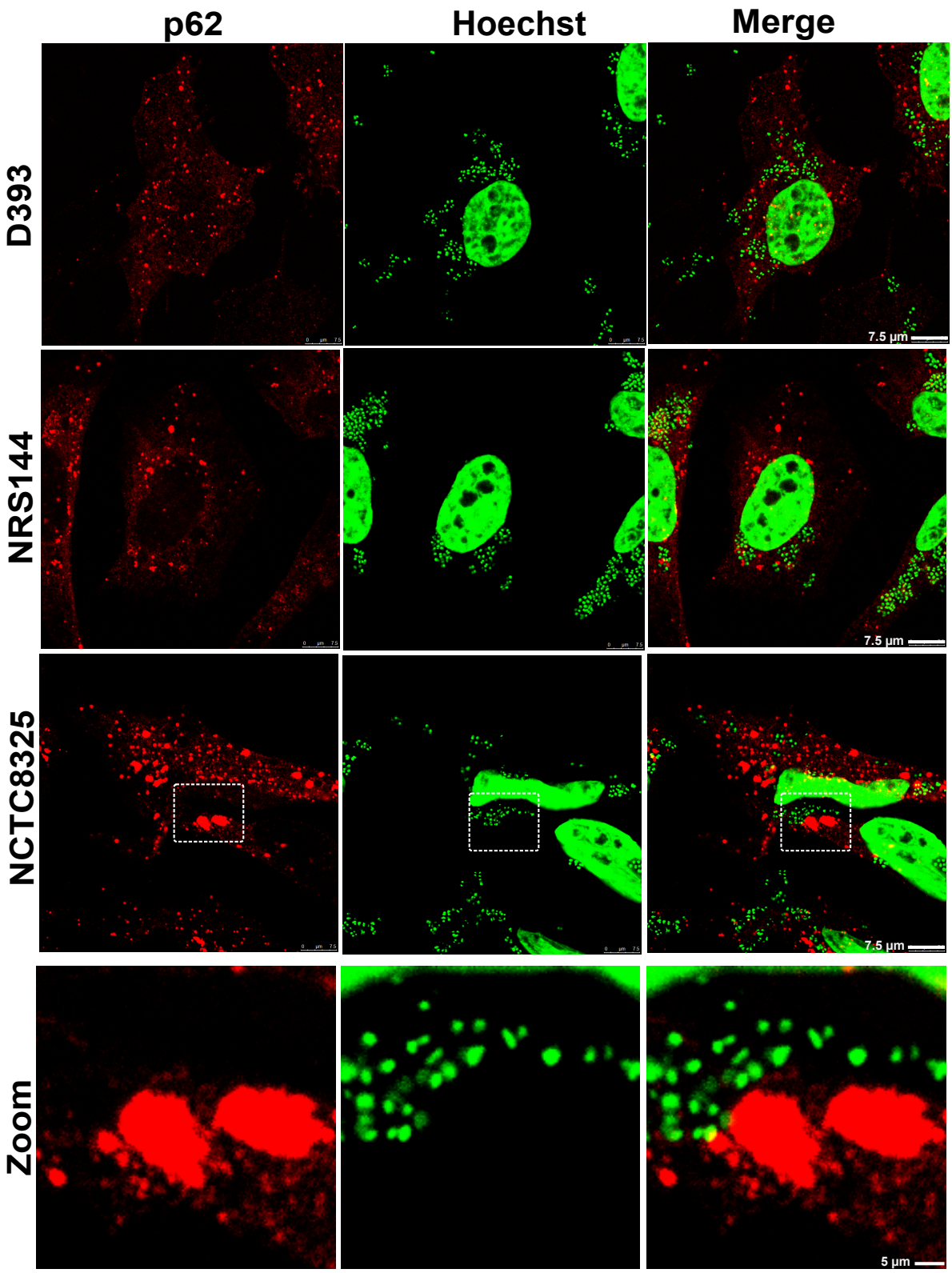

Figure 3.8: Large sized p62 structures formed following infection with wt. *Staphylococcus aureus*. HeLa cells were plated on glass coverslips and then infected with 100 MOI of D393 clonal complex 8, NRS144 agr mutant, NCTC8325 and incubated at 37^{O}C for 3hrs with gentamicin (0.05 mg/ml) (added after 1hr) before fixation and staining with anti-p62/SQSTM1 antibody. Cells were observed by confocal microscopy. Scale bar: 7.5 µm.

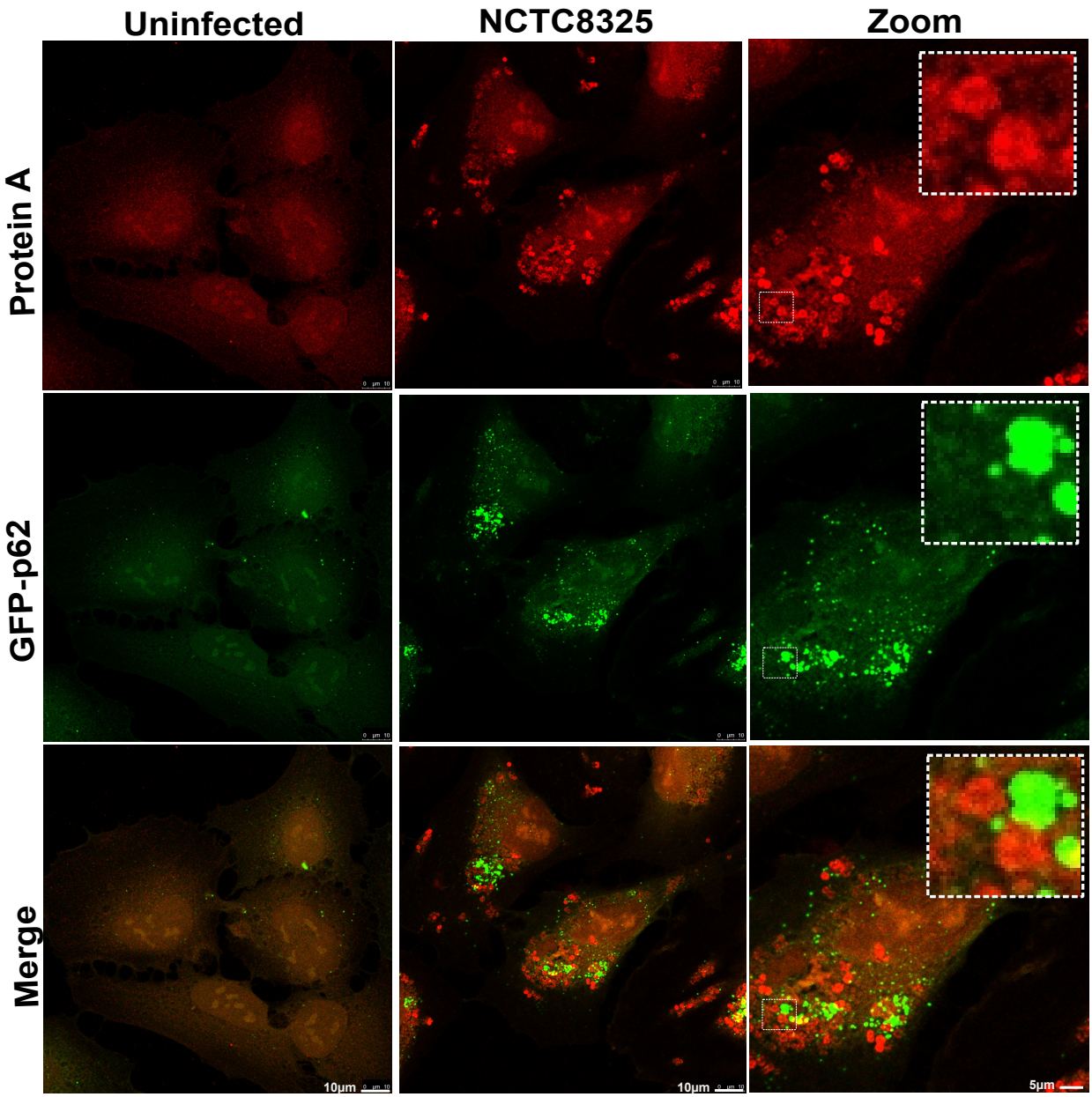

Figure 3.9: Large sized GFP-p62 structures formed following infection with MRSA. GFP-p62/HeLa cells were plated on glass coverslips then infected with 100 MOI NCTC8325 and incubated at 37^{O}C for 3hrs with gentamicin (0.05 mg/ml) (added after 1hr) before fixation and staining with anti-protein A antibody. Cells were observed by confocal microscopy. Scale bar: 10 µm.

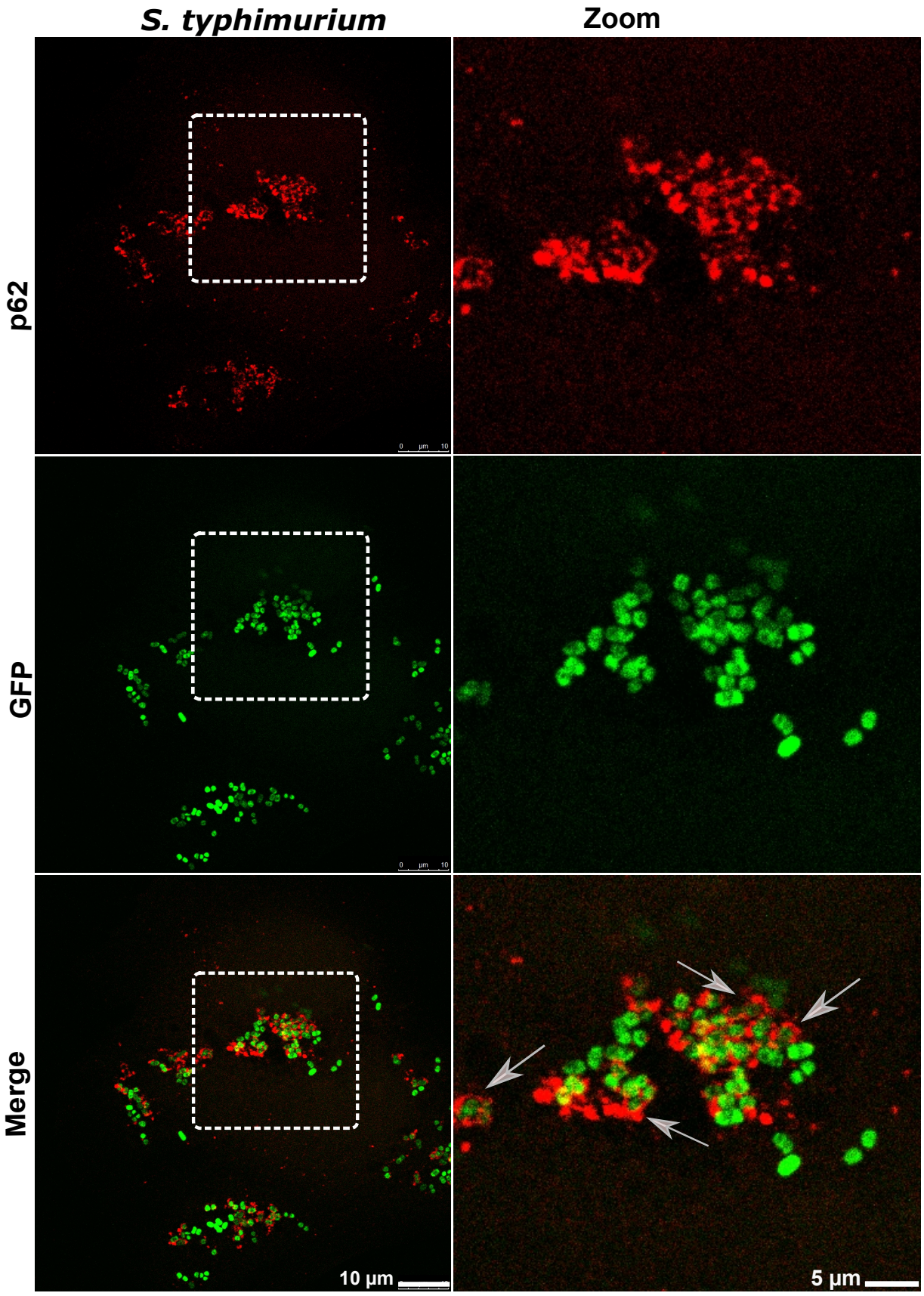

Figure 3.10: Large sized p62 structures formed following infection with *Salmonella enterica* sv. Typhimurium with clear co-localization . HeLa cells were plated on glass coverslips then infected with 1:100 with GFP *Salmonella enterica* sv. Typhimurium and incubated at 37 ^{o}C for 1hr before fixation and staining with anti-p62/SQSTM1 antibody. Infection was via the "*Salmonella* protocol". Cells were observed by confocal microscopy. The arrow shows the co-localization of this bacteria with p62. Scale bar: 10 µm.

In xenophagy, intracellular bacteria are commonly targeted to autophagosomes by ubiquitin-binding adaptor proteins such as p62/Sequestosome1. Furthermore, because p62 is an adaptor protein, its levels accumulate when autophagy degradation is inhibited. On the other hand, p62 levels decrease when autophagy is induced. Therefore, we used p62 as a marker to study levels of autophagic degradative flux following infection with *Salmonella enterica* sv. Typhimurium by imaging.

HeLa cells were infected following the *Salmonella* protocol and then fixed after different times of bacterial interaction (20min., 1-5 hrs) and stained with p62 antibody. As a control, untreated HeLa cells showed low basal levels of p62 positive membrane structures dispersed in the cytoplasm.

We found that the percentage of cells with p62 puncta increased by one hour and this percentage then reduced over time, suggesting that these cells had normal autophagic flux (Figure 3.11). These data suggest that *Salmonella enterica* sv. Typhimurium does not interfere with the homeostatic turnover of the autophagic machinery.

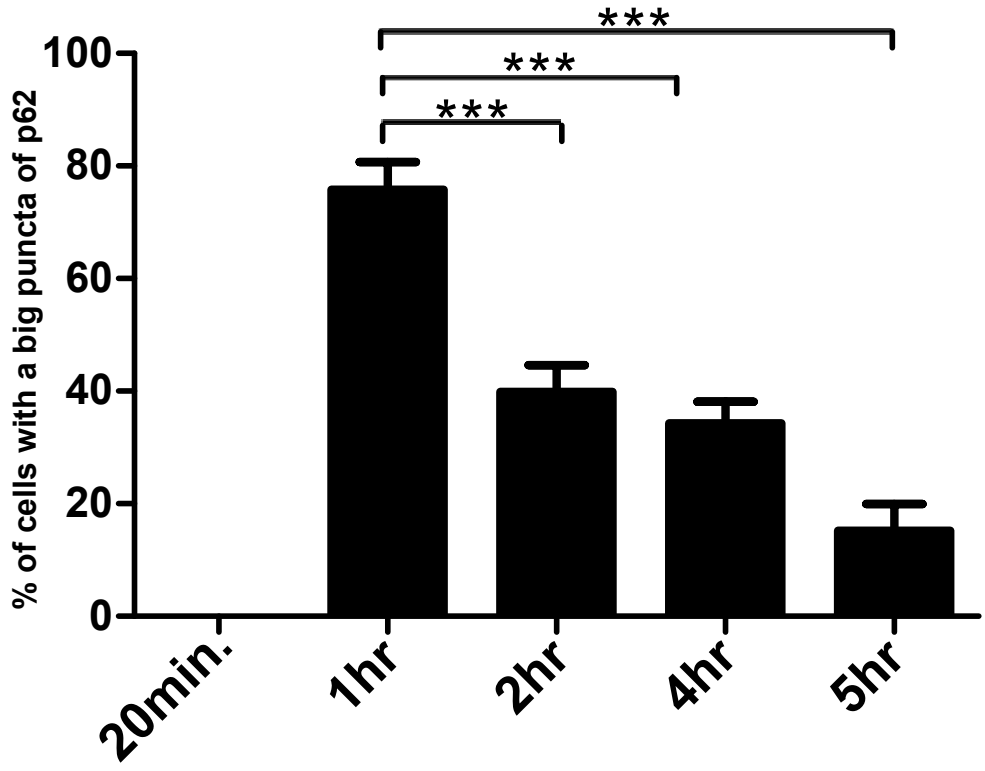

Figure 3.11: The reduction of p62 puncta following infection with *Salmonella enterica* sv. Typhimurium. HeLa cells were plated on glass coverslips then infected with 1:100 MOI of GFP expressing *Salmonella enterica* sv. Typhimurium and incubated at 37^{O}C for 20 min., 1, 2, 3, or 5 hrs with gentamicin (added after 50 min.) before fixation and staining with anti-p62 antibody. The number of infected cells which had p62 puncta was counted using epifluorescence microscopy and then the cells' percentage was calculated as the number of infected cells having p62 puncta divided by the total number of infected cells in the same field multiplied by 100. This experiment was done three times. P value from one-way ANOVA with Tukey multiple comparison test (***P<0.001).

3.2.3. The role of lysosome following infection by *Staphylococcus aureus* or *Salmonella enterica* sv. Typhimurium

As summarised in the introduction, *Staphylococcus aureus* has been proposed to display a complex xenophagy trafficking route. 1) After internalisation in phagosomes, there is pathogen-mediated inhibition of phagosome/ lysosomes fusion. 2) Following this, phagosomes become permeabilised via a mechanism dependent on *Staphylococcus*-secreted toxins. 3) Autophagosomes are recruited to leaky phagosomes (Mestre et al., 2010). 4) Escaping *Staphylococcus aureus*, once captured by autophagosomes, further inhibit fusion of autophagosomes with lysosomes, thereby evading destruction from a fully degradative lysosomal environment. 5) *Staphylococcus aureus* then reside in this specialised niche to further replicate (Schnaith et al., 2007, O'Keeffe et al., 2015).

Since the xenophagy pathways in response to *Staphylococcus aureus* and *Salmonella enterica* sv. Typhimurium infection were different (based on LC3 and p62 markers), we next aimed to clarify how these pathogens interacted with lysosomes using the LAMP-2 marker of late endosome/lysosome and confocal imaging. First, as a control, we confirmed that HeLa cells have basal, relatively small-sized, lysosome structures dispersed in the cytoplasm in uninfected/untreated cells (Figure 3.12). Secondly, the lysosome number, size and LAMP-2 staining intensity all greatly increased when chloroquine was added to the cells to block the autophagy/lysosome pathway.

To examine levels of *Staphylococcus aureus* within lysosomes, we analysed co-localisation of four different *Staphylococcus aureus* strains. HeLa cells were infected with 100 MOI of ATCC29213, NCTC8325, NRS144, or D393 for three hours, fixed and then stained with anti-LAMP-2 antibody. Figure 3.13 shows typical example observations of large swollen lysosomes following infection of HeLa cells with wt. (ATCC29213 or NCTC8325) *Staphylococcus aureus*. Infection with wt *Staphylococcus aureus* led to high numbers of bacteria clustered in the cytoplasm. Only a small fraction of bacteria were surrounded by LAMP-2 membranes.

In contrast, the *agr*-deficient NRS144 strain showed a distinct pattern. These mutant bacteria could be observed in higher levels enclosed in LAMP-2 positive lysosomes. There were also fewer NRS144 bacteria escaping and replicating in the cytoplasm.

The clonal complex 8 genotype (D393) *Staphylococcus aureus* showed an intermediate result, with mildly lower levels of escape from lysosomes and lower free cytosolic bacteria. These results suggest that *Staphylococcus aureus* infection leads to entry and enlargement of lysosomal compartments, even with strains lacking virulence factors or *agr*. Fully virulent *Staphylococcus aureus* have the further ability to avoid lysosome compartments, for example, by preventing fusion with lysosomes or by escaping from lysosomes.

Since levels of lysosome enclosure of *Staphylococcus aureus* appeared to be a critical factor in relationship with virulence, we examined this property closer with higher magnification confocal scanning (Figure 3.14). This analysis further showed that only a small fraction of wildtype *Staphylococcus aureus* were surrounded by enlarged lysosomal membranes three hours post infection. Overall, most of the wildtype NCTC8325 *Staphylococcus aureus* were dispersed in the cytoplasm, but not within any LAMP-2 positive membranes. In contrast, *agr*-deficient *Staphylococcus aureus* were generally well enclosed by lysosomal membranes. This evidence further suggested that *agr*-dependent factors may be inhibiting phagosome-lysosome fusion and/or promoting bacterial escape from lysosomes.

After establishing that wildtype *Staphylococcus aureus* is able to evade lysosomes, we aimed to determine if *Salmonella enterica* sv. Typhimurium similarly is able to escape capture by lysosomes. We infected HeLa cells with the *Salmonella* protocol and observed the interaction with lysosomes over five hours (Figure 3.15). We found that wildtype *Salmonella enterica* sv. Typhimurium were mostly within enlarged (swollen) LAMP-2 positive membranes following infection of HeLa cells; for example, in images from the five-hour time point. By counting the percentage of cells with swollen LAMP-2 positive lysosomes, we found that immediately after infection (20 minutes, 1-hour post infection), there were relatively few swollen *Salmonella*-containing LAMP-2 membranes. However, very clearly, by two hours post infection, there was a drastic increase.

As compared with *Staphylococcus aureus* infection, which produces most bacteria outside of LAMP-2 membranes, *Salmonella* were mostly all within LAMP membranes. This result further highlights how the trafficking of these two pathogens to lysosomes is different. In order to survive and replicate in the phagosome, *Staphylococcus*

aureus exploits the advantage of their virulence factors to block the transport process to avert lysosomal degradation. However, *Salmonella enterica* sv. Typhimurium are transported to lysosomal membranes within two hours post infection, leading to overall degradation of the bacteria. Our results here therefore agree with other work which identified the role of autophagy to clear *Salmonella enterica* sv. Typhimurium and fight this infection (Zheng et al., 2009, Birmingham et al., 2006, Thurston et al., 2009, Wild et al., 2011).

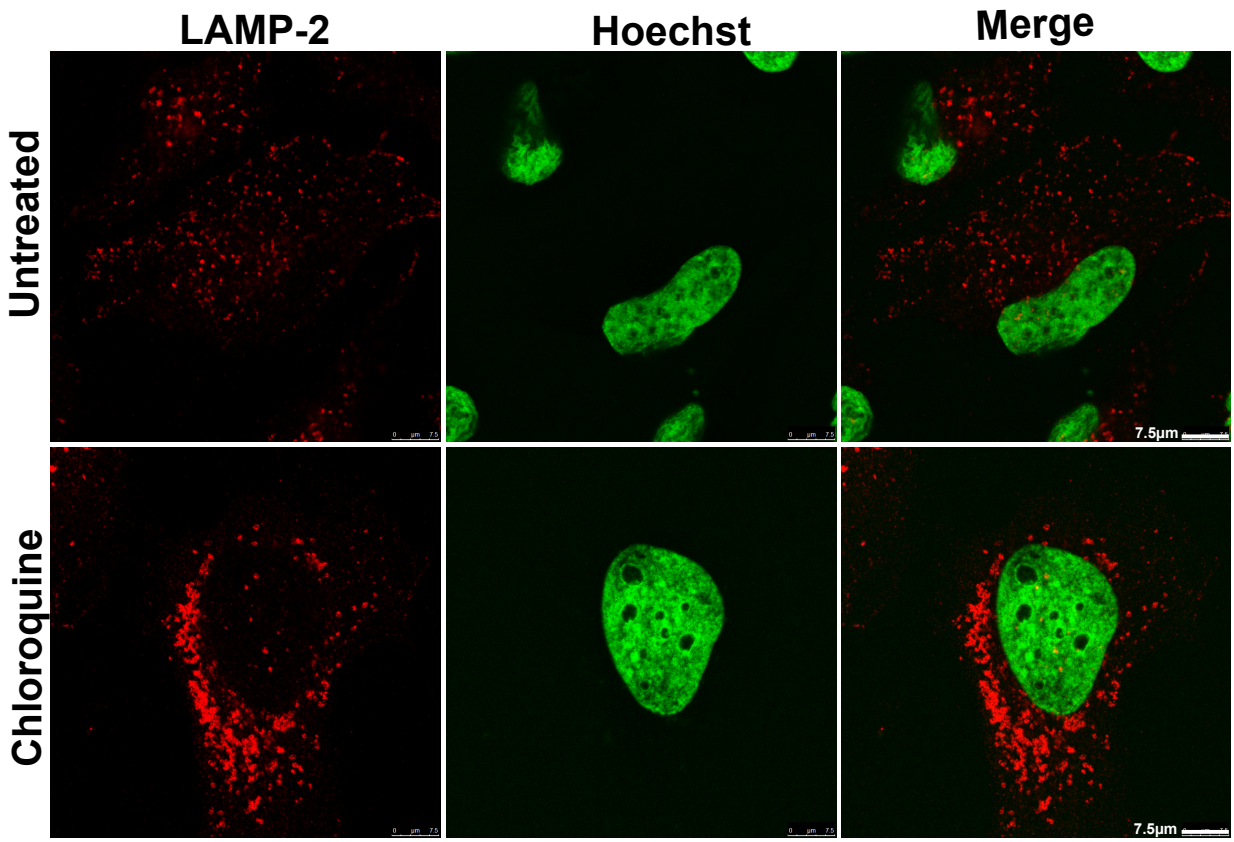

Figure 3.12: Accumulation of swollen lysosomes in HeLa cells following treatment with chloroquine. HeLa cells were plated on glass coverslips. For these control experiments, cells were either left untreated or treated with chloroquine (25 µM) and incubated for 3 hours before fixation and staining with anti-LAMP-2 antibody to detect lysosomes. Cells were observed by confocal microscopy. Scale bar: 7.5 µm.

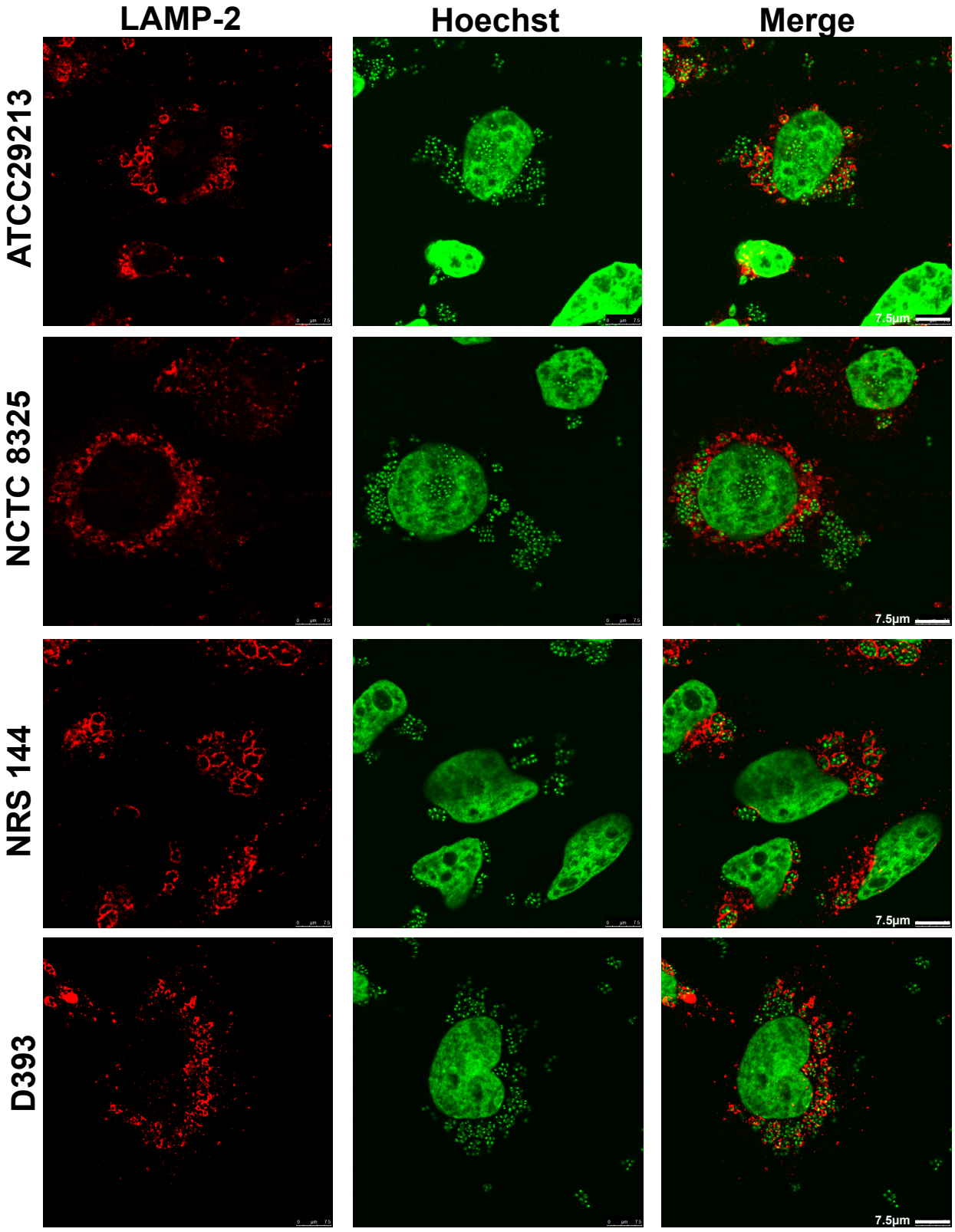

Figure 3.13: Swelling of lysosomes following infection of HeLa cells with agr wt., agr deficient and a clonal complex 8 genotype *Staphylococcus aureus*. HeLa cells were plated on glass coverslips then infected with 100 MOI of ATCC29213, NCTC8325, NRS144, or D393 and incubated at 37^{O}C for 3hrs with gentamicin (0.05 mg/ml) (added after 1hr) before fixation and staining with anti-LAMP-2 antibody. Cells were observed by confocal microscopy. Scale bar: 7.5 µm.

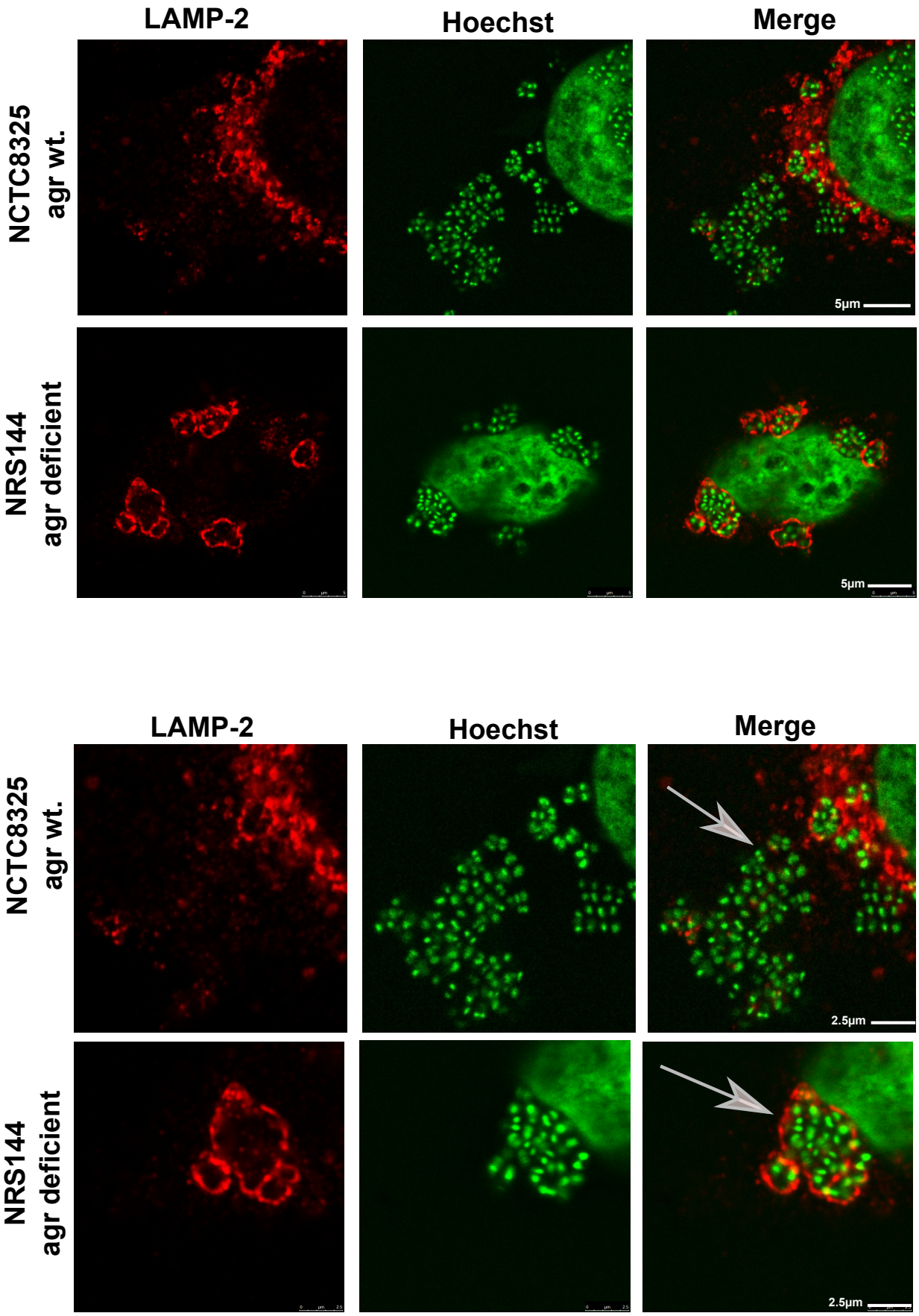

Figure 3.14: Agr wt. but not agr deficient *Staphylococcus aureus* avoid lysosomes following infection of HeLa cells. HeLa cells were plated on glass coverslips then infected with 100 MOI of NRS144, or NCTC8325 and incubated at 37^{O}C for 3hrs with gentamicin (0.05 mg/ml) (added after 1hr) before fixation and staining with anti-LAMP-2 antibody. Cells were observed by confocal microscopy. Scale bar: 2.5 and 5 µm.

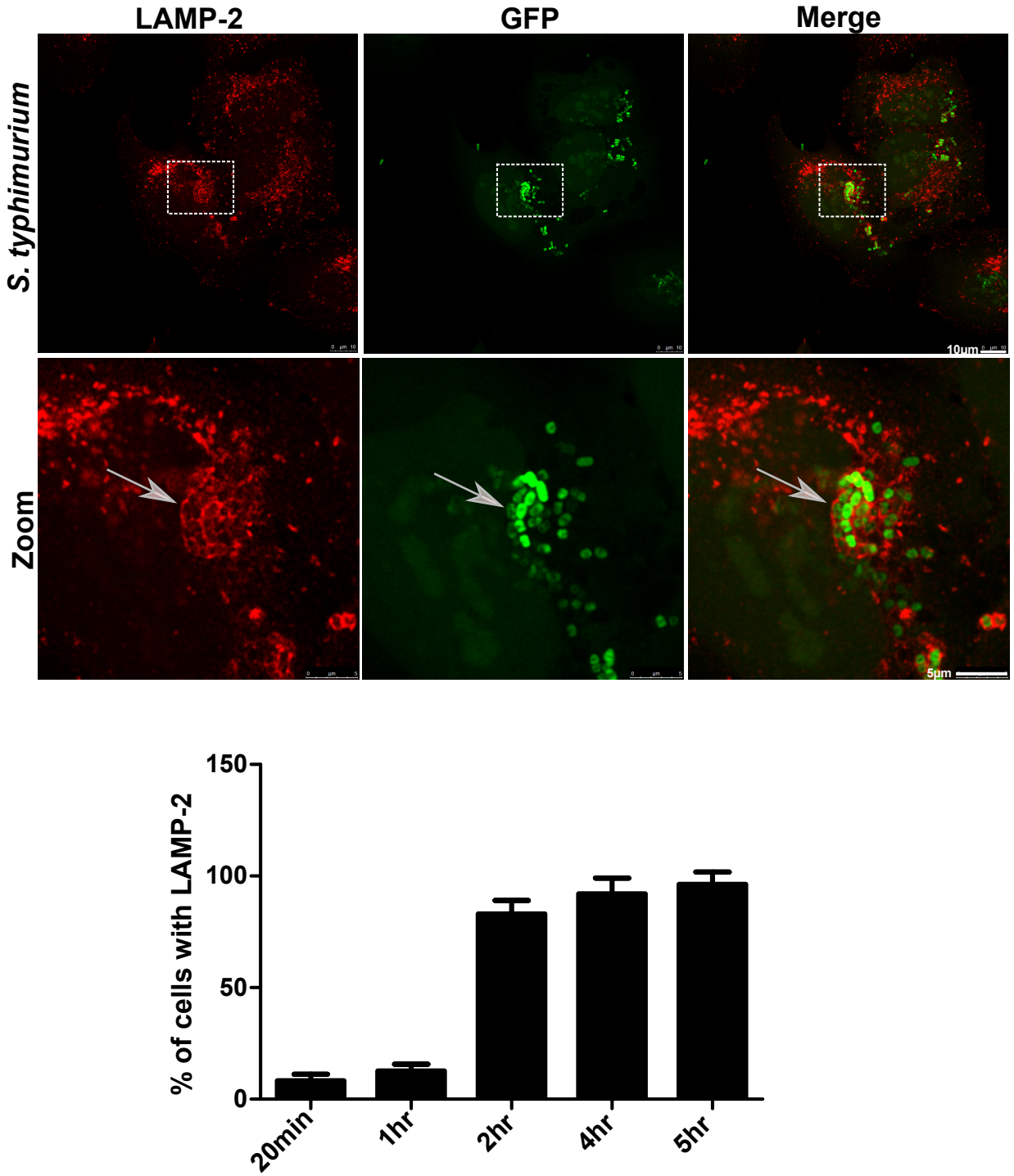

Figure 3.15: ***Salmonella enterica* sv. Typhimurium captured by lysosomes following infection of HeLa cells.** HeLa cells on glass coverslips were infected with 1:100 MOI of GFP expressing *Salmonella enterica* sv. Typhimurium and then incubated at 37 ^{O}C for different times (20min., 1-5hrs) before fixation and staining with anti-LAMP-2 antibody.
Top: Images captured by confocal microscopy from 5hrs postinfection. Scale bar: 10 µm and 5 µm.
Bottom: The numbers of infected cells which have swelling LAMP-2 counted using epifluorescence microscopy and then the cells percentage was calculated as a number of infected cells have LAMP-2 spots divided by the total number of infected cells in the same field multiple by 100.

3.2.4. Measurement of the damage to the endomembrane in host cells following infection by *Staphylococcus aureus* and *Salmonella enterica* sv. Typhimurium

The results above demonstrate that *Staphylococcus aureus* and *Salmonella enterica* sv. Typhimurium traffic differently through the lysosomal system. In the recent years, Galectin-3 has been established as a marker of endomembranes that are damaged (Paz et al., 2010). Galectin-3 belongs to the family of lectin proteins that show affinity for beta-galactosides. Endogenous cellular galectin-3 (Gal3) is often distributed throughout the nucleus and the cytoplasm. On the other hand, beta-galactosides are found on membranes of the Golgi apparatus, surface of cells, post-Golgi secretory and lumen of endocytic compartments (Houzelstein et al., 2004). As a result, normally galectins do not interact with the beta-galactosides. However, rupturing of the endosomal membranes allows Gal3 to interact with luminal glycoproteins (Paz et al., 2010). Galectin members have also been shown to come into contact with beta-galactosides upon lysosomal membrane permeabilisation (LMP) (Aits et al., 2015). Therefore, this evidence helps establish Gal3 as a useful marker for lysosome and vacuole damage.

Accordingly, we wished to investigate lysosomal membrane damage following infection by *Staphylococcus aureus* or *Salmonella enterica* sv. Typhimurium by studying puncta formation of Gal3. In order to test a control for damaged lysosome membranes, L-Leucyl-L-leucine methyl ester (LLOMe) was used. LLOMe builds up in the lysosomes after which it is converted by dipeptidyl peptidase I into its membrane-lytic structure (Leu-Leu) n-OMe. Dipeptidyl peptidase I (DPPI) is a lysosomal thiol protease that facilitates the conversion process (Thiele and Lipsky, 1990, Uchimoto et al., 1999).

HeLa cells were transfected with GFP-Gal3 treated as control with LLOME (2mM) (Figure 3.16). Untreated cells showed a low level of GFP signal. Within three hours of incubation, there was a strong increase in GFP positive membrane structures, labelling the damaged lysosomes.

After establishing the Gal3 assay, we tested infection with *Salmonella enterica* sv. Typhimurium, since these bacteria strongly co-localised with lysosomes within 2–5 hours post infection. Interestingly, extensive puncta of GFP-Galectin3 were found with almost all the cells infected by *Salmonella enterica* sv. Typhimurium for three hours

(Figure 3.17). Most *Salmonella* showed co-localisation with GFP-Gal3. Also, by co-staining for endogenous LC3, we found instances with co-localisation of LC3 on damaged lysosomes containing *Salmonella.* Therefore, the *Salmonella*-containing lysosomes could be fusing with autophagosomes or being targeted by autophagosomes. Overall, the LC3 membrane signal in *Salmonella*-infected cells was the most prominent, going beyond areas of *Salmonella* or lysosomal damage. Therefore, there appears to be strong activation of autophagosome formation. *Salmonella* that traffic to lysosomes act via their virulence factor TTSS to make pores and damage the membrane.

On the other hand, when we performed a similar experiment following infection with MRSA (NCTC8325), we observed an entirely different effect (Figure 3.18). Cells were infected with NCTC8325 for three hours (a time point with high levels of cytosolic bacteria). After NCTC8325 infection, we surprisingly saw low levels of GFP-Gal3 puncta indicating little lysosome damage. Possibly, since wildtype *Staphylococcus aureus* has virulence factors to inhibit fusion of phagosomes with lysosomes, membrane damage is limited.

To further compare with *Salmonella enterica* sv. Typhimurium infection, we incubated cells with NCTC8325 for five hours (Figure 3.19). Similarly, low amounts of EGF-Gal3 puncta were observed in infected cells. To more accurately investigate lysosomal damage, we quantified GFP-Gal3 puncta following the same timeframe of *Salmonella enterica* sv. Typhimurium versus NCTC8325 infection (Figure 3.20). *Salmonella enterica* sv. Typhimurium led to significantly higher lysosomal damage, similar to treatment with LLOMe. These results further suggest that MRSA subvert and avoid lysosomal involvement, while *Salmonella enterica* sv. Typhimurium directly interact with lysosomes.

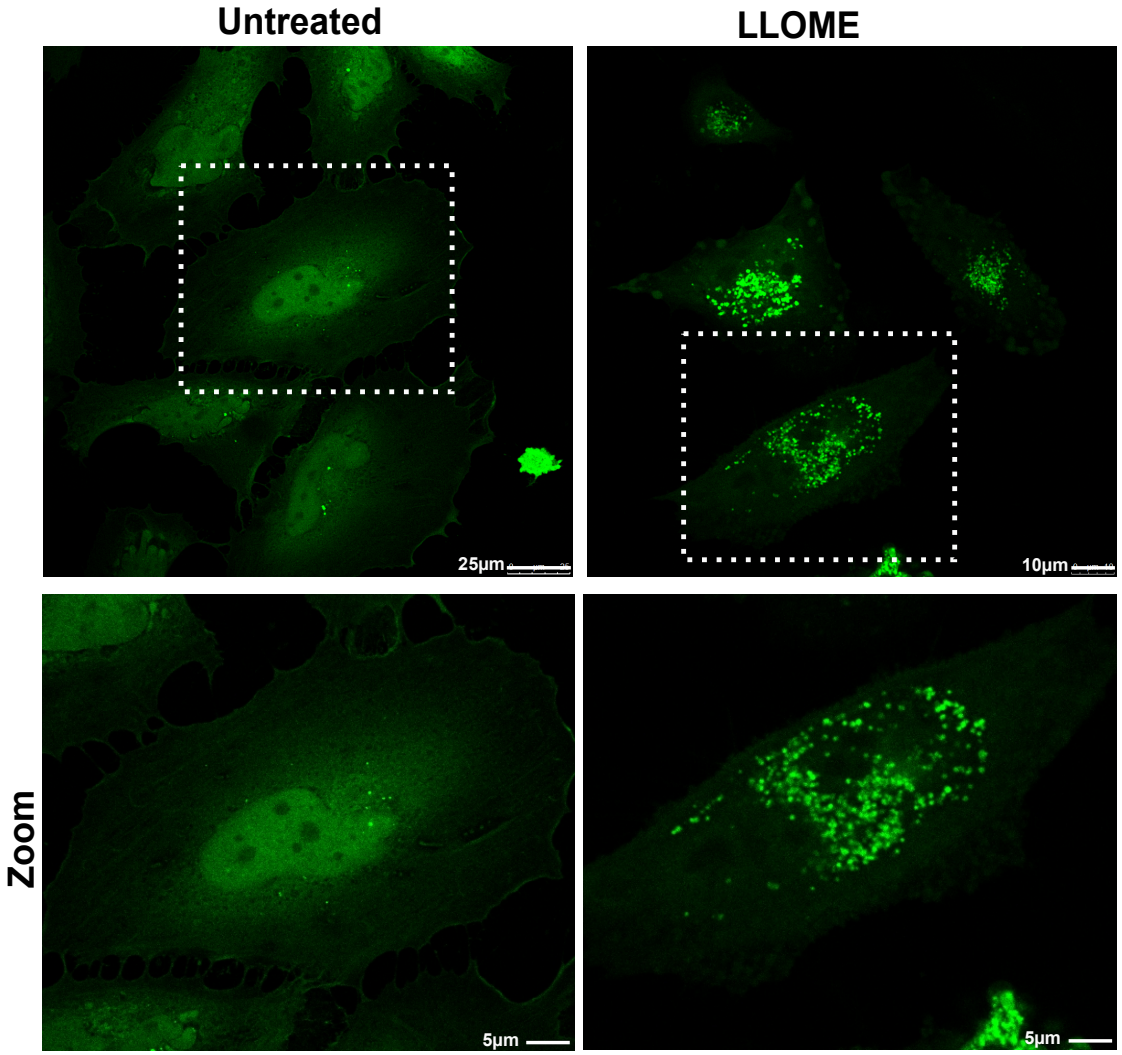

Figure 3.16: Accumulation of galectin3 in HeLa cells following treatment with LLOME. HeLa cells were plated on glass coverslips and then transfected with GFP galectin3 using lipofectamine. These cells were left untreated or treated with LLOME (2 mM concentration) for 3hrs before fixation. Cells were observed by confocal microscopy.

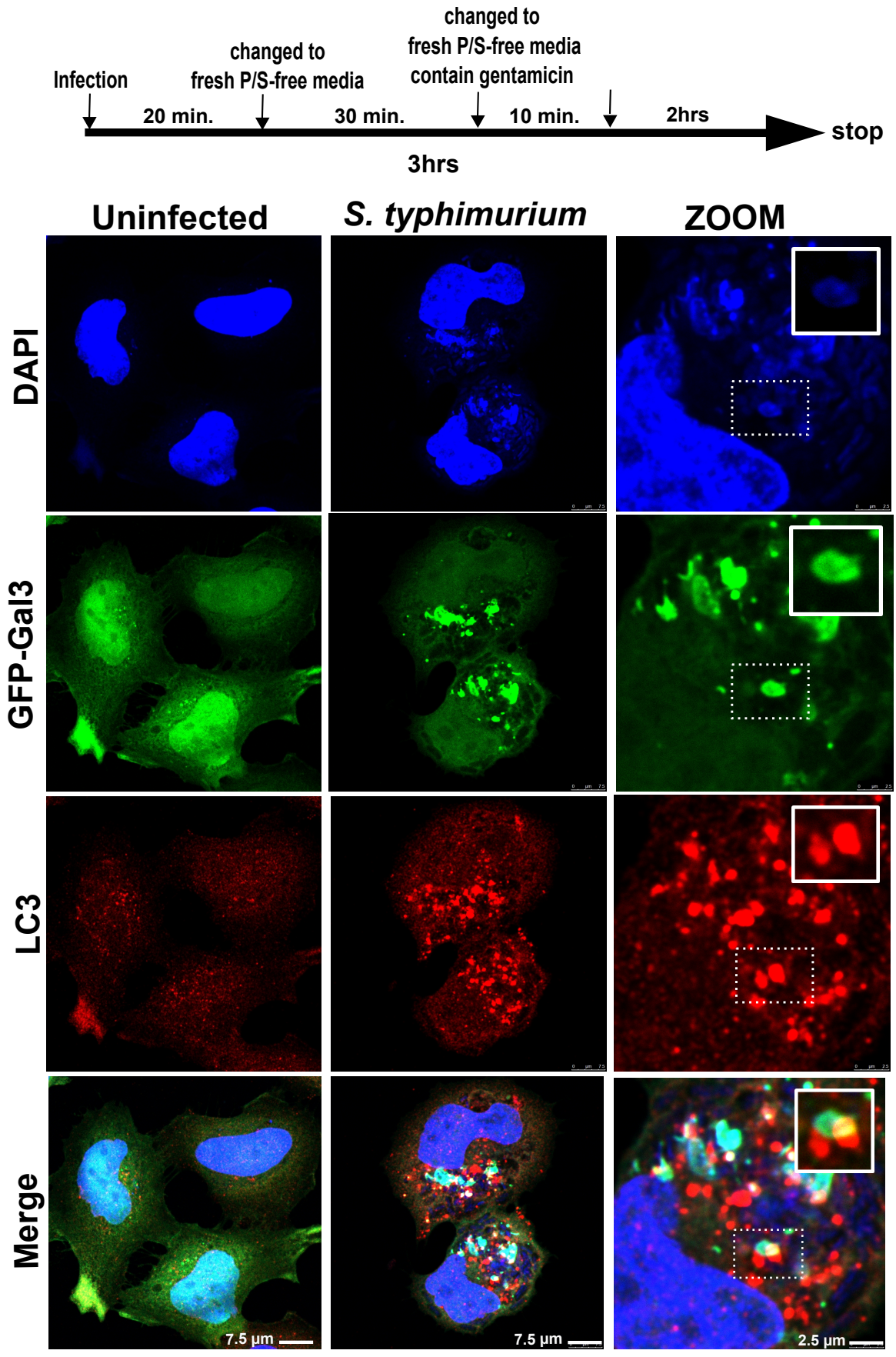

Figure 3.17: The damage of endomembranes in host cells following infection by *Salmonella enterica* sv. Typhimurium. HeLa cells were plated on glass coverslips then transfected with GFP-galectin3 using lipofectamine. These cells then infected with 1:100 MOI of *Salmonella enterica* sv. Typhimurium, then incubated at 37^{o}C for 3hr (from the point of infection) with gentamicin (0.05 mg/ml) (added after 50 minutes of infection) as shown in top diagram before fixation and staining with DAPI and LC3 antibody. Cells were observed by confocal microscopy. This experiment was done three times in different days. Scale bar: 7.5 and 2.5 µm.

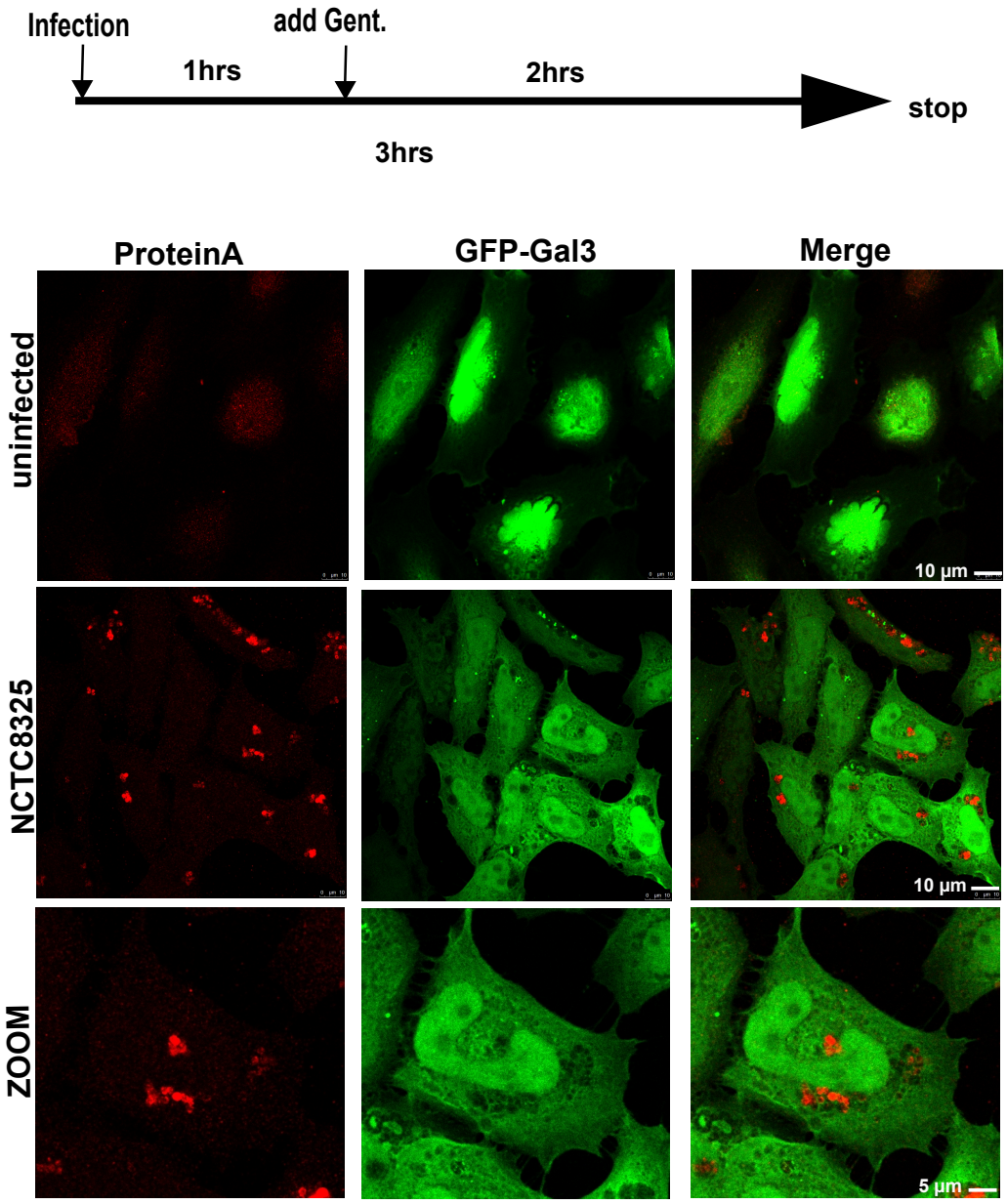

Figure 3.18: No damage of endomembranes following infection of host cells with MRSA. HeLa cells were plated on glass coverslips then transfected with GFP-galectin3 using lipofectamine. These cells infected with 100 MOI of NCTC8325, then incubated at 37^{O}C for 3hrs (from the point of infection) with gentamicin (0.05 mg/ml) (added after one hour of infection) as shown in top diagram. Cell were fixed and stained with protien A antibody. Cells were observed by confocal microscopy. This experiment was done two times. Scale bar: 10 &5 µm.

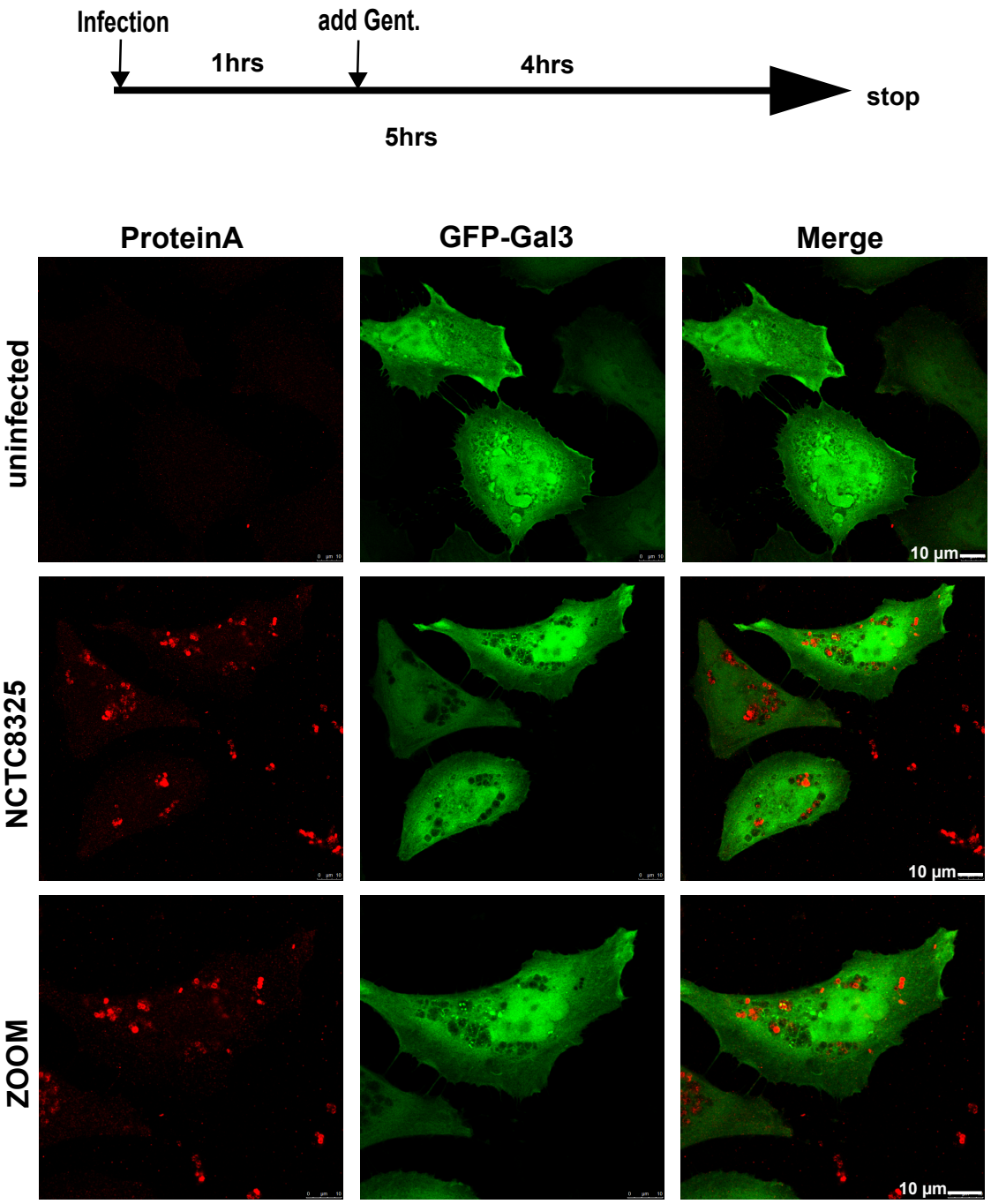

Figure 3.19: No damage of endomembranes following infection of host cells with MRSA. HeLa cells were plated on glass coverslips then transfected with GFP-galectin3 using lipofectamine. These cells were infected with 100 MOI of NCTC8325 as in Figure 3.18 and incubated for 5hrs as shown in top diagram. This experiment was done two times in different days. Scale bar: 10 µm.

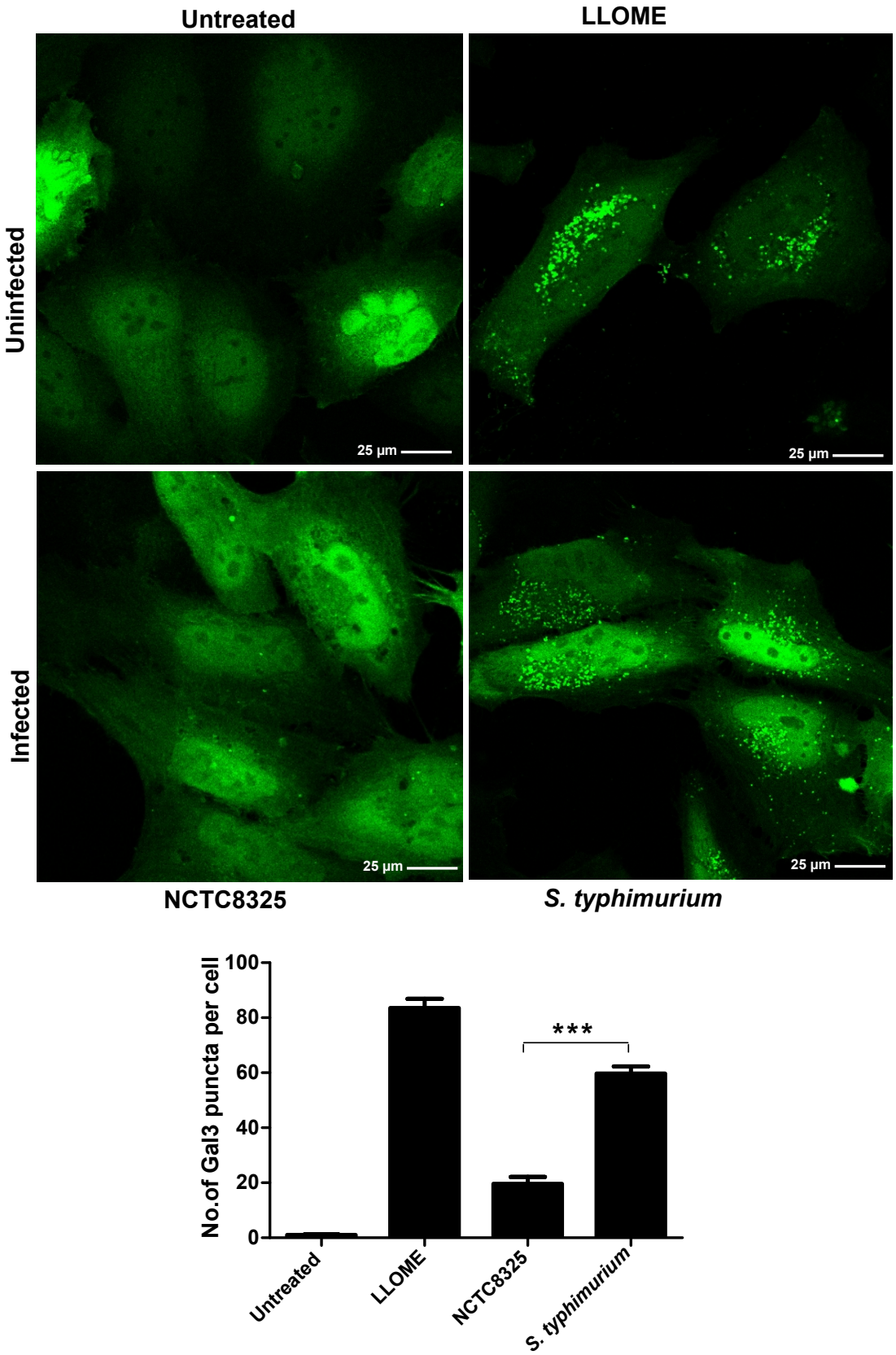

Figure 3.20: Damage of endomembranes in host cells following infection by *Salmonella enterica* sv. Typhimurium in compared with MRSA and the control. HeLa cells were plated on glass coverslips then transfected with GFP-galectin3 using lipofectamine. This cells were then infected with 1:100 MOI of *Salmonella enterica* sv. Typhimurium via " *Salmonella* protocol", or 100 MOI of NCTC8325 via "*Staphylococcus* protocol". Cell were incubated at 37^{O}C for 5hrs (from the point of infection) before fixation. As positive control these cells left without treated or treated with LLOME (2mM concentration) for 3hrs.

Top: Images captured by confocal microscopy. Scale bar: 10 µm and 5 µm.

Bottom: The number of Gal3 puncta was counted from 50 infected cells captured by a confocal microscope. Fifty infected cells were captured from different fields for three coverslips and the average of three independent experiments was taken. P value from t test (***P<0.001).

3.2.5. Analysis of host cell death following *Staphylococcus aureus* infection as compared with *Salmonella enterica* sv. Typhimurium infection

3.2.5.1. Infection with *Staphylococcus aureus*

As discussed above, in order to avoid lysosome degradation, *Staphylococcus aureus* has mechanisms that allow conversion of trafficking from an endosomal pathway to an autophagy pathway to create a special protective niche. After replication, it has been observed that *Staphylococcus aureus* breaks out of the autophagosome-derived replicative niche through the action of α-haemolysin and escapes into the cytoplasm to induce cell death (Campoy and Colombo, 2009, Schnaith et al., 2007). After inducing cell death and lysis, *Staphylococcus aureus* then disperses and goes on to infect neighbouring cells.

According to this scheme, we next wished to investigate the potency of these strains in killing host cells. We studied two different HEK cells lines (standard 293 as compared to 293A, a more adherent selected subtype) as well as HeLa cells. All these cells types are generally well-characterised experimental hosts for bacterial infection and have well-characterised autophagy properties.

Host cells were infected with ATCC29213, D393, NCTC8325 and EMRSA78 *Staphylococcus aureus.* After one hour of infection, gentamicin was added (to inhibit any extracellular bacteria) and these cells were incubated for a total of 72 hours post infection. During this time, any intracellular bacteria undergo their interaction with the cell host and xenophagy defences, culminating in some cases with a lytic infection and apoptotic cell death. At the end time point, plates were fixed, stained to detect remaining live cells and quantified.

We found that all three wildtype, virulent *Staphylococcus aureus* types, ATCC29213, NCTC8325, and EMRSA78, were potently cytotoxic for 293 and HeLa cells. In contrast, the clonal 8 complex *Staphylococcus aureus* D393 was entirely non-cytotoxic (Figure 3.21). These data indicate that the relationship between *Staphylococcus aureus* and host cell killing can vary substantially between *Staphylococcus aureus* genotype, possibly due to *agr*-dependant virulence factors.

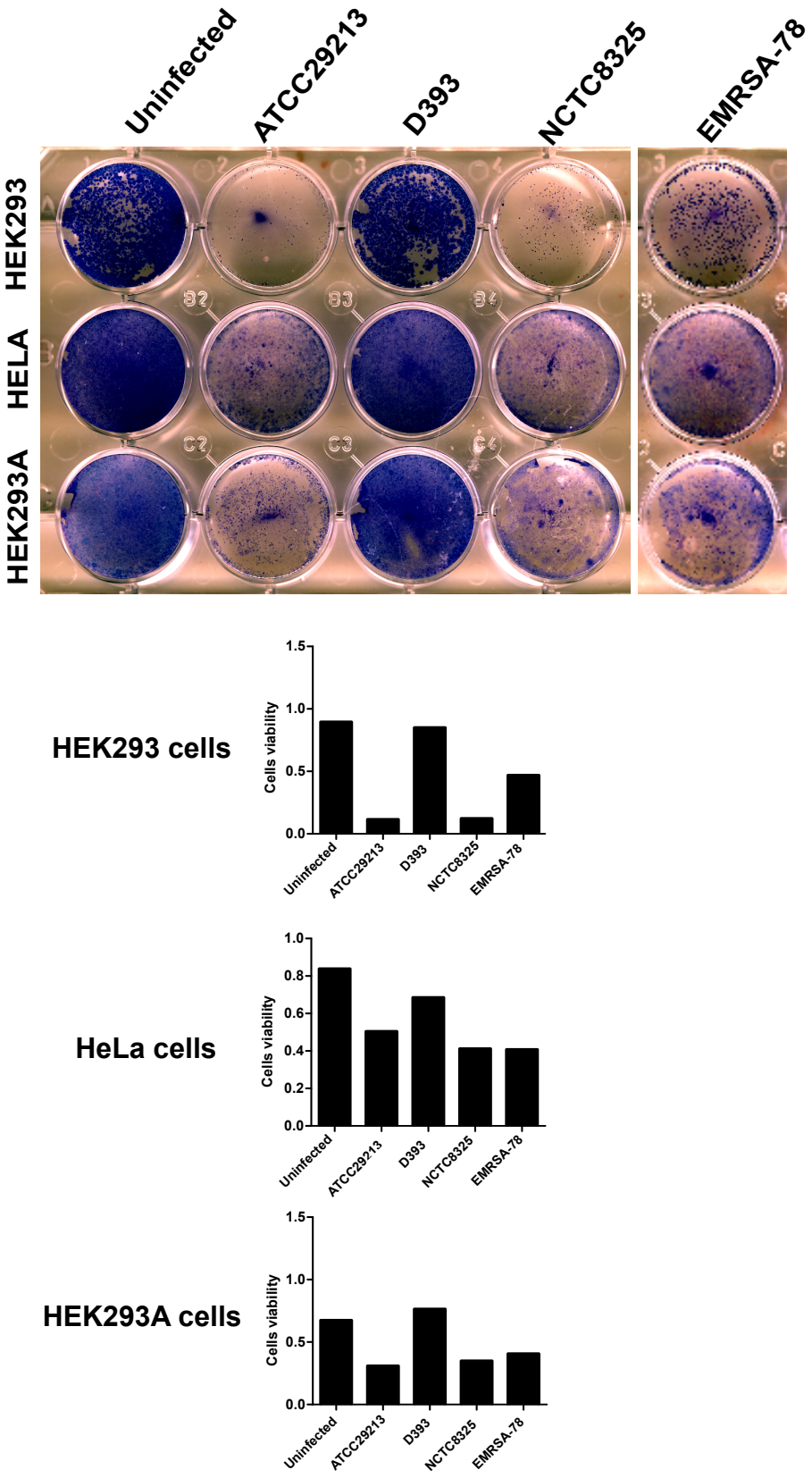

Figure 3.21: Cell killing potencies from different strains of *Staphylococcus aureus* in different host cells. Cells were seeded in a 12 wells plate and infected with ATCC29213, D393, NCTC8325, and EMRSA-78. After 1hr of infection, gentamicin (0.05 mg/ml) was added to inactivate any bacteria which had not invaded cells. Cells were then incubated for 72hrs. Plates were fixed and stained with Giemsa. Cells were quantified by absorbance at 560nm (see methods chapter).

3.2.5.2. The infection of HeLa cells with NCTC8325, NRS144 or D393

In our pilot results on *Staphylococcus aureus* and host cell killing, we found that cell killing varied substantially between *Staphylococcus aureus* genotype, likely depending on *agr* status. Therefore, we wished to more quantitatively measure the trends using HeLa cells as a representative host. Cells were plated and infected with MOI 200 of NCTC8325, D393 or NRS144 and assayed as described above.

Our results confirm that NCTC8325 (*agr* wt) *Staphylococcus aureus* led to strong cell killing, but the NRS144 *agr*-deficient strain was significantly different and did not kill cells (Figure 3.22). In addition, D393 clonal complex 8 *Staphylococcus aureus* was also significantly different from wt and did not show any cell killing activity. These data further suggest that alpha toxin haemolysin is critical to allow this pathogen to replicate and kill their host cells. Clonal 8 complex *Staphylococcus aureus* D393 also is missing this factor, leading to poor escape from the phagolysosome pathway, and thus no cell killing.

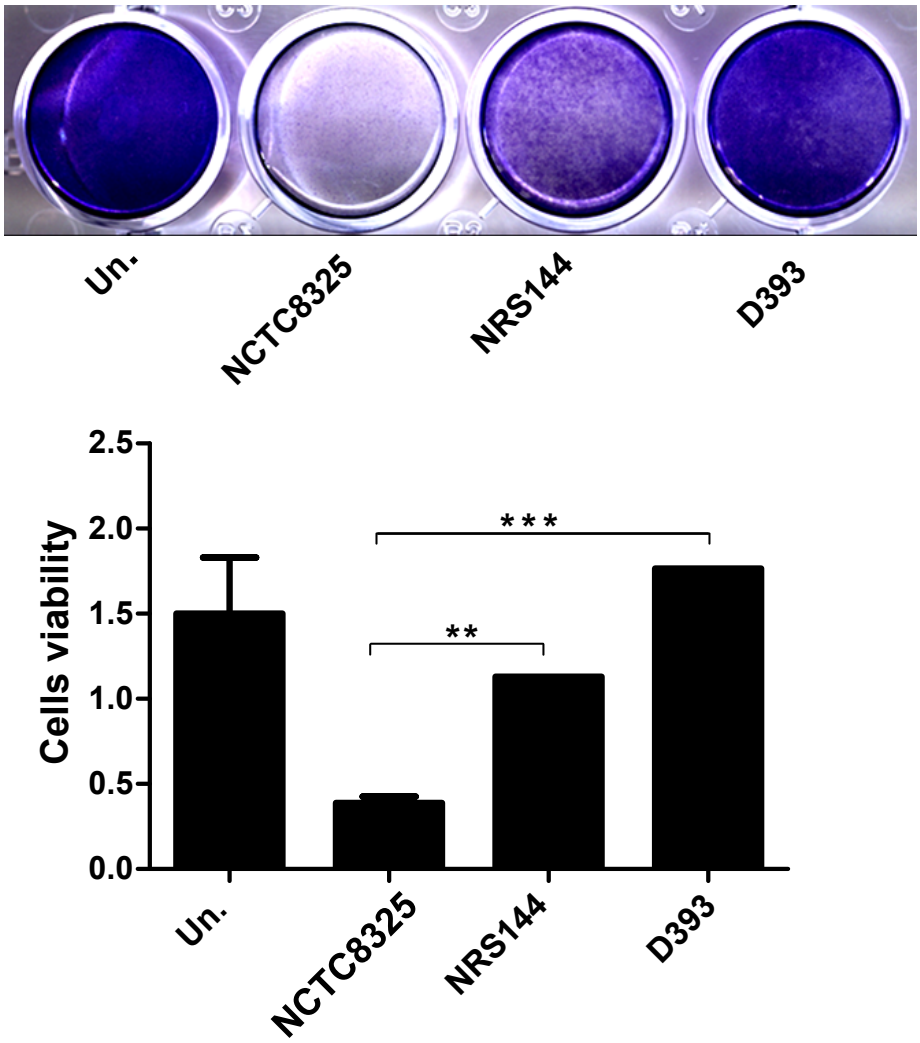

Figure 3.22: Alpha toxin haemolysin is critical for killing host cells. HeLa cells were seeded in a 12 wells plate and infected with NCTC8325, D393 (clonal complex 8) or NRS144 (agr deficient) *Staphylococcus aureus.* After 1hr of infection, gentamicin (0.05 mg/ml) was added to inactivate any bacteria which had not invaded cells. These cells were incubated, fixed, stained and counted as described in Figure 3.21. The average from 3 wells ± SD is shown. P value from one-way ANOVA with Tukey multiple comparison test (**P<0.01, ***P<0.001).

3.2.5.3. Dose dependent killing of HeLa cells with ATCC29213 and NCTC8325

After our initial results on *Staphylococcus aureus* in killing host cells, we wished to characterise in more detail the MOI dependency on host cell killing. HeLa cells were plated and infected with MOI 100-500 for ATCC29213, NCTC8325 or NRS144 and assayed as described.

Our results in Figure 3.23 confirm that *agr* wt but not *agr*-deficient *Staphylococcus aureus* led to strong cell killing following infection of HeLa cells. Cell killing was already strong with 100 MOI and ATCC29213 showed slightly higher cytotoxicity. Also, *agr*-deficient NRS144 did not lead to cell killing, even with very high 500 MOI, indicating that this mutant detective strain was completely non-harmful to cells. Lastly, quantification showed trends consistent with the pattern of cell staining, suggesting that the measurements reflect accurately the levels of cell death. Again, these data highlight that *Staphylococcus aureus* alpha toxin is essential in helping this pathogen replicate and kill their host cell.

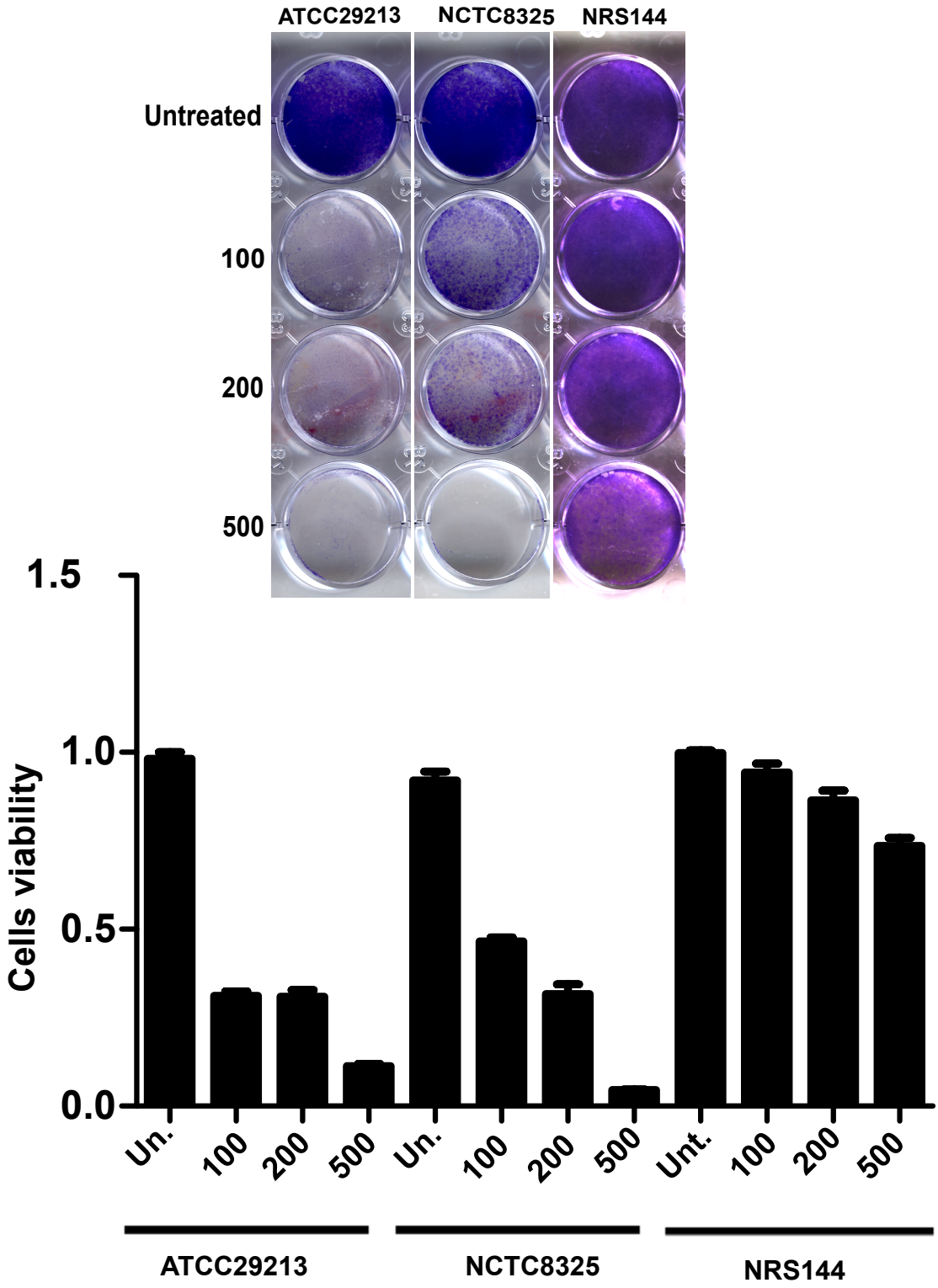

Figure 3.23: Dose dependent infection of HeLa cells with ATCC29213, NCTC8325 *Staphylococcus aureus*. HeLa cells were seeded and infected with ATCC29213, NCTC8325 or NRS144 at 100, 200, 500 MOI. After 1hr of infection, gentamicin (0.05 mg/ml) was added to inactivate any bacteria which had not invaded cells. These cells were incubated, fixed, stained and counted as described in Figure 3.21. Values were normalised to the uninfected control. The average from 3 samples ± SD is shown.

3.2.5.4. Role of ATG5-dependent autophagy in *Staphylococcus aureus* infection

We next aimed to establish in our system the role of ATG5 during xenophagy and infection-related cell death with *Staphylococcus aureus*. As summarised in the introduction, ATG5 through association with ATG12 forms a conjugation complex, which mediates the downstream lipid conjugation of LC3 and association to autophagosomes (Mizushima et al., 2001). Previous studies have shown a role for ATG5 in xenophagy with *Staphylococcus aureus* infection and knockout of this protein reduced replication of this pathogen (Schnaith et al., 2007, Mestre et al., 2010).

Wt and ATG5 knockout MEF were infected by ATCC29213 at MOI 100, 200, or 500. All three of these MOI led to strong cell killing of wild type MEF. Some remaining cells could be detected. These may have been resistant cells or debris from dead cells that pick up the stain, but this did not lead to high background when we quantified the signal. From the ATG5 knockout MEF, we found that full cell killing is inhibited when autophagy is blocked (Figure 3.24). This result confirms the previous findings, that ATG5-dependent autophagy has a role in promoting the *Staphylococcus aureus* niche that enables maximal intracellular growth and full cell death (Schnaith et al., 2007, Mestre et al., 2010).

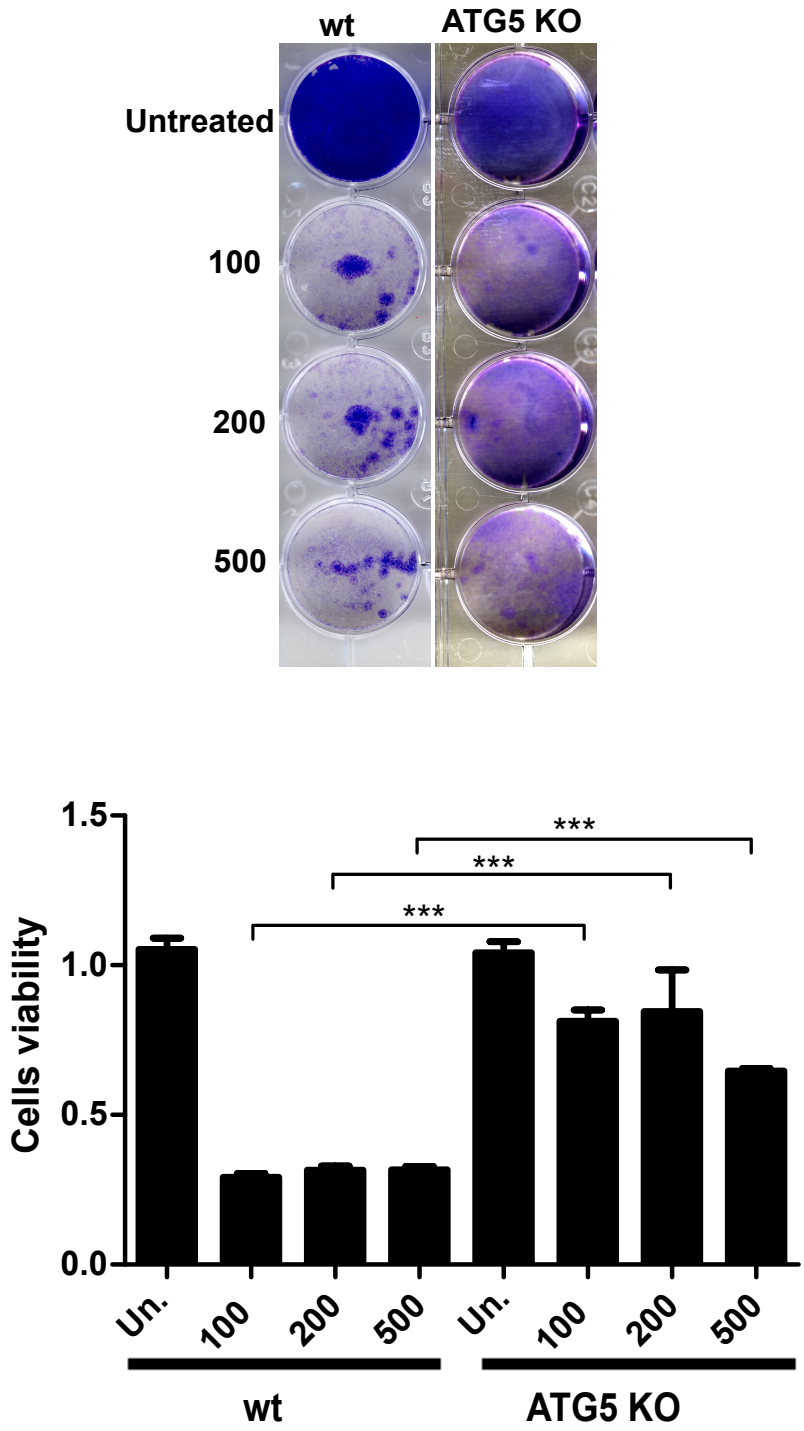

Figure 3.24: The role of ATG5 in xenophagy following infection by *Staphylococcus aureus*. wt. or ATG5 KO. MEF were seeded and infected with *Staphylococcus aureus* ATCC29213 at 100, 200, 500 MOI. After 1hr of infection, gentamicin (0.05 mg/ml) was added to inactivate any bacteria which had not invaded cells. Cells were incubated, fixed, stained and counted as described in Figure 3.21. The average from 3 samples ± SD is shown. P value from one-way ANOVA with Tukey multiple comparison test (***P<0.001).

3.2.5.5. The infection and killing host cells by *Salmonella enterica* sv. Typhimurium

Our previous results showed that *Salmonella enterica* sv. Typhimurium directly interact and traffic to lysosomes. However, we also saw that *Salmonella* then makes pores and damages the lysosomal membrane. Autophagy is activated to fight the infection, but our results showed that this response was highly induced just in the first hours of infection. This suggests that xenophagy of *Salmonella enterica* sv. Typhimurium is mainly an early event and occurs prior to escape by the bacteria into the cytosol, possibly when damage to the SCV is initiated. Therefore, factors that promote SCV damage or limit autophagy would be expected to produce more host cell killing.

We wished to investigate in our system the potency of *Salmonella enterica* sv. Typhimurium in killing host cells. For this we used the *Salmonella* protocol discussed in Figure 3.1B and further incubated for 72 hours. We found that these bacteria were very potent at killing both HEK and HeLa cell hosts (Figure 3.25).

Salmonella enterica sv. Typhimurium, by using specific virulence mechanisms, was found induce host cell death to promote its infection. *Salmonella* produces one set of virulence proteins (SPI-1) to promote invasion of the intestine and a different set (SPI-2) to mediate systemic disease. Significantly, each set of virulence factors mediates a distinct mechanism of host cell death (Guiney, 2005). Autophagy may be used to reduce the pace of killing of host cells by this *Salmonella* bacteria. However, it does not lead to entirely clearing it.

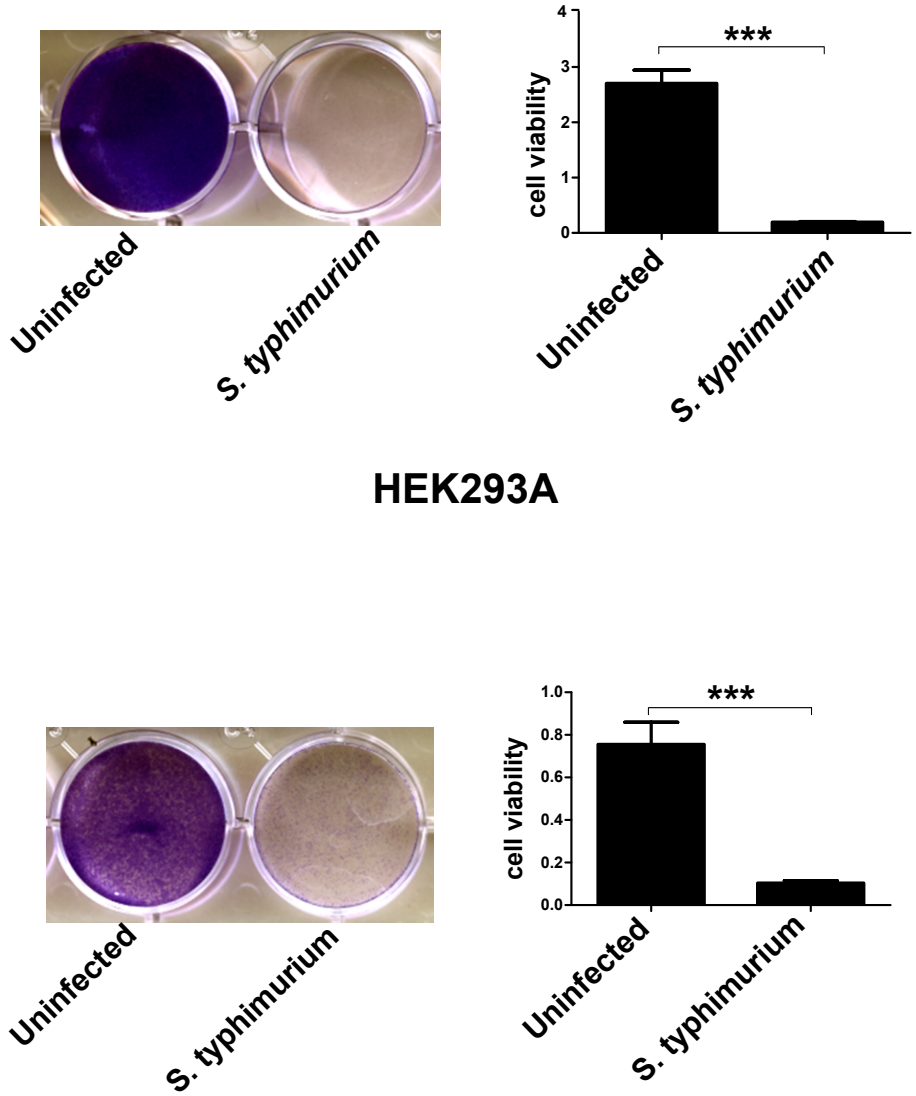

Figure 3.25: Host cell killing potencies from *Salmonella enterica* sv. Typhimurium. HEK293A and HeLa cells were infected with *Salmonella enterica* sv. Typhimurium via the " *Salmonella* protocol". Bacteria were grown until OD= 1.2 - 1.5 and infected cells at 1:100 dilution for 20 min. and then changed to fresh P/S-free media for 30 min. Cells were then changed to fresh P/S-free media contain gentamicin (0.05 mg/ml) and then incubated 72hrs, then fixed, stained and counted as described in Figure 3.21. The average from 3 samples ± SD is shown. P value from t test (***P<0.001).

In the first figures of this chapter, we tested different protocols for producing a *Salmonella enterica* sv. Typhimurium infection in cell cultures. Infection of cells using both protocols did not lead to any LC3 lipidation by western blotting. Infection with *Salmonella enterica* sv. Typhimurium using the *Salmonella* protocol did produce xenophagy markers by cell imaging. Here, we performed one final comparison of the infection protocols.

HeLa cells were infected with either *Salmonella enterica* sv. Typhimurium or *Staphylococcus aureus* using the *Staphylococcus* protocol and further incubated for 72 hours. We clearly saw that infection with *Staphylococcus aureus* led to strong cell killing. By comparison, *Salmonella enterica* sv. Typhimurium performed in parallel failed to show any detectable cell killing. When compared with the earlier result, our results in this procedure show that the cytotoxicity of *Salmonella enterica* sv. Typhimurium strongly depends on how they are handled and presented to cells (Figure 3.26). We propose that *Salmonella* killing probably depends on its growth phase. Infection of cells with *Salmonella enterica* sv. Typhimurium growing in the mid-log phase did not lead to killing. However, *Salmonella* in the late-log phase was highly potent at inducing host cell killing. These findings are similar with those in another research study which established the potential of this bacteria (*Salmonella)* in generating host cell killing when in macrophage, and when this develops in the late-log phase or stationary phase (van der Velden et al., 2000). This other study established the log phase needed to induce SPI-1. Similarly, it also found that the stationary phase was needed to induce SPI-2 (van der Velden et al., 2000). The inducement of SPI-2 in the ileum is done before the penetration of the intestine (Brown et al., 2005). The study also indicated that the *Salmonella* bacteria developing in the mid-log stage did not produce the virulence factor that is necessary for it to penetrate and proliferate in cells.

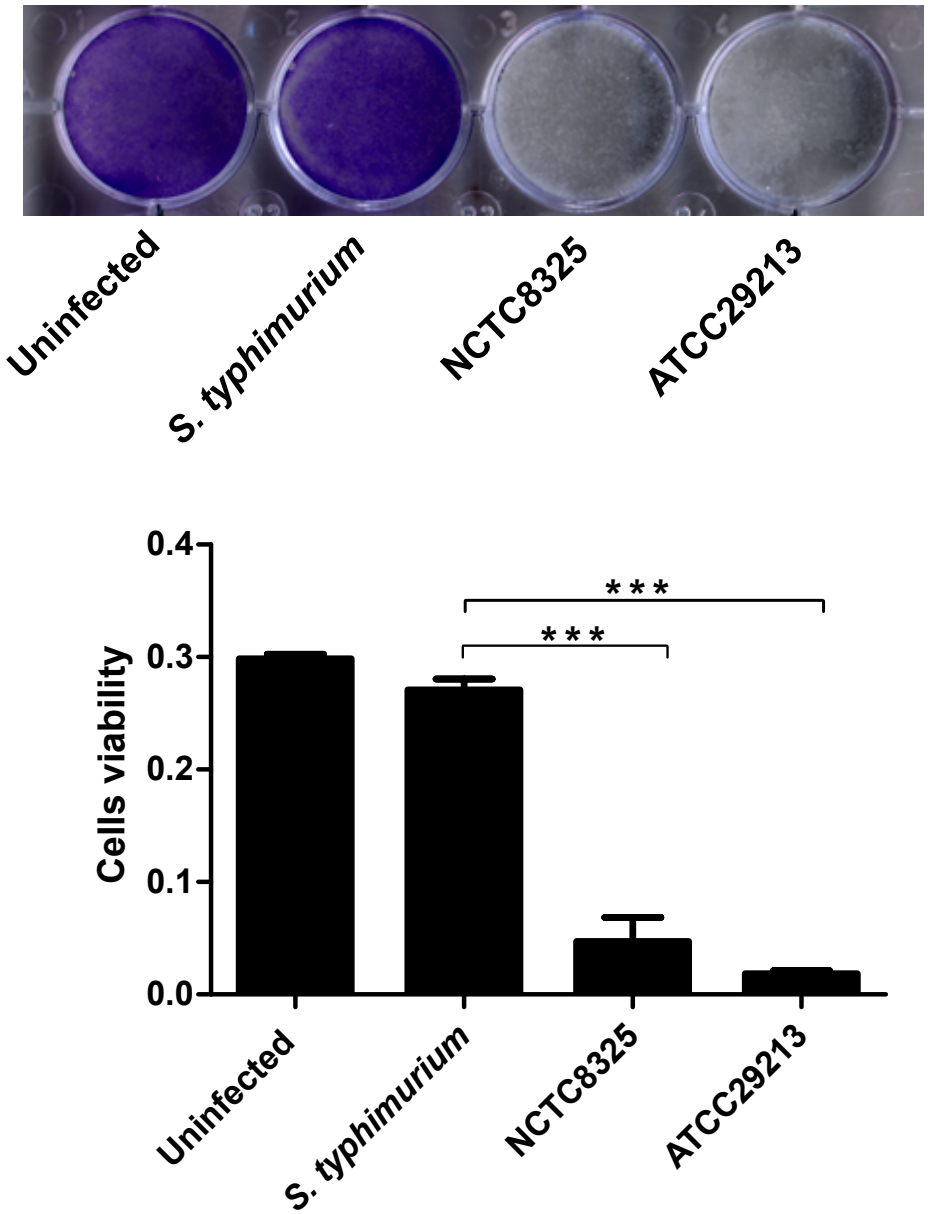

Figure 3.26: *Salmonella enterica* sv. Typhimurium did not kill HeLa cells when grown using the "*Staphylococcus* protocol". HeLa cells were infected with *Salmonella enterica* sv. Typhimurium, NCTC8325 or ATCC29213 at MOI 200. After 1hr of infection, gentamicin was added to inactivate any bacteria which had not invaded cells. Cells were incubated, fixed, stained and counted as described in Figure 3.21. The average from 3 samples ± SD is shown. P value from one-way ANOVA with Tukey multiple comparison test (***P<0.001).

3.3. Discussion

Anti-bacterial xenophagy has been, so far, best characterised with *Salmonella* as the pathogen. In contrast, there have been fewer studies on the association between *Staphylococcus aureus* and autophagy. To propose better approaches for fighting *Staphylococcus aureus* infections in many clinical settings, it is important to better understand how this pathogen interacts and circumvents the defence system of the host cells. Therefore, in this chapter, we aimed to study the autophagy induced by *Staphylococcus aureus* as compared with the better understood xenophagy programme induced following infection with gram-negative *Salmonella enterica* sv. Typhimurium.

3.3.1. The induction of the autophagic response during *Staphylococcus aureus* and *Salmonella enterica* sv. Typhimurium infection

To achieve this aim, we explored multiple readouts of autophagy by biochemical western blotting and imaging to observe bacteria interacting with cellular membrane structures (summarised in Figure 3.27). Using western blotting, we found that three strains of “wildtype” virulent *Staphylococcus aureus* (ATCC29213, NCTC8325 and epidemic MRSA-78) were able to strongly induce LC3 lipidation as a marker of autophagy following the first 3–4 hours of infection in HeLa cells. These results generally agree with other findings (Schnaith et al., 2007), which characterised various strains of *Staphylococcus aureus* on autophagy. This work showed that certain *Staphylococcus aureus* strains induced autophagy based on viewing the formation of membranes labelled with overexpressed GFP-LC3. We used this work as a basis for establishing our experimental system. Here, we collected results that agreed and, furthermore, found strong activation of autophagy across the cell population via biochemical blotting using endogenous LC3. We also extended the study to show that clinical strains of epidemic MRSA isolated from hospitals (Raghukumar et al., 2010) were also potent at stimulating autophagy. However, the *Staphylococcus aureus* NRS144 strain, which lacks the *agr* (*accessory gene regulator*), and also, surprisingly, a clinical isolate with a clonal complex 8 (CC8) genotype from an endo-tracheal aspirate (Sangal et al., 2012) did not induce autophagy.

Staphylococcus aureus has numerous virulence factors which include surface proteins and toxins (Gordon and Lowy, 2008). These factors each contribute vital roles for the stable invasion of host cells. Many of these factors are controlled by the *agr* system (for example, the hla α-haemolysin). Previous research has suggested a model in which α-haemolysin reduces the levels of cAMP in host cells, resulting in activation of autophagy (Mestre and Colombo, 2012). Our finding is in general agreement with this; for example, the importance of a functioning *agr* for autophagy activation. It is possible that the CC8 strain lacks a particular factor under the *agr* which explains the difference in effect with host cell autophagy. Another more recent study has shown that strains with high levels of *agr* activity became associated with autophagosomes (O'Keeffe et al., 2015). In that study, a CC8 strain failed to accumulate autophagosomes (LC3 accumulation) in dendritic cells and did not associate with GFP-LC3 puncta.

To better understand the biology of *Staphylococcus aureus*, we performed parallel studies with the better-understood xenophagy programme following infection with gram-negative *Salmonella enterica* sv. Typhimurium. We found, surprisingly, that *Salmonella enterica* sv. Typhimurium did not stimulate strong lipidation and activation of LC3 (i.e. strong LC3-II protein) in cells infected with *Salmonella enterica* sv. Typhimurium. This result seemed not to agree with the previous studies which found that *Salmonella enterica* sv. Typhimurium can invade host cells and induce poly-ubiquitin modification of bacterial proteins leading to targeting by autophagy (Zheng et al., 2009). It is interesting to note that previous studies of *Salmonella enterica* sv. Typhimurium and autophagy have been reported exclusively with imaging studies of infected cells (Kageyama et al., 2011, Zheng et al., 2009, Birmingham et al., 2005).

Based on the difference between our blotting data and the published results, we decided to try imaging and re-test the xenophagy response by *Salmonella enterica* sv. Typhimurium. Interestingly, using this method, we found these bacteria clearly co-localised with the LC3 membrane in HeLa cells by the first hour of infection in almost all cells of the sample. These results suggest that xenophagy was strongly activated in our HeLa experiments following *Salmonella enterica* sv. Typhimurium invasion but may be at a level below detection by blotting (or unusually without LC3 lipidation). By contrast, xenophagy following gram-positive *Staphylococcus aureus* were dramatic

after a few hours of infection. This indicates that responses are different following infection with *Staphylococcus aureus* and *Salmonella enterica* sv. Typhimurium.

Salmonella enterica sv. Typhimurium was previously shown to invade non-phagocytic cells and modify the SCV to create a specialised vacuolar niche permissive for intracellular growth. As previously noted, not all intracellular *Salmonella enterica* sv. Typhimurium remain within SCVs, but rather, a significant proportion escape into the cytosol early after invasion. These cytosolic bacteria are targeted by the ubiquitination system and recognised by ubiquitin-binding adaptor proteins leading to xenophagy that restricts the infection (Birmingham et al., 2006). Additionally, it was recently discovered that T3SS-1-dependent mechanisms lead to SCV damage at initial stages of *Salmonella enterica* sv. Typhimurium infection. This damage results in exposure of bacteria to the cytosol and autophagy initiation. Autophagy thereby promotes repair of T3SS-1-inflicted damage to SCV membranes (Kreibich et al., 2015). Thus, the low level of escape of this pathogen to the cytoplasm may be another reason why low levels of autophagy were difficult to detect by blotting.

Additionally, it was recently discovered that the role of SifA in the maintenance of SCV integrity makes it critical for the prevention of autophagy initiation. The modulation of certain phosphoinositide 3-phosphate (PI(3)P) through the presence of a myotubularin 4 (MTMR4) are an ideal requirement for *Salmonella enterica* sv. Typhimurium survival. In this way, PI(3)P regulation is also essential for SCV integrity and stability, thus playing an additional role in autophagy modulation (Teo et al., 2016). Moreover, *Salmonella* can recruit FAK (focal adhesion kinase) to the SCV in a manner mediated by SPI-2, and then FAK leads to the suppression of autophagy through activation of the Akt/mTORC1 signalling pathway (Owen et al., 2016). This prevents autonomous cell elimination and prevents the innate TRIF-dependent type1 interferon immune response (Owen et al., 2016). Therefore, the low levels of autophagy were difficult to detect by blotting, possibly because *Salmonella enterica* sv. Typhimurium suppresses autophagy. Overall, it is critical to determine if there are other mechanisms through which *Salmonella* suppresses autophagy to subvert the innate immune response of the host cell.

3.3.2. Infection with *Staphylococcus aureus* is associated with increased accumulation of LC3-II lapidating

In addition, we compared the activation of autophagy induced by bacterial infection with typical autophagy induced by starvation. Our results showed clearly stronger accumulation of LC3-II in the cells with infection, as compared to starvation of cells. This result suggests that there may be increases in the formation of autophagosomes following infection, but these bacterial strains may have also prevented flux of autophagy by preventing acidification of the autophagosome/autolysosome or its fusion with the lysosome. This activation of formation with inhibition of end-stage degradation leads to stronger accumulation of LC3-II. This result agrees with current work, which has found that strains with high levels of *agr* activity were capable of causing autophagosome accumulation (O'Keeffe et al., 2015). Therefore, bacteria induced autophagosomes may have different downstream degradative rates than the more commonly studied smaller starvation-induced autophagosomes.

We studied the accumulation of LC3 over time following infection by *Staphylococcus aureus* as compared with *Salmonella enterica* sv. Typhimurium. Interestingly, infection with MRSA resulted in the persistence of substantial levels of the LC3-II for at least six hours. In comparison, infected HeLa cells with *Salmonella enterica* sv. Typhimurium showed no accumulation of LC3 and the level of LC3 was reduced over time. This result indicated that following infection of HEK293A cells by MRSA (NCTC8325), the constitutive degradation of autophagosomes by lysosomes was prevented, leading to the accumulation of LC3-II. In contrast, *Salmonella enterica* sv. Typhimurium strain SL1344 did not interfere with the homeostatic turnover of the autophagic machinery leading to reduction of the level of LC3. Also, this result suggested that maybe increases in the level of formation of autophagosomes following infection by *Staphylococcus aureus*, as compared with *Salmonella enterica* sv. Typhimurium, was the reason for the accumulation LC3 over time.

3.3.3. p62 as an adaptor molecule showing ubiquitinated cargo following *Staphylococcus aureus* and *Salmonella enterica* sv. Typhimurium infection

Cellular cargo is commonly targeted to autophagosomes by adaptor proteins such as p62/sequestosome1. The p62 adaptor binds to ubiquitinated cellular targets and then interacts with LC3 found in the autophagosome (Pankiv et al., 2007). Prior studies

have noted that *Salmonella enterica* sv. Typhimurium becomes coated by poly-ubiquitinated modifications when it escapes the vacuole and becomes free in the cytosol (Birmingham et al., 2006). The xenophagy pathway is then able to target and neutralise cytosolic *Salmonella enterica* sv. Typhimurium through p62 and other adaptor proteins (Zheng et al., 2009). The observations from our cell system also showed *Salmonella enterica* sv. Typhimurium infection leading to large-sized p62-labelled structures with very clear co-localisation on bacteria. However, this response was highly induced just in the first hours of infection and reduced over time. These images showed p62/sequestosome1 serving as an adaptor molecule targeting *Salmonella enterica* sv. Typhimurium to autophagosomes.

On the other hand, it was less clear from p62 imaging whether *Staphylococcus aureus* also becomes ubiquitinated once within the host cytosol. One interesting finding in this study was the clear accumulation of large-sized structures labelled with endogenous p62 following infection with NCTC8325 wt *Staphylococcus aureus*. This strong alteration of the p62 pathway was not seen following infection with the *agr* mutant or CC8 type *Staphylococcus aureus* that are less potent at activating autophagy. Therefore, infection with *Staphylococcus aureus* strains affecting LC3 also led to accumulation of p62 and possibly ubiquitinated cellular proteins. On the other hand, the large aggregates of p62 did not directly co-localise with NCTC8325. However, they could often be seen just next to the individual *Staphylococcus aureus.* Our results therefore differ on this point with other work, which could show some direct overlap between p62 and *Staphylococcus aureus* signals (Neumann et al., 2016). However, that research used a different *Staphylococcus aureus* strain (SH1000), as well as different cell lines (Murine fibroblasts NIH/3T3). Thus, the extent to which such differences can be attributed to the bacterial strains or host cells needs to be further researched. Our results also suggest that *Staphylococcus aureus* might lead to ubiquitination and p62 targeting of other proteins (or organelles) that become damaged during the bacterial infection. Our results also suggest proteins on *Staphylococcus aureus* may not be ubiquitin modified since the bacteria did not show clear overlap with p62 signals.

Therefore, our results show that both types of bacteria generally lead to increased protein ubiquitination and p62-positive membranes. However, the responses were

different in terms of localisation and only *Salmonella* were closely bound to the p62 adaptor protein.

3.3.4. Targeting of the lysosome during infection by *Staphylococcus aureus* or *Salmonella enterica* sv. Typhimurium

In studying the two different bacteria, we next wished to view the interaction with lysosomes using the LAMP2 marker of late endosome/lysosomes. We found strong lysosome swelling following infection by different *Staphylococcus aureus* strains and *Salmonella enterica* sv. Typhimurium, indicating that these degradative vesicles formed a large part of the intracellular membrane trafficking route for both pathogens.

A key aspect of our data was that the most virulent *Staphylococcus aureus* could avoid being inside lysosomes. The large presence of *Staphylococcus aureus* separate from lysosomal membranes could represent either: 1) a block of fusions between bacteria-containing phagosomes (or autophagosomes) with lysosomes; or 2) escape of bacteria from lysosomes. *Staphylococcus aureus* have been found to escape phagosome-to-lysosome trafficking, which allows intracellular bacterial survival and killing of the host cell (Bayles et al., 1998). It has been shown that the ability of *Staphylococcus aureus* to divert from the endosomal pathway to autophagosomes is driven by factors primarily under the control of the *agr* regulatory system (Schnaith et al., 2007, O'Keeffe et al., 2015). The current model from the literature suggests that α-haemolysin is mainly responsible for the induction of autophagy (Mestre et al., 2010). Thus, this result clearly establishes that the escape step was key for activating autophagy and also for inducing cell death. Overall, *Staphylococcus aureus* appears to critically require a diversion from the endosomal pathway towards the autophagy pathway to form a niche to enable full infection. Therefore, prevention of this diversion may provide the chance for the lysosome endosomal pathway to restrict MRSA infection by delivering this bacteria to the lysosomes.

When compared with *Salmonella enterica* sv. Typhimurium, *Salmonella* were mostly all within LAMP membranes. Our results here therefore agree with other work which identified the role of autophagy to clear *Salmonella enterica* sv. Typhimurium and fight this infection (Zheng et al., 2009, Birmingham et al., 2006). However, Garcia-del Portillo et al. (1993) found, upon infection of HeLa epithelial cells, *Salmonella enterica*

sv. Typhimurium residues in vacuoles that contain lysosomal membrane glycoproteins (lgps). Four to six hours after invasion, intracellular bacteria induce the formation of stable filamentous structures containing lgps that are connected to the bacteria-containing vacuoles. Formation of these lgp-rich structures requires viable intracellular bacteria and is blocked by inhibitors of vacuolar acidification (Garcia-del Portillo et al., 1993). Thus, the LAMP-2 membranes around *Salmonella* could also, in theory, be a niche.

3.3.5. Damage of endomembranes and lysosomes following infection by *Staphylococcus aureus* and *Salmonella enterica* sv. Typhimurium

Since we saw that *Staphylococcus aureus* and *Salmonella enterica* sv. Typhimurium both caused lysosome swelling but with different properties, we looked further into how the lysosomes were affected. In recent years, Galectin-3 has been established as a marker of damaged endomembranes, in particular lysosomal membranes (Aits et al., 2015, Paz et al., 2010). Interestingly, extensive puncta of GFP-Galectin3 were observed within almost all of the cells infected by *Salmonella enterica* sv. Typhimurium. This result indicates high levels of damage on vacuoles or lysosome membrane following infection.

In the current model, when *Salmonella enterica* sv. Typhimurium invades host cells they remain inherent in *Salmonella*-containing vacuoles (SCV) and this is facilitated by its bacterially encoded virulence factors. The vacuoles have been shown become damaged via needle like structures made of SPI-1 T3SSs (Birmingham et al., 2006). Galectin 8 is a related protein that recognises damaged vacuoles and then recruits NDP52 followed by LC3-II, thus linking to autophagosomes (Thurston et al., 2012). In fact, Galectin-1, -9, -3 and -8 members are all capable of binding with glycans on damaged vacuoles (Paz et al., 2010, Thurston et al., 2012, Houzelstein et al., 2004).

In a recent study, lysosomes were identified as being damaged via a different pathway during the pathogenesis of *Listeria monocytogenes*. Studies were able to show that extracellular *Listeria* through secretion of listeriolysin O, which is a pore-generating toxin, alters the integrity of lysosomes in epithelial cells, but not in macrophages (Malet et al., 2017). Listeriolysin O, once it gets inside cells, triggers the lysosome membrane to discharge lysosomal contents such as cathepsins proteases. These cathepsins remain active within its cytosol host and produce unwanted degradation

of cellular components. Similarly, lysosome alteration can result from bacterial pore-generating toxins including pneumolysin and perfringolysin O (Malet et al., 2017). Therefore, different bacteria all appear to lead to lysosome damage using different pathways. Here, we provide the first evidence suggesting that *Salmonella* produces lysosome damage, which would be expected to trigger cell stress, cell lysis and promote infection.

Our results also clearly found co-localisation of LC3 with damaged lysosomes containing *Salmonella*. Therefore, *Salmonella*-containing damaged lysosomes are targeted by autophagosomes. Recent work has described that cells are protected from *Mycobacterium tuberculosis* invasion and lysosomal damage as a result of collaboration between TRIM16 and Galectin-3 in activating selective autophagy (Chauhan et al., 2016). Using lysosomal and phagosomal damage models, it could be shown that TRIM16 recognises endomembrane damage through interactions with Galectin-3, interestingly, in an ULK1-dependent manner (Chauhan et al., 2016).

In contrast, there were much lower levels of lysosomal damage following infection with virulent strains of *Staphylococcus aureus*. These results further demonstrate how *Staphylococcus aureus* follows a unique intracellular route, unlike other types of pathogenic bacteria. Low levels of lysosomal damage are consistent with the current model of *Staphylococcus aureus* trafficking. The key feature, which we observed in our different assays, is that *Staphylococcus aureus* inhibits fusion of phagosomes and autophagosomes with lysosomes to create a niche for replication before release of bacterial progeny into the cytoplasm (Schnaith et al., 2007).

3.3.6. Analysis of cell killing by *Staphylococcus aureus* as compared with *Salmonella enterica* sv. Typhimurium

Our results are consistent with the model (Campoy and Colombo, 2009, Schnaith et al., 2007) in which *Staphylococcus aureus* follows a trafficking pathway from endosomes to autophagy as it seeks to develop a special protective niche. Once within the replicative niche, *Staphylococcus aureus* eventually breaks out via the actions of α-haemolysin to enter into the cytoplasm. Once cell lysis is induced, *Staphylococcus aureus* disperses to infect neighbouring cells.

Following this scheme, we confirmed that *agr* wt strains of *Staphylococcus aureus* were very efficient at killing host cells after infection. In contrast, the *agr* mutant

Staphylococcus aureus NRS144 displayed almost zero ability to induce cell death following infection. The results here are in keeping with other literature suggesting that α-haemolysin is the main virulence factor responsible for the induction of autophagy (Mestre et al., 2010). Also, this study suggested that α-haemolysin led to further interruption of normal autophagic flux within the host cell, hence preventing autophagosome maturation.

Interestingly, the CC8 strain (D393) that we studied did not show any activity in host cell killing despite being isolated from a clinical infection (Sangal et al., 2012). Surprisingly, previous work showed complementary results with another CC8 strain (SH1000) that lacks *agr* (Horsburgh et al., 2002). In this study, the researchers found CC8 bacteria could be killed by dendritic cells (DCs) and macrophages. In addition, *agr* (+) strains, but not *agr*-deficient strains, could escape phagocytosis by dendritic cells causing associated cytotoxicity (O'Keeffe et al., 2015). It is likely that the CC8 strain we have studied also lacks a particular factor such as *agr*, which underlies the difference in effect with host cell autophagy and killing, although there is no evidence for this as yet.

Overall, the results on host cell killing correlate with how potently each *Staphylococcus aureus* strain activates autophagy and avoids lysosomal compartments. Our results also showed that cell killing was greatly inhibited when autophagy was blocked by ATG5 knockout in MEF in keeping with results from other studies (Schnaith et al., 2007, Mestre et al., 2010). Altogether, the results suggest that autophagy has an overall role in promoting the *Staphylococcus aureus* niche that enables maximal intracellular growth and full cell death.

Interestingly, our results also show that host cells in culture can be effectively killed following *Salmonella* infection. However, the potency of killing by *Salmonella* was highly dependent on the growth phase of the bacteria. *Salmonella enterica* sv. Typhimurium collected from the mid-log phase of growth did not cause any host cell death. In contrast, *Salmonella* collected from the late-log phase growth were highly potent for host cell death. Our results are therefore in general agreement with a previous report suggesting that *Salmonella* is more harmful in macrophages when the infection involves bacteria in late-log phase or stationary phase (van der Velden et al., 2000). Furthermore, it was found that SPI-2 was highly induced under the stationary

phase. In agreement, Brown et al. (2005) reported that SPI-2 induction is strong when *Salmonella* are in the ileum prior to the intestinal penetration.

Through its virulence factor, the *Salmonella enterica* sv. Typhimurium (strain SL1344) bacteria was found to be highly cytotoxic to epithelial cells once the infection has lasted for over six hours (Hautefort et al., 2008). Interestingly, our strain also produced the same finding: that autophagy may be used to reduce the pace of killing of host cells by this *Salmonella* bacteria. However, it does not lead to entirely clearing it.

(A) Autophagy with *Salmonella enterica* sv. Typhimurium

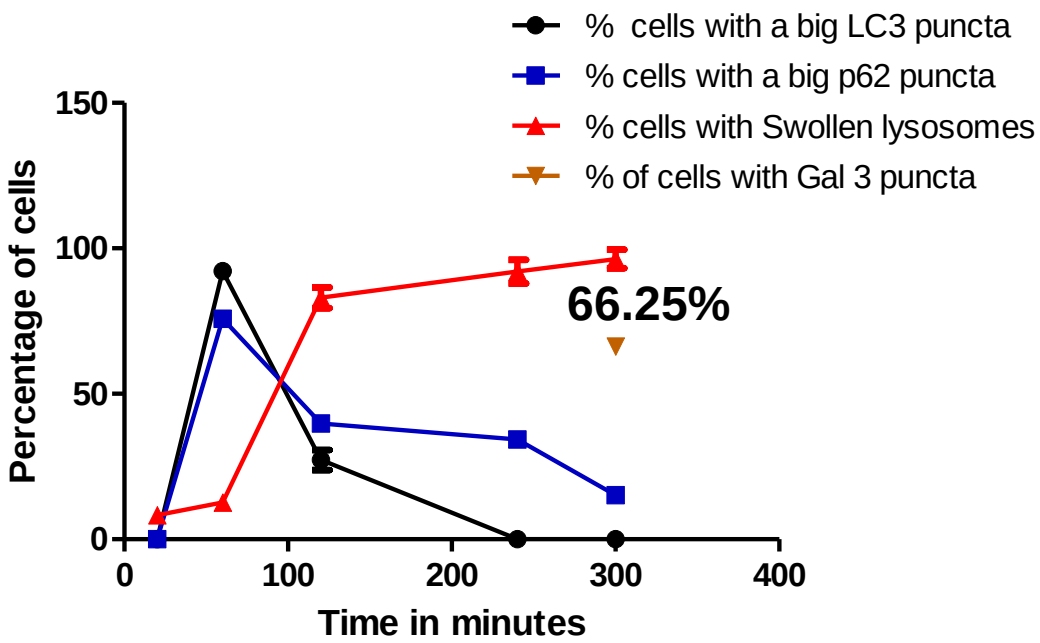

(B) Autophagy with *Staphylococcus aureus*

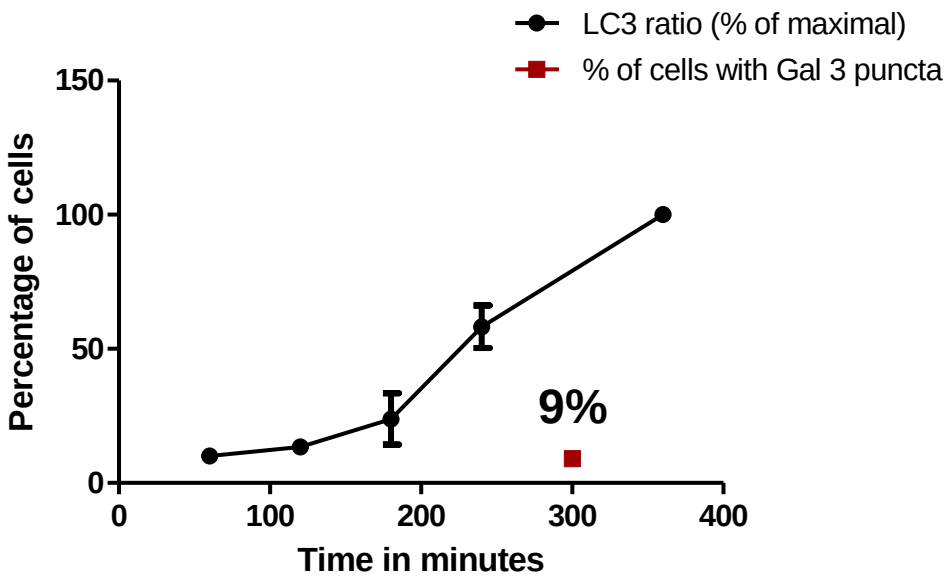

Figure 3.27: Summary of the results of autophagy following infection with *Salmonella enterica* sv. Typhimurium and *Staphylococcus aureus.*

A) The percentage of cells with LC3 and p62 puncta increased following infection with *Salmonella typhimurium* for 1 hour. After 1 hour this percentage reduced over time. However, at 20 minutes and 1 hour post infection, there were relatively few swollen *Salmonella* containing LAMP-2 membranes. However, very clearly, by 2 hours post infection there was a drastic increase. At 5 hours post infection, 66.25% of cells which were infected by *Salmonella* had Gal3 puncta.

B) *Staphylococcus aureu*s strongly induced LC3 lipidation following the first 3 to 4 hours of infection in HeLa cells, and LC3 accumulation increased over time. At 5 hours post infection, just 9% of cells which were infected by *Staphylococcus aureus* had Gal3 puncta.

Chapter 4

The development of ULK1 inhibitors as a novel MRSA infection fighting drug *in vitro*

4. The development of ULK1 inhibitors as a novel MRSA infection fighting drug *in vitro*

4.1. Introduction

4.1.1. Methicillin-resistant *Staphylococcus aureus* as causes of nosocomial infection globally

Methicillin-resistant *Staphylococcus aureus* (MRSA) is the prominent cause of nosocomial infections globally (Chatterjee and Otto, 2013, Hogea et al., 2014). MRSA can spread into the bloodstream and cause sepsis, which is devastating and attributed as the primary cause for shock and circulatory collapse (Xia et al., 2013). MRSA can also spread to other body parts, such as kidneys, lungs, liver, heart and bone marrow, with severe clinical complications caused by endocarditis, osteomyelitis and urethritis (Haim et al., 2010). MRSA is increasingly becoming difficult to treat because of its resistance to numerous known effective antibiotics. Resistant strains of MRSA coupled with further newly evolved strains account for the high mortality rates amongst the worldwide population (Westling, 2009).

4.1.2. Role of autophagy during *Staphylococcus aureus* infection

Restriction of *Staphylococcus aureus* infection was accomplished in culture previously by using ATG5−/− MEFs and in HeLa cells treated with wortmannin to inhibit autophagy (Schnaith et al., 2007). In addition, other studies reported during the course of this project have also shown that targeting the autophagy pathway can restrict *Staphylococcus aureus* infections. Interestingly, these studies have found that *Staphylococcus aureus* can manipulate and subvert autophagy both *in vitro* and *in vivo* (O'Keeffe et al., 2015, Zhu et al., 2018). Overall, *Staphylococcus aureus* appears to critically require a diversion from the endosomal pathway towards the autophagy pathway for the formation of a niche to enable full infection. Therefore, prevention of autophagosome formation suppresses the pathway leading to the niche, thereby restricting the infection.

Our experiments in chapter two confirmed that MRSA are sequestered by autophagosomes within three hours post infection. Most of the bacteria were found outside lysosomes. This confirmed that MRSA may inhibit phagosome/lysosome fusion and reside in a halted autophagosome pathway in order to prevent contact with lysosomes. Gal3 puncta were not strongly detected post infection by MRSA indicating

little damage to lysosomes, possibly because fusion events with lysosomes were lacking.

Moreover, aggregates of p62 did not directly co-localise with MRSA. They could often be seen just next to the individual bacteria, which suggested that the fraction of MRSA which did not co-localise with lysosomes was not free in the cytoplasm. This further supports the halted autophagy model. Following on from previous findings, we proposed to explore approaches for blocking the autophagy process in order to limit this niche site for replication of MRSA.

4.1.3. Role of ULK1 during *Staphylococcus aureus* infection

As summarised in Chapter 1, ULK1 is a serine/threonine kinase that plays an essential role during the early steps of autophagosome biogenesis (Mizushima, 2010). In addition to standard autophagy, ULK1 complex has been shown to be important for regulating the xenophagy response to restrict *Salmonella* growth in host cells (Kageyama et al., 2011). In infected cells, the ULK1, ATG9L and ATG14L complexes each played a role in directing membrane recruitment to help form the autophagosome around the SCV (Kageyama et al., 2011). Inhibition of autophagy in this case would be expected to allow the infection to progress more strongly.

On the other hand, the involvement of ULK1 in autophagy was also studied with *Brucella abortus* (Starr et al., 2012). *Brucella abortus* is a gram-negative bacterium that causes brucellosis in human beings. It was shown that this pathogen subverts the autophagic machinery in order to survive and replicate in ER-derived *Brucella*-containing vacuoles (BCVs). The initiating factors of autophagosomes, such as Beclin-1 or ULK1 are hijacked by the BCVs and turned into autophagosome-like compartments. BCV formation is readily reduced by the depletion of Beclin-1 or ULK1 and also by autophagy's pharmacological inhibition (class III PI3-kinase inhibitor 3-methyladenine and the PI3-kinase inhibitor LY294002). This study further shows that the ULK1 initiation complex can promote xenophagy that, in this case, helps support *Brucella abortus* infection.

Interestingly, the role of the ULK1 complex in xenophagy following infection with *Staphylococcus aureus* has not been studied. WIPI1, which functions downstream of

the ULK1 and Beclin1-PI3-kinase complexes, has been demonstrated to be involved in *Staphylococcus aureus*-related xenophagy (Mauthe et al., 2012). Invading *Staphylococcus aureus* were shown to become entrapped in autophagosome-like WIPI1 positive vesicles.

Moreover, canonical autophagy is involved in xenophagy subsequent to gram-positive bacterial infection. This was shown recently by work which identified c-di-AMP as a vita-PAMP that induces STING dependent endoplasmic reticulum (ER) stress to protect mice against gram-positive bacterial infection. This pathway leads to inactivation of mTOR and induces canonical autophagy. Furthermore, induced autophagy resolves ER stress by removing damaged membranes, a process termed ER-phagy (Moretti et al., 2017). Targeting key autophagy proteins such as ULK1, FIP200, and ATG14 (as part of the canonical Beclin 1 complex) in macrophages impaired LC3 lipidation. Interestingly, the *Staphylococcus aureus* strain MSSA (ATCC) was one of the gram-positive bacteria used in this study to establish this mechanism (Moretti et al., 2017).

Recently, a number of ULK1 kinase inhibitors that block autophagy have been developed (Egan et al., 2015, Petherick et al., 2015, Lazarus and Shokat, 2015). This brings the field nearer to targeting this pathway as a therapeutic method. Interestingly, Petherick et al. (2015) described MRT68921, a strong inhibitor of both ULK1 and ULK2. MRT68921 showed a 15-fold decrease in IC50 for ULK1 (2.9 nM) and an almost 30-fold reduction for ULK2 (1.1 nM), as compared with a related compound MRT67307 (IC50 values of 45 and 38nM, respectively, for ULK1 and ULK2). These authors found MRT68921 to have a strong effect in inhibiting ULK1 and ULK2 *in vitro* activity and blocking mTOR-dependent autophagy in cells. Moreover, a small molecule inhibitor of ULK1, SBI-0206965, blocked phosphorylation of ULK1-dependent phospho-sites in BECN1 and VPS34 (Egan et al., 2015). This compound also selectively hindered the activity of endogenous ULK1 kinase *in vivo*. Although the therapeutic possibilities of these compounds clinically still needs a considerable amount of work to appreciate their clinical capacity, use of ULK1 kinase inhibitors as a novel therapeutic method appears closer.

4.1.4. Hypothesis and aims

The ULK1/2 complex plays an essential role during the early steps of autophagosome formation. We explored approaches for targeting the ULK1 initiation complex with genetic methods or kinase inhibitors in an attempt to reduce the cell killing by MRSA. This goal may help lead to the development of ULK1 inhibitors as drugs to fight MRSA infection in medical applications. Targeting ULK1 would be predicted to prevent formation of double-membrane autophagosomes and prevent *Staphylococcus aureus* niche formation.

The aims of this chapter are:

1- To employ genetic approaches utilising RNAi-mediated gene silencing as well as CRISPR-Cas9 gene editing to target ULK1 and its co-factor, ATG13, in order to restrict Staphylococcal infections in HEK293A and HeLa cells.
2- To use ULK1/2 kinase inhibitors in order to block double-membrane autophagosome formation as a way of preventing Staphylococcal replication and restrict infection.

4.2. Results

4.2.1. Investigation of the involvement of ATG13 in xenophagy following infection by *Salmonella enterica* sv. Typhimurium and *Staphylococcus aureus*

It has been demonstrated that *Staphylococcus aureus* become entrapped in autophagosome-like WIPI1 positive vesicles after infection (Mauthe et al., 2012). To ascertain whether the ULK1 kinase complex is directly involved in the formation of a double-membrane autophagosome following infection by MRSA, we studied the formation of the ATG13 puncta structure. Thus, stable GFP-ATG13/HeLa cells were produced. For additional confirmation, ATG13 antibodies were also used to stain the HeLa cells infected by these different pathogens. As a control, untreated cells or cells starved by EBSS were first studied to show the basal level of ATG13 structures present in uninfected cells, which increased in number and size when the cells were starved by EBSS to induce a standard autophagy response (Figure 4.1).

Firstly, to investigate the involvement of ATG13 in xenophagy, HeLa cells were infected with GFP expressing *Salmonella enterica* sv. Typhimurium (using the *Salmonella* protocol) and then stained with anti-ATG13 antibody. One clear result was that large-sized ATG13 structures formed following infection with clear co-localisation between ATG13 and the invading bacteria (Figure 4.2). This result therefore demonstrates the recruitment of the ULK1/ATG13 complex to membranes around *Salmonella enterica* sv. Typhimurium. This result was then confirmed in the GFP-ATG13/HeLa cells infected by *Salmonella enterica* sv. Typhimurium stained with Hoechst DNA staining (data not shown).

To examine whether ATG13 was involved in the formation of autophagosomes following infection by MRSA (NCTC8325), GFP-ATG13/ HeLa cells were infected with 100 MOI of NCTC8325. Figure 4.3 shows large puncta of ATG13 surrounding MRSA bacteria. This result raised the possibility that ATG13 plays a role during MRSA (NCTC8325) infection. These results together suggested that the ULK1 kinase complex may play essential roles in the formation of double-membrane autophagosomes in xenophagy following infection by either MRSA or *Salmonella enterica* sv. Typhimurium.

To further study ULK1 complex membrane translocation, we quantified numbers of ATG13 puncta. Untreated cells showed a low level of GFP-ATG13 puncta. Within one hour's incubation with EBSS starvation media there was a strong increase in GFP-ATG13 positive structures, as expected for a typical autophagy response. Next, we tested infection with the different pathogens. Surprisingly, the number of GFP-ATG13 puncta was higher when the cells were infected with *Salmonella enterica* sv. Typhimurium as compared with cells infected by MRSA (NCTC8325). This difference may be due to the difference in the time of incubation for different pathogens (Figure 4.4).

According to our results in chapter 2, *Staphylococcus aureus* was able to strongly induce LC3 lipidation as a marker of autophagy following the first 3–4 hours of infection in HeLa cells. However, *Salmonella enterica* sv. Typhimurium was clearly co-localised with the LC3 membrane in HeLa cells by the first hour of infection. Thus, these different pathogens were incubated in different time periods in our experiments: three hours or one hour for *Staphylococcus aureus* and *Salmonella enterica* sv. Typhimurium, respectively.

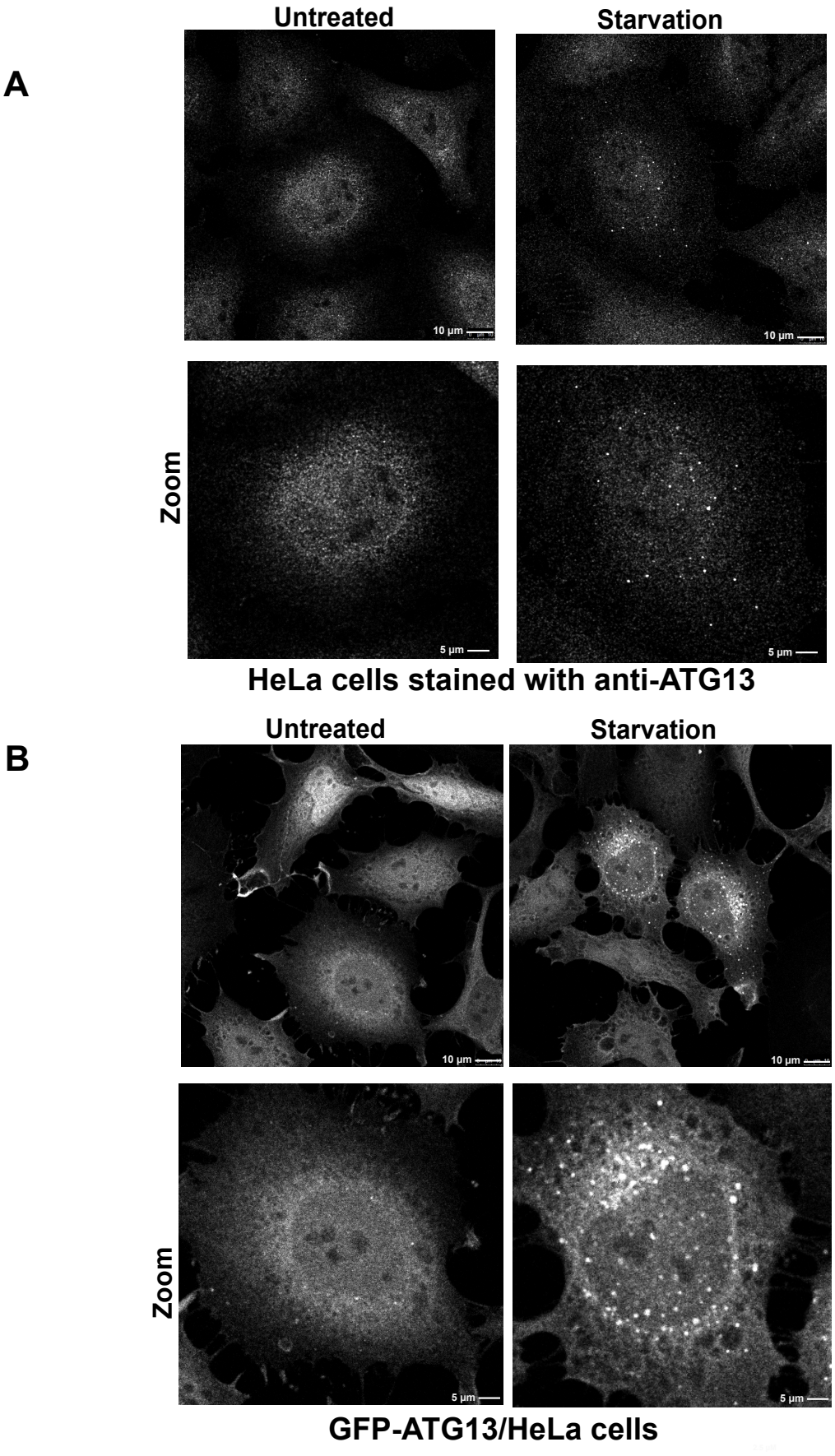

Figure 4.1: Formation of ATG13-labelled autophagosomes in HeLa cells following starvation.

(A) HeLa cells were plated on glass coverslips and then left untreated or starved with EBSS for 1hr. Cell were then fixed and stained with anti-ATG13 and observed by confocal microscopy. Scale bar: 10 & 5 µm.

(B) Stable GFP-ATG13/HeLa cells were plated on glass coverslips then left untreated or starved with EBSS for 1hr. Then fixed and observed by confocal microscopy. Scale bar: 10 &5 µm.

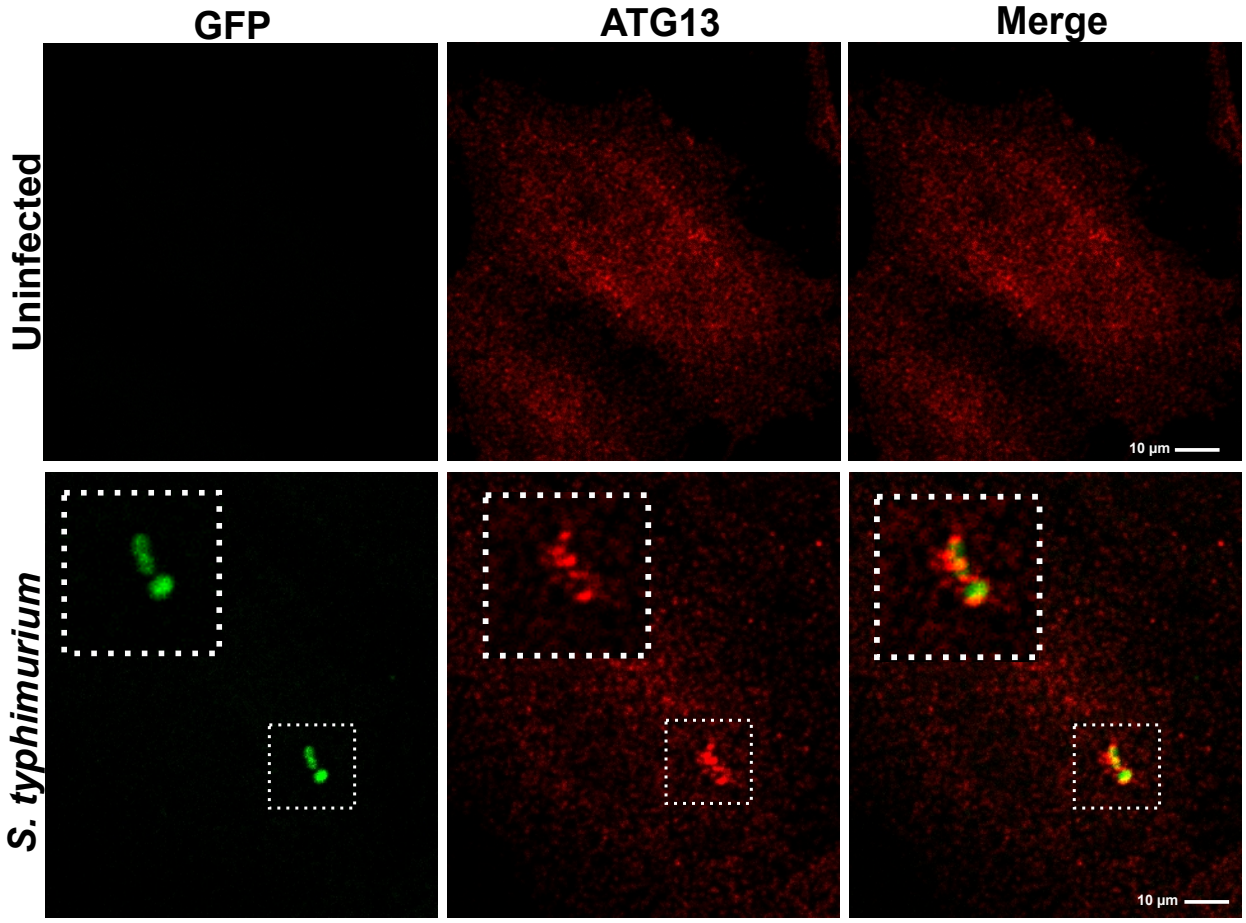

Figure 4.2: Large sized ATG13 structures formed following infection with *Salmonella enterica* sv. Typhimurium with clear co-localization. HeLa cells were plated on glass coverslips and then infected with GFP expressing *Salmonella enterica* sv. Typhimurium at 1:100 MOI via the " *Salmonella* protocol" and then incubated at 37^{O}C for 1hr (gentamicin added after 50 min. of infection). Cells were fixed and stained with ATG13 Ab. Cells were observed by confocal microscopy. Scale bar: 10 µm.

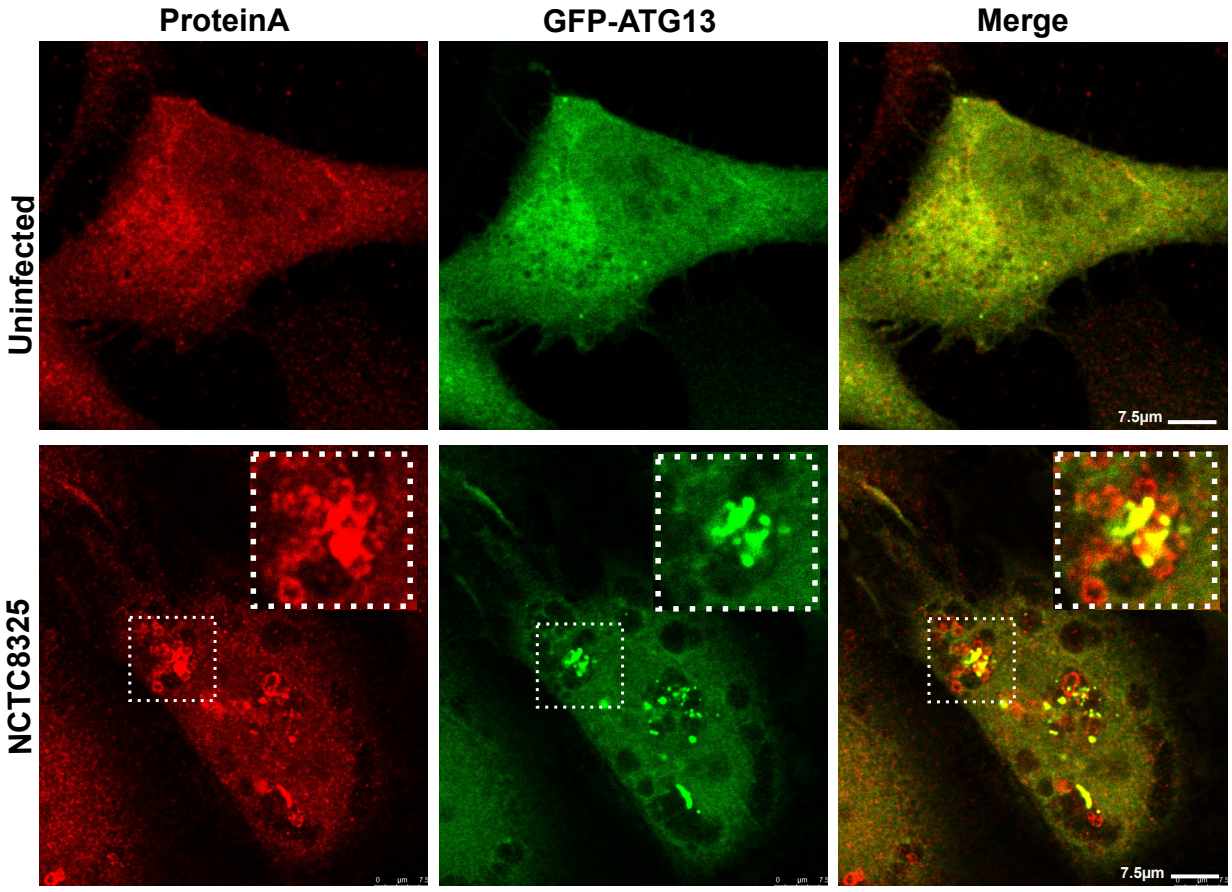

Figure 4.3: Large sized ATG13 structures formed following infection with MRSA with clear co-localization. Stable GFP-ATG13/HeLa cells were plated on glass coverslips and then infected with NCTC8325 at 100 MOI and incubated for 3hr at 37^{O}C (gentamicin added after one hour of infection). Cell were then fixed and stained with protein A antibody. Cells were observed by confocal microscopy. Scale bar: 10 µm.

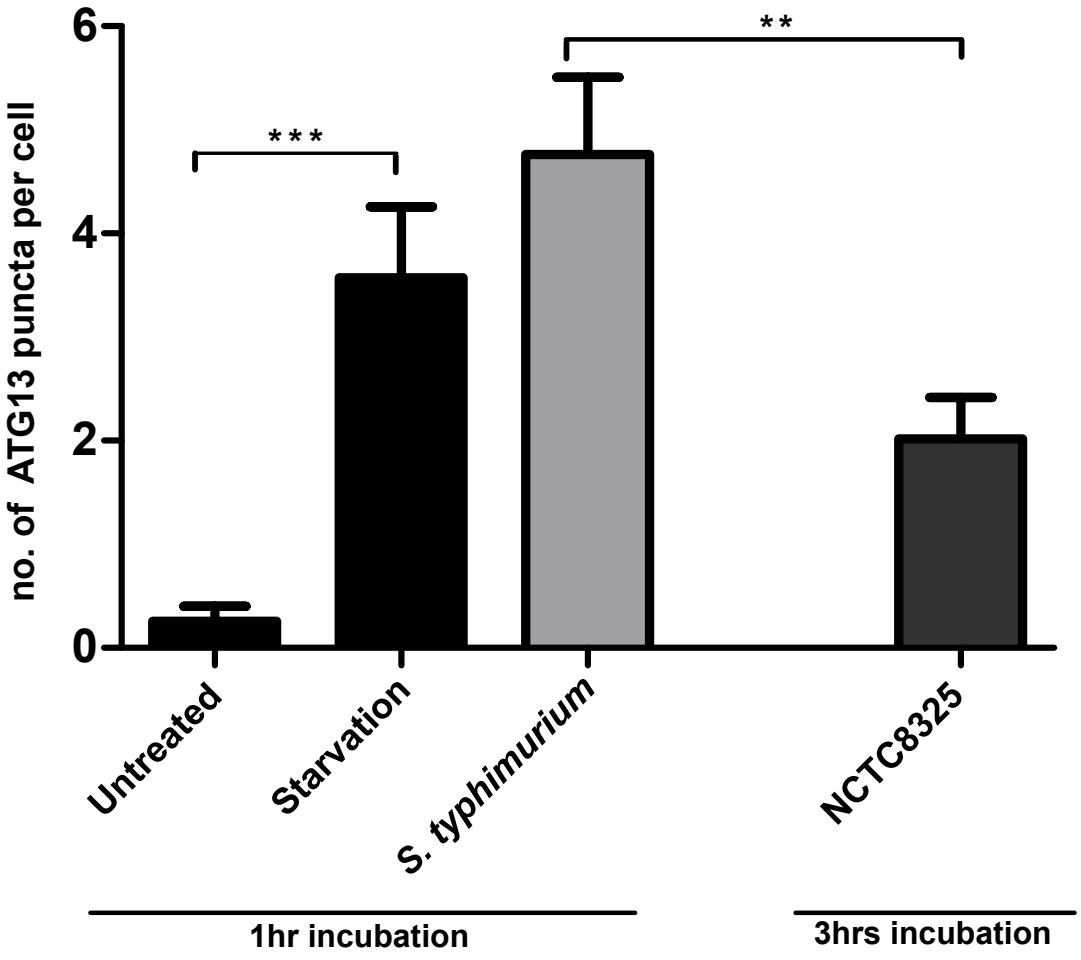

Figure 4.4: ATG13 puncta accumulate following infection with *Salmonella enterica* sv. Typhimurium. Stable GFP-ATG13/HeLa cells were plated on glass coverslips then left untreated, starved with EBSS (1hr), infected with *Salmonella enterica* sv. Typhimurium at 1:100 MOI for 1hr via the "*Salmonella* protocol" or infected with 100 MOI of NCTC8325 for 3hrs via the "*Staphylococcus* protocol". Cells were then fixed and stained with DAPI. The number of ATG13 puncta was counted from 50 infected cells captured by epifluorescence microscopy. Fifty infected cells were captured from different fields for three coverslips and the average of three independent experiments ± SD is shown. P value from one-way ANOVA with Tukey multiple comparison test (**P<0.01, ***P<0.001).

4.2.2. Investigation of the role of the ULK1 complex in xenophagy via gene targeting

4.2.2.1. Investigation of the role of ULK1 in autophagy

After establishing the localisation of the ULK1/ATG13 complex on membranes around MRSA, we then wished to determine if this autophagy pathway is essential for *Staphylococcus aureus* induced cell death. We first used several genetic approaches based on RNAi-mediated gene silencing, as well as the CRISPR gene editing tool, to target ULK1 and its required binding protein ATG13.

Based on our past work, the role of ULK1 is crucial for autophagy, as RNAi-mediated suppression of ULK1 alone could inhibit autophagy in certain cell lines (Chan et al., 2007). Thus, before starting our study of xenophagy, we sought to confirm targeting of ULK1 in our cell systems. ULK1 function was blocked by using shRNA or CRISPR-Cas9, both in HEK293A and HeLa cells. We worked with cell pools generated after transduction with CRISPR-Cas9 or shRNA lentivirus leading to a heterogeneous population. In HEK293A, the shRNA for ULK1 (previously reported by Egan et al., 2011, details in Methods chapter) showed good levels of protein knockdown. By comparison, CRISPR-Cas9 mediated targeting led to even lower ULK1 levels (more efficient targeting).

As a control, amino acid starvation using EBSS and bafilomycin A1 was used to test autophagic flux through LC3-II accumulation. We found that decreasing ULK1 protein using both shRNA and CRISPR inhibited autophagy as shown by the decreased amount of conversion from LC3-I to LC3-II, especially in the bafilomycin condition (Figure 4.5A). Interestingly, the shRNA for ULK1 showed slightly better functional inhibition.

In HeLa, the shRNA for ULK1 showed a better level of protein knockdown as compared to CRISPR-Cas9 mediated targeting (Figure 4.5B). Surprisingly, we found that the strong decrease of ULK1 protein using shRNA did not clearly inhibit the autophagy function. In contrast, in HeLa, the mild loss of ULK1 protein using CRISPR led to better blocking of LC3-II accumulation.

Collectively, these results together confirm that ULK1 is crucial for autophagy in these cell types. Loss of ULK1 occurred but the efficiency of the shRNA and CRISPR-Cas9 vectors depends on cell type. The correlation of ULK1 protein loss and blocking of autophagy is also cell type dependent.

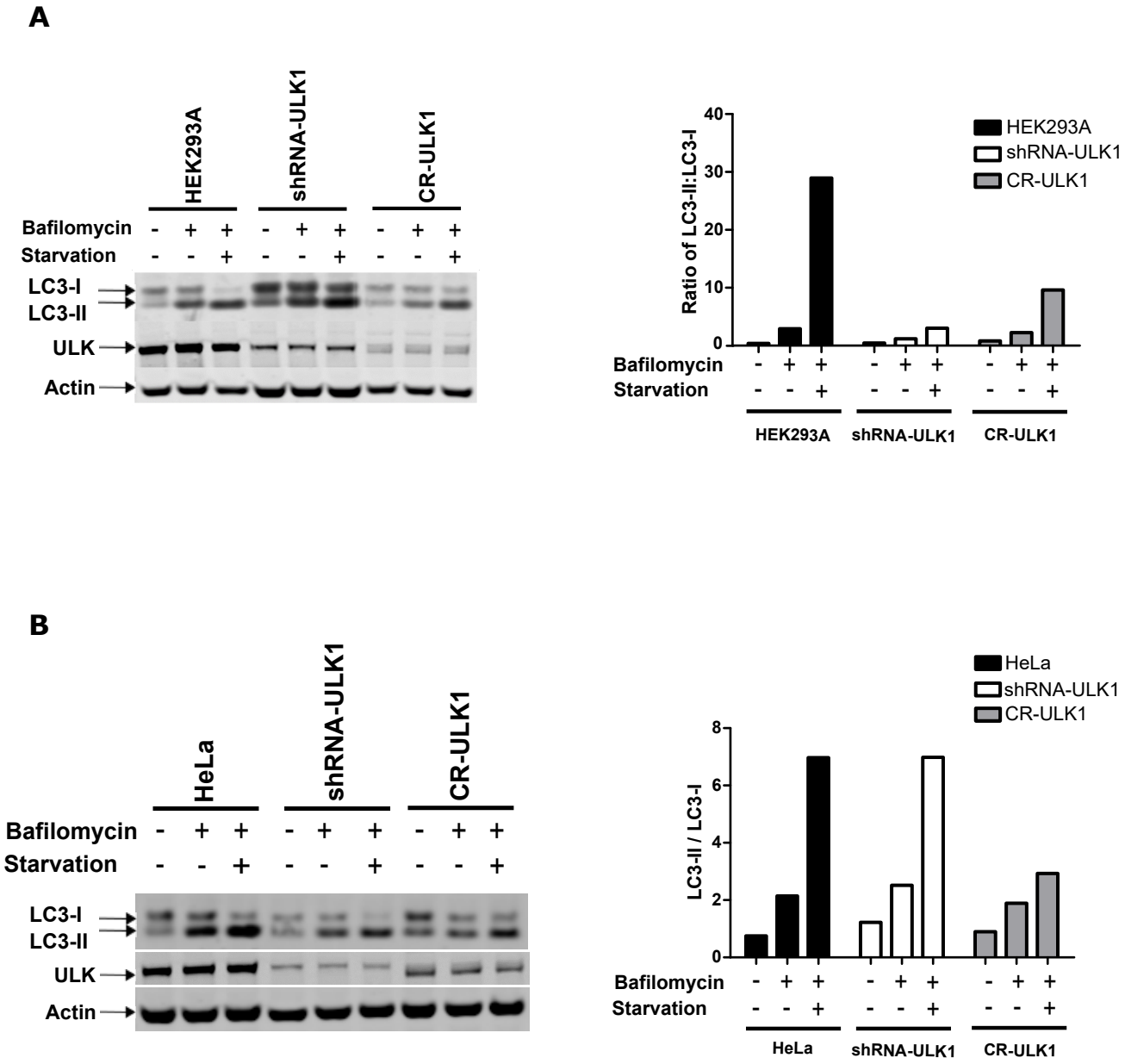

Figure 4.5: Blocking ULK1 inhibited autophagy in HEK293A and HeLa cells. ULK1 was targeted in HEK293A (A) and HeLa (B) cells using shRNA-mediated gene silencing or CRISPR-Cas9 knockout. As control amino acid starvation using EBSS and 10 nM bafilomycin was used. Western blot was used to detect autophagy function through analysis of LC3-II accumulation.

4.2.2.2. Investigation of the role of ULK1 in xenophagy following infection by *Staphylococcus aureus* and *Salmonella enterica* sv. Typhimurium via gene targeting

The ULK1 kinase complex co-localises around *Salmonella enterica* sv. Typhimurium and was important to restrict the infection by this pathogen (Kageyama et al., 2011). In order to establish the role of the ULK complex in xenophagy following infection by MRSA, we used shRNA and the CRISPR editing tool to target ULK1.

Since shRNA and CRISPR-Cas9 for ULK1 gave mixed results in HeLa cells, we further tested these (Figure 4.6A). Again, shRNA for ULK1 showed greater levels of protein loss as compared to CRISPR-Cas9. In terms of function, the shRNA led to a better block of amino acid starvation and bafilomycin A1. Importantly, ULK1 shRNA showed a good block of LC3-II accumulation produced by infection with MRSA.

To ascertain the role of the ULK in xenophagy following infection by MRSA, HeLa ULK1 shRNA cells were infected with MRSA (NCTC8325) and further incubated for 72 hours. We found that the cell destruction was inhibited following infection by MRSA at MOI 100 and 200 but not with 500 MOI (Figure 4.6B).

In comparison with *Salmonella enterica* sv. Typhimurium infection, we found that these cells became very sensitive to destruction by this pathogen (Figure 4.6C), thus indicating the role of autophagy in providing a protective niche for MRSA, and, on the other hand, providing a mechanism to fight infection by *Salmonella enterica* sv. Typhimurium.

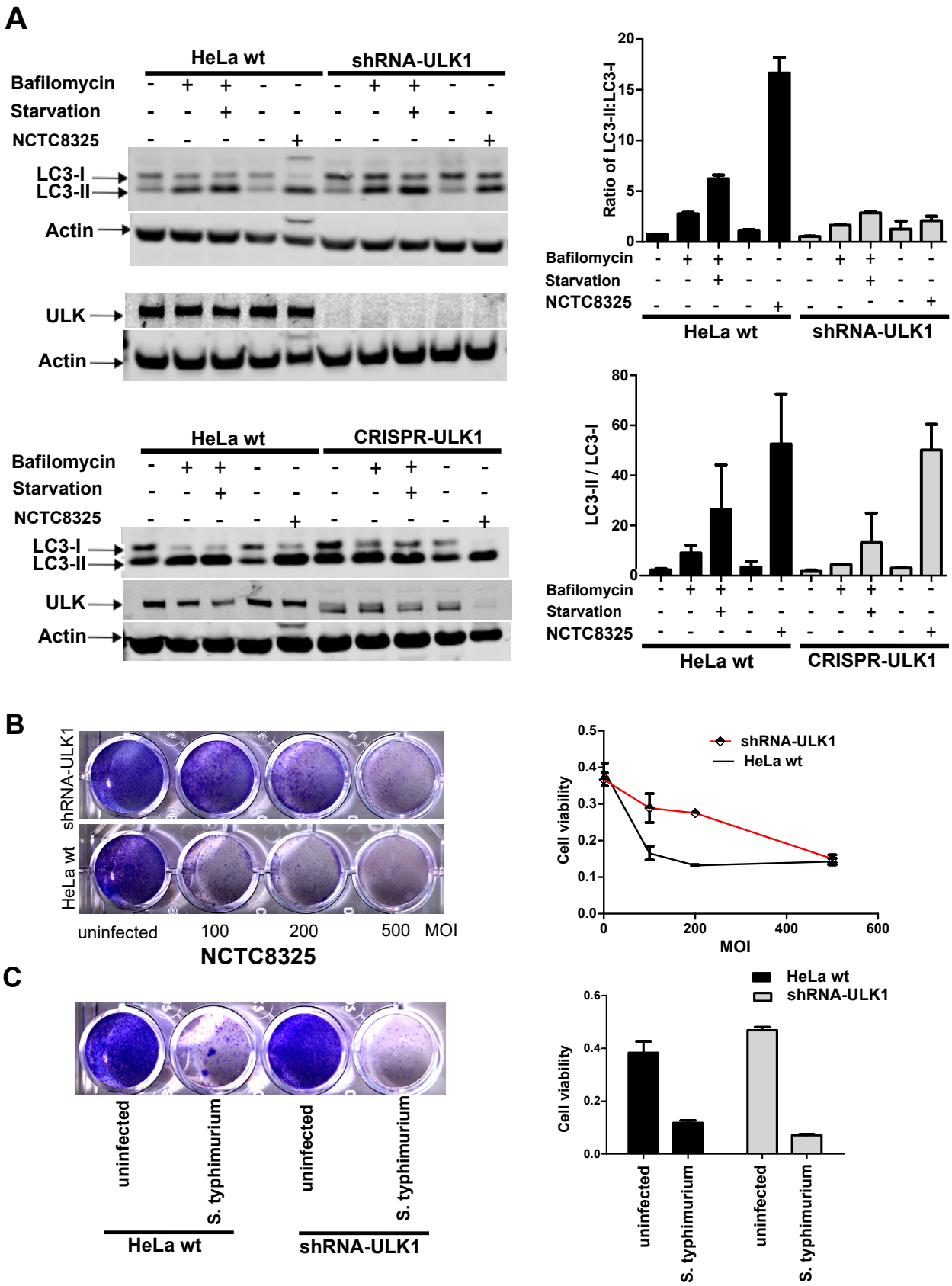

Figure 4.6: ULK1 targeting inhibited cell killing following infection with MRSA and sensitised killing by *Salmonella enterica* sv. Typhimurium. (A) ULK1 was blocked in HeLa cells using shRNA-mediated gene silencing or CRISPR knockout. As control amino acid starvation using EBSS and bafilomycin was used. Western blot was used to detect autophagy function through analysis of LC3-II accumulation. (B) HeLa cells with knockdown in ULK1 were seeded and infected with NCTC8325 at 100, 200, and 500 MOI. Then after 1hr of infection, gentamicin (0.05 mg/ml) was added. Cells were then incubated 72hrs. (C) HeLa cells with ULK1 knockdown were seeded and infected with *Salmonella enterica* sv. Typhimurium at 1:100 MOI. After 50 min.of infection, gentamicin (0.05 mg/ml) was added. Cells were then incubated 72hrs. Cells were fixed, stained with Giemsa and quantified. The average from 3 samples ± SD is shown .

4.2.2.3. Investigation of the role of ATG13 in autophagy

ULK1 in cells appears to be constitutively in complex with ATG13, FIP200, and ATG101 (Mizushima, 2010). Through analysis by siRNA experiments (Hosokawa et al., 2009, Jung et al., 2009), it was found that ATG13 is essential for the autophagy function and is needed for ULK1 localisation to the isolation membrane (Ganley et al., 2009).

After establishing the role of ULK1 in xenophagy, we sought to further identify the role of ATG13 in this process. Firstly, ATG13 was targeted using CRISPR in HEK293A cells (Figure 4.7). We handled cell pools that are produced when the cells are transduced with CRISPR-Cas9. This process led to the development of a heterogeneous population. CRISPR-CAS9 succeeded in strongly reducing ATG13 levels. As a control, amino acid starvation using EBSS and bafilomycin was included in this experiment to enable autophagic flux measurement.

In the control cells, treatment of full nutrient media with bafilomycin showed some increase in LC3-II accumulation level (Lane 1 vs. 2). Control cells under amino acid starvation resulted in a robust increase in bafilomycin-dependent LC3-II levels as expected, indicating autophagy induction (Lane 3). However, CRISPR ATG13 cells showed strongly reduced LC3-II levels in all conditions (Lane 4, 5 and 6). This confirms that CRISPR ATG13 cells are deficient in inducing autophagy. This indicated the important role of ATG13 protein in autophagy and that ATG13 is a prerequisite for autophagy.

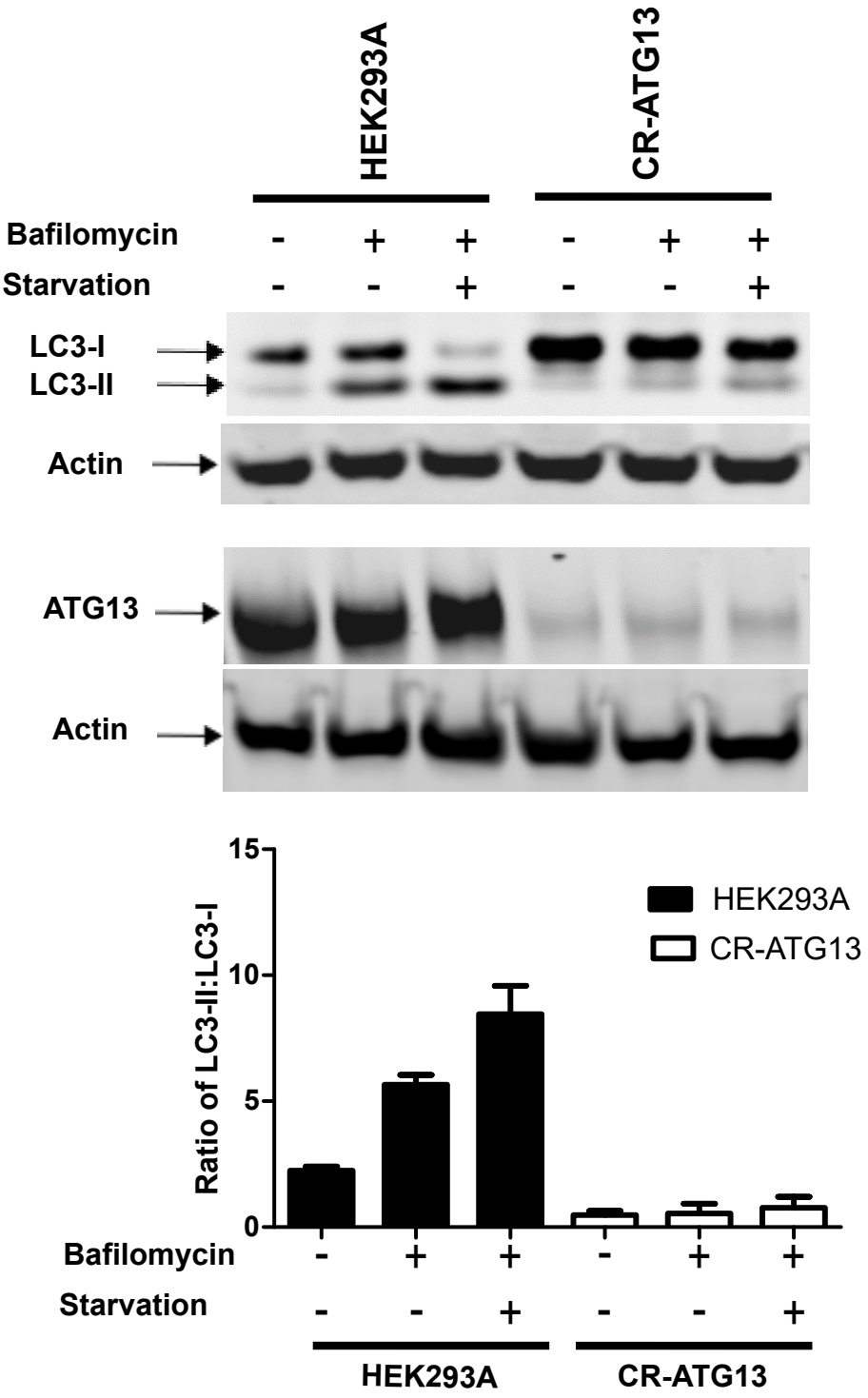

Figure 4.7: Targeting ATG13 inhibited autophagy in HEK293A cells. ATG13 was targeted in HEK293A cells using CRISPR-Cas9 knockout. As control amino acid starvation using EBSS and 10 nM bafilomycin was used. Western blot was used to detect autophagy function through analysis of LC3-II accumulation.

4.2.2.4. Investigation of the role of ATG13 in xenophagy following infection by *Staphylococcus aureus* and *Salmonella enterica* sv. Typhimurium via a gene targeting approach

Based on the strong immunoblot result, CRISPR of ATG13 was further confirmed by the inhibition of autophagy by imaging, through counting the LC3 puncta with starvation conditions.

In an independent line, CRISPR-Cas9 for ATG13 again showed a good level of protein loss (Figure 4.8A). Control HEK293A cells (untreated) showed a low basal level of LC3 positive membrane structures dispersed in the cytoplasm. However, LC3 puncta accumulated following amino acid starvation in wild type HEK293A cells. LC3 puncta size and staining intensity all greatly increased, indicating autophagy induction. In contrast, in ATG13 knockout HEK293A cells, LC3 puncta were inhibited following amino acid starvation, indicating autophagy inhibition (Figure 4.8A). Inhibition of LC3 puncta when blocking ATG13 using CRISPR confirmed that ATG13 is indispensable for autophagy.

To assess the role of the ATG13 in xenophagy following infection with *Staphylococcus aureus* or *Salmonella enterica* sv. Typhimurium, CRISPR targeted cells were then infected with MRSA (NCTC8325) for 72 hours or *Salmonella enterica* sv. Typhimurium for 24 or 48 hours in the presence of gentamicin. CRISPR targeting of ATG13 in HEK293A gave clear resistance to the cells following infection by MRSA (NCTC8325) (Figure 4.8B). On the other hand, as expected, these cells became more sensitive to destruction by *Salmonella enterica* sv. Typhimurium (Figure 4.8C). This further indicated that traffic of *Staphylococcus aureus* into the autophagosomal pathway is required for *Staphylococcus aureus* toxicity. However, restricting infection by *Salmonella enterica* sv. Typhimurium required autophagy. Lastly, CRISPR targeting of ATG13 was effective in affecting these two xenophagy pathways.

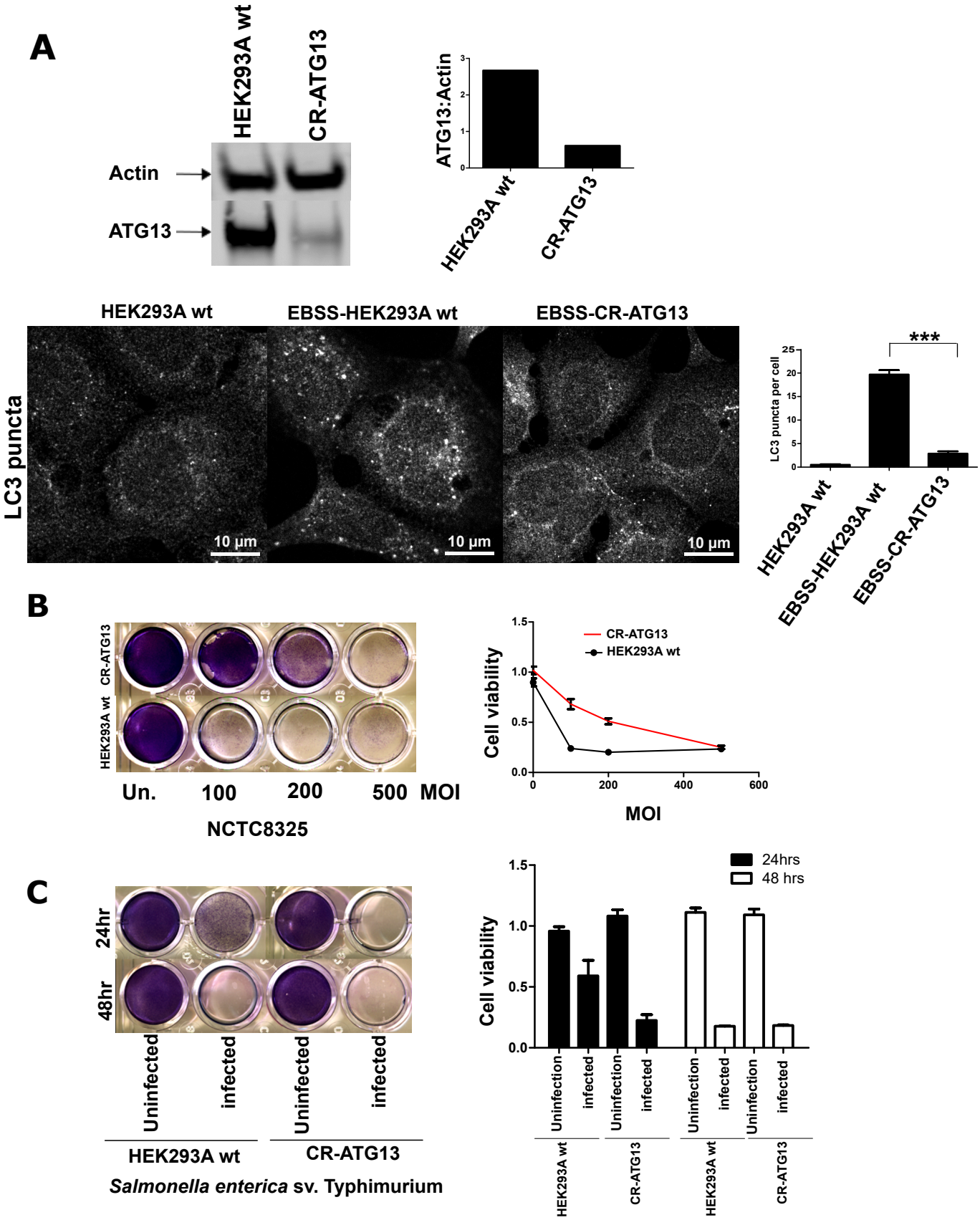

Figure 4.8: ATG13 targeting inhibited cell killing following infection with MRSA and sensitised killing by *Salmonella enterica* sv. Typhimurium. (A) ATG13 was blocked in HEK293A cells using CRISPR. Western blot was used to confirm the knouckout. Imaging was used to detect autophagy through counting LC3 puncta with or without starvation condition. (B) HEK293A cells with knockout in ATG13 were seeded and infected with NCTC8325 at 100, 200 and 500 MOI. Then after 1hr of infection, gentamicin (0.05 mg/ml) was added. Cells were then incubated 72hrs. (C) HEK293A cells with knockout in ATG13 were seeded and infected with *Salmonella enterica* sv. Typhimurium at 1:100 MOI. After 50 min. of infection, gentamicin (0.05 mg/ml) was added. Cells were then incubated 24 or 48hrs. Cells were fixed, stained with Giemsa and quantified. The average from 3 samples ± SD is shown .

4.2.3. The development of ULK1 inhibitors as a novel MRSA infection fighting drug *in vitro*

Restriction of *Staphylococcus aureus* infection was accomplished previously by using wortmannin, an autophagy inhibitor at 50–200 nM concentration (Schnaith et al., 2007). However, this drug was very toxic for the cells and cannot be developed as a therapeutic.

Above, we established the role of the ULK1 kinase complex in reducing cell killing following infection by MRSA. We then wished to examine the development of ULK1 inhibitors as a novel MRSA infection fighting approach.

Several ULK1 inhibitors have recently been developed that block autophagy, for example, MRT68921 and SBI-0206965, bringing the field closer towards targeting this pathway as a therapeutic (Egan et al., 2015, Petherick et al., 2015, Lazarus and Shokat, 2015). Therefore, we tested ULK1 inhibitors including the published MRT68921, and three other unpublished MRT analogues (MRT216403, MRT239016 and MRT238993) obtained from the Medical Research Council Technology/Life Arc (see Methods chapter). The three MRT analogues were produced with the objective of minimising the off-target effects, and as a result of that increasing their precision in inhibiting ULK1. The KS1 drug compound #6, developed by Kevan Shokat and co-workers, (in (Lazarus and Shokat, 2015) as well as SBI-0206965 (Egan et al., 2015) were synthesised in collaboration with Professor. N. Tomkinson from the University of Strathclyde Department of Pure and Applied Chemistry.

4.2.3.1. Pharmacological inhibition of ULK1 inhibited cell killing following infection by *Staphylococcus aureus*

After establishing the role of ULK1 in reducing cell killing via gene targeting, we next wished to investigate the role of ULK1-dependent autophagy using inhibitors. HEK293A were treated with different MRT inhibitors at a high (10 μM) or low (1μM) concentration, and then infected by NCTC8325 *Staphylococcus aureus*. After 48 hours, the presence of any living cells was quantified. It was observed that treating cells with MRT68921 strongly inhibited cell destruction. Interestingly, a low concentration of this inhibitor gives much more resistant cells as compared with high

concentrations. We suggest that the 1 µM concentration was less toxic for cells (in this longer-term experiment) compared with 10 µM (Figure 4.9).

Treatment with the SBI-0206965 inhibitor also gave some resistance, using either a high or low concentration, but the effects were not as strong compared with MRT68921 (Figure 4.9).

Then, we wished to investigate the role of ULK1 during the process of infection using other unpublished MRT analogues (MRT216403, MRT239016 and MRT238993). Interestingly, MRT216403, MRT238993 and MRT239016 (Figure 4.10) with low (1 µM) concentrations did not give strong resistance as compared with high (10 µM) concentrations. This dose dependence suggested that these derivative compounds had less activity at 1 µM to block xenophagy.

Overall, our results in this section demonstrated that we can use ULK1 inhibitors to block xenophagy and improve cell survival during *Staphylococcus aureus* infection.

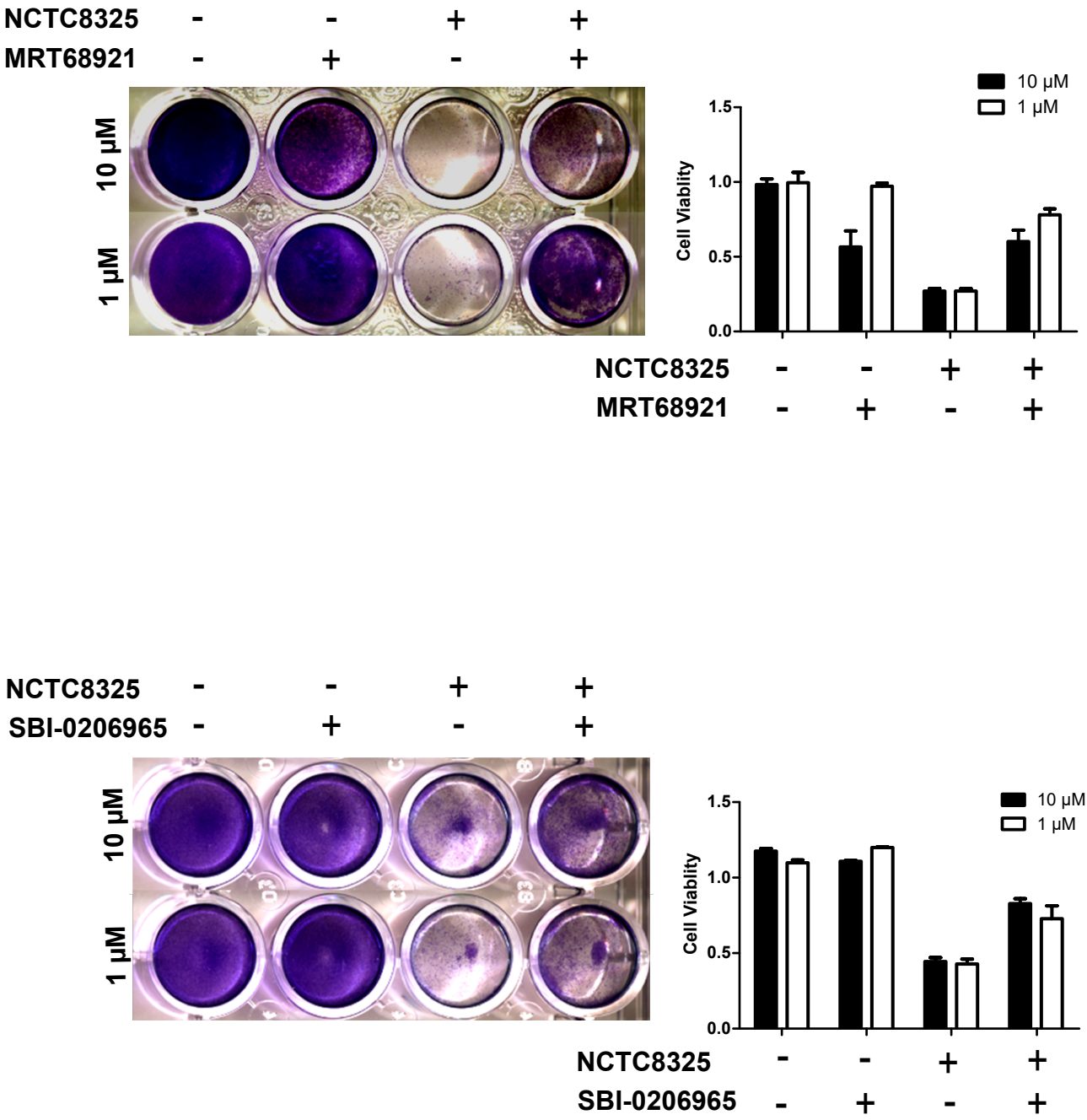

Figure 4.9: ULK1 inhibitors inhibited cell killing following infection with MRSA. HEK293A cells were seeded and infected with NCTC8325 at 200 MOI. At the point of infection, the ULK1 inhibitors were added with 1 µM or 10 µM concentration. After 1hr of infection, gentamicin (0.05 mg/ml) was added and cells were then incubated for 48hrs. Cells were fixed, stained and quantified. The average from 3 samples ± SD is shown.

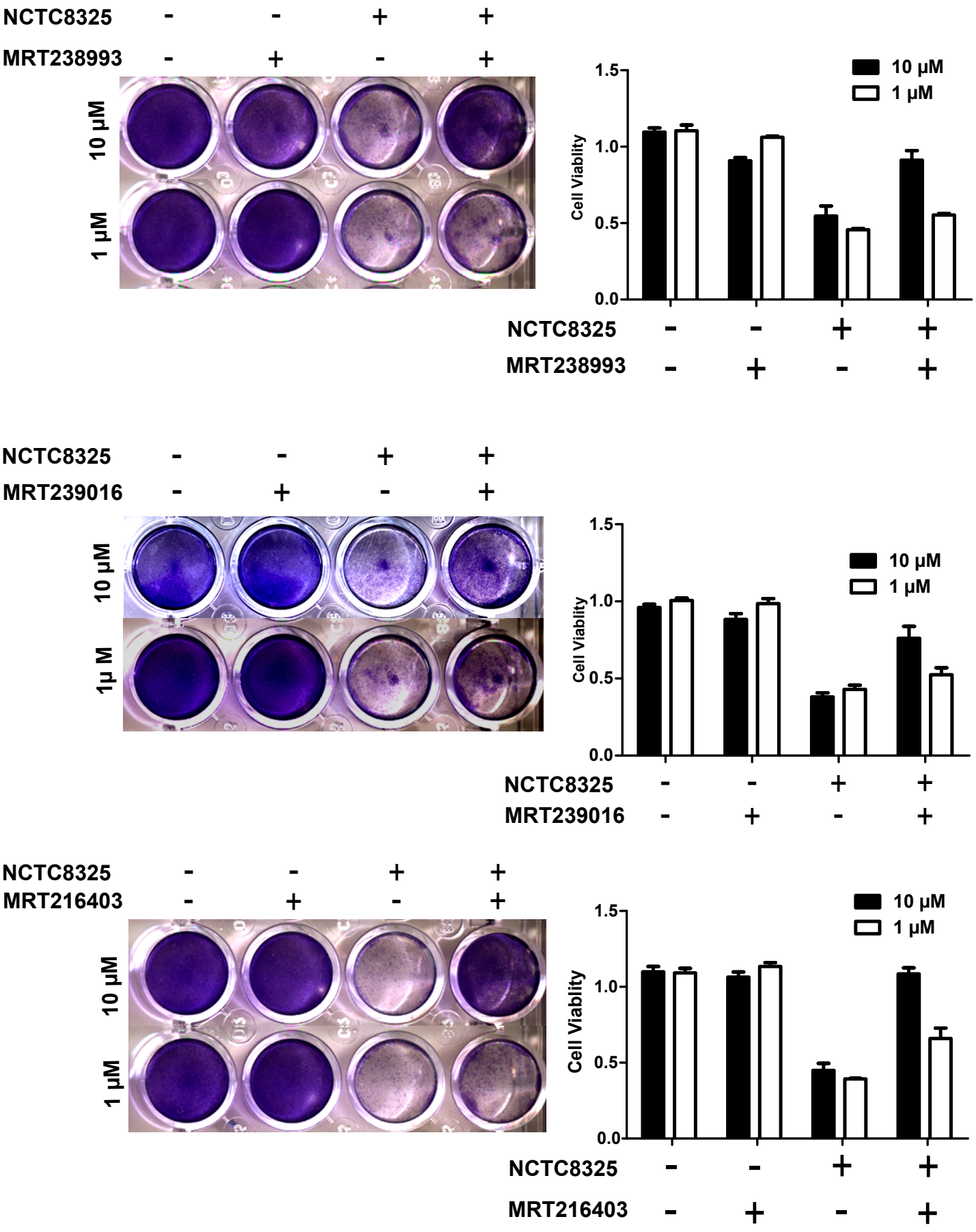

Figure 4.10: ULK1 inhibitors inhibited cell killing following infection with MRSA. HEK293A cells were seeded and infected with NCTC8325 at 200 MOI. At the point of infection, the ULK1 inhibitors were added with 1 µM or 10 µM concentration. After 1hr of infection, gentamicin (0.05 mg/ml) was added and cells were then incubated for 48hrs. Cells were fixed, stained and quantified. The average from 3 samples ± SD is shown.

4.2.3.2. Inhibitors of ULK1 do not block MRSA or *Salmonella enterica* sv. Typhimurium growth *in vitro*

After establishing the role of different ULK1 inhibitors in reducing cell killing following infection by MRSA, we wanted to confirm that ULK1 inhibitors do not directly affect the bacteria (Figure 4.11). Overnight liquid bacterial cultures were diluted (1:100) plus different ULK1 kinase inhibitors and monitored for ability to replicate at 37°C. As a control, parallel bacteria cultures were left to grow without any drugs. From this experiment, we found that none of the ULK1 inhibitors affected *Staphylococcus or Salmonella* growth. To compare, we used gentamicin as a positive control, which fully inhibited growth. This experiment indicated that ULK1 inhibitors do not affect the growth of both bacterial types studied in this thesis.

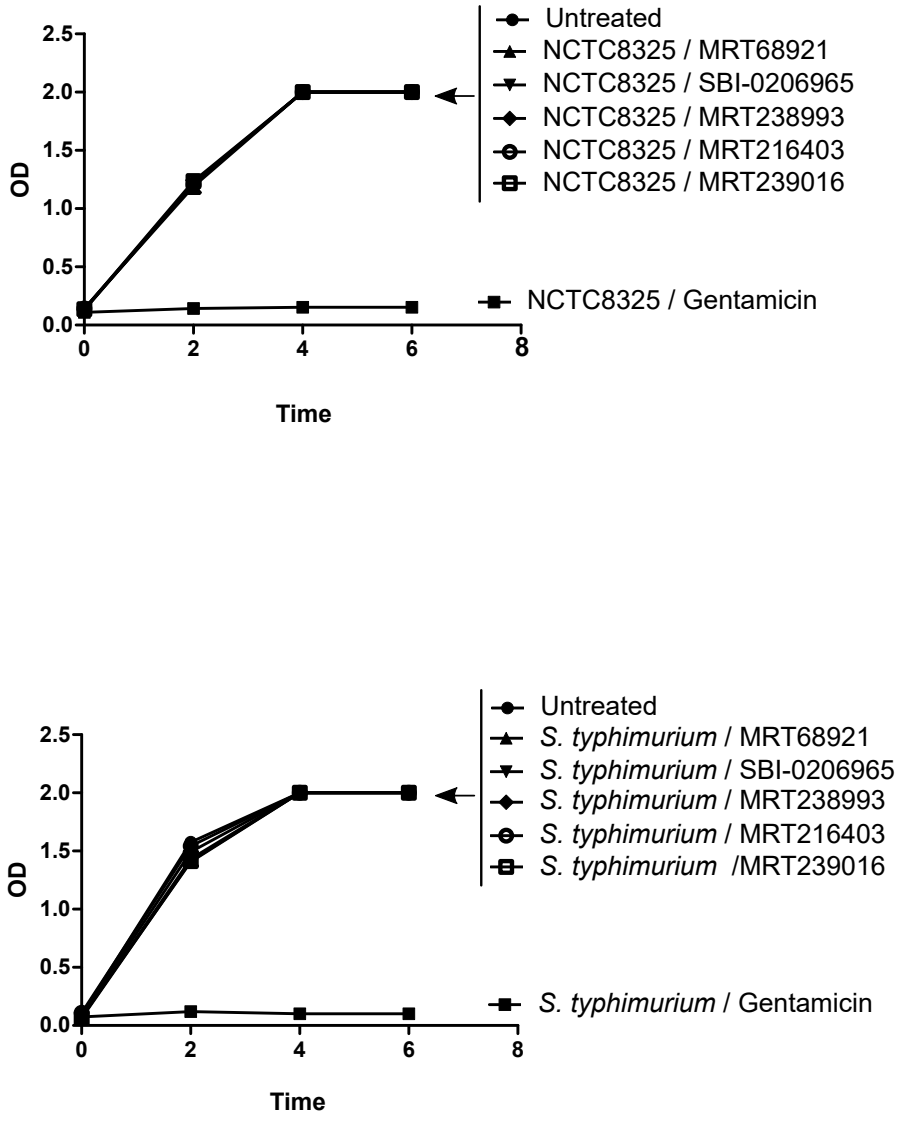

Figure 4.11: Growing MRSA or *Salmonella enterica* sv. Typhimurium in the presence ULK1 inhibitors. NCTC8325 or *Salmonella enterica* sv. Typhimurium were grown overnight and then each strain was diluted at 1:100 for growth time-course test with or without presence of different ULK1 inhibitors (10 μM) or gentamicin (0.05 mg/ml). The optical density (OD) 600 nm was read at various time points following incubation at 37^{O}C.

4.2.3.3. Pharmacological inhibition of ULK1 made cells more sensitive to *Salmonella enterica* sv. Typhimurium

After finding that the different ULK1 inhibitors change cell survival following MRSA infection, we next wished to investigate the role of these inhibitors during *Salmonella enterica* sv. Typhimurium infection. HEK293A were seeded with high confluence (about 60%) and treated with different MRT inhibitors at a high (10 µM) concentration, and then infected by *Salmonella enterica* sv. Typhimurium. After 24 hours the presence of any living cells was quantified.

ULK1 complex has been shown previously to be important for regulating the xenophagy response to restrict *Salmonella* growth in host cells (Kageyama et al., 2011). Thus, as expected, it was observed that ULK1/2 inhibition (blocking autophagy) made the cells more sensitive to cell death following infection by *Salmonella enterica* sv. Typhimurium (Figure 4.12). This indicated that the xenophagy was inhibited when the cells were treated with these ULK1 kinase inhibitors.

Therefore, using the ULK1 inhibitors, we can see the role of xenophagy in providing a protective niche for MRSA; on the other hand, xenophagy provided a mechanism to fight infection by *Salmonella enterica* sv. Typhimurium.

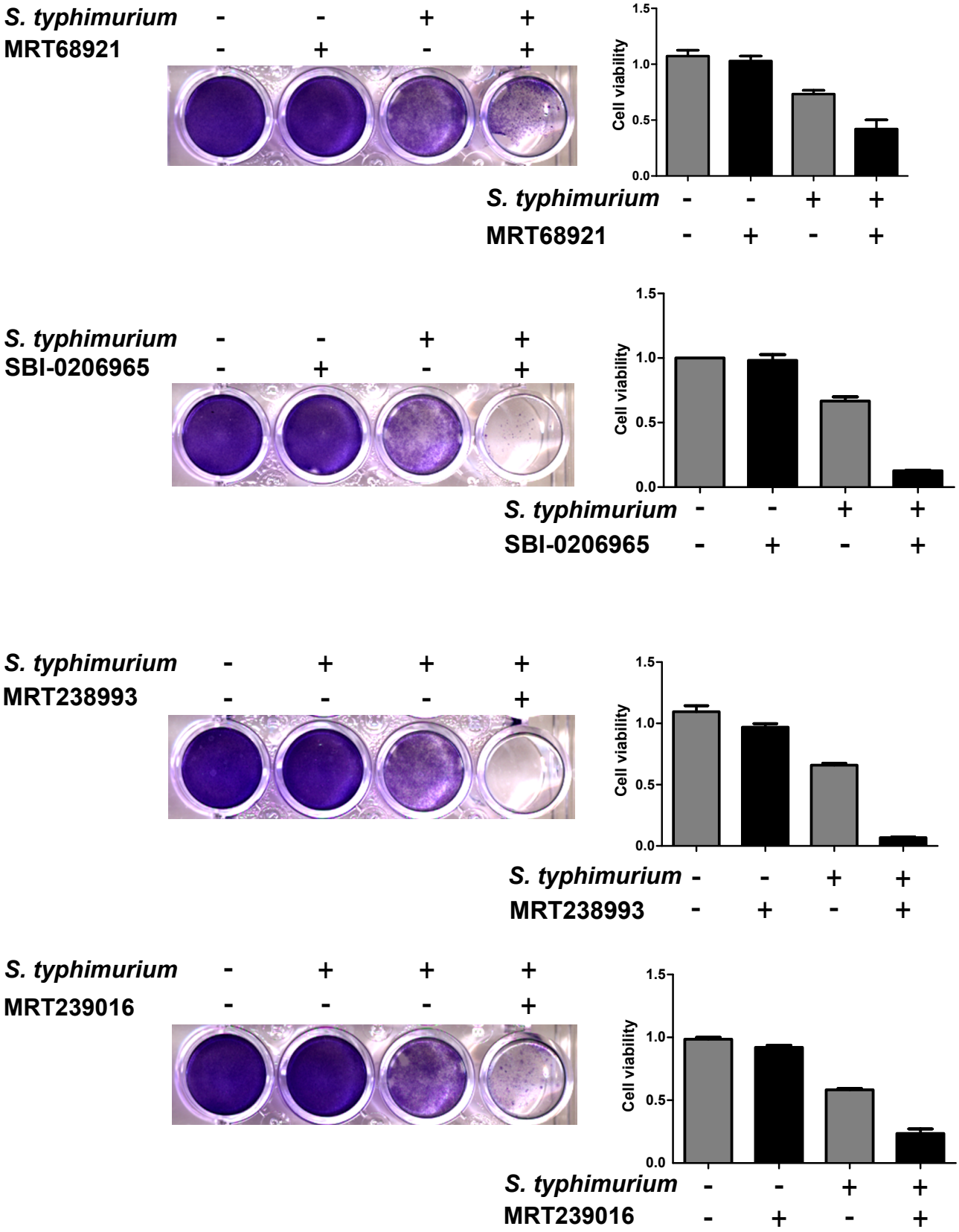

Figure 4.12: The sensitivity of HEK293A cells to be killed by *Salmonella enterica* sv. Typhimurium in the presence ULK1 inhibitors. HEK293A cells were seeded and infected with *Salmonella enterica* sv. Typhimurium at 1:100 MOI. At the point of infection, the ULK1 inhibitors were added. After 50 min. of infection, gentamicin (0.05 mg/ml) was added and cells were then incubated 24hrs. Cells were fixed, stained with Giemsa and quantified. The average from 3 samples ± SD is shown.

4.2.3.4. Pharmacological inhibition of ULK1 blocks autophagy

After establishing the role of different ULK1 inhibitors in reducing cell killing following infection, we then wanted to know how these inhibitors affect autophagy. At first, SBI-0206965, KS1 and MRT68921 drugs were tested at 10 µM concentration to block the function of ULK1 and amino acid starvation-stimulated autophagic flux. Autophagy was detected using western blot detection of LC3-II accumulation. Figure 4.13 shows that control cells untreated in full nutrient media without bafilomycin showed no LC3-II accumulation (Lane 1). Basal LC3-II accumulation was detected upon treatment with bafilomycin (Lane 2). However, further amino acid starvation resulted in a robust increase in bafilomycin-dependent LC3-II levels (and increased LC3 lipidation ratio), as expected (Lane 3), indicating autophagy induction. The three ULK1 inhibitors all significantly decreased bafilomycin-dependent LC3-II lipidation under amino acid starvation. However, MRT68921 was the strongest compared with the other two ULK1 inhibitors (SBI-0206965 and KS1).

Our data therefore confirmed that these different ULK1 inhibitors all have the ability to obstruct autophagy.

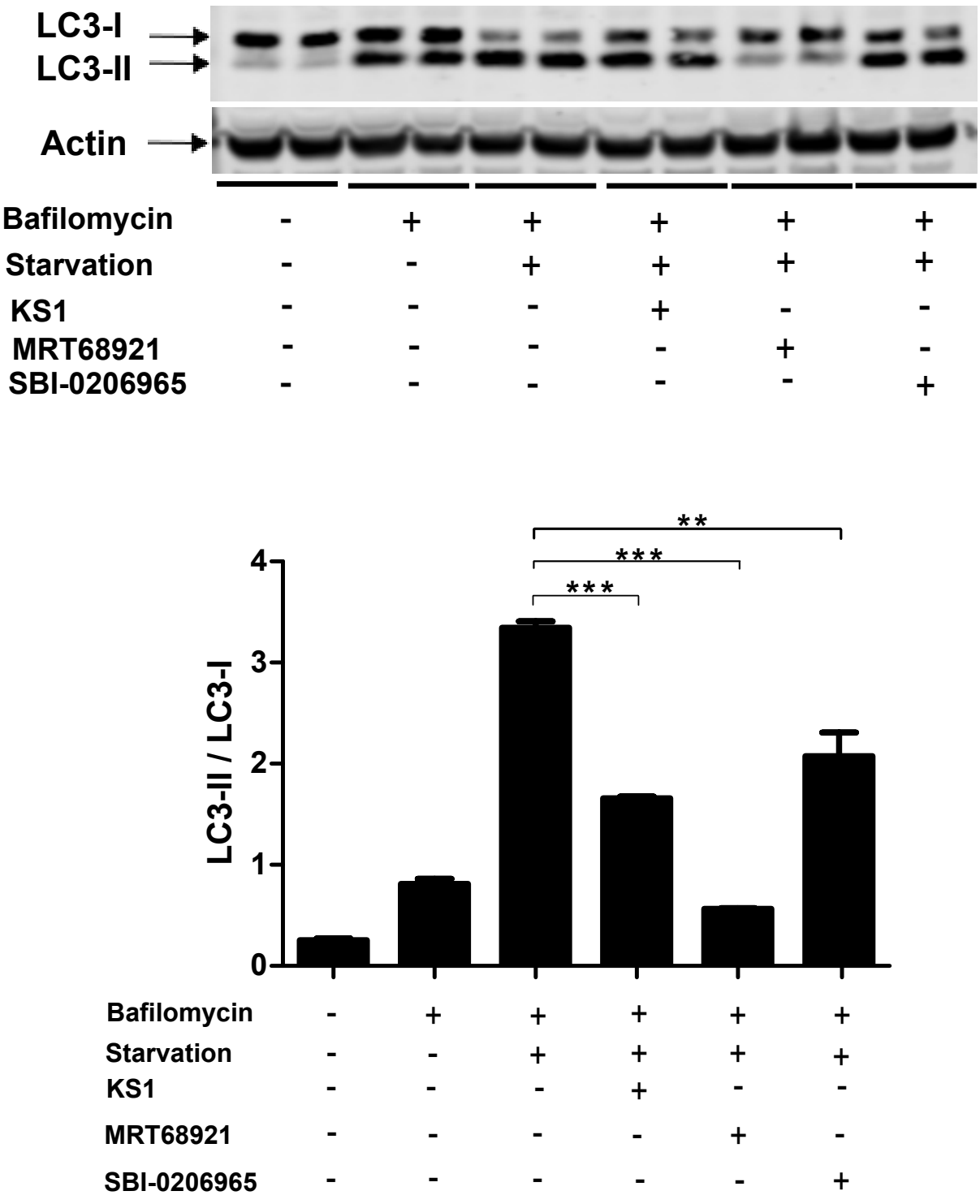

Figure 4.13: ULK1 inhibitors blocked starvation-induced autophagy. HEK293A cells were incubated in EBSS for 2hrs in the presence or absence, KS1, MRT68921 or SBI-0206965 at 10 μM, and 10 nM bafilomycin as indicated. Cell lysates were resolved by NUPAGE gel electrophoresis and the proteins were probed with anti-LC3 antibody. Activation of autophagy pathway was detected by calculating the ratio of LC3-II / LC3-I. The average from 4 samples ± SD is shown. P value from one-way ANOVA with Tukey multiple comparison test.

4.2.3.5. Novel ULK1 inhibitors did not strongly block autophagy

After establishing, in the previous experiment, the levels of autophagy inhibition, we next wanted to test the panel of novel MRT ULK1 inhibitors. For this, MRT216403, MRT239016 and MRT238993 were tested in comparison with MRT68921. Drugs were selected to be tested at 10 μM concentration to block amino acid-starvation stimulated autophagic flux detected by LC3-II accumulation. In Figure 4.14, we again confirmed as a control that bafilomycin alone in the presence of full nutrient led to a basal increase in LC3-II levels (lane 1 vs. 2). Amino acid starvation resulted in a robust increase in bafilomycin-dependent LC3-II levels (Lane 3). As expected, ULK1 inhibitor MRT68921 significantly decreased bafilomycin-dependent LC3-II lipidation (under amino acid starvation conditions). Interestingly, the other three MRT analogues, (MRT216403, MRT239016, or MRT238993) did not decrease the LC3-II accumulation level to similar levels. Therefore, these novel MRT derivatives were not able to strongly inhibit amino acid dependent autophagy in this particular system. Therefore, further work is needed to characterise the activity of these compounds in other autophagy settings.

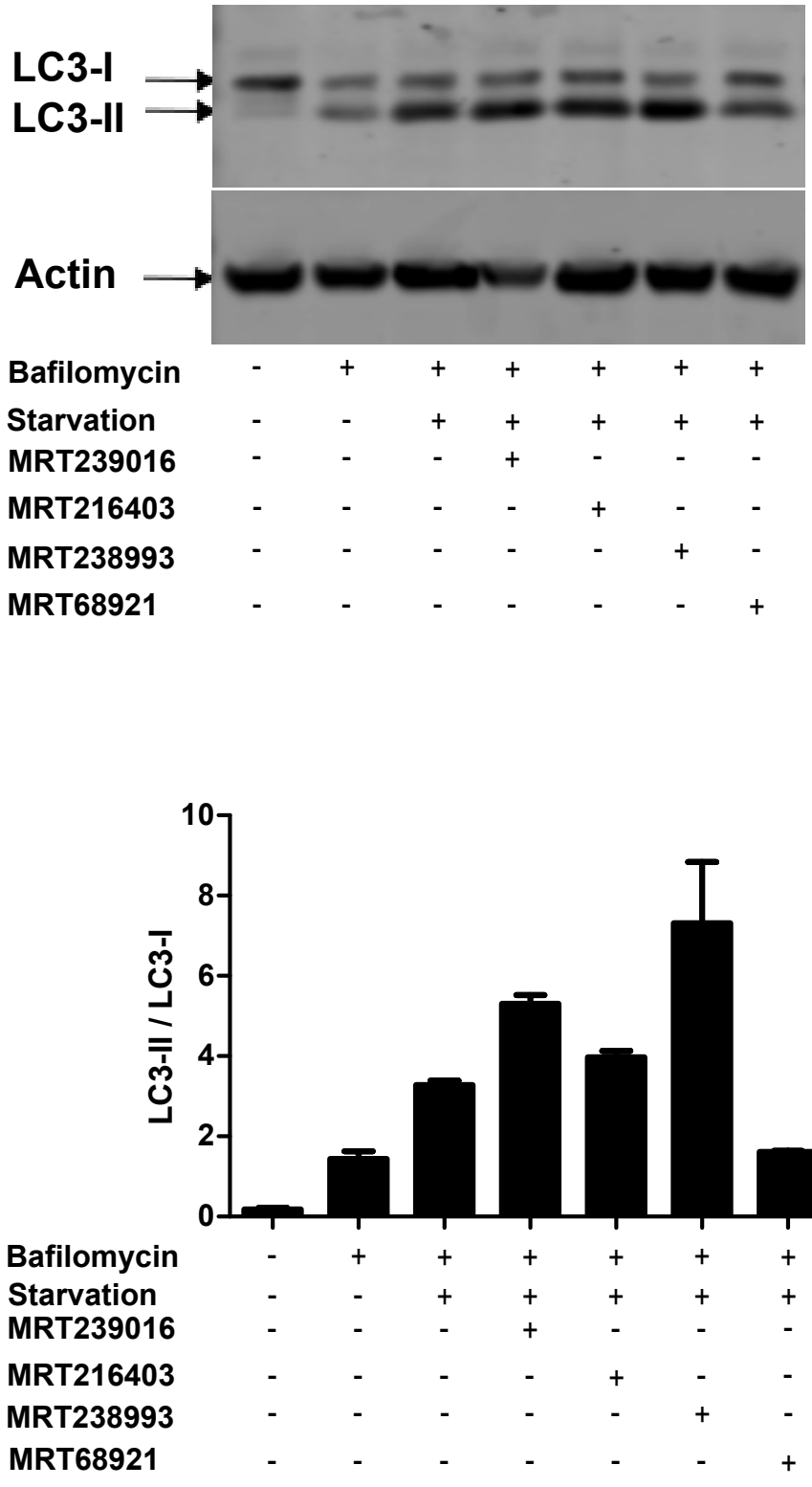

Figure 4.14: MRT68921 but not MRT239016, MRT216403 or MRT238993 ULK1 inhibitors blocked starvation-induced autophagy. HEK293A cells were incubated in EBSS for 2hr in the presence or absence of MRT239016, MRT216403, MRT238993, or MRT68921 and 10 nM bafilomycin as indicated. Cell lysates were resolved by NUPAGE gel electrophoresis and the proteins were probed with anti-LC3 antibody. Activation of autophagy pathway was detected by calculating the ratio of LC3-II / LC3-I. The average from 4 samples ± SD is shown.

4.2.3.6. Pharmacological inhibition of ULK1 blocks LC3 puncta formation

After establishing that SBI-0206965 and MRT68921 drugs have the ability to obstruct autophagy, we further this confirmed using imaging. Untreated control cells showed a basal level of LC3 positive membrane structures dispersed in the cytoplasm with low numbers (Figure 4.15). The number, size, and staining intensity of LC3 all greatly increased when the cells were starved by EBSS, indicating clear autophagy induction. However, treatment with ULK1 kinase inhibitors (MRT68921 and SBI-0206965) under amino acid starvation resulted in a significantly decreased number of LC3 puncta, indicating autophagy inhibition. Again, MRT68921 was stronger than SBI-0206965 in blocking LC3 puncta. Our data indicated that these two different ULK1 inhibitors have the ability to obstruct autophagy but to different levels.

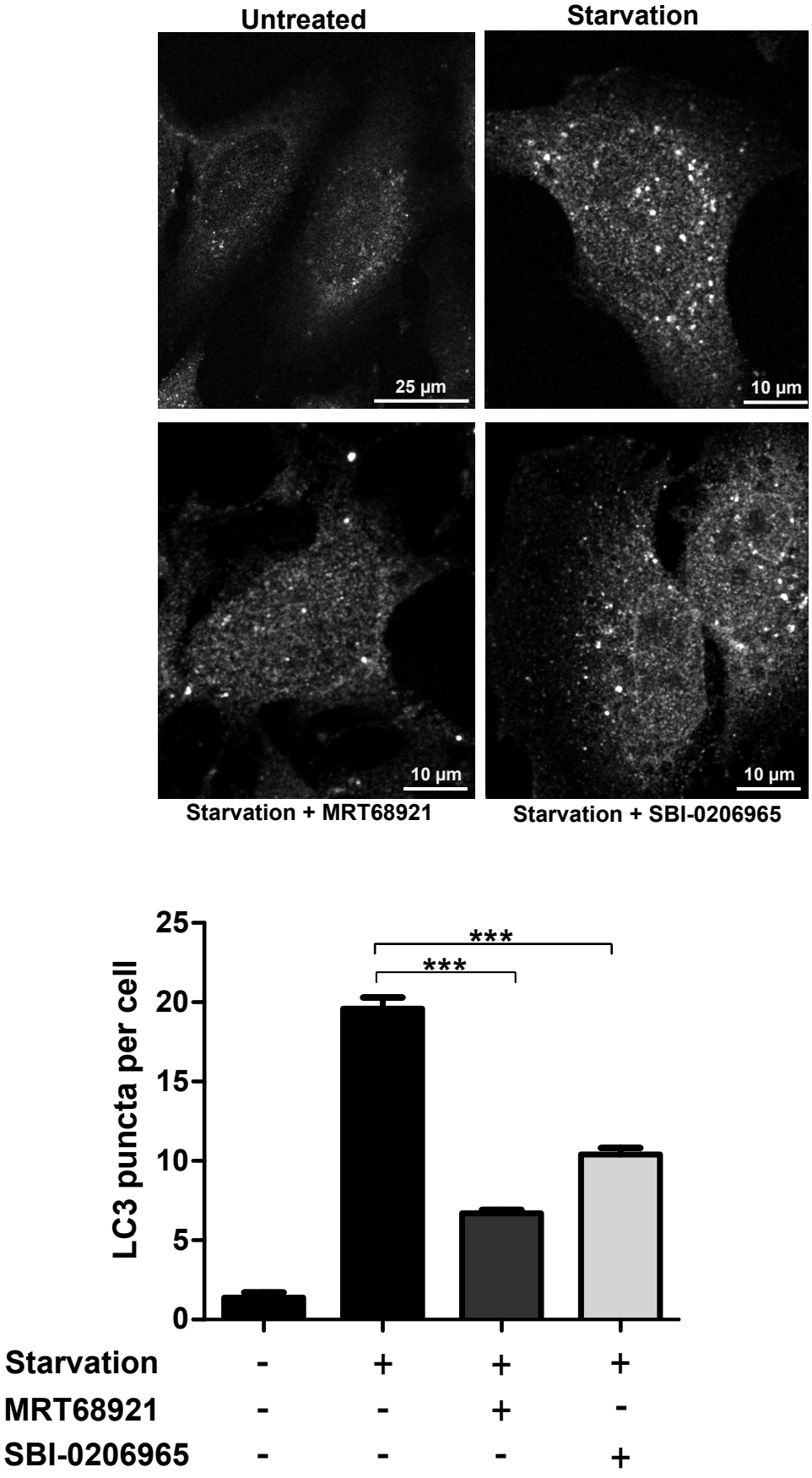

Figure 4.15: ULK1 inhibitors blocked starvation-induced autophagy. HeLa cells were plated on glass coverslips then incubated in EBSS for 2hrs in the presence or absence of MRT68921, or SBI-0206965 (10 μM). Cells were then fixed and stained with anti-LC3 antibody. LC3 puncta were counted under an epifluorescent microscope and then cells observed by confocal microscopy. Scale bar: 10 μm.

4.2.3.7. Pharmacological inhibition of ULK1 inhibited formation of p62-positive aggregate structures

The inhibition of p62 membrane structures in the presence of different ULK1 inhibitors was next tested. In order to do this, stable GFP-p62/HeLa cells (untreated or treated with MRT68921 or SBI-0206965), were infected by NCTC8325. After three hours' infection, the numbers of large GFP-p62 structures increased. However, treatment with MRT68921 reduced the formation of p62-positive large aggregate structures. In this case, we could still detect smaller-sized p62 puncta without any associated MRSA. On the other hand, treatment with SBI-0206965 decreased both the large p62-positive aggregate and smaller p62 structures (Figure 4.16).

To further study p62 aggregate membrane structures, we quantified the numbers of these large puncta. We found that p62-positive aggregate structures significantly decreased when cells were treated with either MRT68921 or SBI-0206965 inhibitors. This result suggested the inhibition of xenophagy following infection by MRSA by these compounds. An interesting observation was the clear aggregation of MRSA in association with big p62 membrane structures around the nuclear membrane. Treatment with inhibitors led to decreased bacterial aggregates. This result further suggested that blocking autophagy by these inhibitors inhibited the bacterial niche for replication and perhaps improved lysosomal clearance.

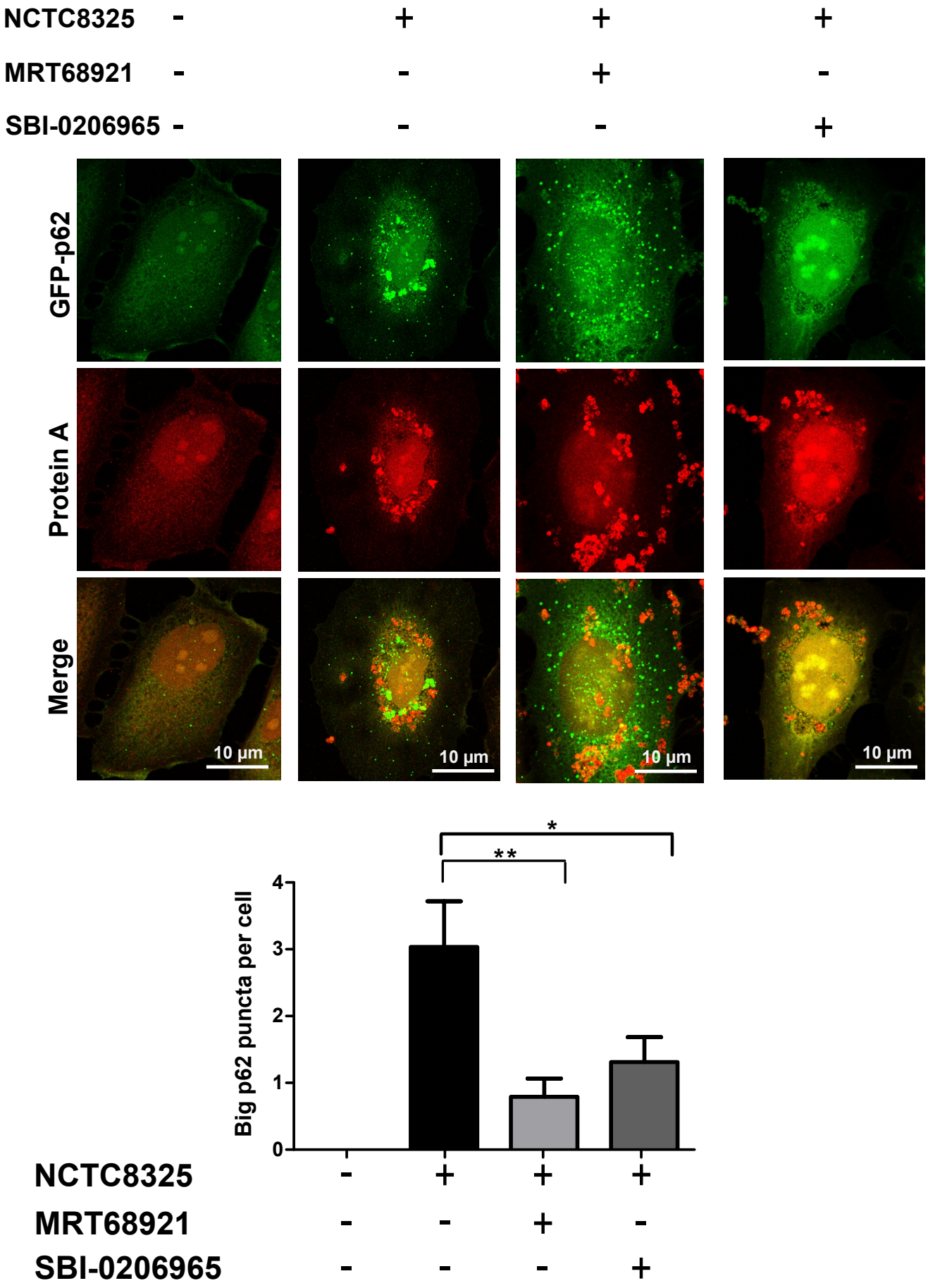

Figure 4.16: Pharmacological inhibition of ULK1 inhibited formation of p62 positive aggregate structures following infection with MRSA. Stable GFP-p62/HeLa cells were plated on glass coverslips and then infected with NCTC8325 at 100 MOI. These were incubated for 3hrs at 37ºC with or without ULK1 inhibitors (10 μM). Subsequently, the cells were fixed and stained with an anti-protein A. Large p62 puncta were counted under an epifluorescent microscope, and then the cells were observed by confocal microscopy. Scale bar: 10 μm.

4.2.3.8. Pharmacological inhibition of ULK1 suppresses infection by MRSA

To date, there have been a range of papers that have examined the interaction between *Staphylococcus aureus* intracellular replication and xenophagy (Liu et al., 2015, O'Keeffe et al., 2015, Schnaith et al., 2007, Mestre and Colombo, 2012, Mestre et al., 2010). For intracellular replication, studies have shown that *Staphylococcus aureus* is able to use autophagosomes as a protective niche (through microscopy and counting the bacterial clusters within the autophagosomes) (Mauthe et al., 2012, Schnaith et al., 2007). In this study, we decided to measure intracellular growth using classical methods: lysing cells and measuring *Staphylococcus aureus* colony forming units (CFU) within cell lysates.

HEK293A cells were seeded and treated with ULK1 inhibitor MRT68921 (1 μM) or SBI-0206965 (10 μM) and then infected with NCTC8325. After one hour of infection, gentamicin was added to inactivate extracellular bacteria. Host cells were then lysed at 3, 6 and 24 hours post gentamicin and cell lysates were cultured on bacterial solid media (Mannitol salt agar). In Figure 4.17, we observed that NCTC8325 *Staphylococcus aureus* is able to replicate in HEK293 cells as detected by CFU. The media agar colour was clearly changed, indicating strong growth of bacteria and fermentation of mannitol leading to phenol red turning to yellow colour. By 24 hours, NCTC8325 fully killed HEK293 host cells. Importantly, the number of bacterial CFU was decreasing when infected cells were treated with ULK1 inhibitors (MRT68921 or SBI-0206965). Interestingly, host cells maintained health 24 to 48 hours after infection with the addition of ULK1 inhibitors (Figure 4.18). These results suggest that the inhibitors can suppress productive *Staphylococcus aureus* infection through blocking ULK1-dependent autophagy. Although the therapeutic possibilities of these compounds clinically still needs a considerable amount of development, ULK1 inhibitors may be a novel approach for fighting infection by MRSA.

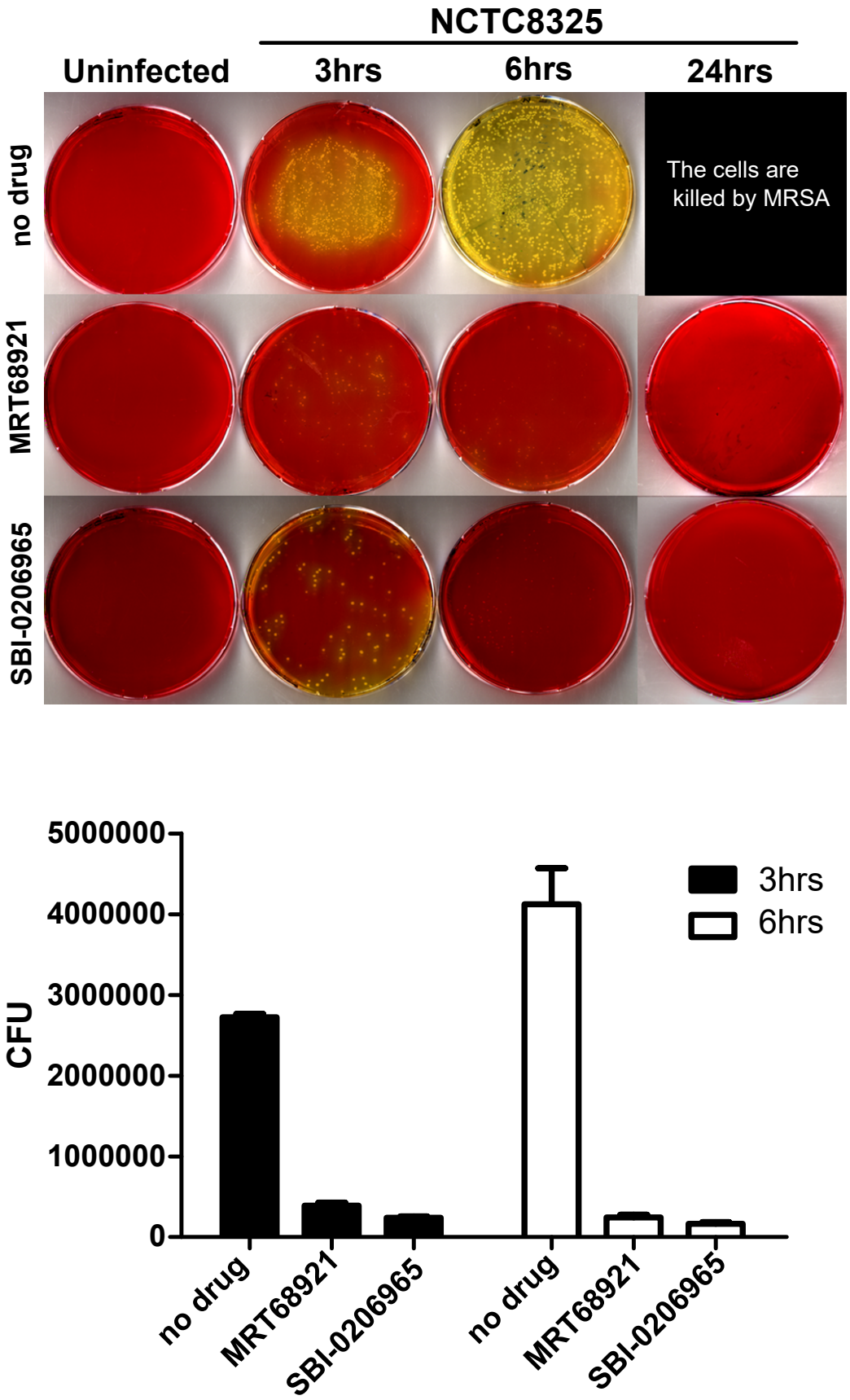

Figure 4.17: Inhibition of MRSA intracellular growth within host cells by ULK1 inhibitors: HEK293A cells were seeded and infected with NCTC8325 at 200 MOI. At the point of infection, ULK1 inhibitors, MRT68921 (1 μM), or SBI-0206965 (10 μM), were added. Then after 1 hour of infection, gentamicin (0.05 mg/ml) was added. Cells were then incubated 3, 6 or 24hrs before lysed. Lysates were diluted at 1/100 and then 50 μl of this dilution was plated on MSA. Plates were incubated at 37^{O}C overnight and colonies then were counted.The average from 3 samples ± SD is shown.

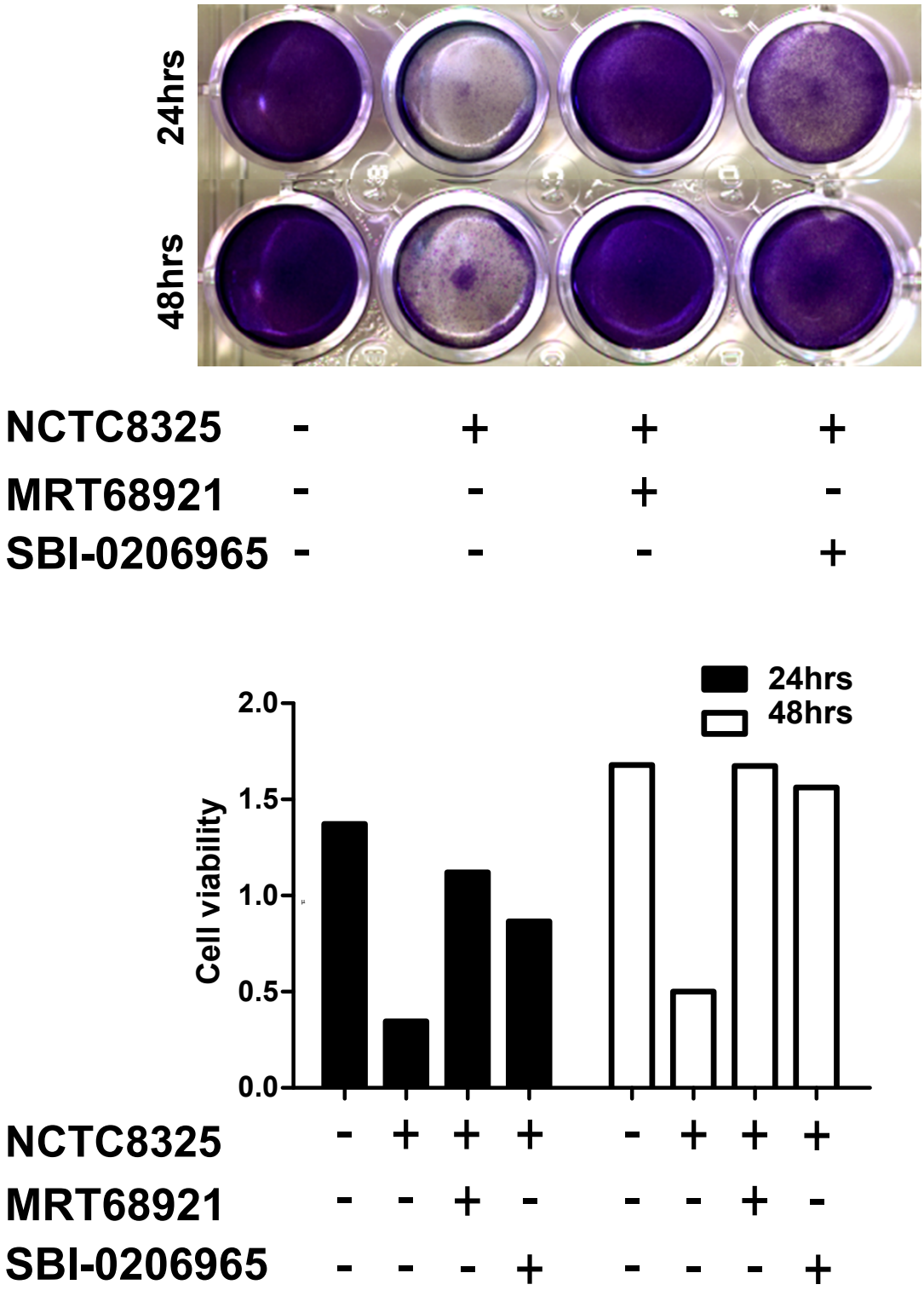

Figure 4.18: Inhibition of MRSA intracellular growth within host cells by ULK1 inhibitors leads to healthy cells. HEK293A cells were seeded and infected with NCTC8325 at 200 MOI. At the point of infection, ULK1 inhibitors, MRT68921 (1 μM), or SBI-0206965 (10 μM), were added. Then after 1hr of infection, gentamicin (0.05 mg/ml) was added. Cells were after incubated 24 or 48hrs and then fixed, stained with Giemsa and quantified.

4.3. Discussion

Currently, the application of host-directed therapies when treating bacterial infections has increased, owing to an increase in the occurrences of antibiotic-resistant bacterial diseases and the scarcity of new antibiotics in development. Invading intracellular bacteria have to continuously battle with the host's innate immunity for survival. Therefore, it is not surprising that most bacterial pathogens have evolved mechanisms to subvert host cell defence. To survive, the bacterial pathogen needs to colonise the host cell and achieve their own niche, avoiding the host's defences, and leaving the infected host cell to support replication and spread the pathogen to another uninfected host.

Formation of an intracellular replicative niche is important in the entire *Staphylococcus aureus* infection tissue process and this involves multiple virulence factors (Fraunholz and Sinha, 2012). *Staphylococcus aureus* is known to survive in a phagosome and secretes toxins (such as α-haemolysin, the metalloprotease aureolysin, protein A, and sortase A) that constrain lysosomal degradation (Jarry and Cheung, 2006, Kubica et al., 2008). Consequently, the survival of *Staphylococcus aureus* inside the intracellular niche has been observed in many cell types including neutrophils (Gresham et al., 2000), osteoblasts and macrophages (Hamza and Li, 2014), sinus cells (Svider et al., 2014), mammary and pulmonary epithelial and endothelial cell lines (Grosz et al., 2014, Jarry et al., 2008).

The diversion of *Staphylococcus aureus* from the endosomal pathway to the autophagy pathway is key to its infection process, by helping to create a protective niche and preventing fusion with lysosomes (Liu et al., 2015, Lopez de Armentia et al., 2017, O'Keeffe et al., 2015, Schnaith et al., 2007). Therefore, targeting autophagosome formation would be expected to prevent creation of the *Staphylococcal* replication niche. Indeed, Schnaith et al. initially demonstrated that intracellular replication of *Staphylococcus aureus* decreases dramatically in ATG5−/− MEFs and in HeLa cells treated with wortmannin, a PI3K inhibitor (Schnaith et al., 2007).

This chapter aimed to study the role of the ULK1 complex in xenophagy following infection by *Staphylococcus aureus* as compared with *Salmonella enterica* sv.

Typhimurium. We first targeted the ULK1 initiation complex using genetic tools and then tested ULK1 inhibitors as a novel therapy to restrict MRSA infection in cells.

An essential role is played by ULK1 during autophagosome formation in *Salmonella* infection xenophagy (Kageyama et al., 2011). In infected cells, the ULK1, ATG9L and ATG14L complexes each played a role in directing membrane recruitment to help form the autophagosome around the SCV (Kageyama et al., 2011). Moreover, recruitment of WIPI2, a factor that functions downstream of the ULK1 and Beclin1-PI3-kinase complexes, has recently been found to play a role in restricting the *Salmonella* proliferation via TBK1 (Thurston et al., 2016). More recently, it has been found that TGF-β-activated kinase 1 (TAK1) becomes activated following *Salmonella enterica* sv. Typhimurium infection leading to AMPK activation. This mechanism in turn activates ULK1 by phosphorylating ULK1S317 and suppressing mTOR activity and ULK1S757 phosphorylation, thereby restricting *Salmonella* proliferation (Liu et al., 2018). These above studies highlight the collaboration of multiple ULK1-dependent pathways following *Salmonella* infection.

Thus, we wanted to ascertain whether the ULK1 kinase complex is also critical in the formation of a double-membrane autophagosome following infection by MRSA. We decided to study ATG13 puncta structures as a marker for the ULK1/2 complex. We showed that ATG13 does localise to the isolation membrane associated with MRSA (and also *Salmonella enterica* sv. Typhimurium) during xenophagy. This suggested key involvement of ULK1 kinase complex in xenophagy following infection with MRSA.

Our next step was to determine whether the ULK1 pathway is essential for *Staphylococcus aureus* induced cell death. We first used genetic approaches based on shRNA-mediated gene silencing, as well as the CRISPR-Cas9 editing tool to target ULK1 and its required binding protein ATG13. We showed that the loss of ULK1 or ATG13 would block standard autophagy assays. Our results here in HEK293A and HeLa cells further confirm that both proteins are indispensable for autophagy.

Following this, we sought to establish whether blocking the ULK1 complex would prevent cell destruction following infection by *Staphylococcus aureus*. Indeed, we found that knockdown of ULK1 or CRISPR knockout of ATG13 could make cells

resistant to killing by *Staphylococcus aureus*. These results indicated that transition of *Staphylococcus aureus* into the autophagosomal pathway is critical for *Staphylococcus aureus* toxicity. On the other hand, knockdown of ULK1 or CRISPR knockout of ATG13 made cells more sensitive to destruction by *Salmonella enterica* sv. Typhimurium indicating the role of autophagy in restricting the infection by this pathogen.

Next, we sought to explore ULK1 inhibitors as a novel MRSA infection fighting strategy. Recently, a number of ULK1 kinase inhibitors that obstruct autophagy have been identified such as MRT68921, SBI-0206965 and KS1 (Egan et al., 2015, Petherick et al., 2015, Lazarus and Shokat, 2015). In addition, we had the opportunity here to study three other unpublished MRT analogues (MRT216403, MRT239016 and MRT238993) developed by collaborators in order to improve target specificity. We first tested the ability of these different inhibitors to block autophagy and found varied results. Interestingly our result found the three MRT analogues, (MRT216403, MRT239016, or MRT238993) did not decrease LC3-II accumulation. Therefore, these novel MRT derivatives were not able to strongly inhibit amino acid dependent autophagy in this particular system. Thus, our group conducted additional investigations in determining effects on ULK1/2 kinase catalytic activity. By measuring ATG13 phosphorylation at Serine 318, other members of the Chan laboratory tested the effects of the different MRT compounds. These studies could demonstrate reduction in ATG13 Ser318 phosphorylation through the combination of MRT68921, MRT238993, KS1 or SBI-0206965 under starvation conditions (Nwadike and Chan, unpublished, PhD Thesis in preparation). These data suggest a poor correlation between inhibition of ULK1 kinase activity with autophagy inhibition, which was unexpected and contrasts with the present accepted model.

We hypothesise that these drugs may be inducing some conformational changes on ULK1 and inhibiting interaction with ATG13, although not fully inhibiting autophagy initiation. This unconventional model is supported by the earlier report showing that starvation-induced autophagy was not inhibited by a non-phosphorylatable ATG13 S318A mutant (Joo et al., 2011). It was suggested in this study that ATG13 phosphorylation at Ser318 is a strong regulation signal for mitophagy, although not

required for starvation induced autophagy, thereby suggesting the possibility of specialised downstream functions being determined by ATG13 phosphorylation.

When we investigated the role of ULK1 inhibitors during the process of infection, interestingly, we found that several of these compounds could inhibit cell destruction following infection by MRSA. On the other hand, ULK1/2 inhibitors (blocking xenophagy) made cells more sensitive to death following infection by *Salmonella enterica* sv. Typhimurium. These results combined suggest that inhibition of ULK1/2 by the drugs can modulate xenophagy, even though starvation autophagy was less affected. Interestingly, measuring *Staphylococcus* growth inside host cells showed there was replication of this pathogen within the first few hours of infection, which led to cell destruction by 24 hours. In contrast, cells treated with SBI-0206965 or MRT68921 ULK1 inhibitors resisted MRSA infection for up to 24 hours. Importantly, these cells stayed healthy and continued cell growth within 48 hours.

This result shows strong correspondence with the previous study that found LC3-PE and Atg16L were still recruited to the SCV in the absence of Atg9L, FIP200 and the PI3K complex (Kageyama et al., 2011). In this study, the researchers suggested that the recruitment of LC3-PE is dependent on a different mechanism to the membrane formation usually occurring in autophagy, for which FIP200 and PI3K are needed. Also, Atg9L, FIP200, and the PI3K complex were important to restrict the infection by *Salmonella* (Kageyama et al., 2011). Our work, therefore, suggests that the formation of the double-membrane autophagosome around the bacteria is important for *Staphylococcus* replication. However, it is important for *Salmonella* restriction. Thus, these inhibitors can fight MRSA infection by preventing the autophagy-dependent niche required for replication.

Our results establish that we can use ULK1 inhibitors to block niche-xenophagy and improve cell survival. A previous study also found that the replication of intracellular *Staphylococcus aureus* was greatly reduced in the presence of wortmannin (PI3K inhibitor). This PI3K inhibitor prevented the initial formation of autophagosomes but unfortunately affects many other pathways (Schnaith et al., 2007).

The involvement of ULK1 in creating a protective niche for bacterial replication has also been suggested with *Brucella abortus* (Starr et al., 2012). This type of infection

was shown to require the autophagic machinery to survive and replicate in ER-derived *Brucella*-containing vacuoles (BCVs). The initiating factors of autophagy such as Beclin1 or ULK1 are hijacked by the BCVs and exploited during the formation of autophagosome-like compartments. BCV formation was readily reduced by the depletion of Beclin1 or ULK1 by siRNA, and also by autophagy's pharmacological inhibition using PI3-kinase inhibitors 3-methyladenine or LY294002. This suggests that *Brucella abortus* infection is promoted by autophagy. ULK1 inhibitors such as the MRT could be further tested in this system.

Other bacterial species also subvert autophagy and reside within autophagosome-like vacuoles, including *Porphyromonas gingivalis* (Dorn et al., 2001). In human coronary artery endothelial (HCAE) cells, the *P. gingivalis* was located within vacuoles morphologically identical to autophagosomes. The early endosomal marker Rab5 was found to co-localise with these vacuoles early after internalisation and these rapidly acquire HsGsa7p (human-specific Gsa7p), which is required for the formation of the autophagosome. At later times, the bacteria traffic to late autophagosomes that contain BiP (the rough endoplasmic reticulum protein) and lysosomal glycoprotein 120 (LGP120). The intracellular survival of *P. gingivalis* decreases over eight hours with the autophagy inhibitors 3-methyladenine and wortmannin (Dorn et al., 2001).

Coxiella burnetii is another bacteria found to subvert autophagy. During epithelial cell and macrophage infection, *C. burnetii* reside within large, acidified, LC3 (+) vacuoles to replicate (Vazquez and Colombo, 2010, Winchell et al., 2014, Beron et al., 2002). Bacteria-containing vacuoles could be labelled by LysoTracker (a marker of acidic compartments) and accumulated monodansylcadaverine (markers of autophagic vacuoles). Pre-treated with 3-methyladenine and wortmannin also blocked *Coxiella* vacuole formation. These autophagosomal features suggest that *Coxiella* also exploits the autophagic pathway for its life cycle (Beron et al., 2002).

As a final example, autophagy also promotes replication of *Legionella pneumophila* although mechanisms slightly differ. During infection in macrophages, *Legionella* reside within a vacuole targeted by LC3 and this trafficking also facilitates survival of *L. pneumophila.* Furthermore, *Legionella* have a mechanism for cleaving conjugated LC3 via the RavZ effector protein to block acidification (Choy et al., 2012).

In general, all of these bacterial pathogens may have evolved different pathways to evade the lysosomal endpoint by exploiting an autophagosome intermediate, thereby fostering a niche permissive for growth (Kirkegaard et al., 2004). If ULK1 inhibitors generally suppress autophagy bacterial niche formation, they may be effective in many different types of infection.

Chapter 5

Genome-wide CRISPR screen reveals novel host factors required for Staphylococcus aureus and *Salmonella enterica* sv. Typhimurium mediated infection

5. Genome-wide CRISPR screen for novel host factors required for *Staphylococcus aureus* or *Salmonella enterica* sv. Typhimurium mediated infection

5.1. Introduction

5.1.1. RNAi-mediated gene silencing

In order to deplete gene function in cellular biology, RNAi-mediated knockdown has become an essential and now routine method to employ (Baumann et al., 2017). The method of gene knockdown is based on obstructing expression of a gene by binding or degrading a particular sequence of mRNA, hence preventing translation into specific proteins. Short double-stranded RNA molecules of about 20–25 nucleotides targeting a gene are traditionally either introduced exogenously (siRNAs) or generated from hairpin-forming precursors (shRNAs). The shRNA can supply the cells, through lenti-viral transmission into the host genome, long-term knockdown of the target gene. Nevertheless, by this method, gene function is minimised, but not absolutely done away with.

In comparison, editing of the genome by use of Clustered Regularly Interspaced Short Palindromic Repeat (CRISPR) directly alters the DNA for the gene in the genome, therefore causing complete removal of gene function. Consequently, CRISPR is regarded as an exciting tool with high potential for gene editing, not only to remove single genes, but with the ability to be used as a screening tool.

5.1.2. CRISPR as genome editing technology

Genome editing technologies have emerged as powerful tools for studying the function of genes in normal and disease settings (Chen et al., 2015, Cong et al., 2013, Hart et al., 2015, Koike-Yusa et al., 2014, Shalem et al., 2014, Wang et al., 2015, Wang et al., 2014). A number of genetic editing technologies have arisen in recent years, including Zinc Finger Nucleases (ZFNs) (Wood et al., 2011, Porteus and Baltimore, 2003), Transcription Activator-like Effector Nucleases (TALENs) (Wood et al., 2011) and CRISPR/Cas9 (Ran et al., 2013). CRISPR/Cas9 is an accessible, quick and well-characterised gene editing tool for researchers. Therefore, researchers have quickly turned to this technology for functional genomic studies (Hsu et al., 2014).

CRISPR was first discovered as a form of adaptive immunity in bacteria and archaea to degrade foreign phage or plasmid DNA (Barrangou et al., 2007). Later, CRISPR-associated protein 9 (Cas9) was described as a missing link for CRISPR function. The CRISPR/Cas9 system consists of two compounds: 1) Cas9 and 2) a guide RNA (gRNA) which function together to induce a double-strand break (DSB) (Jinek et al., 2012). The gRNA contains a twenty-nucleotide target sequence immediately upstream of a Protospacer Adjacent Motif (PAM), linked to a crRNA scaffold. This is sufficient to direct the Cas9 nuclease to the complementary site in the genome and create a DSB, three to four nucleotides upstream of the PAM sequence (Figure 5.1) (Ran et al., 2013, Jinek et al., 2012).

Two types of DNA genome repair are then commonly used by cells: 1) the efficient but error-prone NHEJ pathway (non-homologous end joining); or 2) the less efficient high fidelity HDR pathway (homology-directed repair) (Ran et al., 2013). The NHEJ non-homologous end joining repair pathway is the most active mechanism, capable of rapidly repairing DSB, but in this process there is no validating DNA repair template present. This often results in gene inactivation by the creation of frameshift alleles (Jinek et al., 2013, Mali et al., 2013). By contrast, the alternative HDR pathway utilises a repair template. The experimenter may supply desired base changes within a sequence which are flanked by left and right perfectly homologous arm sequences. Upon double crossover, the desired change is integrated into the genome (San Filippo et al., 2008). Overall, the endogenous repair of DSB using the NHEJ pathway typically results in functional protein disruption (knockout), whereas the HDR pathway can be used to introduce exogenous genetic content (knockin) (Figure 5.2) (San Filippo et al., 2008).

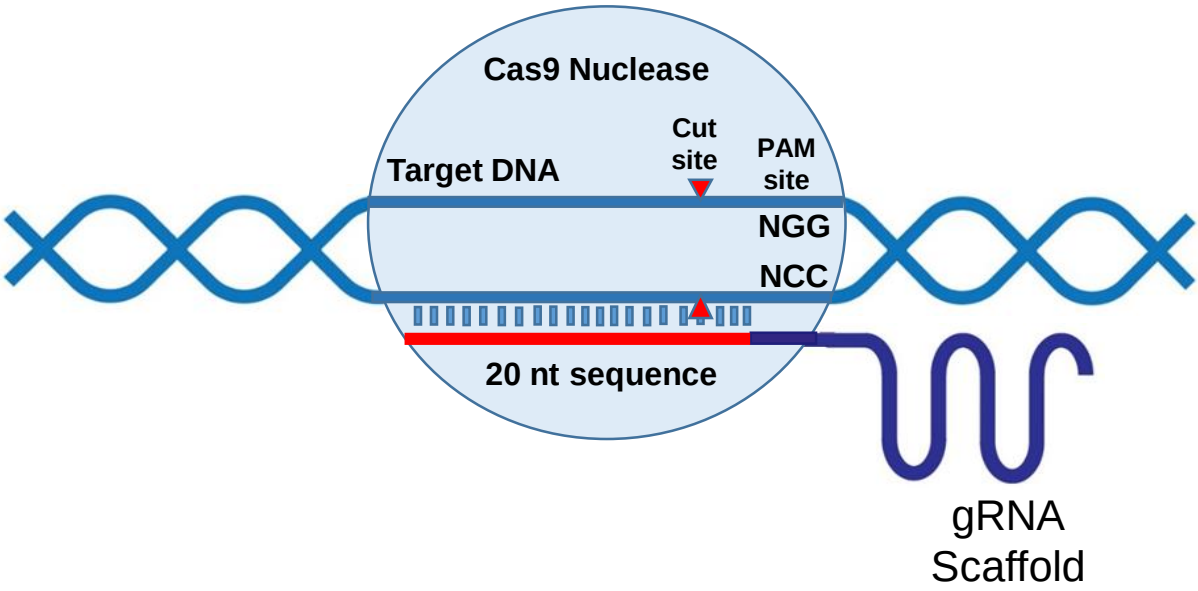

Figure 5.1: The CRISPR-Cas9 System. The Cas9 nuclease from *Streptococcus pyogenes* is targeted to genomic DNA by an sgRNA consisting of a 20-nt guide sequence and a scaffold. The guide sequence pairs with the DNA target, directly upstream of a requisite 5′-NGG adjacent motif (PAM). Cas9 mediates a double strand break 3 bp upstream of the PAM.

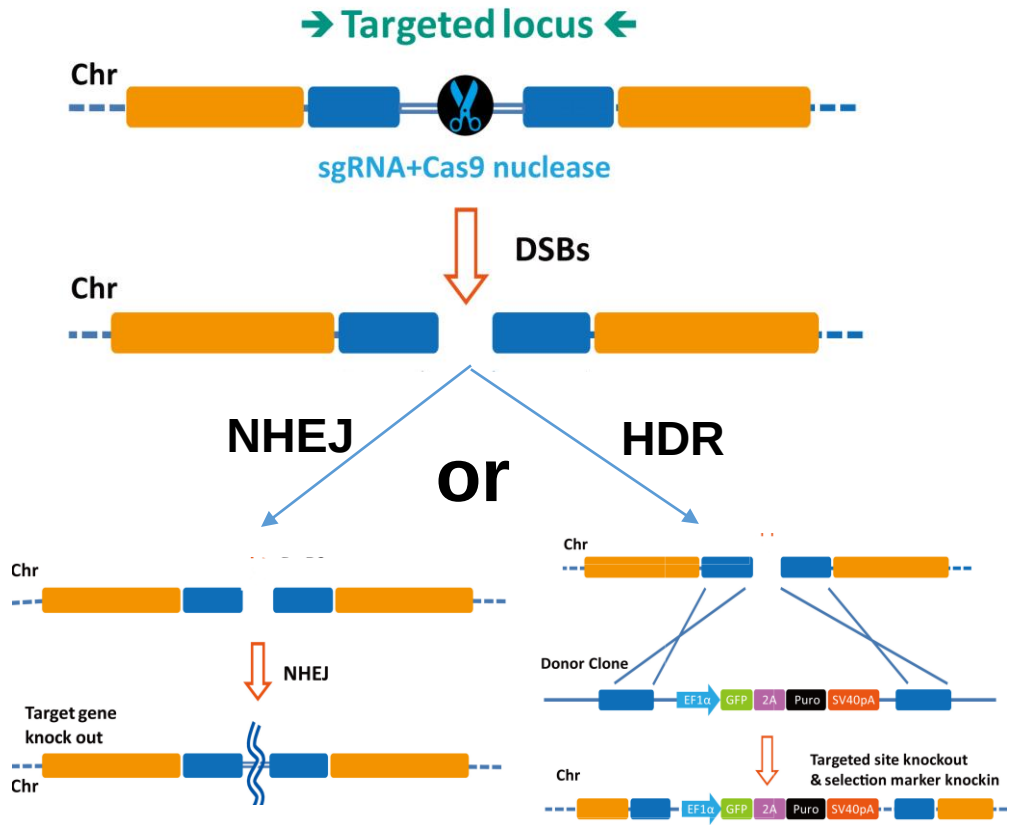

PAM

WT 5-..GGAGGAAGGGCCTGAGTCCGAGCAGAAG-AAGAAGGGCTC..-3
D1 GGAGGAAGGGCCTGAGTCCGAGCAGAAG- -AGAAGGGCTC
+1 GGAGGAAGGGCCTGAGTCCGAGCAGAAGAAAGAAGGGCTC
D2 GGAGGAAGGGCCTGAGTCCGAGCAGAAG- - -GAAGGGCTC
D3 GGAGGAAGGGCCTGAGTCCGAGCAGAAG- - - -AAGGGCTC
D6 GGAGGAAGGGCCTGAGTCCGAGCAGAAG - - - - - -GGGCTC

Figure 5.2: Targeted DNA editing by double strand break induction. Cas9-induced double strand breaks are repaired via one of two types of editing; the efficient but error-prone NHEJ pathway (non-homologous end joining) or the less efficient but high fidelity HDR pathway (homology-directed repair). The NHEJ repair pathway is the most active repair mechanism, capable of rapidly repairing DSBs, but frequently results in small nucleotide insertions or deletions (InDels) at the DSB site. Frameshift mutations lead to changes in the reading frame (change the grouping of the codons) resulting in completely different translation from the original.

5.1.3. CRISPR as a genome-wide forward screening tool

Several groups have adapted the CRISPR approach for high-throughput knockout screens by developing large-scale CRISPR sgRNA libraries targeting every gene in the genome (Shalem et al., 2014, Wang et al., 2014, Zhou et al., 2014). It has been shown that CRISPR technology can be effectively used for large-scale screens in mammalian cells to identify novel genes responsible for a biological process or pathway, opening the door to many new applications, such as drug target identification.

In 2014, the Zhang laboratory (Sanjana et al., 2014, Shalem et al., 2014) produced large Genome-scale CRISPR Knock-Out (GeCKO) pooled libraries (and later an improved second version). These libraries contain over 120,000 gRNAs with six gRNAs per gene for 19,050 human genes (and four gRNAs per miRNA), to ensure redundant representation. Each library is delivered as two half-libraries (A and B). Each library is available in a one-vector (lentiCRISPRv2: Cas9 + gRNA) or two-vector (in which the lentiCas9 and lentiGuideRNA are in separate viruses) format. The two-vector system has been reported to have the advantage of higher titre for the library virus, but this requires the transduction of cells with Cas9 first. After this, the sgRNA library is introduced using the second vector. On the other hand, the one-vector system has the advantage that both Cas9 and gRNA are delivered to each cell uptaking virus in one step.

The Zhang Group (and others) found that after delivering the GeCKO pooled library, the approach can next enable both positive (gain of function) and negative (loss of function) screening in mammalian cells. A positive screen aims to identify the cells with CRISPR targeting which pass a selection mechanism. Most of the cells in this screen will die and not pass the selection mechanism. However, CRISPR may target a gene that ends up giving a positive advantage. A number of genome-wide CRISPR-Cas9 screens in a setting of positive selection have discovered gene mutations that confer drug resistance, resistance to bacterial toxins and genes involved in metastasis (Chen et al., 2015, Koike-Yusa et al., 2014, Parnas et al., 2015, Shalem et al., 2014, Wang et al., 2014, Virreira Winter et al., 2016).

In contrast, a negative screen is used to identify the CRISPR cells which do not survive after applying the selection mechanism. CRISPR gene targeting would be

expected to weaken or sensitise the cell to the selection pressure. This type of screen requires extensive Next Generation Sequencing (NGS) to identify those cells which are absent (or decrease) at the end of the selection. For a negative selection screen, the important control is to see the initial gRNA population in the set of cells before the selection mechanism. NGS on the initial library pool and the remaining cells after the negative selection can be compared to generate a list of gRNAs that have disappeared. A number of negative selection screens by CRISPR-Cas9 have already been reported in a wide range of contexts (Chen et al., 2015, Hart et al., 2015, Sanjana et al., 2014, Shi et al., 2015, Wang et al., 2014). For example, negative selection screening has identified genes required for proliferation and survival of human cancer cell models (Wang et al., 2015). Also, negative selection screens could identify factors essential for cell viability in stem cells such as genes essential for ribosomal structural constituents (Shalem et al., 2014). Overall, GeCKO screening systems have shown high consistency between unique sgRNAs targeting the same gene, low off target modification and a high validation rate of screen hits (Shalem et al., 2014, Sanjana et al., 2014).

5.1.4. Hypothesis and aims

There is a need to find new approaches to combat the emerging resistance in bacterial infections to multiple drugs. There is one strategy which aims to identify new drugs but one would expect eventual resistance to these. Another strategy is to better understand the relationship between the bacteria and host cells. This could lead to the development of host-directed therapies to fight bacterial infections.

The previous chapters discussed how intracellular bacterial pathogens generate niches within the eukaryotic cells which make it possible for them to survive and proliferate (Cornejo et al., 2017, Alix et al., 2011). In establishing these replicative niches, the bacteria hijacked, modified and manipulated cellular pathways, and subverted the host's defence mechanisms. Due to the complex interactions with the pathogen, it is crucial to understand the involvement of the host cellular pathways to find novel ways for fighting bacterial infection. The previous chapter also found that targeting the ULK1 kinase can inhibit the ability of MRSA to produce cell killing.

In this chapter, we aimed to find new genes (such as autophagy regulators) required to form the *Staphylococcus aureus* replicative niche.

1. We performed a genome-wide screen using GeCKO v2 library to identify genes leading to MRSA resistance by positive selection in HEK293A cells.
2. For comparison, we performed a parallel screen using the same HEK293A-CRISPR cell mutant library following positive selection with *Salmonella enterica* sv. Typhimurium infection.

5.2. Results

5.2.1. Optimisation experiments

5.2.1.1. Using Lipofectamine or Calcium phosphate for CRISPR virus production

Before starting work with the full GeCKO library, a number of control experiments were carried out to become familiar with our vector system. In the control experiments, we used the one-vector system lentiCRISPRv2. This same vector was to be used with the GeCKO library. This system enables lentiviral delivery of both Cas9 and sgRNA for targeted gene knockout. Because this vector gives low titre in some cell lines, it was important to perform virus transduction experiments in relation to positive control virus, such as those with shRNA, which is a small plasmid vector and normally gives a high titre.

Firstly, we wanted to establish whether it was more efficient to produce lentivirus with a high titre using Lipofectamine or calcium phosphate transfection into the virus packaging cell. HEK293FT cells were transfected with the lenti CRISPRv2 or LKO.1 shRNA vector by using Lipofectamine or calcium phosphate (for 60 hrs). Then, the lentivirus from the different tests were used to infect the HEK293 cells. The virus titre after puromycin selection was measured by AlamarBlue reagent to detect amounts of viable cells. It was found that Lipofectamine was more efficient than calcium phosphate in transfection, especially with the CRISPR vector but not with the smaller LKO.1 shRNA vector (Figure 5.3). Therefore, Lipofectamine was chosen to use for GeCKO viral production.

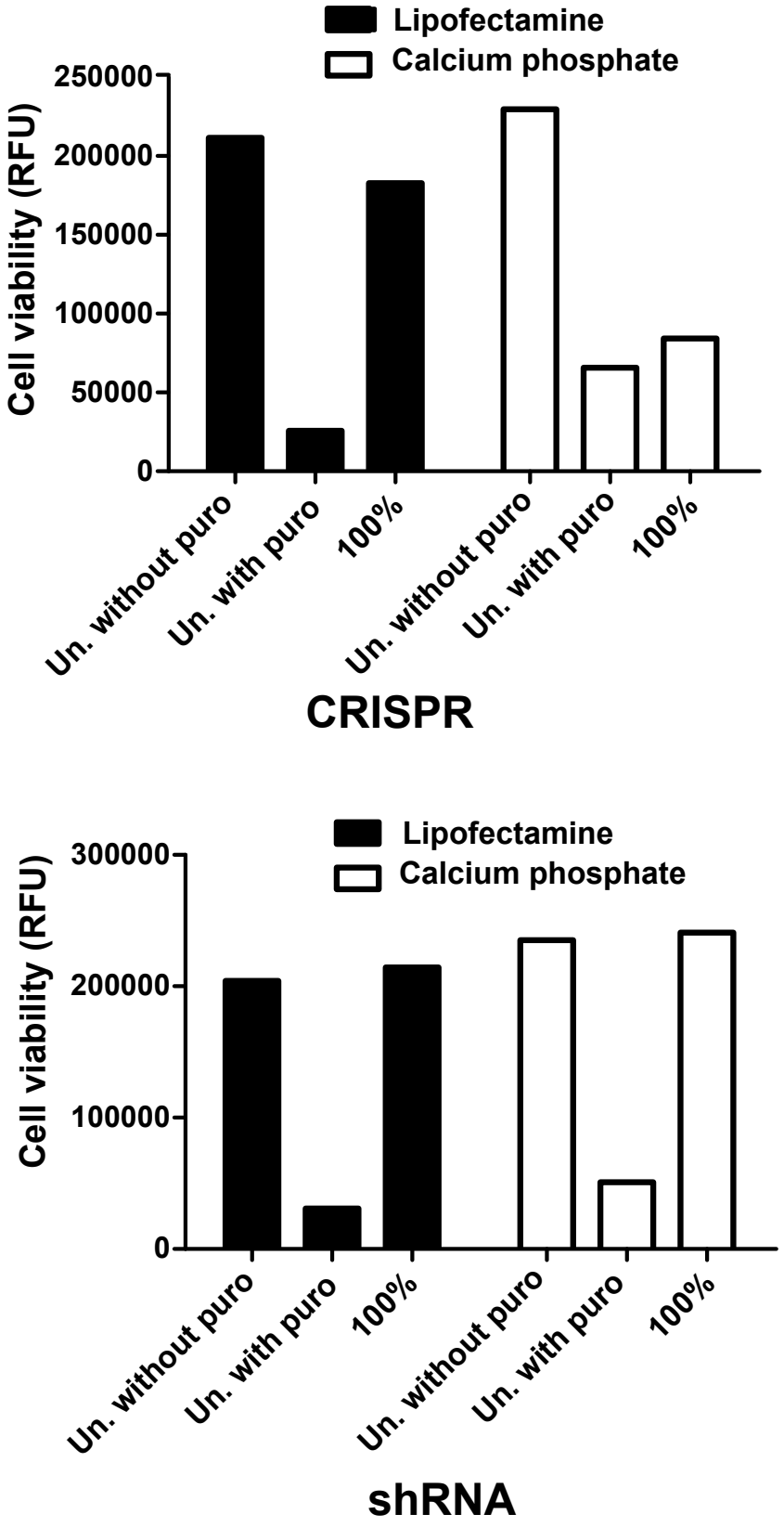

Figure 5.3: Lipofectamine transfection was more efficient than Calcium phosphate in high titre CRISPR lentivirus production. HEK293A cells were transduced by using 100% concentrated CRISPR vector or shRNA vector lentivirus. Cells were selected by puromycin and then the cell viability was measured by using AlamarBlue.

5.2.1.2. Transduction of HEK293A with CRISPR lentivirus as compared with LKO shRNA lentivirus

The next set of control experiments aimed to more carefully quantify if there were significant differences between CRISPR and LKO shRNA lentivirus transduction titre in HEK293A cells. We transduced HEK293A cells with CRISPR or shRNA lentivirus produced by the Lipofectamine 2000 method. After incubation for two days, these cells were selected by puromycin, then the cell viability was measured by AlamarBlue reagent. It was found that CRISPRv2 and LKO shRNA showed similar efficiencies for transduction of 293A cells, both with 100% dilution (neat virus) or when virus was used at 50% concentration (Figure 5.4). Therefore, we became more confident in using the one-vector system (lentiCRISPRv2) in the GeCKO library because this would give a high titre.

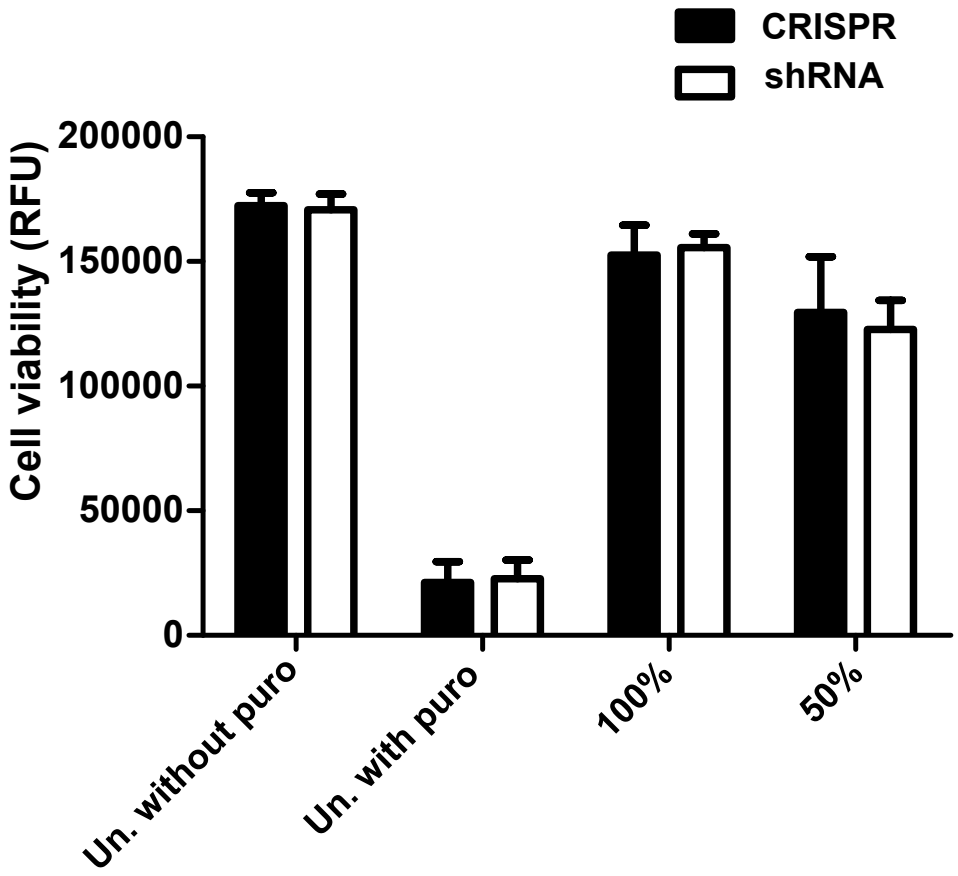

Figure 5.4: CRISPR and shRNA lentivirus titre measurements. HEK293A cells were transduced using 100% or 50% concentrated CRISPR or shRNA lentivirus and incubated two days before selection by puromycin and measurement of the proportion of transduced cells by AlamarBlue. The average from 3 independent experiments± SD is shown.

5.2.1.3. Transducing HEK293A with CRISPR lentivirus using spinfection

In a further control experiment, we tested “the spinfection method” to ascertain if this technique improved cell transduction with CRISPRv2 lentivirus. Normally, this method increases the contact between viral particles and target cells. On the day of the transduction, after adding the viral supernatant on to the cells, we centrifuged the plate at 800 xg for one hour. After incubation for two days, these cells were selected by puromycin, then the cell viability was measured by AlamarBlue. It was found that spinfection improved viral transduction, but by only 5–10% as compared to non spinfection (Figure 5.5). Therefore, this additional manipulation, which introduces more handling and safety considerations, was not dramatically important for viral transduction.

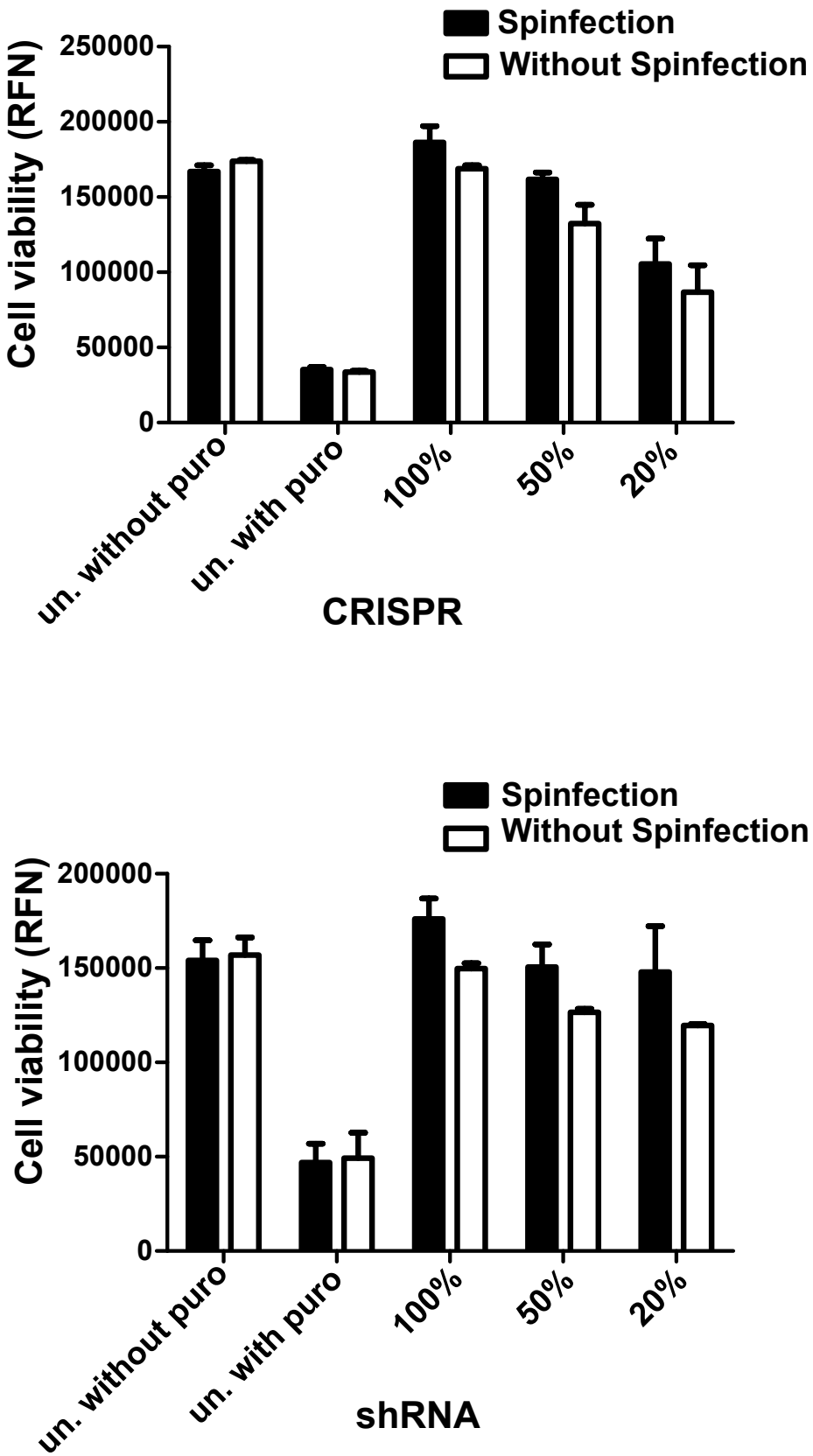

Figure 5.5: Spinfection measurement of transduction efficiency. HEK293A cell were transduced with or without (un.) using spinfection (2000 rpm at 37^{o}C) for 1 hour. Cells were incubated for 2 days before selection by puromycin and cell viablity measurement by AlamarBlue.The average from 3 independent experiments± SD is shown.

5.2.1.4. CRISPRv2 lentivirus production from packaging cells under different densities

As our control experiments found the percentage of HEK293A transduced with CRISPR showed some variability, we tested lentivirus production while controlling confluence of HEK FT packaging cells. High packaging cell confluency can increase virus titre but can inhibit transfection efficiency. We transduced HEK293A using CRISPRv2 lentivirus produced from high or low confluence HEK FT cells. It was found that the confluence of HEK FT cells has a significant role in increasing the titre of a virus; titre is increased when the FT cells confluence steadily increases. This effect is stronger with packaging the CRISPR vector, which is larger than the shRNA vector (Figure 5.6). Therefore, high confluence of HEK FT was critical to increase the GeCKO viral titre.

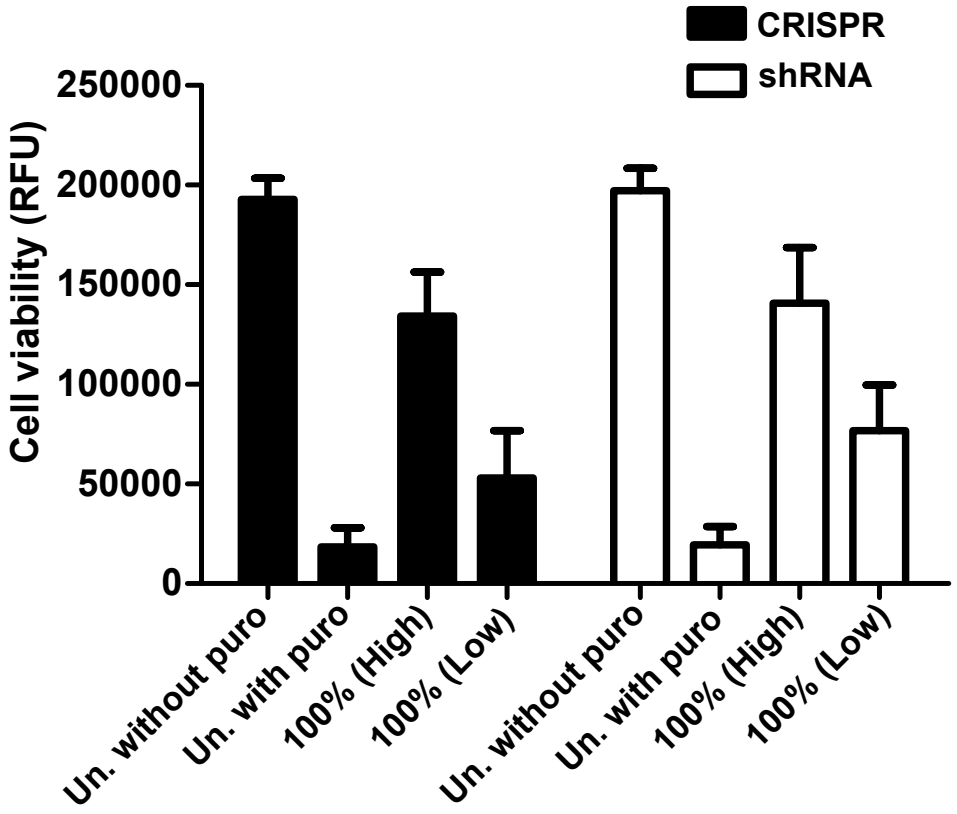

Figure 5.6: Virus titre dependency on 293FT packaging cell confluence. HEK293A were transduced by 100% concentrated CRISPR or shRNA lentivirus produced from high or low 293FT confluence packaging cells. After 2-day incubation, the cells were selected by puromycin then the cell viability was measured by the AlamarBlue. The average from 3 independent experiments± SD is shown.

5.2.1.5. Transduction of HEK293A or HeLa cell with CRISPR lentivirus

In the previous chapter, we found that HEK and HeLa cells were very clearly invaded and killed by both *Staphylococcus aureus* and *Salmonella enterica* sv. Typhimurium. Therefore, in this experiment, we aimed to determine how efficiently each of these cells could be transduced with the CRISPR lentivirus. HEK293A cells and HeLa cells were transduced with the CRISPRv2 lentivirus and then selected by puromycin. The cell viability was measured by AlamarBlue. It was found that the 293A cells were 95-fold better than the HeLa cells in the uptake of the CRISPR lentivirus vector (Figure 5.7). Therefore, we chose HEK293A cells as a more efficient host for the screen.

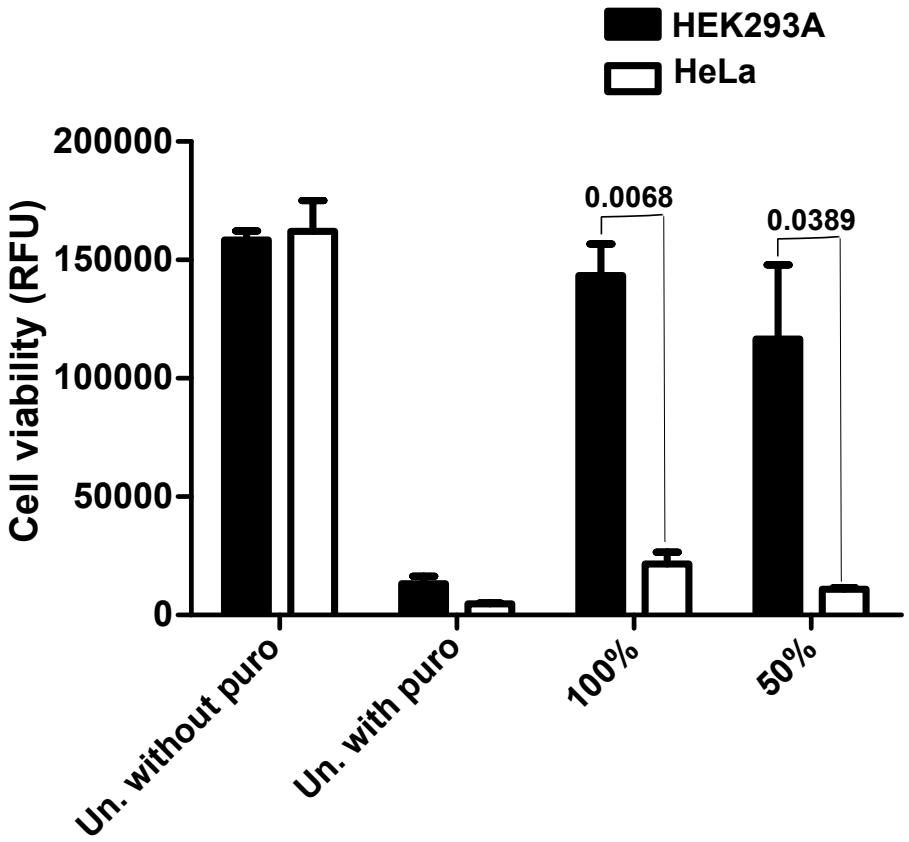

Figure 5.7: 293A cells are better transduced than HeLa using CRISPR lentivirus vectors. HEK293A or HeLa cells were transduced by CRISPR lentivirus at 100% or 50% concentration and then selected by puromycin and cell viability measured by AlamarBlue. The average from 3 independent experiments± SD is shown. P value from one-way ANOVA with Tukey multiple comparison test.

5.2.1.6. Transduction of HEK293A cell with fresh or frozen lentivirus

The full CRISPR library screen will involve large pools of virus stocks and a requirement to work across multiple weeks. Therefore, this control experiment aimed to establish if there were significant differences between fresh and frozen lentivirus stock. We transduced HEK293A cells with 100% (neat) fresh or the same lentivirus which had been frozen for a few days at -80 degree. After incubation for two days, these cells were selected by puromycin then the cell viability was measured. It was found that there was no significant difference between using lentivirus which had been frozen thawed once, as compared to fresh unfrozen virus (Figure 5.8). Therefore, we confirm that freezing would not affect the virus titre.

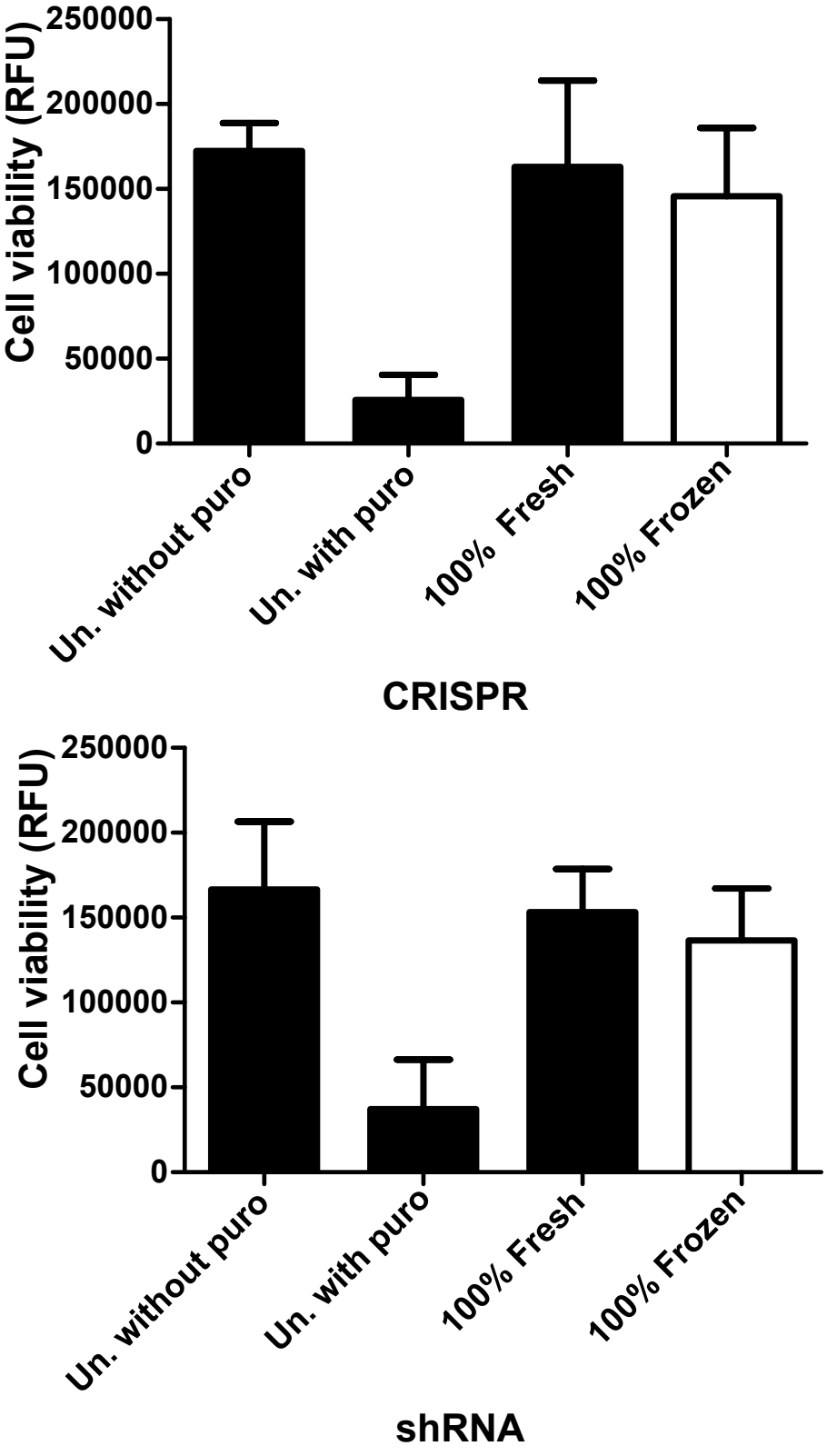

Figure 5.8: Frozen lentivirus retains high titre levels. HEK293A cells were transduced with 100% concentration of fresh or frozen lentivirus and incubated two days before selection by puromycin and measurement of virus titre by AlamarBlue. The average from 3 independent experiments ± SD is shown.

5.2.2. Genome-wide CRISPR screen for host factors required during MRSA or *Salmonella enterica* sv. Typhimurium infection

5.2.2.1. Optimising bacterial MOI for positive selection screening

In order to perform a screen to identify the host genes required for MRSA (NCTC8325) or *Salmonella enterica* sv. Typhimurium toxicity, we proposed to use a genome-wide CRISPRv2 library generated by the Zhang lab (Shalem et al., 2014, Sanjana et al., 2014). This library contains over 120,000 gRNAs with 6 gRNAs per gene for 19,050 human genes (and 4 gRNAs per miRNA).

We firstly determined three different MOI for NCTC8325 (100, 200 and 500) MOI, or *Salmonella enterica* sv. Typhimurium (1:1000, 1:500 and 1:100). HEK293A cells were infected with these different MOI of different pathogens with gentamicin added one hour after infection and then incubated for 72 hours. After the 72-hours incubation, the plates were stained with Giemsa stain to measure cell viability.

A larger number of cells were killed by 200 and 500 NCTC8325 MOI when compared with 100 MOI (Figure 5.9). However, 500 MOI was very stressful to cells, as recorded in our previous experiments in chapter 4. Infection effects from 500 MOI *Staphylococcus aureus* could not be suppressed by either autophagy gene blocking approaches or with ULK1 inhibitors. Thus, 200 MOI MRSA infection was chosen to perform the screen.

On the other hand, most cells were strongly killed following *Salmonella enterica* sv. Typhimurium infection at the 1:100 dilution (Figure 5.9). The 1:1000 or 1:500 diluted *Salmonella* did not produce any clear cell killing. Therefore, the 1:100 dilution was chosen to perform the screen.

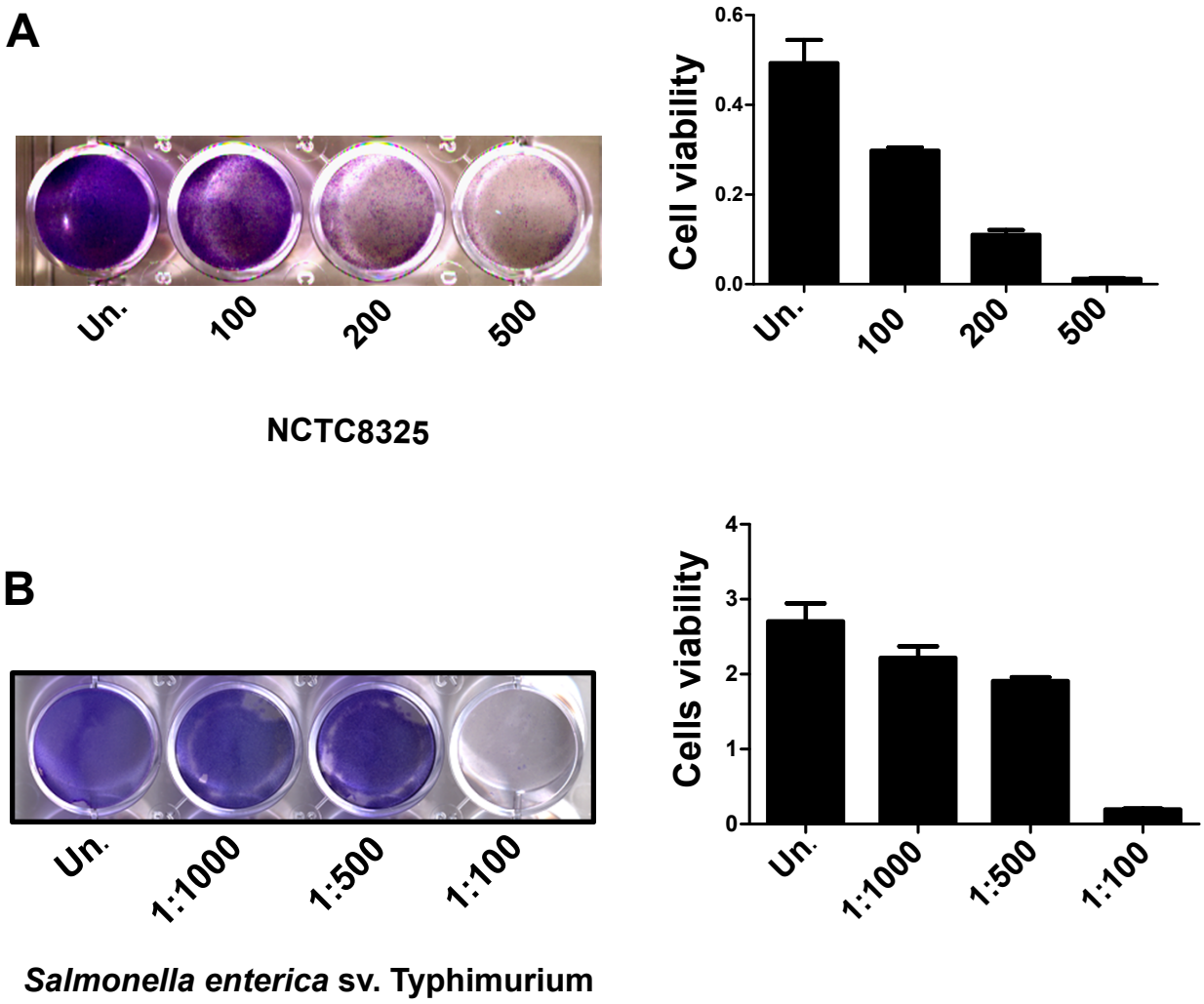

Figure 5.9: Optimising bacterial MOI for positive selection screening.
A) HEK293A cells were seeded and infected with NCTC8325 *Staphylococcus aureus* at 100, 200, 500 MOI via the "*Staphylococcus* protocol". After 1hr of infection, gentamicin (0.05 mg/ml) was added and cells were then incubated for 72hrs. Cells were fixed, stained and quantified. The average from 3 samples ± SD is shown.
B) HEK293A cells were seeded and infected with *Salmonella enterica* sv. Typhimurium at 1:1000, 1:500, 1:100 dilution via the "*Salmonella* protocol". After 50 min. of infection, gentamicin (0.05 mg/ml) was added. Cells were then incubated 72hrs. Cells were fixed, stained with Giemsa and quantified. The average from 3 samples ± SD is shown.

5.2.2.2. Determination of viral titre

A key part of CRISPR/Cas9 functional genetic screens is to generate a large population of cells, in which each cell has only one gene that is targeted by CRISPR. To determine the titre of the CRISPR library stock, HEK293A cells were infected with titrated volumes of virus. Three million cells per well of a 12-well plate were infected with decreasing amounts of virus. After overnight incubation and puromycin selection cell viability was measured by AlamarBlue. Percent transduction was calculated based on cell viability of puromycin resistance cells divided by cell viability of total cells read from wells without puromycin treatment multiplied by 100 (Shalem et al., 2014). From this calculation, it was found that the 250 µl well of the concentrated library virus generated roughly 50% cell survival. With 50% survival, we can predict two things. Firstly, most of the surviving cells should have only one viral particle integration per cell. Second, since the total HEK293A cell pool with the CRISPR library contains 40 million cells with 300x coverage that confirmed a good representation of the library. The multiplicity of infection (MOI) is in this case 0.5 (Figure 5.10).

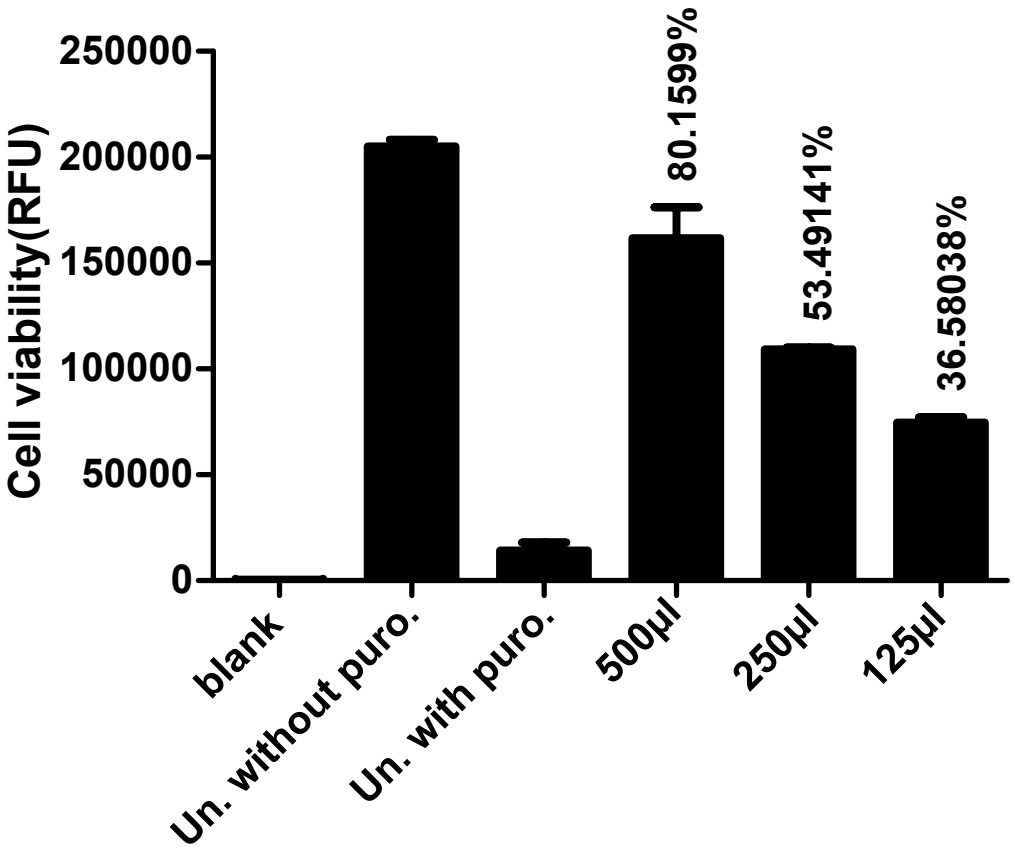

Figure 5.10: Virus titration on HEK293A cell after 72hrs. HEK293A cells were infected with titrated volumes of virus (500 µl, 250 µl, and 125 µl). After overnight incubation and puromycin selection cell viability was measured by AlamarBlue. Percent transduction was then calculated as the cell viability of puromycin resistance cells divided by cell viability of total cells read from wells without puromycin treatment multiplied by 100. The average from 3 experiments± SD is shown.

5.2.2.3. Transduction, positive selection and amplification results

The GeCKO library screen plan is summarised in Figure 5.11. After the GeCKO virus stocks were produced, we started by transducing $80x10^6$ HEK293A cells with the pooled CRISPR library at an MOI of 0.5, followed by selection using puromycin for stable viral integration. After amplification for one week, 60 million of the cells were harvested as an initial population control for next generation sequencing. The remaining cells were plated for bacterial infection with MRSA (NCTC8325) or *Salmonella enterica* sv. Typhimurium for one week to allow outgrowth of resistant mutants. Our goal was therefore to identify single genes that, when lost, caused MRSA (NCTC8325) or *Salmonella enterica* sv. Typhimurium resistance in HEK293A cells. HEK293A non-targeted cells were also included in the infection as a control, to compare with a level of full cell killing. Experiments were conducted in duplicate in order to more clearly detect candidates.

We found that most of the CRISPR pool targeted cells were killed by both bacteria. However, a small amount of cells still survived, and this survival was more than in the non-targeted HEK293A cells by 15-fold. This suggested that some cells targeted by the CRISPR library were resistant (Figure 5.12). These cells were expanded and harvested. We isolated genomic DNA and amplified the gRNA sequences as described by Shalem et al. (2014).

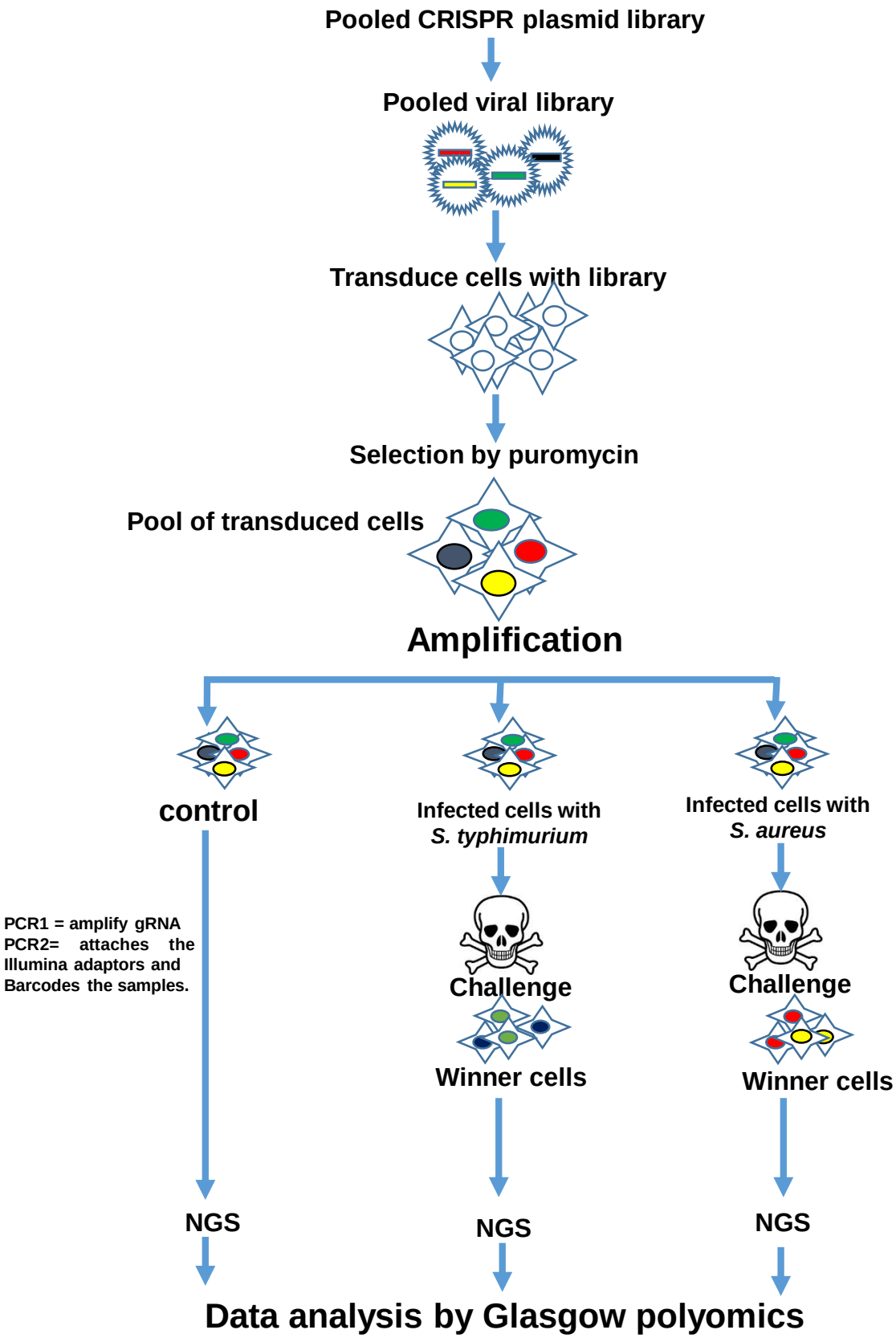

Figure 5.11: Genome-scale CRISPR Knock-Out (GeCKO) pooled libraries screen plan. HEK293A cells are infected with the library followed by puromycin selection. Cells are then split into control and test arms. After infection and positive selection, the genomic DNA is isolated, gRNA sequences amplified and sequenced by next generation sequencing for data analysis.

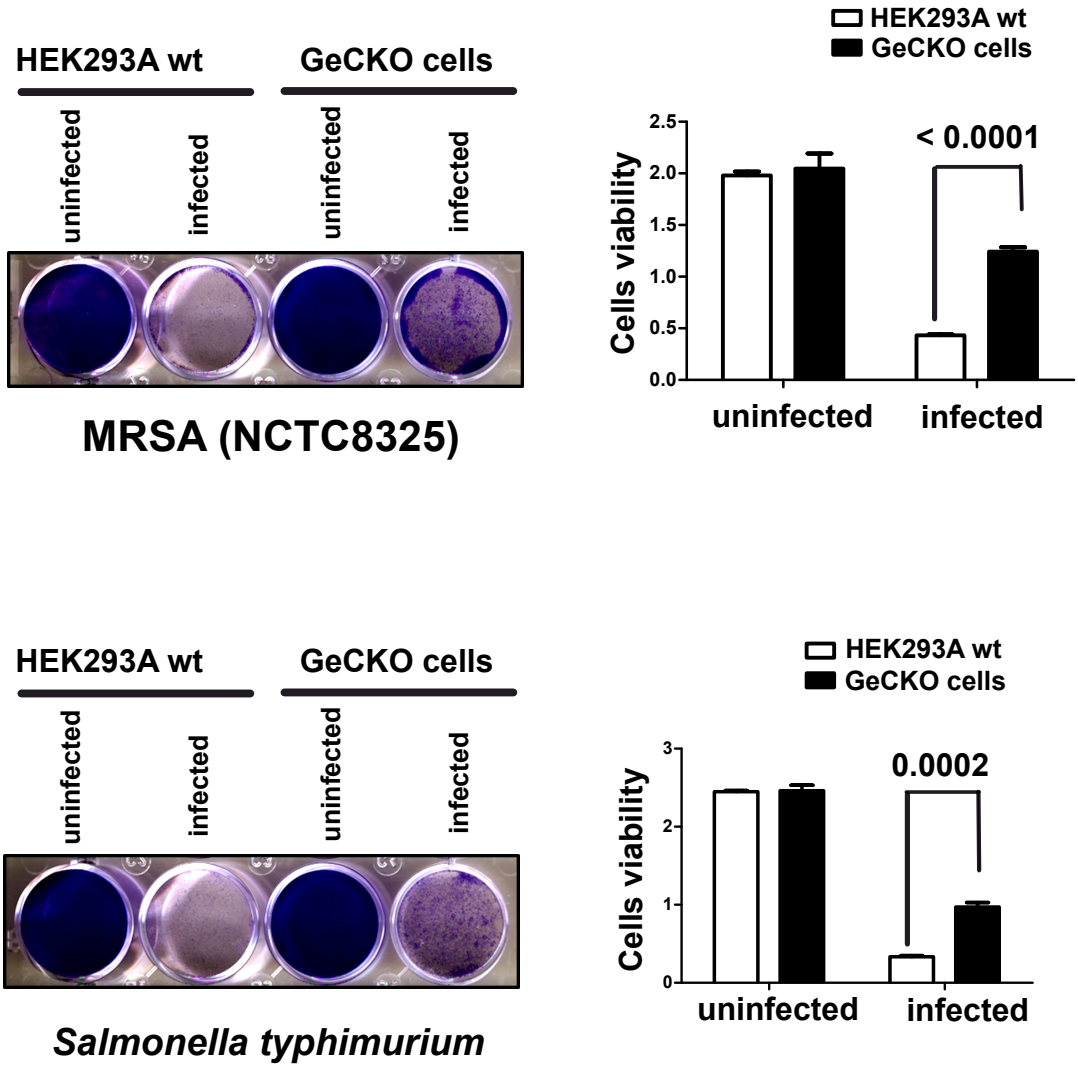

Figure 5.12: Preliminary characterisation showed more resistance in GeCKO library transduced cells as compared with wt cells following infection by MRSA or *Salmonella typhimurium.* HEK293A/wt or GeCKO/HEK293A cells were seeded and infected with NCTC8325 or *Salmonella typhimurium*. These cells were incubated in 37^{O}C for 72hrs after adding gentamicin. Cells were fixed, stained and quantified. The average from 3 samples ± SD is shown. P value from t test.

5.2.2.4. PCR1 and PCR2 amplification results

Two PCRs were used in order to (1) amplify gRNA and (2) add the flanking sequences (Shalem et al., 2014) needed for next generation sequencing, as described in the Methods chapter. Correct amplification was confirmed for the five samples on agarose gel after PCR1 giving a product of 340bp (Figure 5.13). We observed that one sample from the *Salmonella enterica* sv. Typhimurium set did not give a clear product, possibly because of a problem in DNA extraction.

The resulting PCR1 products were processed for the second PCR. Products from the resulting PCR2 were then concentrated on an agarose gel, excised and purified. Product concentrations were confirmed and the average size of fragments was observed to be around 340bp. The samples were finally analysed at the University of Glasgow Polyomics by NGS on a NextSeq500 (Illumina) in collaboration with Dr. Pawel Herzyk.

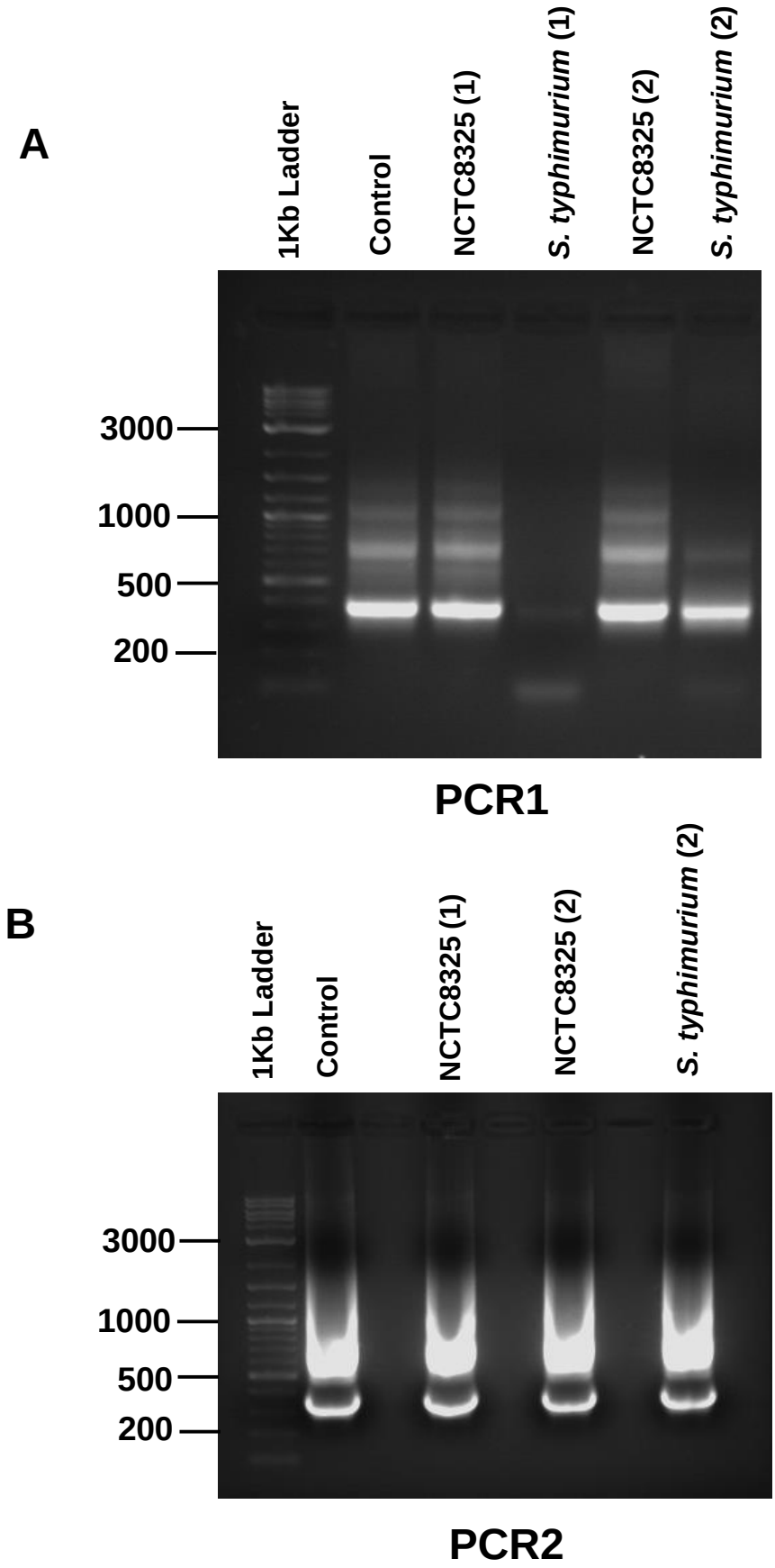

Figure 5.13: Two PCR stages performed for gRNA amplification.
(A) The correct amplification was checked on agarose gel after PCR1. One sample failed to amplify (*S. typhimurium* set one).
(B) Products from the second PCR were cut from this gel for purification and deep sequence analysis.

5.2.2.5. NGS analysis of control cell library before selection

The NGS for the untreated samples were first analysed to confirm the extent of library coverage. We were able to obtain 20,364,492 sequence reads (from a 30 million read sequence run). Of these, 81.4% (16,566,593) could be mapped onto GeCKO gRNA sequences. According to these numbers, only 1,650 of the 119,461 gRNA (1.38%) in the GeCKO library gave a zero count (i.e. not-detectable). Therefore, the initial HEK cell library before selection contained 98.62% of all guides.

The above results indicated that our generation of the GeCKO CRISPR virus, and initial cell library were successful. Furthermore, since the genomic DNA isolation and PCR amplifications were performed in parallel, we gained further confidence and proceeded to read NGS for the samples from cells after bacterial positive selection. For these samples, we analysed only to a depth of 10 million reads since fewer guides RNA sequences were expected in the resistant cells.

5.2.2.5.1. NGS analysis of cell library after MRSA infection

Analysis was done following the Model-based Analysis of Genome-wide CRISPR/Cas9 Knockout (MaGeck) algorithm (Li et al., 2014). The MaGeck method was chosen as an improved computational tool for identification of crucial genes from CRISPR-Cas9 knockout screens.

For each gene, the MaGeck algorithm calculates a robust ranking aggregate (RRA) score based on p-value. For this, the separate p-value ranks of all gRNAs from the same gene are aggregated and statistically analysed to ascertain whether they are significantly different from a purely random rank distribution (Kolde et al., 2012). In our positive selection screen, genes with multiple enriched gRNA leading to resistance were the highest ranked.

For example, in data from the first screen sample following MRSA positive selection (Figure 5.14A), according to the RRA, *ATP9B* was the highest ranking most significantly enriched gene ($p = 0.000048118$) (Figure 5.14B). Interestingly, the number of “good” gRNA (classified by MaGeck for single guides that follow the enrichment pattern) was scored to be six, as can be seen when plotting read counts of each guide (Figure 5.14C).

Also interesting, MaGeck ranked *CNTFR* as the second ranked gene. Surprisingly, the number of good targeting gRNA was just one. A strong effect of just one guide therefore appeared to have had a predominant effect on the RRA ranking.

The other genes ranked in the top ten by MaGeck included: *TMEM185A*, *OR6C3*, *KIAAI024L*, *SLAMF8*, *C15orf61*, *KLHL17*, *ARSK* and *PKD2L2*. For all these genes (besides *SLAMF8*), there were at least three gRNA showing good, clear effect. As discussed below, *KLHL17* (highlighted in the table) was chosen for further confirmation studies.

A

Gene	#gRNA	score	p-value	rank	#good gRNA
ATP9B	6	0.0000090227	0.000048118	1	6
CNTFR	6	0.0000251130	0.000142000	2	1
TMEM185A	6	0.0000279510	0.000161000	3	3
OR6C3	6	0.0000500180	0.000278000	4	4
KIAA1024L	6	0.0000732000	0.000377000	5	4
SLAMF8	6	0.0000753360	0.000386000	6	2
C15orf61	6	0.0000781450	0.000402000	7	3
KLHL17	6	0.0000912220	0.000462000	8	5
ARSK	6	0.0001030000	0.000522000	9	4
PKD2L2	6	0.0001080000	0.000542000	10	5

B

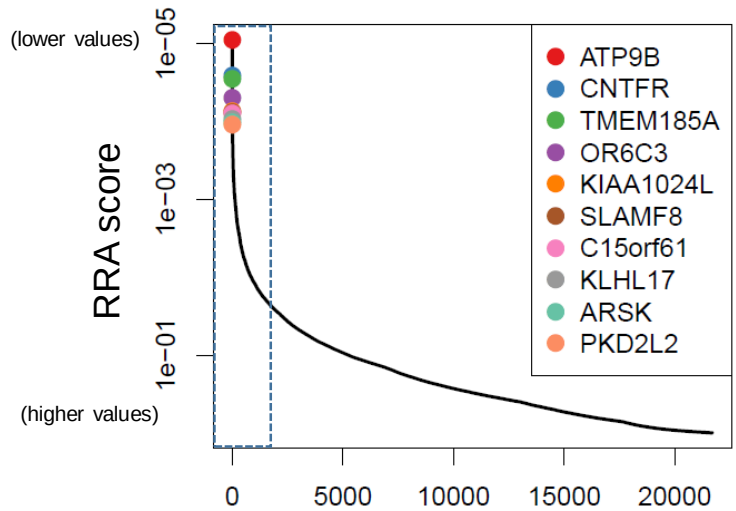

C

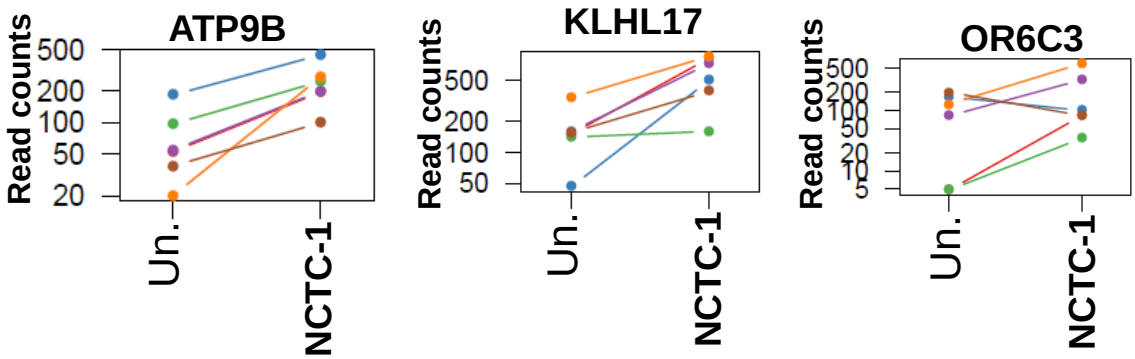

Figure 5.14: Results of NCTC-1 vs untreated comparison in the GeCKO positive selection screen.

(A) Summary generated by MaGeck analysis including: number of targeting gRNAs for each gene in the control (before the selection), RRA score, p-value, ranking of the gene, the number of 'good' gRNAs after the positive selection. Genes shaded in grey chosen for confirmation.

(B) Distribution of RRA score in the comparison NCTC-1 vs untreated positive selection screen. The top 10 genes are shown. Dashed box shows genes P<0.05 (Discussed in Chapter 6).

(C) Read count gRNA detected by MaGeck for selected genes.

MaGeck analysis of replicate 2 from MRSA positive selection gave a complementary set of top ten ranked genes (Figure 5.15A, B). In this replicate, *UPF3A* was the highest ranking most significantly enriched gene (p = 0.000089623). The number of “good” gRNA for *UPF3A* detected by MaGeck to follow the pattern was scored to be five (Figure 5.15C). *TNFRSF25* was the second ranked gene. Surprisingly, the number of good targeting gRNA was just two. Therefore, here, a strong effect of just two guides (out of six) appeared to have had a predominant effect on the RRA ranking.

The other genes ranked in the top ten by MaGeck included: *SLC17A9*, *SSPO*, *AP3D1*, *NLRC4*, *C12orf29*, *FCHSD2*, *PROM1*, and *hsa-mir-6794*. For all these genes (besides *FCHSD2*), there were at least three gRNA showing a good, clear effect. *AP3D1* and *NLRC4* which showed good consistent levels of enrichment of multiple guides were selected for further confirmation, as discussed below.

A

Gene	#gRNA	RRA score	p-value	rank	#good gRNA
UPF3A	6	0.000017365	0.000089623	1	5
TNFRSF25	6	0.000025113	0.000128	2	2
SLC17A9	6	0.000045472	0.00022	3	4
SSPO	6	0.000046836	0.000224	4	3
AP3D1	6	0.000049622	0.000236	5	4
NLRC4	6	0.000074715	0.000336	6	4
C12orf29	6	0.000075336	0.000337	7	3
FCHSD2	6	0.000126000	0.000547	8	1
PROM1	6	0.000135000	0.000589	9	5
hsa-mir-6794	4	0.000135000	0.000589	10	3

B

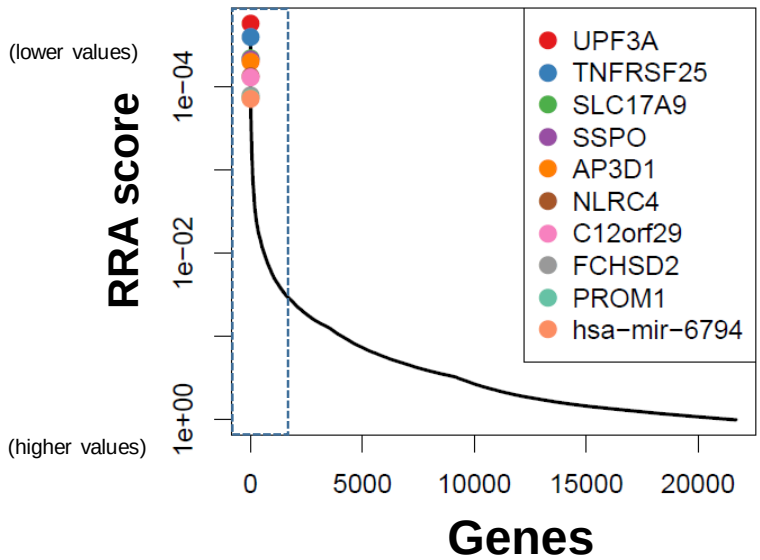

C

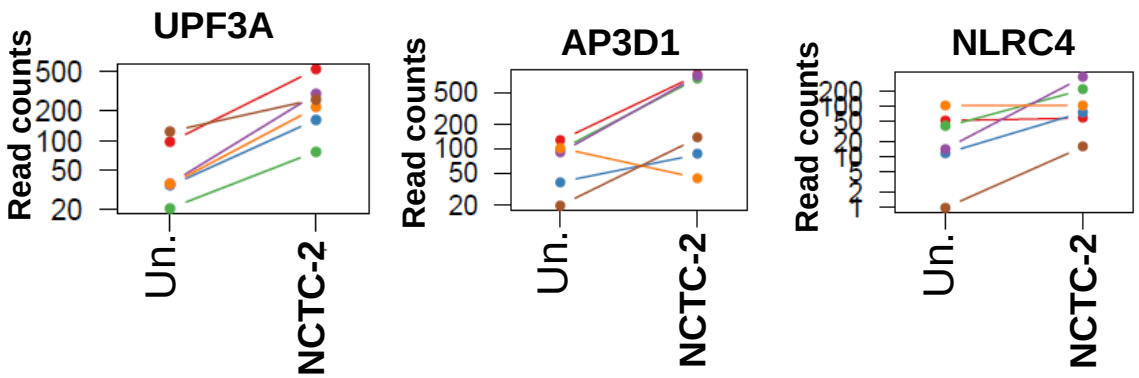

Figure 5.15: Results of NCTC-2 vs untreated comparison in the GeCKO positive selection screen.

(A) Summary generated by MaGeck analysis including: number of targeting gRNAs for each gene in the control (before the selection), RRA score, p-value, ranking of the gene, the number of 'good' gRNAs after the positive selection. Genes shaded in grey chosen for confirmation.

(B) Distribution of RRA score in the comparison NCTC-2 vs untreated positive selection screen. The top 10 genes are shown. Dashed box shows genes P<0.05 (Discussed in Chapter 6).

(C) Read count gRNA detected by MaGeck for selected genes.

The MaGeck algorithm also has the ability to generate gene rankings, combining data from biological replicates, in our case, the two positive selection with MRSA performed independently in parallel. We used MaGeck to rank the most consistently enriched genes across both replicates (Figure 5.16A, B). Using this analysis, *SPRR2A* was the top ranked (P=0.000059521) showing five “good” gRNA with consistent effects.

The second ranked gene *FCHSD2*, again, unexpectedly, showed one good targeting gRNA. Of the other top ten genes, *NLRC4* and *KLHL17* were identified. These two genes were part of the lists when each MRSA replicate was analysed by MaGeck separately (Figures 5.14, 5.15). These two genes are part of the list chosen for further confirmation.

A

Gene	#gRNA	score	p-value	rank	#good gRNA
SPRR2A	5	0.000011678	0.000059521	1	5
FCHSD2	6	0.000025113	0.000135000	2	1
KLHL17	6	0.000049023	0.000249000	3	5
NLRC4	6	0.000069832	0.000353000	4	4
ATP5C1	6	0.000073050	0.000367000	5	4
CNTFR	6	0.000075336	0.000378000	6	2
SLC22A8	6	0.000111000	0.000563000	7	4
RASSF2	6	0.000118000	0.000594000	8	3
CHORDC1	6	0.000126000	0.000634000	9	1
RCL1	6	0.000141000	0.000704000	10	6

B

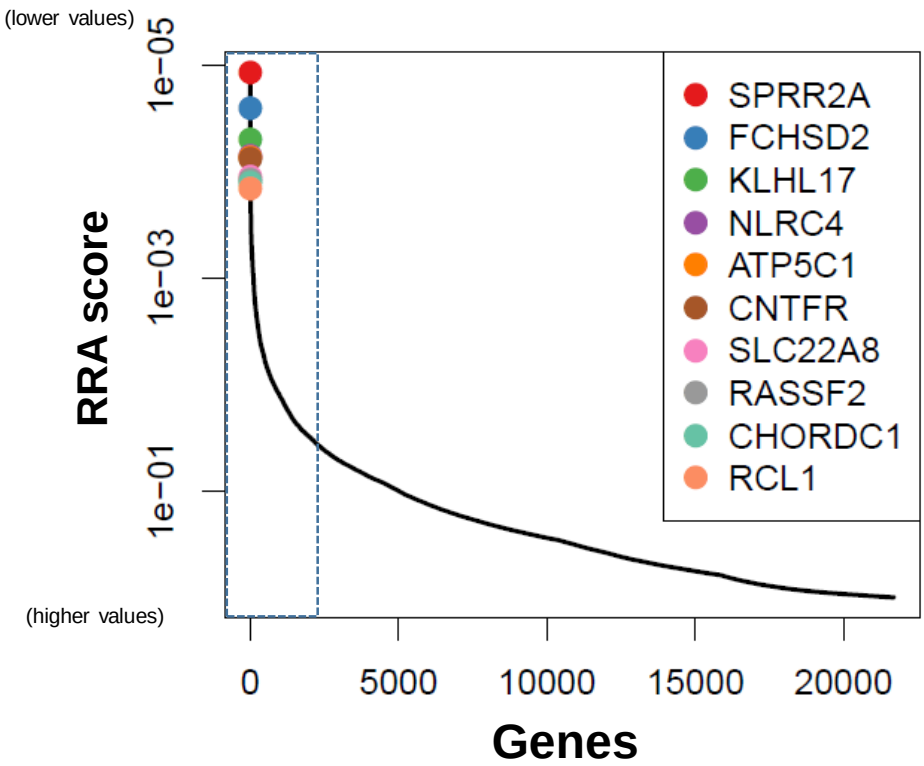

Figure 5.16: Results from combined comparison of NCTC replicate 1 and NCTC replicate 2 vs untreated GeCKO positive selection screen.
(A) Summary generated by MaGeck analysis including: number of targeting gRNAs for each gene in the control (before the selection), RRA score, p-value, ranking of the gene, the number of 'good' gRNAs after the positive selection. Genes shaded in grey chosen for confirmation.
(B) Distribution of RRA score in the comparison NCTC-1&2 vs untreated positive selection screen. The top 10 genes are shown. Dashed box shows genes P<0.05 (Discussed in Chapter 6).

5.2.2.5.2. NGS analysis of cell library after *Salmonella enterica* sv. Typhimurium infection

We carried out positive selection of GeCKO targeted cells using *Salmonella enterica* sv. Typhimurium infection followed by similar MaGeck analysis for gRNA enrichment (Figure 5.17A, B). It was clear that *DAZL* was the most significantly enriched gene (P=0.00006317) with five gRNA showing consistent levels of enrichment (Figure 5.17C).

From MaGeck, *MAP2K3* was the second ranked gene, but with only one good gRNA. Therefore, interestingly, some genes with just a few good guide changes have been detected and ranked relatively high in all MaGeck experiments performed. The other genes in the top ten included *ATXN2*, *TNFRSF25*, *LUZP4*, *CD164*, *FSCN2*, *OR8B8*, *ARHGAP28* and *C5ORF49*. Out of all these genes, at least three gRNA genes showed a good and clear effect, which suggests a generally robust set of candidates. *DAZL*, *CD164* and *ARHGAP28* were selected for validation below. The *Salmonella* screen was performed in duplicate, but the second half of the experiment failed at the level of DNA extraction and PCR amplification. Regardless, we obtained clear trends via the single MaGeck analysis to identify candidate genes required for *Salmonella* infection for further testing.

A

Gene	#gRNA	score	p-value	rank	#good gRNA
DAZL	6	0.000012963	0.00006317	1	5
MAP2K3	6	0.000025113	0.00013100	2	1
TNFRSF25	6	0.000031768	0.00016300	3	4
ATXN2	6	0.000037204	0.00018700	4	3
CD164	6	0.000039864	0.00020200	5	6
LUZP4	6	0.000065940	0.00033000	6	5
FSCN2	6	0.000074222	0.00036700	7	3
C5orf49	6	0.000075336	0.00037400	8	3
ARHGAP28	6	0.000117000	0.00059900	9	5
OR8B8	6	0.000126000	0.00064200	10	3

B

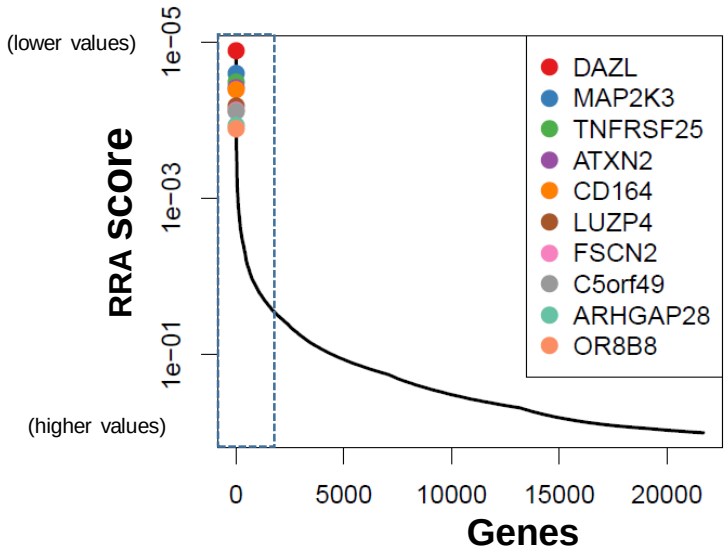

C

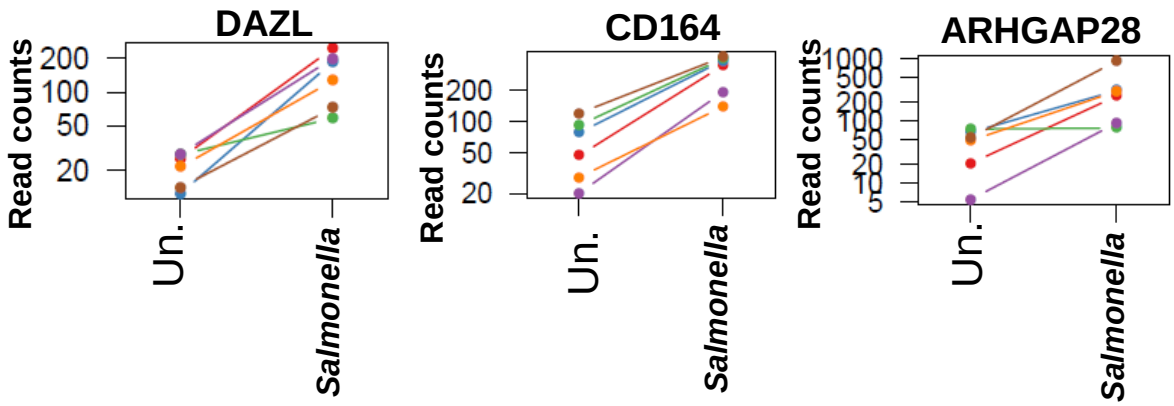

Figure 5.17: Results of *Salmonella* vs untreated Comparison in the GeCKO positive selection screen.

(A) Summary generated by MaGeck analysis including: number of targeting gRNAs for each gene in the control (before the selection), RRA score, p-value, ranking of the gene, the number of 'good' gRNAs after the positive selection. Genes shaded in grey chosen for confirmation.

(B) Distribution of RRA score in the comparison *Salmonella* vs untreated positive selection screen. The top 10 genes are shown. Dashed box shows genes P<0.05 (Discussed in Chapter 6).

(C) Read count gRNA detected by MaGeck for selected genes.

5.2.2.6. Validation results

For both the MRSA and *Salmonella* selection experiments, we selected three hits from the top ten with good gRNA enrichment and potentially interesting mechanisms for validation experiments.

5.2.2.6.1. Validation hits of MRSA screen

From the MRSA (NCTC8325) screen, *NLRC4*, *AP3D1*, and *KLHL17* are potentially interesting genetic modifiers of infection.

NLR family CARD domain-containing protein 4 (*NLRC4*) is an inflammasome family protein that has been suggested to be tasked with the innate immune responses initiation against pathogens by way of CASPASE1 (CASP1) protease activation (Ting et al., 2008). The protein encoded by *NLRC4* was associated with several key proteins via searches of the STRING online interaction database. Proteins interacting with NLRC4 include Tumor protein p53 (TP53), Interleukin 18 (IL18), Interleukin 1, beta (IL1B), Caspase 5 (CASP5), and Caspase recruitment domain family, member 8 (CARD8) as shown in Figure 5.18. NLRC4 is present in the cytosol of myeloid cells, where it controls the activation of caspase-1 and IL-1β processing in response to the presence of intracellular flagellin (Miao et al., 2006, Jha et al., 2017).

The importance of NLRC4-dependent activation of caspase-1 has been highlighted in infection models *in vitro* using *Salmonella enterica* sv. Typhimurium, *Shigella flexneri*, *Legionella pneumophila*, and *Pseudomonas aeruginosa* (Mariathasan et al., 2004, Cohen and Prince, 2013, Lightfield et al., 2011, Man et al., 2014). It has recently been discovered that NLRC4 inflammasome maximal activation in bone-marrow-derived macrophages infected with *Salmonella enterica* sv. Typhimurium, *Burkholderia thailandensis* or *Pseudomonas aeruginosa* requires interferon regulatory factor 8 (IRF8) (Karki et al., 2018). In this way, NAIPS transcription is governed by IRF8 to enable detection of flagellin and T3SS proteins for the activation of the NLRC4 inflammasome.

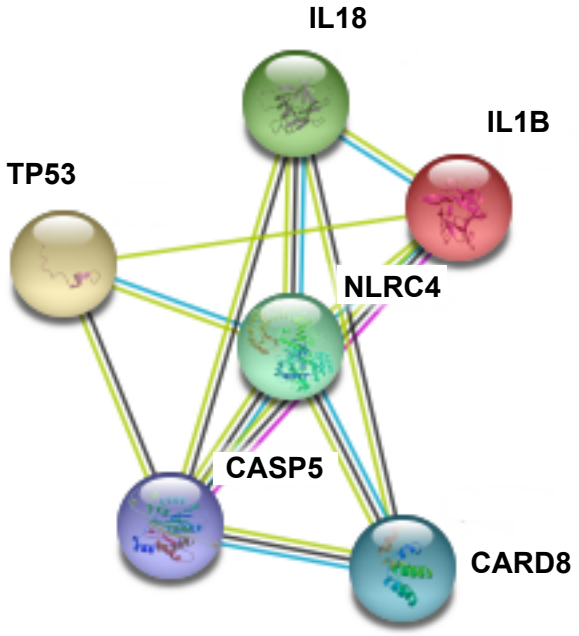

Figure 5.18: *NLRC4* (NLR family CARD domain-containing protein 4) interaction map. Interaction network obtained from the STRING database. The proteins present in the network are Tumor protein p53 (TP53), Interleukin 18 (IL18), Interleukin 1 beta (IL1B), Caspase 5 (CASP5), and Caspase recruitment domain family member 8 (CARD8).

Adaptor-related protein complex 3 delta 1 (*AP3D1*) is part of the AP3 adaptor-like complex which facilitates the budding of vesicles from the Golgi membrane, and may be directly involved in trafficking to lysosomes (Dell'Angelica, 2009). The proteins identified in the *AP3D1* interaction network include VPS41 (vacuolar protein sorting 41), AP3S1 (Adaptor-related protein complex 3, sigma 1 subunit), AP3B1 (Adaptor-related protein complex 3, beta 1 subunit), (AP3M1) Adaptor-related protein complex 3, mu 1 subunit, and (AP3S2) Adaptor-related protein complex 3, sigma 2 subunit (Figure 5.19). VPS41 has also been found to be required for vacuole assembly and vacuole traffic (Radisky et al., 1997).

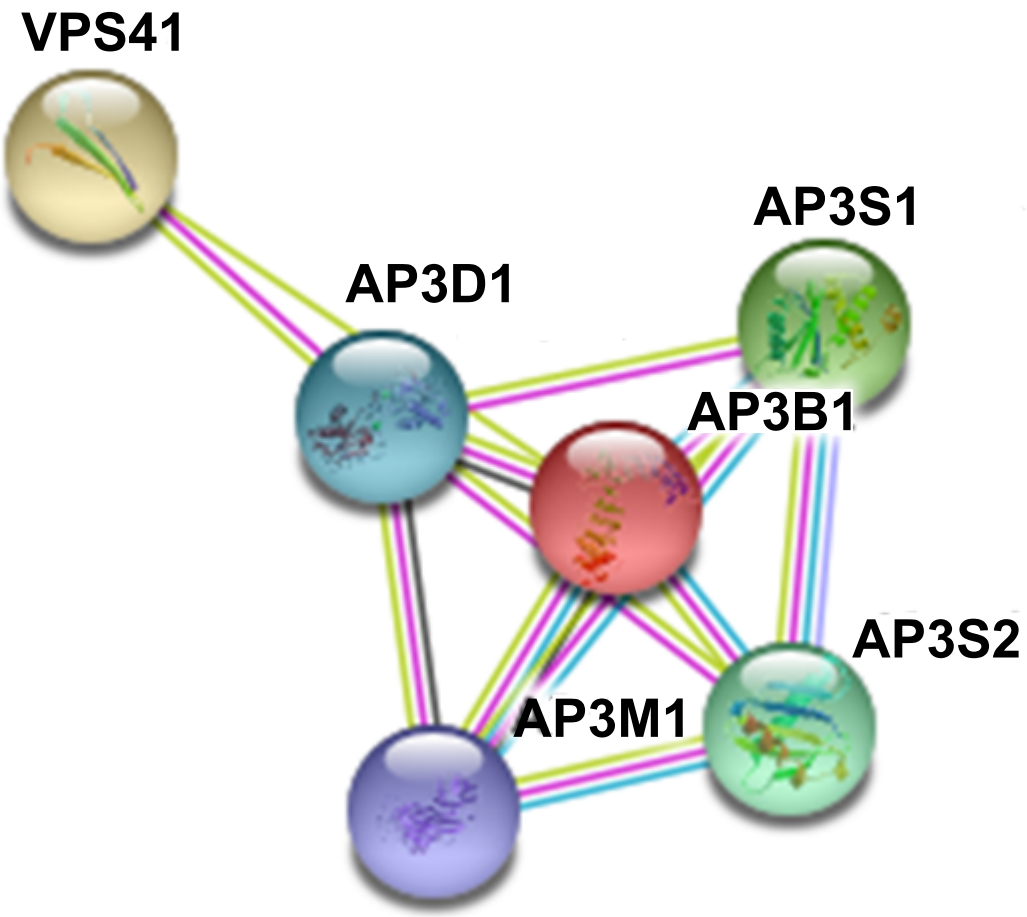

Figure 5.19: *AP3D1* (AP-3 complex subunit delta-1) interaction Map. The STRING database Interaction network. The proteins present in the network are Vacuolar protein sorting 41 (VPS41), Adaptor-related protein complex 3, sigma 1 subunit (AP3S1), Adaptor-related protein complex 3 beta 1 subunit (AP3B1), Adaptor-related protein complex 3 mu 1 subunit (AP3M1), and Adaptor-related protein complex 3 sigma 2 subunit (AP3S2) **.**

The *KLHL17* (Kelch-Like 17) protein is an interesting screen hit. KLHL17 carries an N-terminal BTB domain which is important for dimerization and a C-terminal Kelch domain that mediates binding to F-actin. Kelch domains form a tertiary structure of β-propellers that have a role in extracellular functions, morphology, and binding to other proteins (Dhanoa et al., 2013). From the protein interaction network (Figure 5.20), KLHL17 is predicted to associate with DCN (Decorin), which has been shown to have roles in immunity (Mohan et al., 2011, Neill et al., 2016). Another protein present in the KLHL17 network is ACTC1 (Actin, alpha, cardiac muscle 1).

Importantly, a number of the KLHL family bind to the cullin 3 E3 ubiquitin ligase suggesting that KLHL proteins function in the regulation of ubiquitination (Dhanoa et al., 2013). For example, Keap1 (Kelch-like ECH-associated protein 1) modulates Nrf2 activity and acts as a critical sensor for oxidative and electrophilic stresses (Katoh et al., 2005). Whenever cellular biological stress is not detected, the Keap1-Cul3 E3 ligase ubiquitinates Nrf2 to target degradation via the proteasome. This thereby inhibits Nrf2 activity in the basal state. On the other hand, oxidative and electrophilic stressors inhibit Keap1 ubiquitination activity, thereby facilitating Nrf2 build-up in the nucleus and activation of target genes expression as reviewed in (Suzuki and Yamamoto, 2017).

More recent studies have identified the Keap1/Cul3 pathway to be involved in the regulation of p62 via ubiquitination of K420 in its ubiquitin-associated domain (Lee et al., 2017b). Ubiquitination of the p62 UBA domain by the Keap1/Cul3 complex further increases activity of p62 in sequestering ubiquitinated cargo and recruitment to the growing autophagosome. Interestingly, ubiquitinated p62 also functions as an efficient scaffold adaptor protein to recruit an array of downstream adaptors to bacteria to help maintain a stable complex (Heath et al., 2016). In this mechanism, p62 is ubiquitinated by RNF166 at two different residues: K189 and K91. It is interesting to note that these processes involve both K29- and K33-linked atypical ubiquitin chains. Thus, anti-bacterial degradation function of p62 during xenophagy is facilitated by the activity of the RNF166 ubiquitin ligase (Heath et al., 2016). KLHL17 thus may regulate similar ubiquitination pathways following MRSA infection.

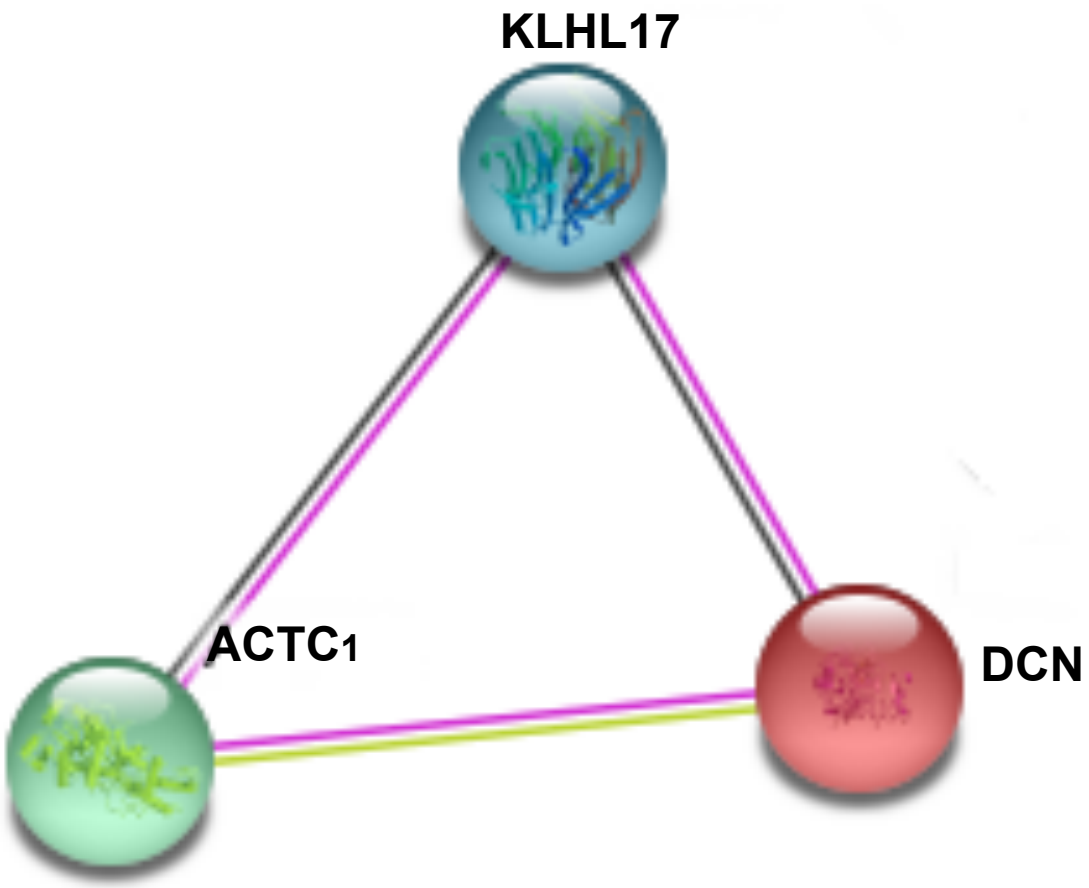

Figure 5.20: *KLHL17* (Kelch-Like 17) interaction Map. The STRING database Interaction network. The proteins present in the network are Decorin (DCN), and Actin, alpha, cardiac muscle 1(ACTC1).

In order to validate hits, six gRNA sequences from each gene were re-cloned into the lentiGuide-Puro vector, confirmed by sequencing and amplified. Lentivirus stocks were made and introduced into HEK293A/Cas9 cells to create CRISPR-targeted lines for each guide of each candidate gene. Use of the smaller lentiGuide-Puro vector (2-vector CRISPR) improves efficiency for re-cloning gRNA sequences. To streamline the process, puro resistant cells carrying the gRNA proceeded immediately to the next step of infection with MRSA (NCTC8325) or *Salmonella enterica* sv. Typhimurium.

Note, we first analysed Cas9 expression levels in our HEK293A/Cas9 stable line. The Cas9 protein was FLAG-tagged. Thus, protein expression was analysed by microscopy following FLAG antibody staining. From this experiment, we found that about 60% of the cells expressed Cas9 (Figure 5.21).

Then, we checked the efficiency of the HEK293/Cas9 cells using the 2-vector CRISPR system. These cells could be efficiently transduced by lentivirus carrying two different gRNA for ATG13, showing strong targeting of protein expression in the total puromycin-resistant cell pools (Figure 5.22). With guide ATG13-03468, the targeting appeared especially strong nearing >90% targeting. Therefore, we concluded that the HEK293/Cas9 cells were a suitable system for the 2-vector CRISPR targeting. There may be sufficient levels of Cas9 for gene editing that we did not detect by FLAG immunostaining and counting.

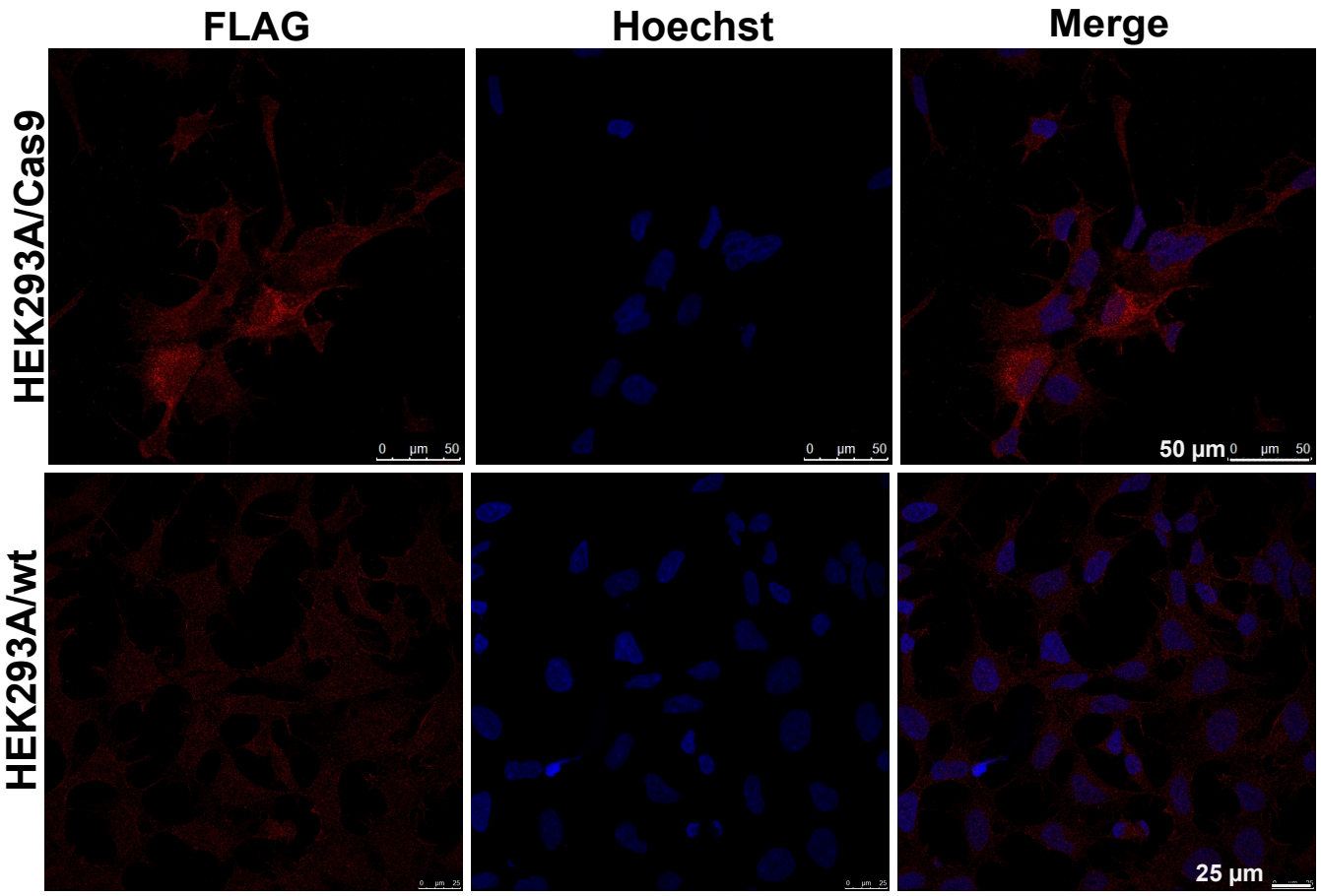

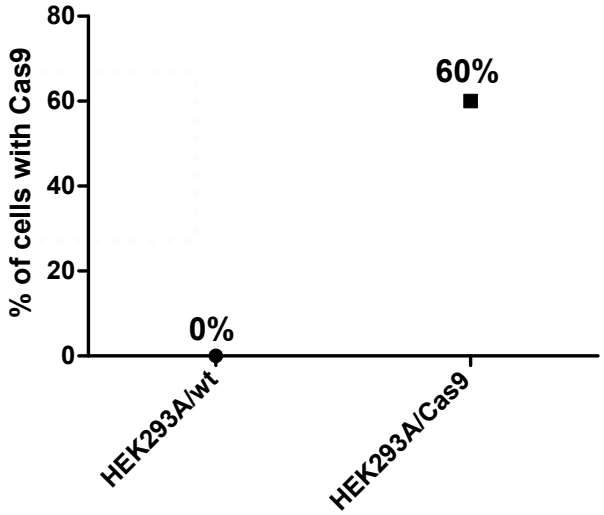

Figure 5.21: The percentage of stable HEK293A blasticidin positive cells expressing Cas9. HEK293A/wt or HEK293A/Cas9-blasticidin cells were plated on glass coverslips then fixed and stained with FLAG antibody. The LentiCas9-Blast vector has a C-terminal FLAG tag on Cas9. The number of cells which have Cas9 were counted using epifluorescent microscopy. Cell images were then captured by confocal microscopy. Scale bar: 50 & 25 µm.

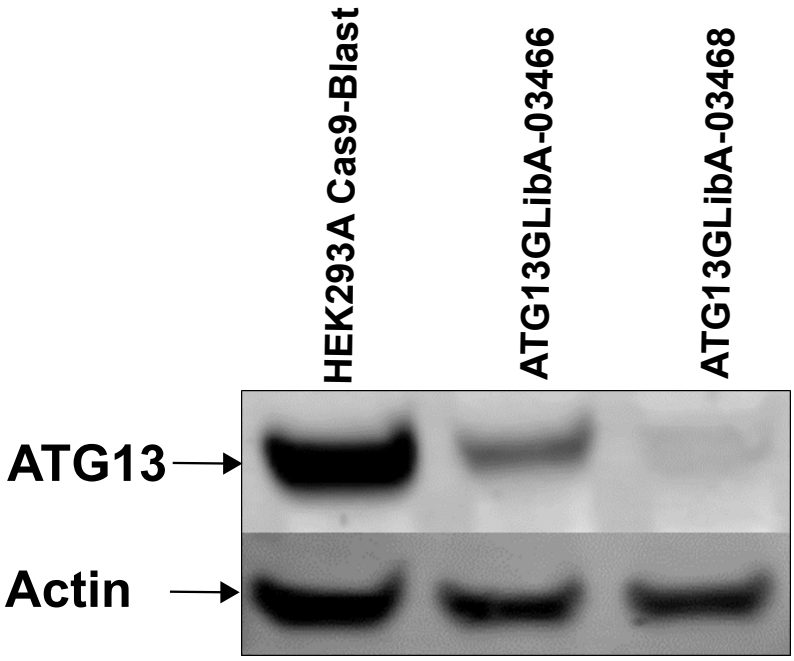

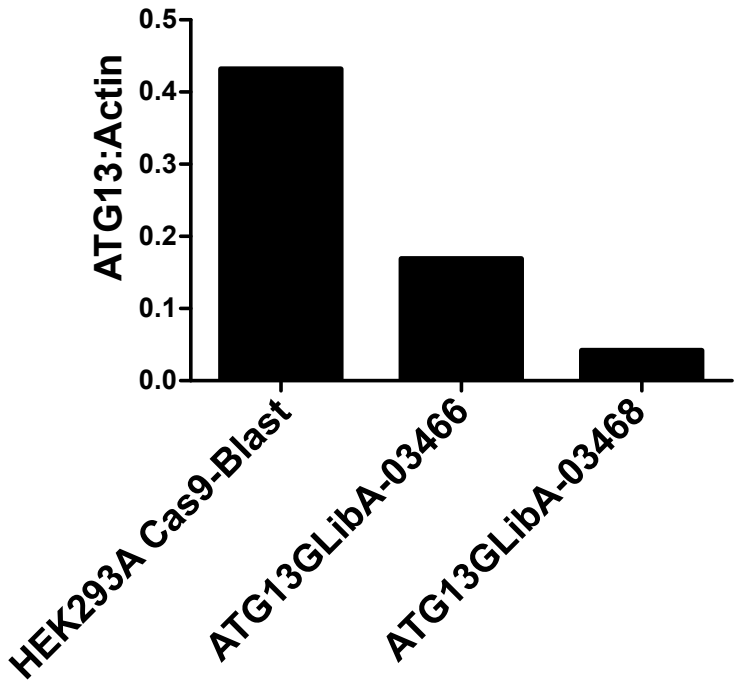

Figure 5.22: The efficiency of HEK293A Cas9 blasticidin cells in knockout of ATG13. HEK293A cells were transduced by gRNAs CRISPR lentivirus for ATG13 at 100% concentration and then selected by puromycin. Efficiency of ATG13 knockout was then confirmed by western blot.

Following this confirmation, HEK293/Cas9 cells were transduced by the different gRNAs for the validation hits and resulting puromycin-resistant cells were infected with MRSA (NCTC8325). Overall, we found good levels of validation across the multiple guides for the three hits selected.

Targeting of *NLRC4* by the NLRC4HGLibA-32090, 32091, NLRC4HGLibB-32047 and 32049 gRNA significantly generated resistance to MRSA (NCTC8325) infection, as compared with the controls HEK293A wildtype (Figure 5.23). For further analysis, we calculated the read count fold-change enrichment for each *NLRC4* gRNA. Interestingly, this analysis found that gRNA #32090, 32047 and 32049 all showed clear enrichment and these were consistent in both MRSA positive selection replicate experiments (Figure 5.24A).

Lastly, we used the BLAT Search tool (UCSC Genome Browser) to map each gRNA sequence across the *NLRC4* gene (Figure 5.24B). We found that all gRNA sequences from the GeCKO library indeed correctly targeted the *NLRC4* gene on chromosome 2. Together, these guides were designed to target either exon 3 or 5, and were directed towards either the forward or reverse strands. Therefore, we have identified a candidate gene and three guide sequences that confirm the initial positive selection result.

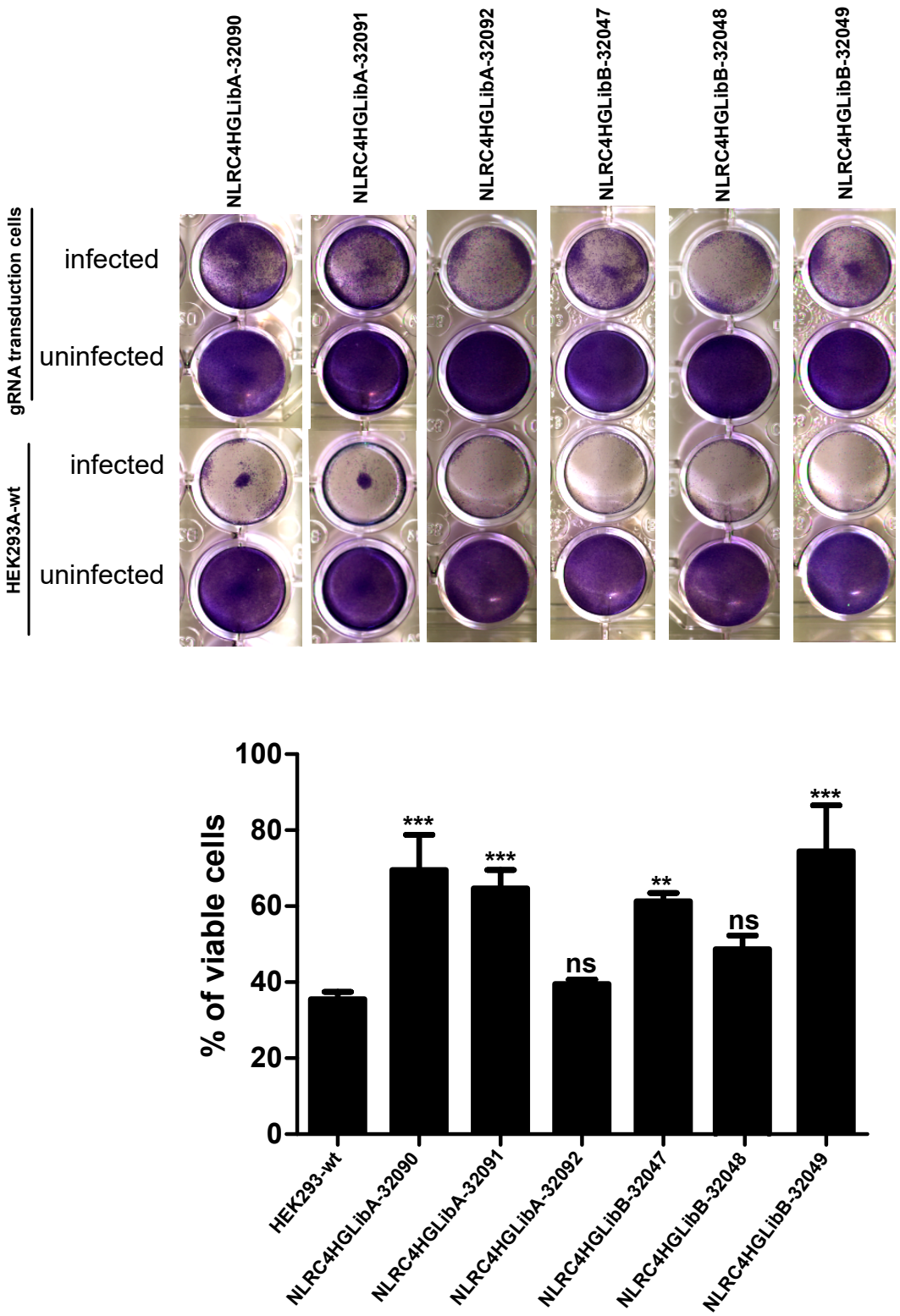

Figure 5.23: gRNAs targeting *NLRC4* results in MRSA resistant cells. HEK293A cells transected with individual gRNAs of *NLRC4* were seeded and infected with NCTC8325 at 200 MOI. After 1hr of infection, gentamicin (0.05 mg/ml) was added and cells were then incubated for 72hrs. Cells were fixed, stained and quantified and the percentage of viable cells was then calculated as described in Figure 5.10. As a control, the HEK/wt cells were included in infection. The average from 3 samples ± SD is shown. P value from one-way ANOVA with Tukey multiple comparison test, comparison to untreated control (**P<0.01, ***P<0.001).

A

gRNA	Control count	Pos. sel. Rep 1	Fold Incr.	Pos. sel. Rep2	Fold Incr.	Validation results
NLRC4HGLibA-32090	10.2	64.2	6.3	73.3	7.2	Significant
NLRC4HGLibA-32091	36.8	53.1	1.4	205.5	5.6	Significant
NLRC4HGLibA-32092	48.9	61.1	1.2	55.5	1.1	Non-Significant
NLRC4HGLibB-32047	12.8	140.4	11.0	365.6	28.6	Significant
NLRC4HGLibB-32048	98.6	101.3	1.0	100.0	1.0	Non-Significant
NLRC4HGLibB-32049	1	60.1	60.1	14.4	14.4	Significant

B

gRNA	Sequence	Cloning Ok?	Size	Identity	Chr	Str	Start	End	Exon
32090	AAACATCATTTGCTGCGAGA	Yes	20	100.0%	2	-	32252548	32252567	3
32091	TATCCATTATGAGCTTTGTA	Yes	20	100.0%	2	+	32241069	32241088	5
32092	GAACCTTACAAAGCTCATAA	Yes	20	100.0%	2	-	32241075	32241094	5
32047	CCATTCAAGTCCTGAAATAG	Yes	20	100.0%	2	+	32252424	32252443	3
32048	GTGGAACTATCCTCTATTTC	Yes	20	100.0%	2	-	32252437	32252456	3
32049	CCGAGCCCTTATTCAAAGAA	Yes	20	100.0%	2	-	32252638	32252657	3

Figure 5.24: Mapping of different gRNA targeting *NLRC4.*
A) Read counts for each guide in control and replicate positive selection. Fold increase was calculated. The validation column shows significantly generated resistance to MRSA (NCTC8325) infections as shown in Figure 4.23.
B) Guide sequences for *NLRC4* were mapped using the BLAT tool (https://genome.ucsc.edu): sequence size, identity, Chromosome, strand, start, end and exon.

Targeting of *AP3D1* by the AP3D1HGLibB-02323, 02324, and 02325 gRNA significantly generated resistance to MRSA (NCTC8325) infection, as compared with the controls HEK293A wildtype (Figure 5.25). We calculated the read count fold-change enrichment for each *AP3D1* gRNA (For further analysis) and found that gRNA #02323, 02324, and 02325 all showed clear enrichment, and these were consistent in both MRSA positive selection replicate experiments (Figure 5.26A).

Figure 4.26B illustrates the use of UCSC Genome Browser (the BLAT Search tool) in mapping every gRNA sequence all over the *AP3D1* gene. We discovered that each and every gRNA sequence from the GeCKO library is in fact accurately targeting the *AP3D1* gene on chromosome 19. These guides were together designed to target either exon 4, 9 or 11, and were directed towards either the forward or reverse strands. We therefore have recognised a candidate gene and three guide sequences, which is a confirmation of the initial positive selection result.

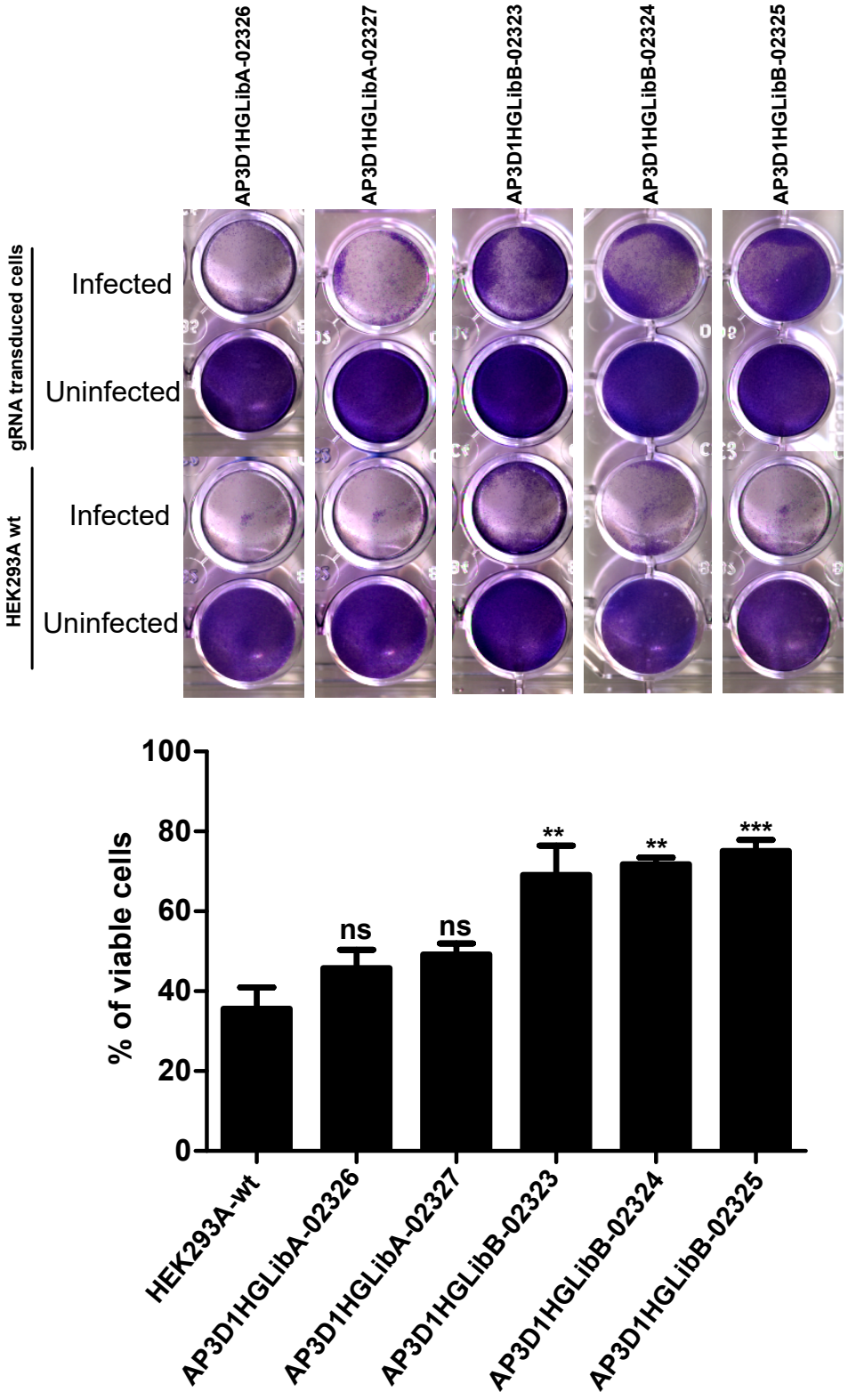

Figure 5.25: gRNAs targeting *AP3D1* results in MRSA resistant cells. HEK293A cells transected with individual gRNAs of *AP3D1* were seeded and infected with NCTC8325 at 200 MOI. After 1hr of infection, gentamicin (0.05 mg/ml) was added and cells were then incubated for 72hrs. Cells were fixed, stained and quantified and the percentage of viable cells was calculated as described in Figure 5.10. As a control, the HEK-wt was included in infection. The average from 3 samples ± SD is shown. P value from one-way ANOVA with Tukey multiple comparison test, comparison to untreated control (**P<0.01, ***P<0.001).

A

gRNA	control count	Pos. sel. Rep 1	Fold Incr.	Pos. sel. Rep2	Fold Incr.	Validation results
AP3D1HGLibA-02325	96.0	65.2	0.7	41.1	0.4	
AP3D1HGLibA-02326	84.0	79.2	0.9	770.1	9.2	Non-Significant
AP3D1HGLibA-02327	91.7	354.1	3.9	717.9	7.8	Non-Significant
AP3D1HGLibB-02323	18.0	58.1	3.2	130.0	7.2	Significant
AP3D1HGLibB-02324	120.1	313.0	2.6	797.9	6.6	Significant
AP3D1HGLibB-02325	36.0	79.2	2.2	81.1	2.3	Significant

B

gRNA	Sequence	Cloning Ok?	Size	Identity	Chr	Str	Strat	End	Exon
02325	CGGTGCCTTCGTGAAAGCTC	No	20	100.0%	19	+	2137046	2137065	4
02326	ACCCACCTTACGGATCTGAT	Yes	20	100.0%	19	+	2137005	2137024	4
02327	TGTGTGAACACCGTGATTGC	Yes	20	100.0%	19	-	2127154	2127173	9
02323	GGATGACTCACAGTTCTGAT	Yes	20	100.0%	19	+	2123347	2123366	11
02324	CCAGTTCTCACCTGCAATCA	Yes	20	100.0%	19	+	2127141	2127160	9
02325	AGCTTTGTGTTCAGAAATTA	Yes	20	100.0%	19	-	2123389	2123408	11

Figure 5.26: Mapping of different gRNA targeting *AP3D1.*
A) Read counts for each guide in control and replicate positive selection. Fold increase was calculated. The validation column shows the significantly generated resistance to MRSA (NCTC8325) infections as shown in Figure 4.25.
B) Guide sequences for *AP3D1* were mapped using the BLAT tool (https://genome.ucsc.edu): sequence size, identity, Chromosome, strand, start, end and exon.

Targeting of *KLHL17* by the KLHL17HGLibA-25141, 25142, KLHL17HGLibB 25106, and 25107 gRNA significantly generated resistance to MRSA (NCTC8325) infection, as compared with the controls HEK293A wildtype (Figure 5.27). We calculated the read count fold-change enrichment for each *KLHL17* gRNA and found that gRNAs which significantly generated resistance for MRSA all showed clear enrichment and these were consistent in both MRSA positive selection replicate experiments (Figure 5.28A).

Using the BLAT Search tool (UCSC Genome Browser) to map each gRNA sequence across the *KLHL17* gene (Figure 5.28B), we found that all gRNA sequences from the GeCKO library indeed correctly targeted the *KLHL17* gene on chromosome 1. Together, these guides were designed to target either exon 2, 3 or 11, and were directed towards either the forward or reverse strands. Therefore, we have identified a candidate gene and four guide sequences that confirm the initial positive selection result.

Together, these results therefore confirm three to four different guide sequences that validate our initial results from the screen for MRSA toxicity.

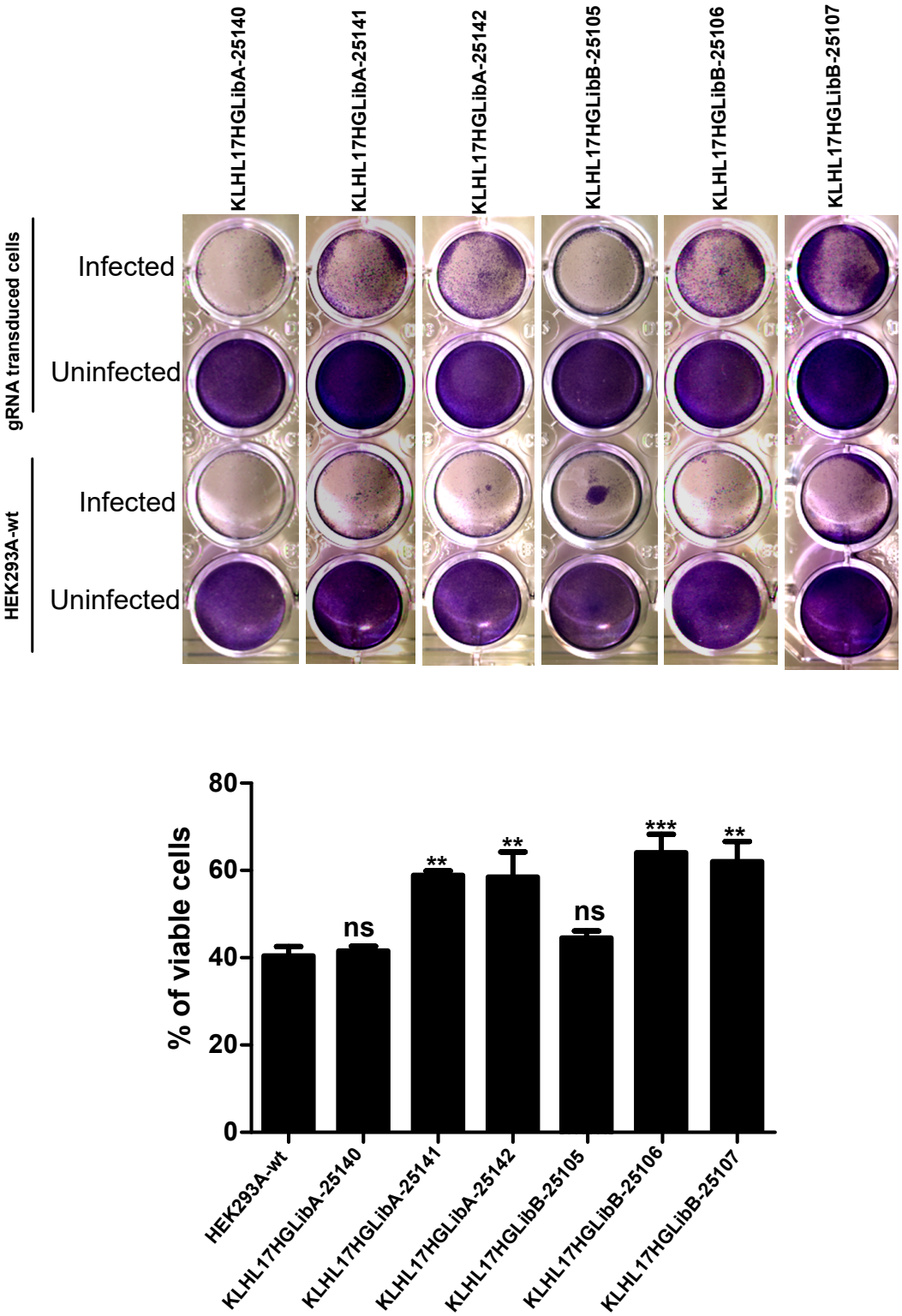

Figure 5.27: gRNAs targeting of *KLHL17* results in MRSA resistant cells. HEK293A cells transduced with individual gRNAs of *KLHL1* were seeded and infected with NCTC8325 at 200 MOI. After 1hr of infection, gentamicin (0.05 mg/ml) was added and cells were then incubated for 72hrs. Cells were fixed, stained and quantified and the percentage of viable cells was calculated as described in Figure 5.10. As a control, the HEK-wt was included in infection. The average from 3 samples ± SD is shown. P value from one-way ANOVA with Tukey multiple comparison test, comparison to untreated control (**P<0.01, ***P<0.001).

A

gRNA	control count	Pos. sel. Rep 1	Fold Incr.	Pos. sel. Rep2	Fold Incr.	Validation results
KLHL17HGLibA-25140	141.5	687.2	4.9	381.1	2.7	Non-Significant
KLHL17HGLibA-25141	303.7	809.6	2.7	2432.7	8.0	Significant
KLHL17HGLibA-25142	138.1	369.2	2.7	223.3	1.6	Significant
KLHL17HGLibB-25105	124.4	149.4	1.2	16.6	0.1	Non-Significant
KLHL17HGLibB-25106	40.3	472.5	11.7	127.8	3.2	Significant
KLHL17HGLibB-25107	133.8	775.5	5.8	325.6	2.4	Significant

B

gRNA	Sequence	Cloning Ok?	Size	Identity	Chr	Str	Strat	End	Exon
25140	TGCGGACCTGCGGATATTCA	Yes	20	100.0%	1	-	964518	964537	11
25141	CGATGTCGTGCAGCGTCACG	Yes	20	100.0%	1	-	961657	961676	3
25142	GCTGCACGACATCGACCCTC	Yes	20	100.0%	1	+	961663	961682	3
25105	GGAGATCCGTGCGCACAAAG	Yes	20	100.0%	1	+	961488	961507	2
25106	GTGCGACATCGTCCTGCACG	Yes	20	100.0%	1	+	961458	961477	2
25107	CGTTGCCCCCTGCCACGTAC	Yes	20	100.0%	1	-	964426	964445	11

Figure 5.28: Mapping of different gRNA targeting *KLHL17.*
A) Read counts for each guide in control and replicate positive selection. Fold increase was calculated. The validation column shows the significantly generated resistance to MRSA (NCTC8325) infections as shown in Figure 4.27.
B) Guide sequences for *KLHL17* were mapped using the BLAT tool (https://genome.ucsc.edu): sequence size, identity, Chromosome, strand, start, end and exon.

5.2.2.6.2. Validation hits of *Salmonella enterica* sv. Typhimurium screen

From the *Salmonella enterica* sv. Typhimurium screen, *DAZL*, *CD164* and *ARHGAP28*, are potentially interesting genetic modifiers of infection.

The overgrowth of clones having a *DAZL* (Deleted in Azoospermia-Like) gene represents an intriguing result from this screen. The *DAZL* gene is specific for germ-cells and is essential in their development and differentiation (Reijo et al., 1995). The protein which encodes by this gene is associated with many proteins, such as the ATP Citrate Lyase (ACLY), Phosphoribosyl Formylglycin Amidine Synthase (PFAS), Cell Division Cycle 40 (CDC40), SNW Domain Containing 1 (SNW1) and DEAH-Box Helicase 8(DHX8), as shown in Figure 5.29. Because the *DAZL* was the most significantly enriched gene (P=0.00006317), with five gRNA showing consistent levels of enrichment, it was chosen for validation.

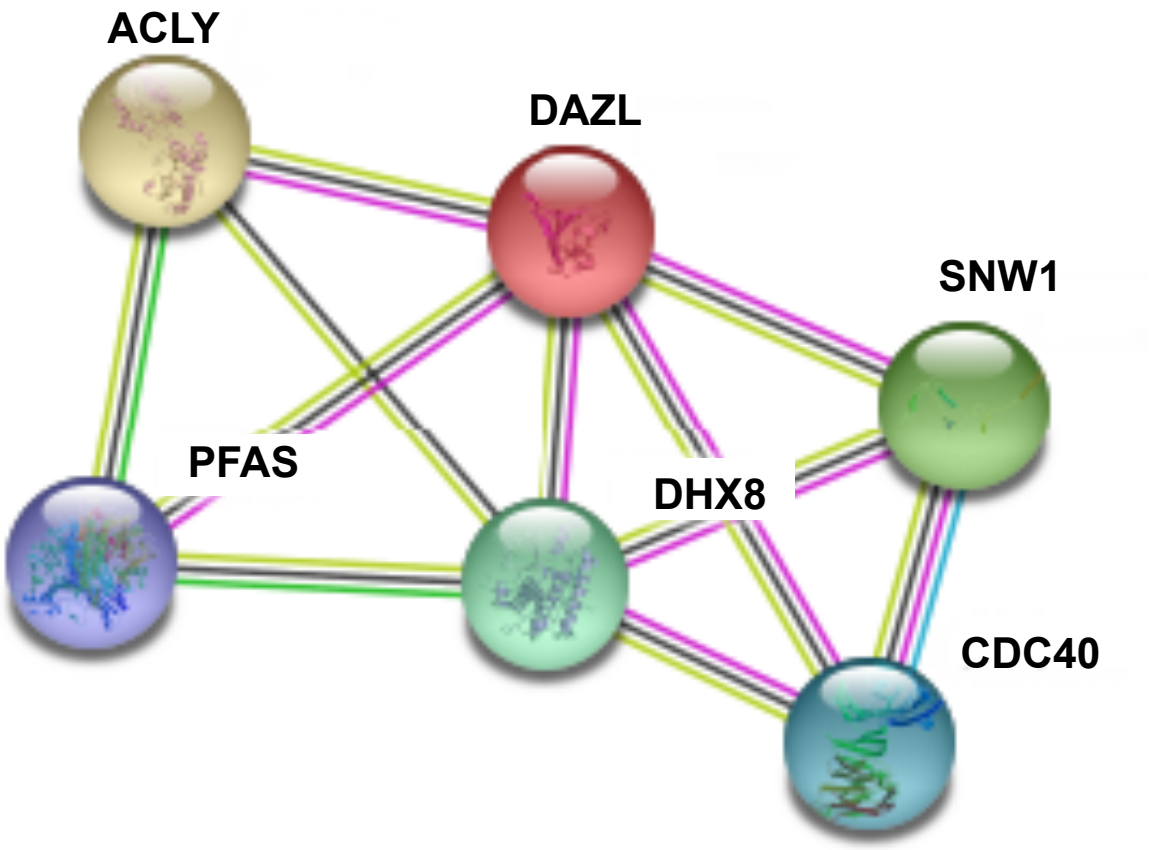

Figure 5.29: *DAZL* (Deleted in Azoospermia-Like) interaction Map. The STRING database Interaction network. The proteins present in the network are the ATP Citrate Lyase (ACLY), Phosphoribosylformylglycinamidine Synthase (PFAS), Cell Division Cycle 40 (CDC40), SNW Domain Containing 1 (SNW1) and DEAH-Box Helicase 8(DHX8).

CD164 (Cluster of differentiation 164) has been demonstrated to be involved in the regulation of proliferation, apoptosis and adhesion (Forde et al., 2007, Doyonnas et al., 2000). From the protein interaction network of *CD164* (Figure 5.30), potential mechanisms are suggested with CXCR4 (Chemokine receptor 4) and CXCR7 (Chemokine receptor 7). CXCR4 is an important receptor in the innate immunity involved in the recognition of a lipopolysaccharide (LPS), which is the main constituent of gram-negative bacterial cell walls (Triantafilou et al., 2008).

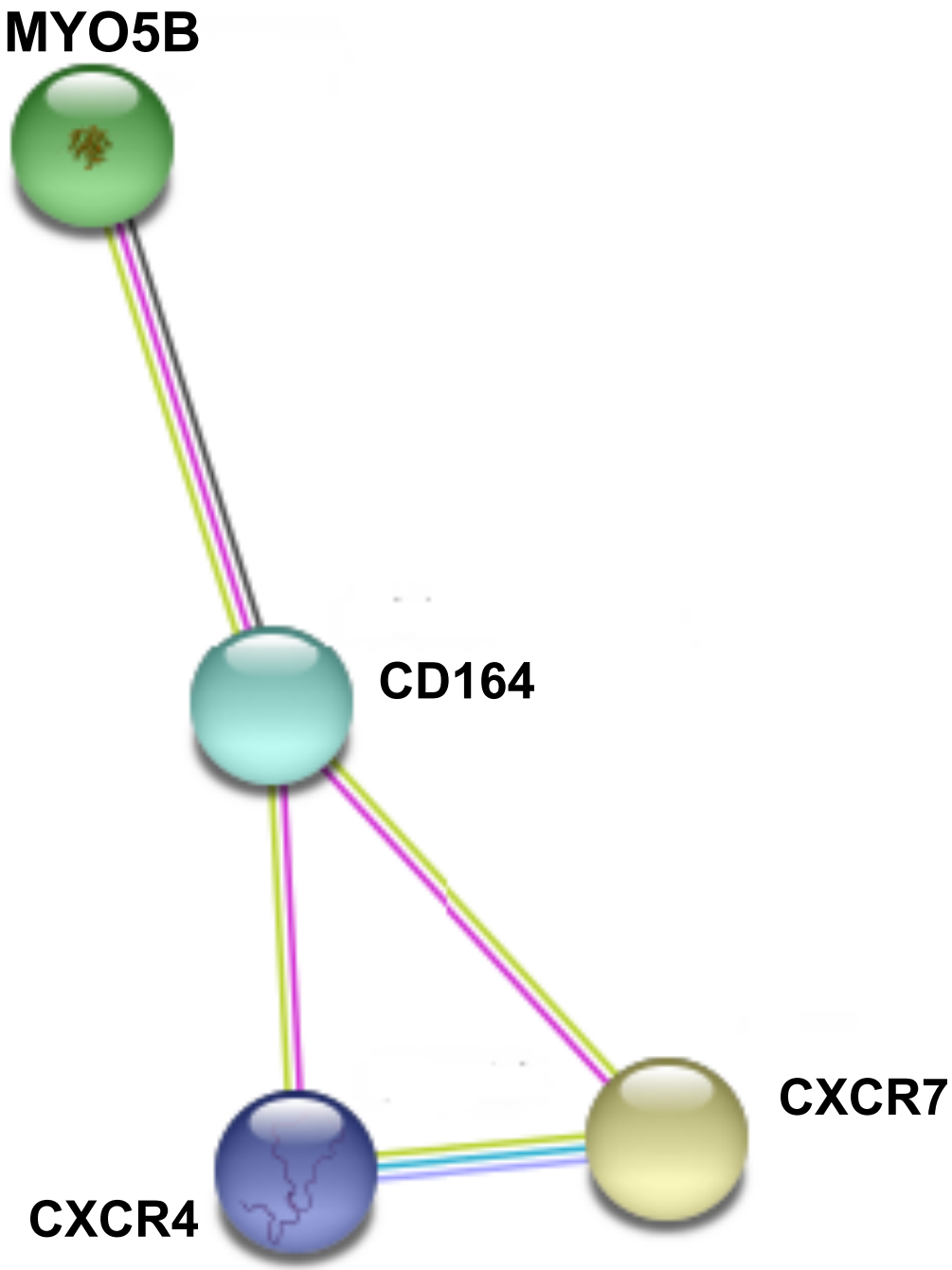

Figure 5.30: *CD164* (Cluster of differentiation 164) interaction Map. The STRING database Interaction network. The proteins present in the network are the C-X-C chemokine receptor type 4 (CXCR-4), C-X-C chemokine receptor type 7 (CXCR-7), and Myosin-Vb (MYO5B).

ARHGAP28 (Rho-Type GTPase-Activating Protein 28) encodes a member of the Rho GTPase activating protein family. From the protein interaction network in Figure 5.31, it can be seen that the proteins associated with this protein are Ras-related C3 botulinum toxin substrate 2 (RAC2), Ras homolog family member D (RHOD), Ras homolog family member C (RHOC), Ras homolog family member D (RHOD), and Ras homolog family member T2 (RHOT2). Rho GTPases are key regulators of innate immune cell functions including cell migration, reactive oxygen species (ROS) production, phagocytosis and degranulation (Bokoch, 2005). One of the closely related GTPase isoforms presented in *ARHGAP28* network is Rac2, which has an important role in innate immunity (Lim et al., 2011). The activation of the Rho GTPases family CDC42 and the RhoG binding protein is carried out by SPI-1 secreted effectors and is crucial for *Salmonella*-induced cytoskeleton rearrangements and bacterial invasion (LaRock et al., 2015, Patel and Galan, 2006).

Research carried out by Keestra et al. (2013) documented that the triggering of small Rho GTPases as a pathogen-instigated activity occurred within the NOD1 signalling pathway. This study identified that activation of RAC1 and CDC42 by *Salmonella* virulence factor (SopE) triggered the NOD1 signalling pathway, with consequent RIP2-mediated induction of NF-κB-dependent inflammatory responses. Likewise, RAC1 intervention is essential in the activation of the NOD1 pathway through peptidoglycan influence. The study also identified that an active constitutive expression of CDC42, RhoA and RAC1 triggered the NOD1 pathway (Keestra et al., 2013).

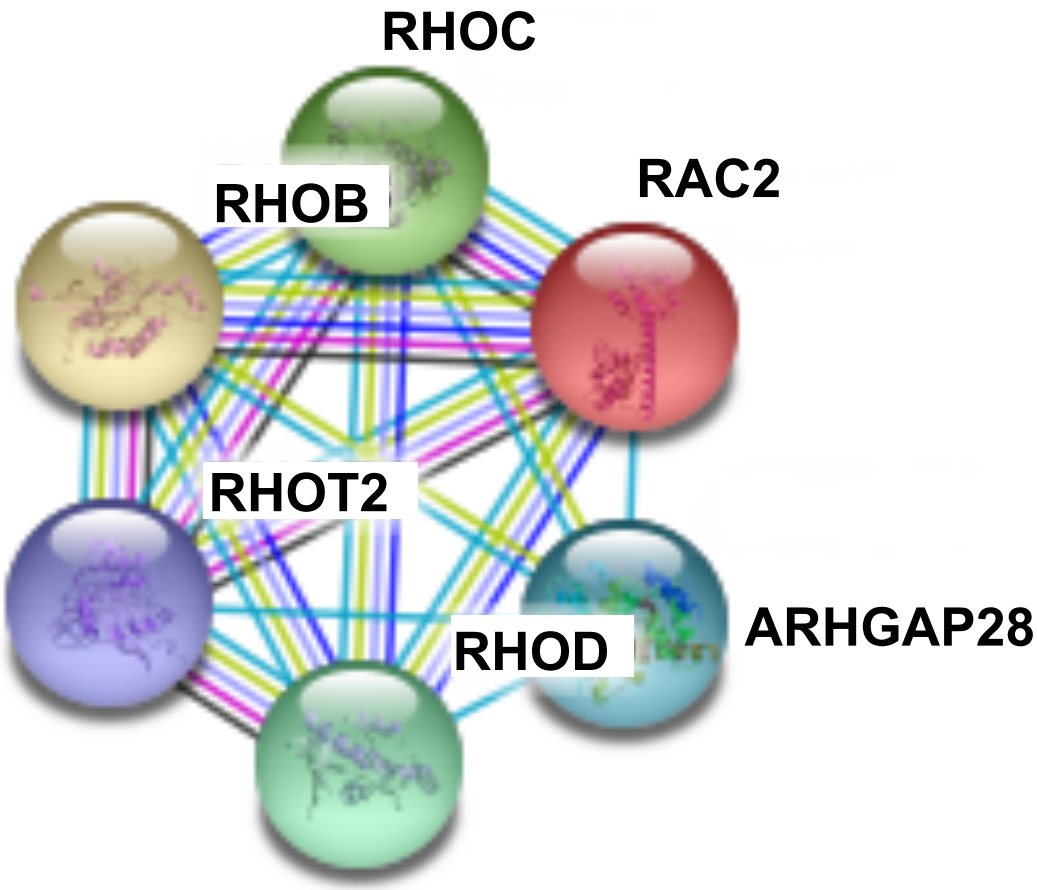

Figure 5.31: *ARHGAP28* (Rho-Type GTPase-Activating Protein 28) interaction Map. The STRING database Interaction network. The proteins present in the network are Ras-related C3 botulinum toxin substrate 2 (RAC2), Ras homolog family member D (RHOD), Ras homolog family member C (RHOC), Ras homolog family member D (RHOD), and Ras homolog family member T2 (RHOT2).

As we performed the procedures above, to validate the three genes from the *Salmonella enterica* sv. Typhimurium screen, HEK293/Cas9 cells were transduced by the six different gRNAs for the validation hits. The resulting puromycin-resistant cells were infected with *Salmonella enterica* sv. Typhimurium. Overall, we also found good levels of validation across the multiple guides for the *DAZL* and *CD164* hits selected.

Targeting of *DAZL* by the DAZLHGLibA-12369, or DAZLHGLibB-12356, 12357 and 12358 gRNA significantly generated resistance to *Salmonella enterica* sv. Typhimurium infection, as compared with the controls HEK293A wildtype (Figure 5.32). When the read count fold-change enrichment for each *DAZL* gRNA was calculated, we discovered that gRNA #12369 or DAZLHGLibB-12356, and 12358 all exhibited enrichment which is clear (Figure 5.33A).

Figure 5.33B clearly shows the use of the UCSC Genome Browser (the BLAT Search tool) in mapping each and every gRNA sequence across the *DAZL* gene. We found that each and every gRNA sequence from the GeCKO library in fact targeted at the *DAZL* gene accurately on chromosome 3. These guides were together meant to aim at exon 3 or 2, and were directed to the reverse or forward strands. We, therefore, have recognised three guide sequences and candidate gene that prove the first positive selection outcome.

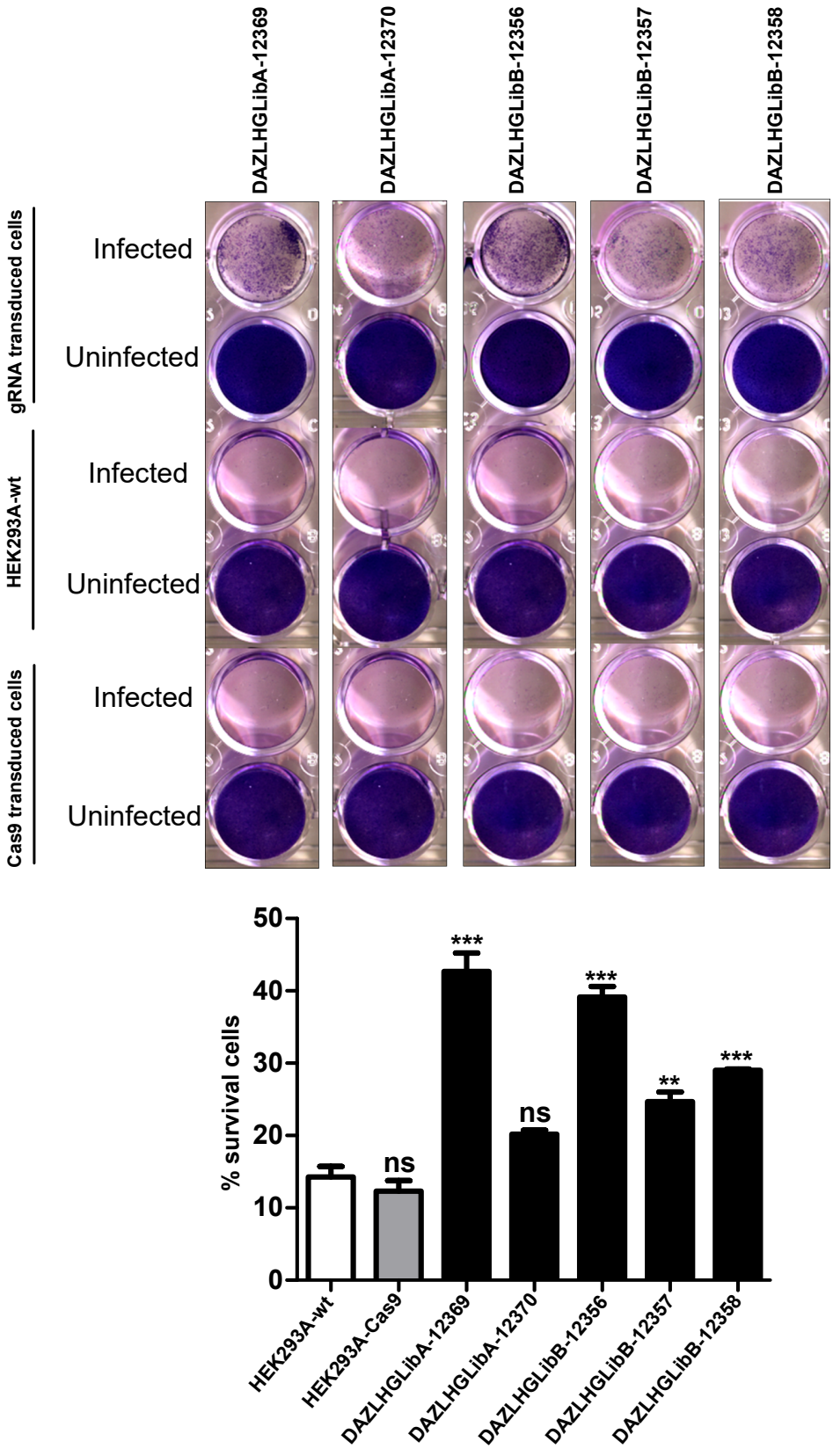

Figure 5.32: gRNA targeting *DAZL* results in *Salmonella enterica* sv. Typhimurium resistant cells. HEK293A cells transduced with individual gRNAs of *DAZL* were seeded and infected with *Salmonella enterica* sv. Typhimurium at 1:100 MOI. After 50 min. of infection, gentamicin (0.05 mg/ml) was added and cells were then incubated for 72hrs. Cells were fixed, stained and quantified and the percentage of viable cells was then calculated as described in Figure 5.10. As a control, the HEK/wt and HEK/Cas9 were included in infection. The average from 3 samples ± SD is shown. P value from one-way ANOVA with Tukey multiple comparison test, comparison to untreated control (**P<0.01, ***P<0.001).

A

gRNA	control count	Pos. sel. count	Fold Incr.	Validation results
DAZLHGLibA-12369	26.9	199.5	7.4	Significant
DAZLHGLibA-12370	13.0	71.0	5.5	Non-Significant
DAZLHGLibA-12371	20.3	125.7	6.2	
DAZLHGLibB-12356	11.4	185.9	16.3	Significant
DAZLHGLibB-12357	26.5	57.4	2.2	Significant
DAZLHGLibB-12358	24.4	246.0	10.1	Significant

B

gRNA	Sequence	Cloning Ok?	Size	Identity	Chr	Str	Strat	End	Exon
12369	CTTCTGGTAAAATATAGCCT	Yes	20	100.0%	3	+	16598499	16598518	2
12370	AAGATAATCACTGATCGAAC	Yes	20	100.0%	3	-	16598102	16598121	3
12371	AGAAGCTTCTTTGCTAGATA	No	20	100.0%	3	-	16598141	16598160	3
12356	TCATCAGCTGCAACCAGCCA	Yes	20	100.0%	3	-	16598519	16598538	2
12357	TGGTTGCAGCTGATGAGGAC	Yes	20	100.0%	3	+	16598523	16598542	2
12358	CCTCCAACAAAAACAGTGTT	Yes	20	100.0%	3	+	16598465	16598484	2

Figure 5.33: Mapping of different gRNA targeting *DAZL*.
A) Read counts for each guide in control and positive selection. Fold increase was calculated. The validation column shows the significantly generated resistance to *Salmonella typhimurium* infections as shown in Figure 4.32.
B) Guide sequences for *DAZL* were mapped using the BLAT tool (https://genome.ucsc.edu): sequence size, identity, Chromosome, strand, start, end and exon.

Targeting of the *CD164* gene by CD164HGLibA-08248, 08249, 08250, CD164HGLibB-08241, 08242, and 08243 sgRNA significantly generated resistance to *Salmonella enterica* sv. Typhimurium infection, as compared with the controls HEK293A wildtype (Figure 5.34). We calculated the read count fold-change enrichment for each *CD164* gRNA and found that all gRNAs which significantly generated resistance for *Salmonella enterica* sv. Typhimurium also showed clear enrichment (Figure 5.35A).

Using the BLAT Search tool (UCSC Genome Browser) to map each gRNA sequence across the *CD164* gene (Figure 5.35B), we found that all gRNA sequences from the GeCKO library indeed correctly targeted the *CD164* gene on chromosome 6. Together, these guides were designed to target either exon 2, 3, 4 or 5, and were directed towards either the forward or reverse strands. Therefore, we have identified a candidate gene and all the six guide sequences that confirm the initial positive selection result.

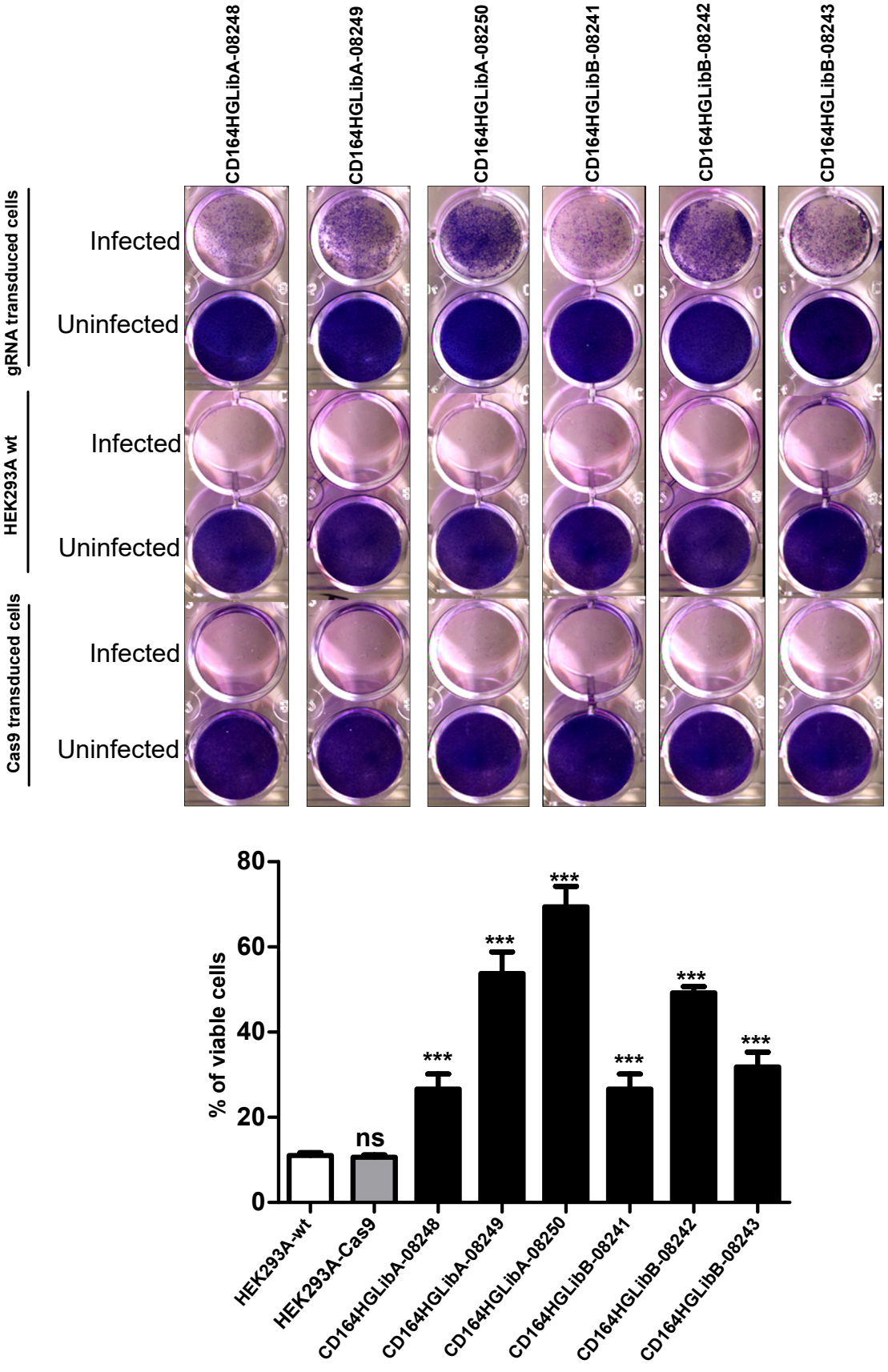

Figure 5.34: gRNA targeting *CD164* results in *Salmonella enterica* sv. Typhimurium resistant cells. HEK293A cells transduced with individual gRNAs of *CD164* were seeded and infected with *Salmonella enterica* sv. Typhimurium at 1:100 MOI. After 50 min. of infection, gentamicin (0.05 mg/ml) was added and cells were then incubated for 72hrs. Cells were fixed, stained and quantified and the percentage of viable cells was then calculated as described in Figure 5.10. As a control, the HEK/wt and HEK/Cas9 cells were included in infection. The average from 3 samples ± SD is shown. P value from one-way ANOVA with Tukey multiple comparison test, comparison to untreated control (***P<0.001).

A

gRNA	control count	Pos. sel. count	Fold Incr.	Validation results
CD164HGLibA-08248	27.7	139.4	5.0	Significant
CD164HGLibA-08249	119.5	426.4	3.6	Significant
CD164HGLibA-08250	77.0	393.6	5.1	Significant
CD164HGLibB-08241	45.6	352.6	7.7	Significant
CD164HGLibB-08242	19.1	194.1	10.2	Significant
CD164HGLibB-08243	91.3	410.0	4.5	Significant

B

gRNA	Sequence	Cloning Ok?	Size	Identity	Chr	Str	Strat	End	Exon
08248	GCAGCTGTTTCGACCTTCAC	Yes	20	100.0%	6	+	109379637	109379656	2
08249	GTGCCAACAGCCAATTCTAC	Yes	20	100.0%	6	-	109376076	109376095	4
08250	AACACGACAGACTTCTGTTC	Yes	20	100.0%	6	-	109377902	109377921	3
08241	TCCAAGACAGTTACTACATC	Yes	20	100.0%	6	-	109370413	109370432	5
08242	AACAGTTAGTGATTGTCAAG	Yes	20	100.0%	6	-	109377927	109377946	3
08243	ACCTGATGTAGTAACTGTCT	Yes	20	100.0%	6	+	109370409	109370428	5

Figure 5.35: Mapping of different gRNA targeting *CD164*.
A) Read counts for each guide in control and positive selection. Fold increase was calculated. The validation column shows the significantly generated resistance to *Salmonella typhimurium* infections as shown in Figure 4.34.
B) Guide sequences for *CD164* were mapped using the BLAT tool (https://genome.ucsc.edu): sequence size, identity, Chromosome, strand, start, end and exon.

Targeting of *ARHGAP28* by different 6 gRNAs, however, did not appear to cause any resistance to infection by *Salmonella enterica* sv. Typhimurium (Figures 5.36). Surprisingly, when we calculated the read count fold-change enrichment for each *ARHGAP28* gRNA, we found that all gRNAs showed clear enrichment (Figure 5.37A).

Using the BLAT Search tool (UCSC Genome Browser) to map each gRNA sequence across the *ARHGAP28 gene* (Figure 5.37B), we found that all gRNA sequences from the GeCKO library indeed correctly targeted the *ARHGAP28* gene on chromosome 18. Together, these guides were designed to target either exon 6, 7, or 8, and were directed towards either the forward or reverse strands.

These results demonstrated that we could confirm two out of three genes chosen for retesting. With both *DAZL* and *CD164*, of test 4 gRNA showed significant confirmation and some of these produced a strong effect, even in CRISPR pooled cell populations. These new candidates enable future studies of potentially interesting mechanisms.

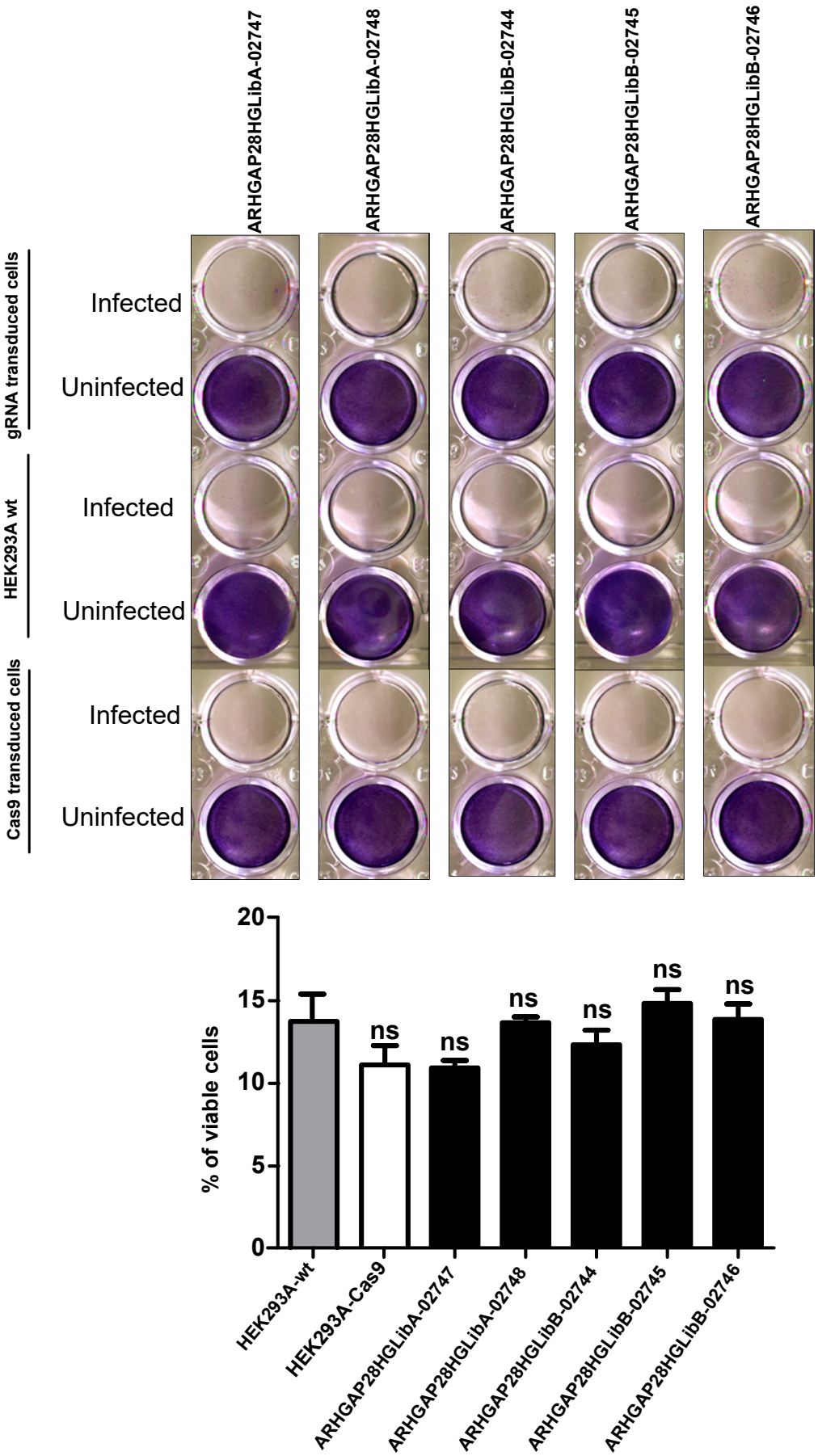

Figure 5.36: gRNA targeting of *ARHGAP28* did not give resistant cells following infection by *Salmonella enterica* sv. Typhimurium. HEK293A cells transduced with individual gRNAs of *ARHGAP28* were seeded and infected with *Salmonella enterica* sv. Typhimurium at 1:100 MOI. After 50 min. of infection, gentamicin (0.05 mg/ml) was added and cells were then incubated for 72hrs. Cells were fixed, stained and quantified and the percentage of viable cells was then calculated as described in Figure 5.10. As a control, the HEK/wt and HEK/Cas9 cells were included in infection. The average from 3 samples ± SD is shown. P value from one-way ANOVA with Tukey multiple comparison test, comparison to untreated control.

A

gRNA	control count	Pos. sel. count	Fold Incr	Validation results
ARHGAP28HGLibA-02746	53.4	937.7	17.5	Non-Significant
ARHGAP28HGLibA-02747	47.7	303.4	6.4	Non-Significant
ARHGAP28HGLibA-02748	19.9	254.2	12.7	
ARHGAP28HGLibB-02744	65.2	311.6	4.8	Non-Significant
ARHGAP28HGLibB-02745	73.8	76.5	1.0	Non-Significant
ARHGAP28HGLibB-02746	4.4	92.9	21.1	Non-Significant

B

gRNA	Sequence	Cloning Ok?	Size	Identity	Chr	Str	Strat	End	Exon
02746	CCACTTATCGCATTCTGAAC	No	20	100.0%	18	-	6868216	6868235	6
02747	CCAGTTCAGAATGCGATAAG	Yes	20	100.0%	18	+	6868213	6868232	6
02748	TGCTTCAGTTAAGCCAAATC	Yes	20	100.0%	18	-	6873431	6873450	8
02744	AATGTTCAGAAAACCAGATT	Yes	20	100.0%	18	+	6873415	6873434	8
02745	AATGACAGCTCTTCAGCCTC	Yes	20	100.0%	18	-	6870622	6870641	7
02746	TGAAGTGTCTTATTCAGAAA	Yes	20	100.0%	18	+	6870642	6870661	7

Figure 5.37. Mapping of different gRNA targeting *ARHGAP28*.
A) Read counts for each guide in control and positive selection. Fold increase was calculated.
B) Guide sequences for *ARHGAP28* were mapped using the BLAT tool (https://genome.ucsc.edu): sequence size, identity, Chromosome, strand, start, end and exon.

5.3. Discussion

One major strategy has been to search for newer drug scaffolds to tackle the appearance of multi-drug resistance in bacteria. The goal is to develop a new drug that kills or attenuates the bacteria, but this strategy has a high risk of the pathogen becoming more resistant to a broader range of drugs. The other strategy calls for understanding the interaction which this pathogen makes with host cells to identify the crucial biological pathways needed to enable infection. Here, we aimed to work towards development of novel therapeutic strategies targeting the genes in host cells required for *Staphylococcus aureus* or *Salmonella enterica* sv. Typhimurium infection.

CRISPR Cas9 technology has revolutionised genome editing by providing a stable and programmable method in mammalian cells. Multiple groups have already reported CRISPR for high-throughput knockout screening by developing large-scale CRISPR sgRNA libraries (Arroyo et al., 2016, Sanjana et al., 2014, Shalem et al., 2014, Wang et al., 2015, Zhong et al., 2015, Zhou et al., 2014). The volume of similar projects currently in progress seems to be growing, based on online CRISPR screening user forums hosted by Google. Here, we proposed to perform a genome-wide CRISPR/Cas9-mediated screen to identify host factors required for *Staphylococcus aureus* and *Salmonella enterica* sv. Typhimurium mediated toxicity. This is an unbiased way to identify different biological pathways required by these two pathogens to produce infection. Also, loss of ULK1 function and autophagy led to resistance to MRSA. Therefore, the MRSA screen could uncover novel autophagy factors.

5.3.1. Optimisation experiments

Before starting the work with this CRISPR library, we optimised a range of lentiviral methodologies. Firstly, we wanted to know for cost/benefit reasons whether it was more efficient to use Lipofectamine (commercial) or calcium phosphate (developed in-house) transfection to generate virus. Lipofectamine was reproducibly more efficient and worth the extra cost for GeCKO viral production. We aimed to improve viral transduction, so we tried spinfection, a more involved method reported to increase contact between viral particles and cells. Spinfection improved viral transduction by just 5–10 percent. Therefore, this additional manipulation, which

introduces more handling and safety considerations, was not dramatically important for viral transduction.

Our previous experiments found that HEK and HeLa cells were clearly invaded and killed by both *Staphylococcus aureus* and *Salmonella enterica* sv. Typhimurium. Therefore, we aimed to determine how each of these cells could be transduced with CRISPR lentivirus. It was found that HEK293A cells were 95% better than the HeLa cells in the uptake of the CRISPR lentivirus vector. Therefore, we chose HEK293A cells as a more efficient host for the screen. Moreover, because sometimes we obtained a variable lentivirus titre, we optimised how this was related to 293FT packaging cell confluence. We found that titre of virus was clearly increased when the FT cells confluence steadily increased. Therefore, high confluence of HEK FT was critical to increase the GeCKO viral titre. Finally, because the CRISPR library screen would involve a large collection of clones and a requirement to work across days, we confirmed that freezing would not affect the virus titre.

These optimisation experiments allowed us to become more familiar with the one-vector system. The genome wide CRISPR Knock-Out (GeCKO) pooled libraries that we used contains over 120,000 gRNAs with six gRNAs per gene for 5' constitutive exons of 19,050 human genes and four gRNAs per miRNA. Multiple unique sgRNAs target the same gene controls for off-target effects of single guides and null background depletion/enrichment. Also, in order to reduce the false positive rate, our design had two biological replicates of the positive selection pressure. Furthermore, in order to favour only one sgRNA per cell, we initially infected cells with low MOI (around 0.5) and we started with a sufficiently large number of cells ($80*10^6$) in order to obtain high representation for the library (300x per guide). We indeed confirmed that our cell library contained 81.4% of all CRISPR gRNA sequences. The other 18% gRNAs were perhaps targeting essential genes and could not be stably tolerated.

5.3.2. MaGeck algorithm method for NGS analysis of cell library

Analysis of gRNA enrichment was done using the model-based Analysis of Genome-wide CRISPR/Cas9 Knockout (MaGeck) algorithm (Li et al., 2014). A previous study had compared MaGeck to other available methods including: methods for statistical evaluation of high-throughput sequencing read counts using NB models (edgeR,

(Robinson et al., 2010) and DESeq (Anders and Huber, 2010); methods designed for genome-scale RNAi screens (RNAi Gene Enrichment Ranking (RIGER) (Luo et al., 2008); and methods for Redundant siRNA Activity (RSA) (Konig et al., 2007). By comparing MaGeck with two RNAi screening algorithms (RIGER and RSA), RIGER showed lower sensitivity when cross compared with MaGeck using data from two negative screening studies (Wang et al., 2014, Koike-Yusa et al., 2014). On the other hand, RSA showed lower specificity and identified higher numbers of genes. MaGeck provided a better overall balanced level of analysis and was able to detect significant genes while giving very few false positives as compared to controls or replicates. The properties of MaGeck proved to be valuable since it was shown to be capable of identifying a number of novel genes and pathways (not reported in original studies) like *EGFR* in datasets from vemurafenib-treated A375 cells carrying activated BRAF (Li et al., 2014).

5.3.3. NGS analysis of cell library after positive selection

Using MaGeck analysis on our own data, we focused on the top ten candidate host genes from each pathogen screen. CRISPR of these genes led to bacterial resistance. Therefore, these genes may be essential for pathogen infection. These hits were ranked based on lowest RRA score and multiple gRNA enrichment. However, variability in cell resistance between the different gRNA targeting the same gene may be due to the variable efficiency of the Cas9 and gRNA complex to introduce double-strand breaks (DSBs). Successful strong disruption of the target gene only occurs if a frameshift mutation is introduced by DNA repair mechanisms in both alleles. Therefore, some cells may have partial mutation or inframe mutations that still encode a functional protein. Differences in efficiency using different gRNAs has been observed in other CRISPR/Cas9 screens (Virreira Winter et al., 2016, Zhou et al., 2014). Recently, it was found that gene knockout efficiency can be influenced by the expression levels of Cas9, the sequence of the gRNA and the chromosomal context (Chen et al., 2015). Despite these challenges, we were able to obtain good rates of confirmation of selected candidates genes.

5.3.4. Validation from hits of MRSA screen

For the validation experiments, we chose three hits from the infection screens based on a combination of lowest p-values and good multiple gRNA enrichment and interesting mechanisms.

We could confirm that CRISPR targeting of *NLRC4* led to resistance to MRSA (NCTC8325). It was earlier demonstrated that the inflammasome pathway containing *NLRC4* protein was activated in response to two bacterial proteins that were part of the pathogen-associated type III secretion systems: flagellin (Franchi et al., 2006) and PrgJ (Miao et al., 2010). Other studies have demonstrated the role which NLRC4 plays in responding against *Salmonella enterica* sv. Typhimurium, *Shigella flexneri*, *Legionella pneumophila* and *Pseudomonas aeruginosa* (Mariathasan et al., 2004, Cohen and Prince, 2013, Lightfield et al., 2011). Interestingly, inflammasome activation can upregulate autophagy in an attempt to protect the host from excessive inflammation (Deretic, 2012). Recently it was found that *Pseudomonas aeruginosa* triggers macrophage autophagy by activation of the NLRP3 Inflammasome in order to escape intracellular killing (Deng et al., 2016). IL-1β decreased the macrophage-mediated killing of *Pseudomonas aeruginosa*, whereas knockdown of ATG7 or Beclin1 restored the IL-1β mediated suppression of bacterial killing. This report suggested a key role for autophagy in modulating inflammasome response during *Pseudomonas aeruginosa* infection. As related to our CRISPR screen, NLRC4 may function in a similar mechanism as NLRP3 during MRSA infection.

A recent study reported at a conference (see Paudel et al., 2017) also suggested that NLRC4 regulates caspase-1 cleavage and IL-1β production in response to MRSA infection. Additionally, NIRC4$^{-/-}$ mice displayed less pneumonia, attenuated pro-inflammatory cytokine production, enhanced bacterial clearance and rescued bacterial burden following MRSA infection (Paudel et al., 2017).

We therefore suggest that depletion of *NLRC4* in our system may inhibit autophagy and the niche of MRSA. To study this, it would be interesting to target *NLRC4* by shRNA or CRISPR and then study the recruitment of autophagy membranes using imaging based on the assays established here. Moreover, pharmacological inhibition of NLRC4 inflammasome or its components can be explored as future work to

modulate infection by MRSA. Future investigation into this candidate would contribute to understanding of the fundamental role of autophagy in the immune response.

Our validation results also found that cells with CRISPR targeting of *AP3D1* became resistant to MRSA (NCTC8325). The protein interaction network of AP3D1 suggests potential mechanisms with VPS41 (vacuole protein sorting 41). Indeed, VPS41 was found to play a central role in trafficking *Coxiella burnetii* bacteria to phagolysosomes through its interaction with p38a-MAPK (Barry et al., 2012). *Coxiella burnetii* is an interesting pathogen for its ability to evolve LPS variations to evade the host response in order to replicate intracellularly (Barry et al., 2012). This CRISPR screen hit therefore suggests a role of AP3D1 (possibly together with VPS41) in MRSA, vacuole traffic.

Moreover, it has been shown that PLEKHM1 plays a role for *Salmonella enterica* sv. Typhimurium pathogenesis via actions of the virulence factor Sif1 (McEwan et al., 2015b). *Salmonella enterica* sv. Typhimurium utilises a complex containing PLEKHM1, Rab7, and VPS41 (HOPS) to tether phagolysosome membranes to the SCV. This membrane remodelling provided a protective niche for proliferation in primary cells, and in tissues, as demonstrated in infected mice (McEwan et al., 2015b). It is therefore possible that AP3D1 may play a similar role as PLEKHM1 for trafficking MRSA to its replicative niche, potentially via VPS41. We would be interested in studying details around the AP3D1 pathway for vesicular traffic and phagolysosomal biogenesis following infection with MRSA as future work.

Interestingly, *AP3D1* is linked by interactome databases to *ATP9B,* which was also present in the top of the MRSA screen with a low p-value (0.000048118). Moreover, both of these factors can be linked via interactome information with autophagy regulation, particularly with the initiation steps (see Figure 6.1). Therefore, further study of these proteins could identify new autophagy regulatory factors which may function for niche formation following infection by MRSA. For example, we could target *AP3D1* by shRNA or CRISPR-Cas9 and then study phagosome biogenesis following MRSA infection by staining with Rab7, Lamp2 and Vps41 (in parallel with autophagy initiation via protein markers such as LC3, ATG13, and ULK1).

Lastly, our validation results found that cells with CRISPR targeting against *KLHL17*, became resistant to MRSA. It was interesting that a range of recent studies have highlighted the involvement of KLHL proteins as E3 ligases in ubiquitination (Mulvaney et al., 2016, Suzuki and Yamamoto, 2017, Tao et al., 2017, Lee et al., 2017b). Other studies have already established Keap1/Cullin 3 to be involved in the ubiquitination of p62 at K420 in its UBA domain (Lee et al., 2017b). Interestingly, ubiquitinated p62 functions as a robust scaffold adaptor protein to recruit bacteria in stable complexes (Heath et al., 2016). This recruitment featured p62 ubiquitination mediated by the novel E3 ligase RNF166 at two different residues: K189 and K91.

Interestingly, in the same study, the E3 ligase, KLHL20, was identified in the primary screen for LC3 co-localisation to bacteria. In addition, KLHL20 has been found to drive K33-mediated ubiquitination of coronin 7, which is involved in post-Golgi trafficking (Heath et al., 2016). Also, KLHL9 and KLHL13 have been previously implicated in the early steps targeting *Salmonella* for antibacterial autophagy (Begun et al., 2015). Therefore, from our screen data, depletion of *KLHL17* may suppress ubiquitination during autophagy and critically disable formation of the MRSA niche.

From the protein interaction network, KLHL17 was predicted to associate with DCN (Decorin). Interestingly, the function of DCN was investigated previously for mediating binding of *Borrelia burgdorferi* (Brown et al., 2001), the causative bacteria for Lyme disease (LD). Deficiency of DCN in mice leads to LD resistance (Brown et al., 2001). Therefore, depletion of *KLHL17* may also decrease DCN activity to prevent MRSA adhesion.

Strikingly, many genes in the KLHL family were significantly identified in our screen when searching through a longer list of candidates (for example, *KLHL21*, *KLHL36*, *KLHL38*, and *KLHL41,* with p-values of 0.00057263, 0.0012089, 0.0021658, and 0.0032654, respectively) (see supplementary Table 7.1). Overall, there is strong scope to study the mechanism of KLHL17 and related family members following infection with MRSA and other types of xenophagy or selective autophagy.

5.3.5. Validation hits of *Salmonella enterica* sv. Typhimurium screen

In this project, we also used CRISPR/Cas9 screening to identify human genes that confer resistance to the *Salmonella enterica* sv. Typhimurium (SL1344) infection.

From this screen, we formed a top ten list of genes with good consistent gRNA enrichment such as *DAZL*, *CD164*, and *ARHGAP28*.

The overgrowth of clones having CRISPR targeting of *DAZL* represents an interesting result from this screen. The *DAZL* gene was shown to be enriched in the germ-cell and was essential for the development and differentiation of the germ-cell layer (Reijo et al., 1995). The *DAZL* gene encodes for a protein found in the nucleus and cytoplasm of fetal germ-cells, as well as the developing oocytes' cytoplasm. In the testis, the protein is restricted in the nucleus of spermatogenia. However, DAZL moves to the cytoplasm during the meiosis stage and persists in spermatids and spermatozoa. *DAZL* amplification during evolution of primates resulted in the *DAZ* gene cluster on the Y chromosome. Different mutations occurring in this gene have been attributed to the development of severe spermatogenic failure and male infertility (Ruggiu et al., 1997, Saunders et al., 2003). Because *DAZL* was the most significantly enriched gene (P=0.00006317), with five gRNA showing consistent levels of enrichment, it was chosen for validation. Indeed, we could confirm that loss of DAZL function leads to bacterial resistance. Therefore, DAZL may represent a real hit although the molecular mechanism during xenophagy remains unclear based on current knowledge.

Our validation results also found that cells with CRISPR against *CD164* became resistant to *Salmonella enterica* sv. Typhimurium. This represents a novel link for this gene in *Salmonella enterica* sv. Typhimurium infection. CD164 functions as an adhesion molecule on the cell surface. Thus, CD164 function may be as a receptor or co-receptor for *Salmonella.* Depletion of this gene may suppress adherence and entry into host cells. Importantly, CD164 binds with CXCR4, which is an important receptor in innate immunity that recognises lipopolysaccharide (LPS) – the main constituent of a gram-negative bacterial cell wall (Triantafilou et al., 2008). This presents a further potential pathway for the involvement of *CD164* during *Salmonella* infection. Thus, a number of clear mechanisms on CD164 function during infection with *Salmonella* arise that can be directly tested for future work.

Interestingly, CXCR4 also plays a critical role in the migration of germ cells (Lee et al., 2017a). As related to our *Salmonella* screen result, *DAZL* function may be involved via a *CXCR4*-dependent pathway that functions in the migration of germ cells, but is

also targeted by *Salmonella*. Thus, study of the mechanism of DAZL following infection with *Salmonella* should involve tests with the CD164-CXCR4 pathway.

5.3.6. Limitations

Above, we showed that we could confirm screen results from both MRSA and *Salmonella* experiments. We could confirm the majority of the top genes with multiple gRNA. Despite this, incomplete resistance for some guides appeared, and some guides failed to give resistant cells. Also, we worked with cell pools generated after transduction with gRNA lentivirus leading to a heterogeneous population. This heterogeneous population can explain the incomplete resistance and differences in survival between targeted genes in pooled populations. To avoid this heterogeneity, we recommend for future validation work that single cell clones be selected for validation. However, we have already seen some strong effects with some cell pools, so effects should further improve.

Notably, there were no bacteria-resistant cells appearing when re-testing gRNAs against *ARHGAP28* even though the initial RRA scored 5/6 gRNA to have this effect. It is possible that this gene is not involved in *Salmonella* infection and was present in the screen off target or false positive effects. We could test for this using other genetic tools such as shRNA and other cell lines. However, the role of Rho GTPases in *Salmonella* invasion via inducing cytoskeleton rearrangements has been established by several studies (Hardt et al., 1998, Criss and Casanova, 2003, Patel and Galan, 2006, Singh et al., 2017). Therefore, we became interested and studied the CRISPR/CAS9 screen hit *ARHGAP28,* possibly in the *Salmonella* invasion step. As future work, we could study Rho and its regulatory factors during the *Salmonella* xenophagy more broadly.

Chapter 6

General Discussion

6. General discussion

Bacterial infections remain one of the major medical challenges worldwide leading to complications and death. Moreover, we face increasing antibiotic resistance, emerging and re-emerging infectious diseases, and faster spread due to global mobility. Invading intracellular bacteria have to continuously battle with the host for survival. Therefore, it is not surprising that most bacterial pathogens have evolved fascinating mechanisms to subvert host cell defence mechanisms. Thus, searching for interaction between the pathogen and the host cells is a good strategy that can be used to develop novel drugs to fight against multi-drug-resistant pathogens.

6.1. Xenophagy following infection by *Staphylococcus aureus* and *Salmonella enterica* sv. Typhimurium

Autophagy is a very critical process that is responsible for elimination of destroyed or damaged intracellular aggregates and organelles. However, the existing studies have found that different autophagy roles exist as a response to bacterial infection, which clearly show the intricate interactions present among the pathogen and host cells. Autophagy has been found to prevent, degrade or restrict some bacteria's replication (Birmingham et al., 2006, Gutierrez et al., 2004, Zhao et al., 2008, Py et al., 2007, Nakagawa et al., 2004). However, studies have also demonstrated that certain types of bacteria require transport via the autophagy membrane for them to complete their cycle of replication (Starr et al., 2012, Mestre et al., 2010, Mestre and Colombo, 2012, Schnaith et al., 2007). For this reason, researchers should be aware that high levels of autophagy do not directly translate to an increased war against pathogenic infections. Different strains of pathogens are different and therefore relate differently to autophagy machinery. In some cases, the host cell of the autophagy machinery is used by the pathogen to proliferate (Starr et al., 2012, Mestre et al., 2010, Mestre and Colombo, 2012, Schnaith et al., 2007). In cases such as these, good treatment would not be achieved through inducing autophagy and, therefore, it would be ideal to direct autophagy to specific bacteria. In this study, we investigated the different role of autophagy in defence against two disease-causing bacteria that are known for their ability to damage cells, *Salmonella enterica* sv. Typhimurium and *Staphylococcus aureus.*

6.1.1. Xenophagy induced the restriction of *Salmonella enterica* sv. Typhimurium infection, but at a limited level does not completely eliminate the bacteria

Our present study clearly indicated the involvement of autophagy as defence mechanisms for clearing *Salmonella enterica* sv. Typhimurium as indicated by the strong formation of large-sized LC3 structures following infection with this bacteria with clear co-localisation. Similarity, the role of p62/sequestosome1 as an adaptor molecule in targeting *Salmonella enterica* sv. Typhimurium that have invaded the cell cytoplasm has been supported by our observation of p62-labelled structures with very clear co-localisation with this pathogen. However, our results also showed that this response was highly induced just in the first hours of infection. Moreover, normal autophagic flux was seen following infection by *Salmonella enterica* sv. Typhimurium. Another important finding in this study was the direct interactions of *Salmonella enterica* sv. Typhimurium and lysosomes.

Nevertheless, the results also showed that *Salmonella* causes pores, as well as injures the lysosomal membrane. Our results were consistent with a model where *Salmonella* traffic to lysosomes via their virulence factor TTSS to make pores and damage the membrane. Importantly, our results also established that epithelial cells can be killed by *Salmonella*.

Collectively, these results confirmed that *Salmonella enterica* sv. Typhimurium invade non-professional phagocytic cells (epithelial cells) and thereafter generate specific vacuoles for replication. These vacuoles fuse with the lysosome and soon escaping *Salmonella* are targeted by autophagy (xenophagy). Xenophagy overall restricts this fraction of bacteria. Another fraction of SCV (the highest fraction) damage the membrane later without autophagy induction. This damage to the SCV ultimately leads to successful escape of this pathogen into the cytoplasm to induce cell death.

Thus, the findings from our study suggested that the xenophagy response was likely to peak in the initial hours of the infection. Such implies that xenophagy associated with *Salmonella enterica* sv. Typhimurium is primarily an early stress response event and may take place before some bacteria eventually escape to the cytosol once the SCV begins disintegrating. This suggests that the activation of autophagy aims to fight infection with *Salmonella enterica* sv. Typhimurium but with only varying limited levels.

Our results were consistent with the overall set of studies that have reported that autophagy is involved in defence mechanisms for clearing *Salmonella enterica* sv. Typhimurium resulting in reduced bacterial survival (Verlhac et al., 2015, Birmingham et al., 2006, Zheng et al., 2009, Tumbarello et al., 2015, Thurston et al., 2009, Wild et al., 2011).

According to our observations following infection with *Salmonella enterica* sv. Typhimurium, autophagy serves in part to reduce the pace of host cell killing by the bacteria. However, xenophagy cannot fully block killing. Therefore, it is suggested that increased autophagy rates would further result in the elimination of bacteria from the cells of the host. In the case of *Salmonella,* increasing autophagy could reduce infection rates.

Recently, BRD5631 and two other selected compounds (BRD34009, BRD2716) were observed to promote antibacterial autophagy independently of the mTOR pathway and inhibited *Salmonella enterica* sv. Typhimurium replication over time (Kuo et al., 2015). This thesis agrees, as future work, that new strategies to increase selective autophagy may help suppress infection of *Salmonella enterica* sv. Typhimurium. For example, other novel compounds that promote non-canonical autophagy without inhibiting mTOR signalling could avoid undesirable side effects which may come from inhibiting mTOR.

6.1.2. *Staphylococcus aureus* moves from the endosomal pathway towards the autophagy pathway to form a replication niche

Our experiments found that *Staphylococcus aureus* are sequestered by autophagosomes within three hours post infection. Moreover, we found that even though this pathogen markedly activates autophagy, normal autophagic flux was interrupted as compared to starvation (typical form of autophagy). The block was comparable with chloroquine treatment which blocks the autophagy/lysosomal pathway. Also, our results clearly showed that some MRSA co-localises within lysosomes. However, we noted that most of the bacteria were found outside lysosomes. This confirmed that MRSA may inhibit a phagosome/lysosome fusion and moves to the autophagosome pathway in order to prevent contact with lysosomes. Also, Galectin3 puncta were not strongly detected post infection by MRSA indicating little damage to lysosomes, possibly because fusion events were inhibited.

Interestingly, we detected p62 puncta following MRSA infection suggestive of selective xenophagy. However, the large aggregates of p62 did not largely co-localise with MRSA. The p62 labelling could be seen just next to the *Staphylococcus aureus.* This observation suggests that a fraction of MRSA in the cytoplasm was sequestered to the double-membrane autophagosomes. Lastly, our results show that *agr* wt but not *agr*-deficient *Staphylococcus aureus* led to strong cell killing following infection HeLa cells.

Overall, these results collectively indicate that *Staphylococcus aureus,* after invasion of the cell, turn from the endosomal pathway towards the autophagy pathway. Then, *Staphylococcus aureus* pervert autophagosome acidification in order to create a protective niche for replication and then escape to the cytoplasm to induce cell death. The results of our study are therefore consistent with the current model from the literature that shows *Staphylococcus aureus* associated with autophagosomes in non-professional and professional phagocytic cells (Mestre et al., 2010, O'Keeffe et al., 2015, Schnaith et al., 2007).

Therefore, diversion of *Staphylococcus aureus* from the endosomal to autophagy pathway is key to its infection process, by helping to create a protective niche and preventing contact with lysosomes. Therefore, with MRSA infection, a strategy may be to target the autophagy genes necessary for niche formation to prevent pathogen replication in the cell and therefore restrict infection. Prevention of traffic to autophagosome may also provide a chance for the phagolysosomal pathway to restrict infection as shown recently in macrophage cells (Zhu et al., 2018). Therefore, it may be beneficial to further study the phagolysosomal process to restrict MRSA infection after blocking autophagy. However, it is critical to remember that while autophagy promotes MRSA in the cell, during *in vivo* infections it becomes further complicated. Autophagy during *in vivo* infection has been found to play a critical role in tolerance following infection by *Staphylococcus aureus*. Autophagy functions offer protection through limiting the toxin's damage by decreasing the level of ADAM10 receptor, in particular on endothelial cells (Maurer et al., 2015a, Maurer et al., 2015b).

Overall, these results highlight the surprising findings that autophagy can have different (opposite) roles against two different pathogens: namely gram-negative *Salmonella enterica* sv. Typhimurium and gram-positive *Staphylococcus aureus*.

Thus, for future work, it may be further useful to test a wider range of human bacterial pathogens. It would be interesting to find out which pathway (positive or negative) is more prevalent across the many bacterial species interacting with mammals.

6.1.3. Targeting ULK1 inhibited cell death following infection with MRSA and sensitised cell death by *Salmonella enterica* sv. Typhimurium

According to our findings, targeting autophagy initiation factors may be a good way to prevent Staphylococcal survival. Our results clearly showed that ATG13 does localise to the isolation membrane associated with MRSA (and also *Salmonella enterica* sv. Typhimurium) during xenophagy. This suggested key involvement of the ULK1 initiation complex in xenophagy following infection with MRSA.

Using genetic approaches to target ULK1 and its required binding protein ATG13, we clearly found that this initiation pathway is essential for *Staphylococcus aureus* induced cell death. Knockdown of ULK1 or CRISPR knockout of ATG13 made cells overall resistant to *Staphylococcus aureus*. These results confirm the autophagy/replication niche model. On the other hand, knockdown of ULK1 or CRISPR knockout of ATG13 made cells more sensitive to destruction by *Salmonella enterica* sv. Typhimurium. Thus, targeting ULK1 using inhibitors may be able to block MRSA infection and improve cell survival.

6.1.4. ULK1 inhibitors are developed as a novel drug to fight MRSA infection *in vitro*

According to our genetic targeting, an essential role is played by ULK1 following MRSA infection. Consequently, targeting the ULK1 complex could possibly inhibit cell killing by *Staphylococcus aureus*, which could help infections and have medical applications in the future.

One clear result from our project is that treatment of cells with different ULK1/2 small molecule inhibitors strongly inhibited cell destruction following infection by MRSA. Using ULK1 inhibitors, replication of *Staphylococcus aureus* was reduced and these cells eventually became very healthy. In agreement with the studies above, ULK1/2

inhibitors (blocking autophagy) made the cells more sensitive to destruction following infection by *Salmonella enterica* sv. Typhimurium.

Therefore, ULK1 inhibitors may be a potential way to prevent Staphylococcal replication and restrict infection. Therapeutic possibilities of ULK1 inhibitor compounds still require a considerable amount of further characterisation to realise clinical capacity. Thus, we propose testing the application of this drug in animal models as future work.

6.2. Genome-wide CRISPR screen discovered the novel host factors required for *Staphylococcus aureus* or *Salmonella enterica* sv. Typhimurium mediated infection

CRISPR Cas9 technology has revolutionised genome editing. This system has been employed to create a simple, RNA programmable method to mediate genome editing in mammalian cells. We employed CRISPR Knock-Out (GeCKO) pooled libraries to screen for genes required during the toxic infection of MRSA (NCTC8325) or *Salmonella enterica* sv. Typhimurium in epithelial cells (HEK293A). Using MaGeck data analysis, we focused on ten candidate host genes from each pathogen screen.

From validation experiments, we confirmed the screen results from both MRSA and *Salmonella* experiments. We could confirm the majority of the top genes with multiple gRNA. Despite this, incomplete resistance for some guides appeared, and some guides failed to give resistant cells. We worked with cell pools generated after transduction with gRNA (i.e. heterogeneous populations). These factors might explain the incomplete resistance and provide strategies for further improvement. Future validation work could investigate whether CRISPR cell clones will have stronger effects. Also, potential hits should be further confirmed by shRNA experiments and more cell lines.

6.3. Future work

The mechanisms of these hits will be interesting for future research. For example, one of the important genes in the MRSA screen was *NLRC4*. Interestingly, the involvement of this gene in MRSA infection was suggested recently by work from a

mouse model (Paudel et al., 2017). Evidence has demonstrated a key functional relationship between autophagy and inflammasomes (Deretic, 2012). We, therefore, hypothesised that *NLRC4* may be important for the induction of autophagy and the MRSA niche. There are several options to study this aspect. We could: 1) Study whether the NLRC4 expression is enhanced in the epithelial cell after MRSA infection through testing the NLRC4 expression by real-time PCR and western blotting. 2) Study if the NLRC4 inflammasome promotes autophagy during MRSA infection by western blotting and fluorescence microscopy to test the amount of the LC3-II protein and the number of LC3 puncta, respectively, in overexpressed NLRC4 cells. 3) Investigate the fundamental role of autophagy in modulation of the immune response. To study this, it would be interesting to target *NLRC4* by shRNA or CRISPR and then study the recruitment of autophagy membranes using imaging based on the assays established here. Depletion of *NLRC4* in our system may inhibit autophagy and the MRSA niche. 4) Using a colony-forming unit assay (CFU), it is also important to study the replication of MRSA intracellularly, which we suggest will be inhibited by the depletion of *NLRC4*. 5) Moreover, pharmacological inhibition of the NLRC4 inflammasome or its components can be explored as future work to modulate infection by MRSA.

Our validation results also found that cells with CRISPR targeting against *KLHL17* became resistant to MRSA. Other recent studies have highlighted the key involvement of the KLHL protein family for ubiquitination regulation (Mulvaney et al., 2016, Suzuki and Yamamoto, 2017, Tao et al., 2017, Lee et al., 2017b). Also, more recent studies have identified Keap1/Cullin 3 to be involved in the ubiquitination of p62 at lysine 420 in its ubiquitin-associated domain (Lee et al., 2017b). The ubiquitinated p62, interestingly, serves the purpose of a scaffold in order to recruit downstream adaptors to bacteria, particularly at early times post infection (Heath et al., 2016). Therefore, we hypothesised that *KLHL17* may lead to ubiquitinated p62, which further leads to recruitment of another adaptor protein to efficiently target the bacteria or its vacuoles to autophagy. This supports our hypothesis that p62 did not largely co-localise with MRSA. The p62 labelling could be seen just next to the *Staphylococcus aureus*. Therefore, inhibition of ubiquitination-related autophagy may result as a consequence of *KLHL17* depletion, thereby preventing the MRSA niche.

The future investigation could explore the wider roles and functions of this very important class of proteins in the process of xenophagy. Possible research could 1) Target *KLHL17* and determine the effects on the recruitment of autophagy adaptor proteins in invading bacteria using imaging approaches; for example, developing a four-colour imaging approach using confocal microscopy to analyse bacteria co-localisation with p62, NDP52, or LC3 proteins. 2) Study if KLHL17 mediates atypical ubiquitination of p62 by co-transfected HEK293 cells with KLHL17, p62 and ubiquitin by infecting them for three hours with MRSA then using immunoprecipitation of p62 under these conditions. 3) Study whether *KLHL17* is necessary for bacterial replication using a colony-forming unit assay (CFU), which we suggest will be inhibited by the depletion of *KLHL17* as compared to a non-targeted control. 4) Additionally, we could study the MRSA infection *in vivo* using a mice model in *KLHL17*$^{-/-}$ mice. We would expect *KLHL17*$^{-/-}$ mice to display less pneumonia, enhanced MRSA clearance and rescued bacterial burden following MRSA infection.

Another gene confirmed to have a role in MRSA resistance is *AP3D1*. The protein encoded by this gene plays a role in vesicular traffic. Interestingly, *AP3D1* could potentially function in a related pathway as *ATP9B,* which was also one of the top MRSA screen hits (p=0.000048118). Both *AP3D1* and *ATP9B* were linked to the autophagy pathway, particularly with the initiation of the autophagy step, via interaction database searches (Figure 6.1). Therefore, we suggest that this gene may also have a role in MRSA trafficking to its autophagosome niche. To study that, we could 1) Target *AP3D1* by shRNA or CRISPR-Cas9 and then study phagosome biogenesis following MRSA infection by staining with Rab7, Lamp2 and Vps41 (in parallel with autophagy initiation via protein markers such as LC3, ATG13 and ULK1). 2) Identify whether *AP3D1* is acting as an autophagy receptor or adaptor molecule in autophagy-deficient MEFs (Atg5 KO, Atg5-/-). 3) We also could use a colony-forming unit assay (CFU) to study the replication of MRSA intracellularly, which we suggest will be inhibited by the depletion of *AP3D1* as compared to a non-targeted control.

On the other hand, studies into the mechanism of proteins encoded by *CD164* and *ARHGAP28,* which were high ranked in the *Salmonella enterica* sv. Typhimurium screen, will also be part of interesting future work. These two genes may be related specifically to the invasion step of *Salmonella*. Rho GTPases play a key role in

Salmonella invasion via inducing actin cytoskeleton rearrangements. Loss of *ARHGAP28* could prevent actin remodelling and prevent bacterial infection. Interestingly, a number of the *ARHGAP* family were significantly present when we looked at a larger set of candidates in the *Salmonella enterica* sv. Typhimurium screen (see supplementary Table 7.4.4). The function of CD164 as a cell adhesion molecule may be for bacterial attachment.

Each screen from our work generated about 1,000 genes that had overall significant ($P<0.05$) effects in the screen, as shown in the supplementary Tables 7.4. 1, 2, 3, and 4. Therefore, deeper network analysis should be used to study the interrelationship of these genes, between the screens, and in conjunction with other resources such as expression and interaction databases. For example, just manually, we found that *ACTC1*, which was present in the interaction network of *KLHL17*, was also significantly presented in this screen with a p-value 0.045946. In addition, many genes in the KLHL family were significantly present in the same screen, such as *KLHL21*, *KLHL36*, *KLHL38*, and *KLHL41,* with p-values of 0.00057263, 0.0012089, 0.0021658, and 0.0032654, respectively (see supplementary Table 7.4.1).

Moreover, in the MRSA screen, a remarkably large number of the *TRIM* family were present with significant p-values. Interestingly, TRIM proteins play a crucial role acting as receptors for specific autophagy of type I interferon response systems as well as inflammasome key components. TRIM family proteins have been shown to recruit and organise autophagy key components, which include ULK1, Beclin-1, ATG16L1, and mammalian homologs of Atg8, with a preference for GABARAP (Kimura et al., 2015, Kimura et al., 2017). From the MRSA screen, we can detect many genes that can be related to the autophagy pathway and, particularly, to upstream processes. Therefore, network analysis may provide further insights into the role of autophagy-related pathways during MRSA xenophagy.

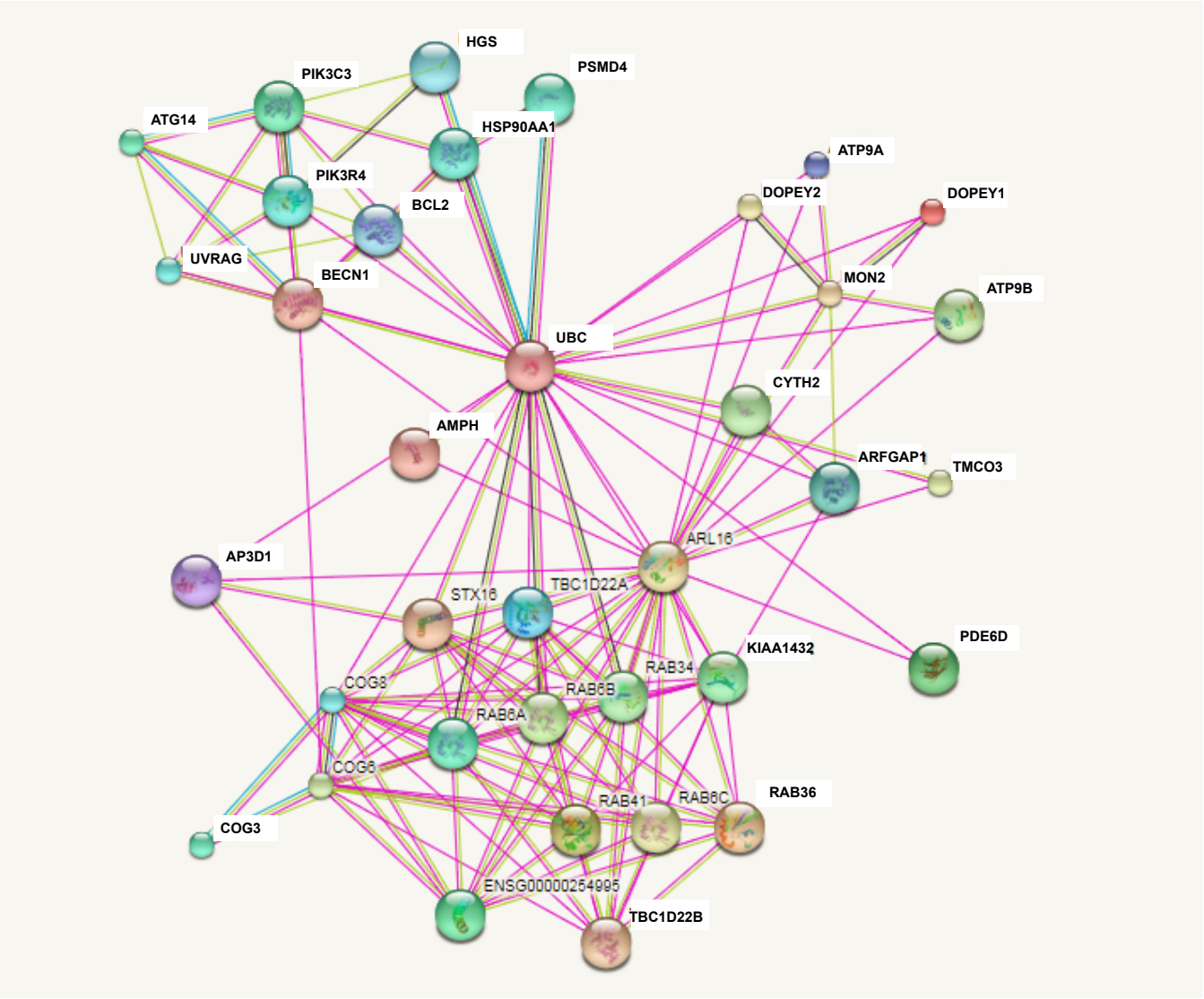

Figure 6.1: *ATP9B* (ATPase Phospholipid Transporting 9B) interaction Map. Via interaction database searches, *AP3D1* is presented in the same pathway as *ATP9B*. Both *AP3D1* and *ATP9B* are linked to the autophagy pathway, particularly with the initiation step.

6.4. Summary models

From our work, we can draw summaries as a model of *Staphylococcus aureus* and *Salmonella enterica* sv. Typhimurium intracellular survival within mammalian cells.

Figure 6.2 shows that once *Staphylococcus aureus* is internalised into a host cell, and depending on the virulence factor (*agr*-dependent factors), some fraction of *Staphylococcus aureus* has the ability to induce and enter autophagy. ULK1 and ATG13 driven factors and membranes assembled around the invading *Staphylococcus aureus*. This autophagy activation promotes intracellular growth of *Staphylococcus aureus* and eventually host cell death. Blocking ULK1 and autophagy by gene-targeting or inhibitors led to the inhibition of bacterial replication and cell killing.

In contrast, Figure 6.3 shows that we believe *Salmonella enterica* sv. Typhimurium does not interfere with the homeostatic turnover of the autophagic machinery. Infection with *Salmonella enterica* sv. Typhimurium led to activation of autophagy (clearly by co-localised LC3 and p62). ULK1 and ATG13 autophagy proteins were assembled around invading *Salmonella enterica* sv. Typhimurium. Blocking ULK1 made the host cells more sensitive to *Salmonella*. *Salmonella enterica* sv. Typhimurium strongly damaged lysosomal membranes and also eventually led to cell death.

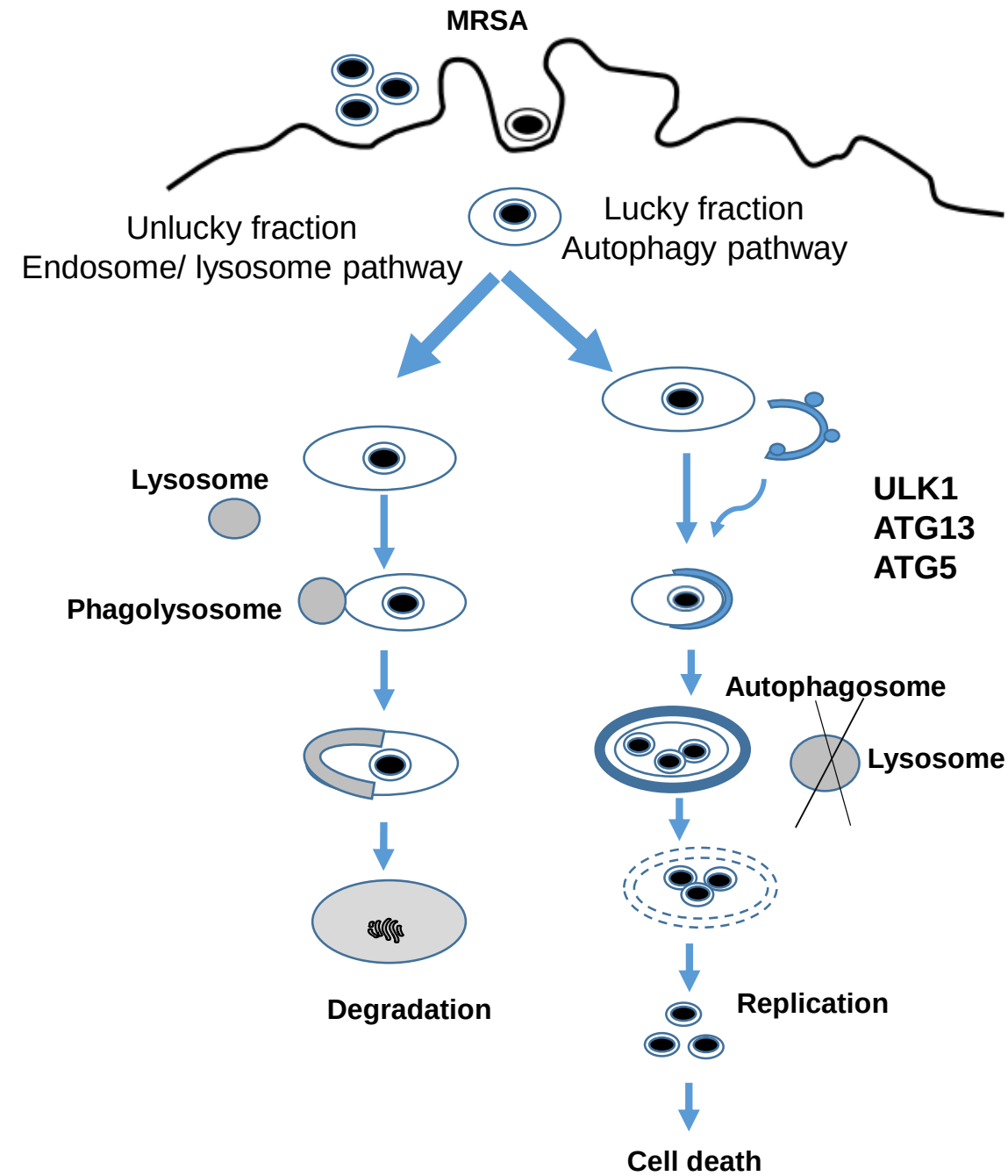

Figure 6.2: MRSA intracellular model. *Staphylococcus aureus* invade nonprofessional phagocytic cells (epithelial cells) and thereafter are targeted by the endosomal pathway, and depending on virulence factors (*agr*-dependent factors), some fraction of *Staphylococcus aureus* has the ability to induce and enter autophagy. ULK1, ATG13 and ATG5 are factors that assemble around the invading *Staphylococcus aureus*. This autophagy activation promotes intracellular growth of *Staphylococcus aureus* and eventually host cell death. Blocking ULK1 and autophagy by gene-targeting or inhibitors led to the inhibition of bacterial replication and cell killing.

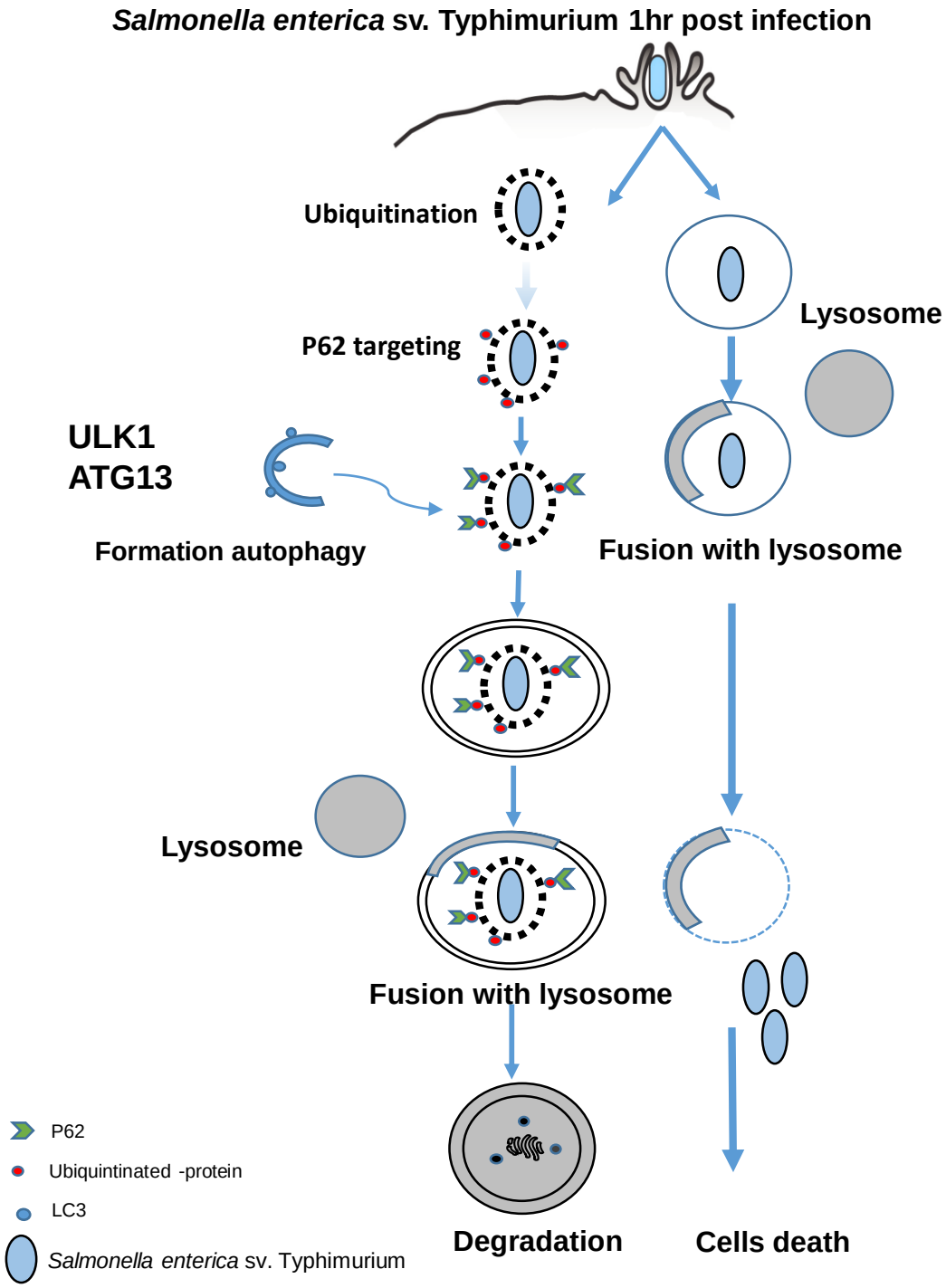

Figure 6.3: *Salmonella enterica* sv. Typhimurium intracellular model. *Salmonella enterica* sv. Typhimurium invade nonprofessional phagocytic cells (epithelial cells) and thereafter generate specific vacuoles for replication. These vacuoles fuse with the lysosome and soon escaping *Salmonella* are targeted by xenophagy. Xenophagy overall restricts this fraction of bacteria. ULK1 and ATG13 autophagy proteins were assembled around invading *Salmonella enterica* sv. Typhimurium. Blocking ULK1 made the host cells more sensitive to *Salmonella*. Another fraction of SCV (the highest fraction) show damage to the membrane later without autophagy induction. This damage to the SCV ultimately leads to successful escape of this pathogen into the cytoplasm to induce cell death.

Supplementary

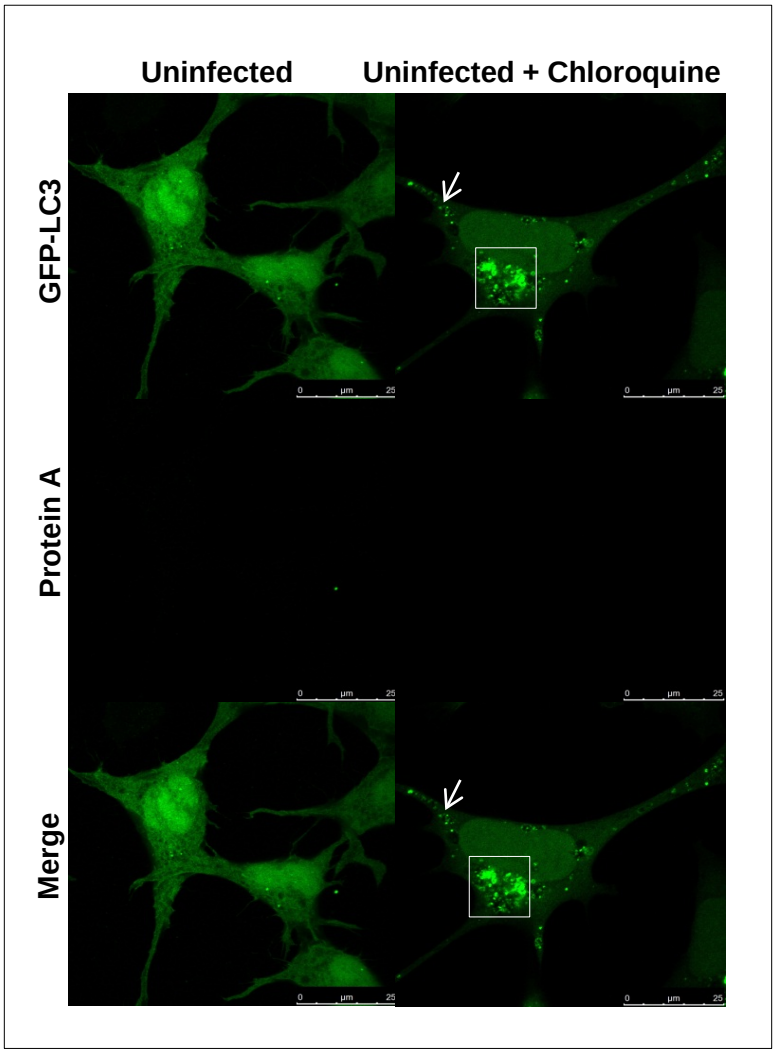

Figure 7.1: The formation of LC3 positive autophagic membranes in chloroquine treated 293-GFP-LC3 cells. Confocal florescence microscopy images of 292-GFP-LC3 cells (passage 20, plated at $0.15X10^6$ cells/well of 24 well dish). For these control experiments, cells were either left untreated or treated with chloroquine and incubated for 3 hours before being fixed. Arrow indicates single autophagosomes. Box indicates where autophagosomes have accumulated as a result of chloroquine treatment. Chloroquine treatment of 293 cells is routinely used as control in our laboratory. Scale bar shown: 25 µm.

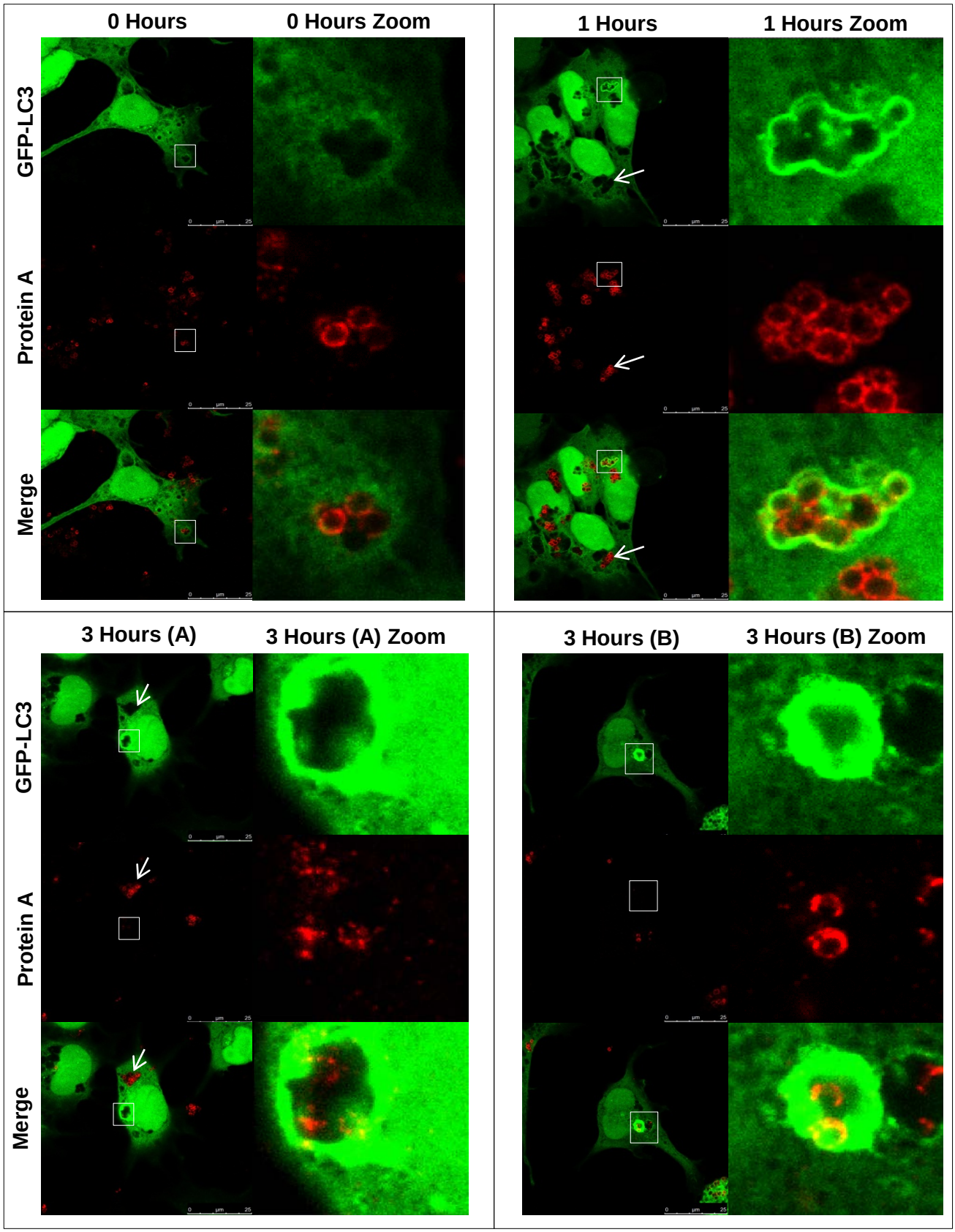

Figure 7.2: The formation of LC3 positive autophagic membranes in 293-GFP-LC3 cells around intracellular EMRSA-15. Confocal microscopy images of 292-GFP-LC3 cells (passage 20, plated at $0.15X10^6$ cells/well of 24 well dish) infected with 100 MOI of EMRSA-15 (Red) for an hour before gentamycin was added. Cells were fixed at 0, 1 and 3 hours post gentamycin and bacteria were stained with anti-protein A antibody, followed by Alexa 555 secondary antibody. Arrows indicate bacteria which are not interacting with autophagy. Box indicates the zoomed area shown to the left. Scale bar shown: 25 µm. Shown are cells from a representative of 3 experiments.

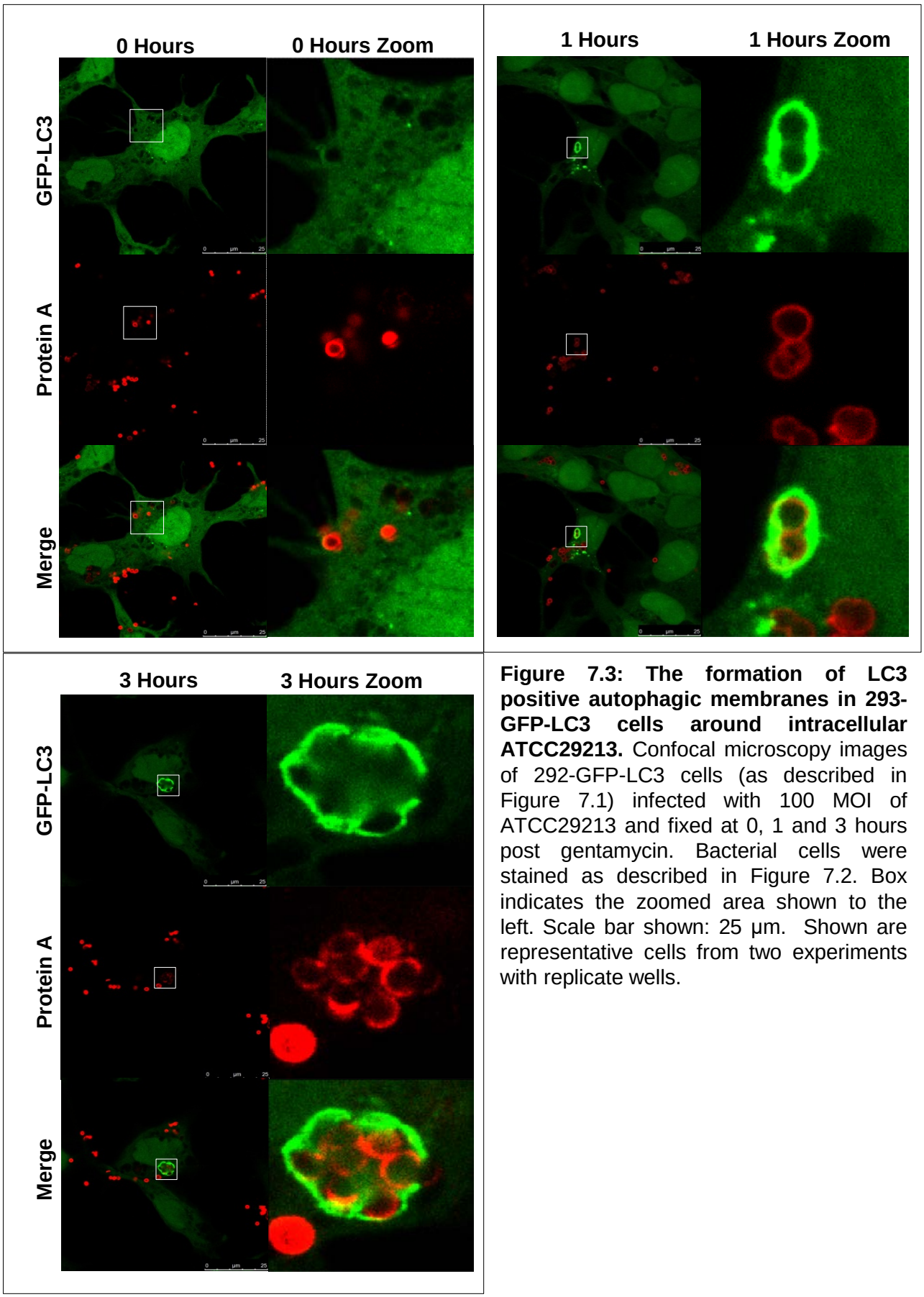

Figure 7.3: The formation of LC3 positive autophagic membranes in 293-GFP-LC3 cells around intracellular ATCC29213. Confocal microscopy images of 292-GFP-LC3 cells (as described in Figure 7.1) infected with 100 MOI of ATCC29213 and fixed at 0, 1 and 3 hours post gentamycin. Bacterial cells were stained as described in Figure 7.2. Box indicates the zoomed area shown to the left. Scale bar shown: 25 µm. Shown are representative cells from two experiments with replicate wells.

7. 4. CRISPR data

7.4.1. Genes listed from the NCTC-1 vs untreated comparison in the GeCKO positive screen.

Gene	# gRNA	score	p-value	rank	# good gRNA
ATP9B	6	9.02E-06	4.81E-05	1	6
CNTFR	6	2.51E-05	0.00014162	2	1
TMEM185A	6	2.80E-05	0.00016077	3	3
OR6C3	6	5.00E-05	0.00027799	4	4
KIAA1024L	6	7.32E-05	0.00037719	5	4
SLAMF8	6	7.53E-05	0.00038609	6	2
C15orf61	6	7.81E-05	0.00040159	7	3
KLHL17	6	9.12E-05	0.00046226	8	5
ARSK	6	0.00010347	0.000522	9	4
PKD2L2	6	0.00010787	0.00054162	10	5
KLHL21	6	0.00011324	0.00057263	11	5
LTBP2	6	0.00012046	0.0006114	12	4
COL11A1	6	0.00012236	0.00062098	13	2
CHORDC1	6	0.00012556	0.00063603	14	1
hsa-mir-6729	4	0.00015935	0.00078153	15	4
ZFAND6	6	0.00016939	0.00083033	16	4
MYO9B	6	0.00017249	0.00084492	17	6
PRPH2	6	0.00017578	0.00086225	18	2
GGA2	6	0.00017928	0.00087867	19	5
SC5D	6	0.00019223	0.00095256	20	5
ZNF425	6	0.0001963	0.00097172	21	4
hsa-mir-326	4	0.0001992	0.00098996	22	2
POLR2B	6	0.00020329	0.0010164	23	6
CPEB4	6	0.00022444	0.0011286	24	5
FBLN5	6	0.00022599	0.0011355	25	4
KLHL36	6	0.00023959	0.0012089	26	4
PLA2G7	6	0.00023998	0.0012107	27	4
PROB1	6	0.00024344	0.0012262	28	6
GBP1	6	0.00026244	0.0013142	29	3
FXYD6	6	0.00026433	0.0013243	30	5
C3orf43	6	0.00027621	0.0013694	31	4
hsa-mir-3923	4	0.00027978	0.0013836	32	3
WWC3	6	0.00029832	0.001473	33	4
DNAJC12	6	0.00029874	0.0014743	34	5
TMX4	6	0.0002998	0.0014803	35	4
ZNF320	5	0.00030533	0.0015026	36	5
C3orf58	6	0.00031452	0.0015487	37	4
hsa-mir-5002	4	0.00031584	0.0015528	38	4
GPRASP1	6	0.00032379	0.0015852	39	4
GIPC2	6	0.00032857	0.0016052	40	4
SAMD15	6	0.00033773	0.0016477	41	6
CTDSPL2	6	0.00035564	0.0017325	42	4
FCHSD2	6	0.00037663	0.0018337	43	3
GJB6	6	0.00039755	0.0019277	44	4
ADRA1D	6	0.00039873	0.0019336	45	6
SAP30	6	0.00040704	0.0019756	46	5
OR8B8	6	0.00042684	0.0020778	47	2
ZNF442	6	0.00043	0.0020965	48	4
UBL3	6	0.00043566	0.0021311	49	6
KLHL38	6	0.00044302	0.0021658	50	6
CEPT1	6	0.00044613	0.0021831	51	5
TPD52L1	6	0.00045424	0.0022187	52	5
MADD	6	0.00046927	0.0022798	53	6
GCKR	6	0.00047375	0.0023031	54	5
IQSEC3	6	0.00047705	0.0023245	55	3
SUPT20HL1	6	0.00049418	0.0024025	56	3
PRRT1	6	0.00050719	0.0024622	57	6
DNM1	6	0.0005237	0.0025384	58	2
MPG	6	0.00052725	0.002553	59	2
E2F7	6	0.0005358	0.0025895	60	6
DCDC2B	6	0.0005384	0.0026036	61	4
GALNT5	6	0.00054481	0.0026347	62	5
OR10G7	6	0.00054887	0.0026524	63	6
TMEM173	6	0.0005707	0.0027551	64	3
ZNF331	6	0.00057247	0.0027619	65	5
ATP5C1	6	0.00057312	0.002766	66	5
STK32A	6	0.00057746	0.0027888	67	3
DTWD1	6	0.00058449	0.0028175	68	4
GRINA	6	0.00058989	0.0028417	69	3
CASKIN2	6	0.00059372	0.0028613	70	6
POLE2	6	0.00061058	0.002948	71	5
ZNF395	6	0.00061201	0.0029526	72	5
KIAA0754	6	0.00061222	0.0029526	73	6
FAM134B	6	0.00061873	0.0029836	74	4
NDUFB5	6	0.00062766	0.0030178	75	3
SOGA3	6	0.00063287	0.0030438	76	4
INO80	6	0.00066132	0.0031843	77	6
BCAT2	6	0.00066166	0.0031865	78	6
MMAA	6	0.00067138	0.0032321	79	5
AIPL1	6	0.00067336	0.0032435	80	4
CNTN6	6	0.00067436	0.0032472	81	5
KLHL41	6	0.00067785	0.0032654	82	5
ENAH	6	0.00070057	0.0033608	83	6
ZMIZ2	6	0.00070993	0.0033954	84	3
KRTAP19-7	6	0.00072405	0.0034597	85	5

CAMK1D	6	0.00072805	0.0034807	86	3
ZNF280C	6	0.00073048	0.0034908	87	6
hsa-mir-595	4	0.00074314	0.0035455	88	2
LUZP4	6	0.00074984	0.0035733	89	4
TMED3	6	0.00077227	0.0036686	90	3
SLMO1	6	0.00077824	0.0036969	91	4
SFXN4	6	0.00079399	0.0037537	92	6
KCNAB1	6	0.00081935	0.0038698	93	6
MIER1	6	0.00082071	0.0038748	94	3
DLG4	6	0.00082791	0.0039081	95	5
FBLN2	6	0.00082844	0.0039104	96	4
HNRNPDL	6	0.00083173	0.0039259	97	6
GDE1	6	0.00083175	0.0039259	98	5
UBE3B	6	0.00083699	0.0039519	99	6
ZNF587B	6	0.00084386	0.0039843	100	5
ZNF597	6	0.00084514	0.0039938	101	3
EXTL1	6	0.00085964	0.0040604	102	4
PAFAH1B1	4	0.00086459	0.0040869	103	4
FRS3	6	0.00086772	0.004101	104	6
NLRC4	6	0.00087076	0.0041142	105	3
CECR1	6	0.00087487	0.0041325	106	6
BOLL	6	0.00087863	0.0041494	107	3
hsa-mir-376c	3	0.00088225	0.0041626	108	2
NAA16	6	0.00089705	0.0042301	109	6
IFNB1	6	0.00089735	0.0042315	110	6
KCTD7	6	0.00091614	0.0043026	111	3
OR10J5	6	0.00092329	0.0043423	112	5
TOMM34	6	0.00092492	0.0043491	113	5
UMOD	6	0.00092881	0.0043692	114	3
CPA4	6	0.00094031	0.0044185	115	4
COLGALT2	6	0.00094988	0.0044595	116	6
hsa-mir-148a	3	0.00096168	0.0045142	117	3
KCNJ5	6	0.00097371	0.0045653	118	6
DDX51	6	0.000979	0.0045927	119	2
CD163L1	6	0.0009884	0.0046255	120	6
PITPNC1	6	0.00099938	0.0046698	121	6
DCAF11	6	0.0010019	0.0046784	122	5
VN1R5	6	0.0010035	0.0046857	123	3
TRIT1	6	0.0010134	0.0047377	124	6
MET	6	0.0010226	0.0047733	125	4
PADI2	6	0.0010246	0.0047822	126	3
TSHR	6	0.0010266	0.0047906	127	5
RASL12	6	0.0010292	0.0048043	128	4
CH25H	6	0.0010323	0.0048189	129	5
LYAR	6	0.0010389	0.0048454	130	4
SLC35G2	6	0.0010612	0.0049357	131	6
PPM1K	6	0.001072	0.0049813	132	5
ZNF549	6	0.0010794	0.0050187	133	2
TXNDC5	6	0.0011022	0.0051213	134	4
UBE2U	6	0.0011079	0.0051487	135	6
CD276	6	0.0011087	0.005151	136	5
ARRDC2	6	0.0011126	0.0051701	137	4
FOXD2	6	0.0011192	0.0051975	138	2
FAM57B	6	0.0011192	0.0051975	139	3
TMEM218	6	0.0011192	0.0051975	140	3
TBK1	6	0.0011295	0.0052426	141	2
ARHGAP28	6	0.0011544	0.0053585	142	2
hsa-mir-4708	4	0.0011756	0.0054515	143	3
OFD1	6	0.0012037	0.0055692	144	6
TPTE2	6	0.0012135	0.0056102	145	5
hsa-mir-3126	4	0.0012156	0.005618	146	4
hsa-mir-4474	4	0.0012233	0.0056463	147	4
TRIM65	6	0.0012354	0.0057015	148	5
RCVRN	6	0.0012503	0.0057699	149	6
TNFAIP8L3	6	0.0012539	0.0057872	150	5
ADH1A	6	0.001255	0.0057936	154	2
C20orf196	6	0.001255	0.0057936	151	2
SPDYE4	6	0.001255	0.0057936	153	4
FAM26D	6	0.001255	0.0057936	152	5
KIAA1024	6	0.0012634	0.0058378	155	5
LRFN5	6	0.0012693	0.0058547	156	4
NEBL	6	0.0012843	0.005919	157	4
XG	6	0.001295	0.0059728	158	4
TMEM82	6	0.0013041	0.0060116	159	4
IFNGR1	6	0.0013043	0.0060121	160	5
HTR1E	6	0.001306	0.0060216	161	5
MGA	6	0.001315	0.0060622	162	6
LEPREL1	6	0.0013405	0.0061785	163	6
RBM48	6	0.0013428	0.0061895	164	6
VWA7	6	0.0013477	0.0062164	165	5
ZNF658	6	0.0013755	0.0063427	166	4
MYLK4	6	0.0013804	0.0063651	167	2
ZNF727	6	0.0013831	0.0063747	168	4
CLRN1	6	0.001389	0.0064029	169	3
CEACAM3	6	0.0014031	0.0064613	170	4
C17orf51	6	0.0014211	0.0065384	171	4
MEP1B	6	0.0014224	0.006543	172	4
C1orf21	6	0.0014306	0.0065799	173	2
C10orf67	6	0.0014459	0.006646	174	6
ZNF648	6	0.0014564	0.0066971	175	5
COL8A1	6	0.0014858	0.0068303	176	6
DNAJB2	6	0.0015281	0.0070191	177	5
FBXO7	6	0.0015292	0.0070237	178	6
IL1RAPL2	6	0.0015309	0.0070296	180	3
RALB	6	0.0015309	0.0070296	181	1
NFE2L3	6	0.0015309	0.0070296	179	2
PPIH	6	0.0015377	0.0070625	182	5
PKN1	6	0.0015433	0.0070848	183	4
PRKAA1	6	0.0015782	0.0072513	184	4
FAM81B	6	0.0015825	0.0072736	185	5
ZNF345	6	0.0016105	0.0074064	186	6

CDHR2	6	0.0016312	0.0075076	187	4
PPARA	6	0.0016452	0.0075756	188	4
WIPI1	6	0.0016581	0.0076403	189	5
HERC6	6	0.0016683	0.0076818	190	4
PRKG2	6	0.0016704	0.0076901	191	5
FAM198B	6	0.0016814	0.0077361	192	2
SPATA31E1	6	0.0016818	0.0077375	193	6
C20orf27	6	0.0016851	0.0077507	194	5
SLC1A6	6	0.0017185	0.0079012	195	4
hsa-mir-486-2	1	0.0017202	0.0079115	196	1
hsa-mir-583	4	0.0017434	0.0080184	197	4
MCMDC2	6	0.0017482	0.0080408	198	4
TMEM51	6	0.0017491	0.0080454	199	4
MS4A6A	6	0.0017516	0.0080577	200	5
CLDN3	6	0.0017566	0.00808	202	1
SSUH2	6	0.0017566	0.00808	201	4
GLB1L	6	0.0017574	0.0080828	203	5
UFSP2	6	0.0017583	0.0080869	204	3
ATAD2B	6	0.0017736	0.0081466	205	6
SCARA5	6	0.0017867	0.0082091	206	6
PINLYP	6	0.0017927	0.008236	207	2
F12	6	0.0018191	0.0083541	208	3
TRMT12	6	0.0018318	0.008418	209	4
C10orf137	6	0.0018416	0.0084581	210	6
FLT3LG	6	0.0018505	0.0085065	211	4
GYG2	6	0.001882	0.0086542	212	4
CAGE1	6	0.001889	0.008683	213	5
NDUFAF3	6	0.0018977	0.0087286	214	4
RRP12	6	0.0019064	0.0087614	215	4
ATP2C1	6	0.0019253	0.0088408	216	6
KANK4	6	0.0019321	0.0088677	217	5
VTN	6	0.0019353	0.0088805	218	5
PATE3	6	0.0019458	0.0089284	219	6
PQBP1	6	0.0019823	0.0090807	220	1
HS3ST3A1	5	0.0019974	0.0091482	221	3
MAGEA12	6	0.00201	0.0092157	222	6
APLNR	6	0.0020231	0.00928	223	4
OR52H1	6	0.0020266	0.0092928	224	4
TAS2R40	6	0.0020324	0.009317	225	3
ZNF385D	6	0.0020343	0.0093274	226	6
C12orf57	6	0.002036	0.0093334	227	5
DHX29	6	0.002042	0.0093603	228	5
ZNF226	6	0.0020604	0.0094355	229	5
ACSL3	6	0.0020612	0.0094378	230	6
NDUFB1	6	0.0020674	0.0094656	231	5
ARL6IP6	6	0.0020711	0.0094802	232	4
PRTN3	6	0.0021076	0.0096349	233	1
MPV17L2	6	0.0021076	0.0096349	234	2
NDUFA5	6	0.0021135	0.0096577	235	6
KRTAP3-1	6	0.0021367	0.0097539	236	6
GPR173	6	0.0021489	0.0098036	237	4
ANXA2	6	0.0021517	0.0098136	238	6
TMEM42	6	0.0021535	0.0098214	239	4
WDR41	6	0.0021543	0.0098232	240	6
hsa-mir-3166	4	0.0021581	0.0098419	241	3
DNAJC25	6	0.0021594	0.0098456	242	5
LAMP5	6	0.00216	0.0098483	243	5
STOML2	6	0.0021759	0.009903	244	4
BROX	6	0.0021828	0.0099395	245	3
XRCC6BP1	6	0.0021982	0.010018	246	5
PGAP3	6	0.0022125	0.010079	247	4
PKP4	6	0.0022234	0.010122	248	5
TBX5	6	0.002233	0.010166	249	1
hsa-mir-4700	4	0.0022478	0.010224	250	4
ADHFE1	6	0.0022498	0.010233	251	4
ESM1	6	0.0022551	0.010252	252	6
MUC20	6	0.0022557	0.010256	253	4
CRYGB	6	0.0022585	0.010267	254	2
SPRED2	6	0.0022839	0.010358	255	3
hsa-mir-598	4	0.0022927	0.010392	256	4
ST6GAL1	6	0.0022988	0.010422	257	5
DHX35	6	0.0023332	0.01057	258	3
RAB3C	6	0.0023358	0.010584	259	4
AVPR2	6	0.0023471	0.01063	260	5
NLGN2	6	0.0023541	0.010665	261	4
P4HA1	6	0.0023703	0.010737	262	4
DUSP12	6	0.0023766	0.010767	263	5
RASSF2	6	0.0023914	0.01083	264	4
UTS2R	6	0.0023984	0.010851	265	5
MMP3	5	0.0024038	0.010877	266	5
GIN1	6	0.0024174	0.010926	267	6
hsa-mir-6079	4	0.0024246	0.010964	268	2
hsa-mir-4305	4	0.0024254	0.010967	269	2
F8	6	0.0024314	0.010997	270	4
SLC29A2	6	0.0024335	0.011005	271	3
NDUFB4	6	0.0024335	0.011005	272	2
TRIM15	6	0.0024428	0.011039	273	6
EPHA8	6	0.0024465	0.011056	274	6
UFSP1	6	0.0024695	0.011151	275	6
TSPYL6	6	0.0025092	0.011305	276	2
hsa-mir-634	4	0.0025256	0.011386	277	4
TNFSF4	6	0.0025288	0.0114	278	6
hsa-mir-18b	4	0.0025523	0.011492	279	3
IL13	6	0.0025579	0.011518	280	5
FSHB	6	0.0025584	0.011518	281	6
FAM32A	6	0.0025588	0.011519	283	4
T	6	0.0025588	0.011519	282	4
GRIA3	6	0.0025681	0.011559	284	4
TULP2	6	0.0025905	0.011644	285	4
PELI2	6	0.0025968	0.011667	286	3
SYK	6	0.0026105	0.011729	287	3

HSD11B1L	6	0.0026159	0.011749	288	4
PKN2	6	0.0026233	0.011776	289	2
OSCAR	6	0.0026331	0.011818	290	5
SPATA25	6	0.0026339	0.011823	291	1
LYZL6	6	0.002635	0.011829	292	4
STX6	6	0.002649	0.011884	293	2
hsa-mir-637	4	0.0026593	0.011931	294	3
WDR11	6	0.002675	0.011996	295	5
WDR96	6	0.0026841	0.012032	296	2
TINF2	6	0.0026856	0.012038	297	5
CSF1	6	0.0026868	0.012042	298	4
DARC	6	0.0026875	0.012046	299	5
AGTPBP1	6	0.0026972	0.012085	300	5
ATRX	6	0.0027111	0.012137	301	3
GPR116	6	0.0027282	0.012208	302	3
ARFGEF1	6	0.002738	0.012236	303	3
KRTAP26-1	6	0.0027396	0.012243	304	5
SGCD	6	0.0027496	0.012278	305	4
UBR2	6	0.0027528	0.012286	306	4
C11orf94	6	0.0027692	0.012345	307	5
ACVR1C	6	0.0027706	0.01235	308	4
TRA2B	6	0.0027788	0.012377	309	5
NCBP2	6	0.0027843	0.012397	311	2
PTCHD4	6	0.0027843	0.012397	310	4
RCHY1	6	0.0027858	0.012402	312	4
MFSD5	6	0.0027862	0.012402	313	4
PIGF	6	0.0027905	0.012416	314	4
hsa-let-7g	4	0.0028264	0.01255	315	1
ASIC5	6	0.002838	0.012594	316	5
FRMD7	6	0.0028388	0.012598	317	3
TIMP3	6	0.0028845	0.012752	318	3
hsa-mir-1323	4	0.0029099	0.012856	319	2
DGKA	6	0.0029126	0.012865	320	4
RCL1	6	0.0029307	0.012927	321	5
STAT4	6	0.0029346	0.012941	322	1
ERC2	6	0.0029631	0.013044	323	3
DNAJB4	6	0.0029724	0.013079	324	4
CAPZA2	6	0.0029821	0.013117	325	5
LEMD1	6	0.0029873	0.013128	326	4
ZUFSP	6	0.002992	0.013147	327	5
hsa-mir-759	4	0.0030071	0.013201	328	2
HYKK	3	0.0030103	0.013212	329	3
LRSAM1	6	0.0030229	0.013253	330	4
ZMYM6NB	6	0.003027	0.01327	331	5
COX7A2	6	0.0030348	0.013296	332	3
ELMO2	6	0.0030428	0.013328	333	5
TNFAIP3	6	0.0030565	0.013377	334	3
SIRPA	6	0.0030638	0.0134	335	5
CAPRIN2	6	0.0030849	0.013479	336	4
FRRS1	6	0.0030897	0.013493	337	4
ZNF493	6	0.0030974	0.013524	338	4
EMID1	6	0.003135	0.013644	339	3
CABLES2	6	0.003137	0.01365	340	4
LEO1	6	0.0031561	0.013717	341	5
COG5	6	0.0031775	0.013782	342	5
LDHD	6	0.0031987	0.013858	343	3
UACA	6	0.0032021	0.013867	344	3
C5orf49	6	0.0032101	0.013896	345	3
CHN1	6	0.0032101	0.013896	346	4
PRSS56	6	0.0032172	0.013925	347	5
THEM4	6	0.0032669	0.014111	348	4
SLC17A9	6	0.0032958	0.014211	349	3
LYPD1	6	0.0033096	0.014255	350	3
GTF2IRD1	6	0.0033103	0.014257	351	2
hsa-mir-6857	4	0.0033275	0.014324	352	2
GRAP2	6	0.0033448	0.014387	353	5
AQP4	6	0.0033624	0.014448	354	4
AGPHD1	5	0.0033815	0.014519	355	4
NSFL1C	6	0.0033854	0.014535	356	4
BRK1	6	0.0034006	0.014587	357	5
CRX	6	0.0034204	0.014657	358	3
ESYT3	6	0.0034284	0.014681	359	4
CCSER1	6	0.0034355	0.014709	360	2
TNFRSF1B	6	0.0035156	0.014983	361	4
NCKAP1	6	0.0035285	0.015029	362	4
CST7	6	0.0035357	0.015054	363	3
HLA-DMB	6	0.0035648	0.015164	364	4
TMEM200A	6	0.0035674	0.015172	365	2
NBN	6	0.0035811	0.015217	366	5
RHCG	6	0.0035822	0.015221	367	4
TBXAS1	6	0.0035958	0.01527	368	4
GPR1	6	0.0036282	0.015371	369	4
GNAZ	6	0.0036358	0.015395	370	3
FICD	6	0.0036358	0.015395	371	3
UTP14C	6	0.0036994	0.015618	372	4
ASXL3	6	0.0037382	0.015753	373	2
CES2	6	0.0037494	0.015794	374	4
hsa-mir-4255	4	0.0037614	0.015836	375	4
AFP	6	0.003775	0.015885	376	5
MAML3	6	0.003786	0.015919	378	3
DUSP14	6	0.003786	0.015919	377	3
EDARADD	6	0.0037971	0.015961	379	4
FITM1	6	0.0038132	0.016019	380	4
TMPRSS13	6	0.0038407	0.016117	381	5
LGMN	6	0.0038439	0.016128	382	5
A4GALT	6	0.0038544	0.016162	383	5
SLC39A14	6	0.0038799	0.016256	385	3
NonTargetingControlGuideForHuman_0700	1	0.0038799	0.016256	388	1
WSB2	6	0.0038799	0.016256	384	3
ZNF682	6	0.0038799	0.016256	387	3
RHOF	6	0.0038799	0.016256	386	3

MINPP1	6	0.003897	0.016312	389	4
FANCF	6	0.0039112	0.016357	390	2
CYP2E1	6	0.0039112	0.016357	391	2
hsa-mir-4433	4	0.0039221	0.016398	392	4
XPO6	6	0.0039246	0.016409	393	4
LYPLAL1	6	0.0039283	0.016419	394	3
DSCR4	6	0.0039382	0.016455	395	5
ANKRD18A	6	0.0039439	0.016474	396	4
UBAC2	6	0.0039634	0.016539	397	4
FAM96A	6	0.003977	0.016581	398	5
CCL15	6	0.0039783	0.016586	399	5
ATAD5	6	0.0039868	0.016616	400	3
UCK2	6	0.0039904	0.01663	401	5
CCDC24	6	0.0040015	0.01667	402	5
TAOK1	6	0.004003	0.016677	403	4
MDK	6	0.0040217	0.016741	404	4
TNN	6	0.0040339	0.016783	405	5
MMD2	6	0.0040364	0.016792	406	2
HAS3	6	0.0040498	0.016838	407	5
KCNA1	6	0.0040658	0.016889	408	3
COQ3	6	0.0040852	0.016965	409	4
MAP2K3	6	0.0040864	0.01697	410	2
SDK2	6	0.0041012	0.017024	411	5
TMEM187	6	0.0041365	0.017145	412	4
CROCC	6	0.0041528	0.017199	413	4
hsa-mir-589	4	0.0041622	0.017236	414	1
BTN2A1	6	0.0041702	0.017268	415	4
PGBD4	6	0.0041838	0.017321	416	5
FREM3	6	0.0041865	0.01733	417	4
NACAD	6	0.0041988	0.017368	418	4
PARS2	6	0.0042673	0.017617	419	3
C1orf35	6	0.0042734	0.017638	420	3
KIAA1598	6	0.0042746	0.017643	421	5
LURAP1	6	0.0042968	0.017722	422	3
ATXN1L	6	0.0043017	0.017737	423	2
CDH9	6	0.0043089	0.017762	424	5
OR4N2	6	0.0043157	0.017786	425	4
ZFR2	6	0.0043302	0.017845	426	3
SMC4	6	0.0043343	0.017857	427	3
C19orf52	6	0.0043617	0.017941	429	2
PNMT	6	0.0043617	0.017941	430	4
CRKL	6	0.0043617	0.017941	428	3
DHX36	6	0.0043814	0.018008	431	4
RPE	6	0.0043971	0.018066	432	4
IFT57	6	0.0044058	0.018095	433	3
hsa-mir-4677	4	0.0044143	0.01812	434	4
OR4C11	6	0.0044232	0.018149	435	5
ZCRB1	6	0.0044237	0.018149	436	4
hsa-mir-4651	4	0.0044292	0.018173	437	1
EMB	6	0.0044688	0.018307	438	5
BCAS1	6	0.0044729	0.018324	439	5
GPHB5	6	0.0044868	0.018376	440	2
RAE1	6	0.0045368	0.01854	441	2
CCL28	6	0.0045538	0.01859	442	5
SLC4A4	6	0.0045601	0.018617	443	4
VAMP4	6	0.0045736	0.018664	444	2
CHCHD10	6	0.0045869	0.018708	445	1
RERG	6	0.0045963	0.018739	446	5
hsa-mir-519c	3	0.0046259	0.01884	447	2
NAPSA	6	0.0046369	0.018874	448	3
PLAGL2	6	0.0046403	0.018885	449	5
CTAGE9	5	0.0046581	0.018945	450	3
CKAP2	6	0.0046655	0.018971	451	4
MSGN1	6	0.0046746	0.019004	452	5
VWA3A	6	0.0046869	0.01904	453	2
AP1S1	6	0.0046948	0.019069	454	3
ZFP14	6	0.0046995	0.019086	455	4
NLK	6	0.0047425	0.019226	456	4
ASF1A	6	0.0047592	0.019281	457	5
hsa-mir-3198-2	4	0.0047604	0.019285	458	2
FIZ1	6	0.0047694	0.019314	459	3
CSNK1G1	6	0.0048111	0.019456	460	5
FLNA	6	0.0048159	0.019468	461	5
CDS1	6	0.0048342	0.019537	462	4
PSMD10	6	0.0048366	0.019552	463	4
LIN7C	6	0.004837	0.019553	466	3
MTAP	6	0.004837	0.019553	467	4
ENY2	6	0.004837	0.019553	468	2
ENHO	6	0.004837	0.019553	464	2
SLC38A11	6	0.004837	0.019553	465	3
GLRA2	6	0.0048492	0.019584	469	4
NBL1	3	0.0048541	0.019602	470	2
PNLIPRP2	6	0.0048595	0.019623	471	5
YIF1A	6	0.0048813	0.019702	472	4
TMC1	6	0.0048985	0.01976	473	2
ELAC1	6	0.0049138	0.01981	474	4
DNAJA3	6	0.0049299	0.019862	475	4
GZF1	6	0.0049304	0.019864	476	5
SPRR2A	5	0.0049337	0.019875	477	5
OR5M10	6	0.0049375	0.019893	478	5
SHOX2	6	0.0049681	0.020004	479	3
CUL9	6	0.0049961	0.020095	480	3
MAZ	6	0.0050163	0.020167	481	5
hsa-mir-3150a	4	0.0050183	0.020174	482	4
TANC2	6	0.0050371	0.020243	483	3
DCDC1	6	0.0050558	0.02031	484	5
CCDC83	6	0.0050871	0.020424	485	3
FUCA1	6	0.0050898	0.020432	486	4
RARRES3	6	0.0050989	0.020468	487	3
SYCP2L	6	0.0051026	0.020482	488	4
PRPF18	6	0.0051371	0.020615	489	1

GOLGA8B	5	0.0051442	0.020644	490	3
NUBPL	6	0.0051781	0.02076	491	5
FAM222B	6	0.0051871	0.020792	492	3
FUBP1	5	0.0052001	0.020834	493	2
DHRS1	6	0.0052032	0.020847	494	3
OSM	6	0.0052078	0.020862	495	4
C2orf53	6	0.0052366	0.020953	496	4
TOP1	6	0.0052371	0.020955	497	4
ZKSCAN7	6	0.0052796	0.021103	498	5
GABRB1	6	0.0053148	0.021215	499	5
LIG4	6	0.005316	0.021219	500	5
C9orf57	6	0.0053325	0.021275	501	5
COX15	6	0.0053621	0.021371	502	2
ALK	6	0.0054012	0.021515	503	5
POC1B-GALNT4	1	0.0054034	0.021524	504	1
HRASLS5	6	0.0054064	0.021533	505	4
DCUN1D4	6	0.0054092	0.021541	506	3
ZNF514	6	0.0054294	0.021619	507	5
DQX1	6	0.0054308	0.021624	508	5
SHROOM4	6	0.0054371	0.021648	509	3
FOXK2	6	0.0054544	0.02171	510	2
USP36	6	0.0054613	0.021736	511	3
MFHAS1	6	0.0054795	0.021797	512	5
NonTargetingControlGuideForHuman_0625	1	0.0055039	0.021889	513	1
ANGPTL3	6	0.0055046	0.021891	514	4
INPP5D	6	0.0055075	0.021903	515	4
hsa-mir-4304	4	0.0055125	0.021922	516	3
IL17B	6	0.0055509	0.022047	517	5
LACE1	6	0.0055548	0.022057	518	2
ARHGAP29	6	0.0055634	0.02208	519	4
TEAD2	6	0.0055823	0.022147	520	2
SP6	6	0.0055871	0.022162	522	3
B3GNT3	6	0.0055871	0.022162	523	2
LMBR1	6	0.0055871	0.022162	521	3
KLHDC8A	6	0.0055871	0.022162	524	4
SRRM4	6	0.0056051	0.022225	525	4
OR5A2	6	0.0056116	0.022245	526	5
FOXC2	6	0.0056201	0.022276	527	5
RPP30	6	0.0056237	0.022285	528	3
RERGL	6	0.005626	0.022292	529	4
ANKRD17	6	0.0056357	0.022328	530	4
MOGAT1	6	0.0056365	0.022332	531	4
DEFB127	6	0.0056514	0.022379	532	4
RBM33	6	0.0056823	0.022481	533	4
CDX2	6	0.0057163	0.022602	534	3
RSAD2	6	0.0057371	0.022683	535	4
S1PR5	6	0.005751	0.022729	536	5
KCTD18	6	0.0057535	0.022738	537	5
RFK	6	0.0057544	0.022741	538	5
SLC22A8	6	0.0057581	0.022754	539	4
C6orf118	6	0.0057814	0.022834	540	2
SLC9C2	6	0.0057841	0.022845	541	3
C1orf94	6	0.0057871	0.022859	542	3
ZFP3	6	0.0057908	0.022871	543	3
IL5	6	0.0058355	0.023041	544	5
ACSL4	6	0.0058367	0.023043	545	4
ITGB1	6	0.005837	0.023043	546	3
SLC25A38	6	0.0058473	0.023077	547	3
TINAG	6	0.0058517	0.023093	548	4
CHTF8	6	0.0058552	0.023107	549	4
PPARGC1A	6	0.0058572	0.023113	550	4
ADRA1A	6	0.0058705	0.023153	551	4
FOLR1	6	0.005887	0.023212	552	3
SLC43A2	6	0.0059176	0.023305	553	4
LILRB5	6	0.0059255	0.023341	554	5
PROX1	6	0.0059744	0.023492	555	3
GABRR1	6	0.0059841	0.023524	556	4
COG7	6	0.005987	0.023534	557	2
GOLPH3	6	0.005987	0.023534	558	2
STAR	6	0.005987	0.023534	559	4
MRVI1	6	0.0059886	0.023543	560	4
hsa-mir-4437	4	0.00599	0.023546	561	4
EFCAB11	6	0.0060005	0.023579	562	2
CRB1	6	0.0060014	0.023585	563	5
MAOA	6	0.0060059	0.023601	564	4
KDELR1	6	0.0060239	0.023662	565	4
CD180	6	0.0060275	0.023672	566	5
OR52E6	6	0.0060404	0.023707	567	4
C5orf28	6	0.0060409	0.023708	568	4
ZNF711	6	0.0060688	0.023802	569	4
OR7A5	6	0.0060698	0.023804	570	4
hsa-mir-4435-1	4	0.0060751	0.023819	571	4
PTAFR	6	0.0060795	0.02383	572	4
TLE4	6	0.0060869	0.023855	573	2
DEPDC7	6	0.0060983	0.023892	574	4
CORO2B	6	0.0061228	0.023976	575	5
FABP4	6	0.0061267	0.023989	576	3
APMAP	6	0.0061451	0.024044	577	5
ELK3	6	0.0061582	0.024087	578	4
IFIT2	6	0.0061892	0.024195	579	5
KIR2DL3	5	0.0062004	0.024225	580	5
TTC34	6	0.0062121	0.024267	581	5
NKAIN1	6	0.0062368	0.024341	583	1
EMC9	6	0.0062368	0.024341	584	2
MT3	6	0.0062368	0.024341	582	2
CLPTM1L	6	0.0062427	0.024355	586	3
FAM177B	6	0.0062427	0.024355	585	3
NNMT	6	0.0062462	0.024368	587	5
hsa-mir-4659a	3	0.0062491	0.024378	588	2
BOLA1	6	0.0062572	0.024402	589	3
hsa-mir-4648	4	0.0063591	0.024745	590	4

LHX1	6	0.0064117	0.024924	592	4
ABCD3	6	0.0064117	0.024924	591	5
HAUS2	6	0.0064501	0.025053	593	4
MPP6	6	0.0064515	0.025055	594	5
PPP1R3G	6	0.0064618	0.025089	595	3
GSDMC	6	0.0064866	0.025181	596	3
LRIG3	6	0.0064918	0.025194	597	5
TTI1	6	0.0065041	0.025232	598	3
IFNW1	6	0.0065486	0.025395	599	4
C4orf6	6	0.0065497	0.025401	600	3
GPX6	6	0.0065771	0.025497	601	4
PRRX2	6	0.0065833	0.025511	602	4
FERMT1	6	0.006586	0.025521	603	5
hsa-mir-4446	4	0.0066133	0.02561	604	3
LOC100505841	6	0.0066201	0.025632	605	3
RNASEH2B	6	0.0066206	0.025635	606	5
RUNDC3B	6	0.0066365	0.025691	607	3
KRTAP19-6	6	0.0066365	0.025691	609	2
TRIO	6	0.0066365	0.025691	608	2
ZNF583	6	0.0066776	0.025824	610	5
AGPAT5	6	0.0066803	0.025833	611	4
ERCC5	6	0.0067045	0.025915	612	4
hsa-mir-5190	4	0.0067068	0.025924	613	4
TACC3	6	0.0067288	0.026005	614	3
TRIM71	6	0.0067405	0.026045	615	3
TUBA1C	6	0.0067895	0.026197	616	5
NR2C1	6	0.0067949	0.026214	618	4
GNL1	6	0.0067949	0.026214	617	4
XPNPEP2	6	0.0067979	0.026227	619	5
RIPK2	6	0.0068261	0.026312	620	3
CABP5	6	0.0068362	0.026349	621	4
TRIM8	6	0.0068362	0.026349	623	2
SSH2	6	0.0068362	0.026349	622	2
GALR1	6	0.0068451	0.026381	624	4
UPF3A	6	0.0068893	0.02654	625	4
METTL21C	6	0.0069108	0.026613	626	5
MRPS22	6	0.0069122	0.026615	627	2
GTF2A1L	6	0.0069243	0.026657	628	5
CDH16	6	0.0069343	0.026687	629	5
MALSU1	6	0.0069361	0.026696	630	1
DMP1	6	0.0069604	0.026776	631	4
DNAH6	6	0.0069751	0.026825	632	5
CECR2	6	0.006986	0.026867	633	2
SORD	6	0.0070033	0.026926	634	5
METTL5	6	0.0070079	0.02694	635	5
SURF1	6	0.007036	0.027036	636	3
C19orf35	6	0.0070392	0.027046	637	3
XRCC6	6	0.0070781	0.027175	638	3
PATL2	6	0.007091	0.02722	639	4
CNPY2	6	0.007109	0.027278	640	5
CBLN2	6	0.0071107	0.027286	641	5
PLTP	6	0.0071608	0.027456	642	2
GPR162	6	0.0071608	0.027456	643	3
hsa-mir-6831	4	0.007169	0.027491	644	3
hsa-mir-890	4	0.0071785	0.027528	645	3
WDR26	6	0.0071791	0.027529	646	3
WDR63	6	0.0071812	0.027535	647	2
MNAT1	6	0.0072001	0.027591	648	5
MINK1	6	0.0072174	0.027649	649	4
CATSPER2	6	0.0072389	0.02772	650	4
ARG2	6	0.0072483	0.027753	651	5
TCEAL4	6	0.0072559	0.027779	652	5
USP3	6	0.0072561	0.02778	653	5
C12orf29	6	0.0072606	0.027793	654	3
CDC42	6	0.0072769	0.027852	655	5
HIPK3	6	0.0072963	0.027922	656	4
HSFY1	5	0.007316	0.027982	657	4
NonTargetingControlGuideForHuman_0047	1	0.0073204	0.027994	658	1
TAS2R9	6	0.0073406	0.028065	659	5
MANBAL	6	0.0073443	0.028075	660	5
SNX19	6	0.0073553	0.028116	661	5
LRFN1	6	0.0073643	0.028143	662	4
ARL4A	6	0.0073658	0.028147	663	3
SLC35E3	6	0.0073854	0.028214	665	2
ARMC1	6	0.0073854	0.028214	666	3
ADNP2	6	0.0073854	0.028214	664	3
hsa-mir-1976	4	0.0074024	0.028267	667	3
GIMAP8	6	0.0074122	0.028294	668	5
GORASP2	6	0.0074259	0.028341	669	5
C3orf30	6	0.0074339	0.028371	670	2
RNASET2	6	0.0074471	0.028417	671	3
ITGA5	6	0.0074599	0.028452	672	5
LRRC42	6	0.0074747	0.028498	673	5
HLA-DQA1	6	0.0074813	0.028518	674	4
RASSF5	6	0.0074886	0.028544	675	5
hsa-mir-1283-1	4	0.007507	0.028608	676	4
GRIA2	6	0.0075286	0.028693	677	5
SCRN2	6	0.0075341	0.028715	678	2
DDB1	6	0.0075601	0.028796	680	3
USP54	6	0.0075601	0.028796	679	2
AURKAIP1	6	0.0075694	0.028825	681	3
PIK3C2A	6	0.0076136	0.028952	682	4
ACE	6	0.0076324	0.029017	683	3
hsa-mir-6788	4	0.0076658	0.029129	684	4
BAX	6	0.0076817	0.029181	685	4
DDX58	6	0.0076849	0.029188	686	4
hsa-mir-3927	4	0.0076957	0.029228	687	3
ACYP2	6	0.0077255	0.029326	688	3
DCDC2	6	0.0077338	0.029355	689	4
DDX46	6	0.0077847	0.029529	690	2
RAB39B	6	0.0077878	0.02954	691	4

NCSTN	6	0.0077898	0.029547	692	3
PSMB2	6	0.0078388	0.02971	693	4
LOC283403	6	0.0078436	0.029721	694	2
IL6	6	0.0078596	0.029774	696	3
ZFYVE19	6	0.0078596	0.029774	695	3
CACHD1	6	0.007876	0.02983	697	4
FAM124A	6	0.0078923	0.029894	698	5
ZNF845	6	0.0079423	0.030059	699	4
DHX40	6	0.0079475	0.030075	700	4
hsa-mir-409	4	0.0079659	0.030131	701	4
MS4A1	6	0.0079785	0.030174	702	5
RGS17	6	0.0079843	0.03019	703	3
OR6K2	6	0.0079932	0.030219	704	4
C8orf42	4	0.0080275	0.030319	705	2
RIMKLA	6	0.0080342	0.030345	706	2
ING5	6	0.0080354	0.030347	707	3
SPANXN5	5	0.0080538	0.030407	708	3
ARR3	6	0.0080549	0.03041	709	4
SPACA7	6	0.008058	0.030418	710	4
DUSP3	6	0.0080768	0.030479	711	2
ZNF74	6	0.0080826	0.030498	712	4
EML6	6	0.008137	0.030666	715	5
MSMO1	6	0.008137	0.030666	714	3
VPS52	6	0.008137	0.030666	713	2
ZNF655	6	0.0081394	0.03067	716	5
CCDC8	6	0.0081506	0.030709	717	4
RNF111	6	0.0081838	0.030811	719	3
FAM76B	6	0.0081838	0.030811	718	3
BUD31	6	0.0081838	0.030811	721	2
PPP1R3B	6	0.0081838	0.030811	720	3
PRKAR1A	6	0.0081838	0.030811	722	2
EFCAB13	6	0.0081857	0.030818	723	4
METTL21A	6	0.0082332	0.030978	724	4
LOC402160	6	0.0082399	0.031	725	4
ACER2	6	0.0082525	0.031045	726	2
TRIM40	6	0.0082779	0.031137	727	3
hsa-mir-1289-2	4	0.0082781	0.031138	728	2
BAGE2	5	0.008289	0.03118	729	4
PCDHB6	6	0.0083248	0.0313	730	5
GEN1	6	0.0083299	0.03132	731	3
CNIH	4	0.0083304	0.031321	732	4
HAPLN3	6	0.0083335	0.031332	733	3
TBC1D14	6	0.008342	0.031359	734	4
FEM1A	6	0.0083465	0.03137	735	4
CDH2	6	0.0083555	0.031396	736	4
ZNF749	6	0.0083628	0.031422	737	5
DEXI	6	0.0083834	0.031479	738	2
C1orf27	6	0.0084087	0.03156	739	5
SLC6A2	6	0.0084301	0.031634	740	3
BPIFA3	6	0.0084635	0.031745	741	5
RHBDF2	6	0.0084714	0.031771	742	4
TAB3	6	0.0084852	0.031816	743	5
TEX33	6	0.0085485	0.032022	744	5
BHLHA15	6	0.0085563	0.032043	745	4
MB	6	0.0085628	0.032064	746	5
SPRR2G	6	0.0085699	0.032081	747	5
NR1D1	6	0.0085828	0.032121	752	2
C10orf35	6	0.0085828	0.032121	750	3
ZADH2	6	0.0085828	0.032121	749	2
PEX6	6	0.0085828	0.032121	753	2
TNFRSF25	6	0.0085828	0.032121	751	2
LELP1	6	0.0085828	0.032121	748	5
PLXNB3	6	0.0085835	0.032123	754	5
G3BP1	6	0.0086179	0.032233	755	5
SIKE1	6	0.0086262	0.032258	756	5
hsa-mir-105-2	3	0.0086593	0.032374	757	3
KRTAP22-2	6	0.008671	0.032409	758	4
NYAP2	6	0.0086827	0.032448	759	5
BTBD3	6	0.0087144	0.032547	760	5
ACAT2	6	0.0087263	0.032582	761	5
LPL	6	0.0087316	0.0326	762	4
PCDH12	6	0.0087358	0.032615	763	3
CYP2W1	6	0.0087605	0.032688	764	5
SLC8B1	3	0.0087701	0.032715	765	3
ZNF165	6	0.0087823	0.032761	766	3
PPP2R3C	6	0.008784	0.032765	767	5
DEFB132	6	0.0088321	0.03292	768	4
TEX26	6	0.0088468	0.032965	769	3
TMEM117	6	0.0088868	0.033105	770	5
ITGA9	6	0.0088892	0.033111	771	4
CCDC36	6	0.0089008	0.033153	772	3
C8A	6	0.0089098	0.033181	773	4
INHBB	6	0.008911	0.033185	774	4
ARHGEF16	6	0.0089318	0.033247	775	2
SCUBE1	6	0.0089318	0.033247	777	2
RNF168	6	0.0089318	0.033247	776	2
IL8	6	0.0089554	0.033324	778	3
FXYD7	6	0.0089955	0.033462	779	3
ZNF527	6	0.0089976	0.033467	780	3
hsa-mir-3650	4	0.0090192	0.033544	781	3
hsa-mir-1183	4	0.0090453	0.033632	782	4
PTH2R	6	0.0090565	0.033666	784	4
HIGD1A	6	0.0090565	0.033666	783	1
hsa-mir-521-2	3	0.0090599	0.033677	785	2
KDM4A	6	0.0090761	0.033732	786	4
GABRA2	6	0.0091062	0.033839	787	4
CLEC2B	6	0.0091162	0.03387	788	4
MRPL22	6	0.0091212	0.033887	789	4
YRDC	6	0.0091229	0.033891	790	5
DYX1C1	6	0.0091312	0.033916	791	4
BTN3A2	6	0.0091322	0.03392	792	5

RGCC	6	0.0091384	0.033939	793	5
ZFP41	6	0.0091429	0.033954	794	5
TRERF1	6	0.0091745	0.034064	795	5
HEXIM2	6	0.009206	0.034159	796	3
CD300LF	6	0.009206	0.034159	797	2
ARHGAP5	6	0.0092875	0.034416	798	4
hsa-mir-6769b	4	0.0093113	0.034495	799	4
GPCPD1	6	0.0093222	0.034534	800	5
C16orf93	6	0.0093306	0.03456	801	2
WFDC10A	6	0.0093349	0.034571	802	4
PRR25	6	0.0093547	0.034638	803	2
TMEM194B	6	0.0093606	0.034654	804	3
DTD1	6	0.0093648	0.034673	805	4
LOC100996485	6	0.0093674	0.034683	806	5
POU4F3	6	0.0093885	0.034743	807	4
CCDC38	6	0.0094045	0.034805	808	3
hsa-mir-5188	4	0.009409	0.034818	809	2
KIF27	6	0.0094247	0.034863	810	5
ARL13B	6	0.0094286	0.034877	811	3
TRIM38	6	0.0094303	0.034883	812	2
ANXA9	6	0.0094801	0.035039	813	4
SORBS2	6	0.0094834	0.035054	814	4
MTERFD1	6	0.0094996	0.035118	815	4
SLC22A14	6	0.0095044	0.035132	816	5
OR13A1	6	0.0095195	0.035185	817	4
CLEC4A	6	0.0095246	0.035208	818	4
BTN1A1	6	0.0095349	0.035243	819	5
TREML1	6	0.0095704	0.035362	820	5
PTGER2	6	0.0095722	0.035368	821	4
PRSS50	6	0.00959	0.035431	822	2
MAP3K4	6	0.0095923	0.035445	823	5
EPSTI1	6	0.0096296	0.035544	824	3
CAB39L	6	0.0096296	0.035544	825	4
UGT8	6	0.0096353	0.035563	826	4
TRAPPC13	6	0.0096472	0.035602	827	5
hsa-mir-5004	4	0.0096593	0.03564	828	2
SP8	6	0.0096638	0.035653	829	4
CCRL1	5	0.0096676	0.035669	830	4
KDM8	6	0.0096768	0.035704	831	4
hsa-mir-4274	4	0.0096836	0.035721	832	4
UGGT1	6	0.0096894	0.035736	833	4
hsa-mir-618	4	0.0097242	0.035833	834	3
SLAMF9	6	0.0097292	0.035849	835	2
hsa-mir-6733	4	0.0097433	0.035893	836	3
HSPA12A	6	0.0097501	0.035915	837	5
DDX19B	6	0.0097532	0.035927	838	2
TESK2	6	0.0097601	0.03595	839	5
MAGED4	6	0.0097609	0.035951	840	5
SLAMF6	6	0.0097801	0.036011	841	3
CCDC158	6	0.009789	0.036037	842	5
ZNF281	6	0.009804	0.036087	843	3
DSCR6	4	0.0098079	0.036101	844	2
STRADA	6	0.0098159	0.036128	845	3
MAN1B1	6	0.0098185	0.036133	846	4
DOK7	6	0.0098518	0.036245	847	2
TMEM60	6	0.0098552	0.036257	848	5
CALU	6	0.0098638	0.036287	849	5
PDCD1LG2	6	0.0098638	0.036287	850	3
hsa-mir-383	4	0.0098815	0.036344	851	4
CA13	6	0.0098914	0.036373	852	4
FNDC9	6	0.0098998	0.036405	853	2
PTPRO	6	0.0099036	0.036414	854	1
NXPE3	6	0.0099036	0.036414	856	4
MYB	6	0.0099036	0.036414	857	5
RAG2	6	0.0099036	0.036414	855	2
MGAT4B	6	0.0099072	0.036426	858	5
CAPN6	6	0.0099072	0.036426	859	5
OR10J3	6	0.009929	0.036491	860	5
ERN2	6	0.009937	0.036521	861	5
PEAK1	6	0.0099463	0.036552	862	5
hsa-mir-5684	4	0.0099749	0.036646	863	3
hsa-mir-760	4	0.009998	0.036723	864	4
THAP6	6	0.010002	0.036736	865	3
SLC47A2	6	0.010024	0.036803	866	5
EIF4ENIF1	6	0.010075	0.036963	867	5
TICAM1	6	0.010081	0.036981	868	5
FOXE3	6	0.010092	0.037017	869	5
TAF9	6	0.010125	0.037124	870	5
TRAPPC12	6	0.010128	0.03713	871	5
WDR45B	6	0.010153	0.037207	873	4
AKAP4	6	0.010153	0.037207	874	4
SOCS7	6	0.010153	0.037207	872	3
STX7	6	0.010165	0.037251	875	3
GBP2	6	0.010174	0.037275	876	3
ZC3H6	6	0.010196	0.037341	877	3
BICD1	6	0.010207	0.037376	878	4
ARFGEF2	6	0.010208	0.037376	879	5
PRRG4	6	0.010212	0.037393	880	5
OR6B3	6	0.010215	0.037403	881	5
DSTN	6	0.010235	0.037472	882	4
ANKRD30B	6	0.01025	0.037513	883	5
BCL9	6	0.010253	0.037523	884	4
hsa-mir-16-2	4	0.010296	0.037669	885	4
PREP	6	0.010299	0.037681	886	4
KATNA1	6	0.010309	0.037709	887	3
WDR78	6	0.010314	0.037723	888	4
TNFSF9	6	0.010327	0.037772	889	2
TCEAL8	6	0.010348	0.037851	890	4
OSTF1	6	0.010379	0.03795	891	4
ABI1	6	0.010391	0.037987	892	4
hsa-mir-4802	4	0.010447	0.038168	893	4

IPMK	6	0.010451	0.03818	894	2
NKX2-8	6	0.010451	0.03818	895	2
CAPN5	6	0.01047	0.038242	896	4
METAP1	6	0.010491	0.038314	897	5
PPP5C	6	0.010498	0.03834	898	3
SLC2A6	6	0.010515	0.038397	899	3
SLCO1C1	6	0.010522	0.038413	900	4
MEAF6	6	0.010526	0.038428	902	5
DPP10	6	0.010526	0.038425	901	5
Dec-01	6	0.010553	0.038515	903	5
PTRF	6	0.010626	0.03877	905	3
C11orf63	6	0.010626	0.03877	904	2
IL10RA	6	0.010644	0.038826	906	5
CTXN3	6	0.010663	0.03888	907	5
CLDN4	6	0.010666	0.038887	908	5
C2orf68	6	0.010725	0.039098	909	1
HNRNPAB	6	0.010735	0.039122	910	4
CXXC4	6	0.010742	0.039146	911	4
TACC1	6	0.010775	0.039258	912	2
hsa-mir-3187	4	0.010795	0.039329	913	4
KCTD15	6	0.010813	0.039393	914	3
WBSCR17	6	0.010819	0.039409	915	3
UBOX5	6	0.010837	0.039463	916	5
PDCD10	6	0.010874	0.039589	917	3
ZAR1	6	0.0109	0.039674	918	5
RNASE12	6	0.010917	0.039724	919	4
SPRED1	6	0.010932	0.039775	920	4
FAM90A1	6	0.010949	0.03983	921	2
CYP3A7	6	0.010949	0.03983	922	2
FBXO34	6	0.010958	0.03986	923	5
CHRM5	6	0.01096	0.039866	925	2
PROZ	6	0.01096	0.039866	924	4
hsa-mir-3651	4	0.010989	0.03996	926	3
OR51G2	6	0.010992	0.03997	927	4
ARHGAP15	6	0.010995	0.039977	928	4
GRHPR	6	0.011013	0.040042	929	3
APBA2	6	0.011014	0.040044	930	4
hsa-mir-4298	4	0.01102	0.040067	931	4
KIAA1217	6	0.011024	0.040081	932	3
CLRN2	6	0.011039	0.040129	933	4
PLEKHM2	6	0.011044	0.040141	934	3
PDE2A	6	0.011058	0.040178	935	3
SPRY4	6	0.01107	0.040214	936	5
CHMP6	6	0.011074	0.040225	937	2
PRDM10	6	0.011082	0.040256	938	4
CCDC129	6	0.011091	0.040286	939	4
C1orf43	6	0.011109	0.040346	940	5
PRAMEF7	5	0.01114	0.040449	941	4
NUDT22	6	0.011146	0.040463	942	5
CYP3A7-CYP3AP1	2	0.011169	0.040539	943	2
C7orf66	6	0.011173	0.040546	944	4
AKAP2	6	0.011203	0.040638	945	5
DEPTOR	6	0.011227	0.040713	946	5
hsa-mir-4278	4	0.011251	0.040788	948	4
TTF2	6	0.011251	0.040783	947	5
MUC7	6	0.011273	0.040856	949	2
SCRIB	6	0.01128	0.04088	950	5
HADH	6	0.011285	0.040893	951	5
NonTargetingControlGuideForHuman_0438	1	0.011297	0.040932	952	1
SEL1L2	6	0.011302	0.040954	953	4
GPX1	6	0.011328	0.041035	954	4
ADAT3	6	0.01134	0.04107	956	5
PPM1G	6	0.01134	0.04107	955	5
TMEM171	6	0.011347	0.04109	957	4
IQCG	6	0.011362	0.041133	958	3
SPRR4	6	0.011383	0.041204	959	4
NCAM2	6	0.011388	0.041217	960	4
FOXJ3	6	0.011392	0.041236	961	5
ARRDC3	6	0.011423	0.041338	962	5
MORC1	6	0.011447	0.041414	966	4
KCNK18	6	0.011447	0.041414	965	3
PSG11	6	0.011447	0.041414	968	5
SPATA2	6	0.011447	0.041414	964	3
SERP2	6	0.011447	0.041414	963	4
PLXNC1	6	0.011447	0.041414	967	2
RLF	6	0.011472	0.04149	969	2
hsa-mir-375	4	0.011482	0.041522	970	2
OR52R1	6	0.011498	0.041575	971	4
SATL1	6	0.01151	0.041612	972	3
ANKRD10	6	0.011535	0.0417	973	4
PILRA	6	0.011561	0.041799	974	4
GYPC	6	0.011577	0.04186	975	5
SLC5A6	6	0.011583	0.04188	976	4
hsa-let-7a-2	4	0.011585	0.041883	977	3
SULF1	6	0.011591	0.041902	978	4
SLFN12L	6	0.011621	0.042006	979	2
ZNF701	5	0.011634	0.042035	980	4
PRAMEF22	4	0.011647	0.042079	981	3
MRPS9	4	0.011664	0.042128	982	3
ATP6V1E2	6	0.011667	0.042133	983	4
TNMD	6	0.011671	0.042142	984	3
PTPLAD1	6	0.011702	0.042239	985	3
BET3L	4	0.011705	0.042248	986	4
ARL2BP	6	0.011711	0.042271	987	3
HM13	6	0.01172	0.042301	988	4
hsa-mir-596	4	0.011734	0.042354	989	3
LIX1L	6	0.011744	0.042391	990	5
CAPN14	6	0.011752	0.042417	991	4
SLC38A10	6	0.01177	0.042467	992	3
PIWIL2	6	0.011788	0.042522	993	4
SCAF4	6	0.011807	0.042585	994	5

IKBKB	6	0.011811	0.042596	995	5
TMEM100	6	0.011813	0.042602	996	4
TEX11	6	0.011818	0.042614	998	5
FAM185A	6	0.011818	0.042614	997	4
NARG2	6	0.01182	0.04262	999	2
RSPRY1	6	0.011823	0.042631	1000	4
TLDC2	6	0.011832	0.042668	1001	5
C17orf74	6	0.011869	0.042788	1002	3
ZIM3	6	0.011888	0.042832	1003	5
PCDHB13	6	0.01191	0.042905	1004	5
UGGT2	6	0.011919	0.042939	1005	2
VSTM2B	6	0.011936	0.042993	1006	5
SLC16A13	6	0.011965	0.043067	1007	4
ZNF121	6	0.011969	0.043081	1008	5
MBD3L2	6	0.011969	0.043081	1009	2
KRIT1	6	0.011977	0.043108	1010	4
NCR1	6	0.012024	0.043248	1011	3
QDPR	6	0.012038	0.043295	1012	4
NMNAT1	6	0.012068	0.043391	1014	2
NAIF1	6	0.012068	0.043391	1015	2
SGK223	6	0.012068	0.043391	1013	2
SCP2D1	6	0.012079	0.043423	1016	4
KIAA2018	6	0.012079	0.043425	1017	5
CXorf57	6	0.012082	0.043435	1018	4
PLAU	5	0.0121	0.043498	1019	1
SHMT1	6	0.012142	0.043634	1020	2
CASP5	6	0.012147	0.043652	1021	5
CASP12	6	0.012181	0.043762	1022	4
PSMB6	6	0.012208	0.043849	1023	2
ZNF778	6	0.012221	0.043886	1024	2
LINGO2	6	0.01223	0.043914	1025	5
FAM83A	6	0.012232	0.043921	1026	4
DEFB4A	5	0.012245	0.043959	1027	2
TM4SF4	6	0.012267	0.044033	1028	3
CSF2RA_X	6	0.012281	0.044077	1029	4
hsa-mir-103a-2	4	0.012283	0.04408	1030	4
VWA5B2	6	0.012297	0.044123	1031	5
C1orf54	6	0.012303	0.044145	1032	3
hsa-mir-3713	4	0.012304	0.044146	1033	3
C2orf42	6	0.012309	0.044167	1034	4
LZTFL1	6	0.012317	0.044195	1035	2
GDF5	6	0.012339	0.044265	1036	5
ICA1L	6	0.012341	0.044271	1037	2
MAMLD1	6	0.012341	0.044272	1038	5
IFNA10	6	0.012353	0.044316	1039	4
FERMT2	6	0.012357	0.04433	1040	5
FAM167A	6	0.012404	0.044477	1041	5
FAM150A	6	0.012446	0.044614	1042	5
SH2B2	6	0.012449	0.044626	1043	5
CENPO	6	0.01246	0.044663	1044	3
EBF3	6	0.012487	0.044754	1045	2
C10orf113	6	0.01252	0.044867	1046	3
MATR3	6	0.012531	0.044904	1047	5
TPMT	6	0.01254	0.044936	1048	4
EDEM2	6	0.012541	0.044937	1049	2
ARPC1A	6	0.012553	0.044982	1050	5
C7orf31	6	0.012563	0.045013	1051	4
C14orf79	6	0.012572	0.045044	1052	5
ARL8B	6	0.012583	0.045085	1053	5
CRYM	6	0.012597	0.045129	1054	5
SMIM6	6	0.012631	0.045226	1055	5
hsa-mir-548f-3	3	0.012645	0.045262	1056	3
CD22	6	0.012653	0.045286	1057	3
OR5H14	6	0.012665	0.045328	1063	2
CASS4	6	0.012665	0.045328	1060	1
ATF4	6	0.012665	0.045328	1058	3
NR5A2	6	0.012665	0.045328	1061	3
CROT	6	0.012665	0.045328	1064	3
APOB	6	0.012665	0.045328	1059	2
SH3BGR	6	0.012665	0.045328	1062	2
PXMP4	6	0.012665	0.045328	1065	2
SAR1A	6	0.012668	0.045335	1066	4
NonTargetingControlGuideForHuman_0297	1	0.012669	0.045339	1067	1
ATXN10	6	0.012709	0.045481	1068	4
MMP26	6	0.012709	0.045481	1069	4
IKBKAP	6	0.012709	0.045481	1070	3
FAM135B	6	0.012728	0.045538	1071	3
GBAS	6	0.012734	0.045559	1072	4
PDE7B	6	0.012782	0.045702	1073	4
ACTC1	6	0.012853	0.045946	1074	5
AP5M1	6	0.012865	0.045973	1075	4
CHST10	6	0.012904	0.046099	1076	2
RGS13	6	0.012913	0.046127	1077	3
SIPA1	6	0.012924	0.046172	1078	2
CCT6B	6	0.012929	0.046182	1079	4
TRAF5	6	0.012946	0.046229	1080	5
SDF2	6	0.012965	0.046285	1081	2
CLEC9A	6	0.012985	0.046349	1082	4
ABCA13	6	0.013006	0.046416	1083	4
EIF2AK1	6	0.013013	0.046437	1084	3
WAS	6	0.013026	0.046483	1085	4
ZFYVE26	6	0.013114	0.046758	1086	5
CAPS2	6	0.013157	0.046899	1087	3
CCP110	6	0.013162	0.046911	1088	3
CCDC64B	6	0.013162	0.046911	1089	2
hsa-mir-511	4	0.013222	0.047109	1090	2
CLEC4C	6	0.013257	0.047211	1091	5
ABCA2	6	0.013286	0.047301	1093	2
C9orf153	6	0.013286	0.047301	1092	5
ODC1	6	0.0133	0.047341	1094	4
ANXA11	6	0.013317	0.047407	1095	4

PSAT1	6	0.01336	0.047544	1096	4
RIPPLY1	6	0.013366	0.047561	1097	3
hsa-mir-93	4	0.013377	0.0476	1098	3
STRIP1	6	0.013395	0.047658	1099	4
CENPC	4	0.013409	0.0477	1100	1
SETD7	6	0.01341	0.047703	1101	3
SLC40A1	6	0.013439	0.047799	1102	4
TTC17	6	0.013449	0.047829	1103	3
KRT40	6	0.013453	0.04784	1104	5
SHROOM1	6	0.01346	0.047866	1105	2
CBX6	6	0.013474	0.047911	1106	3
LGALS16	5	0.013504	0.047998	1107	4
ZNF12	6	0.013509	0.048014	1108	1
SV2A	6	0.01351	0.048016	1109	3
IL15	6	0.013519	0.04804	1110	5
WWC1	6	0.013559	0.048174	1111	1
FAM9A	6	0.013563	0.048189	1112	5
PAIP2B	6	0.013565	0.048193	1113	3
SMURF2	6	0.013576	0.048228	1114	3
PYGB	6	0.013582	0.04825	1115	4
SLCO6A1	6	0.013583	0.048254	1116	3
BLID	6	0.013588	0.048264	1117	5
NEURL4	6	0.013609	0.048327	1118	2
OR9I1	6	0.01366	0.048489	1119	5
PRRG3	6	0.013672	0.04853	1120	4
COPS8	6	0.013703	0.048646	1121	4
CD99_X	6	0.013727	0.048714	1122	5
C6orf10	6	0.013734	0.048733	1123	4
PPP1R13B	6	0.013739	0.04875	1124	4
LRRN3	6	0.013755	0.048804	1125	5
SLC4A1AP	6	0.013758	0.048816	1126	1
RRAS2	6	0.013758	0.048816	1127	2
NDUFA4	6	0.013779	0.048883	1128	3
PLAA	6	0.013785	0.0489	1129	5
C1orf185	6	0.013813	0.048986	1130	3
PCOLCE2	6	0.013823	0.04902	1131	3
ZHX3	6	0.013857	0.049135	1132	4
ATP4B	6	0.013876	0.049188	1133	3
TRPV3	6	0.013898	0.04926	1134	4
PPRC1	6	0.013911	0.049301	1135	3
OR6A2	6	0.013921	0.04933	1136	5
SLC25A29	6	0.013938	0.04939	1137	4
hsa-mir-517a	3	0.013985	0.049534	1138	3
CFB	6	0.014006	0.049613	1139	4
KIFC2	6	0.014016	0.049652	1140	4
GMNN	6	0.01404	0.049721	1141	4
TP53AIP1	6	0.014042	0.049729	1142	5
TMEM45B	6	0.014079	0.049856	1143	5
FSD1	6	0.01408	0.049865	1148	2
TAS1R3	6	0.01408	0.049865	1145	4
LECT1	6	0.01408	0.049865	1147	3
DRD4	6	0.01408	0.049865	1144	5
CCL14	6	0.01408	0.049865	1146	3
EXOC6B	6	0.014161	0.050126	1149	2

7.4. 2. Genes listed from the combined comparison of NCTC replicate 2 vs untreated

Gene	# gRNA	score	p-value	rank	# good gRNA
UPF3A	6	1.74E-05	8.96E-05	1	5
TNFRSF25	6	2.51E-05	0.00012839	2	2
SLC17A9	6	4.55E-05	0.00022007	3	4
SSPO	6	4.68E-05	0.00022417	4	3
AP3D1	6	4.96E-05	0.00023603	5	4
NLRC4	6	7.47E-05	0.00033592	6	4
C12orf29	6	7.53E-05	0.00033728	7	3
FCHSD2	6	0.00012556	0.00054709	8	1
PROM1	6	0.00013539	0.0005886	9	5
hsa-mir-6794	4	0.00013549	0.00058905	10	3
DNAH6	6	0.00014073	0.00061049	11	5
ARL2BP	6	0.00016301	0.00070855	12	3
CHORDC1	6	0.00017578	0.00077103	13	1
hsa-mir-532	4	0.00018316	0.00080707	14	4
DTD1	6	0.00020104	0.00088825	15	3
MBD1	6	0.00020982	0.00092565	16	4
CCDC172	6	0.00022061	0.00097445	17	3
DMRTA1	6	0.00022599	0.00099224	18	1
OSTF1	6	0.00022715	0.00099452	19	4
TREML1	6	0.00023909	0.0010488	20	4
ATP5C1	6	0.00025283	0.0011049	21	4
SCAF11	6	0.00025352	0.0011085	22	4
TRIM38	6	0.00025625	0.0011172	23	3
TMEM14B	6	0.00026661	0.0011615	24	4
REN	6	0.00027621	0.0011943	25	2
ZEB1	6	0.0002941	0.0012705	26	3
LRP2BP	6	0.00029497	0.0012732	27	3
hsa-mir-638	4	0.00030054	0.0012919	28	2
NCSTN	6	0.00030115	0.0012955	29	4
hsa-mir-938	4	0.00031326	0.0013498	30	4
METTL10	6	0.0003135	0.0013498	31	2
CNTFR	6	0.00032642	0.0014009	32	2
RHOQ	6	0.00034301	0.0014657	33	4
hsa-mir-4291	4	0.00035031	0.0014917	34	3
GABRG1	6	0.00036368	0.0015459	35	5
GPR17	6	0.00037663	0.0015998	36	2
PPP3CA	6	0.00038977	0.001649	37	5
SMNDC1	6	0.00039227	0.0016572	38	5

CENPH	3	0.00041611	0.0017676	39	2
OR6K2	6	0.00042069	0.00179	40	4
LRSAM1	6	0.00042113	0.0017913	41	2
PAPSS2	6	0.00042248	0.001795	42	5
UFSP2	6	0.00042684	0.0018105	43	3
C17orf78	6	0.00044465	0.0018894	44	5
ASXL2	6	0.00044542	0.0018939	45	4
TRIM65	6	0.00045115	0.0019227	46	2
PRSS55	6	0.00045115	0.0019227	47	3
R3HCC1	6	0.00045271	0.0019277	48	4
TCP10L2	5	0.00046278	0.0019651	49	4
KIF3A	6	0.00047705	0.002023	50	2
MICU2	6	0.00049497	0.0020896	51	5
HIPK3	6	0.0005155	0.0021776	52	3
ALG11	6	0.00052725	0.0022255	53	3
ATPAF1	6	0.00057604	0.0024226	54	2
ZADH2	6	0.00059813	0.0025197	55	3
PDCL	6	0.00060256	0.0025334	57	2
KDR	6	0.00060256	0.0025334	56	1
GAB4	6	0.00062612	0.0026296	58	4
C1orf43	6	0.00062769	0.0026347	59	5
ADNP	6	0.0006479	0.0027204	60	4
SYCE2	6	0.00067262	0.0028121	61	3
PSMG4	6	0.00067785	0.0028331	62	1
CELSR3	6	0.00068162	0.0028499	63	5
hsa-mir-6786	4	0.00069546	0.0029024	64	3
SLAMF8	6	0.00072185	0.0030004	66	2
ZNF682	6	0.00072185	0.0030004	65	4
GALC	6	0.00072747	0.0030228	67	3
TTC1	6	0.00072805	0.0030255	68	1
PPP1R13B	6	0.00073964	0.0030684	69	5
PPM1K	6	0.00075303	0.0031245	70	4
MSH3	6	0.0007724	0.0032057	71	4
NFXL1	6	0.00077824	0.0032344	72	2
WNT1	6	0.00078251	0.003244	73	4
POLR2B	6	0.00078379	0.003249	74	4
ZNF648	6	0.00079719	0.0033024	75	4
AMER2	6	0.00080363	0.0033266	76	5
T	6	0.00080982	0.0033562	77	2
CEPT1	6	0.00081707	0.0033831	78	3
ADCYAP1R1	6	0.00081883	0.0033927	79	5
SPATA31A4	5	0.00081889	0.0033927	80	4
PRAMEF1	6	0.00082844	0.003431	81	3
QRFPR	6	0.00085719	0.0035583	82	5
NDUFB5	6	0.00087319	0.0036244	83	4
SPATA32	6	0.00092881	0.0038287	84	2
SLC27A2	6	0.0010041	0.0041138	85	2
BUD31	6	0.0010041	0.0041138	86	1
CLPX	6	0.001011	0.0041434	87	4
C6orf141	6	0.0010268	0.0042068	88	4
CYB5R3	6	0.0010408	0.0042702	89	4
SRPX	6	0.0010422	0.0042743	90	4
hsa-mir-567	4	0.0010785	0.0044066	91	4
ACN9	6	0.0010908	0.0044408	92	2
CGGBP1	6	0.0010995	0.0044663	93	3
CLTB	6	0.0011045	0.0044823	94	3
MLXIP	6	0.0011045	0.0044823	95	3
FYB	6	0.0011086	0.0044955	96	4
SSH2	6	0.0011797	0.0047199	97	1
ANKRD10	6	0.0012114	0.0048121	98	4
ADAM10	6	0.0012299	0.0048632	99	3
MRPL47	6	0.0012798	0.0050187	100	4
IFT57	6	0.00128	0.0050191	101	4
GIMAP8	6	0.0012801	0.0050191	102	1
PSD	6	0.0012914	0.0050529	103	4
MRVI1	6	0.0013094	0.0051167	104	3
NECAB2	6	0.0013171	0.0051496	105	3
GABRA2	6	0.0013197	0.0051601	106	4
WARS2	6	0.0013302	0.0051961	107	2
SLC22A8	6	0.0013306	0.0051975	108	3
MTHFS	5	0.0013729	0.0053275	109	2
CLK4	6	0.0013769	0.0053439	110	3
APC	6	0.0013804	0.0053539	111	2
EPS15L1	6	0.0013834	0.0053594	112	3
CFI	6	0.0013946	0.0053836	113	2
USP27X	6	0.0014049	0.0054132	114	3
RECQL5	6	0.0014306	0.0054953	115	1
PNMT	6	0.0014807	0.0056385	116	3
OR56A5	6	0.0014862	0.0056527	117	4
NKX3-2	6	0.0015048	0.0057147	118	3
PRICKLE3	6	0.0015064	0.0057183	119	2
DBX2	6	0.0015123	0.0057348	120	3
LOC100505841	6	0.0015241	0.0057744	121	3
OR4P4	6	0.001526	0.0057795	122	3
MMP16	6	0.0015318	0.0057945	123	4
hsa-mir-6845	4	0.0015394	0.0058219	124	1
SLC35E3	6	0.001556	0.0058679	125	1
FREM3	6	0.001556	0.0058679	126	2
FTMT	6	0.0015573	0.0058698	127	4
TP53BP2	6	0.001559	0.005872	128	3
hsa-mir-6831	4	0.0015707	0.0059062	129	3
CDH18	6	0.0015806	0.0059464	130	4
GPR133	6	0.0016179	0.0060682	131	3

KCNK1	6	0.0016312	0.0061183	132	2
OSTM1	6	0.0016568	0.0062091	133	2
DMTF1	6	0.0016619	0.0062232	134	2
FAM169B	6	0.0016814	0.006278	135	1
TRPA1	6	0.0016938	0.0063177	136	4
LAGE3	6	0.0017306	0.0064308	137	4
GNG7	6	0.0017315	0.0064335	138	1
SLCO1B7	6	0.0017427	0.0064727	139	3
PLXNC1	6	0.0017817	0.0066	140	2
RASSF2	6	0.0017927	0.0066356	141	3
C5orf49	6	0.0018318	0.0067569	142	2
EPC2	6	0.0018448	0.0067938	143	4
FOCAD	6	0.0018635	0.0068495	144	4
C1orf185	6	0.0018905	0.006932	145	4
GNRH1	6	0.0019064	0.0069863	146	3
IQSEC3	6	0.0019071	0.0069877	148	3
ZSCAN20	6	0.0019071	0.0069877	147	2
FABP6	6	0.0019162	0.0070123	149	3
SDC4	6	0.0019187	0.0070223	150	2
WFDC5	6	0.0019506	0.0071149	151	3
RAB7L1	6	0.0019854	0.0072139	152	2
CAB39L	6	0.0019966	0.0072444	153	4
ACPL2	6	0.0020073	0.0072841	154	1
CYP2E1	6	0.0020073	0.0072841	155	2
KIR3DL1	6	0.0020211	0.0073297	156	3
BBS4	6	0.0020297	0.0073516	157	3
GPSM3	6	0.0020777	0.0074994	158	3
DYSF	6	0.0020826	0.0075145	159	3
APEX1	6	0.0021362	0.0076659	160	4
TACSTD2	6	0.0021408	0.0076832	161	2
hsa-mir-1277	4	0.0021545	0.0077247	162	3
FGF1	6	0.0021828	0.0078036	163	1
OVOL2	6	0.0022024	0.0078752	164	3
LAMTOR4	6	0.002233	0.0079664	165	2
SUPT20HL1	6	0.0023076	0.0081785	166	3
TTLL1	6	0.0023082	0.008179	167	4
ITPRIPL1	6	0.0023169	0.0082091	168	4
TAS2R40	6	0.0023833	0.0083984	169	4
PANK3	6	0.0023874	0.0084139	170	4
OR4K14	6	0.0023939	0.0084317	171	4
HDHD2	6	0.0024037	0.0084593	172	3
TMEM89	6	0.0024191	0.0084955	173	2
CEP350	6	0.0024216	0.0085056	174	3
RARRES3	6	0.0024335	0.0085411	175	1
ECHDC2	6	0.0025087	0.0087528	176	1
GRM3	6	0.0025555	0.0088932	177	4
TXNDC9	6	0.0025671	0.0089343	178	4
C9orf153	6	0.0025838	0.008984	179	2
IL11RA	6	0.0026016	0.0090342	180	4
GIGYF2	6	0.0026339	0.009129	181	1
PCBP4	6	0.0026482	0.009176	182	4
ADAMTSL1	6	0.0026489	0.0091778	183	4
C6orf10	6	0.0026781	0.00927	184	4
FUT4	6	0.0026841	0.0092859	185	1
ZNF160	6	0.0027342	0.0094323	186	3
C1orf27	6	0.0027344	0.0094323	187	3
CSF2RB	6	0.0027386	0.0094419	188	4
SP110	6	0.00274	0.0094447	189	4
hsa-let-7g	4	0.0027595	0.0094957	190	1
ZNF385D	6	0.0027759	0.0095418	191	3
FAM167A	6	0.0027843	0.0095655	192	4
TGFBR2	6	0.0027957	0.0095975	193	4
C1orf35	6	0.0028344	0.0097211	194	3
DOCK3	6	0.0029055	0.0099377	195	4
DNAJC8	6	0.0029096	0.0099505	196	2
CLTA	6	0.0029096	0.0099505	197	2
HDX	6	0.0029453	0.010062	198	3
LRRC17	6	0.0029698	0.010144	199	3
TMEM178A	6	0.0029887	0.010209	200	2
SERPINB7	6	0.0029972	0.010233	201	2
TMEM52	6	0.0030098	0.010277	202	1
KRIT1	6	0.0030098	0.010277	203	1
hsa-mir-6090	4	0.0030268	0.010324	204	1
FLT3LG	6	0.0030349	0.010345	205	3
OR10G7	6	0.0030619	0.010433	206	4
MAP2K3	6	0.0030849	0.010506	207	1
KLRD1	6	0.0031316	0.010645	208	4
GHRHR	6	0.0031324	0.010647	209	4
UBE2U	6	0.0031363	0.010659	210	4
FAM221A	6	0.0031623	0.010742	211	4
UBA1	6	0.0031851	0.010809	212	2
MEIS3	6	0.0032231	0.010927	213	3
TLR7	6	0.0032266	0.010938	214	2
GCSAML	6	0.0032302	0.010952	215	3
ZBTB32	6	0.0032361	0.010968	216	3
CEP95	6	0.0032382	0.010974	217	3
DNAJB4	6	0.0032399	0.010979	218	4
SRSF10	6	0.0032443	0.010991	219	2
KCNT2	6	0.0032477	0.011003	220	3
GPRASP1	6	0.0032853	0.011107	223	1
MAP3K8	6	0.0032853	0.011107	221	1
GALNT11	6	0.0032853	0.011107	222	2
PRDM11	6	0.0032889	0.011119	224	4

hsa-mir-486-2	1	0.0033191	0.011213	225	1
HSPA4	6	0.0033228	0.011228	226	3
ELOVL2	6	0.0033732	0.011369	227	2
PPID	6	0.0033854	0.011407	228	2
CREM	6	0.0034216	0.011512	229	4
PTPN2	6	0.0034355	0.011548	230	2
TAAR5	6	0.003477	0.011661	231	2
MALSU1	6	0.0034856	0.011689	232	1
BDKRB2	6	0.0035279	0.01182	233	3
LEMD1	6	0.0035607	0.011935	234	2
MLEC	6	0.0035607	0.011935	235	2
KIAA0754	6	0.003567	0.011951	236	4
RCL1	6	0.0035825	0.011995	237	4
SEC31B	6	0.0035868	0.012002	238	4
SLC32A1	6	0.0036099	0.012072	239	3
ACCSL	6	0.0036347	0.012138	240	4
RCAN1	6	0.0036358	0.012144	241	1
MCMDC2	6	0.0036626	0.01223	242	4
TNFRSF4	6	0.0036796	0.012277	243	2
FSTL4	6	0.003736	0.012437	244	3
GLI1	6	0.003736	0.012437	246	3
KRTAP9-4	6	0.003736	0.012437	245	1
TYR	6	0.0037547	0.012503	247	4
hsa-mir-6080	4	0.003786	0.012585	248	3
SH3KBP1	6	0.003801	0.012635	249	3
TPM2	6	0.0038017	0.012636	250	4
SAMD4B	6	0.0038199	0.012686	251	3
TNFSF15	6	0.0038471	0.012773	252	4
OR5C1	6	0.0038862	0.012891	254	2
AIPL1	6	0.0038862	0.012891	253	2
CD101	6	0.0039039	0.012937	255	3
PHTF2	6	0.0039579	0.013095	256	3
ESF1	6	0.0039634	0.013112	257	2
ZNF585A	6	0.0039863	0.013176	258	1
OPA1	6	0.0040218	0.01329	259	3
KIAA1967	6	0.0040245	0.013296	260	4
WWC3	6	0.0040348	0.01333	261	4
PADI6	6	0.0040364	0.013333	262	2
CD81	6	0.00405	0.013375	263	3
AP1S1	6	0.004062	0.01341	264	4
EFCAB5	4	0.0040788	0.013469	265	1
E2F3	6	0.0040813	0.013482	266	3
RRH	6	0.0040864	0.013498	267	3
STARD3	6	0.0041051	0.013551	268	3
ITGB4	6	0.0041249	0.013602	269	2
LY75	6	0.004133	0.013627	270	4
PCDH18	6	0.0042044	0.013853	271	3
RBM44	6	0.0042115	0.013875	273	1
MT3	6	0.0042115	0.013875	272	1
HEXIM2	6	0.0042513	0.014005	274	3
SOX12	6	0.0042866	0.014113	275	3
SLC13A5	6	0.0043001	0.014148	276	3
CD93	6	0.004305	0.014167	277	3
HAS2	6	0.0043148	0.014198	278	4
MAN2A2	6	0.0043177	0.014208	279	4
TGM6	6	0.0043617	0.014324	280	1
DYNAP	6	0.0043617	0.014324	281	2
ICK	6	0.0044167	0.014475	282	4
CA10	6	0.0044453	0.014568	283	3
PRPS2	6	0.0044538	0.014592	284	4
LMLN	5	0.0044746	0.014654	285	3
KNOP1	6	0.0044972	0.014719	286	4
SPRR2F	4	0.0044989	0.014723	287	3
RHBDF2	6	0.0045194	0.014788	288	3
BRPF3	6	0.004524	0.014798	289	4
PVRIG	6	0.0045368	0.014833	290	2
OLFM2	6	0.0045368	0.014833	293	1
CCDC64B	6	0.0045368	0.014833	292	2
OSBPL10	6	0.0045368	0.014833	291	1
TMPRSS13	6	0.0045438	0.014855	294	4
hsa-mir-5190	4	0.0045473	0.014861	295	3
AGBL4	6	0.0045767	0.014949	296	3
hsa-mir-3920	4	0.0045771	0.01495	297	2
IL1RAP	6	0.0045819	0.014967	298	3
ZNF22	6	0.0046071	0.015043	299	3
ADAMTS9	6	0.0046094	0.015049	300	4
C10orf68	6	0.0046828	0.015266	301	2
KCNN2	6	0.0046869	0.015281	302	1
ORC3	6	0.0047225	0.015385	303	3
PRRG4	6	0.0047355	0.015423	304	4
TSHB	6	0.0047369	0.015426	305	3
DGAT2L6	6	0.0047667	0.015508	306	4
CPNE2	6	0.0047867	0.015562	307	4
ITGB1	6	0.004787	0.015563	308	1
TSGA13	6	0.0048254	0.015676	309	3
UBE2NL	6	0.0048302	0.01569	310	4
KIAA1524	6	0.004849	0.015737	311	2
MTMR2	6	0.0048576	0.015771	312	3
DMTN	6	0.004862	0.015784	314	3
PHF15	6	0.004862	0.015784	313	1
DFFB	6	0.004873	0.01582	315	3
DYNLL1	6	0.0049197	0.015955	316	4
DTWD1	6	0.0049342	0.016002	317	4

ANKRD18A	6	0.004937	0.016011	318	2
PSD2	6	0.004944	0.016034	319	3
CYLD	6	0.0049499	0.016052	320	4
NonTargetingControlGuideForHuman_0700	1	0.0049514	0.016056	321	1
CD4	6	0.0049871	0.016149	322	1
ZFR2	6	0.0050092	0.016216	323	2
COX6C	6	0.0050621	0.016367	324	2
USP3	6	0.0050971	0.016467	325	4
MUC7	6	0.0051371	0.016594	326	1
MSI2	6	0.0052121	0.016819	327	1
EQTN	6	0.0052121	0.016819	328	2
POLE	6	0.0052207	0.016845	329	2
ZNF700	6	0.0052383	0.016893	330	3
FAM162A	6	0.0052604	0.016964	331	4
CAPN13	6	0.0052637	0.016975	332	4
DYX1C1	6	0.0052871	0.017033	333	1
hsa-mir-193a	4	0.0052943	0.017053	334	3
TSPAN5	6	0.005301	0.017073	335	2
MYRIP	6	0.0053527	0.017218	336	2
KRTAP4-7	6	0.0053593	0.017238	337	3
GPR87	6	0.0053674	0.017269	338	4
C16orf74	6	0.0053732	0.017283	339	4
NonTargetingControlGuideForHuman_0492	1	0.0053783	0.017303	340	1
ATP1A3	6	0.005382	0.017314	341	2
ETV3L	6	0.0053871	0.017332	342	2
TRAPPC4	6	0.0053956	0.017361	343	2
ZC4H2	6	0.0054046	0.017382	344	3
CAMK1D	6	0.0054091	0.017395	345	4
CSAG1	6	0.0054371	0.017482	346	1
hsa-mir-485	4	0.0054634	0.01756	347	1
TWF1	6	0.0054871	0.017628	348	1
FAM103A1	6	0.0055279	0.017743	349	3
N4BP2L2	6	0.0055567	0.017828	350	3
ALK	6	0.0055567	0.017828	351	4
GML	6	0.005572	0.017872	352	3
PROZ	6	0.005574	0.017879	353	3
TXNDC12	6	0.0055779	0.01789	354	4
MCTP1	6	0.0055871	0.017921	355	2
SCN4A	6	0.0055871	0.017921	356	1
COX19	6	0.0056191	0.018023	357	2
CHRNB1	6	0.0056629	0.018158	358	3
FANCA	6	0.0056648	0.01816	359	3
KIF6	6	0.0056784	0.018196	360	3
LRRIQ4	6	0.0056871	0.018225	361	2
KIFC1	6	0.0056919	0.01824	362	4
HAUS2	6	0.005736	0.018377	363	3
C11orf93	6	0.0057511	0.018425	364	3
USP24	6	0.0057621	0.018454	365	2
RAB11FIP3	6	0.0057621	0.018454	366	2
LRGUK	6	0.0057674	0.01847	367	3
hsa-mir-759	4	0.0057778	0.018488	368	2
OSBPL5	6	0.0057841	0.018511	369	3
LONRF2	6	0.0057912	0.018532	370	4
PRR5-ARHGAP8	4	0.0058468	0.018696	371	2
hsa-mir-4794	3	0.0058774	0.018783	372	1
C17orf66	6	0.005887	0.018817	373	2
B3GNT8	6	0.0059288	0.018941	375	3
TRIM67	6	0.0059288	0.018941	374	3
RAP2C	6	0.005937	0.018962	376	1
AWAT1	6	0.0059397	0.01897	377	4
hsa-mir-4716	4	0.0059492	0.018996	378	2
MFSD5	6	0.0059606	0.019023	379	4
SLC35A2	6	0.0059668	0.019043	380	4
DAZL	6	0.0059811	0.019083	382	4
OR1N1	6	0.0059811	0.019083	381	4
CHCHD10	6	0.005987	0.0191	383	1
TLN2	6	0.0059916	0.019114	384	4
NUDT10	6	0.0060076	0.019164	385	2
hsa-mir-4433	4	0.0060301	0.019224	386	2
CELF3	6	0.0060369	0.019238	387	1
TMED3	6	0.0060433	0.019252	388	2
hsa-mir-27b	4	0.0060635	0.019306	389	1
CSH1	6	0.0061078	0.019433	390	2
FSIP1	6	0.0061119	0.019439	391	2
ANKEF1	6	0.0061291	0.019488	392	4
KCNRG	6	0.0061349	0.019508	393	4
MAPK7	6	0.0061751	0.019621	394	2
ZFAT	6	0.0061758	0.019623	395	3
FGF12	6	0.0061869	0.019653	396	4
FLJ44313	6	0.0061987	0.019685	397	4
hsa-mir-4708	4	0.0062134	0.019727	398	1
IQGAP3	6	0.0062368	0.019794	399	1
MTTP	6	0.0062491	0.019829	400	4
KCNA1	6	0.0062582	0.019854	401	3
ATP2B1	6	0.0062868	0.019933	402	2
PCBP1	6	0.0063179	0.020023	403	2
SLFN12L	6	0.0063349	0.020069	404	3
CASP8AP2	6	0.0063496	0.020115	405	2
HTR1E	6	0.0063887	0.02023	406	3
LDHAL6A	6	0.0064039	0.020275	407	3
PIK3C2B	6	0.0064117	0.020302	411	4

TRIM8	6	0.0064117	0.020302	408	1
NRG4	6	0.0064117	0.020302	410	2
C16orf70	6	0.0064117	0.020302	409	2
PNLIP	6	0.0064312	0.020363	412	3
DLG4	6	0.0064867	0.020522	413	4
KIAA1024L	6	0.0064945	0.020543	414	3
GPRIN2	6	0.0065116	0.020598	415	2
KRTAP22-2	6	0.0065143	0.02061	416	4
LMBR1	6	0.0065157	0.020612	417	3
DHX35	6	0.006519	0.020625	418	2
TACC1	6	0.0065366	0.020666	419	1
SERHL2	6	0.006566	0.020745	420	2
EWSR1	6	0.0065752	0.020771	421	3
CHMP6	6	0.0065865	0.020805	422	1
C3orf58	6	0.0066189	0.020901	423	4
CLCNKA	6	0.0066306	0.020941	424	2
DNAJC12	6	0.0066362	0.020953	425	4
hsa-mir-8081	4	0.0066442	0.020975	426	2
OR2J3	6	0.0066469	0.020983	427	4
KRBOX1	6	0.0066505	0.020993	428	2
KCNJ12	6	0.0066614	0.02102	430	2
KLHL41	6	0.0066614	0.02102	429	2
ZNF519	6	0.0066754	0.021067	431	2
FGF21	6	0.0066776	0.021074	432	4
GFPT1	6	0.0066804	0.021082	433	2
MMP1	6	0.0066998	0.021133	434	4
TTBK1	6	0.0067199	0.021198	435	4
AMZ2	6	0.0067408	0.021262	436	4
SH2D6	6	0.0067506	0.021294	437	2
TNFSF9	6	0.0067526	0.021299	438	3
hsa-mir-4713	4	0.0067692	0.021345	439	3
VPS52	6	0.0068069	0.021446	440	3
TRIM43B	6	0.0068084	0.02145	441	3
MPG	6	0.0068362	0.021536	443	1
NMU	6	0.0068362	0.021536	445	2
CCK	6	0.0068362	0.021536	442	2
PEX6	6	0.0068362	0.021536	444	2
SATL1	6	0.0068602	0.021613	446	4
IGF1	6	0.0068801	0.021674	447	3
DOPEY2	6	0.0069071	0.021752	448	3
hsa-mir-200b	4	0.0069298	0.021809	449	1
SAMD7	6	0.006935	0.021828	450	3
TMEM19	6	0.0069505	0.021872	451	3
RBMS2	6	0.006986	0.021967	452	2
ST6GAL1	6	0.0070653	0.022204	453	2
GCKR	6	0.0070658	0.022205	454	4
IPMK	6	0.0070825	0.022258	455	4
KCP	6	0.0070859	0.022272	456	2
CREBRF	6	0.0071238	0.022381	457	4
KIAA1244	6	0.0071321	0.022402	458	3
BZRAP1	6	0.0071358	0.022414	459	1
PRRT1	6	0.0071554	0.022473	460	4
KBTBD4	6	0.0072253	0.022674	461	3
TRERF1	6	0.0072281	0.02268	462	4
B3GNT3	6	0.0072357	0.022703	463	2
OGN	6	0.0072357	0.022703	464	1
PDGFC	6	0.0072942	0.022875	465	4
hsa-mir-4774	4	0.0073203	0.022942	466	2
SLC36A1	6	0.0073355	0.022975	467	2
ADSS	6	0.007371	0.023075	468	2
CST7	6	0.0073854	0.023111	469	2
hsa-mir-4308	4	0.0073954	0.02314	470	3
WDR81	6	0.0074219	0.023216	471	4
B3GAT3	6	0.0074853	0.023404	472	2
NUDT3	6	0.0074918	0.023421	473	2
RBM48	6	0.0075059	0.02346	474	4
OPHN1	6	0.0075352	0.02355	475	2
GMFG	6	0.0075431	0.023574	476	4
MBNL3	6	0.0075473	0.023589	477	2
DENND4A	6	0.0075605	0.023624	478	2
PRPSAP2	6	0.0075921	0.023709	479	4
WBSCR17	6	0.0076406	0.023848	480	4
ZNF467	6	0.0076428	0.023854	481	2
ZNF182	6	0.0076508	0.023879	482	2
SMOC1	6	0.0076561	0.02389	483	4
DGCR6	6	0.0076605	0.023906	484	3
THEM5	6	0.0076657	0.023921	485	4
MYLIP	6	0.0076849	0.023977	486	1
RHBDD3	6	0.0076849	0.023977	488	1
TRMT6	6	0.0076849	0.023977	487	3
FAM159B	6	0.0076852	0.023977	489	3
hsa-mir-148a	3	0.0077273	0.0241	490	2
SCN1B	6	0.0077469	0.024165	491	2
hsa-mir-383	4	0.0077969	0.024308	492	3
MUC20	6	0.0078167	0.024358	493	2
DHRS7	6	0.0078189	0.024362	494	4
RGS20	6	0.0078346	0.024409	495	1
TSPAN2	6	0.0078845	0.024554	496	2
CH25H	6	0.0078868	0.024562	497	4
ZNF707	6	0.007894	0.02458	498	4
PGBD3	6	0.0079529	0.024769	499	4
DRD4	6	0.0079843	0.024861	502	2
ANP32E	6	0.0079843	0.024861	501	2

CDT1	6	0.0079843	0.024861	500	1
hsa-mir-3187	4	0.0080299	0.025	503	3
hsa-mir-4264	4	0.0080618	0.025096	504	1
EPS15	6	0.008084	0.025161	505	4
KRCC1	6	0.0080841	0.025162	506	3
FBXO3	6	0.0081093	0.025228	507	3
PPP1R3A	6	0.008134	0.025295	508	2
P2RY12	6	0.0081594	0.025379	509	4
TRPM3	6	0.0082337	0.025585	510	2
hsa-mir-8084	4	0.0082737	0.025693	511	2
NDUFA8	6	0.0082804	0.025711	512	3
ATXN2	6	0.0082836	0.025716	513	1
FAM149B1	6	0.0082911	0.025737	514	2
PREPL	6	0.0083335	0.025852	515	1
GPR110	6	0.0083465	0.025892	516	2
HIVEP3	6	0.0083798	0.025984	517	3
C4orf47	6	0.0084052	0.026054	518	4
PNMA3	6	0.0084231	0.026108	519	4
SMIM15	6	0.0084421	0.026162	520	4
EZR	6	0.0084577	0.026208	521	3
UNC5D	6	0.0084582	0.026209	522	1
MYB	6	0.0084582	0.026209	523	3
ADAM2	6	0.0084582	0.026209	525	1
MAL2	6	0.0084582	0.026209	524	2
NEFL	6	0.0084857	0.026288	526	2
FZD4	6	0.0085373	0.026438	527	4
GAL3ST4	6	0.0085509	0.026473	528	4
EXD2	6	0.0085538	0.026478	529	3
SV2C	6	0.0085585	0.026488	530	3
HAPLN3	6	0.0085828	0.02655	531	1
ENO3	6	0.0085932	0.02658	532	4
ZMYND12	6	0.0086066	0.026616	533	4
FOLR2	6	0.0086146	0.026635	534	2
BHLHA15	6	0.008651	0.026732	535	4
SLC6A7	6	0.0086542	0.026739	536	4
C6orf203	6	0.0086546	0.026739	537	3
ACTA2	6	0.0086597	0.026756	538	2
RRBP1	6	0.0086671	0.026776	539	4
ANGPTL5	6	0.0086735	0.026794	540	4
ZNF280C	6	0.0087053	0.026875	541	3
LRRC8D	6	0.008713	0.026893	542	4
GAP43	6	0.0087357	0.026965	543	4
CHN1	6	0.008751	0.027014	544	3
GCNT7	6	0.0087574	0.027028	547	1
ZIM3	6	0.0087574	0.027028	545	3
ARRDC1	6	0.0087574	0.027028	546	3
ECM1	6	0.0087574	0.027028	548	2
PHOX2A	6	0.0087722	0.027072	549	4
RBM6	6	0.008821	0.027207	550	4
hsa-let-7d	4	0.0088348	0.027252	551	2
ELAVL2	6	0.0088815	0.027383	552	3
SPRR2A	5	0.0088819	0.027383	553	3
MINPP1	6	0.0088866	0.0274	554	3
CNGA3	6	0.0088892	0.027405	555	3
HIST1H4L	6	0.0089098	0.027465	556	3
POLE3	6	0.0089123	0.027476	557	3
SYNGR2	6	0.0089318	0.027525	558	1
CCNI2	6	0.0089325	0.027527	559	3
IFNL4	6	0.0089817	0.027656	560	2
FAM222A	6	0.0090261	0.02779	561	3
hsa-mir-4464	4	0.0090266	0.027792	562	2
CSF1	6	0.0090807	0.02795	563	4
SAPCD2	6	0.0090885	0.027972	564	3
DNAJB2	6	0.0090979	0.027999	565	4
ACR	6	0.0091312	0.028099	566	2
hsa-mir-644a	4	0.0091577	0.028183	567	3
IMPA1	6	0.0091714	0.028221	568	2
NAT1	6	0.0091811	0.028247	569	2
CDK10	6	0.0091946	0.028277	570	3
BCL2A1	6	0.0092498	0.028435	571	2
PLAGL1	6	0.0092556	0.02845	572	2
hsa-mir-634	4	0.0092927	0.028547	573	1
hsa-mir-4305	4	0.0092927	0.028547	574	1
TCTN1	6	0.0093057	0.028587	576	2
TTI1	6	0.0093057	0.028587	575	3
C4orf26	6	0.0093112	0.0286	577	4
HTR3E	6	0.0093303	0.028655	578	3
ACTR1B	6	0.0093488	0.028713	579	3
SH2B2	6	0.0093993	0.028862	580	3
hsa-mir-562	4	0.0094092	0.028888	581	3
ZNF471	6	0.0094303	0.02894	582	1
DENND5A	6	0.0094801	0.029072	583	2
C19orf80	6	0.0094897	0.029107	584	3
hsa-mir-3141	4	0.0095056	0.029155	585	2
GALNT6	6	0.0095125	0.029182	586	4
PLCB2	6	0.0095191	0.029202	587	2
CNNM4	6	0.0095598	0.029302	588	3
SZRD1	6	0.0095763	0.029346	589	4
CNPY2	6	0.0095797	0.029358	590	3
UFM1	6	0.0096312	0.029497	591	3
FGR	6	0.0096353	0.029508	592	4
NUFIP2	6	0.0096629	0.029578	593	4
KIAA1217	6	0.0096818	0.029633	595	2

FXYD6	6	0.0096818	0.029633	594	3
C11orf48	6	0.0097021	0.029686	596	4
MAGED1	6	0.0097292	0.029762	599	1
PLXDC2	6	0.0097292	0.029762	600	3
GUCY1A3	6	0.0097292	0.029762	598	1
LUC7L3	6	0.0097292	0.029762	601	2
YPEL5	6	0.0097292	0.029762	597	2
C19orf60	6	0.009765	0.029866	602	4
SELM	6	0.0097801	0.029912	603	2
DNTTIP1	6	0.0097834	0.029922	604	4
VPS13A	6	0.0098369	0.030064	605	2
hsa-mir-378j	4	0.0098744	0.030176	606	2
ZNF442	6	0.0098786	0.030187	607	2
PDCD5	6	0.0098978	0.030242	608	4
hsa-mir-661	4	0.0099058	0.030257	609	3
DGKA	6	0.0099134	0.030278	610	3
MAS1	6	0.0099238	0.030305	611	2
hsa-mir-4804	4	0.0099575	0.030411	612	1
C1orf151-NBL1	6	0.0099783	0.030465	613	3
hsa-mir-6745	4	0.010023	0.030599	614	3
NTRK1	6	0.010038	0.030639	615	3
TMEM72	6	0.010038	0.03064	616	3
ZNF438	6	0.01005	0.030673	617	2
hsa-mir-4701	4	0.010104	0.030824	618	3
CBS	6	0.010116	0.030849	619	4
hsa-mir-3118-5	1	0.010125	0.030877	620	1
DLGAP5	6	0.010128	0.030882	623	2
CCR6	6	0.010128	0.030882	622	2
PRTN3	6	0.010128	0.030882	625	1
ZNF557	6	0.010128	0.030882	624	2
RAG2	6	0.010128	0.030882	621	2
SLC25A32	6	0.010231	0.031163	626	4
AMELY	5	0.01024	0.03119	627	2
TNFRSF19	6	0.010265	0.031264	629	3
ATF2	6	0.010265	0.031264	628	3
TRIB3	6	0.010272	0.031279	630	2
ILDR1	6	0.010277	0.031293	631	1
GBP1	6	0.010327	0.03143	632	3
C1orf174	6	0.010387	0.031592	633	4
HYAL2	6	0.010391	0.031604	634	2
AAAS	6	0.010422	0.031688	635	3
hsa-mir-4515	4	0.010443	0.03175	636	3
MAP2K2	6	0.010468	0.031824	637	3
DNMT3A	6	0.010476	0.031843	640	2
TNIP3	6	0.010476	0.031843	639	2
ETV1	6	0.010476	0.031843	638	2
MOB4	2	0.010478	0.031846	641	1
FAM110D	6	0.010508	0.031943	642	3
SLC1A6	6	0.010552	0.032065	643	4
AUH	6	0.010573	0.032116	644	2
UGP2	6	0.010575	0.032126	645	3
PHYH	6	0.010576	0.032126	646	1
SRSF11	6	0.010583	0.032144	647	3
PHLDB2	6	0.010613	0.032238	648	3
UCMA	6	0.010618	0.032257	649	4
ABI3	6	0.01066	0.032375	650	4
OR2T11	6	0.010682	0.032431	651	4
ARHGEF12	6	0.010725	0.032565	652	4
PAQR5	6	0.010758	0.032654	653	4
SRD5A1	6	0.010775	0.032697	655	3
TRIP6	6	0.010775	0.032697	654	3
KDM3A	6	0.010796	0.03276	656	4
hsa-mir-148b	4	0.010799	0.032772	657	3
HEXB	6	0.010824	0.032836	658	4
MMP26	6	0.010888	0.033007	659	2
TMEM17	6	0.010924	0.033109	660	2
ZBTB34	6	0.010963	0.033227	661	2
SLC23A3	6	0.010974	0.033255	662	2
NonTargetingControlGuideForHuman_0409	1	0.010978	0.033271	663	1
MCTS1	6	0.010994	0.033318	664	3
PAFAH1B1	4	0.011007	0.033353	665	3
PAGE1	6	0.01101	0.033363	666	2
ROGDI	6	0.011024	0.033402	667	3
PPOX	6	0.011038	0.03344	668	4
SYT10	6	0.011052	0.03348	669	4
STAR	6	0.011083	0.033568	670	2
NR0B1	6	0.011098	0.033615	672	2
KCTD7	6	0.011098	0.033615	671	1
IQGAP1	6	0.011111	0.033648	673	4
IFT46	6	0.011153	0.033757	674	4
DNAJB13	6	0.01117	0.033804	675	4
RFFL	6	0.011223	0.033954	676	1
NR2C1	6	0.01123	0.033975	677	4
NKAIN1	6	0.011231	0.033978	678	3
KLHL25	6	0.011248	0.03402	679	3
TCEA3	6	0.011288	0.03413	680	3
ZNF331	6	0.011295	0.034151	681	4
CD40LG	6	0.011297	0.034161	682	2
HCAR3	6	0.01132	0.034224	683	4
hsa-let-7a-2	4	0.011369	0.034352	684	2
OR6B3	6	0.011372	0.034364	685	2
GPS2	6	0.011398	0.034431	686	2

C14orf28	6	0.011409	0.034463	687	3
KRT73	6	0.011414	0.034479	688	4
PLEKHA6	6	0.011422	0.034495	689	1
ARHGAP29	6	0.011472	0.034626	690	2
KPNA2	6	0.011521	0.034763	691	1
CROCC	6	0.011537	0.034804	692	3
C3orf62	6	0.01155	0.034838	693	4
hsa-mir-6822	4	0.011606	0.035022	694	3
EPCAM	6	0.01161	0.035037	695	2
DNAJC6	6	0.011621	0.035064	696	4
GABRB3	6	0.011645	0.035124	697	4
RBL2	6	0.011646	0.035125	698	2
ANXA11	6	0.011659	0.035153	699	4
ZNF562	6	0.011665	0.035165	700	4
PNLIPRP3	6	0.011672	0.035183	701	4
FAM32A	6	0.01172	0.035314	702	1
GIMAP2	6	0.01172	0.035314	704	1
GJB2	6	0.01172	0.035314	703	1
OCLM	4	0.011733	0.035354	705	2
NonTargetingControlGuideForHuman_0395	1	0.01174	0.035377	706	1
MECP2	6	0.011743	0.035384	707	3
PTPLAD2	6	0.011785	0.035494	708	4
VTCN1	6	0.011814	0.035584	709	3
EMR1	6	0.011841	0.035658	710	3
NKIRAS2	6	0.01186	0.035716	711	2
CARHSP1	6	0.011922	0.035884	712	2
TIFA	6	0.011969	0.03601	713	2
MAGEA10	6	0.011971	0.036019	714	4
C20orf27	6	0.012007	0.036117	715	3
PLEKHA8	6	0.012041	0.036208	716	3
PGM2	6	0.012054	0.036237	717	3
NRXN3	6	0.012065	0.036271	718	4
RNF111	6	0.012068	0.036287	719	2
KCNE1	6	0.01207	0.036291	720	2
VSIG10	6	0.012096	0.036366	721	2
ASIP	6	0.012114	0.036416	722	4
CALU	6	0.012119	0.036431	723	4
ERBB2IP	6	0.012129	0.036453	724	3
ANKRD30B	6	0.012166	0.036562	725	4
PPAPDC1A	6	0.012168	0.036569	727	2
HTRA4	6	0.012168	0.036565	726	1
HLX	6	0.012185	0.036621	728	4
FGFR1OP2	6	0.012203	0.036666	730	4
PRR4	6	0.012203	0.036666	729	3
FAM98C	6	0.012217	0.036705	731	3
TAAR1	6	0.012261	0.036823	732	2
CAP2	6	0.012267	0.036844	733	2
INF2	6	0.012317	0.036992	734	2
SLC17A3	6	0.012427	0.037286	735	2
RUNDC3B	6	0.012466	0.037364	736	1
C9orf3	6	0.012466	0.037364	738	2
ASB15	6	0.012466	0.037364	737	1
hsa-mir-584	4	0.012538	0.037517	739	3
hsa-mir-4437	4	0.012569	0.03758	740	3
TRABD2B	6	0.012578	0.0376	741	3
ZKSCAN7	6	0.012615	0.037668	742	1
COX10	6	0.012621	0.037677	743	3
ERCC6	2	0.012625	0.037688	744	1
NIT2	6	0.012648	0.03773	745	3
CASP12	6	0.012665	0.037775	746	3
RFX5	6	0.012715	0.037881	747	2
CHMP1B	6	0.012725	0.03791	748	3
hsa-mir-137	4	0.012731	0.037924	749	3
C4orf3	6	0.012755	0.03797	750	2
ZNF521	6	0.012764	0.037988	751	1
TBX19	6	0.012814	0.038095	752	1
OR8J3	6	0.012864	0.038201	753	2
SLC39A11	6	0.012877	0.038226	754	2
PDE2A	6	0.012931	0.038339	755	2
LOC388813	5	0.01297	0.03842	756	3
CHDC2	6	0.012986	0.03845	757	3
PLTP	6	0.013112	0.038714	765	1
PARP1	6	0.013112	0.038714	759	1
BOLL	6	0.013112	0.038714	758	1
GPRIN1	6	0.013112	0.038714	760	2
NDUFB4	6	0.013112	0.038714	761	1
MVD	6	0.013112	0.038714	763	1
C2	6	0.013112	0.038714	762	1
GIPC1	6	0.013112	0.038714	764	1
RLF	6	0.013156	0.038812	766	2
PPIL3	6	0.013225	0.038956	767	2
TMEM26	6	0.013251	0.039007	768	3
C6orf89	6	0.013252	0.039009	769	2
C7orf26	6	0.013259	0.039025	770	2
ZFP82	6	0.013266	0.03904	771	3
SLC1A3	6	0.013275	0.03906	772	3
hsa-mir-718	4	0.013282	0.039072	773	2
TEX15	6	0.0133	0.039108	774	3
hsa-mir-4719	1	0.013306	0.039122	775	1
ANK3	6	0.013326	0.03917	776	3
MKNK2	6	0.01336	0.039242	777	2
PCDHGA3	2	0.013361	0.039243	778	2

CDX4	6	0.01341	0.039336	779	1
PPP1R3F	6	0.013424	0.039365	780	3
CYP3A7-CYP3AP1	2	0.013448	0.039417	781	1
DNTTIP2	6	0.013452	0.039426	782	3
ZNF845	6	0.01346	0.039443	783	2
APOA1BP	6	0.013464	0.03945	784	3
C19orf33	6	0.013482	0.039484	785	3
SPANXE	2	0.01349	0.039503	786	1
LUZP2	6	0.013525	0.039583	787	3
IL16	6	0.013559	0.039648	788	2
MMAB	6	0.0136	0.039725	789	3
EFCAB6	6	0.013646	0.039814	790	3
PRR16	6	0.013701	0.039934	791	2
PLEKHM2	6	0.013708	0.039951	792	2
CDK16	6	0.013732	0.039993	793	3
hsa-mir-1302-7	4	0.01375	0.040031	794	3
hsa-mir-579	4	0.013786	0.040103	795	2
ZNF79	6	0.013806	0.040144	796	3
TMEM200B	6	0.013808	0.040148	798	3
LONP2	6	0.013808	0.040148	797	3
NonTargetingControlGuideForHuman_0755	1	0.013866	0.040266	799	1
MED20	6	0.013877	0.040291	800	3
DCUN1D2	6	0.013899	0.040332	801	3
PBX1	6	0.013907	0.040347	804	1
SRRM4	6	0.013907	0.040347	809	2
LRRC46	6	0.013907	0.040347	808	2
VRK1	6	0.013907	0.040347	802	2
LRRK1	6	0.013907	0.040347	803	1
STK32A	6	0.013907	0.040347	806	2
TNKS	6	0.013907	0.040347	811	3
PPARGC1A	6	0.013907	0.040347	805	1
ADHFE1	6	0.013907	0.040347	810	2
PCMTD1	6	0.013907	0.040347	807	1
THG1L	6	0.013908	0.040349	812	3
LRRC19	6	0.013931	0.040394	813	3
C14orf39	6	0.013948	0.040429	814	3
AKAP11	6	0.013958	0.040449	815	3
NMUR1	6	0.01396	0.040453	816	3
DOCK1	6	0.013967	0.040468	817	2
CHI3L1	6	0.014045	0.040633	818	2
TRIM62	6	0.014132	0.04082	819	3
CYP2D6	6	0.014135	0.040829	820	3
LAMC2	6	0.014139	0.040834	821	3
C1orf233	6	0.014186	0.040929	822	2
PCCA	6	0.014254	0.041081	823	1
TCEAL3	6	0.014257	0.041087	824	2
ASB4	6	0.014299	0.041189	825	2
CYP3A4	6	0.014304	0.041201	826	1
hsa-mir-4538	4	0.014337	0.041273	827	1
TIMM21	6	0.014351	0.041302	828	3
MCPH1	6	0.01437	0.041348	829	3
TSHZ3	6	0.014403	0.041411	830	1
BIRC8	6	0.014442	0.041491	831	3
GDE1	6	0.01447	0.041545	832	2
hsa-mir-4710	4	0.01448	0.041564	833	3
hsa-mir-4634	4	0.014489	0.04158	834	2
TGFBR1	6	0.014542	0.041687	835	2
SCG3	6	0.014556	0.041719	836	3
CBFA2T2	6	0.014575	0.041761	837	3
EDDM3A	6	0.014577	0.041764	838	1
VILL	6	0.014606	0.041819	839	2
hsa-mir-7-2	2	0.014608	0.041821	840	2
SGPP1	6	0.014692	0.041979	841	3
GDPD3	6	0.014699	0.041993	842	3
EHBP1	6	0.014771	0.042142	843	2
DCTN2	6	0.014775	0.04215	845	2
GNAS	6	0.014775	0.04215	844	2
AHCYL1	6	0.014811	0.042221	846	2
PATE4	6	0.014829	0.042259	847	2
KRTAP16-1	6	0.014844	0.042286	848	3
TRPC4	6	0.014858	0.042319	849	3
ZNF462	6	0.014892	0.042394	850	3
DDIT4	6	0.014895	0.0424	851	3
hsa-mir-4685	4	0.01492	0.042452	852	3
FDCSP	6	0.014923	0.042458	853	2
SPC25	6	0.014947	0.042515	854	3
TMIGD2	6	0.014949	0.042518	855	2
PARS2	6	0.014959	0.042543	856	3
hsa-mir-6849	4	0.014988	0.042597	857	2
KCNQ5	6	0.014996	0.042609	858	2
SLC38A10	6	0.014998	0.042613	859	1
SPSB3	6	0.015035	0.042691	860	3
LLGL2	6	0.015073	0.042772	862	1
OAF	6	0.015073	0.042772	861	3
IMMP1L	6	0.01509	0.042811	863	3
FAM115A	6	0.015105	0.042837	864	2
DGCR14	6	0.015119	0.042866	865	3
OR51B5	6	0.015161	0.042955	866	3
hsa-mir-361	4	0.015185	0.042994	867	2
RGPD1	6	0.015196	0.043015	868	2
hsa-mir-4729	4	0.015203	0.04303	869	2
MEF2D	6	0.015218	0.043058	870	3

LYPD1	6	0.015221	0.043062	871	2
ARL6IP6	6	0.015233	0.043081	872	3
SRI	6	0.015246	0.043109	876	2
ATAD3B	6	0.015246	0.043109	873	2
METTL21C	6	0.015246	0.043109	875	2
DEFB108B	6	0.015246	0.043109	874	1
OR10K1	6	0.015292	0.043203	877	3
ZNF426	6	0.015312	0.043247	878	3
PPP3R2	6	0.015383	0.043409	879	3
RAB3C	6	0.015414	0.043474	880	3
TJAP1	6	0.015419	0.043485	881	3
KLHL1	6	0.015444	0.043534	882	2
RCSD1	6	0.015456	0.043555	883	2
GPR19	6	0.015471	0.043585	884	3
C6orf25	6	0.015494	0.043631	885	2
BANK1	6	0.015499	0.043642	886	3
UPK3A	6	0.015593	0.043839	887	2
PLK2	6	0.015618	0.043894	888	2
THSD1	6	0.015625	0.043907	889	3
FANCI	6	0.015633	0.043919	890	2
MTPAP	6	0.015643	0.04394	891	1
LRRC27	6	0.015648	0.043953	892	3
ACTRT1	6	0.015662	0.043987	893	2
TRPC3	6	0.015692	0.044043	894	1
CCL21	6	0.015725	0.044109	896	2
FAM222B	6	0.015725	0.044109	895	3
PSMB6	6	0.015742	0.044147	897	1
LMBR1L	6	0.015841	0.044349	898	2
NonTargetingControlGuideForHuman_0221	1	0.015859	0.044391	899	1
ZFP90	6	0.015893	0.04446	900	3
PILRA	6	0.015899	0.044479	901	3
FUBP1	5	0.015949	0.044575	902	3
NonTargetingControlGuideForHuman_0852	1	0.015993	0.044661	903	1
FAM133A	6	0.016002	0.044675	904	3
CASS4	6	0.016014	0.044699	909	1
HIST1H3F	6	0.016014	0.044699	905	1
PPFIBP1	6	0.016014	0.044699	906	3
TBX20	6	0.016014	0.044699	908	1
RIOK1	6	0.016014	0.044699	907	2
ARMCX4	6	0.016142	0.044949	910	3
DDC	6	0.016157	0.044981	911	3
ZC3H12B	6	0.016169	0.045007	912	2
SYT8	6	0.016188	0.045033	913	1
FLNC	6	0.016194	0.045048	914	3
KIAA0319L	6	0.016237	0.045138	915	1
ERV3-1	6	0.01629	0.045252	916	3
ZCCHC17	6	0.016312	0.045299	917	2
C5AR2	6	0.016337	0.045347	918	3
SYNPO2L	6	0.016386	0.04545	919	1
UBE2N	6	0.016436	0.045539	920	2
PTPDC1	6	0.016449	0.045564	921	3
GLOD4	6	0.016485	0.04564	922	2
C19orf47	6	0.016535	0.045741	923	2
HLA-DPB1	6	0.016584	0.045841	924	1
hsa-mir-3148	4	0.016626	0.045933	925	3
CEP192	6	0.016634	0.045947	926	1
LOC391322	6	0.016645	0.045974	927	2
hsa-mir-5091	4	0.016648	0.045977	928	3
GPR173	6	0.016683	0.046051	929	1
FUCA1	6	0.016717	0.04612	930	3
C15orf61	6	0.016725	0.04614	931	2
hsa-mir-548an	4	0.016736	0.046163	933	1
hsa-mir-4779	4	0.016736	0.046163	932	1
C9	6	0.016782	0.046254	934	2
RERGL	6	0.016782	0.046254	935	3
NSD1	6	0.016859	0.046417	937	2
SPG7	6	0.016859	0.046417	936	3
BBS2	6	0.016881	0.046463	938	2
FANK1	6	0.016889	0.046478	939	3
MIA3	6	0.016931	0.046563	940	2
SMC6	6	0.016943	0.046592	941	2
SPINK7	6	0.017076	0.04686	942	3
RPS26	6	0.017085	0.04688	943	2
STARD6	6	0.01712	0.04695	944	2
DDX46	6	0.017129	0.046968	945	2
YRDC	6	0.017174	0.047055	946	2
TCEAL4	6	0.017228	0.047173	947	3
LOC154872	6	0.017251	0.047222	948	2
MEOX2	6	0.017277	0.047278	950	2
C19orf52	6	0.017277	0.047278	952	2
SOX10	6	0.017277	0.047278	949	2
LPAR6	6	0.017277	0.047278	951	1
CACNA1D	6	0.017297	0.047324	953	3
PDXK	6	0.017348	0.04743	954	3
PHTF1	6	0.017359	0.047455	955	2
CKMT2	6	0.017369	0.047475	956	3
NonTargetingControlGuideForHuman_0298	1	0.017382	0.047501	957	1
ZSWIM3	6	0.017413	0.047563	958	3
LAPTM5	6	0.017426	0.047593	959	1
hsa-mir-29b-2	4	0.017447	0.04764	960	1

OR2M4	6	0.01746	0.047665	961	3
LZTS2	6	0.017464	0.047673	962	2
NSUN7	6	0.017475	0.047696	963	2
RNASEH2B	6	0.017525	0.047791	964	2
NonTargetingControlGuideForHuman_0818	1	0.017541	0.047822	965	1
PHEX	6	0.017554	0.047841	966	2
CNRIP1	6	0.017624	0.047991	967	3
BTK	6	0.017671	0.048089	968	2
RPS6KA2	6	0.017673	0.048096	969	3
PAF1	6	0.017721	0.048202	970	3
EXOSC6	6	0.017723	0.048208	971	1
POLR2K	6	0.017731	0.048228	972	3
ZNF586	6	0.017745	0.048258	973	2
TRPM1	6	0.017745	0.048258	974	2
RBFOX1	6	0.017792	0.048353	975	2
YKT6	6	0.017794	0.048358	976	3
MED4	6	0.017898	0.048567	977	2
EMILIN2	6	0.017937	0.048649	978	2
DNAJC1	6	0.017995	0.048769	983	2
ZNF157	6	0.017995	0.048769	985	2
C10orf35	6	0.017995	0.048769	982	3
PPIE	6	0.017995	0.048769	980	1
ZFP2	6	0.017995	0.048769	979	1
FOXH1	6	0.017995	0.048769	981	2
LCN8	6	0.017995	0.048769	984	2
SELPLG	6	0.017995	0.048769	986	1
ZDHHC23	6	0.018032	0.048836	987	3
HMX1	6	0.018046	0.048863	988	3
SMURF2	6	0.018051	0.048876	989	2
FAM149A	6	0.018086	0.04895	990	3
CRNKL1	6	0.018197	0.049154	991	2
IL1R2	6	0.018217	0.04919	992	3
CHRM2	6	0.018246	0.049251	993	3
LZTFL1	6	0.018267	0.049294	994	2
SCAND1	6	0.018285	0.049326	995	2
hsa-mir-129-1	4	0.018287	0.049328	996	3
VMO1	6	0.0183	0.049361	997	3
CDADC1	6	0.018308	0.049372	998	3
VIP	6	0.018317	0.049389	999	1
MMP17	6	0.018348	0.049455	1000	2
FBXO34	6	0.018366	0.049492	1001	2
SMC5	6	0.018432	0.049619	1002	2
BTNL3	6	0.018436	0.049629	1003	3
ANKRD30A	6	0.01844	0.049634	1004	3
METTL21D	6	0.01844	0.049634	1005	1
hsa-mir-328	4	0.018471	0.049712	1006	3
hsa-mir-551b	4	0.018483	0.049736	1007	3
DNAJC9	6	0.018514	0.049795	1008	2
WDR5B	6	0.018523	0.049814	1009	2
DZIP3	6	0.018581	0.04995	1010	3
THRA	6	0.018613	0.05002	1011	2

7.4.3. Genes listed from the NCTC1&2 vs untreated comparison in the GeCKO positive screen.

Gene	# gRNA	score	p-value	rank	# good gRNA
SPRR2A	5	1.17E-05	5.95E-05	1	5
FCHSD2	6	2.51E-05	0.00013523	2	1
KLHL17	6	4.90E-05	0.0002488	3	5
NLRC4	6	6.98E-05	0.00035325	4	4
ATP5C1	6	7.31E-05	0.00036739	5	4
CNTFR	6	7.53E-05	0.00037788	6	2
SLC22A8	6	0.0001114	0.00056305	7	4
RASSF2	6	0.00011765	0.00059407	8	3
CHORDC1	6	0.00012556	0.00063421	9	1
RCL1	6	0.00014065	0.00070353	10	6
TRIM65	6	0.00014619	0.00073272	11	3
PPM1K	6	0.00014886	0.00074321	12	5
LOC100505841	6	0.00015525	0.00077514	13	3
CEPT1	6	0.00017043	0.0008545	14	4
C12orf29	6	0.00017578	0.00088552	15	4
HIPK3	6	0.0001831	0.00093113	16	4
ATP9B	6	0.00019911	0.0010233	17	5
XPNPEP2	6	0.00021776	0.0011136	18	6
TNFRSF25	6	0.00022599	0.0011523	19	3
LRSAM1	6	0.00024208	0.0012404	20	2
OR6K2	6	0.00024925	0.0012709	21	4
DNAJC12	6	0.00025565	0.0013006	22	5
POLR2B	6	0.00027535	0.001395	23	5
IQSEC3	6	0.00027621	0.0013986	24	3
CHN1	6	0.00027641	0.0014	25	4
KRTAP3-1	6	0.00028294	0.0014306	26	6
PRPSAP2	6	0.00031143	0.0015514	27	5
PRRT1	6	0.00031631	0.0015756	28	6
MAP2K3	6	0.00032642	0.0016185	29	2

TMPRSS13	6	0.00035908	0.0017758	30	4
hsa-mir-4700	4	0.00036047	0.0017827	31	4
TAS2R40	6	0.00037663	0.0018625	32	4
hsa-let-7g	4	0.00038501	0.0018962	33	1
NCSTN	6	0.00038519	0.0018967	34	3
KIAA1024L	6	0.00038566	0.0018994	35	4
hsa-mir-4433	4	0.00038979	0.0019163	36	4
GABRG1	6	0.00039195	0.0019277	37	5
hsa-mir-4437	4	0.00039765	0.001951	38	4
CH25H	6	0.00040316	0.0019779	39	4
TGFBR2	6	0.00041846	0.0020481	40	6
T	6	0.00042684	0.002096	41	3
PITPNC1	6	0.00043925	0.0021649	42	6
UFSP2	6	0.00044219	0.0021786	43	3
ADRA1D	6	0.00047362	0.0023286	44	5
C5orf49	6	0.00047705	0.0023487	45	3
ZNF331	6	0.00049235	0.0024164	46	5
SPATA31E1	6	0.0004931	0.002418	47	6
A4GALT	6	0.00049439	0.0024235	48	5
DNAJB2	6	0.00049625	0.002429	49	4
TLR7	6	0.00049774	0.0024367	50	2
SMIM14	6	0.00049939	0.0024456	51	6
ITFG3	6	0.00050917	0.0024924	52	6
ARID3C	6	0.00051204	0.002506	53	5
NMUR1	6	0.00051399	0.0025193	54	6
MMP16	6	0.00052012	0.0025535	55	5
PNMT	6	0.00052725	0.0025895	56	4
MBD1	6	0.00056872	0.0027897	57	6
FUCA1	6	0.00057357	0.002818	58	3
C20orf27	6	0.0005753	0.0028267	59	5
L3MBTL3	6	0.00057833	0.0028399	60	5
UPF3A	6	0.00057871	0.0028413	61	6
GJB6	6	0.00058468	0.0028657	62	6
ADAMTSL1	6	0.00059697	0.0029197	63	6
hsa-mir-383	4	0.00060011	0.0029334	64	4
AP3D1	6	0.00061994	0.0030264	65	5
FREM3	6	0.00062766	0.0030524	66	2
NLK	6	0.00063382	0.0030798	67	4
LY75	6	0.00065722	0.0031906	68	6
C15orf61	6	0.00066816	0.003239	69	3
AGTPBP1	6	0.00067342	0.0032636	70	5
AWAT1	6	0.00067386	0.0032641	71	4
SSH2	6	0.00067785	0.0032837	72	3
PPP1R13B	6	0.00071028	0.0034237	73	5
SUPT20HL1	6	0.00072015	0.0034652	74	3
MPG	6	0.00072805	0.0034985	75	1
DLG4	6	0.00073894	0.0035441	76	6
TMED3	6	0.00075645	0.0036244	77	3
PKN2	6	0.0007582	0.0036317	78	2
GPR173	6	0.00075894	0.0036344	79	6
TP53AIP1	6	0.00075932	0.0036353	80	6
UBE2U	6	0.00077524	0.0037037	81	6
ITGB1	6	0.00077824	0.0037188	82	2
KCNK2	6	0.00077936	0.0037215	83	6
OR10G7	6	0.00079415	0.0037904	84	4
ZNF682	6	0.00079721	0.0038014	85	3
OR13C2	6	0.00080605	0.0038255	86	6
NKX3-2	6	0.00081662	0.0038757	87	3
LOC643802	6	0.00081995	0.0038912	88	6
DNAJB4	6	0.00082434	0.0039108	89	4
RBMY1A1	6	0.00082495	0.0039145	90	6
KLHL41	6	0.00082844	0.0039313	91	4
ZFR2	6	0.00085752	0.0040682	92	3
hsa-mir-148a	3	0.00085935	0.0040805	93	3
hsa-mir-486-2	1	0.00087476	0.0041544	94	1
CAMK1D	6	0.00087999	0.0041731	95	3
ARL6IP6	6	0.00088065	0.004174	96	5
PIH1D2	6	0.00090265	0.0042752	97	6
HSPA4	6	0.00091073	0.0043053	98	4
MAGEA3	6	0.0009132	0.0043136	99	5
ANKRD30B	6	0.00092541	0.0043747	100	4
CYP2E1	6	0.00092881	0.0043847	101	2
PIK3R1	6	0.00093147	0.0044002	102	4
FLT3LG	6	0.00093157	0.0044002	103	4
OR7A5	6	0.00093938	0.0044362	104	4
KRTAP21-2	6	0.00094003	0.0044394	105	6
TLN2	6	0.00094374	0.0044604	106	5
WRAP73	6	0.00094653	0.0044714	107	6
LRP2BP	6	0.00094814	0.0044759	108	3
SLC35E3	6	0.000979	0.0046077	109	1
ZNF727	6	0.001019	0.0047874	110	5
PDCL	6	0.0010292	0.004834	111	3
SEC31B	6	0.0010335	0.0048536	112	4
MAGED4	6	0.0010414	0.0048878	113	5

FAM167A	6	0.0010751	0.0050187	114	5
DNAH6	6	0.0010761	0.005021	115	4
NDUFB5	6	0.0010794	0.0050337	116	4
TPM2	6	0.0011091	0.0051423	117	5
TYR	6	0.0011145	0.0051642	118	5
MALSU1	6	0.0011295	0.0052212	119	1
APLNR	6	0.0011338	0.0052399	120	4
HIST1H4G	6	0.0011399	0.00526	121	5
ENO3	6	0.0011656	0.0053564	122	4
hsa-mir-759	4	0.0011666	0.005363	123	2
PROB1	6	0.0011711	0.0053826	124	5
STK32A	6	0.0011797	0.0054146	125	4
ARHGAP28	6	0.0011978	0.0054853	126	3
PRPH2	6	0.0012299	0.0056011	127	2
SLC17A9	6	0.0012447	0.0056549	129	5
DBX2	6	0.0012447	0.0056549	128	3
PLXNC1	6	0.0012801	0.0057868	130	2
OSTF1	6	0.0013201	0.0059519	131	4
ZNF648	6	0.0013226	0.0059592	132	5
REN	6	0.0013302	0.0059829	133	2
LRRIQ4	6	0.0013328	0.005992	134	4
SAP30	6	0.0013398	0.006018	135	5
ARL8B	6	0.0013535	0.0060709	136	5
E2F3	6	0.0013559	0.0060787	137	2
BOLL	6	0.0013804	0.0061667	138	2
VPS39	6	0.0013805	0.0061667	139	4
CNTN6	6	0.0013944	0.0062146	140	4
OR51G2	6	0.0014017	0.0062406	141	3
hsa-mir-3713	4	0.0014121	0.0062803	142	4
MCMDC2	6	0.0014202	0.0063049	143	5
CHMP6	6	0.0014306	0.0063405	144	3
FITM1	6	0.0014453	0.0063961	145	4
CPNE2	6	0.0014752	0.0065156	146	4
ALG11	6	0.0014807	0.0065393	147	3
CLPX	6	0.0015113	0.0066579	148	3
PNMA3	6	0.0015244	0.0067035	149	5
TTC1	6	0.0015309	0.0067263	150	3
TRPC1	6	0.0015552	0.0068157	151	4
C7orf31	6	0.0015699	0.00687	152	4
CHCHD10	6	0.0015811	0.0069138	153	1
MAPK7	6	0.0016236	0.007073	154	3
MT3	6	0.0016312	0.0071053	155	1
hsa-mir-6831	4	0.0016326	0.0071117	156	3
WWC3	6	0.0016403	0.0071441	157	4
FAM81B	6	0.0016565	0.0072039	158	4
MFSD5	6	0.0016634	0.0072253	159	4
MLXIP	6	0.0016648	0.0072294	160	4
ADRA1B	6	0.0016692	0.0072385	161	4
SLAMF8	6	0.0016814	0.0072814	162	2
PTPRJ	6	0.0016938	0.0073288	163	4
NACAD	6	0.0017033	0.0073626	164	4
BBS4	6	0.0017299	0.0074606	165	4
THSD1	6	0.0017308	0.0074647	166	3
CST7	6	0.0017315	0.0074675	167	3
ZIM3	6	0.0017619	0.0075774	168	5
C6orf10	6	0.0017756	0.0076335	169	5
CGA	6	0.0017759	0.0076349	170	4
DYSF	6	0.0017817	0.0076572	171	3
DTWD1	6	0.0017826	0.0076609	172	4
CSF1	6	0.0018178	0.0078036	173	5
IQCG	6	0.0018235	0.0078314	174	4
C9orf153	6	0.0018318	0.0078593	175	3
MINPP1	6	0.0018381	0.0078821	176	4
CASP12	6	0.0018681	0.0079883	177	5
CD180	6	0.001875	0.0080148	178	5
DYX1C1	6	0.001882	0.0080417	179	2
RERGL	6	0.001889	0.0080663	180	3
WDR11	6	0.0018921	0.00808	181	5
WDR45B	6	0.0019152	0.0081699	182	4
PRTN3	6	0.0019321	0.0082355	183	1
PLCB2	6	0.0019394	0.0082638	184	3
hsa-mir-532	4	0.0019615	0.0083423	185	4
CD93	6	0.0019635	0.0083496	186	4
POU3F4	6	0.0019788	0.0084152	187	4
ACPL2	6	0.0019823	0.0084308	188	2
VN1R5	6	0.0019904	0.0084609	189	3
RBM48	6	0.0019945	0.0084777	190	5
AIPL1	6	0.0019952	0.0084796	191	4
hsa-mir-5190	4	0.0020224	0.0085804	192	4
KCNN2	6	0.0020324	0.0086127	193	2
FXYD6	6	0.0020347	0.0086237	194	4
NonTargetingControlGuideForHuman_0700	1	0.0020383	0.0086374	195	1
CD81	6	0.0020521	0.0086871	196	4
GCKR	6	0.002082	0.0087947	197	5

GPR17	6	0.0020826	0.0087979	198	2
ANKRD10	6	0.0021087	0.0088937	199	5
SCN1B	6	0.0021263	0.0089548	200	2
GPRASP1	6	0.0021327	0.0089758	201	4
MAN2A2	6	0.0021474	0.0090365	202	5
PSD2	6	0.0021524	0.0090579	203	4
hsa-mir-4305	4	0.002158	0.009083	204	1
KCNK10	6	0.0022078	0.0092636	205	4
TMEM19	6	0.002221	0.0093087	206	4
KIAA0754	6	0.0022234	0.0093188	207	5
hsa-mir-634	4	0.0022248	0.0093243	208	3
RARRES3	6	0.002233	0.0093544	209	3
KIAA1598	6	0.0022392	0.0093804	210	5
ARMC6	6	0.0022514	0.0094173	211	5
MET	6	0.0022519	0.0094196	212	4
CCDC172	6	0.0022525	0.0094228	213	3
RLF	6	0.0022555	0.0094351	214	2
MAOA	6	0.0022627	0.0094615	215	4
ZNF385D	6	0.0022791	0.009524	216	4
PRR16	6	0.0023064	0.0096166	217	3
PDE2A	6	0.0023219	0.0096727	218	3
DMRTA1	6	0.0023332	0.0097147	219	1
SV2C	6	0.002353	0.0097867	220	3
PILRA	6	0.0023642	0.0098241	221	3
LRRC3B	6	0.002381	0.0098939	222	3
B3GNT3	6	0.0023833	0.0098989	223	2
WDR47	6	0.0024227	0.010042	224	3
DTD1	6	0.0024335	0.010085	225	3
FAM162A	6	0.0024523	0.010154	226	4
CROCC	6	0.0024638	0.010197	227	5
SP110	6	0.0024673	0.010211	228	4
RNF14	6	0.0024786	0.010257	229	4
TRIM8	6	0.0024836	0.010275	230	3
OR4D1	6	0.0024839	0.010276	231	4
AQP8	6	0.0024884	0.010287	232	5
hsa-mir-27b	4	0.0024922	0.010298	233	2
SCAP	6	0.0024925	0.010298	234	4
GRIK1	6	0.0024993	0.010324	235	5
FAM32A	6	0.0025337	0.01045	236	4
TSKS	6	0.0025461	0.010499	237	3
CPA4	6	0.0025469	0.010501	238	2
GABRA2	6	0.0025692	0.010588	239	5
OSTM1	6	0.0025754	0.01061	240	2
NDUFB4	6	0.0025838	0.010637	241	1
MRVI1	6	0.0026169	0.010731	242	3
PRRG4	6	0.0026302	0.010776	243	4
MUC7	6	0.0026339	0.010789	244	1
COX19	6	0.0026425	0.010821	245	3
SSPO	6	0.0026483	0.010839	246	5
ARHGAP10	4	0.0026575	0.01087	247	4
ZNF280C	6	0.0026614	0.010883	248	4
C6orf141	6	0.0026816	0.010953	249	4
LEMD1	6	0.0026841	0.01096	250	3
MUC20	6	0.0027137	0.011076	251	3
CNPY2	6	0.0027342	0.011155	252	3
HYAL2	6	0.0027365	0.011166	253	2
SH2B2	6	0.0027591	0.011241	254	5
hsa-mir-938	4	0.0027719	0.01129	255	3
NRROS	4	0.0027787	0.011313	256	4
COL11A1	6	0.0027843	0.011337	257	2
LINGO3	6	0.0027902	0.011357	258	5
FAM222B	6	0.0028255	0.01149	259	3
CAPN13	6	0.0028276	0.011502	260	5
LRFN1	6	0.0028318	0.011519	261	4
HAPLN3	6	0.0028344	0.011531	262	2
SAMD15	6	0.0028552	0.011612	263	4
THAP5	6	0.0028757	0.011685	264	4
GIMAP8	6	0.0028845	0.011719	265	4
NonTargetingControlGuideForHuman_0492	1	0.0028922	0.011744	266	1
GIGYF2	6	0.0029346	0.011907	267	2
GBP1	6	0.002936	0.011913	268	3
ZCRB1	6	0.00297	0.01204	269	4
hsa-mir-148b	4	0.0029771	0.012071	270	4
CCDC64B	6	0.0029847	0.012095	271	2
hsa-mir-3927	4	0.0029951	0.012136	272	3
hsa-mir-3187	4	0.0030022	0.01216	273	3
C3orf58	6	0.0030296	0.012258	274	4
PEX6	6	0.0030348	0.012271	275	3
hsa-mir-3126	4	0.0030425	0.012297	276	4
TRIM43B	6	0.0030452	0.012307	277	4
TEX15	6	0.0030535	0.012333	278	5
TACC1	6	0.0030849	0.012448	279	1
PLEKHM2	6	0.0030866	0.012455	280	3
CDH18	6	0.0030951	0.012488	281	5

TNFSF15	6	0.0031324	0.012621	282	5
SCAF11	6	0.0031551	0.012708	283	4
hsa-mir-598	4	0.0031568	0.012712	284	4
hsa-mir-567	4	0.003177	0.012785	285	4
SLC36A1	6	0.0031808	0.012801	286	2
PADI6	6	0.0031851	0.012812	287	3
OR56A5	6	0.0032064	0.012891	288	5
ERICH1	6	0.0032221	0.012955	289	5
UCK2	6	0.0032337	0.012997	290	5
TMEM171	6	0.0032551	0.013077	291	4
SLC2A13	6	0.0032585	0.013088	292	2
PROZ	6	0.003276	0.013145	293	4
ZADH2	6	0.0032853	0.013184	294	2
IYD	6	0.0032994	0.013233	295	5
FAIM	6	0.0033003	0.013236	296	4
TTI1	6	0.0033156	0.013301	297	3
ADAMTS9	6	0.0033377	0.01339	298	5
hsa-mir-4708	4	0.0033609	0.013473	299	2
TMEM211	6	0.0033821	0.013538	300	5
KANK4	6	0.0033854	0.013549	301	3
ARL2BP	6	0.0034343	0.013717	302	3
KRIT1	6	0.0034355	0.013722	303	2
ZBP1	6	0.0034389	0.013736	304	5
hsa-mir-1185-1	4	0.0034454	0.013756	305	4
C12orf42	6	0.0034699	0.013841	306	5
C17orf78	6	0.0034727	0.013847	307	4
BROX	6	0.0034856	0.013889	308	3
DPP10	6	0.0035269	0.014051	309	4
KLHL36	6	0.0035354	0.014077	310	4
PVRIG	6	0.0035357	0.014077	311	4
ZNF519	6	0.0035488	0.01413	312	2
FAM26D	6	0.0035858	0.014248	313	4
ZNF226	6	0.0035939	0.01428	314	5
OR2J3	6	0.0035945	0.014283	315	4
CSF2RB	6	0.0036274	0.014386	316	4
AMZ2	6	0.0036305	0.014396	317	5
MYB	6	0.0036358	0.014416	318	4
GDF5	6	0.0036521	0.014479	319	5
EMD	6	0.0036776	0.014573	320	3
OR4F15	6	0.0036814	0.014587	321	4
CDHR2	6	0.0036859	0.014597	322	3
KCNJ5	6	0.0037007	0.014646	323	5
ALK	6	0.0037034	0.014654	324	4
CLK4	6	0.0037103	0.014678	325	3
KIAA1244	6	0.0037263	0.014737	326	4
IFT57	6	0.003786	0.014942	327	3
ZNF79	6	0.0037936	0.014968	328	5
hsa-mir-4461	4	0.0037951	0.014975	329	4
SLC29A2	6	0.0038361	0.01513	330	3
ZFAND6	6	0.0038412	0.015146	331	4
TRIM38	6	0.0038862	0.015309	332	2
CENPO	6	0.0038915	0.015331	333	5
ERV3-1	6	0.0038973	0.015344	334	3
DCAF11	6	0.0038992	0.015353	335	4
hsa-mir-3198-2	4	0.0039057	0.015375	336	2
ZKSCAN7	6	0.0039362	0.015488	337	4
FAM150A	6	0.003961	0.01557	338	3
ARHGAP5	6	0.0039687	0.015596	339	4
RUNDC3B	6	0.0039863	0.015659	340	3
LRRC17	6	0.003994	0.015686	341	5
SLC17A3	6	0.0040064	0.015731	342	5
hsa-mir-583	4	0.0040105	0.015747	343	4
GABRA3	6	0.0040123	0.015752	344	5
UGGT1	6	0.004017	0.015771	345	4
DHX35	6	0.0040364	0.015841	346	4
SLMO1	6	0.004038	0.015849	347	5
GIPC2	6	0.0040576	0.015915	348	3
ACTC1	6	0.0040705	0.01597	349	5
ANKRD18A	6	0.0040864	0.016041	350	3
PADI1	6	0.0041045	0.01611	351	5
SLC38A10	6	0.0041365	0.016232	352	2
C1orf27	6	0.0041419	0.016251	353	4
FBXO18	6	0.0041531	0.01629	354	3
AMT	6	0.0041616	0.016324	355	4
TMEM52	6	0.0041865	0.016411	356	1
SCIMP	6	0.0041902	0.016418	357	5
C3orf55	6	0.0041936	0.01643	358	5
UGT8	6	0.0042044	0.016472	359	3
ARL4A	6	0.004206	0.016477	360	3
RAB3D	6	0.0042087	0.016491	361	4
FOXC2	6	0.0042254	0.016556	362	4
C19orf52	6	0.0042366	0.016594	363	2
OR52H1	6	0.0042383	0.016599	364	4
RAG2	6	0.0042866	0.016773	365	3

C8orf31	6	0.0042936	0.016799	366	3
FUBP1	5	0.0043245	0.016907	367	3
HIST1H1T	6	0.0043302	0.016927	368	3
CNGA3	6	0.0043344	0.016941	369	4
DDX51	6	0.0043367	0.016946	370	2
GAL3ST4	6	0.0043587	0.017024	371	4
SLC39A11	6	0.0043751	0.017088	372	2
hsa-mir-8084	4	0.0043789	0.0171	373	2
CNPY1	6	0.0043851	0.017121	374	5
PLTP	6	0.0043867	0.017128	375	1
RNASEH2B	6	0.0043915	0.017144	376	4
BCL9	6	0.0043938	0.017152	377	4
HDX	6	0.0043978	0.017169	378	4
C1orf35	6	0.0044367	0.017303	380	3
OVOL2	6	0.0044367	0.017303	379	3
KCNA1	6	0.004442	0.017324	381	3
ARHGEF38	6	0.0044478	0.017351	382	4
RNF111	6	0.0044868	0.017487	383	2
CRYM	6	0.004487	0.017488	384	5
BCL2A1	6	0.0044904	0.017498	385	3
FOCAD	6	0.0044906	0.017501	386	5
C4orf47	6	0.0044978	0.017519	387	5
MNAT1	6	0.0045225	0.017612	388	4
DDX46	6	0.0045368	0.017656	389	2
hsa-mir-182	4	0.0045411	0.017673	390	3
ELAC1	6	0.0045485	0.017699	391	4
KRTAP26-1	6	0.0045548	0.017721	392	5
COX10	6	0.0045699	0.017771	393	4
DCDC2	6	0.004575	0.01779	394	4
DRD4	6	0.0045869	0.017831	395	3
EVL	6	0.0045941	0.017861	396	5
LRFN5	6	0.0045945	0.017863	397	3
hsa-mir-193a	4	0.0045981	0.017876	398	3
CPEB4	6	0.0046029	0.01789	399	4
OR52E8	6	0.0046124	0.017916	400	4
ZNF597	6	0.0046193	0.01794	401	3
GALNT11	6	0.0046365	0.018001	402	3
CELF3	6	0.0046369	0.018002	403	1
GSK3B	6	0.0046433	0.018022	404	5
PSMG4	6	0.0046869	0.018156	405	1
GIMAP1-GIMAP5	5	0.0046927	0.018181	406	4
YRDC	6	0.0047082	0.018236	407	3
C5AR2	6	0.0047225	0.018278	408	4
hsa-mir-595	4	0.0047251	0.018288	409	2
NAPSA	6	0.0047369	0.018328	410	2
PELI2	6	0.0047869	0.018495	411	3
ARHGAP29	6	0.004787	0.018496	412	2
CXorf23	6	0.004812	0.018583	413	5
SGK196	4	0.004823	0.01862	414	4
FAM169B	6	0.004837	0.018667	415	2
NDUFA8	6	0.0048377	0.018672	416	5
hsa-mir-16-2	4	0.004842	0.018682	417	4
RTP1	6	0.0048698	0.018788	418	5
ITGB4	6	0.0048705	0.01879	419	3
ZNF845	6	0.004887	0.018846	420	4
hsa-let-7a-2	4	0.0048964	0.018877	421	2
TNFSF9	6	0.0049138	0.018928	422	3
KRTAP4-7	6	0.0049213	0.01896	423	5
FRMD6	6	0.004931	0.018994	424	3
GTF2IRD1	6	0.004937	0.019017	425	1
ART1	6	0.0049526	0.019071	426	3
SHMT1	6	0.004957	0.019085	427	2
NSUN7	6	0.0049871	0.019183	428	2
ZNF182	6	0.0049961	0.019215	429	3
RETSAT	6	0.0049963	0.019217	430	5
hsa-mir-6857	4	0.0049964	0.019217	431	2
ZNF701	5	0.0049967	0.019218	432	2
ITPRIPL1	6	0.0050049	0.019244	433	5
ESYT3	6	0.0050065	0.019249	434	5
GAB4	6	0.0050211	0.019299	435	3
hsa-mir-5004	4	0.0050279	0.019317	436	2
TPTE2	6	0.0050464	0.019385	437	4
KRTAP22-2	6	0.005068	0.019467	438	5
FAM151B	6	0.0050704	0.019477	439	2
ARRDC3	6	0.0050708	0.019477	440	5
PIK3C3	6	0.0050792	0.019509	441	2
PRICKLE3	6	0.0050836	0.019522	442	2
ROGDI	6	0.0050871	0.019533	443	4
CDH9	6	0.0051059	0.019606	444	4
NHLH2	6	0.0051286	0.019692	445	5
ZFP3	6	0.0051453	0.019761	446	3
TAF4B	6	0.0051674	0.019847	447	3
VPS9D1	6	0.0051693	0.019855	448	4
KRTAP16-1	6	0.0051727	0.019866	449	4

OR10J5	6	0.005205	0.019981	450	4
SPOCK1	6	0.005234	0.020078	451	3
UNC5CL	6	0.0052608	0.020176	452	2
S100A10	6	0.0053189	0.020381	453	5
TSPAN2	6	0.0053371	0.020443	454	2
C17orf112	6	0.005355	0.020503	455	2
GPCPD1	6	0.0053612	0.020526	456	4
C1orf43	6	0.005383	0.020609	457	5
KCTD15	6	0.0053871	0.020627	458	3
ANAPC16	6	0.005391	0.020644	459	3
PKP4	6	0.0054192	0.020737	460	4
SC5D	6	0.0054272	0.020766	461	4
ZNF549	6	0.0054371	0.020803	462	2
VSIG10	6	0.0054454	0.020838	463	3
SPC25	6	0.0054461	0.020839	464	3
TMEM177	6	0.0054537	0.020865	465	3
TRIM71	6	0.0054871	0.020987	466	4
HIST1H4H	6	0.0054993	0.02104	467	4
PARS2	6	0.0055045	0.021052	468	3
ZNF354C	6	0.0055091	0.021069	469	3
SLC6A20	6	0.0055136	0.021083	470	2
GNAQ	6	0.0055145	0.021085	471	4
hsa-mir-378j	4	0.0055301	0.021134	472	2
RECQL5	6	0.0055371	0.021164	473	2
UNCX	6	0.0055586	0.021234	474	3
MRPL47	6	0.0055778	0.021302	475	4
HAUS2	6	0.0055909	0.021345	476	4
C10orf35	6	0.0056121	0.021423	477	5
KAT6B	6	0.0056154	0.021433	478	5
BAX	6	0.0056512	0.021565	479	3
SLC4A4	6	0.0056621	0.021601	480	5
FLNA	6	0.0056668	0.021611	481	5
TSPY1	6	0.0056831	0.021669	482	5
LTBP2	6	0.0056871	0.021682	483	3
ZNF841	6	0.0057233	0.021807	484	3
TOP1	6	0.0057371	0.02186	485	2
CALU	6	0.0057628	0.021961	486	5
WAS	6	0.005786	0.022044	487	4
RBM6	6	0.0058274	0.022204	488	5
GJB2	6	0.005837	0.022236	489	1
FUT1	6	0.0058611	0.022315	490	2
C10orf91	6	0.0058846	0.022405	491	2
PCDH12	6	0.005887	0.022412	492	3
DHX32	6	0.005887	0.022412	493	2
GRIA3	6	0.0059352	0.022579	494	5
TBX19	6	0.005937	0.022586	495	2
HIST1H2BH	6	0.0059647	0.022666	496	5
ZNF557	6	0.005987	0.022745	497	2
RAB3C	6	0.0059991	0.022788	498	4
ENAM	6	0.0060266	0.02288	499	4
FAM151A	6	0.0060302	0.022893	500	5
MED29	6	0.0060365	0.02291	501	5
WDR96	6	0.0060369	0.022912	502	1
C16orf74	6	0.0060695	0.023014	503	4
IRG1	6	0.0060862	0.02307	504	5
IFNL4	6	0.0060869	0.023073	505	4
ATF2	6	0.0061125	0.023161	506	4
ATP6V1D	6	0.0061272	0.023214	507	5
TBX5	6	0.0061369	0.023244	508	1
SELM	6	0.0061847	0.023411	509	2
LZTFL1	6	0.0061869	0.023419	510	2
OR2M7	6	0.0061899	0.023427	511	4
LRRN3	6	0.0062051	0.023472	512	5
GSDMC	6	0.0062178	0.023523	513	4
MTMR2	6	0.0062281	0.023564	514	4
C20orf196	6	0.0062368	0.023601	515	2
IPMK	6	0.0062427	0.023625	516	2
SULF1	6	0.006243	0.023626	517	5
LRGUK	6	0.0062475	0.023646	518	2
EMR1	6	0.0062499	0.023656	519	3
IL11RA	6	0.006255	0.023669	520	5
CYP3A7-CYP3AP1	2	0.0062767	0.023741	521	1
PHOX2A	6	0.0062779	0.023745	522	4
FUT4	6	0.0062868	0.023775	523	1
MMAA	6	0.0062975	0.023815	524	4
CRB1	6	0.006335	0.023945	525	3
PRPF18	6	0.0063367	0.023949	526	1
ACCSL	6	0.0063496	0.023987	527	3
LILRB3	6	0.0063662	0.024045	528	3
PRDM11	6	0.0063802	0.024088	529	5
PPID	6	0.0063867	0.024108	530	2
CCNG1	6	0.0063868	0.024108	531	5
TPBG	6	0.0063887	0.024114	532	3
hsa-mir-4701	4	0.0064181	0.024213	533	4

ASB10	6	0.0064207	0.024225	534	3
GDE1	6	0.0064354	0.024277	535	4
TESK2	6	0.0064623	0.024369	536	4
COLCA2	6	0.0064653	0.02438	537	5
ATHL1	6	0.0064729	0.024409	538	5
MUM1L1	6	0.0064901	0.024469	539	5
CASKIN2	6	0.006492	0.024471	540	5
TNFSF4	6	0.0064946	0.02448	541	4
QRFPR	6	0.0065136	0.02455	542	3
PSMB6	6	0.0065366	0.024625	543	3
KRTAP4-3	6	0.0065581	0.024705	544	5
PAGE1	6	0.0065759	0.024763	545	4
MMP17	6	0.0065809	0.02478	546	3
NFE2L3	6	0.0065865	0.024801	547	1
POU4F2	6	0.0066703	0.025065	548	5
KPNA2	6	0.0066864	0.025118	549	1
C1orf105	6	0.0066897	0.02513	550	4
EMC8	6	0.0067084	0.025196	551	5
hsa-mir-4535	4	0.0067154	0.025219	552	4
ABCC4	6	0.0067339	0.02529	553	5
RCAN1	6	0.0067364	0.025298	554	2
TCEA3	6	0.0067398	0.025309	555	5
hsa-mir-6090	4	0.0067632	0.025384	556	1
ZNF426	6	0.0067732	0.025413	557	3
RPS6KA2	6	0.0067863	0.025453	558	3
UEVLD	6	0.0068153	0.025534	559	5
DNAJC9	6	0.0068362	0.025617	560	2
IST1	6	0.0068364	0.025617	561	3
NANOG	6	0.0068544	0.02568	562	5
ZEB1	6	0.0068564	0.025687	563	2
OR2L5	6	0.0068833	0.025794	564	5
MAS1	6	0.0068862	0.025805	565	4
MCTS1	6	0.0068969	0.025841	566	3
PSG11	6	0.0069213	0.025929	567	5
SLC6A7	6	0.0069218	0.025931	568	4
MAGEB3	6	0.0069313	0.02596	569	5
CDH6	6	0.0069361	0.025982	570	3
METTL21A	6	0.0069417	0.026002	571	4
LOC286238	6	0.0069549	0.026045	572	3
SFMBT2	6	0.0069645	0.026078	573	5
GALC	6	0.0069681	0.026094	574	4
WISP2	6	0.006986	0.026158	575	2
ZC4H2	6	0.0070192	0.026275	576	3
SPINK6	6	0.0070302	0.026313	577	5
IMPA1	6	0.007036	0.026334	578	3
hsa-mir-4439	4	0.0070531	0.026397	579	4
BPIFA3	6	0.0070535	0.026398	580	5
hsa-mir-103a-2	4	0.0070604	0.026422	581	4
EDEM2	6	0.0070653	0.026436	582	2
IL6	6	0.0070859	0.026506	583	1
GORASP2	6	0.0071147	0.026599	584	4
TSHR	6	0.0071273	0.026646	585	4
DOPEY2	6	0.0071358	0.026675	586	4
PCDHB6	6	0.0071526	0.026732	587	4
CD83	6	0.0071548	0.026738	588	5
GLIS3	6	0.007165	0.026777	589	5
hsa-mir-2113	4	0.0071712	0.026795	590	4
KY	6	0.0071786	0.026825	591	2
FLNC	6	0.0071847	0.026842	592	3
ATPAF1	6	0.0071858	0.026847	593	4
CEP350	6	0.0071892	0.026854	594	3
NCKAP1	6	0.0071941	0.02687	595	3
hsa-mir-4255	4	0.0071945	0.026871	596	3
DGKA	6	0.0072044	0.026908	597	3
SLC25A32	6	0.0072208	0.026963	598	5
NEURL4	6	0.0072357	0.027016	599	3
METTL18	6	0.0072405	0.027034	600	5
TRIO	6	0.0072856	0.02719	601	2
DEFB127	6	0.0073127	0.027285	602	4
ZBTB32	6	0.0073188	0.027303	603	4
CSPP1	6	0.0073301	0.027339	604	5
AGGF1	6	0.0073564	0.027431	605	5
UGP2	6	0.0073762	0.027494	606	4
LMBR1L	6	0.0073854	0.027524	607	2
BMF	6	0.0073858	0.027525	608	4
AP1B1	6	0.007392	0.027544	609	2
hsa-mir-8065	4	0.007394	0.027552	610	4
FCER1A	6	0.0074016	0.027575	611	5
RHBDF2	6	0.0074089	0.027593	612	4
HEXIM2	6	0.0074354	0.027697	613	3
ADH6	6	0.0074444	0.02773	614	2
ENTPD8	6	0.007445	0.027735	615	4
KLHL25	6	0.007474	0.027833	616	4
hsa-mir-331	4	0.0074788	0.027847	617	4

hsa-mir-95	4	0.0074925	0.02789	618	3
hsa-mir-4474	4	0.0075239	0.028012	619	3
BZRAP1	6	0.0075352	0.028052	620	2
GFRA3	6	0.0075851	0.028217	621	1
SOX12	6	0.0076345	0.028374	622	5
SPATA25	6	0.007635	0.028376	623	2
IL1RAP	6	0.0076668	0.028481	624	3
C1orf174	6	0.0076669	0.028481	625	5
CD276	6	0.0076734	0.028504	626	5
CCBL2	6	0.0076849	0.028538	627	3
hsa-mir-4509-1	4	0.0076949	0.028571	628	4
DENND4A	6	0.0077095	0.028625	629	3
AFAP1L1	6	0.0077255	0.02868	630	4
HTR1E	6	0.0077311	0.028694	631	4
PKD2L2	6	0.0077348	0.028712	632	4
PSMB10	6	0.0077469	0.02875	633	2
MSGN1	6	0.0077594	0.028796	634	4
ZNF583	6	0.0077847	0.02887	635	3
RASSF5	6	0.0078034	0.028936	636	5
CDRT15L2	6	0.0078129	0.028966	637	4
DUSP3	6	0.0078328	0.029032	638	2
hsa-mir-4802	4	0.0078584	0.029117	639	4
RAB2B	6	0.0078817	0.029199	640	5
KCNC4	6	0.0078845	0.02921	641	3
C17orf105	6	0.0078853	0.029212	642	3
hsa-mir-128-1	4	0.0079227	0.029354	643	4
CDT1	6	0.0079344	0.029394	644	1
MFHAS1	6	0.0079379	0.029404	645	3
MS4A1	6	0.0079423	0.029415	646	4
NonTargetingControlGuideForHuman_0221	1	0.0079482	0.029439	647	1
TMF1	6	0.0079696	0.029508	648	5
SPATA17	6	0.0079836	0.029556	649	4
CD163L1	6	0.0079841	0.029557	650	5
IQGAP3	6	0.0079843	0.029558	651	2
DBF4B	6	0.0080342	0.02972	652	1
CAAP1	6	0.0080436	0.029749	653	5
ESF1	6	0.0080605	0.029811	654	3
ICK	6	0.0080608	0.029811	655	4
RFFL	6	0.0080841	0.029879	656	1
HS3ST3A1	5	0.0080911	0.029896	657	3
hsa-mir-4540	4	0.0080911	0.029896	658	4
TSPAN1	6	0.0081101	0.02995	659	4
USP3	6	0.0081272	0.030002	660	5
C6orf25	6	0.008134	0.030022	661	2
OAZ3	6	0.008136	0.030031	662	3
HMGN5	6	0.0081425	0.030048	663	3
RSPRY1	6	0.0081726	0.030165	664	3
hsa-mir-6833	4	0.0081751	0.030172	665	3
hsa-mir-4490	4	0.0081809	0.030184	666	4
PCBP1	6	0.0082029	0.030253	667	2
SPTBN4	6	0.0082091	0.030276	668	5
EPOR	6	0.0082337	0.030357	669	1
USE1	6	0.0082389	0.03037	670	5
PREP	6	0.008243	0.030382	671	4
SYN3	6	0.0082509	0.03041	672	3
AGTRAP	6	0.0082584	0.030431	673	5
hsa-mir-1976	4	0.0082779	0.030501	674	3
GALNT6	6	0.0082866	0.030531	675	4
AGBL4	6	0.0083054	0.03059	676	5
MAMLD1	6	0.0083229	0.030647	677	5
CNNM1	6	0.0083322	0.030681	678	4
SHROOM1	6	0.0083335	0.030687	679	3
ABI1	6	0.0083633	0.030779	680	4
PLAU	5	0.0083637	0.03078	681	2
LYZL6	6	0.0083817	0.030837	682	4
SHROOM4	6	0.0083834	0.03084	683	2
RET	6	0.008409	0.030926	684	3
SLC1A6	6	0.0084114	0.030936	685	5
MS4A6A	6	0.008425	0.030984	686	5
DNAJC1	6	0.0084332	0.031013	687	2
JMJD8	6	0.0084513	0.031083	688	3
OR8B8	6	0.0084831	0.031188	689	4
METTL10	6	0.008533	0.03137	690	1
TBC1D8	6	0.0085357	0.031382	691	4
RHOJ	6	0.008541	0.031401	692	5
WWC1	6	0.0085828	0.031541	693	2
SNTA1	6	0.0085948	0.031579	694	4
FAM149B1	6	0.0086034	0.031605	695	3
TACC3	6	0.0086041	0.031606	696	3
hsa-mir-18b	4	0.0086427	0.031736	697	3
IGLL1	6	0.0086511	0.031768	698	5
MAPKBP1	6	0.0086595	0.031801	699	5
ZNF700	6	0.0086597	0.031802	700	4
TNFRSF4	6	0.0086826	0.031878	701	3

hsa-mir-1289-2	4	0.008694	0.031915	702	1
KRTAP19-7	6	0.0087275	0.032027	703	3
OGN	6	0.0087324	0.032043	704	2
GBP2	6	0.0087624	0.032154	705	4
ILDR1	6	0.0087823	0.032223	706	2
hsa-mir-4515	4	0.0088012	0.032281	707	3
GPR19	6	0.0088148	0.032325	708	4
ACOX3	6	0.0088297	0.03238	709	3
ACTR1B	6	0.0088321	0.032387	710	2
SMIM20	6	0.0088383	0.032412	711	5
ZNF207	6	0.0088468	0.032438	712	3
FEM1A	6	0.0088525	0.032459	713	2
N4BP1	6	0.0088634	0.032494	714	4
NRSN2	6	0.0089318	0.032715	715	2
DAZ1	6	0.0089367	0.032727	716	5
C19orf33	6	0.0089407	0.032742	717	3
SORBS2	6	0.0089537	0.032783	718	4
NDUFAF6	6	0.0089665	0.03282	719	3
MSTN	6	0.008977	0.032851	720	5
NKAIN1	6	0.0089817	0.03287	721	2
GINM1	6	0.0089856	0.032884	722	5
ORC3	6	0.008995	0.032914	723	4
hsa-mir-1269a	4	0.0090056	0.032949	724	4
SLC40A1	6	0.009007	0.032953	725	3
TPMT	6	0.0090235	0.033014	726	3
PNLIPRP2	6	0.0090315	0.033039	727	3
ZNF514	6	0.0090447	0.033086	728	4
TMEM178A	6	0.0090472	0.033092	729	2
TXNDC9	6	0.0090613	0.033141	730	4
CCDC138	6	0.0090677	0.033167	731	3
RHOXF1	6	0.0090807	0.033203	732	4
POLE	6	0.0090876	0.033221	733	2
hsa-mir-4804	4	0.0090931	0.03324	734	3
GML	6	0.0091251	0.033357	735	3
CD4	6	0.0091312	0.033384	736	3
ACR	6	0.0091396	0.033411	737	2
hsa-mir-3686	4	0.0091515	0.033461	738	2
KBTBD4	6	0.009177	0.033549	739	5
KCTD7	6	0.0091811	0.033559	740	3
ACSL3	6	0.0091832	0.033567	741	5
KRTAP15-1	6	0.0091984	0.033613	742	3
IL13	6	0.0092063	0.033643	743	5
CYB5R2	6	0.0092194	0.033689	744	3
PTGER1	6	0.0092309	0.033724	745	4
AGPAT9	6	0.0092319	0.033728	746	5
THG1L	6	0.0092721	0.033859	747	3
PPARA	6	0.0092774	0.033875	748	4
TREML1	6	0.0092808	0.033887	749	5
FOXD4L5	6	0.0093044	0.033957	750	4
RANGRF	6	0.0093185	0.033997	751	5
OR2T1	6	0.0093248	0.034022	752	5
IGBP1	6	0.0093306	0.03404	753	2
MICU2	6	0.0093424	0.034073	754	5
MAP2K2	6	0.0093804	0.034205	755	3
TP53BP2	6	0.0093807	0.034206	756	3
MGST2	6	0.009391	0.034243	757	4
ANKRD17	6	0.009402	0.034286	758	4
MAN1B1	6	0.0094303	0.034377	759	2
NR2C1	6	0.00945	0.034438	760	3
LUZP4	6	0.0094544	0.034454	761	3
GRM3	6	0.0094661	0.034495	762	3
ZFPL1	6	0.0094696	0.034505	763	4
COX6C	6	0.0094801	0.03454	764	2
PLEKHA8	6	0.0094927	0.034591	765	4
DNAJC5	6	0.0094948	0.034601	766	5
TLR5	6	0.0095332	0.03474	767	5
OR11G2	6	0.0095448	0.034779	768	5
ANK3	6	0.0095625	0.034833	769	3
ETV3L	6	0.0095797	0.0349	770	3
EHD3	6	0.009591	0.034944	771	5
hsa-mir-8067	4	0.0095949	0.034955	772	3
CLTB	6	0.0095959	0.034957	773	3
XCR1	6	0.0096057	0.034989	774	4
hsa-mir-4658	4	0.0096061	0.03499	775	2
hsa-mir-6845	4	0.0096251	0.035047	776	1
hsa-mir-4788	4	0.009645	0.035106	777	3
hsa-mir-644a	4	0.0096467	0.035111	778	3
KLRD1	6	0.0096492	0.035119	779	4
KIAA0319L	6	0.0096794	0.03522	780	1
RYR2	6	0.0096906	0.035255	781	5
MGA	6	0.0096984	0.035284	782	5
KCNK9	6	0.0097012	0.035289	783	4
VPS52	6	0.0097084	0.035311	784	4
RRBP1	6	0.0097274	0.035373	785	3

ZFYVE19	6	0.0097292	0.03538	786	1
DCDC2B	6	0.0097519	0.03546	787	4
GTF2IRD2B	3	0.0097691	0.035516	788	3
MINK1	6	0.0097711	0.035526	789	4
C20orf173	6	0.009779	0.035551	790	2
TIFA	6	0.0098288	0.035714	791	2
hsa-mir-4719	1	0.0098568	0.035806	792	1
VIP	6	0.0098786	0.035881	793	1
NIPA2	6	0.0098872	0.035913	794	4
PAK6	6	0.0099172	0.036007	795	5
C7orf66	6	0.0099285	0.036043	796	4
PBX2	6	0.0099418	0.036089	797	2
TMEM35	6	0.0099659	0.036164	798	2
KIAA0430	6	0.0099675	0.036168	799	5
ACSM2B	6	0.0099714	0.03618	800	5
ANXA9	6	0.0099783	0.036209	801	4
ARR3	6	0.0099954	0.036268	802	4
KIFC1	6	0.0099989	0.036278	803	4
MYOG	6	0.0099993	0.03628	804	5
OR5K4	6	0.01001	0.036315	805	3
OR13C9	6	0.010013	0.036324	806	3
FRMD4B	6	0.010015	0.036333	807	3
ATP8B1	4	0.01004	0.036414	808	4
HAS2	6	0.010044	0.036431	809	3
MN1	6	0.010063	0.036486	810	4
CARF	6	0.010071	0.036512	811	3
OR4B1	6	0.010078	0.036535	813	5
C17orf66	6	0.010078	0.036535	812	3
RGS17	6	0.010105	0.036621	814	2
GCSAML	6	0.010111	0.036639	815	2
GPR22	6	0.010126	0.036681	816	4
TEKT5	6	0.010132	0.0367	817	5
CCDC115	6	0.010177	0.036843	818	2
CDH2	6	0.010193	0.036894	819	4
hsa-mir-7109	4	0.010195	0.036898	820	3
MYLK4	6	0.010227	0.036998	821	1
OR13C8	6	0.010251	0.037071	822	4
CFC1B	3	0.010252	0.037072	823	3
MORC1	6	0.010277	0.037165	824	4
YTHDF2	6	0.010281	0.037177	825	2
GGA2	6	0.010307	0.037257	826	4
RERG	6	0.010311	0.037272	827	5
ZNF160	6	0.010317	0.037291	828	5
TRMT12	6	0.010318	0.037298	829	5
hsa-mir-378b	4	0.010319	0.037299	830	3
TMEM132E	6	0.010327	0.037319	831	4
MATN4	6	0.010377	0.037487	832	4
AGAP11	6	0.010385	0.037508	833	3
PYGM	6	0.0104	0.037555	834	4
C19orf80	6	0.010407	0.037576	835	3
TNMD	6	0.010426	0.037637	836	3
HNRNPDL	6	0.010453	0.037725	837	4
SPATA3	6	0.010481	0.037814	838	3
FIZ1	6	0.010484	0.037818	839	4
DOCK1	6	0.01049	0.037838	840	3
DDX23	6	0.010515	0.037925	841	2
CALD1	6	0.010524	0.037954	842	3
hsa-mir-582	4	0.010526	0.037961	843	3
ESD	6	0.010532	0.037983	844	5
C7orf72	6	0.010541	0.038003	845	5
LGALS9B	6	0.01055	0.038039	846	4
CTNNB1	6	0.010556	0.038062	847	5
ARHGEF16	6	0.010576	0.038122	848	3
NSFL1C	6	0.010613	0.038262	849	5
OR1N1	6	0.010624	0.038305	850	4
TUBA3D	6	0.010626	0.038311	851	3
KRT86	4	0.010655	0.038404	852	2
ODC1	6	0.010669	0.038443	853	3
TM4SF4	6	0.010675	0.038457	854	2
UCHL3	6	0.010691	0.038501	855	5
BTBD16	6	0.010709	0.03857	856	5
CECR2	6	0.010725	0.038625	857	2
BET3L	4	0.01073	0.038638	858	3
PCOLCE2	6	0.010736	0.038661	859	3
PPAN-P2RY11	2	0.010775	0.038774	861	2
RRH	6	0.010775	0.038774	860	2
NTRK1	6	0.010786	0.038813	862	3
ANKRD30A	6	0.010819	0.038913	863	3
OR6B3	6	0.010825	0.038933	864	4
ST6GAL1	6	0.010838	0.03897	865	3
ZNF391	6	0.010867	0.039061	866	5
DEXI	6	0.010874	0.039086	867	1
RPP30	6	0.010875	0.039088	868	4
CEP95	6	0.010914	0.039218	869	3

TXNDC5	6	0.010919	0.039238	870	3
CAP2	6	0.010924	0.039251	871	3
LAMTOR4	6	0.010974	0.039419	872	2
AQP7	6	0.010992	0.039484	873	4
SLC43A2	6	0.011024	0.039577	874	3
TSC22D3	6	0.011034	0.039606	875	4
ACRV1	6	0.011035	0.039612	876	4
CLEC4A	6	0.011036	0.039614	877	3
SLFN12L	6	0.011039	0.039622	878	2
AMER2	6	0.011057	0.039677	879	4
GSTO2	6	0.011062	0.039692	880	4
NonTargetingControlGuideForHuman_0955	1	0.011071	0.039719	881	1
C2orf68	6	0.011074	0.039731	882	2
CORT	6	0.011086	0.039771	883	5
hsa-mir-4464	4	0.011087	0.039776	884	1
TNFRSF1B	6	0.011102	0.039836	885	3
TRIM11	6	0.011108	0.03985	886	4
PGBD3	6	0.011128	0.039909	887	3
ZNF471	6	0.011173	0.040042	888	1
BBS12	6	0.011223	0.04021	889	3
TTL	6	0.011237	0.04025	890	4
GBAS	6	0.011254	0.040313	891	4
PLBD1	6	0.01127	0.040361	892	4
BRCA2	6	0.011273	0.040365	893	3
LOC402160	6	0.011273	0.040365	894	3
NonTargetingControlGuideForHuman_0297	1	0.011297	0.04044	895	1
LEO1	6	0.011302	0.040458	896	5
HDHD2	6	0.011312	0.04049	897	4
ARFGEF1	6	0.011327	0.040529	898	3
EFHD1	6	0.01133	0.040538	899	3
TTBK1	6	0.011331	0.040541	900	5
PAFAH1B1	4	0.011349	0.040601	901	3
PIGF	6	0.011363	0.040636	902	4
AGXT2L1	6	0.011366	0.040645	903	5
TRPM3	6	0.011372	0.040667	904	3
DLGAP5	6	0.011391	0.040723	905	5
TBCCD1	6	0.011396	0.040739	906	4
GJA9	6	0.0114	0.040754	907	4
WDR81	6	0.011407	0.040786	908	3
OCSTAMP	6	0.011472	0.040983	909	2
hsa-mir-6794	4	0.011485	0.041017	910	2
GIPC1	6	0.011521	0.041131	911	1
SATL1	6	0.011568	0.041287	912	3
TMEM72	6	0.011571	0.0413	913	3
ZFP41	6	0.011583	0.041338	914	5
PCDHB10	6	0.011592	0.041362	915	5
NAP1L4	6	0.011608	0.041416	916	4
OLFML2A	6	0.01161	0.041424	917	4
CLDN25	6	0.011621	0.041455	918	3
AOAH	6	0.011626	0.041472	919	5
PHKB	6	0.011637	0.041506	920	4
NonTargetingControlGuideForHuman_0792	1	0.011648	0.041537	921	1
SYCE2	6	0.011652	0.04155	922	3
IGFL2	6	0.011665	0.041584	923	3
RNF212	6	0.011667	0.04159	924	3
MAGEL2	6	0.011671	0.041598	925	2
hsa-mir-4292	4	0.011689	0.041656	926	2
hsa-mir-6733	4	0.011693	0.041676	927	2
C9orf57	6	0.011697	0.041689	928	4
PCBP3	6	0.011719	0.041758	929	5
TRIP6	6	0.01172	0.041763	930	2
TEC	6	0.011722	0.041772	931	5
CHI3L1	6	0.011737	0.041822	932	3
PLSCR1	6	0.011743	0.041845	933	5
SMIM4	6	0.011748	0.041857	934	5
CKMT2	6	0.011769	0.041915	935	2
DQX1	6	0.01177	0.041918	936	4
SPNS1	6	0.011775	0.041932	937	3
SDHC	6	0.011795	0.042005	938	3
TMEM220	6	0.011796	0.042007	939	5
ACIN1	6	0.0118	0.042022	940	5
XK	6	0.011816	0.042069	941	3
TIMP3	6	0.01182	0.042084	942	3
TMEM26	6	0.011826	0.042099	943	3
hsa-mir-1296	4	0.01185	0.042178	944	2
SCAF4	6	0.011869	0.042233	945	4
PCDHA1	6	0.011891	0.042293	946	5
E2F7	6	0.011905	0.042335	947	5
GLRX	6	0.011913	0.042363	948	5
DUSP27	6	0.011919	0.042384	949	3
ADNP	6	0.011936	0.042436	950	3
BRSK2	6	0.011946	0.042468	951	5
TRPM1	6	0.011958	0.042504	952	5
MSANTD3	6	0.011959	0.042507	953	4

INPP5D	6	0.011976	0.042567	954	4
PKN1	6	0.011994	0.042621	955	4
PTGDR	6	0.011998	0.042631	956	4
STOML3	6	0.012012	0.042671	957	4
GLOD4	6	0.012019	0.042689	958	2
NonTargetingControlGuideForHuman_0409	1	0.012025	0.042713	959	1
DGKG	6	0.012068	0.042847	960	1
LOC152586	6	0.012083	0.042889	961	4
EPC1	6	0.012084	0.042893	962	5
C1orf110	6	0.012085	0.042899	963	4
GALR1	6	0.012114	0.043001	964	5
SRA1	6	0.012118	0.043014	965	1
SLC47A2	6	0.012122	0.043029	966	4
CXorf57	6	0.012155	0.043132	967	2
ADAM2	6	0.012217	0.043329	968	1
ARF6	6	0.012248	0.043419	969	3
MAZ	6	0.012253	0.043434	970	4
AFF4	6	0.012256	0.043445	971	3
GRINA	6	0.012267	0.043491	972	3
GPR1	6	0.012287	0.043557	973	3
HTR5A	6	0.012303	0.043604	974	5
MEOX2	6	0.012317	0.043649	975	4
NDUFS3	6	0.012335	0.043704	976	5
CHTF8	6	0.012341	0.043721	977	4
hsa-mir-718	4	0.012373	0.043807	978	2
LCORL	6	0.012376	0.043812	979	3
NonTargetingControlGuideForHuman_0831	1	0.012376	0.043816	980	1
MORN3	6	0.012389	0.043861	981	5
IL15	6	0.012392	0.043866	982	4
PADI4	6	0.012416	0.043941	983	3
hsa-mir-4537	4	0.012448	0.04405	984	1
CCDC85C	6	0.012458	0.044089	985	4
NIPSNAP3A	6	0.012467	0.044126	986	3
ITGA2	6	0.012528	0.044332	987	5
NCR1	6	0.012554	0.044423	988	4
MIER1	6	0.012565	0.044458	989	3
VSTM2B	6	0.012572	0.044482	990	5
KLHDC9	6	0.012607	0.044593	991	3
CAPRIN2	6	0.012615	0.044612	992	3
SP8	6	0.012691	0.044856	993	5
PCDH9	6	0.012696	0.044875	994	5
CHD5	6	0.012715	0.044931	996	2
GPS2	6	0.012715	0.044928	995	2
KIAA1967	6	0.012728	0.04498	997	4
TSGA13	6	0.012738	0.045007	998	3
CLCN2	6	0.012742	0.045019	999	3
hsa-mir-4447	4	0.012744	0.045022	1000	2
SYNJ2BP	6	0.012762	0.045076	1001	5
TNFAIP3	6	0.012767	0.045089	1002	3
OR2G3	6	0.01279	0.045158	1003	4
RBM4	3	0.01279	0.045159	1004	2
CHMP3	6	0.012814	0.045234	1005	2
AUH	6	0.012857	0.045374	1006	3
MTPAP	6	0.012864	0.045391	1007	2
ACSM3	6	0.012892	0.045473	1008	4
ABCA4	6	0.012918	0.045547	1009	2
RBM3	6	0.01292	0.045554	1010	5
PHTF1	6	0.012938	0.045612	1011	3
SNRPC	4	0.012945	0.045635	1012	1
RAD9B	6	0.012963	0.045685	1013	3
hsa-mir-376c	3	0.012965	0.045694	1014	1
hsa-mir-326	4	0.012978	0.045738	1015	1
CD177	6	0.013018	0.04586	1016	5
OR5M10	6	0.013029	0.045897	1017	3
CCIN	6	0.013053	0.045967	1018	5
FSHB	6	0.013062	0.04599	1019	3
SPIN2A	6	0.013064	0.045994	1020	5
hsa-mir-584	4	0.013066	0.046001	1021	2
TRIP11	6	0.013072	0.046026	1022	5
PDE7A	6	0.013112	0.046152	1024	2
GYG1	6	0.013112	0.046151	1023	4
C6orf89	6	0.013129	0.046205	1025	2
ACSS2	6	0.013129	0.046209	1026	5
ASIC5	6	0.013159	0.046304	1027	4
PRKAA1	6	0.013161	0.046309	1028	4
CSAG1	6	0.013162	0.046309	1029	2
PRKAR1B	6	0.013195	0.046412	1030	5
FGF21	6	0.013208	0.046463	1031	3
RFWD2	6	0.013248	0.046578	1032	3
NEFL	6	0.013252	0.04659	1033	3
C1orf141	6	0.013261	0.046617	1034	2
CKAP2	6	0.013273	0.04666	1035	3
ALDOB	6	0.013286	0.0467	1036	3
TCEAL4	6	0.01331	0.046774	1037	3

C19orf47	6	0.013311	0.046776	1038	3
hsa-mir-7-2	2	0.013328	0.046833	1039	2
TAS2R9	6	0.013346	0.046891	1040	4
DZIP1L	6	0.01336	0.046932	1041	1
C8orf22	6	0.013383	0.046998	1042	3
MIP	6	0.013385	0.047007	1043	5
SMARCAD1	6	0.013396	0.04705	1044	3
THSD7B	6	0.013405	0.047084	1045	5
NMU	6	0.01341	0.0471	1046	2
SRF	6	0.013424	0.047148	1047	4
ZNF197	6	0.01343	0.047168	1048	5
OR51B5	6	0.01346	0.04726	1049	2
IPO8	6	0.013495	0.04736	1050	5
BTN3A2	6	0.013497	0.047365	1051	4
MMP3	5	0.013531	0.04747	1052	4
CLPTM1	6	0.013559	0.047554	1053	3
SPG7	6	0.013578	0.04761	1054	3
ANXA11	6	0.01362	0.047745	1055	4
ZNF461	6	0.013625	0.047758	1056	2
PNLIPRP3	6	0.01364	0.047805	1057	4
hsa-mir-4635	4	0.013641	0.04781	1058	3
hsa-mir-562	4	0.013645	0.047821	1059	3
REG1A	6	0.013658	0.047862	1060	3
FOLR2	6	0.013673	0.047907	1061	3
CEACAM3	6	0.013682	0.047938	1062	4
FLT1	6	0.013692	0.047973	1063	5
ZNF442	6	0.013708	0.04803	1064	3
PLVAP	6	0.013726	0.048079	1065	5
SOHLH2	6	0.013733	0.048103	1066	4
C14orf79	6	0.013736	0.048112	1067	3
PARD6B	6	0.01374	0.048124	1068	4
IL8	6	0.013758	0.048183	1069	3
FRRS1	6	0.013765	0.048207	1070	5
CUL9	6	0.013785	0.048265	1071	2
DEFB114	6	0.013789	0.048274	1072	4
CCDC73	5	0.013802	0.048309	1073	4
RASEF	6	0.013806	0.048323	1074	4
FOXH1	6	0.013807	0.048329	1075	2
MXD3	6	0.013818	0.048365	1076	4
PPP1R12C	6	0.013833	0.048413	1077	5
SERPINB2	6	0.013857	0.048491	1078	3
C14orf177	6	0.013862	0.048504	1079	3
TASP1	6	0.013913	0.048667	1080	5
TCP11	6	0.013923	0.048697	1081	5
ARAP1	6	0.013942	0.048754	1082	5
SAMD4B	6	0.013953	0.048792	1083	2
C1orf185	6	0.01396	0.048812	1084	4
POLE3	6	0.013979	0.04887	1085	4
FUBP3	6	0.013981	0.048876	1086	5
SEC22A	6	0.013988	0.048899	1087	4
NonTargetingControlGuideForHuman_0298	1	0.014	0.048938	1088	1
KLHL1	6	0.014006	0.048954	1089	2
GLIPR1L1	6	0.014055	0.049117	1090	4
HLA-C	6	0.014073	0.04917	1091	5
CCL22	6	0.014101	0.049252	1093	4
L3MBTL4	6	0.014101	0.049252	1092	5
CDKN3	6	0.014105	0.049269	1094	4
UTS2R	6	0.014129	0.049349	1095	3
CORO7	6	0.014155	0.049431	1096	2
YTHDF3	6	0.014162	0.049458	1097	4
SCP2D1	6	0.014179	0.049507	1098	4
COMMD3-BMI1	2	0.014188	0.04953	1099	1
CCP110	6	0.014204	0.049575	1100	2
PPP3R2	6	0.014221	0.049615	1101	2
AAAS	6	0.014254	0.0497	1102	2
TRPM4	6	0.014304	0.049836	1103	1
TMEM249	6	0.014313	0.049865	1104	2
VWA7	6	0.014335	0.04992	1105	3
CRYGB	6	0.014349	0.049958	1106	2
CASP2	6	0.014413	0.050111	1107	2

7.4.4. Genes listed from Salmonella vs untreated Comparison in the Gecko positive screen

Gene	# gRNA	score	p-value	rank	# good gRNA
DAZL	6	1.30E-05	6.32E-05	1	5
MAP2K3	6	2.51E-05	0.00013067	2	1
TNFRSF25	6	3.18E-05	0.00016306	3	4
ATXN2	6	3.72E-05	0.00018723	4	3
CD164	6	3.99E-05	0.00020228	5	6
LUZP4	6	6.59E-05	0.00033044	6	5

FSCN2	6	7.42E-05	0.00036739	7	3
C5orf49	6	7.53E-05	0.00037377	8	3
ARHGAP28	6	0.00011726	0.00059863	9	5
OR8B8	6	0.00012556	0.0006415	10	3
ACTR3	6	0.00014701	0.00074276	11	5
FAM167A	6	0.00016183	0.00082257	12	3
IFNL1	6	0.00017169	0.00087366	13	5
TRIM65	6	0.00017578	0.00089144	14	2
NPS	6	0.00017585	0.00089236	15	3
MSANTD3	6	0.00017992	0.00091653	16	3
LNX1	6	0.00018123	0.000922	17	5
PTS	6	0.00018573	0.00094572	18	5
TRPV3	6	0.00019418	0.00098677	19	4
LSM12	6	0.00024202	0.0012381	20	5
BCAS1	6	0.00024974	0.0012686	21	5
LACTB2	6	0.0002499	0.0012696	22	6
CHORDC1	6	0.0002511	0.001275	23	2
EMID1	6	0.0002511	0.001275	24	3
ZC4H2	6	0.00025418	0.0012883	25	5
NUDT10	6	0.0002542	0.0012883	26	3
PRRT1	6	0.00025489	0.001291	27	6
CALN1	6	0.00026751	0.0013571	28	4
NLRC4	6	0.00029035	0.0014629	29	4
TRMT10C	6	0.00029431	0.0014803	30	5
CFI	6	0.00030467	0.0015099	31	3
CNTFR	6	0.00032642	0.0016039	32	2
CECR1	6	0.00033364	0.0016267	33	5
GLIPR1L1	6	0.00033776	0.0016431	34	2
DCST2	6	0.00035997	0.0017425	35	5
AIPL1	6	0.00037663	0.0018109	36	3
AMZ2	6	0.0004005	0.0019044	37	5
TRIM38	6	0.00042684	0.0020189	38	1
CEACAM3	6	0.00044461	0.0021006	39	4
LELP1	6	0.00047705	0.0022365	40	1
SULT6B1	6	0.00049043	0.0022889	41	5
FOXD4L5	6	0.00051969	0.0024002	42	3
PRDX1	6	0.00052258	0.0024112	43	4
UTP14C	6	0.00052272	0.0024112	44	5
ABCB11	6	0.00052725	0.0024276	45	2
EZR	6	0.00055133	0.0025238	46	5
SUSD5	6	0.00055231	0.0025284	47	4
hsa-mir-29b-1	4	0.0005551	0.0025398	48	3
BTBD17	6	0.00057746	0.0026315	49	2
OSM	6	0.00058141	0.0026456	50	2
GDI2	6	0.00060749	0.0027496	51	5
BRWD3	6	0.00062766	0.0028235	52	2
C7orf62	6	0.00063885	0.0028664	53	3
SCP2	6	0.00065017	0.0029092	54	3
TEAD2	6	0.00065927	0.0029462	55	4
TTC1	6	0.00067785	0.0030233	56	1
HTR3B	6	0.00070263	0.0031172	57	3
XKR9	6	0.00071178	0.0031487	58	5
PCBP1	6	0.00072805	0.003213	59	2
hsa-mir-548f-3	3	0.0007383	0.0032504	60	3
hsa-mir-433	4	0.00076198	0.0033334	61	3
SPRED1	6	0.0007685	0.0033603	62	4
SLC25A24	6	0.0007767	0.0033872	63	3
IL1RAP	6	0.00078469	0.0034096	64	4
UBAC2	6	0.00078826	0.0034205	65	3
FAM98A	6	0.0008026	0.0034757	66	3
ZNF442	6	0.00080334	0.0034771	67	2
CD52	6	0.00080334	0.0034771	68	2
SRRM4	6	0.00082071	0.0035414	69	2
PLCG1	6	0.00082984	0.0035833	70	2
H3F3C	6	0.00085505	0.003686	71	4
MBD1	6	0.0008564	0.0036905	72	5
ZNF396	6	0.00085808	0.0036983	73	5
ARFGEF1	6	0.00086431	0.0037256	74	4
CSN3	6	0.00087863	0.0037808	75	3
FAM24B	6	0.00090862	0.0038857	76	3
CYP3A4	6	0.00091422	0.0039049	77	2
GSTA5	6	0.00092412	0.0039405	78	4
WT1	6	0.00092881	0.0039601	79	4
PDCD4	6	0.00094462	0.0040308	80	4
PPIL3	6	0.00094922	0.0040454	81	4
KRTAP25-1	6	0.0009526	0.0040609	82	5
KCNRG	6	0.000953	0.0040622	83	3
ANAPC10	6	0.00095539	0.0040705	84	5
OSBPL10	6	0.000979	0.0041589	85	2
ORC4	6	0.00098526	0.0041831	86	3
hsa-mir-1273c	4	0.0010195	0.0043003	87	2
ZMYM3	6	0.0010292	0.0043409	88	1
SFMBT2	6	0.0010369	0.0043706	89	5
NXPE1	6	0.0010549	0.0044454	90	3
COG4	6	0.0010689	0.0044974	91	2
SAP30	6	0.0011001	0.0046191	92	3
LYRM7	6	0.0011043	0.0046346	93	3
LEMD1	6	0.0011045	0.0046356	94	3
UNK	6	0.00112	0.0047008	95	4
ATP6AP1L	6	0.0011501	0.0048166	96	3
hsa-mir-494	4	0.0011555	0.0048435	97	4
KIF3A	6	0.0011583	0.0048554	98	5
GEMIN6	6	0.0011671	0.0048841	99	3

TPST1	6	0.0011803	0.0049338	100	3
HECTD2	6	0.0012048	0.0050292	101	3
RSPH10B	6	0.0012048	0.0050292	102	1
GIMAP7	6	0.0012265	0.0051063	103	2
SIGMAR1	6	0.0012577	0.0052098	104	3
hsa-mir-4282	4	0.0012778	0.005285	105	3
LAMB4	6	0.0012801	0.0052969	106	2
FXYD4	6	0.0012947	0.0053507	107	4
IL24	6	0.0012989	0.0053708	108	4
CSDC2	6	0.001313	0.0054255	109	4
AARD	6	0.0013204	0.0054561	110	5
CCDC64B	6	0.0013302	0.0054889	111	2
QPCTL	6	0.0013333	0.0055012	112	3
ASIC5	6	0.0013377	0.0055213	113	4
ERO1LB	6	0.0013465	0.0055537	114	4
hsa-mir-27b	4	0.0013554	0.0055938	115	3
AGXT2L1	6	0.0013663	0.0056326	116	4
GSPT1	4	0.0013667	0.0056344	117	2
HCN1	6	0.0013702	0.0056458	118	5
CATSPERG	6	0.0013734	0.0056536	119	4
AGFG1	6	0.0013746	0.005659	120	2
KRIT1	6	0.0013804	0.0056832	121	2
FAM122B	6	0.0014306	0.0058679	122	2
FAM76B	6	0.0014435	0.0059177	123	4
PTPRE	6	0.0014486	0.005935	124	3
MINPP1	6	0.00145	0.0059423	125	5
NAALADL1	6	0.0014723	0.0060239	126	2
DTWD1	6	0.0014807	0.0060595	127	3
FAM46B	6	0.0014923	0.0061088	128	3
TMEM185A	6	0.0015039	0.0061544	129	2
PHEX	6	0.0015115	0.0061785	130	3
ANKRD10	6	0.0015267	0.006241	131	3
FAM107A	6	0.0015309	0.0062547	132	4
ORC2	6	0.0015408	0.0062912	133	4
ATAD5	6	0.001556	0.0063509	134	3
TNPO2	6	0.001556	0.0063509	135	3
DLC1	6	0.0015607	0.0063669	136	3
KLK11	6	0.0015945	0.0064987	137	2
KCNJ5	6	0.0015951	0.006501	138	5
ZNF280C	6	0.0016084	0.0065594	139	4
hsa-mir-580	4	0.0016121	0.0065722	140	2
PSAT1	6	0.0016312	0.006652	141	3
RRAS2	6	0.0016389	0.0066862	142	3
GNAO1	6	0.0016461	0.0067149	143	4
CWC27	6	0.0016606	0.0067728	144	3
ASPG	6	0.0016612	0.0067733	145	3
OR2C1	6	0.0016631	0.006781	146	4
ANKMY1	6	0.0016688	0.0068007	147	4
ZNF461	6	0.0016748	0.0068253	148	4
PLAC8	6	0.0016763	0.0068312	149	4
HFM1	6	0.00168	0.0068403	150	3
GABRB2	6	0.0016814	0.0068467	151	3
DENND4A	6	0.0016944	0.0068919	152	4
TCEB3	6	0.0017034	0.0069215	153	4
IL3RA_X	6	0.0017174	0.0069703	154	5
UPK3A	6	0.0017315	0.0070314	155	2
DARC	6	0.0017605	0.0071436	156	5
THUMPD3	6	0.00178	0.0072184	157	4
BAHD1	6	0.0017817	0.0072267	158	2
SPATA31D3	6	0.0017882	0.0072476	159	5
TIMM10B	6	0.0017991	0.0072974	160	5
DNAI2	6	0.0018059	0.0073206	161	3
PCCA	6	0.0018318	0.0074182	162	2
ZNF613	6	0.0018437	0.0074629	163	4
hsa-mir-938	4	0.0018571	0.0075103	164	2
hsa-mir-1302-1	4	0.0018954	0.0076663	165	2
TMEM178A	6	0.0019071	0.0077046	167	3
CAGE1	6	0.0019071	0.0077046	166	3
UFL1	6	0.0019571	0.007909	168	5
hsa-mir-4445	4	0.0019622	0.0079208	169	2
SH3GL1	6	0.001967	0.0079427	170	4
SCNN1G	6	0.0019771	0.0079824	171	4
PHLDB2	6	0.0019823	0.0080034	172	1
WRAP73	6	0.0019941	0.0080417	173	5
LSM14B	6	0.0020002	0.0080668	174	4
GABRA2	6	0.002001	0.0080672	175	4
PIGB	6	0.0020054	0.0080878	176	4
BTN3A3	6	0.0020304	0.0081717	177	3
OR8U8	3	0.002046	0.0082333	178	2
SPIN1	6	0.0020623	0.0082999	179	3
hsa-mir-1321	4	0.0020708	0.0083336	180	2
USP20	6	0.0020758	0.0083519	181	4
HIST1H3F	6	0.0020826	0.0083747	182	2
RPE	6	0.0020888	0.0083979	183	2
MECP2	6	0.0021327	0.0085452	184	2
MTHFS	5	0.0021537	0.008626	185	2
UHRF1BP1L	6	0.0021605	0.0086488	186	5
ATP1A3	6	0.0021828	0.0087236	187	3
ATP8B4	6	0.0021919	0.0087623	188	2
RASSF9	6	0.0021993	0.0087934	189	3
CXorf23	6	0.0022052	0.0088166	190	4
SMIM21	6	0.0022292	0.008906	191	5
ANKRD30A	6	0.002233	0.0089261	192	2

hsa-mir-3166	4	0.002248	0.0089749	193	4
KL	6	0.0023111	0.0091902	194	5
DUSP11	6	0.0023164	0.0092084	195	3
DNAJB4	6	0.0023441	0.0092983	196	3
SYTL5	6	0.0023479	0.0093138	197	4
APOB	6	0.0023583	0.0093566	200	2
COX7A2	6	0.0023583	0.0093566	199	2
CREM	6	0.0023583	0.0093566	201	1
FGF1	6	0.0023583	0.0093566	198	2
hsa-mir-591	4	0.0023585	0.0093571	202	2
RBM24	6	0.0023942	0.0094948	203	4
TAAR8	6	0.0024836	0.0098296	204	1
ZNF700	6	0.0024984	0.009872	205	3
RAB28	6	0.0025045	0.0098921	207	4
MICA	6	0.0025045	0.0098921	206	4
ZNF740	6	0.0025129	0.009924	208	3
hsa-mir-603	4	0.0025218	0.0099637	209	2
CDCA7	6	0.0025375	0.010016	210	4
HEXB	6	0.0025397	0.010023	211	4
LRRIQ1	6	0.0025425	0.010032	212	5
TEX15	6	0.0025467	0.010041	213	5
RFX1	6	0.0025472	0.010042	214	5
TJP1	6	0.0025486	0.010045	215	5
CYP2C9	4	0.0025712	0.010139	216	3
SLC22A8	6	0.0025754	0.010157	217	3
SLC38A11	6	0.0025761	0.010158	218	4
CLTB	6	0.0025838	0.010182	219	1
ZNF428	6	0.0025838	0.010182	220	3
FEM1C	6	0.0026234	0.010307	221	5
ZNF641	6	0.0026314	0.010343	222	5
MVP	6	0.0026526	0.010429	223	5
MAP3K8	6	0.0026826	0.010538	224	3
BTK	6	0.0026826	0.010538	225	4
ZNF514	6	0.0026958	0.010584	226	3
NCOA2	6	0.0026998	0.010603	227	5
MANEAL	6	0.002711	0.010641	228	4
KRT18	6	0.0027169	0.010664	229	3
CFHR3	6	0.0027235	0.01069	230	2
DNAJC24	6	0.0027407	0.010749	231	4
RNF146	6	0.0027574	0.010804	232	4
GPR98	6	0.0027825	0.010896	233	4
PPP1R3A	6	0.0027843	0.010901	234	1
COMT	6	0.0027843	0.010901	237	2
SPATA2	6	0.0027843	0.010901	236	1
ZNF557	6	0.0027843	0.010901	235	3
HILPDA	6	0.0027858	0.010905	238	3
CSNK2A3	6	0.0027907	0.01092	239	5
TSGA13	6	0.0027964	0.010938	240	5
CGNL1	6	0.0028022	0.010954	241	4
RNF13	6	0.0028224	0.011031	242	4
hsa-mir-548f-5	4	0.0028287	0.011057	243	3
MCMDC2	6	0.0028392	0.011096	244	4
RNF187	6	0.0028487	0.01113	245	3
CLUH	6	0.0028721	0.011204	246	2
CUX2	6	0.0028826	0.011254	247	4
C15orf32	6	0.0028828	0.011254	248	5
DSTN	6	0.0029346	0.011446	249	2
FARS2	6	0.0029631	0.011542	250	2
OGFOD1	6	0.0029711	0.011573	251	4
TMEM225	6	0.0029821	0.011616	252	5
FXYD3	6	0.0029923	0.011657	253	5
STMN3	6	0.003004	0.0117	254	2
C4orf17	6	0.0030314	0.0118	255	3
PRKAA1	6	0.0030348	0.011808	256	3
IAPP	6	0.0030545	0.011877	257	4
SERPINA6	6	0.0030564	0.011885	258	5
TDRP	5	0.0030725	0.011945	259	1
PIGW	6	0.003077	0.011961	260	4
SPTY2D1	6	0.0030781	0.011966	261	4
hsa-mir-562	4	0.0030883	0.012003	262	2
SMYD5	6	0.003097	0.012036	263	2
C11orf58	6	0.0031099	0.012083	265	1
UBL3	6	0.0031099	0.012083	264	2
SEC14L2	6	0.0031504	0.012233	266	5
CHST4	6	0.0031791	0.012333	267	4
SGCG	6	0.0031851	0.012354	268	2
NAIP	6	0.0031928	0.012381	269	5
hsa-mir-4659a	3	0.0032173	0.012471	270	2
C9orf153	6	0.0032352	0.012545	271	2
TEX30	6	0.0032372	0.012551	272	3
CLPTM1	6	0.0032443	0.012574	273	4
hsa-mir-4469	4	0.0032539	0.012609	274	2
NDUFAF6	6	0.0032765	0.012692	275	4
TGM1	6	0.003291	0.01275	276	4
hsa-mir-4718	4	0.0032923	0.012754	277	4
TRPC4	6	0.0032942	0.012761	278	4
TMX4	6	0.0033085	0.012815	279	3
SH3GLB1	6	0.0033103	0.012821	281	4
PRKAR1A	6	0.0033103	0.012821	280	2
hsa-mir-2355	4	0.0033275	0.012884	282	1
ZNF79	6	0.0033504	0.012965	283	4
SRD5A1	6	0.003352	0.01297	284	3
ITSN1	6	0.0033667	0.013018	285	4

RAB10	6	0.0033738	0.013049	286	5
MBOAT7	6	0.0033768	0.013061	287	2
OSGIN2	6	0.0033854	0.013093	288	2
CC2D2B	6	0.0033913	0.013116	289	4
C17orf105	6	0.0034117	0.013189	290	4
VAMP4	6	0.0034386	0.013287	291	2
ZNF550	6	0.0034606	0.013354	293	4
TRIO	6	0.0034606	0.013353	292	2
GAB1	6	0.0034636	0.013368	294	4
PADI1	6	0.0034693	0.013387	295	5
SLC17A3	6	0.0034784	0.013418	296	3
CA1	6	0.0034923	0.013467	297	5
RETSAT	6	0.0034981	0.013491	298	4
LIPE	6	0.0035431	0.013666	299	3
SFRP4	6	0.0035469	0.013679	300	5
PF4	6	0.0035488	0.013681	301	3
SDF2	6	0.0036026	0.013884	302	5
KRTAP21-2	6	0.0036063	0.013895	303	3
ZFP69B	6	0.0036083	0.013906	304	2
C10orf90	6	0.0036089	0.013908	306	5
RIPPLY1	6	0.0036089	0.013908	305	5
CACNA1C	6	0.0036243	0.013963	307	4
NSD1	6	0.003627	0.013971	308	3
FCGR3B	6	0.0036386	0.014019	309	4
ADAMTSL2	6	0.0036466	0.014048	310	5
DOCK1	6	0.0036599	0.014093	311	3
WWC3	6	0.0036859	0.014184	315	3
NTF3	6	0.0036859	0.014184	313	3
MYH15	6	0.0036859	0.014184	312	3
GABRG1	6	0.0036859	0.014184	314	4
IL11RA	6	0.0037079	0.014269	316	3
STAP2	6	0.0037173	0.014303	317	4
PLSCR1	6	0.0037447	0.0144	318	5
hsa-mir-6786	4	0.0037449	0.014401	319	1
OR5H15	6	0.0037515	0.014423	320	4
XAF1	6	0.0037559	0.014442	321	5
GNAZ	6	0.0037559	0.014442	322	5
CDH26	6	0.0037716	0.014497	323	4
CCK	6	0.0038025	0.014607	324	3
ISL1	6	0.0038144	0.014658	325	5
NDUFAF1	6	0.0038202	0.014675	326	2
KCTD10	6	0.0038275	0.014702	327	3
UBAP1L	6	0.0038361	0.014734	328	3
LOC283710	6	0.0038467	0.014775	329	5
GPR87	6	0.0038625	0.014832	330	3
hsa-mir-2114	4	0.0038652	0.014844	331	4
PAQR3	6	0.0038702	0.01486	332	5
PKN2	6	0.0038779	0.014885	334	2
LNP1	6	0.0038779	0.014885	333	4
NonTargetingControlGuideForHuman_0494	1	0.0038799	0.014894	335	1
FCHSD2	6	0.0038862	0.014921	336	2
TUBB2A	6	0.0038943	0.014947	337	4
hsa-mir-548v	4	0.0038982	0.014963	338	2
LRRC8B	6	0.0039277	0.015071	339	3
FXR1	6	0.0039323	0.015086	340	4
IFT172	6	0.0039664	0.015212	341	4
TRIM23	6	0.0039695	0.015224	342	3
ADAP1	6	0.003984	0.015272	343	4
BCL6	6	0.0039863	0.015278	346	2
CLPB	6	0.0039863	0.015278	344	3
MEOX2	6	0.0039863	0.015278	345	2
NSUN7	6	0.0039868	0.015279	347	4
HBS1L	6	0.0039946	0.015311	348	4
MRAP2	6	0.0039993	0.015331	349	5
C6orf141	6	0.0040196	0.015409	350	5
ZNF677	6	0.0040685	0.015602	351	5
RASSF2	6	0.0040831	0.015652	352	3
SLC32A1	6	0.0040864	0.015664	353	2
PTER	6	0.0040988	0.015704	354	4
CD8B	6	0.0041031	0.015718	355	4
PELI1	6	0.0041069	0.015732	356	4
IBA57	6	0.0041365	0.015832	357	2
SH2D4B	6	0.0041548	0.0159	358	2
RHCG	6	0.0041678	0.015959	359	4
NonTargetingControlGuideForHuman_0625	1	0.0041897	0.016049	360	1
RBM44	6	0.0042115	0.016126	362	4
STK38	6	0.0042115	0.016126	361	1
CCDC172	6	0.0042145	0.016139	363	4
RLN1	6	0.0042431	0.016236	364	2
OCA2	6	0.0042488	0.01626	365	3
MFAP4	6	0.0042717	0.016345	366	5
SUPT20HL2	6	0.0042866	0.016402	367	2
C1S	6	0.0043116	0.016488	368	5
PTCD2	6	0.004316	0.0165	369	3
SPESP1	5	0.0043233	0.016523	370	3
TMEM72	6	0.0043322	0.016556	371	2
RNASET2	6	0.0043367	0.01657	372	4
Sep-12	3	0.0043461	0.016598	373	2
RIN2	6	0.0043867	0.016734	374	1
EGR3	6	0.004396	0.016764	375	5
DNMT3L	6	0.0044119	0.016815	376	5

USP17L15	6	0.004432	0.01689	377	3
HYAL2	6	0.0044752	0.017056	378	5
DMD	6	0.0045118	0.017186	381	1
SPATA32	6	0.0045118	0.017186	379	3
PRICKLE3	6	0.0045118	0.017186	380	2
CXorf30	6	0.0045225	0.017222	382	4
TMEM68	6	0.0045534	0.017321	383	5
15-Sep	9	0.0045728	0.017398	384	6
ZKSCAN2	6	0.0045835	0.01744	385	3
CASC10	3	0.0046262	0.017574	386	1
RUNX1	6	0.0046295	0.017585	387	4
C1orf174	6	0.0046381	0.01761	388	3
KRT31	6	0.0046428	0.017626	389	3
ATP11C	6	0.0046429	0.017626	390	5
DCC	6	0.0046621	0.017688	391	3
EXT1	6	0.004668	0.017713	392	2
DNAJC10	6	0.0046787	0.017754	393	5
PPID	6	0.0046869	0.017778	394	4
CHTF8	6	0.0046869	0.017778	395	2
RHBDL3	6	0.004694	0.01781	396	3
CACNB2	6	0.0047182	0.017898	397	3
RDH13	6	0.0047507	0.018007	398	2
ITM2B	6	0.0047572	0.018033	399	4
ARL4A	6	0.0047698	0.018081	400	4
UBXN4	6	0.0047869	0.018147	401	3
DUSP19	6	0.0048052	0.01821	402	5
FSD1	6	0.004837	0.018316	404	3
COX19	6	0.004837	0.018316	403	2
OR2L8	6	0.0048377	0.01832	405	4
MAP9	6	0.0048423	0.018335	406	5
C17orf64	6	0.0048533	0.018376	407	3
LAMTOR4	6	0.0048589	0.018402	408	3
FAM149B1	6	0.0048871	0.018505	409	3
LSP1	6	0.0048933	0.018522	410	3
NDUFB5	6	0.0049066	0.018565	411	4
PLK1S1	6	0.0049173	0.018606	412	3
NR1I3	6	0.0049244	0.018627	413	3
ATXN1	6	0.0049353	0.01867	414	2
RBMS2	6	0.004937	0.018677	415	1
FHL5	6	0.0049635	0.018774	416	2
APOBEC4	6	0.0050166	0.018949	417	3
ZNF397	6	0.0050212	0.018963	418	4
FABP6	6	0.0050223	0.018967	419	2
E2F3	6	0.0050621	0.019103	421	2
OVOL2	6	0.0050621	0.019103	420	3
SNX11	6	0.0051004	0.019235	422	4
POLA1	6	0.0051276	0.01934	423	4
ACTR2	6	0.0051335	0.019362	424	4
G3BP1	6	0.0051549	0.019452	425	5
ST3GAL2	6	0.0051608	0.019472	426	3
NFE2L3	6	0.0051874	0.019563	427	3
C7orf73	5	0.0051962	0.019587	428	4
PIF1	6	0.0052395	0.019715	429	4
TXNDC12	6	0.0052519	0.019749	430	2
WDSUB1	6	0.0052871	0.019843	431	2
NUP54	6	0.0052871	0.019843	432	2
RHOQ	6	0.0053023	0.019884	433	4
TM7SF3	6	0.0053406	0.019986	434	4
TP53I11	6	0.0053856	0.020122	435	3
AK4	6	0.0053871	0.020128	436	4
hsa-mir-4635	4	0.0053967	0.020159	437	2
CCDC90B	6	0.0054134	0.020204	438	4
TEX11	6	0.0054308	0.020247	439	4
HERC5	6	0.0054366	0.020271	440	4
N4BP2L2	6	0.0054371	0.020273	441	1
RNF183	6	0.0054544	0.02032	442	2
GRIA3	6	0.0054644	0.02035	443	4
OR4S2	6	0.005476	0.020377	444	4
ACTR8	6	0.0055432	0.020569	445	4
hsa-mir-3927	4	0.0055867	0.020678	446	2
ATPAF1	6	0.0056121	0.020746	447	1
AFF2	6	0.0056121	0.020746	448	1
ZNF561	6	0.0056121	0.020746	449	1
MYF6	6	0.005659	0.02087	451	3
VRK1	6	0.005659	0.02087	452	3
CKAP2	6	0.005659	0.02087	450	3
CENPI	6	0.0057123	0.021022	453	4
CXCL13	6	0.0057483	0.02112	454	4
CHGA	6	0.0057487	0.021121	455	3
GNAI2	6	0.005862	0.021428	456	2
TPCN2	6	0.0058746	0.02146	457	4
C11orf31	6	0.005882	0.021484	458	3
XKRY	6	0.0059015	0.021534	459	4
OGDH	6	0.005937	0.021639	460	1
THAP8	6	0.0060264	0.021872	461	4
AKAP12	6	0.0060369	0.021902	462	3
MAOA	6	0.0060526	0.021937	463	3
CHPT1	6	0.0060576	0.021954	464	4
HEATR5B	6	0.0061462	0.022192	465	2
KIAA1671	6	0.0061563	0.022215	466	4
SLMO1	6	0.006167	0.022244	467	4
LGSN	6	0.0061869	0.022303	469	3
C16orf70	6	0.0061869	0.022303	468	2

STK32A	6	0.0061869	0.022303	470	2
ELMOD2	6	0.0061869	0.022303	471	2
SDCBP2	6	0.0061912	0.022315	472	3
CNTRL	6	0.0061963	0.022324	473	3
STYXL1	6	0.0062046	0.022343	474	4
ZFR2	6	0.0062046	0.022343	475	3
CD8A	6	0.0062313	0.022417	476	3
hsa-mir-655	4	0.0062571	0.022485	477	3
WDR45B	6	0.0062572	0.022485	478	2
IQGAP2	6	0.006301	0.022611	479	4
EIF3A	6	0.0063184	0.022652	480	4
RNASEH2B	6	0.0063867	0.022836	481	1
BLOC1S6	6	0.0063901	0.022846	482	4
EPX	6	0.0064092	0.022897	483	3
CALU	6	0.0064292	0.022959	484	4
ST6GAL1	6	0.0064367	0.022976	485	2
ABCA8	6	0.006437	0.022977	486	4
APMAP	6	0.0064618	0.023039	487	4
CSAG1	6	0.0064866	0.02311	488	3
IER3IP1	6	0.0064918	0.023122	489	4
ATL1	6	0.0065214	0.023206	490	3
FAM162A	6	0.0065231	0.023211	491	3
HSPB1	6	0.0065493	0.02328	492	4
C8orf47	6	0.0065709	0.023335	493	3
ZNF382	6	0.0065805	0.023359	494	4
F13A1	6	0.0065944	0.023396	495	4
SOSTDC1	6	0.0065989	0.02341	496	4
FAM198B	6	0.0066115	0.023445	498	3
TDRKH	6	0.0066115	0.023445	499	1
TAB1	6	0.0066115	0.023445	497	3
FGFR1OP2	6	0.0066158	0.023457	500	3
hsa-mir-5009	4	0.006625	0.023483	501	2
GIGYF2	6	0.006648	0.023542	503	3
SLC30A6	6	0.006648	0.023542	502	3
KIF17	6	0.0066929	0.023658	504	3
hsa-mir-375	4	0.0067087	0.023704	505	3
FAM111B	6	0.0067298	0.023765	506	3
GPT2	6	0.0067364	0.023784	507	2
FAM19A5	6	0.006738	0.023787	508	2
SCYL2	6	0.0067422	0.023798	509	4
AUH	6	0.0067556	0.023837	510	3
MUC20	6	0.0067757	0.023881	511	2
AMOT	6	0.006816	0.023977	512	2
C19orf77	6	0.0068362	0.024041	513	1
BSX	6	0.0068862	0.02419	514	1
KLC1	6	0.0069054	0.024245	515	4
hsa-mir-548a-1	4	0.0069115	0.024261	516	2
EFCAB11	6	0.0069361	0.024317	517	2
SGPL1	6	0.0069401	0.024328	518	3
TTC39B	6	0.006986	0.024448	519	2
CLVS1	6	0.0069936	0.024473	520	3
TCEB3B	6	0.0069987	0.024487	521	3
INSL4	6	0.007009	0.024511	522	2
AZGP1	6	0.007036	0.024579	523	2
ADRA1B	6	0.0070602	0.024642	524	3
GRIA4	6	0.0071028	0.024766	525	4
MYOF	6	0.0071083	0.024777	526	3
CENPH	3	0.0071276	0.024837	527	1
ZNF430	6	0.0071442	0.02488	528	4
CCZ1	5	0.007183	0.024993	529	4
STRN	6	0.0071858	0.024999	532	1
CLPX	6	0.0071858	0.024999	533	3
CCDC96	6	0.0071858	0.024999	531	2
RBM25	6	0.0071858	0.024999	534	1
GUCY1A3	6	0.0071858	0.024999	530	1
CDADC1	6	0.0072039	0.025047	535	3
KRTAP26-1	6	0.0072276	0.025119	536	4
RHOJ	6	0.0072412	0.025161	537	3
DEFB127	6	0.0072537	0.025195	538	3
KREMEN1	6	0.0072945	0.025305	539	4
MSMO1	6	0.0073059	0.025336	540	3
CYB5R3	6	0.0073113	0.025352	541	4
C5orf20	6	0.0073355	0.025406	542	3
TTBK1	6	0.0073423	0.02542	543	3
CNPY3	6	0.0073501	0.02544	544	4
TADA2A	6	0.0073614	0.02547	545	4
PAMR1	6	0.0073636	0.025476	546	4
KRT17	6	0.0073854	0.02553	547	3
SUPT6H	6	0.0074053	0.025581	548	3
SOHLH2	6	0.0074182	0.025612	549	3
FAM170A	6	0.0074339	0.025652	550	3
PIGU	6	0.0074354	0.025656	551	3
BMPER	6	0.0074536	0.025709	552	3
USP9X	6	0.0074582	0.025721	553	3
SYCE2	6	0.0074655	0.025741	554	2
PIP	6	0.0074853	0.025798	555	1
CABP7	6	0.007516	0.025888	556	4
TTC23L	6	0.0075352	0.025952	557	1
SLC35F6	6	0.0075387	0.02596	558	4
CYP4Z1	6	0.0075552	0.026005	559	4
IP6K3	6	0.0075659	0.02604	560	3
LUZP6	5	0.0075774	0.026074	561	3
NEIL2	6	0.0075834	0.026089	562	3

GDI1	6	0.0075851	0.026091	563	2
C9orf66	6	0.0075976	0.026123	564	2
CD177	6	0.0076109	0.026151	565	3
SMURF2	6	0.0076488	0.026254	566	4
ZNF493	6	0.0076509	0.026261	567	4
JAK1	6	0.0076641	0.02629	568	3
KLHL38	6	0.0076849	0.026344	569	3
LCE2D	5	0.0076931	0.026369	570	4
TNFSF8	6	0.0076958	0.026381	571	3
TAS2R60	6	0.0077063	0.026407	572	3
MNAT1	6	0.0077099	0.026419	573	4
ZDHHC2	6	0.0077148	0.026427	574	3
CNRIP1	6	0.007724	0.026459	575	3
APOL1	6	0.0077348	0.026493	576	2
ST20	6	0.0077523	0.026542	577	2
MAP3K1	6	0.0077658	0.026578	578	4
BANK1	6	0.0077701	0.026586	579	3
SATL1	6	0.0078097	0.026705	580	2
CEACAM20	6	0.0078113	0.026708	581	4
DMXL1	6	0.0078127	0.02671	582	4
RGS13	6	0.0078234	0.026735	583	4
ADHFE1	6	0.0078424	0.026784	584	3
ACSM4	6	0.0078544	0.026822	585	3
COL14A1	6	0.0078555	0.026824	586	3
SLC39A7	6	0.0078598	0.026833	587	3
C12orf29	6	0.0078845	0.026894	588	2
CENPE	6	0.0079084	0.026973	589	3
SPATA22	6	0.0079287	0.027032	590	4
CHMP7	6	0.0079344	0.027049	591	1
hsa-mir-5011	4	0.0079571	0.027105	592	3
LRRC42	6	0.0080269	0.027299	593	3
EVPL	6	0.0080659	0.027405	594	2
DTX2	6	0.0080714	0.027421	595	2
C4orf36	6	0.0080841	0.027459	598	2
KIAA0196	6	0.0080841	0.027459	596	3
LRRC30	6	0.0080841	0.027459	597	1
LOC256021	5	0.0080872	0.027466	599	3
hsa-mir-628	4	0.0081098	0.02752	600	2
hsa-mir-4641	4	0.0081273	0.027566	601	2
MMP9	6	0.0081958	0.027745	602	3
BFSP1	6	0.008212	0.027799	603	4
TRAF3IP3	6	0.0082313	0.027851	604	3
hsa-mir-1292	4	0.0082325	0.027853	605	3
ARF6	6	0.0082337	0.027856	606	1
PPP3CA	6	0.00825	0.027895	607	4
ATG10	6	0.0082726	0.027959	608	4
FAIM	6	0.0082836	0.027987	609	2
APAF1	6	0.0082878	0.027999	610	3
HOXC12	6	0.0083069	0.028045	611	4
WWTR1	6	0.0083124	0.028057	612	3
FBXO4	6	0.0083335	0.028123	613	1
YRDC	6	0.0083834	0.028255	614	2
FADS1	6	0.0083854	0.028263	616	2
C10orf113	6	0.0083854	0.028263	617	3
MVD	6	0.0083854	0.028263	615	2
CYFIP1	6	0.008394	0.028288	618	4
MEP1B	6	0.0084831	0.028534	619	3
CXorf66	6	0.0084944	0.028567	620	4
TRIP12	6	0.008508	0.028614	621	2
LRRC6	6	0.0085564	0.028748	622	4
TRAF3	6	0.0085564	0.028748	623	4
DOCK2	6	0.0085764	0.028805	624	4
MRPS17	6	0.0085828	0.028824	625	4
VILL	6	0.0086078	0.028889	626	3
FBXL14	6	0.0086597	0.029029	627	4
FAHD2B	6	0.0086662	0.029044	628	4
PHF8	6	0.0086735	0.029061	629	4
LIFR	6	0.00869	0.029109	630	3
ZNF654	6	0.0086926	0.029114	631	3
PI15	6	0.0087122	0.029166	632	4
RGS17	6	0.0087324	0.029227	634	2
DPH1	6	0.0087324	0.029227	633	2
C4BPB	6	0.0087324	0.029227	635	3
BAG6	6	0.0087559	0.029303	636	4
SLCO1B1	6	0.0088321	0.02952	637	2
KARS	6	0.0088397	0.029538	638	4
IMMT	6	0.0088525	0.029572	639	4
CORO6	6	0.0089069	0.029725	641	1
ACP2	6	0.0089069	0.029725	640	2
hsa-mir-6798	4	0.0089269	0.029771	642	1
CRLS1	6	0.0089381	0.029792	643	4
GABRR1	6	0.0089382	0.029792	644	3
hsa-mir-411	4	0.008944	0.029809	645	3
NonTargetingControlGuideForHuman_0800	1	0.0089443	0.02981	646	1
MAPK13	6	0.0089817	0.029907	647	2
hsa-mir-8069	4	0.0090266	0.030024	648	3
B3GNT8	6	0.0090365	0.030051	649	3
C19orf81	6	0.0090573	0.0301	650	3
SPANXN5	5	0.0090762	0.030151	651	3
CD36	6	0.009107	0.030235	652	4
CEACAM6	6	0.0091551	0.030369	653	4
MARK3	6	0.0091747	0.030422	654	4

ARRDC1	6	0.0091823	0.03044	655	4
SULT1B1	6	0.0091881	0.030453	656	4
IKZF1	6	0.009201	0.03049	657	4
hsa-mir-802	4	0.0092218	0.030545	658	3
SAMHD1	6	0.0092286	0.030562	659	3
MUM1	6	0.0092309	0.030568	664	3
LRIT3	6	0.0092309	0.030568	663	1
REN	6	0.0092309	0.030568	666	2
PPFIBP1	6	0.0092309	0.030568	660	3
ZFP2	6	0.0092309	0.030568	662	3
SRA1	6	0.0092309	0.030568	665	2
MASP2	6	0.0092309	0.030568	661	3
SLFN12L	6	0.0092614	0.030647	667	2
IL6ST	6	0.0092906	0.030719	668	3
DCD	6	0.0093372	0.03085	669	2
KRTAP22-2	6	0.0093648	0.030926	670	3
C12orf10	6	0.0093993	0.031015	671	3
IQCG	6	0.0094246	0.031076	672	4
hsa-mir-4433	4	0.0094283	0.031082	673	2
PCDHA9	2	0.0094784	0.031208	674	1
UBE2L3	6	0.0095057	0.031291	675	4
ZNF165	6	0.0095134	0.031316	676	4
ST6GAL2	6	0.0095169	0.03133	677	4
LURAP1	6	0.0095195	0.031334	678	4
IMMP1L	6	0.0095299	0.03136	679	3
LPIN2	6	0.0095464	0.031408	680	3
WWC1	6	0.0095486	0.031414	681	3
DYNLRB2	6	0.0095722	0.031484	682	2
DHRS12	6	0.0095806	0.031508	683	4
KCNN2	6	0.0096296	0.031628	684	1
FLT3LG	6	0.0096314	0.031632	685	2
PRSS37	6	0.0096473	0.031671	686	4
INSL5	6	0.0096751	0.031739	687	4
GFRA3	6	0.0096794	0.031749	688	2
GLTSCR1L	6	0.0096968	0.031796	689	4
ATP5J	6	0.0097292	0.03188	690	1
AGPAT3	6	0.0097574	0.031963	691	3
RTEL1	6	0.0097652	0.03199	692	4
CASZ1	6	0.009779	0.032027	693	2
TIFA	6	0.0097807	0.03203	694	4
EPHA3	6	0.0098129	0.032112	695	2
MYLK2	6	0.0098288	0.032158	696	3
TAF9	6	0.0098598	0.032249	697	3
MDP1	6	0.0098698	0.032276	698	3
TGFBR1	6	0.0098786	0.032301	699	1
TRIM67	6	0.0099079	0.03237	700	3
ARHGEF28	6	0.0099128	0.032386	701	4
ERAL1	6	0.0099285	0.032422	702	3
HSF5	6	0.0099491	0.032471	703	3
ZNF81	6	0.0099574	0.032499	704	3
LONRF2	6	0.010015	0.032657	705	3
WDFY2	6	0.010028	0.032693	706	3
ZNF549	6	0.010028	0.032693	707	3
TTC28	6	0.010081	0.032822	708	3
GTSF1	6	0.010083	0.032832	709	4
PAGE1	6	0.010104	0.032887	710	3
LRFN5	6	0.01012	0.032926	711	4
RWDD2A	6	0.010128	0.032943	712	2
hsa-mir-5092	4	0.010138	0.032969	713	3
PROM1	6	0.010144	0.032979	714	2
OR10A3	6	0.010154	0.033002	715	3
OTX1	6	0.010199	0.033112	716	3
TEKT4	6	0.010227	0.033186	717	1
TRIM60	6	0.010232	0.0332	718	4
AGPHD1	5	0.010255	0.033254	719	3
ZNF177	4	0.010257	0.033259	720	2
PPP1R12C	6	0.010276	0.033321	721	4
KCNK18	6	0.010314	0.033418	722	3
hsa-mir-4264	4	0.010329	0.033462	723	2
PLEKHM2	6	0.010342	0.033502	724	3
CUL4A	6	0.010424	0.033714	725	4
RAET1E	6	0.010426	0.033719	729	3
SLC9A4	6	0.010426	0.033719	727	2
ARL3	6	0.010426	0.033719	726	2
CYP4A11	6	0.010426	0.033719	728	4
GHRL	6	0.010426	0.033719	731	3
PPP1R3B	6	0.010426	0.033719	730	2
hsa-mir-4275	4	0.010431	0.033734	732	2
LYPD6B	6	0.010499	0.033913	733	2
hsa-mir-325	4	0.010507	0.033939	734	2
GGA1	6	0.010525	0.033996	735	4
GPRC5B	6	0.010539	0.034033	736	4
WFDC5	6	0.010558	0.034086	737	2
NonTargetingControlGuideForHuman_0031	1	0.010568	0.03411	738	1
PTBP3	6	0.010584	0.034157	739	4
NKAIN3	6	0.010595	0.034188	740	3
OR52K1	6	0.010607	0.034229	741	2
DFFB	6	0.010636	0.03432	742	4
RP1L1	6	0.010675	0.034421	743	1
ARRDC3	6	0.010696	0.034478	744	4
C19orf40	6	0.010722	0.034557	745	3
RNF14	6	0.010723	0.034559	746	4

TROVE2	6	0.010725	0.034564	747	3
KHDRBS1	6	0.010742	0.034607	748	4
OR2F2	6	0.010763	0.034658	749	2
DOPEY2	6	0.010771	0.034682	750	4
GTF3A	6	0.010787	0.034722	751	3
PLCG2	6	0.010822	0.034819	752	3
SH3BGRL	6	0.010825	0.034826	753	2
SPG20	6	0.010836	0.034855	754	3
hsa-mir-532	4	0.010862	0.034921	755	3
AP1S3	6	0.010868	0.034939	756	3
GGCT	6	0.010874	0.03495	757	3
ZNF225	6	0.010893	0.034997	758	3
NPC2	6	0.01092	0.035061	759	4
PRDM14	6	0.010924	0.035072	760	1
TRIM31	6	0.010934	0.035099	761	4
PIGF	6	0.010937	0.035107	762	3
ENPP3	6	0.010974	0.035215	763	2
FAM5B	4	0.010987	0.035253	764	1
SLC22A11	6	0.011024	0.035346	765	2
BMPR1A	6	0.011029	0.035358	766	4
ZC2HC1A	6	0.011045	0.035398	767	2
ATP9A	6	0.01105	0.035409	768	4
NRG2	6	0.011051	0.035413	769	2
hsa-mir-3618	4	0.01106	0.035437	770	3
hsa-mir-944	3	0.011061	0.03544	771	2
ASL	6	0.011066	0.03545	772	4
KIAA0319L	6	0.011074	0.035471	773	1
DCK	6	0.011076	0.03548	774	4
PNLIPRP2	6	0.011086	0.03551	775	4
USP17L2	6	0.011116	0.035591	776	4
GJA10	6	0.011185	0.035768	777	3
TRAT1	5	0.011198	0.035803	778	3
hsa-mir-7844	4	0.011213	0.035844	779	2
OPN3	6	0.011214	0.035847	780	4
MINK1	6	0.011219	0.035856	781	4
KIAA0319	6	0.011305	0.036077	782	3
HADH	6	0.011305	0.036077	783	4
ARSI	6	0.011309	0.036091	784	4
ABCG8	6	0.011321	0.036121	785	3
PFKFB2	6	0.011372	0.03626	787	2
RALGPS1	6	0.011372	0.03626	792	2
TRMT6	6	0.011372	0.03626	793	1
CYP3A7	6	0.011372	0.03626	786	2
MFRP	6	0.011372	0.03626	791	3
UMOD	6	0.011372	0.03626	788	1
C9orf3	6	0.011372	0.03626	794	3
LTBR	6	0.011372	0.03626	790	3
S100A10	6	0.011372	0.03626	789	4
APOD	6	0.011374	0.036265	795	4
COG5	6	0.011382	0.036289	796	3
ANGEL1	6	0.011433	0.036425	797	4
GNAI1	6	0.011446	0.036462	798	3
DPH2	6	0.011468	0.036519	799	4
PPP2R2B	6	0.011475	0.036532	800	3
LRRC70	6	0.011507	0.036621	801	3
SCARB1	6	0.01155	0.03673	802	3
IGSF5	6	0.011555	0.036749	803	3
RASGRP3	6	0.011588	0.036851	804	3
STAMBPL1	6	0.011609	0.036917	805	3
TFAP2B	6	0.011614	0.036931	806	3
OR5L2	6	0.011624	0.036958	807	4
LRRN4	6	0.01165	0.037023	809	4
ANKRD1	6	0.01165	0.037023	808	4
ART4	6	0.011665	0.037058	810	4
VGLL4	6	0.011669	0.037068	811	4
COA3	6	0.011671	0.037072	812	3
AGBL4	6	0.011684	0.037108	813	4
hsa-mir-30c-1	4	0.011689	0.037123	814	3
C9orf117	6	0.011715	0.037192	815	4
ST6GALNAC4	6	0.01172	0.037207	816	2
CAMK1	6	0.011722	0.037212	817	3
ZNF727	6	0.011732	0.037247	818	3
SEMA3E	6	0.011745	0.037279	819	3
C1orf192	6	0.011766	0.037331	820	3
PRPF18	6	0.01177	0.03734	821	1
CNTNAP4	6	0.011782	0.037368	822	3
CFHR2	6	0.01182	0.037481	823	3
OMD	6	0.011823	0.037486	824	4
ATP6V1G2	6	0.011823	0.037486	825	4
hsa-mir-4661	4	0.011837	0.037533	826	3
CDRT15L2	6	0.011847	0.037564	827	3
USP33	6	0.011856	0.037585	828	3
TREML1	6	0.011864	0.037607	829	4
ANKRD30B	6	0.011873	0.037637	830	4
DNMT3B	6	0.011894	0.037687	831	3
L3MBTL4	6	0.011894	0.037687	832	2
hsa-mir-326	4	0.011926	0.037771	833	3
TOR1AIP1	6	0.011932	0.037788	834	3
CRISP3	6	0.011935	0.037798	835	3
KAT6A	6	0.011952	0.037835	836	3
KCNH2	6	0.011965	0.037871	837	2
ZFAND5	6	0.011969	0.037884	838	2
ZFP37	6	0.011981	0.037915	839	3

HIST1H4L	6	0.011994	0.037952	840	4
SLC14A2	6	0.011994	0.037954	841	2
SAA2-SAA4	3	0.011996	0.03796	842	3
PLAC4	6	0.012007	0.037982	843	3
MUC7	6	0.012043	0.038081	844	2
SUMO1	6	0.012043	0.038081	845	1
IL13RA2	6	0.012063	0.038129	846	4
SLC23A2	6	0.012113	0.038279	847	3
BCL7B	6	0.012132	0.038325	848	2
LITAF	6	0.012141	0.038343	849	3
PDZD11	6	0.012165	0.038412	850	4
TRAM1	6	0.012165	0.038412	851	4
GPS2	6	0.012168	0.038418	852	1
TMEM229A	6	0.012175	0.038442	853	4
GIP	6	0.012179	0.038453	854	4
hsa-let-7g	4	0.012215	0.038543	855	2
SYNGR2	6	0.012217	0.038547	856	2
UHRF2	6	0.012241	0.038609	857	3
ADAMTSL3	6	0.012317	0.038822	858	2
TGFBR2	6	0.01236	0.038946	859	3
HEPH	6	0.012366	0.038957	860	3
ZNF658	6	0.012376	0.038981	861	4
GABRA6	6	0.012376	0.038981	862	4
SLC16A6	6	0.012394	0.039021	863	2
HTRA4	6	0.012416	0.039079	864	3
BTF3	6	0.012435	0.039136	865	4
PCSK1N	6	0.012464	0.039214	866	3
LRP8	6	0.012466	0.039224	867	3
CEP41	6	0.012467	0.039229	868	4
CCDC88B	6	0.01248	0.039263	869	2
FAM47C	6	0.0125	0.03931	870	2
NUDT6	6	0.012502	0.039315	871	4
ZNF318	6	0.012516	0.039355	872	1
FAM186B	6	0.012535	0.039409	874	4
OBSL1	6	0.012535	0.039407	873	4
LRRIQ3	6	0.012565	0.039493	875	2
MRPL22	6	0.012615	0.039633	876	3
CLK2	6	0.012625	0.039656	877	4
PTRHD1	6	0.012628	0.039661	878	3
HMGCLL1	6	0.012641	0.03969	879	2
hsa-mir-4291	4	0.012647	0.039702	880	2
SYN2	6	0.012647	0.039702	881	3
C11orf96	6	0.012665	0.03975	882	1
PCDHGC5	2	0.012701	0.039843	883	2
PCDHGA5	2	0.012744	0.039965	884	2
KRTAP10-1	6	0.012749	0.039975	885	3
DTD1	6	0.012769	0.040022	886	3
PSKH2	6	0.012794	0.040084	887	3
TANC1	6	0.01281	0.040123	888	4
DIO1	6	0.012815	0.040136	889	4
hsa-mir-4436b-1	4	0.01283	0.040176	890	2
CEP350	6	0.012831	0.04018	891	4
CBLN1	6	0.012838	0.040198	892	3
SRP72	6	0.01285	0.040232	893	3
SORD	6	0.012857	0.040251	894	4
C4orf22	6	0.012888	0.040331	895	2
PIK3C2B	6	0.012888	0.040331	897	3
RUNDC3B	6	0.012888	0.040331	898	2
LCE1F	6	0.012888	0.040331	896	1
CTAGE5	4	0.012898	0.040354	899	3
IL13RA1	6	0.012908	0.040375	900	2
MYSM1	6	0.012924	0.040421	901	2
LRRC8C	6	0.012952	0.040484	902	4
DSCR4	6	0.01296	0.040507	903	3
ACAT2	6	0.012979	0.040554	904	4
TNRC18	6	0.013006	0.040635	905	3
CATSPER2	6	0.01302	0.040673	906	2
ZBTB1	6	0.013064	0.040788	907	3
hsa-mir-4305	4	0.013075	0.040822	908	3
hsa-mir-548au	3	0.01308	0.040838	909	2
MGAT3	6	0.013087	0.040857	912	2
EEF1B2	6	0.013087	0.040857	911	1
CAMKMT	6	0.013087	0.040857	910	3
GCSAML	6	0.013108	0.04092	913	2
C2	6	0.013126	0.040962	914	3
PDIA6	6	0.01313	0.040973	915	3
POLR1D	6	0.013172	0.041092	916	3
NFATC3	6	0.01318	0.041114	917	3
hsa-mir-559	4	0.013191	0.041139	918	3
SEC31A	6	0.013193	0.041144	919	4
PLCL1	6	0.013197	0.041156	920	3
NCSTN	6	0.013211	0.041203	921	2
HTATSF1	6	0.013224	0.041232	922	4
ADNP	6	0.013231	0.041248	924	3
C22orf26	6	0.013231	0.041247	923	4
NonTargetingControlGuideForHuman_0358	1	0.013247	0.041292	925	1
SLC2A12	6	0.013259	0.041321	926	2
METTL14	6	0.013286	0.041393	928	1
PSMD4	6	0.013286	0.041393	927	2
VN1R2	6	0.0133	0.041425	929	4
SNRPC	4	0.01331	0.04146	930	1
R3HCC1	6	0.013325	0.041495	931	4

hsa-mir-222	4	0.013347	0.041555	932	3
CENPO	6	0.013363	0.041586	933	4
PRR9	6	0.013384	0.041637	934	4
NLRP12	6	0.01341	0.041709	935	2
PTPN5	6	0.013426	0.041753	936	3
GRAP	4	0.013443	0.041803	937	3
KIAA1522	6	0.01346	0.041846	938	3
BCAS4	6	0.013483	0.041905	939	4
SELV	6	0.013483	0.041905	940	2
EFCAB5	4	0.013525	0.042021	941	2
SPIRE1	6	0.013559	0.042107	942	2
RAB8A	6	0.013569	0.042128	943	4
C14orf166B	6	0.01358	0.04216	944	3
NUDT2	6	0.013609	0.042235	945	3
KLHL28	6	0.013695	0.042452	946	4
KRTAP10-2	6	0.013708	0.042487	947	1
ZUFSP	6	0.013717	0.042507	948	4
RNF215	6	0.013758	0.042615	949	1
NYNRIN	6	0.013766	0.042634	950	3
RSPH4A	6	0.013778	0.042664	951	3
FOXJ3	6	0.013807	0.042735	952	2
SERPINA4	6	0.013827	0.042791	953	3
POMGNT1	6	0.013848	0.04284	954	2
C9orf57	6	0.013853	0.042853	955	3
C9orf50	6	0.013857	0.042862	956	2
GALNT14	6	0.013897	0.042972	957	4
MARCO	6	0.013904	0.042989	958	4
PLEKHA6	6	0.013907	0.042998	959	3
SP7	6	0.013914	0.043021	960	3
MGP	6	0.013926	0.04305	961	4
MAB21L1	6	0.013946	0.043108	962	3
ANKDD1B	6	0.013977	0.043182	963	4
OR2AE1	6	0.013981	0.043193	964	2
NARG2	6	0.013981	0.043193	965	2
LOC402160	6	0.013981	0.043194	966	3
YTHDF2	6	0.014014	0.043288	968	3
C12orf77	6	0.014014	0.043288	967	4
ZNF559	6	0.014033	0.043346	969	3
SYNJ1	6	0.014039	0.043356	970	4
SMCR7	1	0.014067	0.043441	971	1
AS3MT	6	0.014074	0.043459	972	4
TMEM57	6	0.014136	0.043626	973	2
CELSR3	6	0.014151	0.043662	974	3
MAP2	6	0.014155	0.04367	975	1
SPSB1	6	0.014168	0.043698	976	2
DNAJC6	6	0.014194	0.043758	977	4
DRAXIN	6	0.014203	0.043781	978	4
TNPO1	6	0.014214	0.043813	980	3
CLRN1	6	0.014214	0.043813	979	3
RNF157	6	0.014254	0.04392	981	2
RAD17	6	0.014259	0.043933	982	3
RNF111	6	0.014264	0.043947	983	3
C1GALT1	6	0.014276	0.043981	984	4
ZNF410	6	0.014289	0.044021	986	2
C11orf68	6	0.014289	0.044021	985	3
SH2B2	6	0.014295	0.044037	987	4
hsa-mir-544b	4	0.014299	0.044047	988	2
NXT1	6	0.014304	0.044067	989	1
C17orf85	6	0.014355	0.044209	990	4
NLRX1	6	0.014356	0.044214	991	4
HRG	6	0.01436	0.04422	992	2
TNFSF9	6	0.014378	0.044276	994	2
WISP3	6	0.014378	0.044276	993	3
NETO1	6	0.014413	0.044366	995	4
CD69	6	0.014491	0.044562	996	3
PCIF1	6	0.014552	0.044716	997	3
OTUB2	6	0.014552	0.044716	998	3
GRM4	6	0.014573	0.044774	999	4
FAF1	6	0.014577	0.044784	1000	4
ST8SIA5	6	0.014586	0.044806	1001	4
CCAR2	6	0.014641	0.044939	1002	4
TSSC1	6	0.014666	0.044995	1003	3
IPO4	6	0.014671	0.04501	1004	3
SLC1A1	6	0.014792	0.04531	1005	4
hsa-mir-1224	4	0.014801	0.045328	1006	3
OTOS	6	0.014823	0.045395	1007	4
B3GAT3	6	0.014825	0.045399	1014	2
UBA1	6	0.014825	0.045399	1013	2
CCT7	6	0.014825	0.045399	1009	2
AP2B1	6	0.014825	0.045399	1010	1
SIGLEC5	6	0.014825	0.045399	1016	1
CYP2E1	6	0.014825	0.045399	1008	2
NRARP	6	0.014825	0.045399	1015	2
FDXACB1	6	0.014825	0.045399	1011	2
PRPF40A	6	0.014825	0.045399	1012	3
hsa-mir-760	4	0.0149	0.045611	1017	2
TNFRSF1B	6	0.014901	0.045616	1018	3
BAX	6	0.014906	0.045626	1019	4
ATG5	6	0.014952	0.045754	1020	3
ISM1	6	0.014972	0.045807	1021	4
ATP6V1D	6	0.014978	0.045826	1022	4
HDHD2	6	0.014981	0.045829	1023	2
hsa-mir-182	4	0.015013	0.045918	1024	2

SLC9A2	6	0.015021	0.045941	1025	3
RBM28	6	0.015048	0.046015	1026	3
ZNF99	6	0.015053	0.04603	1027	4
ZNF426	6	0.015081	0.046099	1028	3
RSAD2	6	0.015099	0.046141	1030	4
hsa-mir-4476	4	0.015099	0.046141	1029	3
HMX1	6	0.015101	0.046148	1031	2
CXorf57	6	0.015102	0.04615	1033	4
TSTD1	6	0.015102	0.04615	1032	4
UNC13A	6	0.015128	0.046215	1034	3
KRBA1	6	0.015156	0.046285	1035	3
TMEM117	6	0.015177	0.046339	1036	3
PRG3	6	0.015197	0.046381	1037	3
TDP2	6	0.015246	0.046517	1038	1
LDB1	6	0.015258	0.046549	1039	3
FXYD7	6	0.015272	0.046597	1040	4
MOSPD2	6	0.015296	0.046655	1041	2
WFDC6	4	0.01533	0.046747	1042	1
hsa-mir-184	4	0.015349	0.046794	1043	3
hsa-mir-4495	2	0.015356	0.046809	1044	2
BOP1	6	0.015377	0.046868	1045	4
ARMC5	6	0.015382	0.046885	1046	3
DLX1	6	0.015383	0.046889	1047	4
MRPL12	6	0.015395	0.046918	1048	1
ANKRD33B	6	0.015409	0.046961	1049	3
TXNDC9	6	0.015441	0.047046	1050	3
OR51I2	6	0.015444	0.047054	1052	3
HMGCS2	6	0.015444	0.047054	1051	4
CCDC25	6	0.015494	0.047177	1053	2
TAF6L	6	0.015544	0.047316	1054	3
C2CD2	6	0.015577	0.047419	1055	3
MECOM	6	0.015616	0.047515	1056	4
KIAA0020	6	0.015643	0.047584	1058	2
LPAR4	6	0.015643	0.047584	1057	2
ZAR1	6	0.015643	0.047584	1059	2
TCEAL3	6	0.015656	0.047617	1060	3
hsa-mir-153-2	3	0.015676	0.047669	1061	2
DUSP14	6	0.01568	0.047682	1062	3
ZNF589	6	0.015691	0.04771	1063	3
SPATA31E1	6	0.0157	0.04773	1064	3
AMPD1	6	0.015742	0.047838	1065	3
CTAGE1	6	0.015791	0.047962	1066	2
ABHD17C	6	0.015803	0.04799	1067	4
SMCHD1	6	0.015833	0.04806	1068	3
ST8SIA1	6	0.015874	0.04817	1069	4
LRSAM1	6	0.015891	0.04821	1070	2
CASQ2	6	0.01595	0.048349	1071	4
SERPINF2	6	0.015974	0.048408	1072	3
CCDC68	6	0.015984	0.048428	1073	4
ZCCHC2	6	0.01599	0.048445	1074	3
SCAP	6	0.016004	0.048483	1075	2
hsa-let-7e	4	0.016025	0.04854	1076	1
NBAS	6	0.016039	0.04858	1077	3
HEMK1	6	0.016053	0.04861	1078	2
LRIG2	6	0.016053	0.04861	1079	3
TMEM66	6	0.016055	0.048614	1080	4
NOX4	6	0.016061	0.048628	1081	3
TSPAN4	6	0.016067	0.048643	1082	4
RAD9B	6	0.016089	0.048703	1083	2
OR5C1	6	0.016092	0.048712	1084	3
DLGAP5	6	0.016094	0.048715	1085	3
ABHD12	6	0.016109	0.048754	1086	4
TMEM120B	6	0.016138	0.048834	1087	2
LINGO3	6	0.016146	0.048853	1088	3
ABI1	6	0.016147	0.048854	1089	3
ARHGAP25	6	0.016188	0.048954	1090	2
UBXN8	6	0.016196	0.048972	1091	2
SETDB1	6	0.016204	0.048992	1092	4
TRIM43B	6	0.016222	0.04904	1093	3
OGN	6	0.016224	0.049044	1094	3
PKN1	6	0.016237	0.049077	1095	2
ENTPD5	6	0.016241	0.049087	1096	3
ERCC8	6	0.016281	0.049201	1097	4
SCGB1D2	6	0.016282	0.049205	1098	2
LIPN	6	0.016286	0.049214	1099	4
PRCD	6	0.016294	0.049234	1100	4
MBNL3	6	0.016319	0.049291	1101	4
OR13A1	6	0.016322	0.0493	1102	3
MAGEE2	6	0.016336	0.049338	1103	4
PEA15	6	0.016337	0.049339	1104	4
ESD	6	0.016359	0.049396	1105	4
CPEB1	6	0.016386	0.049462	1106	1
ITPKC	6	0.016386	0.049462	1107	4
SIGLEC8	6	0.016478	0.049679	1108	3
CROT	6	0.016485	0.049693	1109	2
FGFBP3	6	0.016521	0.049788	1110	4
SERPINB7	6	0.016539	0.049834	1111	2
PODXL2	6	0.016562	0.049884	1112	4
ATP6V1H	6	0.016584	0.049944	1113	3
NonTargetingControlGuideForHuman_0409	1	0.016595	0.049979	1114	1
UBE2U	6	0.0166	0.049986	1115	4
hsa-mir-4479	4	0.016606	0.050002	1116	3

References

ABDERRAZAK, A., COUCHIE, D., DARWEESH MAHMOOD, D. F., ELHAGE, R., VINDIS, C., LAFFARGUE, M., MATEO, V., BUCHELE, B., AYALA, M. R., GAAFARY, M. E., SYROVETS, T., SLIMANE, M. N., FRIGUET, B., FULOP, T., SIMMET, T., HADRI, K. E. & ROUIS, M. 2015. Response to Letter Regarding Article, "Anti-inflammatory and Antiatherogenic Effects of the Inflammasome NLRP3 Inhibitor Arglabin in ApoE2.Ki Mice Fed a High-Fat Diet". *Circulation,* 132**,** e250-1.

AHMED, S., MEGHJI, S., WILLIAMS, R. J., HENDERSON, B., BROCK, J. H. & NAIR, S. P. 2001. Staphylococcus aureus fibronectin binding proteins are essential for internalization by osteoblasts but do not account for differences in intracellular levels of bacteria. *Infect Immun,* 69**,** 2872-7.

AITS, S., KRICKER, J., LIU, B., ELLEGAARD, A. M., HAMALISTO, S., TVINGSHOLM, S., CORCELLE-TERMEAU, E., HOGH, S., FARKAS, T., HOLM JONASSEN, A., GROMOVA, I., MORTENSEN, M. & JAATTELA, M. 2015. Sensitive detection of lysosomal membrane permeabilization by lysosomal galectin puncta assay. *Autophagy,* 11**,** 1408-24.

ALEMU, E. A., LAMARK, T., TORGERSEN, K. M., BIRGISDOTTIR, A. B., LARSEN, K. B., JAIN, A., OLSVIK, H., OVERVATN, A., KIRKIN, V. & JOHANSEN, T. 2012. ATG8 family proteins act as scaffolds for assembly of the ULK complex: sequence requirements for LC3-interacting region (LIR) motifs. *J Biol Chem,* 287**,** 39275-90.

ALIBAYOV, B., BABA-MOUSSA, L., SINA, H., ZDENKOVA, K. & DEMNEROVA, K. 2014. Staphylococcus aureus mobile genetic elements. *Mol Biol Rep,* 41**,** 5005-18.

ALIX, E., MUKHERJEE, S. & ROY, C. R. 2011. Subversion of membrane transport pathways by vacuolar pathogens. *J Cell Biol,* 195**,** 943-52.

ALVA-MURILLO, N., LOPEZ-MEZA, J. E. & OCHOA-ZARZOSA, A. 2014. Nonprofessional phagocytic cell receptors involved in Staphylococcus aureus internalization. *Biomed Res Int,* 2014**,** 538546.

AMER, A. O. & SWANSON, M. S. 2005. Autophagy is an immediate macrophage response to Legionella pneumophila. *Cell Microbiol,* 7**,** 765-78.

ANDERS, S. & HUBER, W. 2010. Differential expression analysis for sequence count data. *Genome Biol,* 11**,** R106.

ARROYO, J. D., JOURDAIN, A. A., CALVO, S. E., BALLARANO, C. A., DOENCH, J. G., ROOT, D. E. & MOOTHA, V. K. 2016. A Genome-wide CRISPR Death Screen Identifies Genes Essential for Oxidative Phosphorylation. *Cell Metab,* 24**,** 875-885.

ASHFORD, T. P. & PORTER, K. R. 1962. Cytoplasmic components in hepatic cell lysosomes. *J Cell Biol,* 12**,** 198-202.

ASHIDA, H., KIM, M. & SASAKAWA, C. 2014. Exploitation of the host ubiquitin system by human bacterial pathogens. *Nat Rev Microbiol,* 12**,** 399-413.

AXE, E. L., WALKER, S. A., MANIFAVA, M., CHANDRA, P., RODERICK, H. L., HABERMANN, A., GRIFFITHS, G. & KTISTAKIS, N. T. 2008. Autophagosome formation from membrane compartments enriched in phosphatidylinositol 3-phosphate and dynamically connected to the endoplasmic reticulum. *The Journal of Cell Biology,* 182**,** 685-701.

BANDYOPADHYAY, U., KAUSHIK, S., VARTICOVSKI, L. & CUERVO, A. M. 2008. The chaperone-mediated autophagy receptor organizes in dynamic protein complexes at the lysosomal membrane. *Mol Cell Biol,* 28**,** 5747-63.

BARNETT, T. C., LIEBL, D., SEYMOUR, L. M., GILLEN, C. M., LIM, J. Y., LAROCK, C. N., DAVIES, M. R., SCHULZ, B. L., NIZET, V., TEASDALE, R. D. & WALKER, M. J. 2013. The globally

disseminated M1T1 clone of group A Streptococcus evades autophagy for intracellular replication. *Cell Host Microbe,* 14**,** 675-82.

BARRANGOU, R., FREMAUX, C., DEVEAU, H., RICHARDS, M., BOYAVAL, P., MOINEAU, S., ROMERO, D. A. & HORVATH, P. 2007. CRISPR provides acquired resistance against viruses in prokaryotes. *Science,* 315**,** 1709-12.

BARRY, A. O., BOUCHERIT, N., MOTTOLA, G., VADOVIC, P., TROUPLIN, V., SOUBEYRAN, P., CAPO, C., BONATTI, S., NEBREDA, A., TOMAN, R., LEMICHEZ, E., MEGE, J. L. & GHIGO, E. 2012. Impaired stimulation of p38alpha-MAPK/Vps41-HOPS by LPS from pathogenic Coxiella burnetii prevents trafficking to microbicidal phagolysosomes. *Cell Host Microbe,* 12**,** 751-63.

BAUMANN, V., LORENZER, C., THELL, M., WINKLER, A. M. & WINKLER, J. 2017. RNAi-Mediated Knockdown of Protein Expression. *Methods Mol Biol,* 1654**,** 351-360.

BAYLES, K. W., WESSON, C. A., LIOU, L. E., FOX, L. K., BOHACH, G. A. & TRUMBLE, W. R. 1998. Intracellular Staphylococcus aureus escapes the endosome and induces apoptosis in epithelial cells. *Infect Immun,* 66**,** 336-42.

BEGUN, J., LASSEN, K. G., JIJON, H. B., BAXT, L. A., GOEL, G., HEATH, R. J., NG, A., TAM, J. M., KUO, S. Y., VILLABLANCA, E. J., FAGBAMI, L., OOSTING, M., KUMAR, V., SCHENONE, M., CARR, S. A., JOOSTEN, L. A., VYAS, J. M., DALY, M. J., NETEA, M. G., BROWN, G. D., WIJMENGA, C. & XAVIER, R. J. 2015. Integrated Genomics of Crohn's Disease Risk Variant Identifies a Role for CLEC12A in Antibacterial Autophagy. *Cell Rep,* 11**,** 1905-18.

BENTO, C. F., RENNA, M., GHISLAT, G., PURI, C., ASHKENAZI, A., VICINANZA, M., MENZIES, F. M. & RUBINSZTEIN, D. C. 2016. Mammalian Autophagy: How Does It Work? *Annu Rev Biochem,* 85**,** 685-713.

BERON, W., GUTIERREZ, M. G., RABINOVITCH, M. & COLOMBO, M. I. 2002. Coxiella burnetii localizes in a Rab7-labeled compartment with autophagic characteristics. *Infect Immun,* 70**,** 5816-21.

BEUZON, C. R., MERESSE, S., UNSWORTH, K. E., RUIZ-ALBERT, J., GARVIS, S., WATERMAN, S. R., RYDER, T. A., BOUCROT, E. & HOLDEN, D. W. 2000. Salmonella maintains the integrity of its intracellular vacuole through the action of SifA. *Embo j,* 19**,** 3235-49.

BIRMINGHAM, C. L., CANADIEN, V., KANIUK, N. A., STEINBERG, B. E., HIGGINS, D. E. & BRUMELL, J. H. 2008. Listeriolysin O allows Listeria monocytogenes replication in macrophage vacuoles. *Nature,* 451**,** 350-4.

BIRMINGHAM, C. L., JIANG, X., OHLSON, M. B., MILLER, S. I. & BRUMELL, J. H. 2005. Salmonella-induced filament formation is a dynamic phenotype induced by rapidly replicating Salmonella enterica serovar typhimurium in epithelial cells. *Infect Immun,* 73**,** 1204-8.

BIRMINGHAM, C. L., SMITH, A. C., BAKOWSKI, M. A., YOSHIMORI, T. & BRUMELL, J. H. 2006. Autophagy controls Salmonella infection in response to damage to the Salmonella-containing vacuole. *J Biol Chem,* 281**,** 11374-83.

BOKOCH, G. M. 2005. Regulation of innate immunity by Rho GTPases. *Trends Cell Biol,* 15**,** 163-71.

BOWMAN, L., ZEDEN, M. S., SCHUSTER, C. F., KAEVER, V. & GRUNDLING, A. 2016. New Insights into the Cyclic Di-adenosine Monophosphate (c-di-AMP) Degradation Pathway and the Requirement of the Cyclic Dinucleotide for Acid Stress Resistance in Staphylococcus aureus. *J Biol Chem,* 291**,** 26970-26986.

BROWN, E. L., WOOTEN, R. M., JOHNSON, B. J., IOZZO, R. V., SMITH, A., DOLAN, M. C., GUO, B. P., WEIS, J. J. & HOOK, M. 2001. Resistance to Lyme disease in decorin-deficient mice. *J Clin Invest,* 107**,** 845-52.

BROWN, N. F., VALLANCE, B. A., COOMBES, B. K., VALDEZ, Y., COBURN, B. A. & FINLAY, B. B. 2005. Salmonella pathogenicity island 2 is expressed prior to penetrating the intestine. *PLoS Pathog,* 1**,** e32.

BRUMELL, J. H. & GRINSTEIN, S. 2004. Salmonella redirects phagosomal maturation. *Curr Opin Microbiol,* 7**,** 78-84.

BRUMELL, J. H., STEELE-MORTIMER, O. & FINLAY, B. B. 1999. Bacterial invasion: Force feeding by Salmonella. *Curr Biol,* 9**,** R277-80.

BRUMELL, J. H., TANG, P., MILLS, S. D. & FINLAY, B. B. 2001. Characterization of Salmonella-induced filaments (Sifs) reveals a delayed interaction between Salmonella-containing vacuoles and late endocytic compartments. *Traffic,* 2**,** 643-53.

BRUMELL, J. H., TANG, P., ZAHARIK, M. L. & FINLAY, B. B. 2002. Disruption of the Salmonella-containing vacuole leads to increased replication of Salmonella enterica serovar typhimurium in the cytosol of epithelial cells. *Infect Immun,* 70**,** 3264-70.

BUCHMEIER, N. A. & HEFFRON, F. 1991. Inhibition of macrophage phagosome-lysosome fusion by Salmonella typhimurium. *Infect Immun,* 59**,** 2232-8.

CAMPOY, E. & COLOMBO, M. I. 2009. Autophagy in intracellular bacterial infection. *Biochim Biophys Acta,* 1793**,** 1465-77.

CANTALUPO, G., ALIFANO, P., ROBERTI, V., BRUNI, C. B. & BUCCI, C. 2001. Rab-interacting lysosomal protein (RILP): the Rab7 effector required for transport to lysosomes. *Embo j,* 20**,** 683-93.

CEMMA, M. & BRUMELL, J. H. 2012. Interactions of pathogenic bacteria with autophagy systems. *Curr Biol,* 22**,** R540-5.

CEMMA, M., KIM, P. K. & BRUMELL, J. H. 2011. The ubiquitin-binding adaptor proteins p62/SQSTM1 and NDP52 are recruited independently to bacteria-associated microdomains to target Salmonella to the autophagy pathway. *Autophagy,* 7**,** 341-5.

CHA-MOLSTAD, H., YU, J. E., FENG, Z., LEE, S. H., KIM, J. G., YANG, P., HAN, B., SUNG, K. W., YOO, Y. D., HWANG, J., MCGUIRE, T., SHIM, S. M., SONG, H. D., GANIPISETTI, S., WANG, N., JANG, J. M., LEE, M. J., KIM, S. J., LEE, K. H., HONG, J. T., CIECHANOVER, A., MOOK-JUNG, I., KIM, K. P., XIE, X. Q., KWON, Y. T. & KIM, B. Y. 2017. p62/SQSTM1/Sequestosome-1 is an N-recognin of the N-end rule pathway which modulates autophagosome biogenesis. *Nat Commun,* 8**,** 102.

CHAN, E. Y., KIR, S. & TOOZE, S. A. 2007. siRNA screening of the kinome identifies ULK1 as a multidomain modulator of autophagy. *J Biol Chem,* 282**,** 25464-74.

CHAN, E. Y., LONGATTI, A., MCKNIGHT, N. C. & TOOZE, S. A. 2009. Kinase-inactivated ULK proteins inhibit autophagy via their conserved C-terminal domains using an Atg13-independent mechanism. *Mol Cell Biol,* 29**,** 157-71.

CHATTERJEE, S. S. & OTTO, M. 2013. Improved understanding of factors driving methicillin-resistant Staphylococcus aureus epidemic waves. *Clin Epidemiol,* 5**,** 205-17.

CHAUHAN, S., KUMAR, S., JAIN, A., PONPUAK, M., MUDD, M. H., KIMURA, T., CHOI, S. W., PETERS, R., MANDELL, M., BRUUN, J. A., JOHANSEN, T. & DERETIC, V. 2016. TRIMs and Galectins Globally Cooperate and TRIM16 and Galectin-3 Co-direct Autophagy in Endomembrane Damage Homeostasis. *Dev Cell,* 39**,** 13-27.

CHAUHAN, S., MANDELL, M. A. & DERETIC, V. 2015. IRGM governs the core autophagy machinery to conduct antimicrobial defense. *Mol Cell,* 58**,** 507-21.

CHEN, S., SANJANA, N. E., ZHENG, K., SHALEM, O., LEE, K., SHI, X., SCOTT, D. A., SONG, J., PAN, J. Q., WEISSLEDER, R., LEE, H., ZHANG, F. & SHARP, P. A. 2015. Genome-wide CRISPR screen in a mouse model of tumor growth and metastasis. *Cell,* 160**,** 1246-60.

CHEN, Y., HE, J., TIAN, M., ZHANG, S. Y., GUO, M. R., KASIMU, R., WANG, J. H. & OUYANG, L. 2014. UNC51-like kinase 1, autophagic regulator and cancer therapeutic target. *Cell Prolif,* 47**,** 494-505.

CHOY, A., DANCOURT, J., MUGO, B., O'CONNOR, T. J., ISBERG, R. R., MELIA, T. J. & ROY, C. R. 2012. The Legionella effector RavZ inhibits host autophagy through irreversible Atg8 deconjugation. *Science,* 338**,** 1072-6.

COHEN, T. S. & PRINCE, A. S. 2013. Activation of inflammasome signaling mediates pathology of acute P. aeruginosa pneumonia. *J Clin Invest,* 123**,** 1630-7.

CONG, L., RAN, F. A., COX, D., LIN, S., BARRETTO, R., HABIB, N., HSU, P. D., WU, X., JIANG, W., MARRAFFINI, L. A. & ZHANG, F. 2013. Multiplex genome engineering using CRISPR/Cas systems. *Science,* 339**,** 819-23.

COONEY, R., BAKER, J., BRAIN, O., DANIS, B., PICHULIK, T., ALLAN, P., FERGUSON, D. J., CAMPBELL, B. J., JEWELL, D. & SIMMONS, A. 2010. NOD2 stimulation induces autophagy in dendritic cells influencing bacterial handling and antigen presentation. *Nat Med,* 16**,** 90-7.

CORNEJO, E., SCHLAERMANN, P. & MUKHERJEE, S. 2017. How to rewire the host cell: A home improvement guide for intracellular bacteria. *J Cell Biol,* 216**,** 3931-3948.

CRISS, A. K. & CASANOVA, J. E. 2003. Coordinate regulation of Salmonella enterica serovar Typhimurium invasion of epithelial cells by the Arp2/3 complex and Rho GTPases. *Infect Immun,* 71**,** 2885-91.

DAVIS, B. K., WEN, H. & TING, J. P. 2011. The inflammasome NLRs in immunity, inflammation, and associated diseases. *Annu Rev Immunol,* 29**,** 707-35.

DE DUVE, C. & WATTIAUX, R. 1966. Functions of lysosomes. *Annu Rev Physiol,* 28**,** 435-92.

DELGADO, M., SINGH, S., DE HARO, S., MASTER, S., PONPUAK, M., DINKINS, C., ORNATOWSKI, W., VERGNE, I. & DERETIC, V. 2009. Autophagy and pattern recognition receptors in innate immunity. *Immunol Rev,* 227**,** 189-202.

DELL'ANGELICA, E. C. 2009. AP-3-dependent trafficking and disease: the first decade. *Curr Opin Cell Biol,* 21**,** 552-9.

DENG, Q., WANG, Y., ZHANG, Y., LI, M., LI, D., HUANG, X., WU, Y., PU, J. & WU, M. 2016. Pseudomonas aeruginosa Triggers Macrophage Autophagy To Escape Intracellular Killing by Activation of the NLRP3 Inflammasome. *Infect Immun,* 84**,** 56-66.

DEOSARAN, E., LARSEN, K. B., HUA, R., SARGENT, G., WANG, Y., KIM, S., LAMARK, T., JAUREGUI, M., LAW, K., LIPPINCOTT-SCHWARTZ, J., BRECH, A., JOHANSEN, T. & KIM, P. K. 2013. NBR1 acts as an autophagy receptor for peroxisomes. *J Cell Sci,* 126**,** 939-52.

DERETIC, V. 2008. Autophagy, an immunologic magic bullet: Mycobacterium tuberculosis phagosome maturation block and how to bypass it. *Future Microbiol,* 3**,** 517-24.

DERETIC, V. 2012. Autophagy as an innate immunity paradigm: expanding the scope and repertoire of pattern recognition receptors. *Curr Opin Immunol,* 24**,** 21-31.

DEVENISH, R. J. & LAI, S. C. 2015. Autophagy and burkholderia. *Immunol Cell Biol,* 93**,** 18-24.

DHANOA, B. S., COGLIATI, T., SATISH, A. G., BRUFORD, E. A. & FRIEDMAN, J. S. 2013. Update on the Kelch-like (KLHL) gene family. *Hum Genomics,* 7**,** 13.

DI BARTOLOMEO, S., CORAZZARI, M., NAZIO, F., OLIVERIO, S., LISI, G., ANTONIOLI, M., PAGLIARINI, V., MATTEONI, S., FUOCO, C., GIUNTA, L., D'AMELIO, M., NARDACCI, R.,

ROMAGNOLI, A., PIACENTINI, M., CECCONI, F. & FIMIA, G. M. 2010. The dynamic interaction of AMBRA1 with the dynein motor complex regulates mammalian autophagy. *J Cell Biol,* 191**,** 155-68.

DOOLEY, H. C., RAZI, M., POLSON, H. E., GIRARDIN, S. E., WILSON, M. I. & TOOZE, S. A. 2014. WIPI2 links LC3 conjugation with PI3P, autophagosome formation, and pathogen clearance by recruiting Atg12-5-16L1. *Mol Cell,* 55**,** 238-52.

DORN, B. R., DUNN, W. A. & PROGULSKE-FOX, A. 2001. Porphyromonas gingivalis Traffics to Autophagosomes in Human Coronary Artery Endothelial Cells. *Infection and Immunity,* 69**,** 5698-5708.

DORTET, L., MOSTOWY, S., SAMBA-LOUAKA, A., GOUIN, E., NAHORI, M. A., WIEMER, E. A., DUSSURGET, O. & COSSART, P. 2011. Recruitment of the major vault protein by InlK: a Listeria monocytogenes strategy to avoid autophagy. *PLoS Pathog,* 7**,** e1002168.

DOYONNAS, R., YI-HSIN CHAN, J., BUTLER, L. H., RAPPOLD, I., LEE-PRUDHOE, J. E., ZANNETTINO, A. C. W., SIMMONS, P. J., BUHRING, H. J., LEVESQUE, J. P. & WATT, S. M. 2000. CD164 Monoclonal Antibodies That Block Hemopoietic Progenitor Cell Adhesion and Proliferation Interact with the First Mucin Domain of the CD164 Receptor. *The Journal of Immunology,* 165**,** 840-851.

DUPONT, N., LACAS-GERVAIS, S., BERTOUT, J., PAZ, I., FRECHE, B., VAN NHIEU, G. T., VAN DER GOOT, F. G., SANSONETTI, P. J. & LAFONT, F. 2009. Shigella phagocytic vacuolar membrane remnants participate in the cellular response to pathogen invasion and are regulated by autophagy. *Cell Host Microbe,* 6**,** 137-49.

EDWARDS, A. M., POTTS, J. R., JOSEFSSON, E. & MASSEY, R. C. 2010. Staphylococcus aureus host cell invasion and virulence in sepsis is facilitated by the multiple repeats within FnBPA. *PLoS Pathog,* 6**,** e1000964.

EFEYAN, A., ZONCU, R., CHANG, S., GUMPER, I., SNITKIN, H., WOLFSON, R. L., KIRAK, O., SABATINI, D. D. & SABATINI, D. M. 2013. Regulation of mTORC1 by the Rag GTPases is necessary for neonatal autophagy and survival. *Nature,* 493**,** 679-83.

EGAN, D. F., CHUN, M. G., VAMOS, M., ZOU, H., RONG, J., MILLER, C. J., LOU, H. J., RAVEENDRA-PANICKAR, D., YANG, C. C., SHEFFLER, D. J., TERIETE, P., ASARA, J. M., TURK, B. E., COSFORD, N. D. & SHAW, R. J. 2015. Small Molecule Inhibition of the Autophagy Kinase ULK1 and Identification of ULK1 Substrates. *Mol Cell,* 59**,** 285-97.

EGAN, D. F., SHACKELFORD, D. B., MIHAYLOVA, M. M., GELINO, S., KOHNZ, R. A., MAIR, W., VASQUEZ, D. S., JOSHI, A., GWINN, D. M., TAYLOR, R., ASARA, J. M., FITZPATRICK, J., DILLIN, A., VIOLLET, B., KUNDU, M., HANSEN, M. & SHAW, R. J. 2011. Phosphorylation of ULK1 (hATG1) by AMP-activated protein kinase connects energy sensing to mitophagy. *Science,* 331**,** 456-61.

FABREGA, A. & VILA, J. 2013. Salmonella enterica serovar Typhimurium skills to succeed in the host: virulence and regulation. *Clin Microbiol Rev,* 26**,** 308-41.

FAHMI, T., PORT, G. C. & CHO, K. H. 2017. c-di-AMP: An Essential Molecule in the Signaling Pathways that Regulate the Viability and Virulence of Gram-Positive Bacteria. *Genes (Basel),* 8.

FASIHI, Y., SAFFARI, F., MANSOURI, S. & KALANTAR-NEYESTANAKI, D. 2017. The emergence of vancomycin-resistant Staphylococcus aureus in an intensive care unit in Kerman, Iran. *Wien Med Wochenschr*.

FILOMENI, G., DE ZIO, D. & CECCONI, F. 2015. Oxidative stress and autophagy: the clash between damage and metabolic needs. *Cell Death Differ,* 22**,** 377-88.

FISKIN, E., BIONDA, T., DIKIC, I. & BEHRENDS, C. 2016. Global Analysis of Host and Bacterial Ubiquitinome in Response to Salmonella Typhimurium Infection. *Mol Cell,* 62**,** 967-981.

FONTAYNE, A., DANG, P. M., GOUGEROT-POCIDALO, M. A. & EL-BENNA, J. 2002. Phosphorylation of p47phox sites by PKC alpha, beta II, delta, and zeta: effect on binding to p22phox and on NADPH oxidase activation. *Biochemistry,* 41**,** 7743-50.

FORDE, S., TYE, B. J., NEWEY, S. E., ROUBELAKIS, M., SMYTHE, J., MCGUCKIN, C. P., PETTENGELL, R. & WATT, S. M. 2007. Endolyn (CD164) modulates the CXCL12-mediated migration of umbilical cord blood CD133+ cells. *Blood,* 109**,** 1825-33.

FOSTER, T. J. 2004. The Staphylococcus aureus "superbug". *J Clin Invest,* 114**,** 1693-6.

FRANCHI, L., AMER, A., BODY-MALAPEL, M., KANNEGANTI, T. D., OZOREN, N., JAGIRDAR, R., INOHARA, N., VANDENABEELE, P., BERTIN, J., COYLE, A., GRANT, E. P. & NUNEZ, G. 2006. Cytosolic flagellin requires Ipaf for activation of caspase-1 and interleukin 1beta in salmonella-infected macrophages. *Nat Immunol,* 7**,** 576-82.

FRAUNHOLZ, M. & SINHA, B. 2012. Intracellular Staphylococcus aureus: live-in and let die. *Front Cell Infect Microbiol,* 2**,** 43.

FUJITA, N., HAYASHI-NISHINO, M., FUKUMOTO, H., OMORI, H., YAMAMOTO, A., NODA, T. & YOSHIMORI, T. 2008. An Atg4B mutant hampers the lipidation of LC3 paralogues and causes defects in autophagosome closure. *Mol Biol Cell,* 19**,** 4651-9.

FUJITA, N., MORITA, E., ITOH, T., TANAKA, A., NAKAOKA, M., OSADA, Y., UMEMOTO, T., SAITOH, T., NAKATOGAWA, H., KOBAYASHI, S., HARAGUCHI, T., GUAN, J. L., IWAI, K., TOKUNAGA, F., SAITO, K., ISHIBASHI, K., AKIRA, S., FUKUDA, M., NODA, T. & YOSHIMORI, T. 2013. Recruitment of the autophagic machinery to endosomes during infection is mediated by ubiquitin. *J Cell Biol,* 203**,** 115-28.

GALLAGHER, L. E., RADHI, O. A., ABDULLAH, M. O., MCCLUSKEY, A. G., BOYD, M. & CHAN, E. Y. W. 2017. Lysosomotropism depends on glucose: a chloroquine resistance mechanism. *Cell Death Dis,* 8**,** e3014.

GALLAGHER, L. E., WILLIAMSON, L. E. & CHAN, E. Y. 2016. Advances in Autophagy Regulatory Mechanisms. *Cells,* 5.

GALLUZZI, L., BAEHRECKE, E. H., BALLABIO, A., BOYA, P., BRAVO-SAN PEDRO, J. M., CECCONI, F., CHOI, A. M., CHU, C. T., CODOGNO, P., COLOMBO, M. I., CUERVO, A. M., DEBNATH, J., DERETIC, V., DIKIC, I., ESKELINEN, E. L., FIMIA, G. M., FULDA, S., GEWIRTZ, D. A., GREEN, D. R., HANSEN, M., HARPER, J. W., JAATTELA, M., JOHANSEN, T., JUHASZ, G., KIMMELMAN, A. C., KRAFT, C., KTISTAKIS, N. T., KUMAR, S., LEVINE, B., LOPEZ-OTIN, C., MADEO, F., MARTENS, S., MARTINEZ, J., MELENDEZ, A., MIZUSHIMA, N., MUNZ, C., MURPHY, L. O., PENNINGER, J. M., PIACENTINI, M., REGGIORI, F., RUBINSZTEIN, D. C., RYAN, K. M., SANTAMBROGIO, L., SCORRANO, L., SIMON, A. K., SIMON, H. U., SIMONSEN, A., TAVERNARAKIS, N., TOOZE, S. A., YOSHIMORI, T., YUAN, J., YUE, Z., ZHONG, Q. & KROEMER, G. 2017. Molecular definitions of autophagy and related processes. *Embo j,* 36**,** 1811-1836.

GANLEY, I. G., LAM DU, H., WANG, J., DING, X., CHEN, S. & JIANG, X. 2009. ULK1.ATG13.FIP200 complex mediates mTOR signaling and is essential for autophagy. *J Biol Chem,* 284**,** 12297-305.

GARCIA-DEL PORTILLO, F., ZWICK, M. B., LEUNG, K. Y. & FINLAY, B. B. 1993. Salmonella induces the formation of filamentous structures containing lysosomal membrane glycoproteins in epithelial cells. *Proc Natl Acad Sci U S A,* 90**,** 10544-8.

GARZONI, C. & KELLEY, W. L. 2009. Staphylococcus aureus: new evidence for intracellular persistence. *Trends Microbiol,* 17**,** 59-65.

GELINO, S. & HANSEN, M. 2012. Autophagy - An Emerging Anti-Aging Mechanism. *J Clin Exp Pathol,* Suppl 4.

GENG, J., BABA, M., NAIR, U. & KLIONSKY, D. J. 2008. Quantitative analysis of autophagy-related protein stoichiometry by fluorescence microscopy. *J Cell Biol,* 182**,** 129-40.

GOBERDHAN, D. C., WILSON, C. & HARRIS, A. L. 2016. Amino Acid Sensing by mTORC1: Intracellular Transporters Mark the Spot. *Cell Metab,* 23**,** 580-9.

GOMES, L. C. & DIKIC, I. 2014. Autophagy in antimicrobial immunity. *Mol Cell,* 54**,** 224-33.

GORDON, R. J. & LOWY, F. D. 2008. Pathogenesis of methicillin-resistant Staphylococcus aureus infection. *Clin Infect Dis,* 46 Suppl 5**,** S350-9.

GRESHAM, H. D., LOWRANCE, J. H., CAVER, T. E., WILSON, B. S., CHEUNG, A. L. & LINDBERG, F. P. 2000. Survival of Staphylococcus aureus Inside Neutrophils Contributes to Infection. *The Journal of Immunology,* 164**,** 3713-3722.

GROSZ, M., KOLTER, J., PAPROTKA, K., WINKLER, A. C., SCHAFER, D., CHATTERJEE, S. S., GEIGER, T., WOLZ, C., OHLSEN, K., OTTO, M., RUDEL, T., SINHA, B. & FRAUNHOLZ, M. 2014. Cytoplasmic replication of Staphylococcus aureus upon phagosomal escape triggered by phenol-soluble modulin alpha. *Cell Microbiol,* 16**,** 451-65.

GUINEY, D. G. 2005. The role of host cell death in Salmonella infections. *Curr Top Microbiol Immunol,* 289**,** 131-50.

GUO, W., SUN, Y., LIU, W., WU, X., GUO, L., CAI, P., WU, X., WU, X., SHEN, Y., SHU, Y., GU, Y. & XU, Q. 2014. Small molecule-driven mitophagy-mediated NLRP3 inflammasome inhibition is responsible for the prevention of colitis-associated cancer. *Autophagy,* 10**,** 972-85.

GUTIERREZ, M. G., MASTER, S. S., SINGH, S. B., TAYLOR, G. A., COLOMBO, M. I. & DERETIC, V. 2004. Autophagy is a defense mechanism inhibiting BCG and Mycobacterium tuberculosis survival in infected macrophages. *Cell,* 119**,** 753-66.

GWINN, D. M., SHACKELFORD, D. B., EGAN, D. F., MIHAYLOVA, M. M., MERY, A., VASQUEZ, D. S., TURK, B. E. & SHAW, R. J. 2008. AMPK phosphorylation of raptor mediates a metabolic checkpoint. *Mol Cell,* 30**,** 214-26.

HAILEY, D. W., RAMBOLD, A. S., SATPUTE-KRISHNAN, P., MITRA, K., SOUGRAT, R., KIM, P. K. & LIPPINCOTT-SCHWARTZ, J. 2010. Mitochondria supply membranes for autophagosome biogenesis during starvation. *Cell,* 141**,** 656-67.

HAIM, M., TROST, A., MAIER, C. J., ACHATZ, G., FEICHTNER, S., HINTNER, H., BAUER, J. W. & ONDER, K. 2010. Cytokeratin 8 interacts with clumping factor B: a new possible virulence factor target. *Microbiology,* 156**,** 3710-21.

HAMASAKI, M., FURUTA, N., MATSUDA, A., NEZU, A., YAMAMOTO, A., FUJITA, N., OOMORI, H., NODA, T., HARAGUCHI, T., HIRAOKA, Y., AMANO, A. & YOSHIMORI, T. 2013. Autophagosomes form at ER-mitochondria contact sites. *Nature,* 495**,** 389-93.

HAMZA, T. & LI, B. 2014. Differential responses of osteoblasts and macrophages upon Staphylococcus aureus infection. *BMC Microbiol,* 14**,** 207.

HANADA, T., NODA, N. N., SATOMI, Y., ICHIMURA, Y., FUJIOKA, Y., TAKAO, T., INAGAKI, F. & OHSUMI, Y. 2007. The Atg12-Atg5 conjugate has a novel E3-like activity for protein lipidation in autophagy. *J Biol Chem,* 282**,** 37298-302.

HARA, T., TAKAMURA, A., KISHI, C., IEMURA, S., NATSUME, T., GUAN, J. L. & MIZUSHIMA, N. 2008. FIP200, a ULK-interacting protein, is required for autophagosome formation in mammalian cells. *J Cell Biol,* 181**,** 497-510.

HARAGA, A., OHLSON, M. B. & MILLER, S. I. 2008. Salmonellae interplay with host cells. *Nat Rev Microbiol,* 6**,** 53-66.

HARDT, W. D., CHEN, L. M., SCHUEBEL, K. E., BUSTELO, X. R. & GALAN, J. E. 1998. S. typhimurium encodes an activator of Rho GTPases that induces membrane ruffling and nuclear responses in host cells. *Cell,* 93**,** 815-26.

HARNETT, M. M., PINEDA, M. A., LATRE DE LATE, P., EASON, R. J., BESTEIRO, S., HARNETT, W. & LANGSLEY, G. 2017. From Christian de Duve to Yoshinori Ohsumi: More to autophagy than just dining at home. *Biomed J,* 40**,** 9-22.

HART, T., CHANDRASHEKHAR, M., AREGGER, M., STEINHART, Z., BROWN, K. R., MACLEOD, G., MIS, M., ZIMMERMANN, M., FRADET-TURCOTTE, A., SUN, S., MERO, P., DIRKS, P., SIDHU, S., ROTH, F. P., RISSLAND, O. S., DUROCHER, D., ANGERS, S. & MOFFAT, J. 2015. High-Resolution CRISPR Screens Reveal Fitness Genes and Genotype-Specific Cancer Liabilities. *Cell,* 163**,** 1515-26.

HAUTEFORT, I., THOMPSON, A., ERIKSSON-YGBERG, S., PARKER, M. L., LUCCHINI, S., DANINO, V., BONGAERTS, R. J., AHMAD, N., RHEN, M. & HINTON, J. C. 2008. During infection of epithelial cells Salmonella enterica serovar Typhimurium undergoes a time-dependent transcriptional adaptation that results in simultaneous expression of three type 3 secretion systems. *Cell Microbiol,* 10**,** 958-84.

HAYASHI-NISHINO, M., FUJITA, N., NODA, T., YAMAGUCHI, A., YOSHIMORI, T. & YAMAMOTO, A. 2009. A subdomain of the endoplasmic reticulum forms a cradle for autophagosome formation. *Nat Cell Biol,* 11**,** 1433-7.

HE, C. & KLIONSKY, D. J. 2009. Regulation mechanisms and signaling pathways of autophagy. *Annu Rev Genet,* 43**,** 67-93.

HEATH, R. J., GOEL, G., BAXT, L. A., RUSH, J. S., MOHANAN, V., PAULUS, G. L. C., JANI, V., LASSEN, K. G. & XAVIER, R. J. 2016. RNF166 Determines Recruitment of Adaptor Proteins during Antibacterial Autophagy. *Cell Rep,* 17**,** 2183-2194.

HEO, J. M., ORDUREAU, A., PAULO, J. A., RINEHART, J. & HARPER, J. W. 2015. The PINK1-PARKIN Mitochondrial Ubiquitylation Pathway Drives a Program of OPTN/NDP52 Recruitment and TBK1 Activation to Promote Mitophagy. *Mol Cell,* 60**,** 7-20.

HERRERO, A., MENDOZA, M. C., RODICIO, R. & RODICIO, M. R. 2008. Characterization of pUO-StVR2, a virulence-resistance plasmid evolved from the pSLT virulence plasmid of Salmonella enterica serovar Typhimurium. *Antimicrob Agents Chemother,* 52**,** 4514-7.

HOGEA, C., VAN EFFELTERRE, T. & ACOSTA, C. J. 2014. A basic dynamic transmission model of Staphylococcus aureus in the US population. *Epidemiol Infect,* 142**,** 468-78.

HOLDEN, D. W. 2002. Trafficking of the Salmonella vacuole in macrophages. *Traffic,* 3**,** 161-9.

HOMER, C. R., KABI, A., MARINA-GARCIA, N., SREEKUMAR, A., NESVIZHSKII, A. I., NICKERSON, K. P., CHINNAIYAN, A. M., NUNEZ, G. & MCDONALD, C. 2012. A dual role for receptor-interacting protein kinase 2 (RIP2) kinase activity in nucleotide-binding oligomerization domain 2 (NOD2)-dependent autophagy. *J Biol Chem,* 287**,** 25565-76.

HORN, J., STELZNER, K., RUDEL, T. & FRAUNHOLZ, M. 2017. Inside job: Staphylococcus aureus host-pathogen interactions. *Int J Med Microbiol*.

HOSOKAWA, N., HARA, T., KAIZUKA, T., KISHI, C., TAKAMURA, A., MIURA, Y., IEMURA, S., NATSUME, T., TAKEHANA, K., YAMADA, N., GUAN, J. L., OSHIRO, N. & MIZUSHIMA,

N. 2009. Nutrient-dependent mTORC1 association with the ULK1-Atg13-FIP200 complex required for autophagy. *Mol Biol Cell,* 20**,** 1981-91.

HOUZELSTEIN, D., GONCALVES, I. R., FADDEN, A. J., SIDHU, S. S., COOPER, D. N., DRICKAMER, K., LEFFLER, H. & POIRIER, F. 2004. Phylogenetic analysis of the vertebrate galectin family. *Mol Biol Evol,* 21**,** 1177-87.

HOWDEN, B. P., MCEVOY, C. R., ALLEN, D. L., CHUA, K., GAO, W., HARRISON, P. F., BELL, J., COOMBS, G., BENNETT-WOOD, V., PORTER, J. L., ROBINS-BROWNE, R., DAVIES, J. K., SEEMANN, T. & STINEAR, T. P. 2011. Evolution of multidrug resistance during Staphylococcus aureus infection involves mutation of the essential two component regulator WalKR. *PLoS Pathog,* 7**,** e1002359.

HSU, P. D., LANDER, E. S. & ZHANG, F. 2014. Development and applications of CRISPR-Cas9 for genome engineering. *Cell,* 157**,** 1262-78.

HUANG, J. & BRUMELL, J. H. 2014. Bacteria-autophagy interplay: a battle for survival. *Nat Rev Microbiol,* 12**,** 101-14.

HUANG, J., CANADIEN, V., LAM, G. Y., STEINBERG, B. E., DINAUER, M. C., MAGALHAES, M. A., GLOGAUER, M., GRINSTEIN, S. & BRUMELL, J. H. 2009. Activation of antibacterial autophagy by NADPH oxidases. *Proc Natl Acad Sci U S A,* 106**,** 6226-31.

HUETT, A., HEATH, R. J., BEGUN, J., SASSI, S. O., BAXT, L. A., VYAS, J. M., GOLDBERG, M. B. & XAVIER, R. J. 2012. The LRR and RING domain protein LRSAM1 is an E3 ligase crucial for ubiquitin-dependent autophagy of intracellular Salmonella Typhimurium. *Cell Host Microbe,* 12**,** 778-90.

HUTAGALUNG, A. H. & NOVICK, P. J. 2011. Role of Rab GTPases in membrane traffic and cell physiology. *Physiol Rev,* 91**,** 119-49.

ICHIMURA, Y., KUMANOMIDOU, T., SOU, Y. S., MIZUSHIMA, T., EZAKI, J., UENO, T., KOMINAMI, E., YAMANE, T., TANAKA, K. & KOMATSU, M. 2008. Structural basis for sorting mechanism of p62 in selective autophagy. *J Biol Chem,* 283**,** 22847-57.

INOKI, K., LI, Y., XU, T. & GUAN, K. L. 2003a. Rheb GTPase is a direct target of TSC2 GAP activity and regulates mTOR signaling. *Genes Dev,* 17**,** 1829-34.

INOKI, K., ZHU, T. & GUAN, K. L. 2003b. TSC2 mediates cellular energy response to control cell growth and survival. *Cell,* 115**,** 577-90.

IRVING, A. T., MIMURO, H., KUFER, T. A., LO, C., WHEELER, R., TURNER, L. J., THOMAS, B. J., MALOSSE, C., GANTIER, M. P., CASILLAS, L. N., VOTTA, B. J., BERTIN, J., BONECA, I. G., SASAKAWA, C., PHILPOTT, D. J., FERRERO, R. L. & KAPARAKIS-LIASKOS, M. 2014. The immune receptor NOD1 and kinase RIP2 interact with bacterial peptidoglycan on early endosomes to promote autophagy and inflammatory signaling. *Cell Host Microbe,* 15**,** 623-35.

ITAKURA, E., KISHI, C., INOUE, K. & MIZUSHIMA, N. 2008. Beclin 1 forms two distinct phosphatidylinositol 3-kinase complexes with mammalian Atg14 and UVRAG. *Mol Biol Cell,* 19**,** 5360-72.

ITO, T., KUWAHARA-ARAI, K., KATAYAMA, Y., UEHARA, Y., HAN, X., KONDO, Y. & HIRAMATSU, K. 2014. Staphylococcal Cassette Chromosome mec (SCCmec) analysis of MRSA. *Methods Mol Biol,* 1085**,** 131-48.

ITOH, T. & DE CAMILLI, P. 2006. BAR, F-BAR (EFC) and ENTH/ANTH domains in the regulation of membrane-cytosol interfaces and membrane curvature. *Biochim Biophys Acta,* 1761**,** 897-912.

IVANOV, S. & ROY, C. R. 2009. NDP52: the missing link between ubiquitinated bacteria and autophagy. *Nat Immunol,* 10**,** 1137-9.

JAPPE, U., HEUCK, D., STROMMENGER, B., WENDT, C., WERNER, G., ALTMANN, D. & WITTE, W. 2008. Staphylococcus aureus in dermatology outpatients with special emphasis on community-associated methicillin-resistant strains. *J Invest Dermatol,* 128**,** 2655-64.

JARRY, T. M. & CHEUNG, A. L. 2006. Staphylococcus aureus escapes more efficiently from the phagosome of a cystic fibrosis bronchial epithelial cell line than from its normal counterpart. *Infect Immun,* 74**,** 2568-77.

JARRY, T. M., MEMMI, G. & CHEUNG, A. L. 2008. The expression of alpha-haemolysin is required for Staphylococcus aureus phagosomal escape after internalization in CFT-1 cells. *Cell Microbiol,* 10**,** 1801-14.

JENNINGS, E., THURSTON, T. L. M. & HOLDEN, D. W. 2017. Salmonella SPI-2 Type III Secretion System Effectors: Molecular Mechanisms And Physiological Consequences. *Cell Host Microbe,* 22**,** 217-231.

JETT, B. D. & GILMORE, M. S. 2002. Internalization of Staphylococcus aureus by human corneal epithelial cells: role of bacterial fibronectin-binding protein and host cell factors. *Infect Immun,* 70**,** 4697-700.

JHA, S., BRICKEY, W. J. & TING, J. P. 2017. Inflammasomes in Myeloid Cells: Warriors Within. *Microbiol Spectr,* 5.

JIANG, P., NISHIMURA, T., SAKAMAKI, Y., ITAKURA, E., HATTA, T., NATSUME, T. & MIZUSHIMA, N. 2014. The HOPS complex mediates autophagosome-lysosome fusion through interaction with syntaxin 17. *Mol Biol Cell,* 25**,** 1327-37.

JINEK, M., CHYLINSKI, K., FONFARA, I., HAUER, M., DOUDNA, J. A. & CHARPENTIER, E. 2012. A programmable dual-RNA-guided DNA endonuclease in adaptive bacterial immunity. *Science,* 337**,** 816-21.

JINEK, M., EAST, A., CHENG, A., LIN, S., MA, E. & DOUDNA, J. 2013. RNA-programmed genome editing in human cells. *Elife,* 2**,** e00471.

JOACHIM, J., JEFFERIES, H. B., RAZI, M., FRITH, D., SNIJDERS, A. P., CHAKRAVARTY, P., JUDITH, D. & TOOZE, S. A. 2015. Activation of ULK Kinase and Autophagy by GABARAP Trafficking from the Centrosome Is Regulated by WAC and GM130. *Mol Cell,* 60**,** 899-913.

JONGSMA, M. L., BERLIN, I., WIJDEVEN, R. H., JANSSEN, L., JANSSEN, G. M., GARSTKA, M. A., JANSSEN, H., MENSINK, M., VAN VEELEN, P. A., SPAAPEN, R. M. & NEEFJES, J. 2016. An ER-Associated Pathway Defines Endosomal Architecture for Controlled Cargo Transport. *Cell,* 166**,** 152-66.

JOO, J. H., DORSEY, F. C., JOSHI, A., HENNESSY-WALTERS, K. M., ROSE, K. L., MCCASTLAIN, K., ZHANG, J., IYENGAR, R., JUNG, C. H., SUEN, D. F., STEEVES, M. A., YANG, C. Y., PRATER, S. M., KIM, D. H., THOMPSON, C. B., YOULE, R. J., NEY, P. A., CLEVELAND, J. L. & KUNDU, M. 2011. Hsp90-Cdc37 chaperone complex regulates Ulk1- and Atg13-mediated mitophagy. *Mol Cell,* 43**,** 572-85.

JUNG, C. H., JUN, C. B., RO, S. H., KIM, Y. M., OTTO, N. M., CAO, J., KUNDU, M. & KIM, D. H. 2009. ULK-Atg13-FIP200 complexes mediate mTOR signaling to the autophagy machinery. *Mol Biol Cell,* 20**,** 1992-2003.

KABEYA, Y., MIZUSHIMA, N., UENO, T., YAMAMOTO, A., KIRISAKO, T., NODA, T., KOMINAMI, E., OHSUMI, Y. & YOSHIMORI, T. 2000. LC3, a mammalian homologue of yeast Apg8p, is localized in autophagosome membranes after processing. *Embo j,* 19**,** 5720-8.

KAGEYAMA, S., OMORI, H., SAITOH, T., SONE, T., GUAN, J. L., AKIRA, S., IMAMOTO, F., NODA, T. & YOSHIMORI, T. 2011. The LC3 recruitment mechanism is separate from Atg9L1-

dependent membrane formation in the autophagic response against Salmonella. *Mol Biol Cell,* 22**,** 2290-300.

KAHL, B. C., GOULIAN, M., VAN WAMEL, W., HERRMANN, M., SIMON, S. M., KAPLAN, G., PETERS, G. & CHEUNG, A. L. 2000. Staphylococcus aureus RN6390 replicates and induces apoptosis in a pulmonary epithelial cell line. *Infect Immun,* 68**,** 5385-92.

KARANASIOS, E., STAPLETON, E., MANIFAVA, M., KAIZUKA, T., MIZUSHIMA, N., WALKER, S. A. & KTISTAKIS, N. T. 2013. Dynamic association of the ULK1 complex with omegasomes during autophagy induction. *J Cell Sci,* 126**,** 5224-38.

KARIUKI, S., REVATHI, G., KARIUKI, N., KIIRU, J., MWITURIA, J. & HART, C. A. 2006. Characterisation of community acquired non-typhoidal Salmonella from bacteraemia and diarrhoeal infections in children admitted to hospital in Nairobi, Kenya. *BMC Microbiol,* 6**,** 101.

KARKI, R., LEE, E., PLACE, D., SAMIR, P., MAVULURI, J., SHARMA, B. R., BALAKRISHNAN, A., MALIREDDI, R. K. S., GEIGER, R., ZHU, Q., NEALE, G. & KANNEGANTI, T. D. 2018. IRF8 Regulates Transcription of Naips for NLRC4 Inflammasome Activation. *Cell*.

KATOH, Y., IIDA, K., KANG, M. I., KOBAYASHI, A., MIZUKAMI, M., TONG, K. I., MCMAHON, M., HAYES, J. D., ITOH, K. & YAMAMOTO, M. 2005. Evolutionary conserved N-terminal domain of Nrf2 is essential for the Keap1-mediated degradation of the protein by proteasome. *Arch Biochem Biophys,* 433**,** 342-50.

KAWAI, T. & AKIRA, S. 2009. The roles of TLRs, RLRs and NLRs in pathogen recognition. *Int Immunol,* 21**,** 317-37.

KEESTRA-GOUNDER, A. M., TSOLIS, R. M. & BAUMLER, A. J. 2015. Now you see me, now you don't: the interaction of Salmonella with innate immune receptors. *Nat Rev Microbiol,* 13**,** 206-16.

KEESTRA, A. M., WINTER, M. G., AUBURGER, J. J., FRASSLE, S. P., XAVIER, M. N., WINTER, S. E., KIM, A., POON, V., RAVESLOOT, M. M., WALDENMAIER, J. F., TSOLIS, R. M., EIGENHEER, R. A. & BAUMLER, A. J. 2013. Manipulation of small Rho GTPases is a pathogen-induced process detected by NOD1. *Nature,* 496**,** 233-7.

KHAMINETS, A., BEHL, C. & DIKIC, I. 2016. Ubiquitin-Dependent And Independent Signals In Selective Autophagy. *Trends Cell Biol,* 26**,** 6-16.

KIM, J., KUNDU, M., VIOLLET, B. & GUAN, K. L. 2011. AMPK and mTOR regulate autophagy through direct phosphorylation of Ulk1. *Nat Cell Biol,* 13**,** 132-41.

KIM, P. K., HAILEY, D. W., MULLEN, R. T. & LIPPINCOTT-SCHWARTZ, J. 2008. Ubiquitin signals autophagic degradation of cytosolic proteins and peroxisomes. *Proc Natl Acad Sci U S A,* 105**,** 20567-74.

KIMURA, T., JAIN, A., CHOI, S. W., MANDELL, M. A., JOHANSEN, T. & DERETIC, V. 2017. TRIM-mediated precision autophagy targets cytoplasmic regulators of innate immunity

Autophagy, 13**,** 989-990.

KIMURA, T., JAIN, A., CHOI, S. W., MANDELL, M. A., SCHRODER, K., JOHANSEN, T. & DERETIC, V. 2015. TRIM-mediated precision autophagy targets cytoplasmic regulators of innate immunity. *J Cell Biol,* 210**,** 973-89.

KIRKEGAARD, K., TAYLOR, M. P. & JACKSON, W. T. 2004. Cellular autophagy: surrender, avoidance and subversion by microorganisms. *Nat Rev Microbiol,* 2**,** 301-14.

KIRKIN, V., LAMARK, T., SOU, Y. S., BJORKOY, G., NUNN, J. L., BRUUN, J. A., SHVETS, E., MCEWAN, D. G., CLAUSEN, T. H., WILD, P., BILUSIC, I., THEURILLAT, J. P., OVERVATN, A., ISHII, T., ELAZAR, Z., KOMATSU, M., DIKIC, I. & JOHANSEN, T. 2009. A role for NBR1 in autophagosomal degradation of ubiquitinated substrates. *Mol Cell,* 33**,** 505-16.

KLIONSKY, D. J. 2008. Autophagy revisited: a conversation with Christian de Duve. *Autophagy,* 4**,** 740-3.

KNODLER, L. A. & CELLI, J. 2011. Eating the strangers within: host control of intracellular bacteria via xenophagy. *Cell Microbiol,* 13**,** 1319-27.

KOIKE-YUSA, H., LI, Y., TAN, E. P., VELASCO-HERRERA MDEL, C. & YUSA, K. 2014. Genome-wide recessive genetic screening in mammalian cells with a lentiviral CRISPR-guide RNA library. *Nat Biotechnol,* 32**,** 267-73.

KOLDE, R., LAUR, S., ADLER, P. & VILO, J. 2012. Robust rank aggregation for gene list integration and meta-analysis. *Bioinformatics,* 28**,** 573-80.

KONIG, R., CHIANG, C. Y., TU, B. P., YAN, S. F., DEJESUS, P. D., ROMERO, A., BERGAUER, T., ORTH, A., KRUEGER, U., ZHOU, Y. & CHANDA, S. K. 2007. A probability-based approach for the analysis of large-scale RNAi screens. *Nat Methods,* 4**,** 847-9.

KOPITZ, J., KISEN, G. O., GORDON, P. B., BOHLEY, P. & SEGLEN, P. O. 1990. Nonselective autophagy of cytosolic enzymes by isolated rat hepatocytes. *J Cell Biol,* 111**,** 941-53.

KOZAK, G. K., MACDONALD, D., LANDRY, L. & FARBER, J. M. 2013. Foodborne outbreaks in Canada linked to produce: 2001 through 2009. *J Food Prot,* 76**,** 173-83.

KRAFT, C., KIJANSKA, M., KALIE, E., SIERGIEJUK, E., LEE, S. S., SEMPLICIO, G., STOFFEL, I., BREZOVICH, A., VERMA, M., HANSMANN, I., AMMERER, G., HOFMANN, K., TOOZE, S. & PETER, M. 2012. Binding of the Atg1/ULK1 kinase to the ubiquitin-like protein Atg8 regulates autophagy. *Embo j,* 31**,** 3691-703.

KRAFT, C., REGGIORI, F. & PETER, M. 2009. Selective types of autophagy in yeast. *Biochim Biophys Acta,* 1793**,** 1404-12.

KREIBICH, S., EMMENLAUER, M., FREDLUND, J., RAMO, P., MUNZ, C., DEHIO, C., ENNINGA, J. & HARDT, W. D. 2015. Autophagy Proteins Promote Repair of Endosomal Membranes Damaged by the Salmonella Type Three Secretion System 1. *Cell Host Microbe,* 18**,** 527-37.

KREISWIRTH, B. N., LOFDAHL, S., BETLEY, M. J., O'REILLY, M., SCHLIEVERT, P. M., BERGDOLL, M. S. & NOVICK, R. P. 1983. The toxic shock syndrome exotoxin structural gene is not detectably transmitted by a prophage. *Nature,* 305**,** 709-12.

KRUT, O., UTERMOHLEN, O., SCHLOSSHERR, X. & KRONKE, M. 2003. Strain-Specific Association of Cytotoxic Activity and Virulence of Clinical Staphylococcus aureus Isolates. *Infection and Immunity,* 71**,** 2716-2723.

KUBICA, M., GUZIK, K., KOZIEL, J., ZAREBSKI, M., RICHTER, W., GAJKOWSKA, B., GOLDA, A., MACIAG-GUDOWSKA, A., BRIX, K., SHAW, L., FOSTER, T. & POTEMPA, J. 2008. A potential new pathway for Staphylococcus aureus dissemination: the silent survival of S. aureus phagocytosed by human monocyte-derived macrophages. *PLoS One,* 3**,** e1409.

KUMA, A., HATANO, M., MATSUI, M., YAMAMOTO, A., NAKAYA, H., YOSHIMORI, T., OHSUMI, Y., TOKUHISA, T. & MIZUSHIMA, N. 2004. The role of autophagy during the early neonatal starvation period. *Nature,* 432**,** 1032-6.

KUO, S. Y., CASTORENO, A. B., ALDRICH, L. N., LASSEN, K. G., GOEL, G., DANCIK, V., KUBALLA, P., LATORRE, I., CONWAY, K. L., SARKAR, S., MAETZEL, D., JAENISCH, R., CLEMONS, P. A., SCHREIBER, S. L., SHAMJI, A. F. & XAVIER, R. J. 2015. Small-molecule enhancers of autophagy modulate cellular disease phenotypes suggested by human genetics. *Proc Natl Acad Sci U S A,* 112**,** E4281-7.

KURODA, M., OHTA, T., UCHIYAMA, I., BABA, T., YUZAWA, H., KOBAYASHI, I., CUI, L., OGUCHI, A., AOKI, K.-I., NAGAI, Y., LIAN, J., ITO, T., KANAMORI, M., MATSUMARU, H.,

MARUYAMA, A., MURAKAMI, H., HOSOYAMA, A., MIZUTANI-UI, Y., TAKAHASHI, N. K., SAWANO, T., INOUE, R.-I., KAITO, C., SEKIMIZU, K., HIRAKAWA, H., KUHARA, S., GOTO, S., YABUZAKI, J., KANEHISA, M., YAMASHITA, A., OSHIMA, K., FURUYA, K., YOSHINO, C., SHIBA, T., HATTORI, M., OGASAWARA, N., HAYASHI, H. & HIRAMATSU, K. 2001. Whole genome sequencing of meticillin-resistant Staphylococcus aureus. *The Lancet,* 357**,** 1225-1240.

LAM, G. Y., FATTOUH, R., MUISE, A. M., GRINSTEIN, S., HIGGINS, D. E. & BRUMELL, J. H. 2011. Listeriolysin O suppresses phospholipase C-mediated activation of the microbicidal NADPH oxidase to promote Listeria monocytogenes infection. *Cell Host Microbe,* 10**,** 627-34.

LAMARK, T., SVENNING, S. & JOHANSEN, T. 2017. Regulation of selective autophagy: the p62/SQSTM1 paradigm. *Essays Biochem,* 61**,** 609-624.

LAPLANTE, M. & SABATINI, D. M. 2012. mTOR signaling in growth control and disease. *Cell,* 149**,** 274-93.

LAROCK, D. L., CHAUDHARY, A. & MILLER, S. I. 2015. Salmonellae interactions with host processes. *Nat Rev Microbiol,* 13**,** 191-205.

LATASA, C., ROUX, A., TOLEDO-ARANA, A., GHIGO, J. M., GAMAZO, C., PENADES, J. R. & LASA, I. 2005. BapA, a large secreted protein required for biofilm formation and host colonization of Salmonella enterica serovar Enteritidis. *Mol Microbiol,* 58**,** 1322-39.

LAZAROU, M., SLITER, D. A., KANE, L. A., SARRAF, S. A., WANG, C., BURMAN, J. L., SIDERIS, D. P., FOGEL, A. I. & YOULE, R. J. 2015. The ubiquitin kinase PINK1 recruits autophagy receptors to induce mitophagy. *Nature,* 524**,** 309-314.

LAZARUS, M. B. & SHOKAT, K. M. 2015. Discovery and structure of a new inhibitor scaffold of the autophagy initiating kinase ULK1. *Bioorg Med Chem,* 23**,** 5483-8.

LEDEBOER, N. A., FRYE, J. G., MCCLELLAND, M. & JONES, B. D. 2006. Salmonella enterica serovar Typhimurium requires the Lpf, Pef, and Tafi fimbriae for biofilm formation on HEp-2 tissue culture cells and chicken intestinal epithelium. *Infect Immun,* 74**,** 3156-69.

LEE, J. H., PARK, J. W., KIM, S. W., PARK, J. & PARK, T. S. 2017a. C-X-C chemokine receptor type 4 (CXCR4) is a key receptor for chicken primordial germ cell migration. *J Reprod Dev,* 63**,** 555-562.

LEE, J. W., PARK, S., TAKAHASHI, Y. & WANG, H. G. 2010. The association of AMPK with ULK1 regulates autophagy. *PLoS One,* 5**,** e15394.

LEE, Y., CHOU, T. F., PITTMAN, S. K., KEITH, A. L., RAZANI, B. & WEIHL, C. C. 2017b. Keap1/Cullin3 Modulates p62/SQSTM1 Activity via UBA Domain Ubiquitination. *Cell Rep,* 19**,** 188-202.

LEGAKIS, J. E., YEN, W. L. & KLIONSKY, D. J. 2007. A cycling protein complex required for selective autophagy. *Autophagy,* 3**,** 422-32.

LEVINE, B., MIZUSHIMA, N. & VIRGIN, H. W. 2011. Autophagy in immunity and inflammation. *Nature,* 469**,** 323-35.

LEVINE, B., SINHA, S. C. & KROEMER, G. 2008. Bcl-2 family members: Dual regulators of apoptosis and autophagy. *Autophagy,* 4**,** 600-606.

LI, J., CHAI, Q. Y. & LIU, C. H. 2016. The ubiquitin system: a critical regulator of innate immunity and pathogen-host interactions. *Cell Mol Immunol,* 13**,** 560-76.

LI, S., WANDEL, M. P., LI, F., LIU, Z., HE, C., WU, J., SHI, Y. & RANDOW, F. 2013. Sterical hindrance promotes selectivity of the autophagy cargo receptor NDP52 for the danger receptor galectin-8 in antibacterial autophagy. *Sci Signal,* 6**,** ra9.

LI, W., XU, H., XIAO, T., CONG, L., LOVE, M. I., ZHANG, F., IRIZARRY, R. A., LIU, J. S., BROWN, M. & LIU, X. S. 2014. MAGeCK enables robust identification of essential genes from genome-scale CRISPR/Cas9 knockout screens. *Genome Biol,* 15**,** 554.

LI, W. W., LI, J. & BAO, J. K. 2012. Microautophagy: lesser-known self-eating. *Cell Mol Life Sci,* 69**,** 1125-36.

LIANG, C., FENG, P., KU, B., DOTAN, I., CANAANI, D., OH, B. H. & JUNG, J. U. 2006. Autophagic and tumour suppressor activity of a novel Beclin1-binding protein UVRAG. *Nat Cell Biol,* 8**,** 688-99.

LIGHTFIELD, K. L., PERSSON, J., TRINIDAD, N. J., BRUBAKER, S. W., KOFOED, E. M., SAUER, J. D., DUNIPACE, E. A., WARREN, S. E., MIAO, E. A. & VANCE, R. E. 2011. Differential requirements for NAIP5 in activation of the NLRC4 inflammasome. *Infect Immun,* 79**,** 1606-14.

LIM, M. B., KUIPER, J. W., KATCHKY, A., GOLDBERG, H. & GLOGAUER, M. 2011. Rac2 is required for the formation of neutrophil extracellular traps. *J Leukoc Biol,* 90**,** 771-6.

LIN, X., YANG, T., WANG, S., WANG, Z., YUN, Y., SUN, L., ZHOU, Y., XU, X., AKAZAWA, C., HONG, W. & WANG, T. 2014. RILP interacts with HOPS complex via VPS41 subunit to regulate endocytic trafficking. *Sci Rep,* 4**,** 7282.

LIU, P. F., CHENG, J. S., SY, C. L., HUANG, W. C., YANG, H. C., GALLO, R. L., HUANG, C. M. & SHU, C. W. 2015. IsaB Inhibits Autophagic Flux to Promote Host Transmission of Methicillin-Resistant Staphylococcus aureus. *J Invest Dermatol,* 135**,** 2714-2722.

LIU, T., ZHANG, L., JOO, D. & SUN, S. C. 2017. NF-kappaB signaling in inflammation. *Signal Transduct Target Ther,* 2.

LIU, W., JIANG, Y., SUN, J., GENG, S., PAN, Z., PRINZ, R. A., WANG, C., SUN, J., JIAO, X. & XU, X. 2018. Activation of TGF-beta-activated kinase 1 (TAK1) restricts Salmonella Typhimurium growth by inducing AMPK activation and autophagy. *Cell Death Dis,* 9**,** 570.

LOFFLER, B., TUCHSCHERR, L., NIEMANN, S. & PETERS, G. 2014. Staphylococcus aureus persistence in non-professional phagocytes. *Int J Med Microbiol,* 304**,** 170-6.

LOPEZ DE ARMENTIA, M. M., AMAYA, C. & COLOMBO, M. I. 2016. Rab GTPases and the Autophagy Pathway: Bacterial Targets for a Suitable Biogenesis and Trafficking of Their Own Vacuoles. *Cells,* 5.

LOPEZ DE ARMENTIA, M. M., GAURON, M. C. & COLOMBO, M. I. 2017. Staphylococcus aureus Alpha-Toxin Induces the Formation of Dynamic Tubules Labeled with LC3 within Host Cells in a Rab7 and Rab1b-Dependent Manner. *Front Cell Infect Microbiol,* 7**,** 431.

LUO, B., CHEUNG, H. W., SUBRAMANIAN, A., SHARIFNIA, T., OKAMOTO, M., YANG, X., HINKLE, G., BOEHM, J. S., BEROUKHIM, R., WEIR, B. A., MERMEL, C., BARBIE, D. A., AWAD, T., ZHOU, X., NGUYEN, T., PIQANI, B., LI, C., GOLUB, T. R., MEYERSON, M., HACOHEN, N., HAHN, W. C., LANDER, E. S., SABATINI, D. M. & ROOT, D. E. 2008. Highly parallel identification of essential genes in cancer cells. *Proc Natl Acad Sci U S A,* 105**,** 20380-5.

LUPFER, C., THOMAS, P. G., ANAND, P. K., VOGEL, P., MILASTA, S., MARTINEZ, J., HUANG, G., GREEN, M., KUNDU, M., CHI, H., XAVIER, R. J., GREEN, D. R., LAMKANFI, M., DINARELLO, C. A., DOHERTY, P. C. & KANNEGANTI, T. D. 2013. Receptor interacting protein kinase 2-mediated mitophagy regulates inflammasome activation during virus infection. *Nat Immunol,* 14**,** 480-8.

MA, Y., ZHANG, L., LU, J., SHUI, T., CHEN, J., YANG, J., YUAN, J., LIU, Y. & YANG, D. 2017. A Negative Feedback Loop Between Autophagy and Immune Responses in Mycobacterium leprae Infection. *DNA Cell Biol,* 36**,** 1-9.

MAEJIMA, I., TAKAHASHI, A., OMORI, H., KIMURA, T., TAKABATAKE, Y., SAITOH, T., YAMAMOTO, A., HAMASAKI, M., NODA, T., ISAKA, Y. & YOSHIMORI, T. 2013. Autophagy sequesters damaged lysosomes to control lysosomal biogenesis and kidney injury. *Embo j,* 32**,** 2336-47.

MALET, J. K., COSSART, P. & RIBET, D. 2017. Alteration of epithelial cell lysosomal integrity induced by bacterial cholesterol-dependent cytolysins. *Cell Microbiol,* 19.

MALI, P., YANG, L., ESVELT, K. M., AACH, J., GUELL, M., DICARLO, J. E., NORVILLE, J. E. & CHURCH, G. M. 2013. RNA-guided human genome engineering via Cas9. *Science,* 339**,** 823-6.

MAN, S. M., HOPKINS, L. J., NUGENT, E., COX, S., GLUCK, I. M., TOURLOMOUSIS, P., WRIGHT, J. A., CICUTA, P., MONIE, T. P. & BRYANT, C. E. 2014. Inflammasome activation causes dual recruitment of NLRC4 and NLRP3 to the same macromolecular complex. *Proc Natl Acad Sci U S A,* 111**,** 7403-8.

MARCUS, S. L., BRUMELL, J. H., PFEIFER, C. G. & FINLAY, B. B. 2000. Salmonella pathogenicity islands: big virulence in small packages. *Microbes Infect,* 2**,** 145-56.

MARI, M., GRIFFITH, J., RIETER, E., KRISHNAPPA, L., KLIONSKY, D. J. & REGGIORI, F. 2010. An Atg9-containing compartment that functions in the early steps of autophagosome biogenesis. *J Cell Biol,* 190**,** 1005-22.

MARIATHASAN, S., NEWTON, K., MONACK, D. M., VUCIC, D., FRENCH, D. M., LEE, W. P., ROOSE-GIRMA, M., ERICKSON, S. & DIXIT, V. M. 2004. Differential activation of the inflammasome by caspase-1 adaptors ASC and Ipaf. *Nature,* 430**,** 213-8.

MARTENS, S. 2016. No ATG8s, no problem? How LC3/GABARAP proteins contribute to autophagy. *J Cell Biol,* 215**,** 761-763.

MATSUNAGA, K., SAITOH, T., TABATA, K., OMORI, H., SATOH, T., KUROTORI, N., MAEJIMA, I., SHIRAHAMA-NODA, K., ICHIMURA, T., ISOBE, T., AKIRA, S., NODA, T. & YOSHIMORI, T. 2009. Two Beclin 1-binding proteins, Atg14L and Rubicon, reciprocally regulate autophagy at different stages. *Nat Cell Biol,* 11**,** 385-96.

MAURER, K., REYES-ROBLES, T., ALONZO, F., 3RD, DURBIN, J., TORRES, V. J. & CADWELL, K. 2015a. Autophagy mediates tolerance to Staphylococcus aureus alpha-toxin. *Cell Host Microbe,* 17**,** 429-40.

MAURER, K., TORRES, V. J. & CADWELL, K. 2015b. Autophagy is a key tolerance mechanism during Staphylococcus aureus infection. *Autophagy,* 11**,** 1184-6.

MAUTHE, M., YU, W., KRUT, O., KRONKE, M., GOTZ, F., ROBENEK, H. & PROIKAS-CEZANNE, T. 2012. WIPI-1 Positive Autophagosome-Like Vesicles Entrap Pathogenic Staphylococcus aureus for Lysosomal Degradation. *Int J Cell Biol,* 2012**,** 179207.

MAZURKIEWICZ, P., THOMAS, J., THOMPSON, J. A., LIU, M., ARBIBE, L., SANSONETTI, P. & HOLDEN, D. W. 2008. SpvC is a Salmonella effector with phosphothreonine lyase activity on host mitogen-activated protein kinases. *Mol Microbiol,* 67**,** 1371-83.

MCCLELLAND, M., SANDERSON, K. E., SPIETH, J., CLIFTON, S. W., LATREILLE, P., COURTNEY, L., PORWOLLIK, S., ALI, J., DANTE, M., DU, F., HOU, S., LAYMAN, D., LEONARD, S., NGUYEN, C., SCOTT, K., HOLMES, A., GREWAL, N., MULVANEY, E., RYAN, E., SUN, H., FLOREA, L., MILLER, W., STONEKING, T., NHAN, M., WATERSTON, R. & WILSON, R. K. 2001. Complete genome sequence of Salmonella enterica serovar Typhimurium LT2. *Nature,* 413**,** 852-6.

MCEWAN, D. G., POPOVIC, D., GUBAS, A., TERAWAKI, S., SUZUKI, H., STADEL, D., COXON, F. P., MIRANDA DE STEGMANN, D., BHOGARAJU, S., MADDI, K., KIRCHOF, A., GATTI, E., HELFRICH, M. H., WAKATSUKI, S., BEHRENDS, C., PIERRE, P. & DIKIC, I. 2015a. PLEKHM1 regulates autophagosome-lysosome fusion through HOPS complex and LC3/GABARAP proteins. *Mol Cell,* 57**,** 39-54.

MCEWAN, D. G., RICHTER, B., CLAUDI, B., WIGGE, C., WILD, P., FARHAN, H., MCGOURTY, K., COXON, F. P., FRANZ-WACHTEL, M., PERDU, B., AKUTSU, M., HABERMANN, A., KIRCHOF, A., HELFRICH, M. H., ODGREN, P. R., VAN HUL, W., FRANGAKIS, A. S., RAJALINGAM, K., MACEK, B., HOLDEN, D. W., BUMANN, D. & DIKIC, I. 2015b. PLEKHM1 regulates Salmonella-containing vacuole biogenesis and infection. *Cell Host Microbe,* 17**,** 58-71.

MCGOURTY, K., THURSTON, T. L., MATTHEWS, S. A., PINAUD, L., MOTA, L. J. & HOLDEN, D. W. 2012. Salmonella inhibits retrograde trafficking of mannose-6-phosphate receptors and lysosome function. *Science,* 338**,** 963-7.

MERCER, C. A., KALIAPPAN, A. & DENNIS, P. B. 2009. A novel, human Atg13 binding protein, Atg101, interacts with ULK1 and is essential for macroautophagy. *Autophagy,* 5**,** 649-62.

MERCER, T. J., GUBAS, A. & TOOZE, S. A. 2018. A Molecular Perspective of Mammalian Autophagosome Biogenesis. *J Biol Chem*.

MESQUITA, F. S., THOMAS, M., SACHSE, M., SANTOS, A. J., FIGUEIRA, R. & HOLDEN, D. W. 2012. The Salmonella deubiquitinase SseL inhibits selective autophagy of cytosolic aggregates. *PLoS Pathog,* 8**,** e1002743.

MESTRE, M. B. & COLOMBO, M. I. 2012. cAMP and EPAC are key players in the regulation of the signal transduction pathway involved in the alpha-hemolysin autophagic response. *PLoS Pathog,* 8**,** e1002664.

MESTRE, M. B., FADER, C. M., SOLA, C. & COLOMBO, M. I. 2010. Alpha-hemolysin is required for the activation of the autophagic pathway in Staphylococcus aureus-infected cells. *Autophagy,* 6**,** 110-25.

MIAO, E. A., ALPUCHE-ARANDA, C. M., DORS, M., CLARK, A. E., BADER, M. W., MILLER, S. I. & ADEREM, A. 2006. Cytoplasmic flagellin activates caspase-1 and secretion of interleukin 1beta via Ipaf. *Nat Immunol,* 7**,** 569-75.

MIAO, E. A., MAO, D. P., YUDKOVSKY, N., BONNEAU, R., LORANG, C. G., WARREN, S. E., LEAF, I. A. & ADEREM, A. 2010. Innate immune detection of the type III secretion apparatus through the NLRC4 inflammasome. *Proc Natl Acad Sci U S A,* 107**,** 3076-80.

MIZUSHIMA, N. 2010. The role of the Atg1/ULK1 complex in autophagy regulation. *Curr Opin Cell Biol,* 22**,** 132-9.

MIZUSHIMA, N., YAMAMOTO, A., HATANO, M., KOBAYASHI, Y., KABEYA, Y., SUZUKI, K., TOKUHISA, T., OHSUMI, Y. & YOSHIMORI, T. 2001. Dissection of Autophagosome Formation Using Apg5-Deficient Mouse Embryonic Stem Cells. *The Journal of Cell Biology,* 152**,** 657-668.

MOCHIDA, K., OIKAWA, Y., KIMURA, Y., KIRISAKO, H., HIRANO, H., OHSUMI, Y. & NAKATOGAWA, H. 2015. Receptor-mediated selective autophagy degrades the endoplasmic reticulum and the nucleus. *Nature,* 522**,** 359-62.

MOHAN, R. R., TOVEY, J. C., SHARMA, A., SCHULTZ, G. S., COWDEN, J. W. & TANDON, A. 2011. Targeted decorin gene therapy delivered with adeno-associated virus effectively retards corneal neovascularization in vivo. *PLoS One,* 6**,** e26432.

MOREAU, K., LACAS-GERVAIS, S., FUJITA, N., SEBBANE, F., YOSHIMORI, T., SIMONET, M. & LAFONT, F. 2010. Autophagosomes can support Yersinia pseudotuberculosis replication in macrophages. *Cell Microbiol,* 12**,** 1108-23.

MORETTI, J., ROY, S., BOZEC, D., MARTINEZ, J., CHAPMAN, J. R., UEBERHEIDE, B., LAMMING, D. W., CHEN, Z. J., HORNG, T., YERETSSIAN, G., GREEN, D. R. & BLANDER, J. M. 2017. STING Senses Microbial Viability to Orchestrate Stress-Mediated Autophagy of the Endoplasmic Reticulum. *Cell,* 171**,** 809-823 e13.

MORTIMORE, G. E. & SCHWORER, C. M. 1977. Induction of autophagy by amino-acid deprivation in perfused rat liver. *Nature,* 270**,** 174-6.

MORTON, S., HESSON, L., PEGGIE, M. & COHEN, P. 2008. Enhanced binding of TBK1 by an optineurin mutant that causes a familial form of primary open angle glaucoma. *FEBS Lett,* 582**,** 997-1002.

MULVANEY, K. M., MATSON, J. P., SIESSER, P. F., TAMIR, T. Y., GOLDFARB, D., JACOBS, T. M., CLOER, E. W., HARRISON, J. S., VAZIRI, C., COOK, J. G. & MAJOR, M. B. 2016. Identification and Characterization of MCM3 as a Kelch-like ECH-associated Protein 1 (KEAP1) Substrate. *J Biol Chem,* 291**,** 23719-23733.

NAKAGAWA, I., AMANO, A., MIZUSHIMA, N., YAMAMOTO, A., YAMAGUCHI, H., KAMIMOTO, T., NARA, A., FUNAO, J., NAKATA, M., TSUDA, K., HAMADA, S. & YOSHIMORI, T. 2004. Autophagy defends cells against invading group A Streptococcus. *Science,* 306**,** 1037-40.

NAKAYASU, E. S., SYDOR, M. A., BROWN, R. N., SONTAG, R. L., SOBREIRA, T. J., SLYSZ, G. W., HUMPHRYS, D. R., SKARINA, T., ONOPRIENKO, O., DI LEO, R., DEATHERAGE KAISER, B. L., LI, J., ANSONG, C., CAMBRONNE, E. D., SMITH, R. D., SAVCHENKO, A. & ADKINS, J. N. 2015. Identification of Salmonella Typhimurium Deubiquitinase SseL Substrates by Immunoaffinity Enrichment and Quantitative Proteomic Analysis. *J Proteome Res,* 14**,** 4029-38.

NEILL, T., SCHAEFER, L. & IOZZO, R. V. 2016. Decorin as a multivalent therapeutic agent against cancer. *Adv Drug Deliv Rev,* 97**,** 174-85.

NEUMANN, Y., BRUNS, S. A., ROHDE, M., PRAJSNAR, T. K., FOSTER, S. J. & SCHMITZ, I. 2016. Intracellular Staphylococcus aureus eludes selective autophagy by activating a host cell kinase. *Autophagy,* 12**,** 2069-2084.

NG, A. C., EISENBERG, J. M., HEATH, R. J., HUETT, A., ROBINSON, C. M., NAU, G. J. & XAVIER, R. J. 2011. Human leucine-rich repeat proteins: a genome-wide bioinformatic categorization and functional analysis in innate immunity. *Proc Natl Acad Sci U S A,* 108 Suppl 1**,** 4631-8.

NGUYEN, T. N., PADMAN, B. S., USHER, J., OORSCHOT, V., RAMM, G. & LAZAROU, M. 2016. Atg8 family LC3/GABARAP proteins are crucial for autophagosome-lysosome fusion but not autophagosome formation during PINK1/Parkin mitophagy and starvation. *J Cell Biol,* 215**,** 857-874.

NOAD, J., VON DER MALSBURG, A., PATHE, C., MICHEL, M. A., KOMANDER, D. & RANDOW, F. 2017. LUBAC-synthesized linear ubiquitin chains restrict cytosol-invading bacteria by activating autophagy and NF-kappaB. *Nat Microbiol,* 2**,** 17063.

NODA, N. N., KUMETA, H., NAKATOGAWA, H., SATOO, K., ADACHI, W., ISHII, J., FUJIOKA, Y., OHSUMI, Y. & INAGAKI, F. 2008. Structural basis of target recognition by Atg8/LC3 during selective autophagy. *Genes Cells,* 13**,** 1211-8.

NODA, N. N., OHSUMI, Y. & INAGAKI, F. 2010. Atg8-family interacting motif crucial for selective autophagy. *FEBS Lett,* 584**,** 1379-85.

NOVIKOFF, A. B. & ESSNER, E. 1962. Cytolysomes and mitochondrial degeneration. *J Cell Biol,* 15**,** 140-6.

O'HARA, F. P., GUEX, N., WORD, J. M., MILLER, L. A., BECKER, J. A., WALSH, S. L., SCANGARELLA, N. E., WEST, J. M., SHAWAR, R. M. & AMRINE-MADSEN, H. 2008. A geographic variant of the Staphylococcus aureus Panton-Valentine leukocidin toxin and the origin of community-associated methicillin-resistant S. aureus USA300. *J Infect Dis,* 197**,** 187-94.

O'KEEFFE, K. M., WILK, M. M., LEECH, J. M., MURPHY, A. G., LAABEI, M., MONK, I. R., MASSEY, R. C., LINDSAY, J. A., FOSTER, T. J., GEOGHEGAN, J. A. & MCLOUGHLIN, R. M. 2015. Manipulation of Autophagy in Phagocytes Facilitates Staphylococcus aureus Bloodstream Infection. *Infect Immun,* 83**,** 3445-57.

OBARA, K. & OHSUMI, Y. 2008. Dynamics and function of PtdIns(3)P in autophagy. *Autophagy,* 4**,** 952-4.

OGAWA, M., YOSHIMORI, T., SUZUKI, T., SAGARA, H., MIZUSHIMA, N. & SASAKAWA, C. 2005. Escape of intracellular Shigella from autophagy. *Science,* 307**,** 727-31.

OHASHI, Y. & MUNRO, S. 2010. Membrane delivery to the yeast autophagosome from the Golgi-endosomal system. *Mol Biol Cell,* 21**,** 3998-4008.

ORENSTEIN, S. J. & CUERVO, A. M. 2010. Chaperone-mediated autophagy: molecular mechanisms and physiological relevance. *Semin Cell Dev Biol,* 21**,** 719-26.

OTTO, M. 2010. Looking toward basic science for potential drug discovery targets against community-associated MRSA. *Med Res Rev,* 30**,** 1-22.

OWEN, K. A., ANDERSON, C. J. & CASANOVA, J. E. 2016. Salmonella Suppresses the TRIF-Dependent Type I Interferon Response in Macrophages. *MBio,* 7**,** e02051-15.

PADER, V., HAKIM, S., PAINTER, K. L., WIGNESHWERARAJ, S., CLARKE, T. B. & EDWARDS, A. M. 2016. Staphylococcus aureus inactivates daptomycin by releasing membrane phospholipids. *Nat Microbiol,* 2**,** 16194.

PANKIV, S., CLAUSEN, T. H., LAMARK, T., BRECH, A., BRUUN, J. A., OUTZEN, H., OVERVATN, A., BJORKOY, G. & JOHANSEN, T. 2007. p62/SQSTM1 binds directly to Atg8/LC3 to facilitate degradation of ubiquitinated protein aggregates by autophagy. *J Biol Chem,* 282**,** 24131-45.

PARK, J. M., JUNG, C. H., SEO, M., OTTO, N. M., GRUNWALD, D., KIM, K. H., MORIARITY, B., KIM, Y. M., STARKER, C., NHO, R. S., VOYTAS, D. & KIM, D. H. 2016. The ULK1 complex mediates MTORC1 signaling to the autophagy initiation machinery via binding and phosphorylating ATG14. *Autophagy,* 12**,** 547-64.

PARNAS, O., JOVANOVIC, M., EISENHAURE, T. M., HERBST, R. H., DIXIT, A., YE, C. J., PRZYBYLSKI, D., PLATT, R. J., TIROSH, I., SANJANA, N. E., SHALEM, O., SATIJA, R., RAYCHOWDHURY, R., MERTINS, P., CARR, S. A., ZHANG, F., HACOHEN, N. & REGEV, A. 2015. A Genome-wide CRISPR Screen in Primary Immune Cells to Dissect Regulatory Networks. *Cell,* 162**,** 675-86.

PATEL, J. C. & GALAN, J. E. 2006. Differential activation and function of Rho GTPases during Salmonella-host cell interactions. *J Cell Biol,* 175**,** 453-63.

PATTINGRE, S., BAUVY, C., CARPENTIER, S., LEVADE, T., LEVINE, B. & CODOGNO, P. 2009. Role of JNK1-dependent Bcl-2 phosphorylation in ceramide-induced macroautophagy. *J Biol Chem,* 284**,** 2719-28.

PAUDEL, S., GHIMIRE, L., CAI, S., JIN, L. & JEYASEELAN, S. 2017. Methicillin -Resistant Staphylococcus Aureus Exploits Nlrc4 inflammasome To Dampen Pulmonary Host Defenses. *American Journal of Respiratory and critical care Medicine* 195.

PAZ, I., SACHSE, M., DUPONT, N., MOUNIER, J., CEDERFUR, C., ENNINGA, J., LEFFLER, H., POIRIER, F., PREVOST, M. C., LAFONT, F. & SANSONETTI, P. 2010. Galectin-3, a marker for vacuole lysis by invasive pathogens. *Cell Microbiol,* 12**,** 530-44.

PEI, G., BUIJZE, H., LIU, H., MOURA-ALVES, P., GOOSMANN, C., BRINKMANN, V., KAWABE, H., DORHOI, A. & KAUFMANN, S. H. E. 2017. The E3 ubiquitin ligase NEDD4 enhances killing of membrane-perturbing intracellular bacteria by promoting autophagy. *Autophagy,* 13**,** 2041-2055.

PENGO, N., AGROTIS, A., PRAK, K., JONES, J. & KETTELER, R. 2017. A reversible phospho-switch mediated by ULK1 regulates the activity of autophagy protease ATG4B. *Nat Commun,* 8**,** 294.

PERRIN, A. J., JIANG, X., BIRMINGHAM, C. L., SO, N. S. & BRUMELL, J. H. 2004. Recognition of bacteria in the cytosol of Mammalian cells by the ubiquitin system. *Curr Biol,* 14**,** 806-11.

PERRY, V. H., CUNNINGHAM, C. & HOLMES, C. 2007. Systemic infections and inflammation affect chronic neurodegeneration. *Nat Rev Immunol,* 7**,** 161-7.

PETHERICK, K. J., CONWAY, O. J., MPAMHANGA, C., OSBORNE, S. A., KAMAL, A., SAXTY, B. & GANLEY, I. G. 2015. Pharmacological inhibition of ULK1 kinase blocks mammalian target of rapamycin (mTOR)-dependent autophagy. *J Biol Chem,* 290**,** 28726.

POLAJNAR, M., DIETZ, M. S., HEILEMANN, M. & BEHRENDS, C. 2017. Expanding the host cell ubiquitylation machinery targeting cytosolic Salmonella. *EMBO Rep,* 18**,** 1572-1585.

POLSON, H. E., DE LARTIGUE, J., RIGDEN, D. J., REEDIJK, M., URBE, S., CLAGUE, M. J. & TOOZE, S. A. 2010. Mammalian Atg18 (WIPI2) localizes to omegasome-anchored phagophores and positively regulates LC3 lipidation. *Autophagy,* 6**,** 506-22.

PORTEUS, M. H. & BALTIMORE, D. 2003. Chimeric nucleases stimulate gene targeting in human cells. *Science,* 300**,** 763.

POWERS, M. E. & BUBECK WARDENBURG, J. 2015. Host autophagy combating S. aureus: alpha-toxin will be tolerated. *Cell Host Microbe,* 17**,** 419-20.

PRUNEDA, J. N., DURKIN, C. H., GEURINK, P. P., OVAA, H., SANTHANAM, B., HOLDEN, D. W. & KOMANDER, D. 2016. The Molecular Basis for Ubiquitin and Ubiquitin-like Specificities in Bacterial Effector Proteases. *Mol Cell,* 63**,** 261-276.

PUENTE, C., HENDRICKSON, R. C. & JIANG, X. 2016. Nutrient-regulated Phosphorylation of ATG13 Inhibits Starvation-induced Autophagy. *J Biol Chem,* 291**,** 6026-35.

PY, B. F., LIPINSKI, M. M. & YUAN, J. 2007. Autophagy limits Listeria monocytogenes intracellular growth in the early phase of primary infection. *Autophagy,* 3**,** 117-25.

QAZI, S. N. A., HARRISON, S. E., SELF, T., WILLIAMS, P. & HILL, P. J. 2004. Real-Time Monitoring of Intracellular Staphylococcus aureus Replication. *Journal of Bacteriology,* 186**,** 1065-1077.

QIN, L., WANG, X., ZHANG, S., FENG, S., YIN, L. & ZHOU, H. 2016. Lipopolysaccharide-induced autophagy participates in the control of pro-inflammatory cytokine release in grass carp head kidney leukocytes. *Fish Shellfish Immunol,* 59**,** 389-397.

RADISKY, D. C., SNYDER, W. B., EMR, S. D. & KAPLAN, J. 1997. Characterization of VPS41, a gene required for vacuolar trafficking and high-affinity iron transport in yeast. *Proc Natl Acad Sci U S A,* 94**,** 5662-6.

RAGHUKUMAR, R., VALI, L., WATSON, D., FEARNLEY, J. & SEIDEL, V. 2010. Antimethicillin-resistant Staphylococcus aureus (MRSA) activity of 'pacific propolis' and isolated prenylflavanones. *Phytother Res,* 24**,** 1181-7.

RAN, F. A., HSU, P. D., WRIGHT, J., AGARWALA, V., SCOTT, D. A. & ZHANG, F. 2013. Genome engineering using the CRISPR-Cas9 system. *Nat Protoc,* 8**,** 2281-2308.

RANDOW, F. & YOULE, R. J. 2014. Self and nonself: how autophagy targets mitochondria and bacteria. *Cell Host Microbe,* 15**,** 403-11.

REGGIORI, F., KOMATSU, M., FINLEY, K. & SIMONSEN, A. 2012. Autophagy: more than a nonselective pathway. *Int J Cell Biol,* 2012**,** 219625.

REGGIORI, F. & UNGERMANN, C. 2017. Autophagosome Maturation and Fusion. *J Mol Biol,* 429**,** 486-496.

REIJO, R., LEE, T. Y., SALO, P., ALAGAPPAN, R., BROWN, L. G., ROSENBERG, M., ROZEN, S., JAFFE, T., STRAUS, D., HOVATTA, O. & ET AL. 1995. Diverse spermatogenic defects in humans caused by Y chromosome deletions encompassing a novel RNA-binding protein gene. *Nat Genet,* 10**,** 383-93.

RIKIHISA, Y. 1984. Glycogen autophagosomes in polymorphonuclear leukocytes induced by rickettsiae. *Anat Rec,* 208**,** 319-27.

ROBINSON, M. D., MCCARTHY, D. J. & SMYTH, G. K. 2010. edgeR: a Bioconductor package for differential expression analysis of digital gene expression data. *Bioinformatics,* 26**,** 139-40.

ROGOV, V., DOTSCH, V., JOHANSEN, T. & KIRKIN, V. 2014. Interactions between autophagy receptors and ubiquitin-like proteins form the molecular basis for selective autophagy. *Mol Cell,* 53**,** 167-78.

ROGOV, V. V., SUZUKI, H., FISKIN, E., WILD, P., KNISS, A., ROZENKNOP, A., KATO, R., KAWASAKI, M., MCEWAN, D. G., LOHR, F., GUNTERT, P., DIKIC, I., WAKATSUKI, S. & DOTSCH, V. 2013. Structural basis for phosphorylation-triggered autophagic clearance of Salmonella. *Biochem J,* 454**,** 459-66.

ROLLIN, G., TAN, X., TROS, F., DUPUIS, M., NASSIF, X., CHARBIT, A. & COUREUIL, M. 2017. Intracellular Survival of Staphylococcus aureus in Endothelial Cells: A Matter of Growth or Persistence. *Front Microbiol,* 8**,** 1354.

ROY, D., LISTON, D. R., IDONE, V. J., DI, A., NELSON, D. J., PUJOL, C., BLISKA, J. B., CHAKRABARTI, S. & ANDREWS, N. W. 2004. A process for controlling intracellular bacterial infections induced by membrane injury. *Science,* 304**,** 1515-8.

RUGGIU, M., SPEED, R., TAGGART, M., MCKAY, S. J., KILANOWSKI, F., SAUNDERS, P., DORIN, J. & COOKE, H. J. 1997. The mouse Dazla gene encodes a cytoplasmic protein essential for gametogenesis. *Nature,* 389**,** 73-7.

RUIZ-RAMOS, J., VIDAL-CORTES, P., DIAZ-LAMAS, A., REIG-VALERO, R., ROCHE-CAMPO, F., DEL VALLE-ORTIZ, M., NUVIALS-CASALS, X., ORTIZ-PIQUER, M., ANDALUZ-OJEDA, D., TAMAYO-LOMAS, L., BLASCO-NAVALPOTRO, M. A., RODRIGUEZ-AGUIRREGABIRIA, M., AGUADO, J. & RAMIREZ, P. 2017. Ventilator-associated pneumonia by methicillin-susceptible Staphylococcus aureus: do minimum inhibitory concentrations to vancomycin and daptomycin matter? *Eur J Clin Microbiol Infect Dis,* 36**,** 1569-1575.

RUSSELL, R. C., TIAN, Y., YUAN, H., PARK, H. W., CHANG, Y. Y., KIM, J., KIM, H., NEUFELD, T. P., DILLIN, A. & GUAN, K. L. 2013. ULK1 induces autophagy by phosphorylating Beclin-1 and activating VPS34 lipid kinase. *Nat Cell Biol,* 15**,** 741-50.

SAITOH, T., FUJITA, N., HAYASHI, T., TAKAHARA, K., SATOH, T., LEE, H., MATSUNAGA, K., KAGEYAMA, S., OMORI, H., NODA, T., YAMAMOTO, N., KAWAI, T., ISHII, K., TAKEUCHI, O., YOSHIMORI, T. & AKIRA, S. 2009. Atg9a controls dsDNA-driven

dynamic translocation of STING and the innate immune response. *Proc Natl Acad Sci U S A,* 106**,** 20842-6.

SAN FILIPPO, J., SUNG, P. & KLEIN, H. 2008. Mechanism of eukaryotic homologous recombination. *Annu Rev Biochem,* 77**,** 229-57.

SANGAL, V., GIRVAN, E. K., JADHAV, S., LAWES, T., ROBB, A., VALI, L., EDWARDS, G. F., YU, J. & GOULD, I. M. 2012. Impacts of a long-term programme of active surveillance and chlorhexidine baths on the clinical and molecular epidemiology of meticillin-resistant Staphylococcus aureus (MRSA) in an Intensive Care Unit in Scotland. *Int J Antimicrob Agents,* 40**,** 323-31.

SANJANA, N. E., SHALEM, O. & ZHANG, F. 2014. Improved vectors and genome-wide libraries for CRISPR screening. *Nat Methods,* 11**,** 783-784.

SAUNDERS, P. T., TURNER, J. M., RUGGIU, M., TAGGART, M., BURGOYNE, P. S., ELLIOTT, D. & COOKE, H. J. 2003. Absence of mDazl produces a final block on germ cell development at meiosis. *Reproduction,* 126**,** 589-97.

SAXTON, R. A. & SABATINI, D. M. 2017. mTOR Signaling in Growth, Metabolism, and Disease. *Cell,* 168**,** 960-976.

SCHEIDEL, J., AMSTEIN, L., ACKERMANN, J., DIKIC, I. & KOCH, I. 2016. In Silico Knockout Studies of Xenophagic Capturing of Salmonella. *PLoS Comput Biol,* 12**,** e1005200.

SCHLUMBERGER, M. C. & HARDT, W. D. 2006. Salmonella type III secretion effectors: pulling the host cell's strings. *Curr Opin Microbiol,* 9**,** 46-54.

SCHNAITH, A., KASHKAR, H., LEGGIO, S. A., ADDICKS, K., KRONKE, M. & KRUT, O. 2007. Staphylococcus aureus subvert autophagy for induction of caspase-independent host cell death. *J Biol Chem,* 282**,** 2695-706.

SCHRODER, A., KLAND, R., PESCHEL, A., VON EIFF, C. & AEPFELBACHER, M. 2006. Live cell imaging of phagosome maturation in Staphylococcus aureus infected human endothelial cells: small colony variants are able to survive in lysosomes. *Med Microbiol Immunol,* 195**,** 185-94.

SCHWORER, C. M. & MORTIMORE, G. E. 1979. Glucagon-induced autophagy and proteolysis in rat liver: mediation by selective deprivation of intracellular amino acids. *Proc Natl Acad Sci U S A,* 76**,** 3169-73.

SENDI, P. & PROCTOR, R. A. 2009. Staphylococcus aureus as an intracellular pathogen: the role of small colony variants. *Trends Microbiol,* 17**,** 54-8.

SETO, S., TSUJIMURA, K. & KOIDE, Y. 2011. Rab GTPases regulating phagosome maturation are differentially recruited to mycobacterial phagosomes. *Traffic,* 12**,** 407-20.

SHAHNAZARI, S. & BRUMELL, J. H. 2011. Mechanisms and consequences of bacterial targeting by the autophagy pathway. *Curr Opin Microbiol,* 14**,** 68-75.

SHAHNAZARI, S., YEN, W. L., BIRMINGHAM, C. L., SHIU, J., NAMOLOVAN, A., ZHENG, Y. T., NAKAYAMA, K., KLIONSKY, D. J. & BRUMELL, J. H. 2010. A diacylglycerol-dependent signaling pathway contributes to regulation of antibacterial autophagy. *Cell Host Microbe,* 8**,** 137-46.

SHAID, S., BRANDTS, C. H., SERVE, H. & DIKIC, I. 2013. Ubiquitination and selective autophagy. *Cell Death Differ,* 20**,** 21-30.

SHALEM, O., SANJANA, N. E., HARTENIAN, E., SHI, X., SCOTT, D. A., MIKKELSON, T., HECKL, D., EBERT, B. L., ROOT, D. E., DOENCH, J. G. & ZHANG, F. 2014. Genome-scale CRISPR-Cas9 knockout screening in human cells. *Science,* 343**,** 84-87.

SHANG, L., CHEN, S., DU, F., LI, S., ZHAO, L. & WANG, X. 2011. Nutrient starvation elicits an acute autophagic response mediated by Ulk1 dephosphorylation and its subsequent dissociation from AMPK. *Proc Natl Acad Sci U S A,* 108**,** 4788-93.

SHAW, S. Y., TRAN, K., CASTORENO, A. B., PELOQUIN, J. M., LASSEN, K. G., KHOR, B., ALDRICH, L. N., TAN, P. H., GRAHAM, D. B., KUBALLA, P., GOEL, G., DALY, M. J., SHAMJI, A. F., SCHREIBER, S. L. & XAVIER, R. J. 2013. Selective modulation of autophagy, innate immunity, and adaptive immunity by small molecules. *ACS Chem Biol,* 8**,** 2724-2733.

SHI, C. S. & KEHRL, J. H. 2008. MyD88 and Trif target Beclin 1 to trigger autophagy in macrophages. *J Biol Chem,* 283**,** 33175-82.

SHI, J., WANG, E., MILAZZO, J. P., WANG, Z., KINNEY, J. B. & VAKOC, C. R. 2015. Discovery of cancer drug targets by CRISPR-Cas9 screening of protein domains. *Nat Biotechnol,* 33**,** 661-7.

SHPILKA, T., WEIDBERG, H., PIETROKOVSKI, S. & ELAZAR, Z. 2011. Atg8: an autophagy-related ubiquitin-like protein family. *Genome Biol,* 12**,** 226.

SINGH, V., DAVIDSON, A. C., HUME, P. J., HUMPHREYS, D. & KORONAKIS, V. 2017. Arf GTPase interplay with Rho GTPases in regulation of the actin cytoskeleton. *Small GTPases***,** 1-8.

SINHA, B. & FRAUNHOLZ, M. 2010. Staphylococcus aureus host cell invasion and post-invasion events. *Int J Med Microbiol,* 300**,** 170-5.

SINHA, B. & HERRMANN, M. 2005. Mechanism and consequences of invasion of endothelial cells by Staphylococcus aureus. *Thromb Haemost,* 94**,** 266-77.

SMITH, M. D., HARLEY, M. E., KEMP, A. J., WILLS, J., LEE, M., ARENDS, M., VON KRIEGSHEIM, A., BEHRENDS, C. & WILKINSON, S. 2017. CCPG1 Is a Non-canonical Autophagy Cargo Receptor Essential for ER-Phagy and Pancreatic ER Proteostasis. *Dev Cell*.

SONTAG, R. L., NAKAYASU, E. S., BROWN, R. N., NIEMANN, G. S., SYDOR, M. A., SANCHEZ, O., ANSONG, C., LU, S. Y., CHOI, H., VALLEAU, D., WEITZ, K. K., SAVCHENKO, A., CAMBRONNE, E. D. & ADKINS, J. N. 2016. Identification of Novel Host Interactors of Effectors Secreted by Salmonella and Citrobacter. *mSystems,* 1.

STAPLETON, P. D. & TAYLOR, P. W. 2002. Methicillin resistance in Staphylococcus aureus: mechanisms and modulation. *Sci Prog,* 85**,** 57-72.

STARR, T., CHILD, R., WEHRLY, T. D., HANSEN, B., HWANG, S., LOPEZ-OTIN, C., VIRGIN, H. W. & CELLI, J. 2012. Selective subversion of autophagy complexes facilitates completion of the Brucella intracellular cycle. *Cell Host Microbe,* 11**,** 33-45.

STECHER, B., HAPFELMEIER, S., MULLER, C., KREMER, M., STALLMACH, T. & HARDT, W. D. 2004. Flagella and chemotaxis are required for efficient induction of Salmonella enterica serovar Typhimurium colitis in streptomycin-pretreated mice. *Infect Immun,* 72**,** 4138-50.

STENMARK, H. 2009. Rab GTPases as coordinators of vesicle traffic. *Nat Rev Mol Cell Biol,* 10**,** 513-25.

STOLZ, A., ERNST, A. & DIKIC, I. 2014. Cargo recognition and trafficking in selective autophagy. *Nat Cell Biol,* 16**,** 495-501.

STROBEL, M., PFORTNER, H., TUCHSCHERR, L., VOLKER, U., SCHMIDT, F., KRAMKO, N., SCHNITTLER, H. J., FRAUNHOLZ, M. J., LOFFLER, B., PETERS, G. & NIEMANN, S. 2016. Post-invasion events after infection with Staphylococcus aureus are strongly dependent on both the host cell type and the infecting S. aureus strain. *Clin Microbiol Infect,* 22**,** 799-809.

SUN, Q., FAN, W., CHEN, K., DING, X., CHEN, S. & ZHONG, Q. 2008. Identification of Barkor as a mammalian autophagy-specific factor for Beclin 1 and class III phosphatidylinositol 3-kinase. *Proc Natl Acad Sci U S A,* 105**,** 19211-6.

SUZUKI, H., TABATA, K., MORITA, E., KAWASAKI, M., KATO, R., DOBSON, R. C., YOSHIMORI, T. & WAKATSUKI, S. 2014. Structural basis of the autophagy-related LC3/Atg13 LIR complex: recognition and interaction mechanism. *Structure,* 22**,** 47-58.

SUZUKI, T. & YAMAMOTO, M. 2017. Stress-sensing mechanisms and the physiological roles of the Keap1-Nrf2 system during cellular stress. *J Biol Chem,* 292**,** 16817-16824.

SVIDER, P. F., HUSAIN, Q., MAURO, K. M., FOLBE, A. J., BAREDES, S. & ELOY, J. A. 2014. Impact of mentoring medical students on scholarly productivity. *Int Forum Allergy Rhinol,* 4**,** 138-42.

TAKAHASHI, Y., COPPOLA, D., MATSUSHITA, N., CUALING, H. D., SUN, M., SATO, Y., LIANG, C., JUNG, J. U., CHENG, J. Q., MULE, J. J., PLEDGER, W. J. & WANG, H. G. 2007. Bif-1 interacts with Beclin 1 through UVRAG and regulates autophagy and tumorigenesis. *Nat Cell Biol,* 9**,** 1142-51.

TAKESHIGE, K., BABA, M., TSUBOI, S., NODA, T. & OHSUMI, Y. 1992. Autophagy in yeast demonstrated with proteinase-deficient mutants and conditions for its induction. *J Cell Biol,* 119**,** 301-11.

TAO, S., LIU, P., LUO, G., ROJO DE LA VEGA, M., CHEN, H., WU, T., TILLOTSON, J., CHAPMAN, E. & ZHANG, D. D. 2017. p97 Negatively Regulates NRF2 by Extracting Ubiquitylated NRF2 from the KEAP1-CUL3 E3 Complex. *Mol Cell Biol,* 37.

TEO, W. X., KERR, M. C. & TEASDALE, R. D. 2016. MTMR4 Is Required for the Stability of the Salmonella-Containing Vacuole. *Front Cell Infect Microbiol,* 6**,** 91.

THIELE, D. L. & LIPSKY, P. E. 1990. Mechanism of L-leucyl-L-leucine methyl ester-mediated killing of cytotoxic lymphocytes: dependence on a lysosomal thiol protease, dipeptidyl peptidase I, that is enriched in these cells. *Proc Natl Acad Sci U S A,* 87**,** 83-7.

THURSTON, T. L., BOYLE, K. B., ALLEN, M., RAVENHILL, B. J., KARPIYEVICH, M., BLOOR, S., KAUL, A., NOAD, J., FOEGLEIN, A., MATTHEWS, S. A., KOMANDER, D., BYCROFT, M. & RANDOW, F. 2016. Recruitment of TBK1 to cytosol-invading Salmonella induces WIPI2-dependent antibacterial autophagy. *Embo j,* 35**,** 1779-92.

THURSTON, T. L., RYZHAKOV, G., BLOOR, S., VON MUHLINEN, N. & RANDOW, F. 2009. The TBK1 adaptor and autophagy receptor NDP52 restricts the proliferation of ubiquitin-coated bacteria. *Nat Immunol,* 10**,** 1215-21.

THURSTON, T. L., WANDEL, M. P., VON MUHLINEN, N., FOEGLEIN, A. & RANDOW, F. 2012. Galectin 8 targets damaged vesicles for autophagy to defend cells against bacterial invasion. *Nature,* 482**,** 414-8.

TING, J. P., LOVERING, R. C., ALNEMRI, E. S., BERTIN, J., BOSS, J. M., DAVIS, B. K., FLAVELL, R. A., GIRARDIN, S. E., GODZIK, A., HARTON, J. A., HOFFMAN, H. M., HUGOT, J. P., INOHARA, N., MACKENZIE, A., MALTAIS, L. J., NUNEZ, G., OGURA, Y., OTTEN, L. A., PHILPOTT, D., REED, J. C., REITH, W., SCHREIBER, S., STEIMLE, V. & WARD, P. A. 2008. The NLR gene family: a standard nomenclature. *Immunity,* 28**,** 285-7.

TONG, S. Y., DAVIS, J. S., EICHENBERGER, E., HOLLAND, T. L. & FOWLER, V. G., JR. 2015. Staphylococcus aureus infections: epidemiology, pathophysiology, clinical manifestations, and management. *Clin Microbiol Rev,* 28**,** 603-61.

TRAVASSOS, L. H., CARNEIRO, L. A., RAMJEET, M., HUSSEY, S., KIM, Y. G., MAGALHAES, J. G., YUAN, L., SOARES, F., CHEA, E., LE BOURHIS, L., BONECA, I. G., ALLAOUI, A., JONES,

N. L., NUNEZ, G., GIRARDIN, S. E. & PHILPOTT, D. J. 2010. Nod1 and Nod2 direct autophagy by recruiting ATG16L1 to the plasma membrane at the site of bacterial entry. *Nat Immunol,* 11**,** 55-62.

TRIANTAFILOU, M., LEPPER, P. M., BRIAULT, C. D., AHMED, M. A., DMOCHOWSKI, J. M., SCHUMANN, C. & TRIANTAFILOU, K. 2008. Chemokine receptor 4 (CXCR4) is part of the lipopolysaccharide "sensing apparatus". *Eur J Immunol,* 38**,** 192-203.

TUMBARELLO, D. A., MANNA, P. T., ALLEN, M., BYCROFT, M., ARDEN, S. D., KENDRICK-JONES, J. & BUSS, F. 2015. The Autophagy Receptor TAX1BP1 and the Molecular Motor Myosin VI Are Required for Clearance of Salmonella Typhimurium by Autophagy. *PLoS Pathog,* 11**,** e1005174.

UCHIMOTO, T., NOHARA, H., KAMEHARA, R., IWAMURA, M., WATANABE, N. & KOBAYASHI, Y. 1999. Mechanism of apoptosis induced by a lysosomotropic agent, L-Leucyl-L-Leucine methyl ester. *Apoptosis,* 4**,** 357-62.

VAN DER VELDEN, A. W., LINDGREN, S. W., WORLEY, M. J. & HEFFRON, F. 2000. Salmonella pathogenicity island 1-independent induction of apoptosis in infected macrophages by Salmonella enterica serotype typhimurium. *Infect Immun,* 68**,** 5702-9.

VAN WIJK, S. J., FISKIN, E., PUTYRSKI, M., PAMPALONI, F., HOU, J., WILD, P., KENSCHE, T., GRECCO, H. E., BASTIAENS, P. & DIKIC, I. 2012. Fluorescence-based sensors to monitor localization and functions of linear and K63-linked ubiquitin chains in cells. *Mol Cell,* 47**,** 797-809.

VAN WIJK, S. J. L., FRICKE, F., HERHAUS, L., GUPTA, J., HOTTE, K., PAMPALONI, F., GRUMATI, P., KAULICH, M., SOU, Y. S., KOMATSU, M., GRETEN, F. R., FULDA, S., HEILEMANN, M. & DIKIC, I. 2017. Linear ubiquitination of cytosolic Salmonella Typhimurium activates NF-kappaB and restricts bacterial proliferation. *Nat Microbiol,* 2**,** 17066.

VAZQUEZ-TORRES, A., XU, Y., JONES-CARSON, J., HOLDEN, D. W., LUCIA, S. M., DINAUER, M. C., MASTROENI, P. & FANG, F. C. 2000. Salmonella pathogenicity island 2-dependent evasion of the phagocyte NADPH oxidase. *Science,* 287**,** 1655-8.

VAZQUEZ, C. L. & COLOMBO, M. I. 2010. Coxiella burnetii modulates Beclin 1 and Bcl-2, preventing host cell apoptosis to generate a persistent bacterial infection. *Cell Death Differ,* 17**,** 421-38.

VERLHAC, P., GREGOIRE, I. P., AZOCAR, O., PETKOVA, D. S., BAGUET, J., VIRET, C. & FAURE, M. 2015. Autophagy receptor NDP52 regulates pathogen-containing autophagosome maturation. *Cell Host Microbe,* 17**,** 515-25.

VIRREIRA WINTER, S., ZYCHLINSKY, A. & BARDOEL, B. W. 2016. Genome-wide CRISPR screen reveals novel host factors required for Staphylococcus aureus alpha-hemolysin-mediated toxicity. *Sci Rep,* 6**,** 24242.

VLADIMER, G. I., MARTY-ROIX, R., GHOSH, S., WENG, D. & LIEN, E. 2013. Inflammasomes and host defenses against bacterial infections. *Curr Opin Microbiol,* 16**,** 23-31.

VON MUHLINEN, N., AKUTSU, M., RAVENHILL, B. J., FOEGLEIN, A., BLOOR, S., RUTHERFORD, T. J., FREUND, S. M., KOMANDER, D. & RANDOW, F. 2012. LC3C, bound selectively by a noncanonical LIR motif in NDP52, is required for antibacterial autophagy. *Mol Cell,* 48**,** 329-42.

WANG, L., YAN, J., NIU, H., HUANG, R. & WU, S. 2018. Autophagy and Ubiquitination in Salmonella Infection and the Related Inflammatory Responses. *Front Cell Infect Microbiol,* 8**,** 78.

WANG, T., BIRSOY, K., HUGHES, N. W., KRUPCZAK, K. M., POST, Y., WEI, J. J., LANDER, E. S. & SABATINI, D. M. 2015. Identification and characterization of essential genes in the human genome. *Science,* 350**,** 1096-101.

WANG, T., WEI, J. J., SABATINI, D. M. & LANDER, E. S. 2014. Genetic screens in human cells using the CRISPR-Cas9 system. *Science,* 343**,** 80-4.

WATTIAU, P., BOLAND, C. & BERTRAND, S. 2011. Methodologies for Salmonella enterica subsp. enterica subtyping: gold standards and alternatives. *Appl Environ Microbiol,* 77**,** 7877-85.

WEI, Y., PATTINGRE, S., SINHA, S., BASSIK, M. & LEVINE, B. 2008. JNK1-mediated phosphorylation of Bcl-2 regulates starvation-induced autophagy. *Mol Cell,* 30**,** 678-88.

WEIDBERG, H., SHPILKA, T., SHVETS, E., ABADA, A., SHIMRON, F. & ELAZAR, Z. 2011. LC3 and GATE-16 N termini mediate membrane fusion processes required for autophagosome biogenesis. *Dev Cell,* 20**,** 444-54.

WEIDBERG, H., SHVETS, E., SHPILKA, T., SHIMRON, F., SHINDER, V. & ELAZAR, Z. 2010. LC3 and GATE-16/GABARAP subfamilies are both essential yet act differently in autophagosome biogenesis. *Embo j,* 29**,** 1792-802.

WESTLING, K. 2009. Cost-effectiveness analysis of treatment of methicillin-resistant Staphylococcus aureus bacteremia and endocarditis is a difficult issue. *Clin Infect Dis,* 49**,** 699-701.

WILD, P., FARHAN, H., MCEWAN, D. G., WAGNER, S., ROGOV, V. V., BRADY, N. R., RICHTER, B., KORAC, J., WAIDMANN, O., CHOUDHARY, C., DOTSCH, V., BUMANN, D. & DIKIC, I. 2011. Phosphorylation of the autophagy receptor optineurin restricts Salmonella growth. *Science,* 333**,** 228-33.

WILKE, G. A. & BUBECK WARDENBURG, J. 2010. Role of a disintegrin and metalloprotease 10 in Staphylococcus aureus alpha-hemolysin-mediated cellular injury. *Proc Natl Acad Sci U S A,* 107**,** 13473-8.

WILLIAMS, A., SARKAR, S., CUDDON, P., TTOFI, E. K., SAIKI, S., SIDDIQI, F. H., JAHREISS, L., FLEMING, A., PASK, D., GOLDSMITH, P., O'KANE, C. J., FLOTO, R. A. & RUBINSZTEIN, D. C. 2008. Novel targets for Huntington's disease in an mTOR-independent autophagy pathway. *Nat Chem Biol,* 4**,** 295-305.

WINCHELL, C. G., GRAHAM, J. G., KURTEN, R. C. & VOTH, D. E. 2014. Coxiella burnetii type IV secretion-dependent recruitment of macrophage autophagosomes. *Infect Immun,* 82**,** 2229-38.

WOLD, M. S., LIM, J., LACHANCE, V., DENG, Z. & YUE, Z. 2016. ULK1-mediated phosphorylation of ATG14 promotes autophagy and is impaired in Huntington's disease models. *Mol Neurodegener,* 11**,** 76.

WONG, Y. C. & HOLZBAUR, E. L. 2014. Optineurin is an autophagy receptor for damaged mitochondria in parkin-mediated mitophagy that is disrupted by an ALS-linked mutation. *Proc Natl Acad Sci U S A,* 111**,** E4439-48.

WOOD, A. J., LO, T. W., ZEITLER, B., PICKLE, C. S., RALSTON, E. J., LEE, A. H., AMORA, R., MILLER, J. C., LEUNG, E., MENG, X., ZHANG, L., REBAR, E. J., GREGORY, P. D., URNOV, F. D. & MEYER, B. J. 2011. Targeted genome editing across species using ZFNs and TALENs. *Science,* 333**,** 307.

XIA, J., GAO, J., KOKUDO, N., HASEGAWA, K. & TANG, W. 2013. Methicillin-resistant Staphylococcus aureus antibiotic resistance and virulence. *Biosci Trends,* 7**,** 113-21.

XU, Y., JAGANNATH, C., LIU, X. D., SHARAFKHANEH, A., KOLODZIEJSKA, K. E. & EISSA, N. T. 2007. Toll-like receptor 4 is a sensor for autophagy associated with innate immunity. *Immunity,* 27**,** 135-44.

YANG, Z. & KLIONSKY, D. J. 2010. Eaten alive: a history of macroautophagy. *Nat Cell Biol,* 12**,** 814-22.

YOO, S. M. & JUNG, Y. K. 2018. A Molecular Approach to Mitophagy and Mitochondrial Dynamics. *Mol Cells,* 41**,** 18-26.

YOSHIDA, Y., YASUDA, S., FUJITA, T., HAMASAKI, M., MURAKAMI, A., KAWAWAKI, J., IWAI, K., SAEKI, Y., YOSHIMORI, T., MATSUDA, N. & TANAKA, K. 2017. Ubiquitination of exposed glycoproteins by SCF(FBXO27) directs damaged lysosomes for autophagy. *Proc Natl Acad Sci U S A,* 114**,** 8574-8579.

YOSHIKAWA, Y., OGAWA, M., HAIN, T., YOSHIDA, M., FUKUMATSU, M., KIM, M., MIMURO, H., NAKAGAWA, I., YANAGAWA, T., ISHII, T., KAKIZUKA, A., SZTUL, E., CHAKRABORTY, T. & SASAKAWA, C. 2009. Listeria monocytogenes ActA-mediated escape from autophagic recognition. *Nat Cell Biol,* 11**,** 1233-40.

YOUNG, A. R., CHAN, E. Y., HU, X. W., KOCHL, R., CRAWSHAW, S. G., HIGH, S., HAILEY, D. W., LIPPINCOTT-SCHWARTZ, J. & TOOZE, S. A. 2006. Starvation and ULK1-dependent cycling of mammalian Atg9 between the TGN and endosomes. *J Cell Sci,* 119**,** 3888-900.

YU, L., CHEN, Y. & TOOZE, S. A. 2018. Autophagy pathway: Cellular and molecular mechanisms. *Autophagy,* 14**,** 207-215.

YUK, J. M., YOSHIMORI, T. & JO, E. K. 2012. Autophagy and bacterial infectious diseases. *Exp Mol Med,* 44**,** 99-108.

ZALCKVAR, E., BERISSI, H., MIZRACHY, L., IDELCHUK, Y., KOREN, I., EISENSTEIN, M., SABANAY, H., PINKAS-KRAMARSKI, R. & KIMCHI, A. 2009. DAP-kinase-mediated phosphorylation on the BH3 domain of beclin 1 promotes dissociation of beclin 1 from Bcl-XL and induction of autophagy. *EMBO Rep,* 10**,** 285-92.

ZEDEN, M. S., SCHUSTER, C. F., BOWMAN, L., ZHONG, Q., WILLIAMS, H. D. & GRUNDLING, A. 2018. Cyclic-di-adenosine monophosphate (c-di-AMP) is required for osmotic regulation in Staphylococcus aureus but dispensable for viability in anaerobic conditions. *J Biol Chem*.

ZHAO, Z., FUX, B., GOODWIN, M., DUNAY, I. R., STRONG, D., MILLER, B. C., CADWELL, K., DELGADO, M. A., PONPUAK, M., GREEN, K. G., SCHMIDT, R. E., MIZUSHIMA, N., DERETIC, V., SIBLEY, L. D. & VIRGIN, H. W. 2008. Autophagosome-independent essential function for the autophagy protein Atg5 in cellular immunity to intracellular pathogens. *Cell Host Microbe,* 4**,** 458-69.

ZHENG, Y. T., SHAHNAZARI, S., BRECH, A., LAMARK, T., JOHANSEN, T. & BRUMELL, J. H. 2009. The adaptor protein p62/SQSTM1 targets invading bacteria to the autophagy pathway. *J Immunol,* 183**,** 5909-16.

ZHONG, C., YIN, Q., XIE, Z., BAI, M., DONG, R., TANG, W., XING, Y. H., ZHANG, H., YANG, S., CHEN, L. L., BARTOLOMEI, M. S., FERGUSON-SMITH, A., LI, D., YANG, L., WU, Y. & LI, J. 2015. CRISPR-Cas9-Mediated Genetic Screening in Mice with Haploid Embryonic Stem Cells Carrying a Guide RNA Library. *Cell Stem Cell,* 17**,** 221-32.

ZHONG, Y., WANG, Q. J., LI, X., YAN, Y., BACKER, J. M., CHAIT, B. T., HEINTZ, N. & YUE, Z. 2009. Distinct regulation of autophagic activity by Atg14L and Rubicon associated with Beclin 1-phosphatidylinositol-3-kinase complex. *Nat Cell Biol,* 11**,** 468-76.

ZHOU, C., MA, K., GAO, R., MU, C., CHEN, L., LIU, Q., LUO, Q., FENG, D., ZHU, Y. & CHEN, Q. 2017. Regulation of mATG9 trafficking by Src- and ULK1-mediated phosphorylation in basal and starvation-induced autophagy. *Cell Res,* 27**,** 184-201.

ZHOU, Y., ZHU, S., CAI, C., YUAN, P., LI, C., HUANG, Y. & WEI, W. 2014. High-throughput screening of a CRISPR/Cas9 library for functional genomics in human cells. *Nature,* 509**,** 487-91.

ZHU, Y., LI, H., DING, S. & WANG, Y. 2018. Autophagy inhibition promotes phagocytosis of macrophage and protects mice from methicillin-resistant staphylococcus aureus pneumonia. *J Cell Biochem*.